

**UCLA**

**UCLA Electronic Theses and Dissertations**

**Title**

Atomically Precise, Multivalent Organomimetic Cluster Nanomolecules

**Permalink**

<https://escholarship.org/uc/item/78c1n2wf>

**Author**

Qian, Elaine Anne

**Publication Date**

2019

Peer reviewed|Thesis/dissertation

UNIVERSITY OF CALIFORNIA

Los Angeles

Atomically Precise, Multivalent  
Organomimetic Cluster Nanomolecules

A dissertation submitted in partial satisfaction of the  
requirements for the degree Doctor of Philosophy  
in Bioengineering

by

Elaine Anne Qian

2019



© Copyright by

Elaine Anne Qian

2019

## ABSTRACT OF THE DISSERTATION

Atomically Precise, Multivalent  
Organomimetic Cluster Nanomolecules

by

Elaine Anne Qian

Doctor of Philosophy in Bioengineering

University of California, Los Angeles, 2019

Professor Heather D. Maynard, Co-Chair

Professor Alexander Michael Spokoyny, Co-Chair

This dissertation describes efforts in assembling atomically precise and structurally robust hybrid nanomolecules featuring an inorganic dodecaborate cluster scaffold, as well as work in applying the functionalized nanomolecules to study multivalent interactions with proteins. Specifically, this dissertation describes two bioconjugation strategies – perfluoroaryl-thiol nucleophilic aromatic substitution ( $S_{\text{N}}\text{Ar}$ ) chemistry and transition metal-mediated chemistry – for constructing well-defined and tunable cluster-based nanomolecules. Both conjugation approaches offer excellent chemoselectivity toward thiols and facilitate the rapid perfunctionalization of the cluster core with a wide scope of thiol-based molecules and macromolecules. The resulting nanomolecules exhibit high structural stability under biologically relevant conditions because of

the full covalency of all the bonding interactions. Importantly, these assemblies can be rationally engineered to engender specific, multivalent recognition of a variety of protein targets with high avidity. In a biomedically relevant example, biocompatible glycosylated nanomolecules are able to inhibit the protein-protein interactions between a dendritic cell receptor and a viral envelope glycoprotein, thereby preventing the cell uptake of the glycoprotein.

The dissertation of Elaine Anne Qian is approved.

Timothy J. Deming

Zhen Gu

Heather D. Maynard, Committee Co-Chair

Alexander Michael Spokoyny, Committee Co-Chair

University of California, Los Angeles

2019

*To my husband, Alex, and my parents, Xin and Fu Min, for their unwavering love and support.*

## TABLE OF CONTENTS

LIST OF FIGURES	xiv
LIST OF TABLES	xxiv
ACKNOWLEDGMENTS	xxv
VITA	xxvii
CHAPTER ONE: Synthesis and Applications of Perfunctionalized Boron Clusters	1
Introduction to Biological Applications	1
Delivery of $^{10}\text{B}$ for Boron Neutron Capture Therapy (BNCT)	1
Delivery of Chemotherapy Drugs	5
Diagnostic Imaging	7
Multivalent Protein Binders	8
CHAPTER TWO: Atomically Precise Organomimetic Cluster Nanomolecules Assembled via Perfluoroaryl-Thiol $\text{S}_{\text{N}}\text{Ar}$ Chemistry	11
Abstract	11
Introduction	12
Results and Discussion	15
Conclusions	27
Experimental Section	29
General considerations	29
Materials	29
Instruments	30
2D diffusion-ordered (DOSY) $^1\text{H}$ NMR spectroscopy	31

High resolution transmission electron microscopy (HRTEM)	31
Size exclusion chromatography-multi angle light scattering (SEC-MALS)	32
Surface plasmon resonance (SPR)	32
X-ray data collection and processing parameters	33
Microwave synthesis	34
Synthesis of <b>1</b>	35
Synthesis of <b>2</b>	35
Synthesis of 4-pentafluorophenyl(hydroxymethyl) benzene	36
Synthesis of 4-pentafluorophenyl(bromomethyl) benzene	37
Synthesis of <b>3</b>	38
Synthesis of <b>2a</b>	40
Synthesis of <b>2b</b>	41
Synthesis of <b>2c</b>	42
Synthesis of <b>2d</b>	43
Synthesis of <b>2e</b>	45
Synthesis of <b>2f</b>	46
Synthesis of <b>2i</b>	47
Synthesis of <b>j</b>	48
Synthesis of <b>2j</b>	49
Synthesis of <b>2k</b>	50
Synthesis of <b>2l</b>	51
Synthesis of <b>3a</b>	52
Synthesis of <b>3b</b>	54

Synthesis of <b>3c</b>	55
Synthesis of <b>3d</b>	57
Synthesis of <b>3e</b>	58
Synthesis of <b>3f</b>	59
Synthesis of <b>3g</b>	60
Synthesis of <b>3h</b>	61
Synthesis of <b>3i</b>	62
Synthesis of <b>3j</b>	63
Synthesis of <b>3k</b>	64
Synthesis of <b>3l</b>	65
Stability studies of <b>2i</b> under biologically relevant conditions	67
Computational work	69
CHAPTER THREE: Multivalent Cluster Nanomolecules for Inhibiting Protein-Protein Interactions	81
Abstract	81
Introduction	82
Results and Discussion	84
Conclusions	97
Experimental Section	98
General considerations	98
Materials	98
Instruments	99
Synthesis of <b>1</b>	100



Synthesis of <b>2</b>	100
Synthesis of <b>2a</b>	101
Synthesis of <b>2b</b>	102
Synthesis of <b>2c</b>	104
Synthesis of <b>2d</b>	105
Synthesis of sulfone-bridged linker	106
Synthesis of <b>3</b>	108
Synthesis of <b>3a</b>	109
Synthesis of <b>3b</b>	110
Synthesis of <b>3c</b>	111
Synthesis of <b>3d</b>	112
SPR procedure and supplementary data	113
Cell proliferation assay	117
Confocal microscopy procedure and supplementary data	117
Computational work	128
CHAPTER FOUR: An Organometallic Strategy for Assembling Atomically Precise Hybrid Nanomaterials	130
Abstract	130
Introduction	131
Results and Discussion	133
Conclusions	147
Experimental Section	148
General considerations	148

Materials	148
Instruments and methods	149
Synthesis of Me-DalPhos	151
Synthesis of (Me-DalPhos)AuCl	151
Synthesis of B <sub>12</sub> (OCH <sub>2</sub> C <sub>6</sub> H <sub>4</sub> ) <sub>12</sub>	151
Synthesis of [B <sub>12</sub> (OCH <sub>2</sub> C <sub>6</sub> H <sub>4</sub> ((Me-DalPhos)AuCl) <sub>12</sub> ][SbF <sub>6</sub> ] <sub>11</sub> ( <b>[1]</b> )[SbF <sub>6</sub> ] <sub>11</sub> )	153
General procedure for conjugation reactions with <b>[1]</b> [SbF <sub>6</sub> ] <sub>11</sub>	155
Synthesis of [K <sub>2</sub> ][B <sub>12</sub> (OCH <sub>2</sub> C <sub>6</sub> H <sub>4</sub> SPh) <sub>12</sub> ] ( <b>[K<sub>2</sub>][2]</b> )	156
Synthesis of [K <sub>2</sub> ][B <sub>12</sub> (OCH <sub>2</sub> C <sub>6</sub> H <sub>4</sub> SC <sub>6</sub> H <sub>4</sub> ) <sub>12</sub> ] ( <b>[K<sub>2</sub>][3]</b> )	157
Synthesis of [K <sub>2</sub> ][B <sub>12</sub> (OCH <sub>2</sub> C <sub>6</sub> H <sub>4</sub> SCH <sub>2</sub> C <sub>6</sub> H <sub>5</sub> ) <sub>12</sub> ] ( <b>[K<sub>2</sub>][4]</b> )	157
Synthesis of [K <sub>2</sub> ][B <sub>12</sub> (OCH <sub>2</sub> C <sub>6</sub> H <sub>4</sub> (cyclohexanethiol)) <sub>12</sub> ] ( <b>[K<sub>2</sub>][5]</b> )	158
Synthesis of [K <sub>2</sub> ][B <sub>12</sub> (OCH <sub>2</sub> C <sub>6</sub> H <sub>4</sub> (1-thioglycerol)) <sub>12</sub> ] ( <b>[K<sub>2</sub>][6]</b> )	159
Synthesis of [K <sub>2</sub> ][B <sub>12</sub> (OCH <sub>2</sub> C <sub>6</sub> H <sub>4</sub> (2-mercaptoethanol)) <sub>12</sub> ] ( <b>[K<sub>2</sub>][7]</b> )	160
Synthesis of [K <sub>2</sub> ][B <sub>12</sub> (OCH <sub>2</sub> C <sub>6</sub> H <sub>4</sub> ( <i>m</i> PEG <sub>350</sub> thiol)) <sub>12</sub> ] ( <b>[K<sub>2</sub>][8]</b> )	160
Synthesis of [Na <sub>14</sub> ][B <sub>12</sub> (OCH <sub>2</sub> C <sub>6</sub> H <sub>4</sub> (2-thioethanesulfonate)) <sub>12</sub> ] ( <b>[Na<sub>14</sub>][9]</b> )	161
Synthesis of [H <sub>3</sub> NC(CH <sub>2</sub> OH) <sub>3</sub> /Na] <sub>14</sub> [B <sub>12</sub> (OCH <sub>2</sub> C <sub>6</sub> H <sub>4</sub> (2-thioethanesulfonate)) <sub>12</sub> ] ( <b>[H<sub>3</sub>NC(CH<sub>2</sub>OH)<sub>3</sub>/Na]<sub>14</sub>[9]</b> )	162
Synthesis of [K <sub>2</sub> ][B <sub>12</sub> (OCH <sub>2</sub> C <sub>6</sub> H <sub>4</sub> S(CH <sub>2</sub> ) <sub>5</sub> CH <sub>3</sub> ) <sub>12</sub> ] ( <b>[K<sub>2</sub>][10]</b> )	163
Synthesis of [K <sub>2</sub> ][B <sub>12</sub> (OCH <sub>2</sub> C <sub>6</sub> H <sub>4</sub> SC <sub>6</sub> F <sub>5</sub> ) <sub>12</sub> ] ( <b>[K<sub>2</sub>][11]</b> )	164
Synthesis of [H <sub>3</sub> NC(CH <sub>2</sub> OH) <sub>3</sub> ] <sub>2</sub> [B <sub>12</sub> (OCH <sub>2</sub> C <sub>6</sub> H <sub>4</sub> (2-thio-5-trifluoromethylpyridine)) <sub>12</sub> ] ( <b>[H<sub>3</sub>NC(CH<sub>2</sub>OH)<sub>3</sub>]<sub>2</sub>[12]</b> )	165
Synthesis of [K <sub>2</sub> ][B <sub>12</sub> (OCH <sub>2</sub> C <sub>6</sub> H <sub>4</sub> (2-mercaptobenzothiazole)) <sub>12</sub> ] ( <b>[K<sub>2</sub>][13]</b> )	166
Synthesis of [K <sub>2</sub> ][B <sub>12</sub> (OCH <sub>2</sub> C <sub>6</sub> H <sub>4</sub> (2-thio-5-(4-pyridyl)-1,3,4-oxadiazole)) <sub>12</sub> ] ( <b>[K<sub>2</sub>][14]</b> )	167

Synthesis of $[\text{K}_2][\text{B}_{12}(\text{OCH}_2\text{C}_6\text{H}_4(3\text{-thio-1,2,4-triazole}))_{12}]$ ( $[\text{K}_2][\mathbf{15}]$ )	167
Synthesis of $[\text{K}_2][\text{B}_{12}(\text{OCH}_2\text{C}_6\text{H}_4\text{SePh})_{12}]$ ( $[\text{K}_2][\mathbf{16}]$ )	168
Synthesis of $[\text{H}_3\text{NC}(\text{CH}_2\text{OH})_3][\text{B}_{12}(\text{OCH}_2\text{C}_6\text{H}_4(\text{glutathione}))_{12}]$ ( $[\text{H}_3\text{NC}(\text{CH}_2\text{OH})_3][\mathbf{17}]$ )	169
Synthesis of $[\text{Na}_2][\text{B}_{12}(\text{OCH}_2\text{C}_6\text{H}_4(1\text{-thio-}\beta\text{-D-glucose}))_{12}]$ ( $[\text{Na}_2][\mathbf{18}]$ )	170
Synthesis of $[\text{Na}_2][\text{B}_{12}(\text{OCH}_2\text{C}_6\text{H}_4(1\text{-thio-}\beta\text{-D-galactose}))_{12}]$ ( $[\text{Na}_2][\mathbf{19}]$ )	171
Synthesis of $[\text{Na}_2][\text{B}_{12}(\text{OCH}_2\text{C}_6\text{H}_4(1\text{-thio-}\alpha\text{-D-mannose}))_{12}]$ ( $[\text{Na}_2][\mathbf{20}]$ )	172
Synthesis of $[\text{B}_{12}(\text{OCH}_2\text{C}_6\text{H}_4\text{SC}_6\text{H}_4(\text{Me-DalPhos})\text{AuCl})_{12}][\text{SbF}_6]_{10}$ ( $[\mathbf{21}][\text{SbF}_6]_{10}$ )	174
General procedure for conjugation reactions with $[\mathbf{21}][\text{SbF}_6]_{10}$	175
Synthesis of $[\text{H}_3\text{NC}(\text{CH}_2\text{OH})_3]_2[\text{B}_{12}(\text{OCH}_2\text{C}_6\text{H}_4\text{SC}_6\text{H}_4\text{SPh})_{12}]$ ( $[\text{H}_3\text{NC}(\text{CH}_2\text{OH})_3]_2[\mathbf{22}]$ )	176
Synthesis of $[\text{H}_3\text{NC}(\text{CH}_2\text{OH})_3]_2[\text{B}_{12}(\text{OCH}_2\text{C}_6\text{H}_4\text{SC}_6\text{H}_4(5\text{-(4-pyridyl)-oxadiazole-2-thiol}))_{12}]$ ( $[\text{H}_3\text{NC}(\text{CH}_2\text{OH})_3]_2[\mathbf{23}]$ )	176
Synthesis of $[\text{H}_3\text{NC}(\text{CH}_2\text{OH})_3]_2[\text{B}_{12}(\text{OCH}_2\text{C}_6\text{H}_4\text{SC}_6\text{H}_4(2\text{-thio-5-trifluoromethylpyridine}))_{12}]$ ( $[\text{H}_3\text{NC}(\text{CH}_2\text{OH})_3]_2[\mathbf{24}]$ )	176
Synthesis of $[\text{H}_3\text{NC}(\text{CH}_2\text{OH})_3]_2[\text{B}_{12}(\text{OCH}_2\text{C}_6\text{H}_4\text{SC}_6\text{H}_4(2\text{-mercaptoethanol}))_{12}]$ ( $[\text{H}_3\text{NC}(\text{CH}_2\text{OH})_3]_2[\mathbf{25}]$ )	177
Synthesis of $[\text{H}_3\text{NC}(\text{CH}_2\text{OH})_3]_2[\text{B}_{12}(\text{OCH}_2\text{C}_6\text{H}_4\text{SC}_6\text{H}_4\text{S}(\text{CH}_2)_5\text{CH}_3)_{12}]$ ( $[\text{H}_3\text{NC}(\text{CH}_2\text{OH})_3]_2[\mathbf{26}]$ )	177
Synthesis of $[\text{Na}_2][\text{B}_{12}(\text{OCH}_2\text{C}_6\text{H}_4\text{SC}_6\text{H}_4(1\text{-thio-}\beta\text{-D-galactose}))_{12}]$ ( $[\text{Na}_2][\mathbf{27}]$ )	178
Synthesis of $[\text{H}_3\text{NC}(\text{CH}_2\text{OH})_3]_2[\text{B}_{12}(\text{OCH}_2\text{C}_6\text{H}_4\text{SC}_6\text{H}_4(N\text{-}(tert\text{-butoxycarbonyl})\text{-L-cysteine methyl ester}))_{12}]$ ( $[\text{H}_3\text{NC}(\text{CH}_2\text{OH})_3]_2[\mathbf{28}]$ )	178
Synthesis of $[\text{H}_3\text{NC}(\text{CH}_2\text{OH})_3]_2[\text{B}_{12}(\text{OCH}_2\text{C}_6\text{H}_4\text{SC}_6\text{H}_4(2\text{-mercaptobenzothiazole}))_{12}]$ ( $[\text{H}_3\text{NC}(\text{CH}_2\text{OH})_3]_2[\mathbf{29}]$ )	179

Synthesis of $[\text{H}_3\text{NC}(\text{CH}_2\text{OH})_3]_2[\text{B}_{12}(\text{OCH}_2\text{C}_6\text{H}_4\text{SC}_6\text{H}_4\text{SC}_6\text{H}_4\text{I})_{12}]$ ( $[\text{H}_3\text{NC}(\text{CH}_2\text{OH})_3]_2[\mathbf{30}]$ )	179
Synthesis of (1-thio- $\beta$ -D-galactose) $_2\text{C}_6\text{H}_4$	180
Stability studies of $[\text{Na}_2][\text{B}_{12}(\text{OCH}_2\text{C}_6\text{H}_4(1\text{-thio-}\beta\text{-D-glucose}))_{12}]$ under biologically relevant conditions	181
Monitoring the conjugation reaction between $[\mathbf{1}][\text{SbF}_6]_{11}$ and $\text{Na}[1\text{-thio-}\beta\text{-D-galactose}]$ by $^{31}\text{P}$ NMR spectroscopy	183
Procedure for (Me-DalPhos)AuCl recovery after conjugation reactions	185
Surface plasmon resonance (SPR) measurements	188
Concanavalin A (ConA)	188
Shiga Toxin 1, B Subunit (Stx1B)	189
DC-SIGN ECD	191
Confocal microscopy studies with DC-SIGN	193
Free D-mannose control	197
$[\text{K}_2][\mathbf{8}]$ control	198
$[\text{Na}_2][\mathbf{20}]$ inhibitor	199
Computational studies	200
Systems and methods	200
Calculated structures	201
Binding of $[\mathbf{18}]^{2-}$ with ConA	203
Binding of $[\mathbf{19}]^{2-}$ and $[\mathbf{8}]^{2-}$ with Stx1B	205
Binding of $[\mathbf{20}]^{2-}$ with DC-SIGN	208
X-ray crystallographic details	209

$B_{12}(OCH_2C_6H_4I)_{12}$	209
$[B_{12}(OCH_2C_6H_4((Me-DalPhos)AuCl))_{12}][SbF_6]_{11} ([1][SbF_6]_{11})$	211
APPENDICES	215
Supplementary Data Relevant to Chapter Two	215
Supplementary Data Relevant to Chapter Three	398
Supplementary Data Relevant to Chapter Four	445
A Cluster-based Approach for Peptide Macrocyclization	548
REFERENCES	556

## LIST OF FIGURES

**Figure 1.1.** (A) Illustration of BNCT, a binary strategy for the treatment of cancer. (B) Some BNCT candidates used in preclinical and clinical settings. 2

**Figure 1.2.** (A) Chemical structure and (B) 3D representation of the dodeca(*nido-o*-carboranyl)-substituted dodecaborate cluster. 4

**Figure 1.3.** (A) Trimodal closomer drug-delivery system, CDDS-1, which features targeting, imaging, and cell-killing abilities. (B) Confocal microscopy images of CDDS-1 showing its colocalization with lysosomes. 6

**Figure 1.4.** (A) cRGD peptide-labeled,  $Gd^{3+}$ -DOTA chelates carrying dodecaborate cluster MRI contrast agents. (B) Resulting strong contrast enhancement in T1-weighted MRI scans of mice for up to 4 h after injection. 8

**Figure 1.5.** (A) Pentafluoroaryl-based dodecaborate clusters undergoing efficient  $S_NAr$  reactions with a variety of thiolated molecules. Single-crystal X-ray structures of (B) *hypercloso*- $B_{12}(OCH_2C_6F_5)_{12}$  and (C) *hypercloso*- $B_{12}(OCH_2-4-(C_6F_5)-C_6H_4)_{12}$ . 9

**Figure 1.6.** Snapshot after 20 ns of a molecular dynamics simulation between a glycosylated OCN and the tetrameric lectin ConA. The carbohydrate binding sites of ConA are highlighted. 10

**Figure 2.1.** Comparison of features between the thiol-capped AuNPs and the OCNs. (a) Thiol-capped AuNPs between 5 and 100 nm can be easily prepared *via* self-assembly to give rise to polydisperse hybrid particles that comprise weak, non-covalent gold–thiolate bonds (40–50 kcal mol<sup>-1</sup>). These AuNPs often undergo ligand-exchange processes that can compromise the structural integrity of the particles. (b) Uniform and robust OCNs can be assembled efficiently with atomic precision and full covalency in the size range 2–10 nm *via* perfluoroaryl-thiol  $S_NAr$  chemistry under mild conditions. The formed carbon–sulfur bond (80–90 kcal mol<sup>-1</sup>) is significantly stronger

compared with the gold-sulfur interaction, and results in nanomolecules that feature high structural stabilities. 13

**Figure 2.2.** Synthesis and characterization of the perfluoroaryl-perfunctionalized dodecaborate clusters and the subsequent modification with thiols. (a) Perfunctionalization of **1** with rigid pentafluoroaryl-terminated linkers yields pure clusters **2** and **3**, after isolation. (b,c) Ball-and-stick and space-filling representations of the single-crystal X-ray structures of **2** and **3**, respectively. Size measurements of the crystal structures reveal that **2** is 1.9 nm and **3** is 2.7 nm (lengthwise). B, pink; O, red; C, grey; F, purple. (d) “Click”-like modification of cluster **2** with the 1-hexanethiol reagent and the corresponding  $^{19}\text{F}$  and  $^{11}\text{B}$  NMR spectra associated with the transformation from the starting material **2** to the functionalized product **2a**. Specifically, perfunctionalization of **2** with 1-hexanethiol results in a shift of the *meta*-F resonance and the complete disappearance of the *para*-F resonance as well as a characteristic upfield shift of the boron singlet resulting from the reduction of the cluster. TBA, tetrabutylammonium. 16

**Figure 2.3.** Characterization of the PEGylated OCNs **2i–2k** and **3i–3k**. (a) Plot of the particle sizes of the PEGylated OCNs **2i–2k** and **3i–3k** obtained *via* 2D DOSY  $^1\text{H}$  NMR experiments. The plot reveals a trend of a gradual increase in the sizes of the OCNs, both as a function of the cluster precursor dimension and of the chain length of the PEG reagent. The size of **3i** is larger than expected, probably because of aggregation. (b) TEM images of a negatively stained sample of **3i** reveal the presence of nearly monodisperse particles with an average size of 1.9 nm, consistent with the expected size of **3i**. (c) GPC traces of **2k** and **3k** measured in water further confirm the monodispersity of the samples ( $D = 1.003 \pm 0.02$  and  $1.081 \pm 0.007$ , respectively). (d) MD-calculated structures of the PEGylated nanomolecules in pure water after 21 ns of simulation

indicate a trend in the sizes of the OCNs consistent with that observed through the 2D DOSY experiments. RI = refractive index; a.u., arbitrary units. 24

**Figure 2.4.** Multivalent binding of the glycosylated OCN **2l** to the lectin ConA. (a) ESI-HRMS of **2l** supports its proposed structure and composition (see inset for the MD simulated structure of **2l** in an aqueous environment). (b) SPR sensorgram indicates that the measured binding response is dependent on the concentration of **2l**. Furthermore, it suggests multivalent binding interactions between **2l** and ConA as well as minimal binding of the PEGylated cluster **2i** and D-glucose controls to ConA. (c) A snapshot at 20 ns of a MD simulation showcases the interactions between four **2l** particles (I, II, III, and IV) and ConA. (d–f) MD-simulation close-up snapshots of three of the **2l** particles (I (d), II (e) and III (f)) binding to ConA at the known monosaccharide-binding residues (coloured and labelled). Calcd, calculated; obsd, observed. 26

**Figure S2.1.** Nanoparticles snapshots in water after 21 ns of simulations. Scale bar is 1 nm. A) **2i** B) **3i** C) **2j** D) **3j** E) **2k** F) **3k**. 70

**Figure S2.2.** Nanoparticles snapshots in 0.08 M buffer solution at pH=7.4 (salt) after 31 ns of simulations. Scale bar is 1 nm. A) **2i** B) **3i** C) **2j** D) **3j** E) **2k** F) **3k**. 71

**Figure S2.3.** RDFs of **2i–k** and **3i–k** NPs.  $g'(r)$  calculated for A) boron-PEG oxygen atoms in water and B) boron-PEG oxygen atoms in ionic solution.  $g(r)$  calculated for C) boron-terminal C atoms in water and D) boron-terminal C atoms in ionic solutions. 72

**Figure S2.4.** Distributions of  $r_{\text{gyr}}$  in a) water and b) ionic solutions. 75

**Figure S2.5.** A) Tetramer of Con A and sugar-coated particles. B) Tetramer of Con A and  $\beta$ -D glucoses. Details of glucose binding shown in both cases. 77

**Figure S2.6.** Nearest distances between SPs ligands and the Con A tetramer. 78

**Figure S2.7.** Nearest distances between  $\beta$ -D glucose molecules and the Con A tetramer. 79



**Figure 3.1.** Synthesis of perfluoroaryl-perfunctionalized clusters and their reactivities toward an unprotected thiolated saccharide. (a) Clusters **2** and **3** are readily prepared from **1** with the assistance of a microwave reactor. (b) Conversion rates of  $S_NAr$  reactions between **2/3** and 1-thio- $\beta$ -D-glucose sodium salt, as monitored by  $^{19}F$  NMR spectroscopy, reveal the significantly enhanced reactivity of **3** over **2**. (c)  $^{19}F$  NMR spectra of **3** in DMF and **3c** after conjugation with 1-thio- $\beta$ -D-glucose sodium salt in DMF or mixed aqueous/organic media. \*NaF signal. 86

**Figure 3.2.** Multivalent binding interactions between mannose-functionalized nanomolecules and DC-SIGN. (a, d) SPR sensorgrams reveal dose-dependent multivalent binding of **2a** and **3a** to DC-SIGN, respectively, while the controls PEGylated clusters (**2d** and **3d**) and D-mannose exhibit minimal to no binding to DC-SIGN. In all SPR experiments, the flow rate is 5  $\mu$ L/min, and the analytes are injected for 6 minutes, followed by buffer flow. (b, e) Snapshots after 40 ns of MD simulations of the binding interactions between **2a/3a** and DC-SIGN. (c, f) Zoomed-in snapshots reveal each nanomolecule binding to the carbohydrate recognition sites of DC-SIGN. 90

**Figure 3.3.** Mannose-functionalized clusters are capable of inhibiting protein-protein interactions. (a, b) SPR-based competitive binding studies suggest that **2a** and **3a** effectively compete against immobilized gp120 to bind free DC-SIGN, which leads to reduced binding responses. 93

**Figure 3.4.** Biocompatible mannose-coated cluster nanomolecules can serve as multivalent inhibitors to prevent the DC-SIGN-mediated cell uptake of gp120. (a) Glycosylated clusters can potentially inhibit the uptake of viral glycoproteins such as gp120 by blocking cell-surface DC-SIGN. Figure is not drawn to scale. (b) Mannose-coated and PEGylated clusters exhibit no apparent toxicity toward Raji DC-SIGN<sup>+</sup> cells at least up to 50  $\mu$ M, as assessed by an MTS assay. (c) DC-SIGN-dependent cell uptake of gp120-FITC is inhibited by mannose-coated clusters (**2a**

and <b>3a</b> ), as indicated by confocal microscopy analysis. However, the controls PEGylated clusters ( <b>2d</b> and <b>3d</b> ) and D-mannose do not affect the uptake of gp120-FITC.	95
<b>Figure S3.1.</b> SPR sensorgrams of <b>2c</b> injected over DC-SIGN ECD.	114
<b>Figure S3.2.</b> SPR sensorgrams of <b>3c</b> injected over DC-SIGN ECD.	115
<b>Figure S3.3.</b> SPR sensorgrams of <b>2b</b> injected over DC-SIGN ECD.	115
<b>Figure S3.4.</b> SPR sensorgrams of <b>3b</b> injected over DC-SIGN ECD.	115
<b>Figure S3.5.</b> SPR sensorgrams of DC-SIGN ECD and <b>2b</b> , <b>2d</b> , or D-mannose co-injected over gp120.	116
<b>Figure S3.6.</b> SPR sensorgrams of DC-SIGN ECD and <b>3b</b> , <b>3d</b> , or D-mannose co-injected over gp120.	117
<b>Figure S3.7.</b> Confocal microscopy images of Raji cells exposed to gp120-FITC and water (brightfield, green, overlay).	119
<b>Figure S3.8.</b> Confocal microscopy images of Raji DC-SIGN+ cells exposed to gp120-FITC and water (brightfield, green, overlay).	120
<b>Figure S3.9.</b> Confocal microscopy images of Raji DC-SIGN+ cells exposed to gp120-FITC and 10 $\mu$ M <b>2a</b> (brightfield, green, overlay).	121
<b>Figure S3.10.</b> Confocal microscopy images of Raji DC-SIGN+ cells exposed to gp120-FITC and 25 $\mu$ M <b>2a</b> (brightfield, green, overlay).	122
<b>Figure S3.11.</b> Confocal microscopy images of Raji DC-SIGN+ cells exposed to gp120-FITC and 10 $\mu$ M <b>3a</b> (brightfield, green, overlay).	123
<b>Figure S3.12.</b> Confocal microscopy images of Raji DC-SIGN+ cells exposed to gp120-FITC and 25 $\mu$ M <b>3a</b> (brightfield, green, overlay).	124

- Figure S3.13.** Confocal microscopy images of Raji DC-SIGN+ cells exposed to gp120-FITC and 25  $\mu$ M **2d** (brightfield, green, overlay). 125
- Figure S3.14.** Confocal microscopy images of Raji DC-SIGN+ cells exposed to gp120-FITC and 25  $\mu$ M **3d** (brightfield, green, overlay). 126
- Figure S3.15.** Confocal microscopy images of Raji DC-SIGN+ cells exposed to gp120-FITC and 25  $\mu$ M D-mannose (brightfield, green, overlay). 127
- Figure S3.16.** Changes in the number of hydroxy groups (3-OH and 4-OH) on mannose binding to DC-SIGN over 40 ns. 129
- Figure 4.1.** (Left) Hybrid thiol-capped AuNPs feature non-covalent, weak Au–S bonds (40-50 kcal/mol). (Right) This work presents a class of atomically precise nanoclusters built upon robust and comparatively stronger C–S linkages (80-90 kcal/mol). 132
- Figure 4.2.** (A) Synthetic protocol for the preparation of  $[1][SbF_6]_{11}$ . (B) Solid-state structure of  $[1][SbF_6]_{11}$  (center), and zoomed-in image of a single Au(III) organometallic fragment (left) with thermal ellipsoids rendered at the 30% probability level and with hydrogen atoms and counteranions omitted, and space-filling diagram (right). For crystallographic details see the Supporting Information. 136
- Figure 4.3.** (A, B) Scheme for reactions of  $[1][SbF_6]_{11}$  with thiol-containing substrates. (C) Substrate scope for conjugation reactions. All cluster conjugates were isolated and characterized ( $^1H$  and  $^{11}B$  NMR spectroscopy, HR-ESI-MS(–)) after purification (see the Supporting Information for experimental details and characterization data). 138
- Figure 4.4.** (A) “Layer-by-layer” assembly strategy for building nanoclusters that are modularly extended in size. (B)  $^{31}P\{^1H\}$  NMR spectrum of  $[21][SbF_6]_{10}$ . (C) Synthetic scheme for reactions of  $[21][SbF_6]_{10}$  and thiol-containing substrates. (D) Substrate scope for conjugation reactions. All

cluster conjugates were observed *in situ* by ESI-MS(-) (see the Supporting Information for experimental details and characterization data). 141

**Figure 4.5.** (A) Calculated structure of  $[\mathbf{18}]^{2-}$ . (B)  $^{11}\text{B}$  NMR stability studies of  $[\mathbf{18}]^{2-}$  in fetal bovine serum monitored over the course of 14 days indicating the cluster maintains its structural integrity under these conditions. (C) ESI-MS(-) of  $[\mathbf{18}]^{2-}$ . (D) Snapshots of MD simulations (after 20 ns) depicting the multivalent binding interactions between  $[\mathbf{18}]^{2-}$  (one molecule per binding site) and ConA (left),  $[\mathbf{19}]^{2-}$  and Stx1B (middle), and  $[\mathbf{20}]^{2-}$  and DC-SIGN (right). (E) SPR sensorgrams with calculated  $K_D$  values for direct binding measurements of each nanocluster and its respective protein target depicted in (D). (F) Confocal microscopy images of Raji DC-SIGN+ cells incubated with FITC-tagged gp120 and DMSO (control, left) and with  $[\text{Na}_2][\mathbf{20}]$  (right, 50  $\mu\text{M}$ ), showing significant inhibition of DC-SIGN mediated cellular entry of gp-120 in the presence of the  $[\text{Na}_2][\mathbf{20}]$  inhibitor. 143

**Figure S4.1.** (A) General scheme for conjugation reactions of  $[\mathbf{1}][\text{SbF}_6]_{11}$  with thiol-containing substrates. (B) Scope of nanocluster thio-conjugates. 155

**Figure S4.2.** (A) General scheme for conjugation reactions of  $[\mathbf{21}][\text{SbF}_6]_{10}$  with thiol-containing substrates. (B) Scope of nanocluster thio-conjugates. All species were observed *in situ* by ESI-MS(-). 175

**Figure S4.3.** Reaction scheme for the preparation of  $(1\text{-thio-}\beta\text{-D-galactose})_2\text{C}_6\text{H}_4$ . 180

**Figure S4.45.**  $^{31}\text{P}\{^1\text{H}\}$  NMR spectra taken of an initial DMF solution of  $[\mathbf{1}][\text{SbF}_6]_{11}$  before addition of  $\text{Na}[1\text{-thio-}\beta\text{-D-galactose}]$  (top), and of the crude reaction mixture 15 min after substrate addition (bottom) (DMF, 162 MHz, 25  $^\circ\text{C}$ ). 184

**Figure S4.5.**  $^1\text{H}$  NMR spectra of mixture collected from conjugation reactions before purification (*top*) and recovered (Me-DalPhos)AuCl post purification (*bottom*) ( $\text{CD}_2\text{Cl}_2$ , 400 MHz, 25 °C).

186

**Figure S4.6.**  $^{31}\text{P}\{^1\text{H}\}$  NMR spectrum of recovered (Me-DalPhos)AuCl after purification ( $\text{CD}_2\text{Cl}_2$ , 162 MHz, 25 °C).

187

**Figure S4.7.** SPR sensorgram for the binding of  $[\text{Na}_2][\text{B}_{12}(\text{OCH}_2\text{C}_6\text{H}_4(1\text{-thio-}\beta\text{-D-glucose}))_{12}]$  (0.5, 1, 2, 4 mg/L concentrations) to ConA with  $[\text{K}_2][\text{B}_{12}(\text{OCH}_2\text{C}_6\text{H}_4(m\text{PEG}_{350}\text{ thiol}))_{12}]$  (4 mg/L) and free D-glucose (30 mg/L) controls.

189

**Figure S4.8.** SPR sensorgram for the binding of  $[\text{Na}_2][\text{B}_{12}(\text{OCH}_2\text{C}_6\text{H}_4(1\text{-thio-}\beta\text{-D-galactose}))_{12}]$  (15, 30, 45, 60 mg/L concentrations) to Stx1B with  $(1\text{-thio-galactose})_2\text{C}_6\text{H}_4$  (100 mg/L) and free D-galactose (100 mg/L) controls.

190

**Figure S4.9.** SPR sensorgram for the binding of  $[\text{K}_2][\text{B}_{12}(\text{OCH}_2\text{C}_6\text{H}_4(m\text{PEG}_{350}\text{thiol}))_{12}]$  (40, 60, 80, 100 mg/L concentrations) to Stx1B.

191

**Figure S4.10.** SPR sensorgram for the binding of  $[\text{Na}_2][\text{B}_{12}(\text{OCH}_2\text{C}_6\text{H}_4(1\text{-thio-}\alpha\text{-D-mannose}))_{12}]$  (1, 2, 3, 4 mg/L concentrations) to DC-SIGN with  $[\text{K}_2][\text{B}_{12}(\text{OCH}_2\text{C}_6\text{H}_4(m\text{PEG}_{350}\text{ thiol}))_{12}]$  (8 mg/L) and free D-mannose (20 mg/L) controls.

192

**Figure S4.11.** Confocal laser scanning microscopy images (bright field, fluorescence, and overlay) of Raji DC-SIGN+ cells incubated with gp120-FITC (83 nM) and (A) DMSO as a control; (B) free D-mannose (50  $\mu\text{M}$  solution in DMSO); (C)  $[\text{K}_2][\mathbf{8}]$  (50  $\mu\text{M}$  solution in DMSO); (D)  $[\text{Na}_2][\mathbf{20}]$  (50  $\mu\text{M}$  solution in DMSO), demonstrating significant reduction in cellular uptake of gp120-FITC in the presence of the  $[\text{Na}_2][\mathbf{20}]$  inhibitor, and no observable reduction in gp120-FITC cellular uptake for the control experiments (B, C).

194

<b>Figure S4.12.</b> Two sets of confocal microscopy images of Raji cells (no DC-SIGN) exposed to gp120-FITC and DMSO (bright field, fluorescence, and overlay).	195
<b>Figure S4.13.</b> Two sets of confocal microscopy images of Raji DC-SIGN+ cells exposed to gp120-FITC and DMSO (bright field, fluorescence, and overlay).	196
<b>Figure S4.14.</b> Two sets of confocal microscopy images of Raji DC-SIGN+ cells exposed to gp120-FITC and free D-mannose (50 $\mu$ M) (bright field, fluorescence, and overlay).	197
<b>Figure S4.15.</b> Two sets of confocal microscopy images of Raji DC-SIGN+ cells exposed to gp120-FITC and [K <sub>2</sub> ][ <b>8</b> ] (50 $\mu$ M) (bright field, fluorescence, and overlay).	198
<b>Figure S4.16.</b> Two sets of confocal microscopy images of Raji DC-SIGN+ cells exposed to gp120-FITC and [K <sub>2</sub> ][ <b>20</b> ] (50 $\mu$ M) (bright field, fluorescence, and overlay).	199
<b>Figure S4.17.</b> Calculated structure of [ <b>18</b> ] <sup>2-</sup> . Gray: C; white: H; red: O; yellow: S; pink: B.	201
<b>Figure S4.18.</b> Calculated structure of [ <b>19</b> ] <sup>2-</sup> . Gray: C; white: H; red: O; yellow: S; pink: B.	202
<b>Figure S4.19.</b> Calculated structure of [ <b>20</b> ] <sup>2-</sup> . Gray: C; white: H; red: O; yellow: S; pink: B.	202
<b>Figure S4.20.</b> Calculated structure of [ <b>8</b> ] <sup>2-</sup> . Gray: C; white: H; red: O; yellow: S; pink: B.	203
<b>Figure S4.21.</b> Binding of four independent [ <b>18</b> ] <sup>2-</sup> molecules to the four distinct binding sites of ConA. (a) Initial configuration of the four [ <b>18</b> ] <sup>2-</sup> clusters with ConA. (b) Final configuration after the 20 ns simulation. (c) Zoomed-in image of [ <b>18</b> ] <sup>2-</sup> -1 interacting with one of the four sugar binding pockets. (d) Zoomed-in image of [ <b>18</b> ] <sup>2-</sup> -2 binding to the surrounding residues of the pocket. (e) Zoomed-in image of [ <b>18</b> ] <sup>2-</sup> -3 showing the glucose ligands spanning the binding pocket.	204
<b>Figure S4.22.</b> Plot displaying the number of ligands of the [ <b>18</b> ] <sup>2-</sup> -1 - [ <b>18</b> ] <sup>2-</sup> -4 clusters that interact with the specific binding pocket of ConA over the course of the 20 ns simulation.	205

- Figure S4.23.** Binding of  $[\mathbf{19}]^{2-}$  to Stx1B. (a) Initial configuration at sites 1 and 2. (b) Final binding configuration at sites 1 and 2 after 20 ns. (c) Initial configuration at site 3. (d, e) Two views of the final binding configuration at site 3 after 20 ns. 206
- Figure S4.24.** Plot displaying the number of ligands of the  $[\mathbf{19}]^{2-}$  cluster that interact with the specific binding sites of Stx1B over the course of the 20 ns simulation. 206
- Figure S4.25.** Binding of  $[\mathbf{8}]^{2-}$  to Stx1B. (a) Initial configuration at sites 1 and 2. (b) Final binding configuration at sites 1 and 2 after 20 ns. (c) Initial configuration at site 3. (d, e) Two views of the final binding configuration at site 3 after 20 ns. 207
- Figure S4.26.** Plot displaying the number of ligands of the  $[\mathbf{8}]^{2-}$  cluster that interact with the specific binding sites of Stx1B over the course of the 20 ns simulation. 207
- Figure S4.27.** Binding of  $[\mathbf{20}]^{2-}$  to DC-SIGN. (a) Initial configuration. (b) Configuration at 10 ns with zoomed-in image. (c) Final binding configuration after 20 ns. 208
- Figure S4.28.** Plot displaying the number of ligands of the  $[\mathbf{20}]^{2-}$  cluster that interact with the specific binding pocket of DC-SIGN over the course of the 20 ns simulation. 208
- Figure S4.29.** Solid-state structure of  $\text{B}_{12}(\text{OCH}_2\text{C}_6\text{H}_4\text{I})_{12}$  with thermal ellipsoids rendered at the 50% probability level with PLATON<sup>218</sup> and with hydrogen atoms omitted for clarity. 209
- Figure S4.30.** Solid-state structure of  $[\mathbf{1}]^{1+}$  with thermal ellipsoids rendered at the 50% probability level with PLATON<sup>218</sup> and with hydrogen atoms and  $\text{SbF}_6^-$  anions omitted for clarity. 211
- Figure S4.31.** Solid-state structure of  $[\mathbf{1}]^{1+}$  (left) with zoomed-in image (right) displaying the benzyl group  $\pi$ -stacking interactions. 212

## LIST OF TABLES

<b>Table 2.1.</b> Conjugation scope for <b>2</b> and <b>3</b> .	19
<b>Table 2.2.</b> PEGylation and glycosylation of <b>2</b> and <b>3</b> .	20
<b>Table S2.1.</b> Crystal data for <b>[3]</b> <sup>0</sup>	34
<b>Table S2.2.</b> Initial studies and reaction optimization	40
<b>Table S2.3.</b> Radii of gyration, $\langle r_{\text{gyr}} \rangle$ , and their confidence intervals for PEGylated species in water and salt solutions	74
<b>Table 3.1.</b> Glycosylation and PEGylation of clusters <b>2</b> and <b>3</b>	88
<b>Table S4.1.</b> Crystallographic and structure refinement information for $\text{B}_{12}(\text{OCH}_2\text{C}_6\text{H}_4\text{I})_{12}$	210
<b>Table S4.2.</b> Crystallographic and structure refinement information for <b>[1][SbF<sub>6</sub>]</b> <sub>11</sub>	213



## ACKNOWLEDGMENTS

I would like to start by thanking my Ph.D. advisor, Professor Alexander M. Spokoyny, for his guidance, support, and encouragement throughout my graduate career. I will forever be grateful for the invaluable opportunity he offered me, a first-year bioengineer, to venture into the field of chemistry and tackle an exciting multidisciplinary project. Working on the project in his laboratory has taught me not only valuable research skills, but also important life lessons that I will always treasure.

I would also like to thank the other members of my doctoral committee: Professors Heather D. Maynard, Timothy J. Deming, Zhen Gu, and Dean Ho. Thank you for your time and helpful input on my research, and for challenging me to integrate knowledge from different fields in my studies.

Over the past five year, the Spokoyny laboratory has felt like a second home, and its members has felt like family. I am especially thankful for the wisdom from the incredible postdoctoral researchers Dr. Julia Stauber, Dr. Liban Saleh, Dr. Xin Mu, and Dr. Jon Axtell, the camaraderie with fellow graduate students Alex Wixtrom, Dahee Jung, Marco Messina, Rafal Dziedzic, and Kent Kirlikovali, and the friendships with former undergraduate students Azin Saebi, Elamar Hakim Moully, Jena Kim, Parker Beatty, Sylvia Chow, Daniel Mosallaei, and Monica Kirollos.

I am very grateful to the NIH for a three-year training fellowship in the UCLA Chemistry-Biology Interface (CBI) program. Under the leadership of Professor Heather D. Maynard, the program advanced my training by exposing me to cutting-edge research through seminars, retreats, symposia, and an internship at MIT. Lastly, I would like to thank the UCLA Graduate Division for a Dissertation Year Fellowship.

Chapter one is an excerpt of Axtell, J. C.; Saleh, L. M. A.; Qian, E. A.; Wixtrom, A. I.; Spokoyny, A. M. Synthesis and applications of perfunctionalized boron clusters. *Inorg. Chem.* **2018**, *57*, 2333–2350. All authors co-wrote the manuscript.

Chapter two is a version of Qian, E. A.; Wixtrom, A. I.; Axtell, J. C.; Saebi, A.; Jung, D.; Rehak, P.; Han, Y.; Hakim Mouly, E.; Mosallaei, D.; Chow, S.; Messina, M. S.; Wang, J. Y.; Royappa, A. T.; Rheingold, A. L.; Maynard, H. D.; Král, P.; Spokoyny, A. M. Atomically precise organomimetic cluster nanomolecules assembled via perfluoroaryl-thiol  $S_NAr$  chemistry. *Nat. Chem.* **2017**, *9*, 333–340. E.A.Q., A.I.W., J.C.A., A.S., D.J., E.H.M., D.M., S.C., M.S.M., J.Y.W., and A.T.R. were responsible for the experimental studies. P.R. and Y.H. were responsible for the computational studies.

Chapter three is a version of Qian, E. A.; Han, Y.; Messina, M. S.; Maynard, H. D.; Král, P.; Spokoyny, A. M. Multivalent cluster nanomolecules for inhibiting protein-protein interactions. *Bioconjugate Chem.* **2019**, *30*, 2594–2603. E.A.Q. and M.S.M. were responsible for the experimental studies. Y.H. was responsible for the computational studies.

Chapter four is a version of Stauber, J. M.; Qian, E. A.; Han, Y.; Rheingold, A. L.; Král, P.; Fujita, D.; Spokoyny, A. M. An organometallic strategy for assembling atomically precise hybrid nanomaterials. *Submitted*. J.M.S., E.A.Q., A.L.R, and D.F. were responsible for the experimental studies. Y.H. was responsible for the computational studies.

## VITA

### EDUCATION

<b>University of California, Los Angeles</b> <i>M.S., Bioengineering</i>	Los Angeles, CA June 2016
<b>Vanderbilt University</b> <i>B.E., Biomedical Engineering</i>	Nashville, TN May 2014

### RESEARCH AND WORK EXPERIENCE

**UCLA Technology Development Group** Los Angeles, CA  
*Technology Fellow (Business Development & Technology Transfer)* February 2019 – August 2019

- Created non-confidential written and presentation documents based on disclosures/publications for marketing innovations across life sciences and engineering

**UCLA Chemistry & Biochemistry** Los Angeles, CA  
*Ph.D. Researcher (Spokoiny Group)* October 2014 – August 2019

- Launched and led an interdisciplinary project on building novel atomically precise, robust cluster nanomolecules
- Demonstrated the ability to fine-tune multivalent interactions between nanomolecules and proteins

*Teaching Assistant* January 2015 – June 2015

- Led discussion sections for 2 undergraduate chemistry courses

**MIT Chemistry** Cambridge, MA  
*Visiting Researcher (Pentelute Group)* August 2017 – December 2017

- Spearheaded a project on innovative peptide macrocyclization strategies

**Amgen** Thousand Oaks, CA  
*Intern (Therapeutic Discovery – Protein Technologies)* May 2013 – August 2013

- Tested the ability of small-molecule proteostasis regulators to improve protein expression in mammalian cells

**Vanderbilt University Chemical & Biomolecular Engineering** Nashville, TN  
*Undergraduate Researcher (Young Group)* May 2012 – May 2014

- Demonstrated the effects of anti-apoptotic genes on mammalian cell proliferation, lactate level, and caspase activity

### HONORS AND AWARDS

UCLA Bioengineering Outstanding Ph.D. Award	2019
UCLA Dissertation Year Fellowship	2018 – 2019
UCLA Research Showcase Fellowship Award for ACS National Meeting	2017, 2019
UCLA Seaborg Symposium Poster Award	2018
ACS Women Chemists Committee/Merck Research Award	2017
ACS Women Chemists Committee/Eli Lilly Travel Award	2017
UC Systemwide Bioengineering Symposium Rapid Fire Talk Award	2017
NIH Training Fellowship/Chemistry-Biology Interface Training Program	2015 – 2018
Vanderbilt Biomedical Engineering Honors Program	2012 – 2014
Vanderbilt School of Engineering Dean's List	2012 – 2014
Vanderbilt School of Engineering Summer Research Fellowship	2012

### PUBLICATIONS

- Stauber, J. M.; Qian, E. A.; Han, Y.; Rheingold, A. L.; Král, P.; Fujita, D.; Spokoiny, A. M. An Organometallic-Based Strategy for Assembling Atomically Precise Thiol-Capped Gold Nanoparticle Mimics. **2019**, *submitted*.

- Qian, E. A.; Han, Y.; Messina, M. S.; Maynard, H. D.; Král, P.; Spokoyny, A. M. Multivalent Cluster Nanomolecules for Inhibiting Protein-Protein Interactions. *Bioconjugate Chem.* **2019**, *30*, 2594–2603.
- Barton, J. L.;<sup>†</sup> Wixtrom, A. I.;<sup>†</sup> Kowalski, J. A.;<sup>†</sup> Qian, E. A.; Jung, D.; Brushett, F. R.; Spokoyny, A. M. Perfunctionalized Dodecaborate Clusters as Stable Metal-Free Active Materials for Charge Storage. *ACS Appl. Energy Mater.* **2019**, *2*, 4907–4913.
- Jung, D.; Raffan-Montoya, F.; Ramachandran, R.; Zhang, Y.; Islamoglu, T.; Marin, G.; Qian, E. A.; Dziedzic, R. M.; Farha, O. K.; Stoliarov, S. I.; Spokoyny, A. M. Cross-Linked Porous Polyurethane Materials Featuring Dodecaborate Clusters as Inorganic Polyol Equivalents. *Chem. Commun.* **2019**, *55*, 8852–8855.
- Axtell, J. C.; Saleh, L. M. A.; Qian, E. A.; Wixtrom, A. I.; Spokoyny, A. M. Synthesis and Applications of Perfunctionalized Boron Clusters. *Inorg. Chem.* **2018**, *57*, 2333–2350.
- Wixtrom, A. I.; Parvez, Z. A.; Savage, M. D.; Qian, E. A.; Jung, D.; Khan, S. I.; Rheingold, A. L.; Spokoyny, A. M. Tuning the Electrochemical Potential of Perfunctionalized Dodecaborate Clusters Through Vertex Differentiation. *Chem. Commun.* **2018**, *54*, 5867–5870.
- Qian, E. A.; Wixtrom, A. I.; Axtell, J. C.; Saebi, A.; Jung, D.; Rehak, P.; Han, Y.; Hakim Mouly, E.; Mosallaei, D.; Chow, S.; Messina, M. S.; Wang, J. Y.; Royappa, A. T.; Rheingold, A. L.; Maynard, H. D.; Král, P.; Spokoyny, A. M. Atomically Precise Organomimetic Cluster Nanomolecules Assembled *via* Perfluoroaryl-Thiol  $S_NAr$  Chemistry. *Nat. Chem.* **2017**, *9*, 333–340.
- Wixtrom, A. I.; Shao, Y.; Jung, D.; Machan, C. W.; Kevork, S. N.; Qian, E. A.; Axtell, J. C.; Khan, S. I.; Kubiak, C. P.; Spokoyny, A. M. Rapid Synthesis of Redox-Active Dodecaborane  $B_{12}(OR)_{12}$  Clusters Under Ambient Conditions. *Inorg. Chem. Front.* **2016**, *3*, 711–717.
- Templeton, N.; Lewis, A.; Dorai, H.; Qian, E. A.; Campbell, M.; Smith, K. D.; Lang, S.; Betenbaugh, M. J.; Young, J. D. Bcl-2 $\Delta$  Expression Enhances Mitochondrial Metabolism and Limits Lactate Production in CHO Cells. *Metab. Eng.* **2014**, *25*, 92–102.

#### SELECTED PRESENTATIONS (9/22)

- UCLA Bioengineering Research Day – Graduate Student Speaker Presentation, Los Angeles, CA, “Atomically Precise Organomimetic Nanomolecules,” February 8, 2019.
- SoCal Bioinorganic Chemistry Conference – Poster Session, Pasadena, CA, “Atomically Precise Organomimetic Cluster Nanomolecules (OCNs),” December 8, 2018.
- UCLA Chemistry-Biology Interface Day – Graduation Talk, Los Angeles, CA, “Atomically Precise Organomimetic Cluster Nanomolecules (OCNs),” September 20, 2018.
- ACS National Meeting – Merck Research Award Symposium, Washington, D.C., “Atomically Precise, Tunable Organomimetic Cluster Nanomolecules (OCNs),” August 20, 2017.
- UC Systemwide Bioengineering Symposium – Rapid Fire Talk & Poster Session, Los Angeles, CA, “Atomically Precise, Tunable Cluster Nanomolecules,” June 28, 2017.
- UCLA Molecular Biology Institute Annual Retreat – Poster Session, Ventura, CA, “Atomically Precise Organomimetic Cluster Nanomolecules (OCNs),” April 22, 2017.
- ACS National Meeting – Division of Inorganic Chemistry: Nanoscience Symposium, Eli Lilly Travel Award Poster Session, & UCLA Research Showcase Poster Session, San Francisco, CA, “Atomically Precise Organomimetic Cluster Nanomolecules (OCNs),” April 4–5, 2017.
- UC Symposium for the Chemical Sciences – Poster Session, Lake Arrowhead, CA, “Synthesis of Atomically Precise, Tunable Nanomolecules from Organomimetic Clusters,” March 22, 2016.
- Amgen Therapeutic Discovery Interns Presentations, Thousand Oaks, CA, “Exploring Protein Expression Improvement in Mammalian Cells with Proteostasis Regulators,” August 9, 2013.

#### PATENTS

Spokoyny, A., Maynard, H. D., Qian, E. A., Messina, M. S., Wixtrom, A., Axtell, J., Kirlikovali, K., Gonzalez, A. Novel Three-Dimensional Boron-Rich Clusters. U.S. Patent Application 16/077,415, filed February 2017.

## CHAPTER ONE

*An excerpt of*

### **Synthesis and Applications of Perfunctionalized Boron Clusters**

Jonathan C. Axtell, Liban M. A. Saleh, Elaine A. Qian,

Alex I. Wixtrom, and Alexander M. Spokoyny.

*Inorg. Chem.* **2018**, *57*, 2333–2350.

#### **Introduction to Biological Applications**

A number of boron cluster derivatives are attractive candidates for a broad range of biomedical applications because of their exceptional stability and biocompatibility, availability of  $^{10}\text{B}$  nuclei (20% natural abundance), and tunability.<sup>1–4</sup> Over the past few decades, many biological applications of boron clusters have been explored, most notably in the areas of drug delivery and imaging for the diagnosis and treatment of cancer<sup>2,5</sup> and, only most recently, in the area of probing protein–biomolecule interactions.<sup>6</sup>

#### **Delivery of $^{10}\text{B}$ for Boron Neutron Capture Therapy (BNCT)**

The most widely investigated research area within boron cluster-based drug delivery is undoubtedly BNCT, a binary therapeutic strategy for the treatment of cancer (Figure 1.1A). The concept of BNCT was first proposed in 1936 by Locher<sup>7</sup> and has since captured the attention of many researchers because of its elegant design. As described by Hawthorne and others, the beauty of BNCT lies in the fact that both of its essential components, nonradioactive  $^{10}\text{B}$  nuclei and low-

energy thermal neutrons, are nontoxic by themselves; however, together they initiate an energetic nuclear decomposition reaction that typically cannot extend past the diameter of a cell.<sup>2,8,9</sup> On the basis of this principle, BNCT was proposed as a safer alternative to many of the single-component radiation and chemotherapy approaches for the treatment of cancer. Many boron-containing compounds have been investigated for BNCT with generally unsuccessful results, with the exception of L-*p*-dihydroxyborylphenylalanine (BPA; Figure 1.1B), which is still being used in clinical settings today.<sup>2,10,11</sup> Between 1959 and 1960, the discovery of polyhedral borane anions *closo*-[B<sub>10</sub>H<sub>10</sub>]<sup>2-</sup> and *closo*-[B<sub>12</sub>H<sub>12</sub>]<sup>2-</sup><sup>12-14</sup> sparked renewed interest in BNCT, given the exceptional stability of these species and their high boron content. The sodium salt of [B<sub>10</sub>H<sub>10</sub>]<sup>2-</sup> (Figure 1.1B) was tested in animals, and while it showed promising results, it later failed in a clinical trial.<sup>15,16</sup> Two thiol-containing derivatives, Na<sub>2</sub>[B<sub>10</sub>Cl<sub>8</sub>(SH)<sub>2</sub>] and Na<sub>2</sub>[B<sub>12</sub>H<sub>11</sub>SH] (BSH; Figure 1.1B), were identified as potential drug candidates from studies using mouse tumor models.<sup>16,17</sup> Although Na<sub>2</sub>[B<sub>10</sub>Cl<sub>8</sub>(SH)<sub>2</sub>] proved too toxic in mice, BSH exhibited more favorable properties and has since been extensively used in clinical trials.<sup>2,10,18</sup>

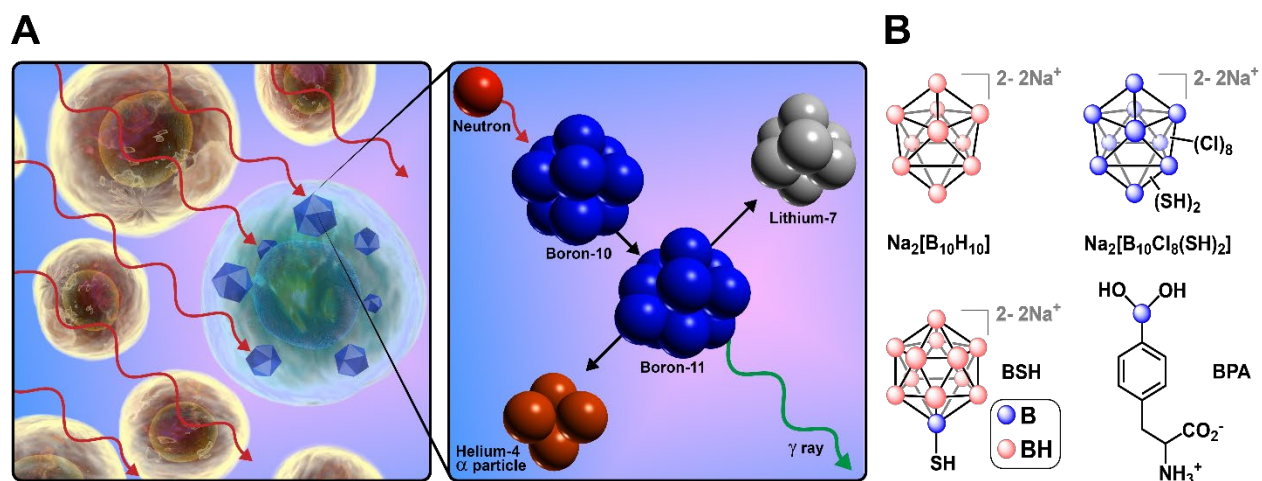


**Figure 1.1.** (A) Illustration of BNCT, a binary strategy for the treatment of cancer. (B) Some BNCT candidates used in preclinical and clinical settings.

However, despite the relative success of BPA and BSH in clinical trials, an important challenge remains to selectively deliver sufficiently large amounts of  $^{10}\text{B}$  nuclei to the tumor tissue (approximately  $20\text{--}35\ \mu\text{g g}_{\text{tumor}}^{-1}$  or  $10^9$  atoms  $\text{cell}^{-1}$ ), which is critical to the success of BNCT.<sup>9,19</sup> Therefore, two general approaches have been taken to tackle this issue. The first strategy involves the incorporation of boron into biomolecules with tumor-targeting abilities such as peptides and proteins, nucleic acids, carbohydrates, and porphyrins,<sup>20,21</sup> while the second approach uses liposomes and nanoparticles to deliver  $^{10}\text{B}$  atoms to tumor tissues.<sup>21–25</sup> In particular, many boron-encapsulated and boron-lipid liposomes have shown promising results in their ability to selectively deliver therapeutic quantities of  $^{10}\text{B}$  atoms into tumor cells for effective BNCT.<sup>26–34</sup>

However, while the liposome-based approach has been successful, this system is inherently inefficient because only around 5–10 % of the total mass arises from boron.<sup>35,36</sup> In an attempt to improve the efficiency, boron-cluster-based nanoparticles have been proposed as alternative BNCT agents. Toward this end, Hawthorne and colleagues synthesized ester-linked<sup>35</sup> and ether-linked<sup>36</sup> derivatives of the dodecaborate core with pendant *nido-o*-carboranyl substituents, which in total contain roughly 40% boron content by mass. The sodium salt of the ether-linked cluster (Figure 1.2) was found to be water-soluble and subsequently evaluated for its suitability as a BNCT agent in a series of toxicity and biodistribution studies in animals.<sup>36</sup> The results from these studies indicate that the compound is nontoxic to mice at a therapeutic dose and tumor-selective (the tumor-to-blood ratio is 9.4); however, in this particular study, its accumulation in tumor tissues ( $10.5\ \mu\text{g g}_{\text{tumor}}^{-1}$ ) was half of the therapeutic amount necessary for BNCT. Nevertheless, this strategy of using cluster-based nanoparticles as BNCT agents is appealing because of its high boron content, modularity, and low toxicity.

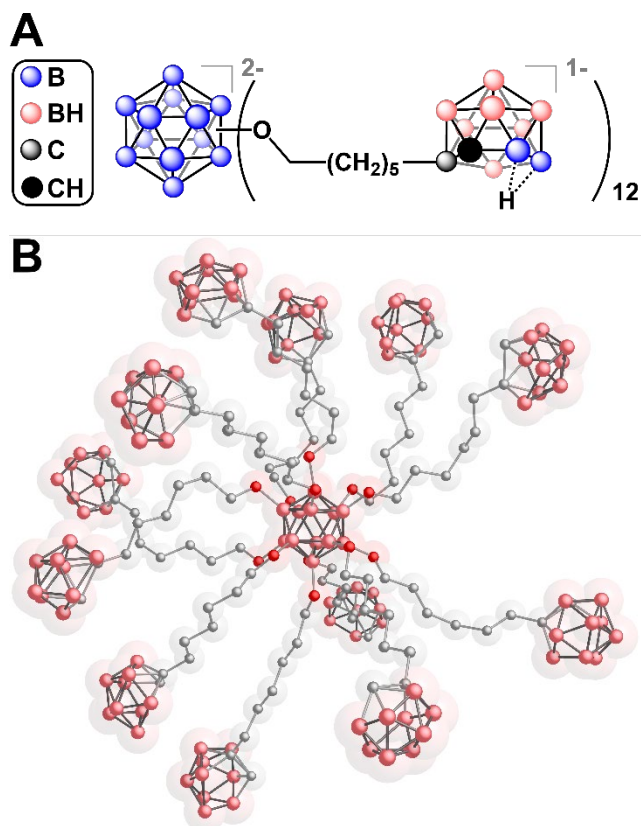


**Figure 1.2.** (A) Chemical structure and (B) 3D representation of the dodeca(*nido-o*-carboranyl)-substituted dodecaborate cluster.

Very recently, Kovalska and co-workers reported a spectroscopic and calorimetric binding study of perhalogenated decaborate ( $[\text{B}_{10}\text{X}_{10}]^{2-}$ , where X = Cl, Br, or I) and dodecaborate ( $[\text{B}_{12}\text{X}_{12}]^{2-}$ , where X = Cl or I) dianions to bovine and human serum albumins (BSA and HSA, respectively) toward potential use in BNCT.<sup>37</sup> It was shown through isothermal titration calorimetry and fluorescence quenching experiments that the halogenated boron clusters displayed a greater affinity toward albumin binding ( $\sim 4\text{--}5$  clusters per protein,  $K \sim 10^4\text{--}10^6 \text{ M}^{-1}$ ) than the parent cluster,  $[\text{B}_n\text{H}_n]^{2-}$  ( $n = 10$  or  $12$ ; 2 clusters per protein,  $K \sim 10^3 \text{ M}^{-1}$ ). Circular dichroism studies suggested that no significant change in the secondary protein structure had occurred even at the highest concentrations of clusters species tested. This is consistent with the inefficient



fluorescence quenching of HSA, which contains a Tyr residue buried within the protein manifold, relative to BSA, which contains both buried and surface Tyr residues. In a similar study, Losytskyy *et al.* studied the binding of oligoether- and ammonium-substituted decaborate anions to BSA, HSA, immunoglobulin IgG, b-lactoglobulin, and lysozyme.<sup>38</sup> It was found that the functionalized, charge-compensated B<sub>10</sub>-based monoanions formed stronger interactions with these protein substrates than with unfunctionalized decaborate and dodecaborate dianions. These studies present an additional delivery system for high-boron-content molecules *in vitro* and suggest that perhalogenated boron clusters may be potentially useful in BNCT applications.

### **Delivery of Chemotherapy Drugs**

In addition to their function as BNCT agents, boron clusters have recently been developed as nanocarriers for the delivery of various chemotherapy drugs. Within the past few years, Hawthorne and colleagues have constructed several heterofunctional cluster-based drug-delivery systems. For example, Bondarev *et al.* demonstrated the synthesis of a vertex-differentiated dodecaborate cluster scaffold, *closo*-[B<sub>12</sub>(OH)<sub>11</sub>NH<sub>3</sub>]<sup>-</sup>, which is further functionalized with an amide-bound fluorescein and 11 carboplatin analogues bound through carbamate linkages.<sup>39</sup> This species is found to localize in the nuclei of A549 cancer cells and shows potent cytotoxicity against both platinum-sensitive and platinum-resistant cell lines. In another example by Sarma *et al.*, a trimodal targeted drug-delivery system was assembled from a heteroperfunctionalized dodecaborate dianion, *closo*-[B<sub>12</sub>(OH)<sub>11</sub>(OR)]<sup>2-</sup>, by conjugating one vertex to a fluorescein molecule *via* click chemistry and the 11 other vertices to a branched linker featuring both the targeting molecule glucosamine and the anticancer drug chlorambucil (Figure 1.3A).<sup>40</sup>

Interestingly, the targeted cluster colocalized with the lysosomes (Figure 1.3B) and mitochondria within Jurkat cancer cells and exhibited 15-fold-enhanced cytotoxicity compared to the non-targeted cluster against cells overexpressing the receptor for glucosamine. In a different approach to assembling the cluster-based nanocarriers, the encapsulation of a hydrophobic chemotherapy agent doxorubicin by the dendritic dodecaborate clusters in a manner reminiscent of its encapsulation by the poly(amidoamine) dendrimers was disclosed,<sup>41,42</sup> thus laying the groundwork for potential delivery into cancer cells using functionalized dodecaborates.

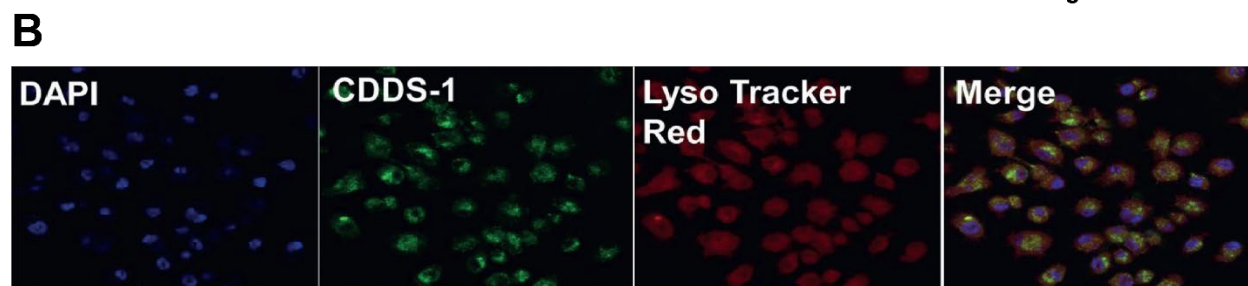
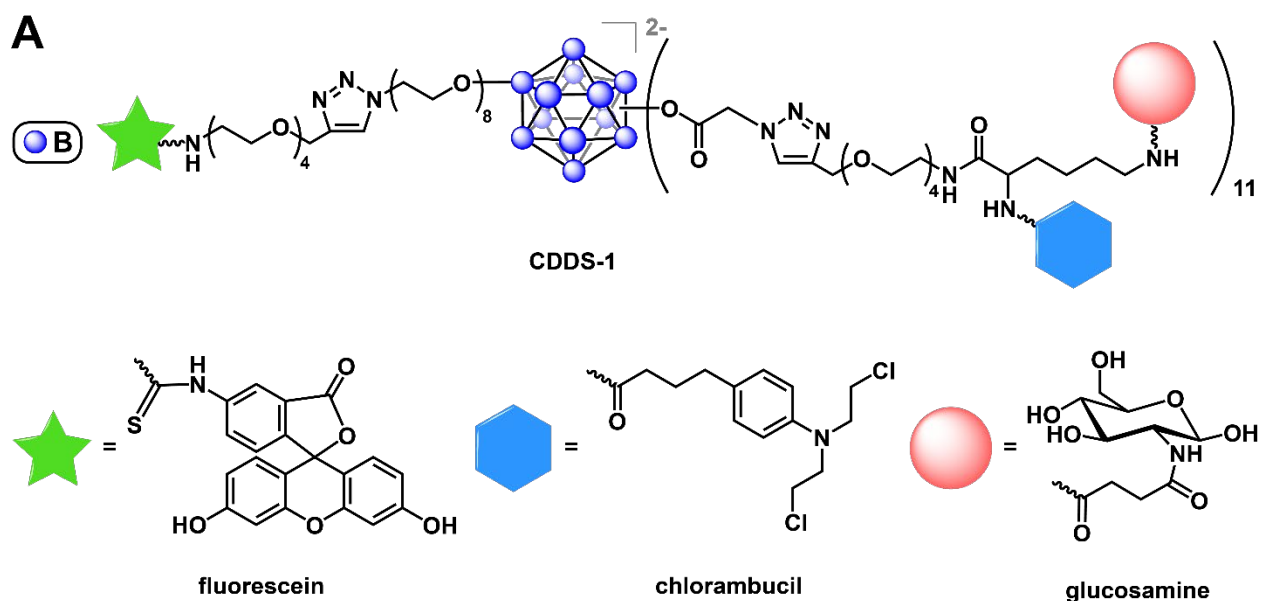


**Figure 1.3.** (A) Trimodal dendritic drug-delivery system, CDDS-1, which features targeting, imaging, and cell-killing abilities. (B) Confocal microscopy images of CDDS-1 showing its colocalization with lysosomes.

## Diagnostic Imaging

In addition to their applications in drug delivery for various types of cancer treatments, many derivatives of boron clusters have also been investigated for potential applications in diagnostic imaging. In fact, for decades, radiolabeled boron clusters have been studied as X-ray contrast agents because the incorporation of radiolabels on boron clusters can lead to higher chemical stability of the radiolabels.<sup>5</sup> However, while there have been numerous reports on the radiolabeling of boron clusters,<sup>5,43,44</sup> the vast majority have focused on the radiolabeled carborane derivatives and therefore will not be discussed here.

We will instead examine the development of high-performance all-boron cluster-based contrast agents for a more modern imaging technique, magnetic resonance imaging (MRI). MRI has emerged as one of the most important tools for the diagnosis of diseases; however, there is a need to develop larger MRI contrast agents that can overcome the issues of low relaxivity values, short plasma half-lives, and low contrast typically associated with low-molecular-weight contrast agents, while remaining well-defined.<sup>45-48</sup> To tackle this challenge, Hawthorne and colleagues reported the synthesis of both the non-targeted<sup>45</sup> and targeted<sup>48</sup> (Figure 1.4A) dodecaborate cluster-based MRI contrast agents that feature multiple gadolinium(III) complexes and further demonstrated that these compounds provided significantly enhanced image contrast in addition to tumor-targeting ability provided by the RGD (cRGD) peptide (Figure 1.4B).

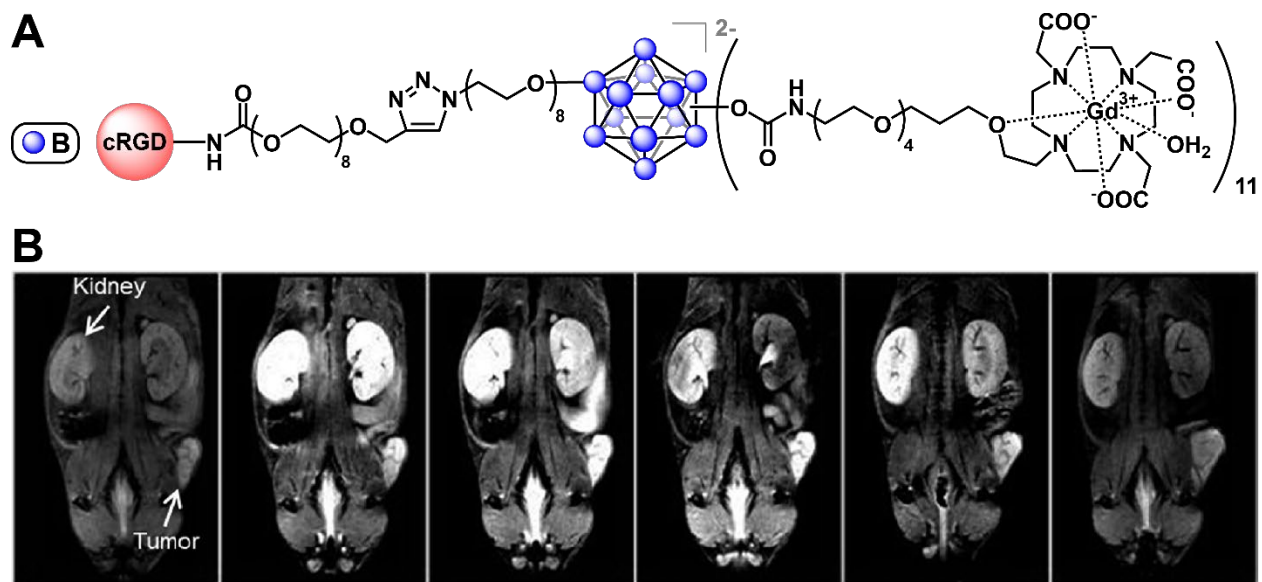


**Figure 1.4.** (A) cRGD peptide-labeled,  $\text{Gd}^{3+}$ -DOTA chelates carrying dodecaborate cluster MRI contrast agents. (B) Resulting strong contrast enhancement in T1-weighted MRI scans of mice for up to 4 h after injection.

### Multivalent Protein Binders

We recently reported a strategy to rapidly assemble atomically precise, highly tunable organomimetic cluster nanomolecules (OCNs) *via* perfluoroaryl-thiol  $\text{S}_{\text{N}}\text{Ar}$  chemistry (Figure 1.5).<sup>6</sup> This approach is reminiscent of the facile assembly method of the thiol-capped gold nanoparticles; however, the resulting OCNs are monodisperse and structurally robust under a range of biologically relevant conditions because of covalently linked substituents on the cluster core.

When this strategy was employed, the pentafluoroarylated dodecaborate clusters were perfunctionalized with a broad scope of thiolated (macro)molecules, including unprotected peptides, saccharides, and polymers. Furthermore, a glycosylated OCN was shown to be capable of *multivalent* interactions with Concanavalin A (ConA; Figure 1.6), resulting in binding affinities that are orders of magnitude higher than those observed for a single carbohydrate-lectin interaction. Taken together, this work showcases how one might rationally design and synthesize

well-defined nanomolecules that can be useful in (1) elucidating multivalent binding mechanisms and (2) potentially probing or inhibiting protein–biomolecule interactions.

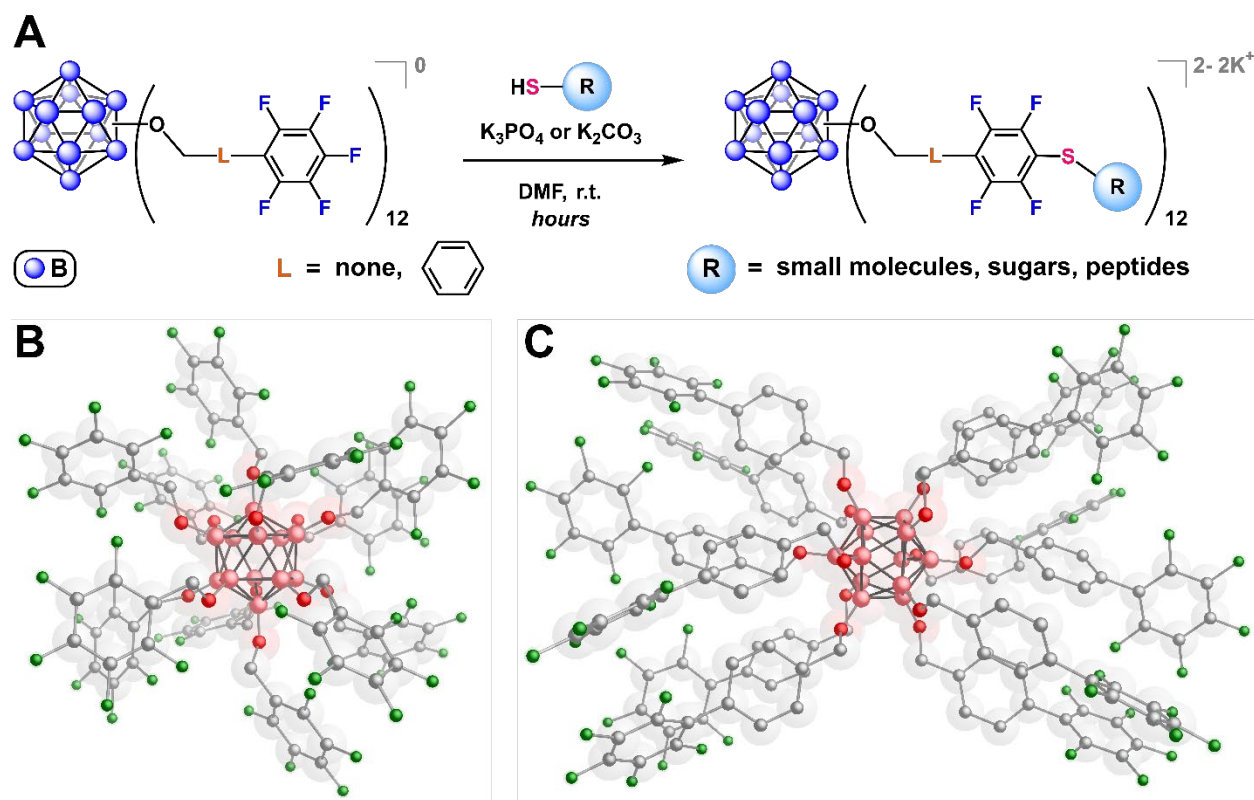


**Figure 1.5.** (A) Pentafluoroaryl-based dodecaborate clusters undergoing efficient  $\text{S}_{\text{N}}\text{Ar}$  reactions with a variety of thiolated molecules. Single-crystal X-ray structures of (B) *hypercloso*- $\text{B}_{12}(\text{OCH}_2\text{C}_6\text{F}_5)_{12}$  and (C) *hypercloso*- $\text{B}_{12}(\text{OCH}_2\text{-4-(C}_6\text{F}_5\text{)-C}_6\text{H}_4)_{12}$ .

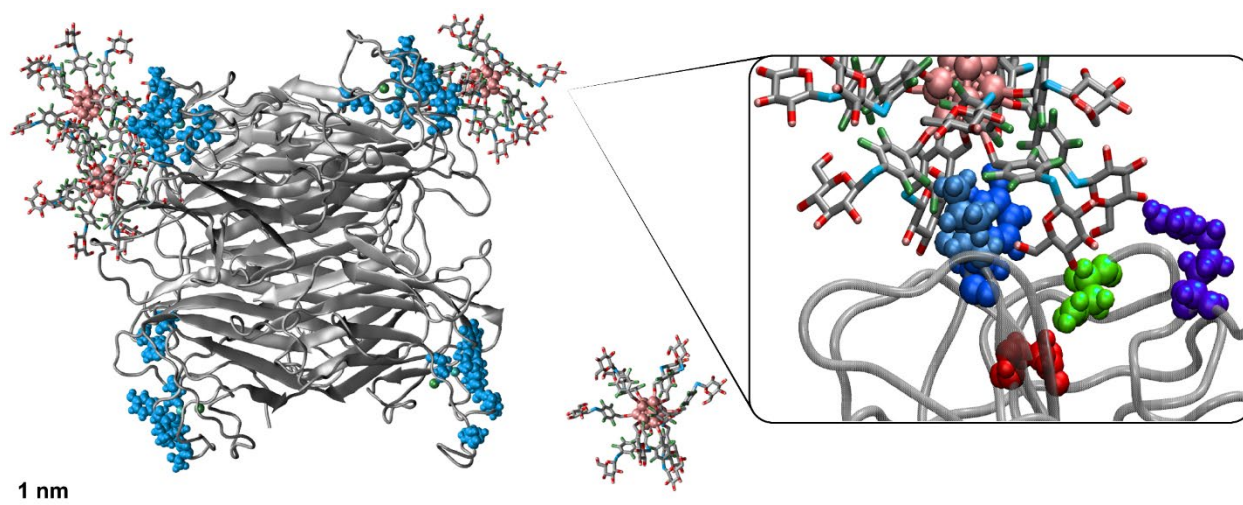


**Figure 1.6.** Snapshot after 20 ns of a molecular dynamics simulation between a glycosylated OCN and the tetrameric lectin ConA. The carbohydrate binding sites of ConA are highlighted.

## CHAPTER TWO

### **Atomically Precise Organomimetic Cluster Nanomolecules Assembled via Perfluoroaryl-Thiol $S_NAr$ Chemistry**

Elaine A. Qian, Alex I. Wixtrom, Jonathan C. Axtell, Azin Saebi, Dahee Jung, Pavel Rehak, Yanxiao Han, Elamar Hakim Mouly, Daniel Mosallaei, Sylvia Chow, Marco S. Messina, Jing Yang Wang, A. Timothy Royappa, Arnold L. Rheingold, Heather D. Maynard, Petr Král, and Alexander M. Spokoyny.

*Nat. Chem.* **2017**, *9*, 333–340.

#### **Abstract**

The majority of biomolecules are intrinsically atomically precise, an important characteristic that enables rational engineering of their recognition and binding properties. However, imparting a similar precision to hybrid nanoparticles has been challenging because of the inherent limitations of existing chemical methods and building blocks. Here we report a new approach to form atomically precise and highly tunable hybrid nanomolecules with well-defined three-dimensionality. Perfunctionalization of atomically precise clusters with pentafluoroaryl-terminated linkers produces size-tunable rigid cluster nanomolecules. These species are amenable to facile modification with a variety of thiol-containing molecules and macromolecules. Assembly proceeds at room temperature within hours under mild conditions, and the resulting nanomolecules exhibit high stabilities because of their full covalency. We further demonstrate how these nanomolecules grafted with saccharides can exhibit dramatically improved binding affinity

towards a protein. Ultimately, the developed strategy allows the rapid generation of precise molecular assemblies to investigate multivalent interactions.

## **Introduction**

Natural systems feature very complex three-dimensional (3D) molecular architectures that can interact with a high degree of specificity and fidelity. Among the well-established interaction modes, multivalency has been known to enable myriad biological events by strengthening individually weak interactions between biomolecules that are either native or foreign to the organism.<sup>49</sup> Multivalent interactions can be found in such diverse processes as infection (viral/bacterial proteins–cell receptors), immune recognition (antibodies–cell receptors/antigens, cytokines–cell receptors), and gene expression regulation (transcription factors–DNA), because of the higher avidity and better recognition compared with the corresponding monovalent bindings.<sup>49,50</sup>

Inspired by nature's design, chemists have taken an interest in developing synthetic multivalent ligands with the ability to bind specific target receptors with a high affinity to (1) elucidate the mechanistic details of multivalent interactions and (2) promote or inhibit biological interactions of interest.<sup>51</sup> Many examples of synthetic scaffolds have emerged over the past several decades,<sup>52,53,62–66,54–61</sup> which include, but are not limited to, polymeric nanoparticles,<sup>52,53</sup> dendrimers<sup>54,55</sup> and hybrid nanoparticles.<sup>56–64</sup> Specifically, the advent of nanotechnology and the development of surface-functionalized metal nanoparticles has provided an extremely powerful class of multivalent scaffolds. For example, gold nanoparticles (AuNPs) capped with thiolated ligands can feature biocompatibility and stability, which enables them for applications that require



binding and recognition capabilities.<sup>58,59</sup> Hybrid AuNP systems are especially attractive because of the synthetic ease of producing systems that are well-defined and tunable in size. Nevertheless, it is well known that thiolated ligands often can desorb or undergo exchange processes with other surfactants in solution over short periods of time, and furthermore, various electrochemical conditions or elevated temperatures ( $>60\text{ }^{\circ}\text{C}$ ) dramatically accelerate these processes.<sup>58,67–70</sup> These events can be explained primarily by the relatively weak nature of the gold–thiolate bond ( $40\text{--}50\text{ kcal mol}^{-1}$ ).<sup>67</sup> Processes of thiol–ligand exchange also readily occur on smaller Au-based cluster molecules ( $\leq 5\text{ nm}$ ), which potentially limits the ability of researchers to create atomically precise hybrid nanomolecules that remain compositionally well-defined under biologically relevant conditions (for example, in serum).<sup>69,71</sup>

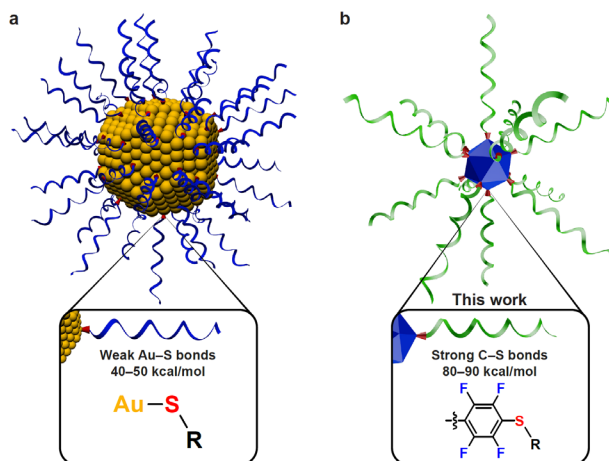


**Figure 2.1.** Comparison of features between the thiol-capped AuNPs and the OCNs. (a) Thiol-capped AuNPs between 5 and 100 nm can be easily prepared *via* self-assembly to give rise to polydisperse hybrid particles that comprise weak, non-covalent gold–thiolate bonds ( $40\text{--}50\text{ kcal mol}^{-1}$ ). These AuNPs often undergo ligand-exchange processes that can compromise the structural integrity of the particles. (b) Uniform and robust OCNs can be assembled efficiently with atomic precision and full covalency in the size range 2–10 nm *via* perfluoroaryl–thiol  $\text{S}_{\text{N}}\text{Ar}$  chemistry under mild conditions. The formed carbon–sulfur bond ( $80\text{--}90\text{ kcal mol}^{-1}$ ) is significantly stronger compared with the gold–sulfur interaction, and results in nanomolecules that feature high structural stabilities.

Here we report a new strategy to build robust atomically precise hybrid nanomolecules using air-stable inorganic clusters<sup>72–78</sup> densely decorated with perfluoroaromatic functional groups. Using this organomimetic strategy,<sup>77</sup> we show that one can mimic the rigid surface of a Au-based nanoparticle core and simultaneously produce assemblies that are fully covalent and thus stable under relatively harsh conditions (Figure 2.1). Specifically, we demonstrate how dodecaborate clusters<sup>14,40,77,79–82</sup> that feature a dense layer of rigid pentafluoroaryl functional groups can serve as excellent scaffolds for constructing atomically precise multivalent organomimetic cluster nanomolecules (OCNs). The perfluoroaryls are able to undergo facile “click”-like nucleophilic aromatic substitution (S<sub>N</sub>Ar) with a wide range of thiols at room temperature within hours, which creates robust carbon–sulfur bonds (80–90 kcal mol<sup>-1</sup>)<sup>83</sup> and thereby produces nanomolecules decorated with well-defined functional surfaces. This approach affords the functional advantages of using dendrimers while at the same time mimicking the synthetic ease with which thiol-capped AuNPs are normally constructed. Unlike the majority of dendritic scaffolds,<sup>84,85</sup> the resulting assemblies are highly rigid and can be synthesized and purified within hours. Furthermore, these OCNs are purely covalent and therefore feature improved stability in serum and various pH environments. Finally, we demonstrate the first example of using a hybrid inorganic cluster scaffold as a highly competent multivalent recognition platform for binding a protein system.

## Results and Discussion

Given the high reactivity of the perfluoroarenes with thiol-based nucleophiles,<sup>86-90</sup> we hypothesized that perfluoroaryl-thiol S<sub>N</sub>Ar chemistry could be utilized to conjugate various thiolated groups onto perfluoroaryl-containing clusters efficiently under mild conditions at room temperature. Recently, our laboratory reported a rapid perfunctionalization strategy of the [B<sub>12</sub>(OH)<sub>12</sub>]<sup>2-</sup> cluster (**1**), originally discovered by Hawthorne and co-workers,<sup>14,40,79,80</sup> that features a wide scope of substituents.<sup>81</sup> Using this method, we synthesized perfunctionalized clusters grafted with rigid linkers containing peripheral pentafluoroaryl moieties (Figure 2.2a). Specifically, perfunctionalized cluster scaffolds **2** and **3** can be synthesized in good yields under 30 minutes and isolated after purification by silica gel column chromatography in their neutral form as air-stable solids soluble in the majority of common polar organic solvents (see the Supporting Information for experimental details and characterization data). The single crystal X-ray structures of **2** and **3** reveal the highly rigid nature of these scaffolds (Figure 2.2b,c, respectively). Importantly, by virtue of using size-tunable linker precursor in the synthesis of **2** and **3**, the resulting rigid cluster species can be rationally controlled in size (**2** is approximately 1.9 and **3** is about 2.7 nm lengthwise, as measured from the single crystal structures). These clusters represent a new class of atomically precise scaffolds that offer unique rigidity and structural covalency, making them topologically reminiscent of both dendrimers and small metal nanoparticles.

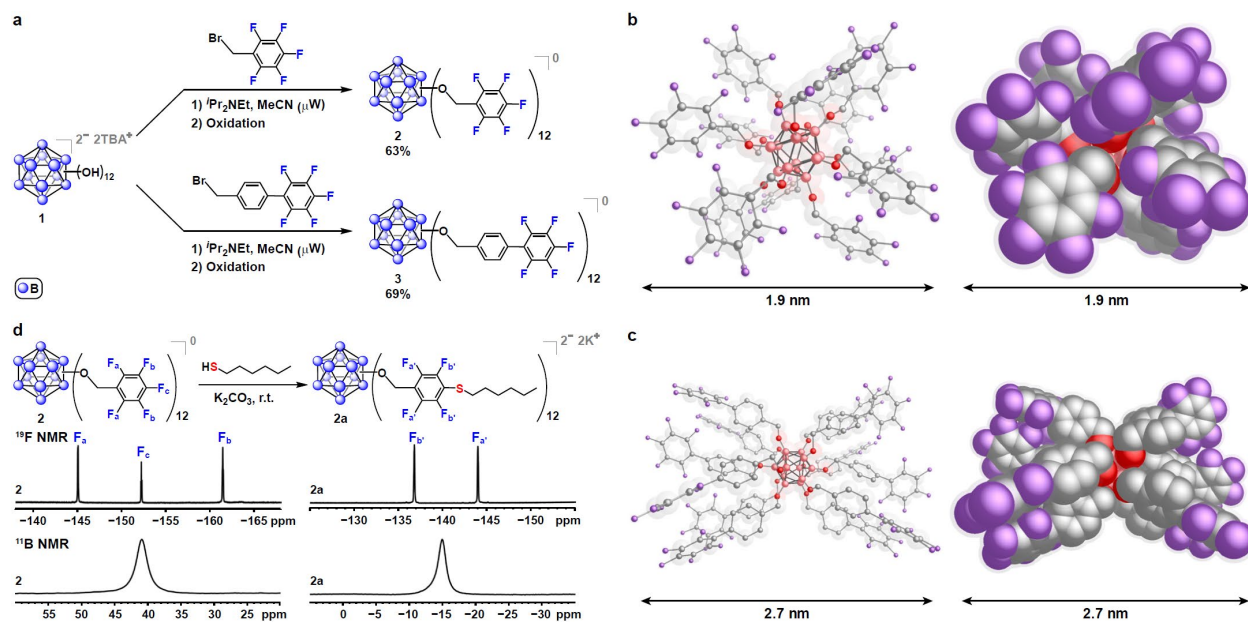


**Figure 2.2.** Synthesis and characterization of the perfluoroaryl-perfunctionalized dodecaborate clusters and the subsequent modification with thiols. (a) Perfunctionalization of **1** with rigid pentafluoroaryl-terminated linkers yields pure clusters **2** and **3**, after isolation. (b,c) Ball-and-stick and space-filling representations of the single-crystal X-ray structures of **2** and **3**, respectively. Size measurements of the crystal structures reveal that **2** is 1.9 nm and **3** is 2.7 nm (lengthwise). B, pink; O, red; C, grey; F, purple. (d) “Click”-like modification of cluster **2** with the 1-hexanethiol reagent and the corresponding  $^{19}\text{F}$  and  $^{11}\text{B}$  NMR spectra associated with the transformation from the starting material **2** to the functionalized product **2a**. Specifically, perfunctionalization of **2** with 1-hexanethiol results in a shift of the *meta*-F resonance and the complete disappearance of the *para*-F resonance as well as a characteristic upfield shift of the boron singlet resulting from the reduction of the cluster. TBA, tetrabutylammonium.

To test our hypothesis that **2** and **3** could be fully functionalized by thiols *via*  $\text{S}_{\text{N}}\text{Ar}$  reaction, we commenced conjugation studies between **2** and 1-hexanethiol (**a**). Cluster **2** was mixed with 12 equiv. of thiol **a** in dimethylformamide (DMF) in the presence of base and left stirring under  $\text{N}_2$  atmosphere to mitigate the undesired oxidation of the thiol reagent. Notably, the initially dark red solution quickly turned colourless.  $^{11}\text{B}$  NMR spectroscopy of this colourless solution revealed a singlet resonance at  $\delta$  -15 characteristic of a reduced cluster in a  $[\mathbf{2}]^{2-}$  oxidation state,<sup>81,82</sup> which is consistent with the reducing capacity of the thiolate species when exposed to  $[\mathbf{2}]^0$  (Figure 2.2d).

Therefore, for all subsequent optimization studies we utilized an extra equivalent of the thiol reagent to account for this reduction.  $^{19}\text{F}$  NMR spectroscopy was utilized to monitor the conversion of **2** to **2a**, given the diagnostic change associated with this transformation (Figure 2.2d – disappearance of the *para*-F resonance and significant downfield shift of the *meta*-F resonances in **2a** compared to the starting material **2**). A base screen identified potassium carbonate ( $\text{K}_2\text{CO}_3$ ) as the optimal reagent leading to the substantial conversion resulting in the formation of perfunctionalized cluster **2a** (see the Supporting Information for experimental details). After additional optimization using  $\text{K}_2\text{CO}_3$ , we found that using 13.3 equiv. of **a** and 30 equiv. of  $\text{K}_2\text{CO}_3$  resulted in a nearly quantitative (>99%) substitution of **2**, producing the 12-fold substituted OCN **2a** (Table 2.1, entry 1; Figure 2.2d). The crude product was dried and then purified *via* silica gel column chromatography and isolated as an oily substance in 70% yield (see the Supporting Information for experimental details). Electrospray ionization-high resolution mass spectrometry (ESI-HRMS),  $^1\text{H}$ ,  $^{11}\text{B}$ , and  $^{19}\text{F}$  NMR spectroscopy of purified **2a** are consistent with its proposed structure and composition (see the Supporting Information for characterization data). We further found that **2** could be fully conjugated with aromatic (**b**) and benzylic (**c**) thiols. Both reactions proceeded nearly quantitatively within 24 hours at room temperature using potassium phosphate ( $\text{K}_3\text{PO}_4$ ), leading to pure OCNs **2b** and **2c** (Table 2.1, entries 2 and 3), respectively, after isolation in good yields (see the Supporting Information for experimental details and characterization data). Importantly, results with **2a–2c** indicate that the developed chemistry can operate with a wide range of thiol-based species spanning a significant window of nucleophilicities (pKa of aliphatic thiols is approximately 17, aromatic – 10). Overall, these experiments suggest that using the developed method, it is possible to rapidly assemble OCNs *via*  $\text{S}_{\text{N}}\text{Ar}$  chemistry under very mild and operationally simple conditions mimicking the simplicity of the thiol-capped AuNPs

assembly. Furthermore, unlike the previously developed Huisgen “click” cycloaddition and carbamate functionalization strategies of inherently non-rigid B<sub>12</sub>-based clusters, which require elevated temperatures, long reaction times (days) and a large excess of reagents (4–5 fold per vertex), the perfluoroaryl-thiol S<sub>N</sub>Ar chemistry described here proceeds using significantly milder conditions.<sup>40,80</sup>

Thiol-capped AuNP constructs are also extremely attractive given the chemical orthogonality of the gold-thiol interaction compared to other ligands, which provides an opportunity to use a wide variety of unprotected thiol reagents for facile and programmable self-assembly. Therefore, we decided to probe the degree to which S<sub>N</sub>Ar chemistry on perfluorinated clusters can mimic this attractive feature. To evaluate the thiol-selectivity of our approach, we performed conjugation reactions between **2** and thiols featuring additional nucleophilic groups such as alcohols and amines. Consistent with the previous work by Pentelute and co-workers with unprotected peptides,<sup>89,90</sup> we found that the model thiol species (**d–f**) all reacted with **2** through the thiol site selectively to form the desired perfunctionalized OCNs **2d–2f** (Table 2.1, entries 4–6) within 24 hours as confirmed by <sup>19</sup>F NMR spectroscopy (see the Supporting Information for experimental details and characterization data). This finding is important as it suggests that this chemistry can be used to selectively conjugate thiol reagents containing multiple nucleophilic functional groups and fundamentally takes advantage of the mild conditions developed here, which allow one to guide the kinetic selectivity between the thiol and pentafluoroaryl fragment.<sup>88–90</sup> Most importantly, this chemoselectivity is reminiscent of that observed in the assembly of thiol-capped AuNPs.

**Table 2.1.** Conjugation scope for **2** and **3**.

Entry	Symbol	L	R	Time (h)	<i>in situ</i> yield <sup>a</sup> (%)	Isolated yield <sup>b</sup> (%)
1	<b>2a</b>	none		24	99	70
2	<b>2b</b>	none		24	99	90
3	<b>2c</b>	none		24	99	94
4	<b>2d</b>	none		24	99	40
5	<b>2e</b>	none		24	99	30
6	<b>2f</b>	none		24	99	49
7	<b>3a</b>			7 <sup>c</sup>	99	87
8	<b>3b</b>			7 <sup>c</sup>	99	85
9	<b>3c</b>			5	99	81
10	<b>3d</b>			2	99	81
11	<b>3e</b>			4	99	59
12	<b>3f</b>			3	99	33
13	<b>3g</b>			3	99	49
14	<b>3h<sup>d</sup></b>			6	99	29

<sup>a</sup>Yield determined by <sup>19</sup>F NMR spectroscopy; <sup>b</sup>Isolated yields after purification; <sup>c</sup>Small-scale reactions show full conversion within 1 h; <sup>d</sup>Additional 36 equiv. isopropoxytrimethylsilane (<sup>i</sup>PrMe<sub>3</sub>Si) was employed to scavenge fluoride (F<sup>-</sup>) by-product. r.t., room temperature.

**Table 2.2.** PEGylation and glycosylation of **2** and **3**.

Entry	Symbol	L	R	Time (h)	<i>in situ</i> yield <sup>a</sup> (%)	Isolated yield <sup>b</sup> (%)
1	<b>2i</b>	none		24	99	81
2	<b>2j</b>	none		24	99	19
3	<b>2k</b>	none		24	99	41
4	<b>2l<sup>c</sup></b>	none		24	99	17
5	<b>3i</b>			5	99	78
6	<b>3j</b>			4	99	21
7	<b>3k</b>			20 <sup>d</sup>	99	54
8	<b>3l<sup>c</sup></b>			5	99	32

<sup>a</sup>Yield determined by <sup>19</sup>F NMR spectroscopy; <sup>b</sup>Isolated yields after purification; <sup>c</sup>**2l** and **3l** underwent partial K<sup>+</sup>/Na<sup>+</sup> counterion exchange during the deprotection reaction with NaOMe; <sup>d</sup>Small-scale reaction shows full conversion within 5 h.

With the successful perfunctionalization of **2** (*vide supra*), we hypothesized that the larger-sized cluster **3** could not only be perfunctionalized with the same thiols to create a new generation of OCNs that are modularly extended in size, but could also accommodate 12-fold conjugation with bulkier substrates. Indeed, under the same conditions as described above for functionalization of **2**, cluster **3** undergoes clean and facile perfunctionalization chemistry with thiols **a–f**, yielding **3a–3f** (Table 2.1, entries 7–12; see the Supporting Information for experimental details and characterization data). Importantly, when using **3** instead of **2**, we observed a significantly faster



conversion rate leading to perfunctionalized clusters (under six hours versus 24 hours), consistent with the surface of **3** being less sterically encumbered than **2**. Therefore, using **3** allowed full substitution with a bulky cysteine derivative (**g**) as well as a small, unprotected peptide sequence C-A-G (**h**), yielding **3g** and **3h**, respectively (Table 2.1, entries 13 and 14; see the Supporting Information for experimental details and characterization data).

Next, to test whether more complex molecular architectures could also be introduced onto the clusters, we turned our attention to poly(ethylene glycol) (PEG).<sup>52,70,91,92</sup> Complete 12-fold conjugation between **2** and commercially available mPEG-thiol ( $MW_{\text{avg}} = 356$  Da) occurred within 24 hours at room temperature, yielding OCN **2i** (Table 2.2, entry 1; see the Supporting Information for experimental details and characterization data). Subsequently, larger mPEG-thiols ( $MW_{\text{avg}} = 766$  Da and 2,000 Da) were tested and similarly afforded **2j** and **2k**, respectively, in quantitative conversions based on <sup>19</sup>F NMR spectroscopy (Table 2.2, entries 2 and 3; see the Supporting Information for experimental details and characterization data). As expected, PEGylation conferred considerable hydrophilicity to these clusters: **2i–2k** are readily soluble in water. Owing to the full covalency of PEGylated OCNs, we hypothesized that these species should be structurally stable under biological conditions. Using **2i** as a model, we conducted stability studies in biologically relevant media (see the Supporting Information for experimental details and data). A purified sample of **2i** was exposed to cell culture media containing fetal bovine serum (FBS) for five days at room temperature, and no changes or degradation products were observed by monitoring this sample *via* <sup>19</sup>F and <sup>11</sup>B NMR spectroscopy. Similarly, no degradation occurred when this sample was incubated for an additional five days at 37 °C. Importantly, samples of **2i** were dissolved in buffers of various pH (5, 7, and 9) for five days, and these were found to remain structurally intact as well. These results suggest that OCNs retain their structural integrity under

the wide range of biologically relevant conditions. We then decided to investigate the stability of the conjugation linkage between the cluster core and the thiol. Given the full covalency of **2i**, we expected that it should not undergo ligand-exchange, a process that commonly occurs with many ligand-capped AuNPs.<sup>70</sup> Significantly, no thiol-exchange occurred when **2i** (0.8 mM) was exposed to 2-mercaptoethanol (20 mM) over a period of 11 days. Similar results were obtained with 2 mM glutathione (GSH). Overall, these experiments clearly demonstrate that the OCNs constructed *via* the S<sub>N</sub>Ar approach feature superior robustness compared to many AuNP-based assemblies.<sup>58,69</sup>

PEGylated OCNs were characterized by a number of techniques to ensure their proposed nearly monodisperse composition (while the OCN cores are monodisperse, the PEG chains used in this study feature some compositional variability because of the inherent limitations of PEG oligomer synthesis).<sup>93</sup> First, we conducted 2D diffusion ordered spectroscopy (2D DOSY) <sup>1</sup>H NMR experiments with purified samples of **2i–2k** and the more extended OCNs **3i–3k** (Table 2.2, entries 5–7; see the Supporting Information for experimental details and characterization data) in D<sub>2</sub>O (see the Supporting Information for 2D DOSY method and plots). Based on the diffusion constants obtained from these DOSY experiments, the respective hydrodynamic diameters were estimated (Figure 2.3a). As expected, the results reveal a gradual increase in the sizes of the PEGylated clusters, both as a function of the cluster core size (from **2** to **3**) and the length of the PEG chain used. The size of **3i** measured by 2D DOSY was larger than expected, most likely because of aggregation under the conditions the measurement was performed, which suggests the small number of PEG units in **3i** could not fully stabilize the hydrophobic core against self-aggregation. To determine the size of a single non-aggregated OCN **3i**, we performed additional transmission electron microscopy (TEM) experiments on **3i** (Figure 2.3b; see the Supporting Information for experimental details). The TEM images reveal the presence of nearly

monodisperse particles with an average size of 1.9 nm, which is in agreement with the expected value for a non-aggregated single particle. Consistent with these results, gel permeation chromatography (GPC) traces of **2k** and **3k** in water (Figure 2.3c) also reveal nearly monodisperse samples ( $D = 1.003 \pm 0.02$ ,  $1.081 \pm 0.007$ , respectively; see the Supporting Information for experimental details). Furthermore, we performed molecular dynamics (MD) simulations of species **2i–2k** and **3i–3k** in water and calculated their hydrodynamic radii and radii of gyration (snapshots after 21 ns in Figure 2.3d; see the Supporting Information for experimental details). The results are in good agreement with the non-aggregated OCN sizes measured by TEM, and furthermore exhibit a trend similar to the one observed by 2D DOSY  $^1\text{H}$  NMR spectroscopy. A small discrepancy arises between the sizes estimated based on computational studies/TEM and 2D DOSY  $^1\text{H}$  NMR spectroscopy and is likely due to some aggregation of the particles under the conditions employed in 2D DOSY  $^1\text{H}$  NMR spectroscopy experiments. Overall, our measurements clearly show that using the developed  $\text{S}_{\text{N}}\text{Ar}$  assembly strategy, one can rationally prepare robust and nearly monodisperse samples of size-tunable PEGylated OCNs.

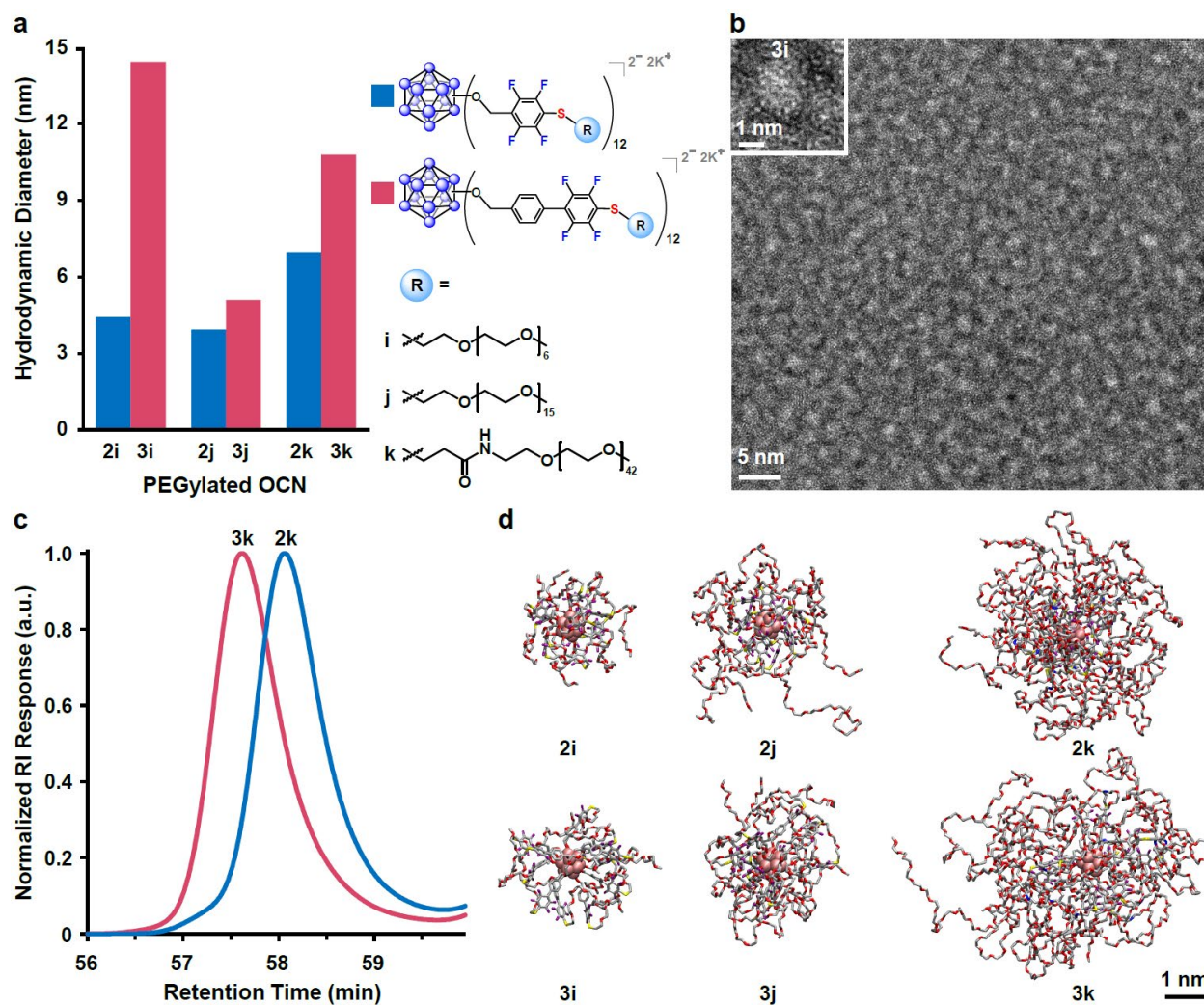


**Figure 2.3.** Characterization of the PEGylated OCNs **2i–2k** and **3i–3k**. (a) Plot of the particle sizes of the PEGylated OCNs **2i–2k** and **3i–3k** obtained *via* 2D DOSY  $^1\text{H}$  NMR experiments. The plot reveals a trend of a gradual increase in the sizes of the OCNs, both as a function of the cluster precursor dimension and of the chain length of the PEG reagent. The size of **3i** is larger than expected, probably because of aggregation. (b) TEM images of a negatively stained sample of **3i** reveal the presence of nearly monodisperse particles with an average size of 1.9 nm, consistent with the expected size of **3i**. (c) GPC traces of **2k** and **3k** measured in water further confirm the monodispersity of the samples ( $D = 1.003 \pm 0.02$  and  $1.081 \pm 0.007$ , respectively). (d) MD-calculated structures of the PEGylated nanomolecules in pure water after 21 ns of simulation indicate a trend in the sizes of the OCNs consistent with that observed through the 2D DOSY experiments. RI = refractive index; a.u., arbitrary units.

After demonstrating the scope of the developed chemistry with various classes of thiols, we next aimed to coat the scaffold clusters with recognition moieties in order to develop OCNs

capable of multivalent binding interactions. In nature, multivalent glycoconjugates such as glycoproteins and glycolipids can bind lectins with relatively high avidity, thereby bypassing the fundamental limitation of weak monosaccharide binding (dissociation constants ( $K_D$ ) ranging between mM and  $\mu$ M).<sup>84,94–98</sup> We hypothesized that cluster **2** and **3** can serve as a rigid, tunable scaffold for three-dimensional, precise display of carbohydrates. Using commercially available carbohydrate precursor 1-thio- $\beta$ -D-glucose tetraacetate, we have synthesized functionalized OCNs **2I** and **3I** featuring 12 appended glucose molecules (Table 2.2, entries 4 and 8; Figure 2.4a; see the Supporting Information for experimental details and characterization data). We then conducted surface plasmon resonance (SPR) experiments with a Biacore T100 instrument to monitor and quantify binding interactions between the glycosylated OCN **2I** and a model lectin Concanavalin A (ConA) at pH 7.4 (see the Supporting Information for experimental details). ConA was covalently attached to the Au-coated sensor chip's dextran layer *via* conventional amide coupling,<sup>99</sup> and binding between ConA and the injected analyte was measured as a change in refractive index (RI) and expressed in response units (RU). From the binding sensorgrams (Figure 2.4b), it is clear that the measured binding response was dependent on the concentration of **2I** in the injected sample. Furthermore, when two controls (**2i** and D-glucose) were injected at the highest mass concentration of **2I** shown ( $2.0 \text{ mg L}^{-1}$ ), minimal to no binding was observed. When the binding curves of **2I** were fitted to the Langmuir 1:1 binding model, the  $K_D$  value was estimated to be 54 nM, which corresponds to a 6,500-fold increase in affinity when compared to the  $K_D$  between ConA and methyl D-glucopyranoside.<sup>99</sup> These results are consistent with the  $K_D$  value previously reported by Munoz and co-workers between ConA and a 3<sup>rd</sup> generation D-glucose-functionalized glycodendrimer (15.8 nM, 27 saccharides). This result is significant since it demonstrates that a similar multivalent effect can be achieved by using a rigid OCN scaffold

featuring significantly fewer (12 vs. 27) saccharides. Furthermore, compared to the glycodendrimer used in the work of Munoz and co-workers, which requires 8 synthetic steps, glycosylated OCNs can be rapidly constructed in 3 steps with an  $S_NAr$  conjugation done under 24 hours (Huisgen click cycloaddition conjugations on large dendritic assemblies normally take several days for completion).<sup>100</sup> Lastly, we note that the OCNs generated here are fully covalent and therefore feature enhanced stability properties compared to the species synthesized *via* coordination-based self-assembly.<sup>101</sup>

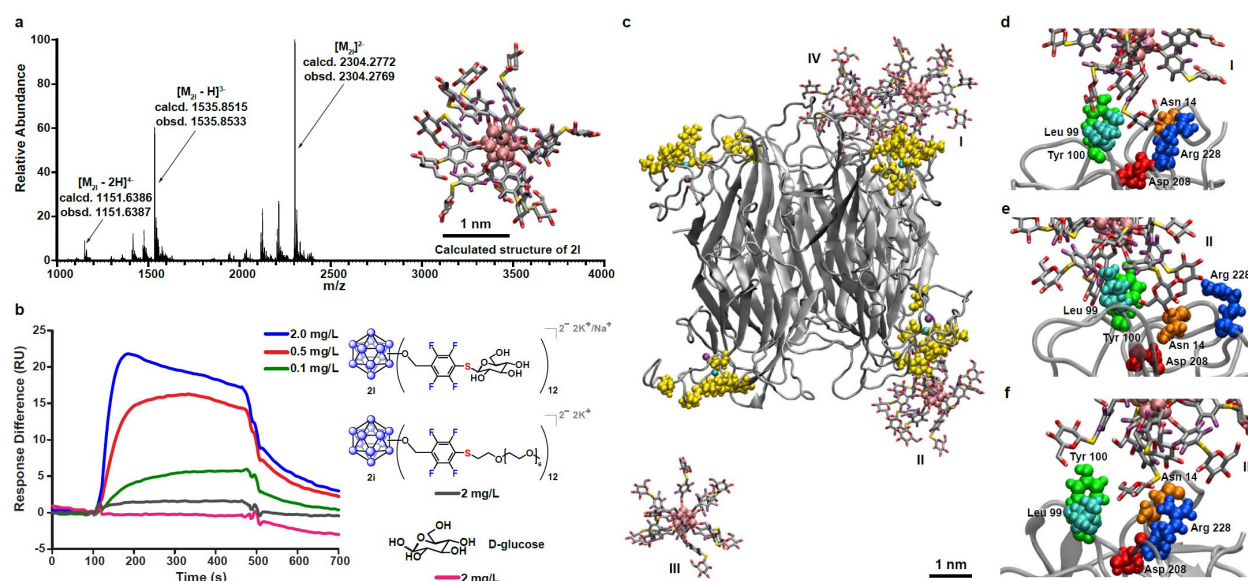


**Figure 2.4.** Multivalent binding of the glycosylated OCN **2I** to the lectin ConA. (a) ESI-HRMS of **2I** supports its proposed structure and composition (see inset for the MD simulated structure of **2I** in an aqueous environment). (b) SPR sensorgram indicates that the measured binding response is dependent on the concentration of **2I**. Furthermore, it suggests multivalent binding interactions between **2I** and ConA as well as minimal binding of the PEGylated cluster **2i** and D-glucose controls to ConA. (c) A snapshot at 20 ns of a MD simulation showcases the interactions between four **2I** particles (I, II, III, and IV) and ConA. (d–f) MD-simulation close-up snapshots of three of the **2I** particles (I (d), II (e) and III (f)) binding to ConA at the known monosaccharide-binding residues (coloured and labelled). Calcd, calculated; obsd, observed.

We hypothesized that the glycosylated OCN's dramatically enhanced affinity over D-glucose toward ConA can be explained by the cluster glycoside effect,<sup>84</sup> and in order to better

understand the mechanistic details of binding between **21** and ConA, we performed MD simulations of the interactions between **21** and ConA in water (see snapshots of the simulations in Figure 2.4c–f; see the Supporting Information for experimental details). Our calculation results are consistent with the experimental observations – that **21** exhibits much higher affinity than the monovalent D-glucose molecule toward ConA’s saccharide-binding sites. Furthermore, the higher affinity can be attributed to the multivalent statistical/rebinding effect provided by the densely functionalized surface filled with monosaccharide ligands positioned around the OCN cluster.<sup>51,99</sup>

## Conclusions

We have developed a new strategy that allows a rapid assembly of fully covalent nanoparticles with atomic precision. Specifically, we demonstrated that the rigid clusters densely decorated with perfluoroaryl-containing functional groups undergo efficient conjugation with a variety of thiols *via* S<sub>N</sub>Ar chemistry under very mild conditions at room temperature. Importantly, this chemistry is operationally reminiscent of the chemoselective assembly conditions associated with thiol-capped AuNPs. Furthermore, similarly to thiol-capped AuNPs, these OCNs can be easily tuned in size and surface chemistry by choosing a specific thiol reagent. OCNs exhibit dramatically improved structural stability under a wide range of biologically relevant conditions because of the full covalency of all the bonding interactions that comprise these nanomolecules. Finally, using this assembly strategy we show how one can design and synthesize nanomolecules that feature a 3D densely packed layer of saccharides that can participate in multivalent binding with a natural lectin and lead to a dramatic increase in binding affinity. This work ultimately opens

a new avenue to create highly tailored synthetic mimics of ligand-capped AuNPs that feature rigid and fully covalent atomically precise assemblies.



## Experimental Section

### General considerations

Microwave synthesis reactions and all post-microwave work-up and characterization were performed under ambient conditions. For the purposes of this manuscript, “ambient conditions” refer to room temperature (20 - 28 °C) and uncontrolled laboratory air.

### Materials

Deuterated solvents were purchased from Cambridge Isotope Laboratories. MilliQ water described in this manuscript refers to purified potable water with a resistivity at 25 °C of  $\leq 18.2$  M $\Omega$ ·cm. [NEt<sub>3</sub>H]<sub>2</sub>[B<sub>12</sub>H<sub>12</sub>] was purchased from Boron Specialties. EtOH (200 proof) was purchased from Decon Labs. Fmoc-L-amino acids (>98.5%) were purchased from Chem-Impex International, Inc. Piperidine (99%) was purchased from Spectrum. CaCl<sub>2</sub>·2 H<sub>2</sub>O ( $\geq 99\%$ ), MgCl<sub>2</sub>·6 H<sub>2</sub>O ( $\geq 99\%$ ), MnCl<sub>2</sub>·4 H<sub>2</sub>O ( $\geq 98\%$ ), diethyl ether (anhydrous,  $\geq 99.9\%$ ), glycine (98%), and Gibco minimum essential medium were purchased from Fisher Scientific. Thiophenol (99%) and poly(ethylene glycol) methyl ether (average MW 750 Da, MW range 715 – 785 Da) were purchased from Acros Organics. HBS-P pH 7.4 buffer (10 mM HEPES, 0.005% v/v Tween P20) and 1 M ethanolamine-HCl (pH 8.5) were purchased from GE Healthcare Life Sciences. Fetal bovine serum was purchased from ScienCell Research Laboratories. FeCl<sub>3</sub>·6 H<sub>2</sub>O ( $\geq 97\%$ ), CsOH·1 H<sub>2</sub>O ( $\geq 99.5\%$ ), H<sub>2</sub>O<sub>2</sub> (30% in H<sub>2</sub>O), [N<sup>n</sup>Bu<sub>4</sub>]OH (40% in H<sub>2</sub>O), trifluoroacetic acid (TFA, 99%), triisopropylsilane (98%), *N,N*-dimethylformamide (DMF,  $\geq 99.8\%$ ; anhydrous, 99.8%), MeCN ( $\geq 99.9\%$ ), CH<sub>2</sub>Cl<sub>2</sub> ( $\geq 99.5\%$ ), ethyl acetate ( $\geq 99.5\%$ ), hexanes ( $\geq 98.5\%$ ), MeOH ( $\geq 99.8\%$ ), *N,N*-

diisopropylethylamine ( $\geq 99\%$ ), tetrabutylammonium hexafluorophosphate ( $\geq 99.0\%$ , electrochemical grade), 1,2-ethanedithiol ( $\geq 98\%$ ), 1-hexanethiol (95%), benzyl mercaptan (99%), cysteamine (95%), 2-mercaptoethanol ( $\geq 99\%$ ), 1-thioglycerol ( $\geq 97\%$ ), *O*-(2-mercaptoethyl)-*O*'-methyl-hexa(ethylene glycol) (average  $M_n$  356.48 Da,  $\geq 95\%$ ), *O*-(2-mercaptoethyl)-*O*'-methylpolyethylene glycol (average  $M_w$  2,000 Da), 1-thio- $\beta$ -D-glucose tetraacetate (97%), *N*-(*tert*-Butoxycarbonyl)-L-cysteine methyl ester (97%), isopropoxytrimethylsilane (98%),  $K_3PO_4$  ( $\geq 98\%$ ),  $K_2CO_3$  ( $\geq 99\%$ ), Tris ( $\geq 99\%$ ), and triethylamine ( $\geq 99\%$ ) were purchased from Sigma-Aldrich. All reagents were used as received unless otherwise indicated.

## Instruments

Bruker AV300, AV400, AV500, and DRX500 spectrometers were used to obtain  $^1H$ ,  $^{11}B$ ,  $^{13}C\{^1H\}$ , and  $^{19}F$  NMR spectra and Bruker Topspin software was used to process the NMR data.  $^1H$  and  $^{13}C\{^1H\}$  NMR spectra were referenced to residual solvent resonances in deuterated solvents (due to high humidity,  $H_2O$  resonances are often present).  $^{11}B$  and  $^{19}F$  NMR spectra were referenced to  $BF_3 \cdot Et_2O$  and  $CFCl_3$  external standards, respectively, at  $\delta$  0.0. *in situ*  $^{11}B$  and  $^{19}F$  NMR spectroscopy was run unlocked and unshimmed.  $^{11}B$  NMR spectra were baseline-corrected using the cubic spline correction tool within the Bruker Topspin software. Mass spectrometry data were acquired using a Thermo Scientific Q-Exactive Plus instrument with a quadrupole mass filter and Orbitrap mass analyzer or a Waters LCT Premier TOF system with ACQUITY LC and autosampler. IR spectroscopy was acquired on solid samples using a PerkinElmer Spectrum Two FT-IR spectrometer equipped with a diamond universal ATR probe. High resolution transmission electron microscopy (HRTEM) images were acquired with a FEI Titan electron microscope

operating at 300 kV. Size exclusion chromatography-multi angle light scattering (SEC-MALS) was conducted on a GE AKTA PURE chromatographic system equipped with a WYATT miniDawn Treos MALS, WYATT optilab T-rEX RI detector, one Tosoh PWXL guard column (6.0 mm ID x 4.0 cm, 12  $\mu\text{m}$ ), and one Tosoh G4000PWxl (7.8 mm ID x 30 cm, 10  $\mu\text{m}$ ) column. Surface plasmon resonance (SPR) experiments were run on a GE Healthcare Life Sciences Biacore T100 instrument. Purification of peptides was done using a Waters HPLC system equipped with a UV/Vis detector set at  $\lambda = 214 \text{ nm}$ .

### **2D diffusion-ordered (DOSY) $^1\text{H}$ NMR spectroscopy**

2D DOSY experiments on purified samples of PEGylated OCNs were performed in  $\text{D}_2\text{O}$  at 30  $^\circ\text{C}$  on a Bruker AV 300 spectrometer. The data were processed with the standard Bruker Topspin software – the T1/T2 *vargrad* fitting function was used to determine the diffusion coefficients. 2D DOSY plots were created with the Bruker Topspin software. Hydrodynamic diameters were estimated based on the diffusion coefficients using the Stokes-Einstein Equation.

### **High resolution transmission electron microscopy (HRTEM)**

HRTEM samples were prepared by dropping 5  $\mu\text{L}$  of 25  $\mu\text{g}/\text{mL}$  aqueous sample solutions onto carbon copper grids (Ted Pella). The samples were then blotted once with a filter paper and then left to air-dry for 10 minutes. Then, 3  $\mu\text{L}$  of a 2% w/w uranyl acetate aqueous solution was dropped on the grids, and subsequently blotted after 2 minutes.

### **Size exclusion chromatography-multi angle light scattering (SEC-MALS)**

Samples for SEC-MALS were prepared by dissolving sample in MilliQ water and filtering sample through a 0.20  $\mu\text{m}$  PTFE Fisherbrand syringe filter. Eluent was Millipore filtered MilliQ water with 0.02%  $\text{NaN}_3$  at 12  $^\circ\text{C}$  (flow rate: 0.70 mL/min). Chromatograms were analyzed using Astra 6.0 software.

### **Surface plasmon resonance (SPR)**

All experiments were performed on a Biacore T100 instrument with a Series S CM5 chip (GE Healthcare Life Sciences). The procedure used here was modified from a published procedure by Safina *et al.*<sup>102</sup> The running buffer was 10 mM HEPES buffer (pH 7.4) with 0.005% Tween P20, 1 mM  $\text{CaCl}_2$ , 1 mM  $\text{MgCl}_2$ , and 1 mM  $\text{MnCl}_2$ . 5  $\mu\text{L}/\text{min}$  flow rate was used throughout the experiments. First, a reference channel (flow cell 1) was prepared by activating the surface with a 0.4 M EDC and 0.1 M NHS (1:1 v/v) mixture during 30 minutes, then 1 M ethanolamine HCl (pH 8.5) during 40 minutes. Then, the sample channel (flow cell 2) was activated using under the EDC/NHS conditions, followed by injection of 0.1 mg/mL ConA for 40 minutes and then 1 M ethanolamine HCl for 30 minutes for blocking. Analyte samples of 0.022  $\mu\text{M}$  to 130  $\mu\text{M}$  were injected in tandem over both cells for 6 minutes. Surfaces were regenerated by injecting 10 mM HCl for 2 minutes followed by injecting 10 mM glycine HCl (pH 2.5) for 2 minutes. Binding curves at various analyte concentrations were fitted to the Langmuir 1:1 binding model for an estimation of the binding constants. For the purpose of figure presentation, the sensorgrams were processed using the smoothing function in the OriginPro data analysis software.

## X-ray data collection and processing parameters

For **2**, a single crystal was mounted on a nylon loop using perfluoropolyether oil and cooled rapidly to 100 K with a stream of cold dinitrogen. Diffraction data were measured using a Bruker APEX-II CCD diffractometer using Mo- $K\alpha$  radiation. The cell refinement and data reduction were carried out using Bruker SAINT and the structure was solved with SHELXS-97. All subsequent crystallographic calculations were performed using SHELXL-2013. For **3**, single-crystal diffraction data were collected at 100(2) K on a Bruker Apex II CCD diffractometer with Mo  $K\alpha$  radiation ( $\lambda = 0.71073 \text{ \AA}$ ). After correcting for absorption and polarization effects, structure solution and refinement were carried out using the SHELXT<sup>103</sup>, XL<sup>104</sup> and Olex2<sup>105</sup> software suites. Non-hydrogen atoms were refined with anisotropic thermal displacement parameters, and hydrogen atoms were placed in suitable riding positions.

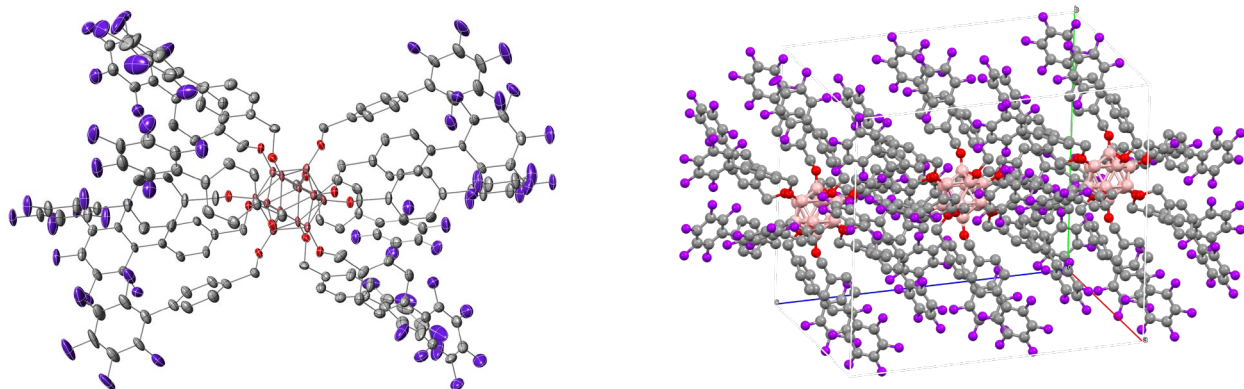


**Table S2.1.** Crystal data for [3]<sup>0</sup>

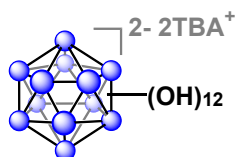
compound	<b>3</b>
empirical formula	C <sub>78</sub> H <sub>36</sub> B <sub>6</sub> F <sub>30</sub> O <sub>6</sub>
fw	1703.95
temp / K	100
wavelength / Å	0.71073 Å
space group	<i>P</i> -1
<i>a</i> / Å	19.211(3)
<i>b</i> / Å	19.674(3)
<i>c</i> / Å	22.866(4)
$\alpha$ / deg	97.606(5)
$\beta$ / deg	114.089(5)
$\gamma$ / deg	109.756(5)
<i>V</i> / Å <sup>3</sup>	7047.9(18)
<i>Z</i>	2
<i>d</i> (calcd) / Mg·m <sup>-3</sup>	1.606
abs coeff / mm <sup>-1</sup>	0.153
R indices:	<i>R</i> <sub>I</sub> = 0.1771
	<i>R</i> <sub>w</sub> = 0.2030

### Microwave synthesis

Microwave reactions were performed using a CEM Discover SP microwave synthesis reactor. Except where noted otherwise, all reactions were performed in glass 10 mL microwave reactor vials purchased from CEM with silicone/PTFE caps. Flea micro PTFE-coated stir bars (10 mm x 3 mm) were used in the vials with magnetic stirring set to high and 15 seconds of premixing prior

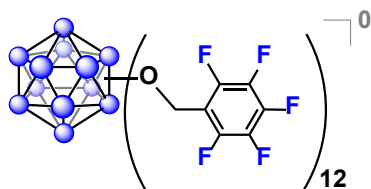
to the temperature ramping. All microwave reactions were carried out at 140 °C with the pressure release limit set to 250 psi (no reactions exceeded this limit to trigger venting) and the maximum wattage set to 250 W (the power applied was dynamically controlled by the microwave instrument and did not exceed this limit for any reactions). Column chromatography was performed using 2.0 - 2.25 cm inner diameter glass fritted chromatography columns with 20-30 cm of slurry-packed silica gel to ensure full separation of reagents and products. Unfiltered pressurized air was used to assist column chromatography.

### Synthesis of 1



The [N<sup>n</sup>Bu<sub>4</sub>]<sub>2</sub> salt of [B<sub>12</sub>(OH)<sub>12</sub>]<sup>2-</sup> was prepared according to the procedures detailed in Wixtrom *et al.* 2016.<sup>81</sup> From this point, N<sup>n</sup>Bu<sub>4</sub> will be referred to as TBA. Note: **1** is air-stable, but hygroscopic. Store under inert atmosphere or in a sealed desiccator to prevent excess absorption of water over extended periods of time in storage.

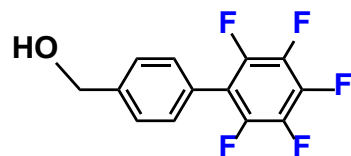
### Synthesis of 2



Previously reported protocol<sup>82</sup> used to synthesize compound **2** – procedure is duplicated here. Compound **1** (300 mg, 0.366 mmol) was transferred out of a nitrogen filled glovebox, opened to

the air, and dissolved in 4 mL acetonitrile in a 30 mL glass microwave vial. *N,N*-diisopropylethylamine (1.21 mL, 6.96 mmol) and 2,3,4,5,6-pentafluorobenzyl bromide (6.86 mL, 45.4 mmol) were added along with a magnetic stir bar, the vial was sealed with a Teflon/silicone cap, and the reaction mixture was heated under microwave conditions at 140°C with high stirring for 15 minutes. The volatiles were removed via rotary evaporation, and the excess reagent was eluted through a silica column with 65/35 hexanes/ethyl acetate, and the pink/purple product mixture was eluted with acetone. The acetone was removed via rotary evaporation and the residue was dissolved in ~5 mL 90/5/5 ethanol/acetonitrile/H<sub>2</sub>O. FeCl<sub>3</sub>·6H<sub>2</sub>O (1.88 g, 6.96 mmol) was added and the mixture was left to stir for 24 hours. The mixture was concentrated *in vacuo*. The residue (while still in the round bottom flask) was rinsed three times with water. The residue was then taken up in toluene and extracted three times with water. The organic fractions were combined and dried under vacuum. The resulting solid was charged with hexane and isolated by filtration to afford an orange/yellow solid (574 mg, 63%). <sup>1</sup>H NMR (500 MHz, CDCl<sub>3</sub>): δ 5.23 (s, 24H). <sup>11</sup>B NMR (160 MHz, CDCl<sub>3</sub>): δ 40.9. <sup>13</sup>C {<sup>1</sup>H} NMR (126 MHz, CDCl<sub>3</sub>): δ 60.1. <sup>19</sup>F NMR (376 MHz, CDCl<sub>3</sub>): δ -145.1 (d, 24F, *-ortho*), -152.2 (t, 12F, *-para*), -161.3 – -161.5 (m, 24F, *-meta*). HRMS (Q-Exactive Plus): *m/z* calculated for C<sub>8</sub>H<sub>8</sub>B<sub>12</sub>O<sub>12</sub> (M<sup>-</sup>), 2494.1499 Da; found, 2494.1631 Da. Crystallized from CDCl<sub>3</sub> at room temperature for 1 week to obtain a single crystal for X-ray diffraction analysis.

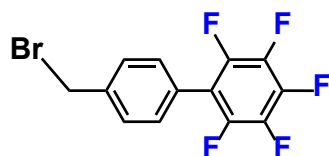
### Synthesis of 4-pentafluorophenyl(hydroxymethyl) benzene





A solution of 4-pentafluorophenyl benzaldehyde (0.900 g, 3.30 mmol) and sodium borohydride (0.150 g, 3.96 mmol) in 14 mL tetrahydrofuran and 7 mL ethanol was prepared and placed under a positive nitrogen flow. The mixture was stirred at room temperature for 24 hours. The resulting dark solution was diluted with water (30 mL) and extracted with methylene chloride (30 mL). The organic layer was washed three times with H<sub>2</sub>O, dried over MgSO<sub>4</sub>, and filtered through Celite. The solvent was then dried *in vacuo*. The residue was purified by flash chromatography (eluent: DCM; R<sub>f</sub> = 0.4) through a silica column, using UV light for TLC visualization. The resulting solution was dried under vacuum, providing 4-pentafluorophenyl(hydroxymethyl) benzene as a white solid (0.705 g, 78%). <sup>1</sup>H NMR (400 MHz, CDCl<sub>3</sub>): δ 7.49 (d, 2H, Ar), 7.42 (d, 2H, Ar), 4.76 (d, 2H, CH<sub>2</sub>OH), 2.05 (t, 1H, CH<sub>2</sub>OH). <sup>13</sup>C {<sup>1</sup>H} NMR (126 MHz, CDCl<sub>3</sub>): δ 144.3, 142.3, 140.6, 138.1, 130.5, 127.2, 126.3, 115.8, 64.9. <sup>19</sup>F NMR (376 MHz, CDCl<sub>3</sub>): δ -143.3 (q, 2F, *-ortho*), -155.5 (t, 1F, *-para*), -162.2 (m, 2F, *-meta*).

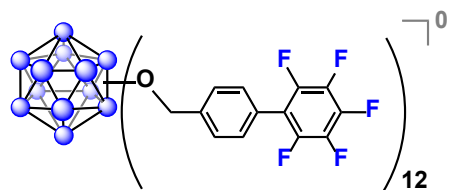
### Synthesis of 4-pentafluorophenyl(bromomethyl) benzene



A flask containing 4-pentafluorophenyl(hydroxymethyl) benzene (1.00 g, 3.65 mmol) was purged with nitrogen and 30 mL of dry methylene chloride was charged into the flask. The solution was placed in ice bath and PBr<sub>3</sub> (346 μL, 3.65 mmol) was added *via* syringe. The reaction mixture was stirred overnight, during which time the mixture turned yellow. The resulting mixture was then diluted with 100 mL distilled H<sub>2</sub>O. The organic layer was separated and washed 3 times with saturated NaCl solution. Organic layer was collected and dried over MgSO<sub>4</sub>, then filtered through

Celite. Solvent was evaporated and the residue was purified by flash chromatography (hexane/CH<sub>2</sub>Cl<sub>2</sub>, 2:1; R<sub>f</sub> = 0.75) through a silica column, using UV light for TLC visualization. The resulting solution was dried under vacuum, providing 4-pentafluorophenyl(bromomethyl) benzene as a white solid (0.773 g, 63%). <sup>1</sup>H NMR (400 MHz, CDCl<sub>3</sub>): δ 7.53 (d, 2H, Ar), 7.42 (d, 2H, Ar), 4.54 (s, 2H, CH<sub>2</sub>Br). <sup>13</sup>C{<sup>1</sup>H} NMR (126 MHz, CDCl<sub>3</sub>): δ 144.3, 140.7, 139.1, 138.0, 130.7, 129.5, 126.6, 115.4, 32.6. <sup>19</sup>F NMR (376 MHz, CDCl<sub>3</sub>): δ -143.1 (q, 2F, *-ortho*), -155.1 (t, 1F, *-para*), -162.0 (m, 2F, *-meta*).

### Synthesis of 3



Compound **1** (75.0 mg, 0.092 mmol) was added to a 10 mL glass microwave vial and transferred out of a nitrogen-filled glovebox, opened to the air, and dissolved in 1.5 mL acetonitrile. *N,N*-diisopropylethylamine (0.3 mL, 1.73 mmol) and 4-pentafluorophenyl(bromomethyl) benzene (0.8334 g, 2.47 mmol) were added along with a flea micro stir bar, the vial was sealed with a PTFE/silicone cap, and the mixture was heated at 140 °C with stirring in the microwave for 30 minutes. The volatiles were removed *via* rotary evaporation, and the remaining reagent was eluted first through a slurry-packed silica gel column with 80/20 hexanes/CH<sub>2</sub>Cl<sub>2</sub>, and the pink/purple product mixture was eluted with acetone followed by CH<sub>2</sub>Cl<sub>2</sub>. *Note: The eluted fraction containing the reagent ligand can be purified by eluting through a silica column with 90/10 hexanes/CH<sub>2</sub>Cl<sub>2</sub>, and after drying thoroughly it can be used for subsequent synthesis of 3. Recycling the ligand in*

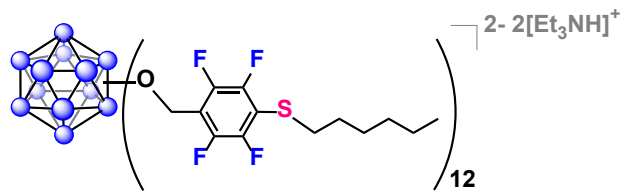
*this manner can minimize unnecessary repetition of ligand synthesis.* The volatiles were removed *via* rotary evaporation, and the remaining charged 2-/1- product mixture was dissolved in 5 mL 90/10 EtOH/MeCN. FeCl<sub>3</sub>·6H<sub>2</sub>O (0.3 g, 1.11 mmol) was added and the mixture was left to stir for 24 hours. Following oxidation, the solvent mixture was removed *via* rotary evaporation, and a red-orange band containing the neutral product was separated from the FeCl<sub>3</sub>·6H<sub>2</sub>O through a slurry-packed silica gel column with CH<sub>2</sub>Cl<sub>2</sub>. The CH<sub>2</sub>Cl<sub>2</sub> was removed *via* rotary evaporation and the final neutral product **2** was dried under high vacuum to obtain an isolated yield of 266.5 mg (85%). Compound **2** is a dark red-orange solid. <sup>1</sup>H NMR (500 MHz, CD<sub>2</sub>Cl<sub>2</sub>): δ 7.21 - 7.33 (m, 48H, C<sub>6</sub>H<sub>4</sub>), 5.50 (s, 24H, OCH<sub>2</sub>). <sup>11</sup>B{<sup>1</sup>H} NMR (128 MHz, CD<sub>2</sub>Cl<sub>2</sub>): δ 42.4. <sup>19</sup>F NMR (376 MHz, CD<sub>2</sub>Cl<sub>2</sub>): δ -144.2 (q, 24F, *-ortho*), -156.5 (t, 12F, *-para*), -163.4 – -163.5 (m, 24F, *-meta*). HRMS (Q-Exactive Plus): *m/z* calculated for C<sub>165</sub>H<sub>72</sub>B<sub>12</sub>F<sub>60</sub>O<sub>12</sub> (M<sup>-</sup>), 3407.5289 Da; found, 3407.5278 Da. X-ray quality crystals of **3** were grown from a cooling solution of boiling 1:1 EtOH:MeOH.

**Table S2.2.** Initial studies and reaction optimization

Entry	Base	Yield <sup>a</sup> (%)
1	NEt <sub>3</sub>	3
2	Tris	7
3	K <sub>3</sub> PO <sub>4</sub>	72
4	K <sub>2</sub> CO <sub>3</sub>	87

<sup>a</sup>Yield determined by <sup>19</sup>F NMR spectroscopy. r.t., room temperature. Tris, tris(hydroxymethyl)aminomethane.

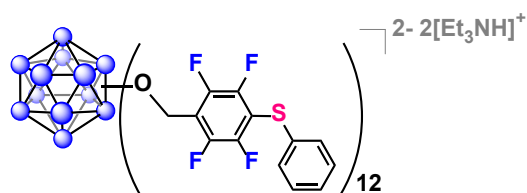
### Synthesis of 2a



**2** (5.0 mg, 0.0020 mmol) and K<sub>2</sub>CO<sub>3</sub> (8.4 mg, 0.061 mmol) were added along with a flea micro stir bar to a 4-mL glass vial, which was then sealed with a PTFE/silicone cap under ambient conditions. The vial was then purged and backfilled with N<sub>2</sub> three times before being transferred into the glovebox. In the glovebox, the vial was opened and 150 μL anhydrous DMF was added, followed by 1-hexanethiol (3.76 μL, 0.027 mmol). The vial was sealed again and set to stir at 400 rpm for 22 hours. The vial was transferred out of the glovebox, and its contents were transferred into an NMR tube for *in situ* <sup>19</sup>F NMR spectroscopy to ensure nearly quantitative conversion and *in situ* <sup>11</sup>B NMR spectroscopy to ensure structural integrity of the cluster. The crude mixture was

then transferred into a 20-mL glass vial and lyophilized for solvent removal. A 5 3/4" glass Pasteur pipet column was prepared using glass wool and 4" of silica gel, and the pipet was flushed with triethylamine (2X column volumes). The crude product mixture containing **2a** was loaded onto the column with 80/20 hexanes/ethyl acetate (sonication was used to aid dissolution), and the remaining reagent was eluted with 80/20 hexanes/ethyl acetate. A very slightly yellow band containing **2a** was eluted with MeCN, and the fractions containing **2a** (as assessed by TLC) were combined and volatiles were removed *via* rotary evaporation followed by lyophilization overnight to obtain an isolated yield of 5.4 mg (70%). <sup>1</sup>H NMR (400 MHz, CD<sub>3</sub>CN): δ 5.42 (br s, 24H, OCH<sub>2</sub>), 3.12 (q, 12H, [(CH<sub>3</sub>CH<sub>2</sub>)<sub>3</sub>NH]<sup>+</sup>), 2.89 – 2.82 (m, 24H, SCH<sub>2</sub>), 1.49 - 1.39 (m, 24H, SCH<sub>2</sub>CH<sub>2</sub>), 1.36 – 1.26 (br m, 24H, S(CH<sub>2</sub>)<sub>2</sub>(CH<sub>2</sub>)<sub>3</sub>CH<sub>3</sub>), 1.24 (t, 18H, [(CH<sub>3</sub>CH<sub>2</sub>)<sub>3</sub>NH]<sup>+</sup>), 1.21 – 1.10 (br m, 48H, S(CH<sub>2</sub>)<sub>2</sub>(CH<sub>2</sub>)<sub>3</sub>CH<sub>3</sub>), 0.83 – 0.74 (m, 36H, S(CH<sub>2</sub>)<sub>5</sub>CH<sub>3</sub>). <sup>11</sup>B {<sup>1</sup>H} NMR (128 MHz, CD<sub>3</sub>CN): δ -15.8. <sup>19</sup>F NMR (376 MHz, CD<sub>3</sub>CN): δ -137.4 (br m, 24F, *-meta*<sup>88</sup>), -145.1 (br m, 24F, *-ortho*<sup>88</sup>). MS (LCT Premier): *m/z* calculated for C<sub>156</sub>H<sub>180</sub>B<sub>12</sub>F<sub>48</sub>O<sub>12</sub>S<sub>12</sub> (M<sup>2-</sup>), 1836.52 Da; found, 1836.29 Da.

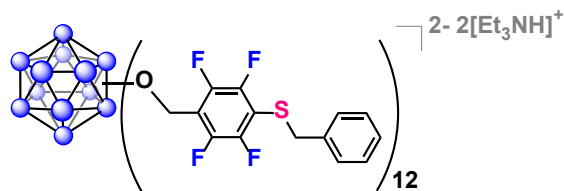
### Synthesis of 2b



**2** (5.0 mg, 0.0020 mmol) and K<sub>3</sub>PO<sub>4</sub> (9 mg, 0.042 mmol) were added along with a flea micro stir bar to a 4-mL glass vial, which was then sealed with a PTFE/silicone cap under ambient conditions. The vial was then purged and backfilled with N<sub>2</sub> three times before being transferred into the glovebox. In the glovebox, the vial was opened and 150 μL anhydrous DMF was added, followed

by thiophenol (2.66  $\mu\text{L}$ , 0.026 mmol). The vial was sealed again and set to stir at 400 rpm for 25 hours. The vial was transferred out of the glovebox, and its contents were transferred into an NMR tube for *in situ*  $^{19}\text{F}$  NMR spectroscopy to ensure nearly quantitative conversion and *in situ*  $^{11}\text{B}$  NMR spectroscopy to ensure structural integrity of the cluster. The crude mixture was then transferred into a 20-mL glass vial and lyophilized for solvent removal. A 5  $\frac{3}{4}$ " glass Pasteur pipet column was prepared using glass wool and 4" of silica gel, and the pipet was flushed with triethylamine (2X column volumes). The crude product mixture containing **2b** was loaded onto the column with 35/65 ethyl acetate/hexanes (sonication was used to aid dissolution), and the remaining reagent was eluted with 35/65 ethyl acetate/hexanes. A very slightly yellow band containing **2b** was eluted with MeCN, and the fractions containing **2b** (as assessed by TLC) were combined and volatiles were removed *via* rotary evaporation followed by lyophilization overnight to obtain an isolated yield of 6.8 mg (90%).  $^1\text{H}$  NMR (400 MHz,  $\text{CD}_3\text{CN}$ ):  $\delta$  7.22 – 7.14 (br m, 60H, S-Ar), 5.49 (br s, 24H, OCH<sub>2</sub>), 3.11 (q, 12H, [(CH<sub>3</sub>CH<sub>2</sub>)<sub>3</sub>NH]<sup>+</sup>), 1.23 (t, 18H, [(CH<sub>3</sub>CH<sub>2</sub>)<sub>3</sub>NH]<sup>+</sup>).  $^{11}\text{B}\{^1\text{H}\}$  NMR (128 MHz,  $\text{CD}_3\text{CN}$ ):  $\delta$  -15.7.  $^{19}\text{F}$  NMR (376 MHz,  $\text{CD}_3\text{CN}$ ):  $\delta$  -136.4 (m, 24F, -*meta*), -144.1 (m, 24F, -*ortho*). HRMS (Q-Exactive Plus): *m/z* calculated for  $\text{C}_{156}\text{H}_{84}\text{B}_{12}\text{F}_{48}\text{O}_{12}\text{S}_{12}$  ( $\text{M}^{2-}$ ), 1788.1481 Da; found, 1788.1514 Da.

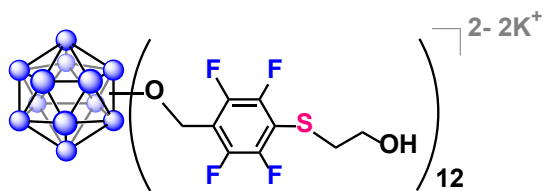
### Synthesis of 2c



**2** (5.0 mg, 0.0020 mmol) and  $\text{K}_3\text{PO}_4$  (8.1 mg, 0.038 mmol) were added along with a flea micro stir bar to a 4-mL glass vial, which was then sealed with a PTFE/silicone cap under ambient

conditions. The vial was then purged and backfilled with N<sub>2</sub> three times before being transferred into the glovebox. In the glovebox, the vial was opened and 150 μL anhydrous DMF was added, followed by benzyl mercaptan (3.53 μL, 0.030 mmol). The vial was sealed again and set to stir at 400 rpm for 24 hours. The vial was transferred out of the glovebox, and its contents were transferred into an NMR tube for *in situ* <sup>19</sup>F NMR spectroscopy to ensure nearly quantitative conversion and *in situ* <sup>11</sup>B NMR spectroscopy to ensure structural integrity of the cluster. The crude mixture was then transferred into a 20-mL glass vial and lyophilized for solvent removal. A 5 3/4" glass Pasteur pipet column was prepared using glass wool and 4" of silica gel, and the pipet was flushed with triethylamine (2X column volumes). The crude product mixture containing **2c** was loaded onto the column with 35/65 ethyl acetate/hexanes (sonication was used to aid dissolution), and the remaining reagent was eluted with 35/65 ethyl acetate/hexanes. A very slightly yellow band containing **2c** was eluted with MeCN, and the fractions containing **2c** (as assessed by TLC) were combined and volatiles were removed *via* rotary evaporation followed by lyophilization overnight to obtain an isolated yield of 7.4 mg (93.5%). <sup>1</sup>H NMR (400 MHz, CD<sub>3</sub>CN): δ 7.20 – 7.04 (br m, 60H, SCH<sub>2</sub>-Ar), 5.39 (br s, 24H, OCH<sub>2</sub>), 4.05 (m, 24H, SCH<sub>2</sub>), 3.11 (q, 12H, [(CH<sub>3</sub>CH<sub>2</sub>)<sub>3</sub>NH]<sup>+</sup>), 1.23 (t, 18H, [(CH<sub>3</sub>CH<sub>2</sub>)<sub>3</sub>NH]<sup>+</sup>). <sup>11</sup>B{<sup>1</sup>H} NMR (128 MHz, CD<sub>3</sub>CN): δ -15.8. <sup>19</sup>F NMR (376 MHz, CD<sub>3</sub>CN): δ -136.8 (m, 24F, *-meta*), -144.8 (m, 24F, *-ortho*). HRMS (Q-Exactive Plus): *m/z* calculated for C<sub>168</sub>H<sub>108</sub>B<sub>12</sub>F<sub>48</sub>O<sub>12</sub>S<sub>12</sub> (M<sup>2-</sup>), 1872.2420 Da; found, 1872.2469 Da.

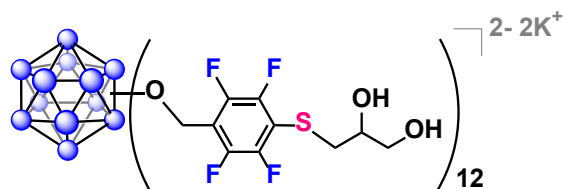
## Synthesis of **2d**



**2** (5.0 mg, 0.0020 mmol) and  $K_3PO_4$  (10.4 mg, 0.049 mmol) were added along with a flea micro stir bar to a 4-mL glass vial, which was then sealed with a PTFE/silicone cap under ambient conditions. The vial was then purged and backfilled with  $N_2$  three times before being transferred into the glovebox. In the glovebox, the vial was opened and 150  $\mu$ L anhydrous DMF was added, followed by 2-mercaptoethanol (2.26  $\mu$ L, 0.032 mmol). The vial was sealed again and set to stir at 400 rpm for 24 hours. The vial was transferred out of the glovebox, and its contents were transferred into an NMR tube for *in situ*  $^{19}F$  NMR spectroscopy to ensure nearly quantitative conversion and *in situ*  $^{11}B$  NMR spectroscopy to ensure structural integrity of the cluster. The crude mixture was then transferred into a 20-mL glass vial and lyophilized for solvent removal. A 1.25 cm x 35 cm glass column was packed with Sephadex LH20 medium in MeOH (23 cm packed height), and the crude product mixture containing **2d** was loaded onto the column with MeOH. 15 1-2 mL fractions were collected, dried *via* rotary evaporation, and subjected to characterization *via*  $^1H$ ,  $^{11}B$ , and  $^{19}F$  NMR spectroscopy. The pure product fractions as indicated by NMR spectroscopy were combined and dried *via* rotary evaporation to obtain an isolated yield of 2.6 mg (40 %).  $^1H$  NMR (400 MHz,  $CD_3OD$ ):  $\delta$  5.50 (br s, 24H,  $OCH_2$ ), 3.64 (t, 24H,  $CH_2CH_2OH$ ), 3.00 (t,  $SCH_2CH_2$ ).  $^{11}B$  NMR (128 MHz,  $CD_3OD$ ):  $\delta$  -15.7.  $^{19}F$  NMR (376 MHz,  $CD_3OD$ ):  $\delta$  -137.6 – -137.7 (m, 24F, *-meta*), -145.1 – -145.2 (m, 24F, *-ortho*). HRMS (Q-Exactive Plus): *m/z* calculated for  $C_{108}H_{84}B_{12}F_{48}O_{24}S_{12}$  ( $M^{2-}$ ), 1596.1176 Da; found, 1596.1233 Da.

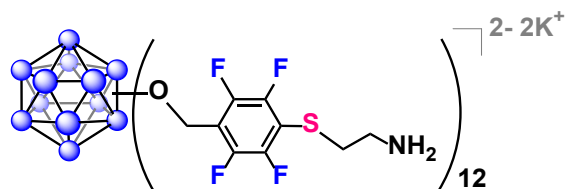


## Synthesis of 2e



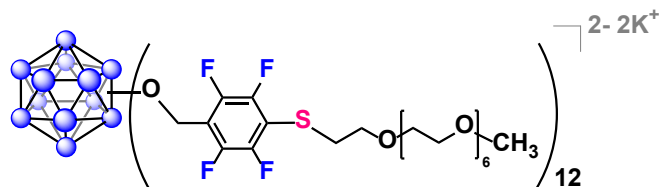
**2** (5.0 mg, 0.0020 mmol) and  $K_3PO_4$  (10.2 mg, 0.048 mmol) were added along with a flea micro stir bar to a 4-mL glass vial, which was then sealed with a PTFE/silicone cap under ambient conditions. The vial was then purged and backfilled with  $N_2$  three times before being transferred into the glovebox. In the glovebox, the vial was opened and 150  $\mu$ L anhydrous DMF was added, followed by thioglycerol (3.12  $\mu$ L, 0.036 mmol). The vial was sealed again and set to stir at 400 rpm for 24 hours. The vial was transferred out of the glovebox, and its contents were transferred into an NMR tube for *in situ*  $^{19}F$  NMR spectroscopy to ensure nearly quantitative conversion and *in situ*  $^{11}B$  NMR spectroscopy to ensure structural integrity of the cluster. The crude mixture was then transferred into a 20-mL glass vial and lyophilized for solvent removal. A 1.25 cm x 35 cm glass column was packed with Sephadex LH20 medium in MeOH (23 cm packed height), and the crude product mixture containing **2e** was loaded onto the column with MeOH. 15 1-2 mL fractions were collected, dried *via* rotary evaporation, and subjected to characterization *via*  $^1H$ ,  $^{11}B$ , and  $^{19}F$  NMR spectroscopy. The pure product fractions as indicated by NMR spectroscopy were combined and dried *via* rotary evaporation to obtain an isolated yield of 2.2 mg (30 %).  $^1H$  NMR (400 MHz,  $CD_3OD$ ):  $\delta$  5.50 (br s, 24H,  $OCH_2$ ), 3.69 – 3.64 (m, 12H,  $SCH_2CH(OH)$ ), 3.60 – 3.53 (m, 24H,  $CH(OH)CH_2OH$ ), 3.07 – 2.93 (m, 24H,  $SCH_2CH(OH)$ ).  $^{11}B$  NMR (128 MHz,  $CD_3OD$ ):  $\delta$  -15.6.  $^{19}F$  NMR (376 MHz,  $CD_3OD$ ):  $\delta$  -137.5 – -137.6 (m, 24F, *-meta*), -145.1 (m, 24F, *-ortho*). HRMS (Q-Exacte Plus):  $m/z$  calculated for  $C_{120}H_{108}B_{12}F_{48}O_{36}S_{12}$  ( $M^{2-}$ ), 1776.1810 Da; found, 1776.1894 Da.

## Synthesis of **2f**



**2** (5.0 mg, 0.0020 mmol) and K<sub>2</sub>CO<sub>3</sub> (2.6 mg, 0.019 mmol) were added along with a flea micro stir bar to a 4-mL glass vial, which was then sealed with a PTFE/silicone cap under ambient conditions. The vial was then purged and backfilled with N<sub>2</sub> three times before being transferred into the glovebox. In the glovebox, the vial was opened and 150 μL anhydrous DMF was added, followed by cysteamine (3.7 mg, 0.048 mmol). The vial was sealed again and set to stir at 400 rpm for 23 hours. The vial was transferred out of the glovebox, and its contents were transferred into an NMR tube for *in situ* <sup>19</sup>F NMR spectroscopy to ensure nearly quantitative conversion and *in situ* <sup>11</sup>B NMR spectroscopy to ensure structural integrity of the cluster. The crude mixture was then transferred into a 20-mL glass vial and lyophilized for solvent removal. A 1.25 cm x 35 cm glass column was packed with Sephadex LH20 medium in 40/60 MeOH/MeCN (23 cm packed height), and the crude product mixture containing **2f** was loaded onto the column with 40/60 MeOH/MeCN. 15 1-2 mL fractions were collected, dried *via* rotary evaporation, and subjected to characterization *via* <sup>1</sup>H, <sup>11</sup>B, and <sup>19</sup>F NMR spectroscopy. The pure product fractions as indicated by NMR spectroscopy were combined and dried *via* rotary evaporation to obtain an isolated yield of 3.2 mg (49 %). <sup>1</sup>H NMR (400 MHz, CD<sub>3</sub>OD): δ 5.51 (br s, 24H, OCH<sub>2</sub>), 2.94 (t, 24H, SCH<sub>2</sub>CH<sub>2</sub>), 2.72 (t, CH<sub>2</sub>CH<sub>2</sub>NH<sub>2</sub>). <sup>11</sup>B NMR (128 MHz, CD<sub>3</sub>OD): δ -15.4. <sup>19</sup>F NMR (376 MHz, CD<sub>3</sub>OD): δ -137.6 (m, 24F, *-meta*), -144.4 – -144.6 (m, 24F, *-ortho*). MS (LCT Premier): *m/z* calculated for C<sub>108</sub>H<sub>96</sub>B<sub>12</sub>F<sub>48</sub>N<sub>12</sub>O<sub>12</sub>S<sub>12</sub> (M<sup>2-</sup>), 1590.21 Da; found, 1590.07 Da.

## Synthesis of **2i**

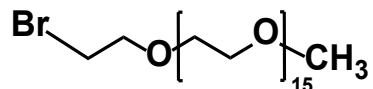


**2** (8 mg, 0.0032 mmol) and  $\text{K}_3\text{PO}_4$  (16.6 mg, 0.078 mmol) were added along with a flea micro stir bar to a 4-mL glass vial, which was then sealed with a PTFE/silicone cap under ambient conditions. The vial was then purged and backfilled with  $\text{N}_2$  three times before being transferred into the glovebox. In the glovebox, the vial was opened and 240  $\mu\text{L}$  anhydrous DMF was added, followed by mPEGthiol<sub>356</sub> (20.63  $\mu\text{L}$ , 0.064 mmol). The vial was sealed again and set to stir at 400 rpm for 28 hours. The vial was transferred out of the glovebox, and its contents were transferred into an NMR tube for *in situ*  $^{19}\text{F}$  NMR spectroscopy to ensure nearly quantitative conversion and *in situ*  $^{11}\text{B}$  NMR spectroscopy to ensure structural integrity of the cluster. The crude mixture was then transferred into a 20-mL glass vial and lyophilized for solvent removal. A 1.25 cm x 35 cm glass column was packed with Sephadex LH20 medium in MeOH (23 cm packed height), and the crude product mixture containing **2i** was loaded onto the column with MeOH. 15 1-2 mL fractions were collected, dried *via* rotary evaporation, and subjected to characterization *via*  $^1\text{H}$ ,  $^{11}\text{B}$ , and  $^{19}\text{F}$  NMR spectroscopy. The pure product fractions as indicated by NMR spectroscopy were combined and dried *via* rotary evaporation to obtain an isolated yield of 16.9 mg (81 %).  $^1\text{H}$  NMR (400 MHz,  $\text{CD}_3\text{OD}$ ):  $\delta$  5.51 (br s, 24H,  $\text{OCH}_2$ ), 3.63 – 3.50 (m, 312H,  $\text{SCH}_2\text{CH}_2\text{O}(\text{CH}_2\text{CH}_2\text{O})_6$ ), 3.35 – 3.33 (m, 36H,  $(\text{CH}_2\text{CH}_2\text{O})_6\text{CH}_3$ ), 3.08 (t, 24H,  $\text{SCH}_2$ ).  $^{11}\text{B}$  NMR (128 MHz,  $\text{CD}_3\text{OD}$ ):  $\delta$  -15.7.  $^{19}\text{F}$  NMR (376 MHz,  $\text{CD}_3\text{OD}$ ):  $\delta$  -137.2 – -137.3 (m, 24F, *-meta*), -144.8 (m, 24F, *-ortho*). HRMS (Q-

Exactive Plus):  $m/z$  calculated for  $C_{264}H_{396}B_{12}F_{48}O_{96}S_{12}$  ( $M^{2-}$ ), 3265.1552 Da; found, 3265.1444 Da.

## Synthesis of j

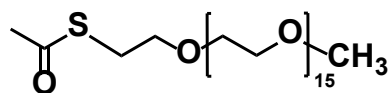
### 1. Synthesis of j-Br



In a round bottom flask, mPEG<sub>750</sub> (7.50 g, 10.00 mmol) and CBr<sub>4</sub> (3.98 g, 12.00 mmol) were dissolved in 40 mL of acetonitrile. To the stirring solution, PPh<sub>3</sub> (3.15 g, 6.00 mmol) was added in small portions over 30 minutes. The mixture was then left stirring at room temperature for 4 hours. After 4 hours, the solvent was then removed *in vacuo* and the resulting yellow-orange oil was dissolved in 20 mL of H<sub>2</sub>O and left at 4 °C overnight, producing a white precipitate. The mixture was filtered through Celite\* on a glass frit and the filtrate was washed twice with 5 mL of toluene. The aqueous layer was dried *in vacuo* to yield the desired product as an orange oil (7.08 g, 87%). <sup>1</sup>H NMR (400 MHz, CDCl<sub>3</sub>): δ 3.55 – 3.51 (m, 62H, CH<sub>2</sub>O(CH<sub>2</sub>CH<sub>2</sub>O)<sub>15</sub>), 3.43 (m, 2H, BrCH<sub>2</sub>), 3.26 (s, 3H, (CH<sub>2</sub>CH<sub>2</sub>O)<sub>15</sub>CH<sub>3</sub>).

\*Celite was pretreated on the frit by washing with 30 mL of H<sub>2</sub>O before the mixture was filtered.

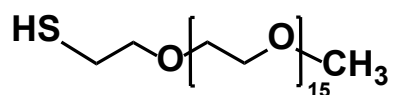
### 2. Synthesis of j-SAc



To a solution of **j-Br** (1.07 g, 1.32 mmol) in 35 mL of ethanol, potassium thioacetate (0.20 g, 1.75 mmol) was added in one portion. The mixture was refluxed at 120 °C for 5 hours. The resulting suspension was filtered through Celite and the filtrate was dried under vacuum, affording a brown

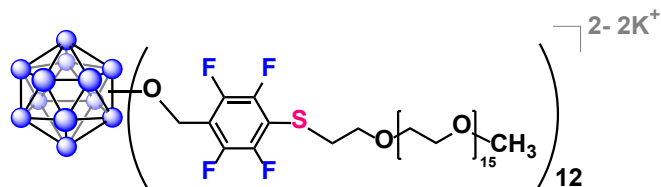
oil. The oil was dissolved in 40 mL of chloroform and the organic phase was washed twice with H<sub>2</sub>O. The organic layer was dried over Na<sub>2</sub>SO<sub>4</sub> and filtered through Celite. The solvent was removed *in vacuo*, providing **j-SAc** (0.64 g, 74%). <sup>1</sup>H NMR (400 MHz, CDCl<sub>3</sub>): δ 3.64 – 3.61 (m, 62H, CH<sub>2</sub>O(CH<sub>2</sub>CH<sub>2</sub>O)<sub>15</sub>), 3.36 (s, 3H, (CH<sub>2</sub>CH<sub>2</sub>O)<sub>15</sub>CH<sub>3</sub>), 3.07 (t, 2H, SCH<sub>2</sub>), 2.32 (s, 3H, SCOCH<sub>3</sub>).

### 3. Synthesis of **j**



**j-SAc** (405 mg, 0.5 mmol) was charged with 5 mL of 1M HCl and was refluxed at 110 °C for 2 hours under a blanket of Ar. The solvent was removed *in vacuo*. The residue was dissolved in 10 mL of DCM and the organic phase was washed twice with water. The organic layer was separated and dried over Na<sub>2</sub>SO<sub>4</sub> and filtered through Celite. The solution was dried under vacuum to yield the desired product as a brown oil (319 mg, 83%). Product was stored under inert atmosphere. <sup>1</sup>H NMR (400 MHz, CD<sub>2</sub>Cl<sub>2</sub>): δ 3.58 – 3.59 (m, 62H, CH<sub>2</sub>O(CH<sub>2</sub>CH<sub>2</sub>O)<sub>15</sub>), 3.32 (s, 3H, (CH<sub>2</sub>CH<sub>2</sub>O)<sub>15</sub>CH<sub>3</sub>), 2.67 (dt, 2H, SHCH<sub>2</sub>), 1.61 (t, 1H, SHCH<sub>2</sub>).

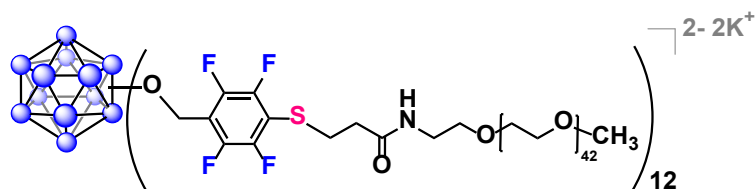
### Synthesis of **2j**



**2** (5.0 mg, 0.0020 mmol) and K<sub>3</sub>PO<sub>4</sub> (19.2 mg, 0.090 mmol) were added along with a flea micro stir bar to a 4-mL glass vial, which was then sealed with a PTFE/silicone cap under ambient conditions. The vial was then purged and backfilled with N<sub>2</sub> three times before being transferred

into the glovebox. In the glovebox, the vial was opened and 150  $\mu\text{L}$  anhydrous DMF was added, followed by mPEGthiol<sub>766</sub> (48.1  $\mu\text{L}$ , 0.069 mmol). The vial was sealed again and set to stir at 400 rpm for 24 hours. The vial was transferred out of the glovebox, and its contents were transferred into an NMR tube for *in situ*  $^{19}\text{F}$  NMR spectroscopy to ensure nearly quantitative conversion and *in situ*  $^{11}\text{B}$  NMR spectroscopy to ensure structural integrity of the cluster. The crude mixture was then transferred into a 20-mL glass vial and lyophilized for solvent removal. A 1.25 cm x 35 cm glass column was packed with Sephadex G50 medium in water (23 cm packed height), and the crude product mixture containing **2j** was loaded onto the column with water. 15 1-2 mL fractions were collected, dried *via* lyophilization, and subjected to characterization *via*  $^1\text{H}$ ,  $^{11}\text{B}$ , and  $^{19}\text{F}$  NMR spectroscopy. The pure product fractions as indicated by NMR spectroscopy were combined and dried *via* lyophilization to obtain an isolated yield of 4.4 mg (19%).  $^1\text{H}$  NMR (400 MHz,  $\text{CD}_3\text{OD}$ ):  $\delta$  5.50 (br s, 24H,  $\text{OCH}_2$ ), 3.63 – 3.53 (m, 744H,  $\text{SCH}_2\text{CH}_2\text{O}(\text{CH}_2\text{CH}_2\text{O})_{15}$ ), 3.35 (m, 36H,  $(\text{CH}_2\text{CH}_2\text{O})_{15}\text{CH}_3$ ), 3.08 (t, 24H,  $\text{SCH}_2$ ).  $^{11}\text{B}$  NMR (128 MHz,  $\text{CD}_3\text{OD}$ ):  $\delta$  -16.0.  $^{19}\text{F}$  NMR (376 MHz,  $\text{CD}_3\text{OD}$ ):  $\delta$  -137.2 (m, 24F, *-meta*), -144.8 (m, 24F, *-ortho*).

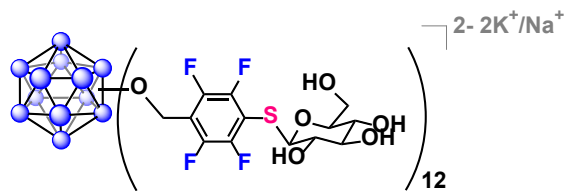
### Synthesis of **2k**



**2** (5.0 mg, 0.0020 mmol) and  $\text{K}_3\text{PO}_4$  (13.4 mg, 0.063 mmol) were added along with a flea micro stir bar to a 4-mL glass vial, which was then sealed with a PTFE/silicone cap under ambient conditions. The vial was then purged and backfilled with  $\text{N}_2$  three times before being transferred

into the glovebox. In the glovebox, the vial was opened and 150  $\mu\text{L}$  anhydrous DMF was added, followed by mPEGthiol<sub>2000</sub> (101.0 mg, 0.051 mmol). The vial was sealed again and set to stir at 400 rpm for 24 hours. The vial was transferred out of the glovebox, and its contents were transferred into an NMR tube for *in situ*  $^{19}\text{F}$  NMR spectroscopy to ensure nearly quantitative conversion and *in situ*  $^{11}\text{B}$  NMR spectroscopy to ensure structural integrity of the cluster. The crude mixture was then transferred into a 20-mL glass vial and lyophilized for solvent removal. A 1.25 cm x 35 cm glass column was packed with Sephadex G50 medium in water (23 cm packed height), and the crude product mixture containing **2k** was loaded onto the column with water. 15 1-2 mL fractions were collected, dried *via* lyophilization, and subjected to characterization *via*  $^1\text{H}$ ,  $^{11}\text{B}$ , and  $^{19}\text{F}$  NMR spectroscopy. The pure product fractions as indicated by NMR spectroscopy were combined and dried *via* lyophilization to obtain an isolated yield of 21.5 mg (41 %).  $^1\text{H}$  NMR (400 MHz,  $\text{CD}_3\text{OD}$ ):  $\delta$  5.50 (br s, 24H,  $\text{OCH}_2$ ), 3.82 – 3.45 (m, 2100H,  $\text{SCH}_2\text{CH}_2(\text{CONH})\text{CH}_2\text{CH}_2\text{O}(\text{CH}_2\text{CH}_2\text{O})_{42}$ ), 3.36 (s, 36H,  $(\text{CH}_2\text{CH}_2\text{O})_{42}\text{CH}_3$ ), 3.09 (t, 24H,  $\text{SCH}_2\text{CH}_2$ ).  $^{11}\text{B}$  NMR (128 MHz,  $\text{CD}_3\text{OD}$ ):  $\delta$  -16.0.  $^{19}\text{F}$  NMR (376 MHz,  $\text{CD}_3\text{OD}$ ):  $\delta$  -137.0 – -137.1 (m, 24F, *-meta*), -144.8 (m, 24F, *-ortho*). GPC trace of **2k** measured in water with 0.02%  $\text{NaN}_3$  at 12  $^\circ\text{C}$  gives a  $\text{Đ}$  (polydispersity index) of 1.003 (see Figure 2.3c in main text).

### Synthesis of **2l**

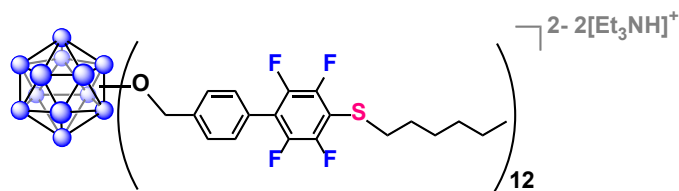


**2** (5.0 mg, 0.0020 mmol) and  $\text{K}_3\text{PO}_4$  (13.0 mg, 0.061 mmol) were added along with a flea micro stir bar to a 4-mL glass vial, which was then sealed with a PTFE/silicone cap under ambient

conditions. The vial was then purged and backfilled with N<sub>2</sub> three times before being transferred into the glovebox. In the glovebox, the vial was opened and 150 μL anhydrous DMF was added, followed by 1-thio-β-D-glucose tetraacetate (25.0 mg, 0.069 mmol). The vial was sealed again and set to stir at 400 rpm for 24 hours. The vial was transferred out of the glovebox, and its contents were transferred into an NMR tube for *in situ* <sup>19</sup>F NMR spectroscopy to ensure nearly quantitative conversion and *in situ* <sup>11</sup>B NMR spectroscopy to ensure structural integrity of the cluster. The crude mixture was then transferred into a 20-mL glass vial and lyophilized for solvent removal. The resulting residue was treated with NaOMe (6.0 mg, 0.11 mmol) in 1 mL MeOH for 2 hours. The volatiles were removed *via* rotary evaporation. A 1.25 cm x 35 cm glass column was packed with Sephadex G50 medium in water (23 cm packed height), and the crude product mixture containing **2I** was loaded onto the column with water. 15 1-2 mL fractions were collected, dried *via* lyophilization, and subjected to characterization *via* <sup>1</sup>H, <sup>11</sup>B, and <sup>19</sup>F NMR spectroscopy. The pure product fractions as indicated by NMR spectroscopy were combined and dried *via* lyophilization to obtain an isolated yield of 1.6 mg (17 %). <sup>1</sup>H NMR (400 MHz, D<sub>2</sub>O): δ 5.64 – 5.45 (br s, 24H, OCH<sub>2</sub>), 4.03 – 3.20 (m, 84H, SCHCH<sub>2</sub>OH(CHOH)<sub>3</sub>CHO). <sup>11</sup>B NMR (128 MHz, D<sub>2</sub>O): δ -16.3. <sup>19</sup>F NMR (376 MHz, D<sub>2</sub>O): δ -134.3 – -135.6 (m, 24F, -*meta*), -143.5 (m, 24F, -*ortho*). HRMS (Q-Exactive Plus): *m/z* calculated for C<sub>156</sub>H<sub>156</sub>B<sub>12</sub>F<sub>48</sub>O<sub>72</sub>S<sub>12</sub> (M<sup>2-</sup>), 2304.2772 Da; found, 2304.2769 Da.

### Synthesis of **3a**

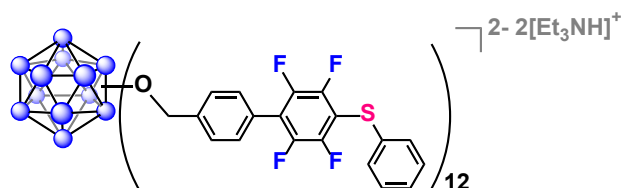




**3** (10.0 mg, 0.0029 mmol) and  $\text{K}_2\text{CO}_3$  (22.0 mg, 0.159 mmol) were added along with a flea micro stir bar to a 4-mL glass vial, which was then sealed with a PTFE/silicone cap under ambient conditions. The vial was then purged and backfilled with  $\text{N}_2$  three times before being transferred into the glovebox. In the glovebox, the vial was opened and 300  $\mu\text{L}$  anhydrous DMF was added, followed by 1-hexanethiol (5.42  $\mu\text{L}$ , 0.038 mmol). The vial was sealed again and set to stir at 400 rpm for 7 hours. The vial was transferred out of the glovebox, and its contents were transferred into an NMR tube for *in situ*  $^{19}\text{F}$  NMR spectroscopy to ensure nearly quantitative conversion and *in situ*  $^{11}\text{B}$  NMR spectroscopy to ensure structural integrity of the cluster. The crude mixture was then transferred into a 20-mL glass vial and lyophilized for solvent removal. A 5  $\frac{3}{4}$ " glass Pasteur pipet column was prepared using glass wool and 4" of silica gel, and the pipet was flushed with triethylamine (2X column volumes). The crude product mixture containing **3a** was loaded onto the column with 80/20 hexanes/ethyl acetate (sonication was used to aid dissolution), and the remaining reagent was eluted with 80/20 hexanes/ethyl acetate. A very slightly yellow band containing **3a** was eluted with MeCN, and the fractions containing **3a** (as assessed by TLC) were combined and volatiles were removed *via* rotary evaporation followed by lyophilization overnight to obtain an isolated yield of 12.2 mg (87%).  $^1\text{H}$  NMR (400 MHz,  $\text{CD}_3\text{CN}$ ):  $\delta$  7.64 – 7.50 (br m, 24H,  $\text{OCH}_2\text{-Ar}$ ), 7.25 – 7.15 (br m, 24H,  $\text{OCH}_2\text{-Ar}$ ), 5.60 (br s, 24H,  $\text{OCH}_2$ ), 3.06 (q, 12H,  $[(\text{CH}_3\text{CH}_2)_3\text{NH}]^+$ ), 2.93 (t, 24H,  $\text{SCH}_2$ ), 1.61 - 1.49 (m, 24H,  $\text{SCH}_2\text{CH}_2$ ), 1.44 – 1.34 (br m, 24H,  $\text{S}(\text{CH}_2)_2(\text{CH}_2)_3\text{CH}_3$ ), 1.30 – 1.21 (br m, 48H,  $\text{S}(\text{CH}_2)_2(\text{CH}_2)_3\text{CH}_3$ ), 1.18 (t, 18H,  $[(\text{CH}_3\text{CH}_2)_3\text{NH}]^+$ ), 0.89 – 0.80 (m, 36H,  $\text{S}(\text{CH}_2)_5\text{CH}_3$ ).  $^{11}\text{B}\{^1\text{H}\}$  NMR (128 MHz,  $\text{CD}_3\text{CN}$ ):  $\delta$  -15.1.  $^{19}\text{F}$  NMR (376

MHz, CD<sub>3</sub>CN):  $\delta$  -136.7 (q, 24F, *-meta*), -145.2 (q, 24F, *-ortho*). HRMS (Q-Exactive Plus):  $m/z$  calculated for C<sub>228</sub>H<sub>228</sub>B<sub>12</sub>F<sub>48</sub>O<sub>12</sub>S<sub>12</sub> (M<sup>2-</sup>), 2292.7115 Da; found, 2292.7157 Da.

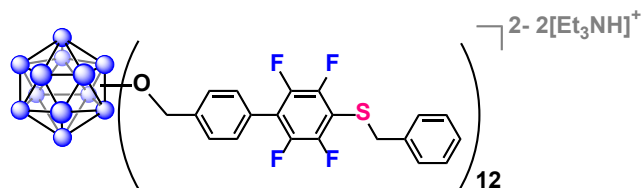
### Synthesis of **3b**



**3** (10.0 mg, 0.0029 mmol) and K<sub>3</sub>PO<sub>4</sub> (18.9 mg, 0.089 mmol) were added along with a flea micro stir bar to a 4-mL glass vial, which was then sealed with a PTFE/silicone cap under ambient conditions. The vial was then purged and backfilled with N<sub>2</sub> three times before being transferred into the glovebox. In the glovebox, the vial was opened and 300  $\mu$ L anhydrous DMF was added, followed by thiophenol (3.89  $\mu$ L, 0.038 mmol). The vial was sealed again and set to stir at 400 rpm for 7 hours. The vial was transferred out of the glovebox, and its contents were transferred into an NMR tube for *in situ* <sup>19</sup>F NMR spectroscopy to ensure nearly quantitative conversion and *in situ* <sup>11</sup>B NMR spectroscopy to ensure structural integrity of the cluster. The crude mixture was then transferred into a 20-mL glass vial and lyophilized for solvent removal. A 5 <sup>3</sup>/<sub>4</sub>" glass Pasteur pipet column was prepared using glass wool and 4" of silica gel, and the pipet was flushed with triethylamine (2X column volumes). The crude product mixture containing **3b** was loaded onto the column with 35/65 ethyl acetate/hexanes (sonication was used to aid dissolution), and the remaining reagent was eluted with 35/65 ethyl acetate/hexanes. A very slightly yellow band containing **3b** was eluted with MeCN, and the fractions containing **3b** (as assessed by TLC) were combined and volatiles were removed *via* rotary evaporation followed by lyophilization overnight

to obtain an isolated yield of 11.7 mg (85%).  $^1\text{H}$  NMR (400 MHz,  $\text{CD}_3\text{CN}$ ):  $\delta$  7.65 – 7.48 (br m, 24H,  $\text{OCH}_2\text{-Ar}$ ), 7.34 – 7.20 (br m, 60H and 24H,  $\text{S-Ar}$  and  $\text{OCH}_2\text{-Ar}$ ), 5.61 (br s, 24H,  $\text{OCH}_2$ ), 3.09 (q, 12H,  $[(\text{CH}_3\text{CH}_2)_3\text{NH}]^+$ ), 1.21 (t, 18H,  $[(\text{CH}_3\text{CH}_2)_3\text{NH}]^+$ ).  $^{11}\text{B}\{^1\text{H}\}$  NMR (128 MHz,  $\text{CD}_3\text{CN}$ ):  $\delta$  -15.1.  $^{19}\text{F}$  NMR (376 MHz,  $\text{CD}_3\text{CN}$ ):  $\delta$  -135.9 (m, 24F, *-meta*), -145.2 (m, 24F, *-ortho*). HRMS (Q-Exactive Plus):  $m/z$  calculated for  $\text{C}_{228}\text{H}_{132}\text{B}_{12}\text{F}_{48}\text{O}_{12}\text{S}_{12}$  ( $\text{M}^{2-}$ ), 2244.3359 Da; found, 2244.3381 Da.

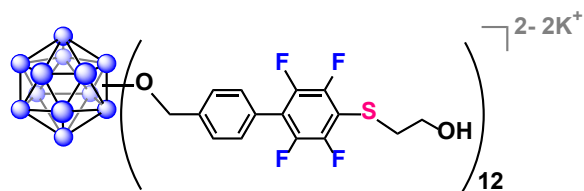
### Synthesis of **3c**



**3** (10.0 mg, 0.0029 mmol) and  $\text{K}_3\text{PO}_4$  (22.5 mg, 0.106 mmol) were added along with a flea micro stir bar to a 4-mL glass vial, which was then sealed with a PTFE/silicone cap under ambient conditions. The vial was then purged and backfilled with  $\text{N}_2$  three times before being transferred into the glovebox. In the glovebox, the vial was opened and 300  $\mu\text{L}$  anhydrous DMF was added, followed by benzyl mercaptan (4.48  $\mu\text{L}$ , 0.038 mmol). The vial was sealed again and set to stir at 400 rpm for 5 hours. The vial was transferred out of the glovebox, and its contents were transferred into an NMR tube for *in situ*  $^{19}\text{F}$  NMR spectroscopy to ensure nearly quantitative conversion and *in situ*  $^{11}\text{B}$  NMR spectroscopy to ensure structural integrity of the cluster. The crude mixture was then transferred into a 20-mL glass vial and lyophilized for solvent removal. A 5  $\frac{3}{4}$ " glass Pasteur pipet column was prepared using glass wool and 4" of silica gel, and the pipet was flushed with triethylamine (2X column volumes). The crude product mixture containing **3c** was loaded onto the

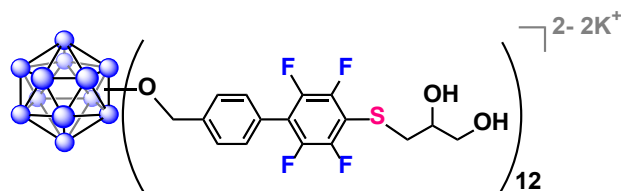
column with 35/65 ethyl acetate/hexanes (sonication was used to aid dissolution), and the remaining reagent was eluted with 35/65 ethyl acetate/hexanes. A very slightly yellow band containing **3c** was eluted with MeCN, and the fractions containing **3c** (as assessed by TLC) were combined and volatiles were removed *via* rotary evaporation followed by lyophilization overnight to obtain an isolated yield of 11.6 mg (81%). <sup>1</sup>H NMR (400 MHz, CD<sub>3</sub>CN): δ 7.59 – 7.52 (br d, 24H, OCH<sub>2</sub>-Ar), 7.26 – 7.15 (br m, 60H and 24H, SCH<sub>2</sub>-Ar and OCH<sub>2</sub>-Ar), 5.60 (br s, 24H, OCH<sub>2</sub>), 4.11 (br s, 24H, SCH<sub>2</sub>), 3.06 (q, 12H, [(CH<sub>3</sub>CH<sub>2</sub>)<sub>3</sub>NH]<sup>+</sup>), 1.18 (t, 18H, [(CH<sub>3</sub>CH<sub>2</sub>)<sub>3</sub>NH]<sup>+</sup>). <sup>11</sup>B{<sup>1</sup>H} NMR (128 MHz, CD<sub>3</sub>CN): δ -15.1. <sup>19</sup>F NMR (376 MHz, CD<sub>3</sub>CN): δ -135.9 (q, 24F, *-meta*), -145.1 (q, 24F, *-ortho*). HRMS (Q-Exactive Plus): *m/z* calculated for C<sub>240</sub>H<sub>156</sub>B<sub>12</sub>F<sub>48</sub>O<sub>12</sub>S<sub>12</sub> (M<sup>2-</sup>), 2328.9298 Da; found, 2328.9363 Da.

### Synthesis of **3d**



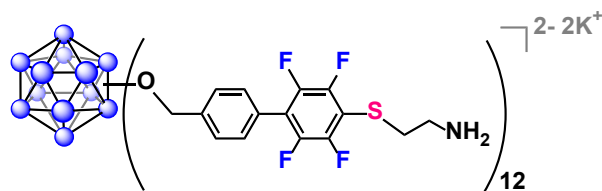
**3** (10.0 mg, 0.0029 mmol) and K<sub>3</sub>PO<sub>4</sub> (12.3 mg, 0.058 mmol) were added along with a flea micro stir bar to a 4-mL glass vial, which was then sealed with a PTFE/silicone cap under ambient conditions. The vial was then purged and backfilled with N<sub>2</sub> three times before being transferred into the glovebox. In the glovebox, the vial was opened and 300 μL anhydrous DMF was added, followed by 2-mercaptoethanol (2.69 μL, 0.038 mmol). The vial was sealed again and set to stir at 400 rpm for 4 hours. The vial was transferred out of the glovebox, and its contents were transferred into an NMR tube for *in situ* <sup>19</sup>F NMR spectroscopy to ensure nearly quantitative conversion and *in situ* <sup>11</sup>B NMR spectroscopy to ensure structural integrity of the cluster. The crude mixture was then transferred into a 20-mL glass vial and lyophilized for solvent removal. A 1.25 cm x 35 cm glass column was packed with Sephadex LH20 medium in MeOH (23 cm packed height), and the crude product mixture containing **3d** was loaded onto the column with MeOH. 15 1-2 mL fractions were collected, dried *via* rotary evaporation, and subjected to characterization *via* <sup>1</sup>H, <sup>11</sup>B, and <sup>19</sup>F NMR spectroscopy. The pure product fractions as indicated by NMR spectroscopy were combined and dried *via* rotary evaporation to obtain an isolated yield of 10.0 mg (81 %). <sup>1</sup>H NMR (400 MHz, CD<sub>3</sub>OD): δ 7.61 – 7.45 (br m, 24H, OCH<sub>2</sub>-Ar), 7.24 – 7.13 (br m, 24H, OCH<sub>2</sub>-Ar), 5.65 (br m, 24H, OCH<sub>2</sub>), 3.73 (t, 24H, CH<sub>2</sub>CH<sub>2</sub>OH), 3.10 (t, SCH<sub>2</sub>CH<sub>2</sub>). <sup>11</sup>B NMR (128 MHz, CD<sub>3</sub>OD): δ -15.1. <sup>19</sup>F NMR (376 MHz, CD<sub>3</sub>OD): δ -136.8 – -136.9 (m, 24F, -*meta*), -145.4 – -145.5 (m, 24F, -*ortho*). HRMS (Q-Exactive Plus): *m/z* calculated for C<sub>180</sub>H<sub>132</sub>B<sub>12</sub>F<sub>48</sub>O<sub>24</sub>S<sub>12</sub> (M<sup>2-</sup>), 2052.3054 Da; found, 2052.3080 Da.

### Synthesis of **3e**



**3** (10.0 mg, 0.0029 mmol) and K<sub>3</sub>PO<sub>4</sub> (13.1 mg, 0.062 mmol) were added along with a flea micro stir bar to a 4-mL glass vial, which was then sealed with a PTFE/silicone cap under ambient conditions. The vial was then purged and backfilled with N<sub>2</sub> three times before being transferred into the glovebox. In the glovebox, the vial was opened and 300 μL anhydrous DMF was added, followed by thioglycerol (3.30 μL, 0.038 mmol). The vial was sealed again and set to stir at 400 rpm for 4 hours. The vial was transferred out of the glovebox, and its contents were transferred into an NMR tube for *in situ* <sup>19</sup>F NMR spectroscopy to ensure nearly quantitative conversion and *in situ* <sup>11</sup>B NMR spectroscopy to ensure structural integrity of the cluster. The crude mixture was then transferred into a 20-mL glass vial and lyophilized for solvent removal. A 1.25 cm x 35 cm glass column was packed with Sephadex LH20 medium in MeOH (23 cm packed height), and the crude product mixture containing **3e** was loaded onto the column with MeOH. 15 1-2 mL fractions were collected, dried *via* rotary evaporation, and subjected to characterization *via* <sup>1</sup>H, <sup>11</sup>B, and <sup>19</sup>F NMR spectroscopy. The pure product fractions as indicated by NMR spectroscopy were combined and dried *via* rotary evaporation to obtain an isolated yield of 7.9 mg (59 %). <sup>1</sup>H NMR (400 MHz, CD<sub>3</sub>OD): δ 7.59 – 7.45 (br m, 24H, OCH<sub>2</sub>-Ar), 7.23 – 7.16 (br m, 24H, OCH<sub>2</sub>-Ar), 5.64 – 5.60 (br m, 24H, OCH<sub>2</sub>), 3.78 – 3.72 (m, 12H, SCH<sub>2</sub>CH(OH)), 3.65 – 3.57 (m, 24H, CH(OH)CH<sub>2</sub>OH), 3.17 – 3.02 (m, 24H, SCH<sub>2</sub>CH(OH)). <sup>11</sup>B NMR (128 MHz, CD<sub>3</sub>OD): δ -15.1. <sup>19</sup>F NMR (376 MHz, CD<sub>3</sub>OD): δ -136.6 – -136.7 (m, 24F, *-meta*), -145.5 (m, 24F, *-ortho*). HRMS (Q-Exactive Plus): *m/z* calculated for C<sub>192</sub>H<sub>156</sub>B<sub>12</sub>F<sub>48</sub>O<sub>36</sub>S<sub>12</sub> (M<sup>2-</sup>), 2232.3688 Da; found, 2232.3752 Da.

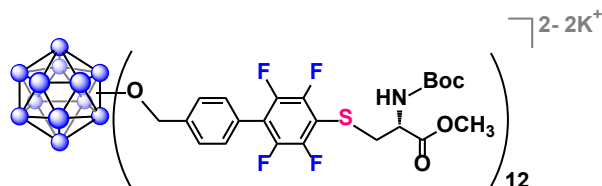
### Synthesis of **3f**



**3** (10.0 mg, 0.0029 mmol) and K<sub>2</sub>CO<sub>3</sub> (8.1 mg, 0.059 mmol) were added along with a flea micro stir bar to a 4-mL glass vial, which was then sealed with a PTFE/silicone cap under ambient conditions. The vial was then purged and backfilled with N<sub>2</sub> three times before being transferred into the glovebox. In the glovebox, the vial was opened and 300 μL anhydrous DMF was added, followed by cysteamine (4.9 mg, 0.064 mmol). The vial was sealed again and set to stir at 400 rpm for 4 hours. The vial was transferred out of the glovebox, and its contents were transferred into an NMR tube for *in situ* <sup>19</sup>F NMR spectroscopy to ensure nearly quantitative conversion and *in situ* <sup>11</sup>B NMR spectroscopy to ensure structural integrity of the cluster. The crude mixture was then transferred into a 20-mL glass vial and lyophilized for solvent removal. A 1.25 cm x 35 cm glass column was packed with Sephadex LH20 medium in 40/60 MeOH/MeCN (23 cm packed height), and the crude product mixture containing **3f** was loaded onto the column with 40/60 MeOH/MeCN. 15 1-2 mL fractions were collected, dried *via* rotary evaporation, and subjected to characterization *via* <sup>1</sup>H, <sup>11</sup>B, and <sup>19</sup>F NMR spectroscopy. The pure product fractions as indicated by NMR spectroscopy were combined and dried *via* rotary evaporation to obtain an isolated yield of 4.0 mg (33 %). <sup>1</sup>H NMR (400 MHz, 33/67 CD<sub>3</sub>OD/CD<sub>3</sub>CN): δ 7.55 – 7.52 (br m, 24H, OCH<sub>2</sub>-Ar), 7.21 – 7.18 (br m, 24H, OCH<sub>2</sub>-Ar), 5.60 – 5.54 (br m, 24H, OCH<sub>2</sub>), 2.95 (t, 24H, SCH<sub>2</sub>CH<sub>2</sub>), 2.70 (t, CH<sub>2</sub>CH<sub>2</sub>NH<sub>2</sub>). <sup>11</sup>B NMR (128 MHz, 33/67 CD<sub>3</sub>OD/CD<sub>3</sub>CN): δ -15.2. <sup>19</sup>F NMR (376 MHz, 33/67 CD<sub>3</sub>OD/CD<sub>3</sub>CN): δ -136.0 – -136.5 (m, 24F, -*meta*), -145.1 – -145.6 (m, 24F, -*ortho*). MS

(LCT Premier):  $m/z$  calculated for  $C_{180}H_{144}B_{12}F_{48}N_{12}O_{12}S_{12}$  ( $M^{2-}$ ), 2046.40 Da; found, 2046.31 Da.

### Synthesis of **3g**

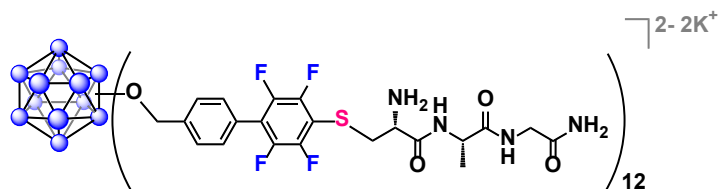


**3** (10.0 mg, 0.0029 mmol) and  $K_3PO_4$  (18.7 mg, 0.088 mmol) were added along with a flea micro stir bar to a 4-mL glass vial, which was then sealed with a PTFE/silicone cap under ambient conditions. The vial was then purged and backfilled with  $N_2$  three times before being transferred into the glovebox. In the glovebox, the vial was opened and 300  $\mu$ L anhydrous DMF was added, followed by *N*-(*tert*-Butoxycarbonyl)-L-cysteine methyl ester (8.16  $\mu$ L, 0.040 mmol). The vial was sealed again and set to stir at 400 rpm for 3 hours. The vial was transferred out of the glovebox, and its contents were transferred into an NMR tube for *in situ*  $^{19}F$  NMR spectroscopy to ensure nearly quantitative conversion and *in situ*  $^{11}B$  NMR spectroscopy to ensure structural integrity of the cluster. The crude mixture was then transferred into a 20-mL glass vial and lyophilized for solvent removal. A 1.25 cm x 35 cm glass column was packed with Sephadex LH20 medium in MeOH (23 cm packed height), and the crude product mixture containing **3g** was loaded onto the column with MeOH. 15 1-2 mL fractions were collected, dried *via* rotary evaporation, and subjected to characterization *via*  $^1H$ ,  $^{11}B$ , and  $^{19}F$  NMR spectroscopy. The pure product fractions as indicated by NMR spectroscopy were combined and dried *via* rotary evaporation to obtain an isolated yield of 8.8 mg (49 %).  $^1H$  NMR (400 MHz,  $CD_3OD$ ):  $\delta$  7.52 (d, 24H,  $OCH_2$ -Ar), 7.19



(d, 24H, OCH<sub>2</sub>-Ar), 5.63 (br s, 24H, OCH<sub>2</sub>), 4.37 – 4.34 (br m, 12H, SCH<sub>2</sub>CH), 3.69 (m, 36H, OCH<sub>3</sub>), 3.49 – 3.44 (br m, 24H, SCH<sub>2</sub>), 1.35 – 1.33 (m, 108H, C(CH<sub>3</sub>)<sub>3</sub>). <sup>11</sup>B NMR (128 MHz, CD<sub>3</sub>OD): δ -15.1. <sup>19</sup>F NMR (376 MHz, CD<sub>3</sub>OD): δ -135.9 – -136.0 (m, 24F, -*meta*), -144.8 – -145.1 (m, 24F, -*ortho*). HRMS (Q-Exactive Plus): *m/z* calculated for C<sub>264</sub>H<sub>264</sub>B<sub>12</sub>F<sub>48</sub>N<sub>12</sub>O<sub>60</sub>S<sub>12</sub> (M<sup>2-</sup>), 2994.7487 Da; found, 2994.7404 Da.

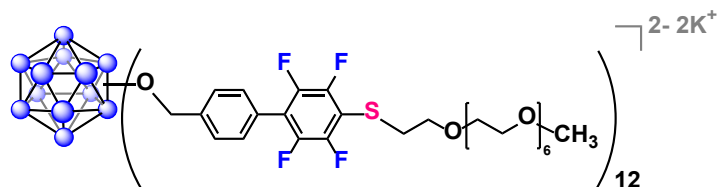
### Synthesis of 3h



**3** (10.0 mg, 0.0029 mmol) and K<sub>3</sub>PO<sub>4</sub> (56.1 mg, 0.264 mmol) were added along with a flea micro stir bar to a 4-mL glass vial, which was then sealed with a PTFE/silicone cap under ambient conditions. The vial was then purged and backfilled with N<sub>2</sub> three times before being transferred into the glovebox. In the glovebox, the vial was opened and 300 μL anhydrous DMF was added, followed by unprotected C-A-G-TFA (synthesized using conventional Fmoc solid-phase peptide synthesis protocol<sup>106</sup>) (17.8 mg, 0.049 mmol) and isopropoxytrimethylsilane (18.8 μL, 0.106 mmol). The vial was sealed again and set to stir at 400 rpm for 6 hours. The vial was transferred out of the glovebox, and its contents were transferred into an NMR tube for *in situ* <sup>19</sup>F NMR spectroscopy to ensure nearly quantitative conversion and *in situ* <sup>11</sup>B NMR spectroscopy to ensure structural integrity of the cluster. The crude mixture was then transferred into a 20-mL glass vial and lyophilized for solvent removal. A 1.25 cm x 35 cm glass column was packed with Sephadex LH20 medium in H<sub>2</sub>O/ACN (23 cm packed height), and the crude product mixture containing **3h**

was loaded onto the column with H<sub>2</sub>O/ACN. 15 1-2 mL fractions were collected, dried *via* lyophilization, and subjected to characterization *via* <sup>1</sup>H, <sup>11</sup>B, and <sup>19</sup>F NMR spectroscopy. The pure product fractions as indicated by NMR spectroscopy were combined and dried *via* lyophilization to obtain an isolated yield of 5.3 mg (29 %). <sup>1</sup>H NMR (400 MHz, D<sub>2</sub>O/CD<sub>3</sub>CN): δ 7.44 (br m, 24H, OCH<sub>2</sub>-Ar), 7.09 – 7.08 (br m, 24H, OCH<sub>2</sub>-Ar), 5.50 (br s, 24H, O-CH<sub>2</sub>), 3.77 – 3.68 (br m, 24H, (CONH)CH<sub>2</sub>(CONH<sub>2</sub>)), 3.48 – 3.45 (br t, 12H, SCH<sub>2</sub>CH), 3.15 – 3.10 (br m, 24H, SCH<sub>2</sub>), 1.26 – 1.24 (d, 36H, CCH<sub>3</sub>). <sup>11</sup>B NMR (128 MHz, D<sub>2</sub>O/CD<sub>3</sub>CN): δ -15.8. <sup>19</sup>F NMR (376 MHz, D<sub>2</sub>O/CD<sub>3</sub>CN): δ -135.4 – -135.5 (m, 24F, -*meta*), -144.7 – -144.8 (m, 24F, -*ortho*). MS (LCT Premier): *m/z* calculated for C<sub>252</sub>H<sub>252</sub>B<sub>12</sub>F<sub>48</sub>N<sub>48</sub>O<sub>48</sub>S<sub>12</sub> (M<sup>2-</sup>), 3072.79 Da; found, 3072.60 Da.

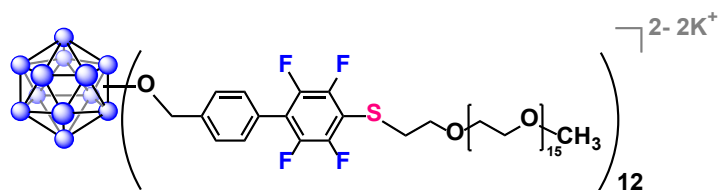
### Synthesis of 3i



**3** (10.0 mg, 0.0029 mmol) and K<sub>3</sub>PO<sub>4</sub> (8.5 mg, 0.040 mmol) were added along with a flea micro stir bar to a 4-mL glass vial, which was then sealed with a PTFE/silicone cap under ambient conditions. The vial was then purged and backfilled with N<sub>2</sub> three times before being transferred into the glovebox. In the glovebox, the vial was opened and 300 μL anhydrous DMF was added, followed by mPEGthiol<sub>356</sub> (12.27 μL, 0.038 mmol). The vial was sealed again and set to stir at 400 rpm for 5 hours. The vial was transferred out of the glovebox, and its contents were transferred into an NMR tube for *in situ* <sup>19</sup>F NMR spectroscopy to ensure nearly quantitative conversion and *in situ* <sup>11</sup>B NMR spectroscopy to ensure structural integrity of the cluster. The crude mixture was

then transferred into a 20-mL glass vial and lyophilized for solvent removal. A 1.25 cm x 35 cm glass column was packed with Sephadex LH20 medium in MeOH (23 cm packed height), and the crude product mixture containing **3i** was loaded onto the column with MeOH. 15 1-2 mL fractions were collected, dried *via* rotary evaporation, and subjected to characterization *via*  $^1\text{H}$ ,  $^{11}\text{B}$ , and  $^{19}\text{F}$  NMR spectroscopy. The pure product fractions as indicated by NMR spectroscopy were combined and dried *via* rotary evaporation to obtain an isolated yield of 17.1 mg (78 %).  $^1\text{H}$  NMR (400 MHz,  $\text{CD}_3\text{OD}$ ):  $\delta$  7.64 – 7.46 (br m, 24H,  $\text{OCH}_2\text{-Ar}$ ), 7.26 – 7.18 (br m, 24H,  $\text{OCH}_2\text{-Ar}$ ), 5.65 – 5.61 (br m, 24H,  $\text{OCH}_2$ ), 3.70 (t, 24H,  $\text{SCH}_2\text{CH}_2$ ), 3.62 – 3.44 (m, 288H,  $\text{SCH}_2\text{CH}_2\text{O}(\text{CH}_2\text{CH}_2\text{O})_6$ ), 3.30 – 3.28 (m, 36H,  $(\text{CH}_2\text{CH}_2\text{O})_6\text{CH}_3$ ), 3.14 (t, 24H,  $\text{SCH}_2$ ).  $^{11}\text{B}$  NMR (128 MHz,  $\text{CD}_3\text{OD}$ ):  $\delta$  -15.3.  $^{19}\text{F}$  NMR (376 MHz,  $\text{CD}_3\text{OD}$ ):  $\delta$  -136.4 – -136.5 (m, 24F, *-meta*), -145.3 (m, 24F, *-ortho*). HRMS (Q-Exactive Plus):  $m/z$  calculated for  $\text{C}_{336}\text{H}_{444}\text{B}_{12}\text{F}_{48}\text{O}_{96}\text{S}_{12}$  ( $\text{M}^{2-}$ ), 3721.3430 Da; found, 3721.3395 Da.

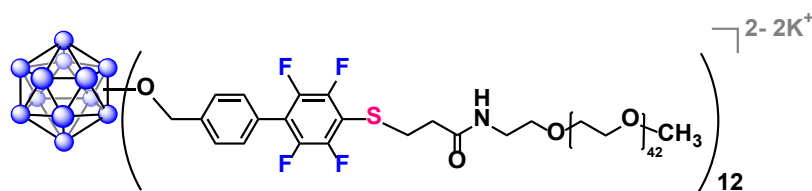
### Synthesis of **3j**



**3** (10.0 mg, 0.0029 mmol) and  $\text{K}_3\text{PO}_4$  (32.0 mg, 0.151 mmol) were added along with a flea micro stir bar to a 4-mL glass vial, which was then sealed with a PTFE/silicone cap under ambient conditions. The vial was then purged and backfilled with  $\text{N}_2$  three times before being transferred into the glovebox. In the glovebox, the vial was opened and 300  $\mu\text{L}$  anhydrous DMF was added, followed by mPEGthiol<sub>766</sub> (44.1  $\mu\text{L}$ , 0.063 mmol). The vial was sealed again and set to stir at 400

rpm for 4 hours. The vial was transferred out of the glovebox, and its contents were transferred into an NMR tube for *in situ*  $^{19}\text{F}$  NMR spectroscopy to ensure nearly quantitative conversion and *in situ*  $^{11}\text{B}$  NMR spectroscopy to ensure structural integrity of the cluster. The crude mixture was then transferred into a 20-mL glass vial and lyophilized for solvent removal. A 1.25 cm x 35 cm glass column was packed with Sephadex LH20 medium in MeOH (23 cm packed height), and the crude product mixture containing **3j** was loaded onto the column with MeOH. 15 1-2 mL fractions were collected, dried *via* rotary evaporation, and subjected to characterization *via*  $^1\text{H}$ ,  $^{11}\text{B}$ , and  $^{19}\text{F}$  NMR spectroscopy. The pure product fractions as indicated by NMR spectroscopy were combined and dried *via* rotary evaporation to obtain an isolated yield of 7.7 mg (21 %).  $^1\text{H}$  NMR (400 MHz,  $\text{CD}_3\text{OD}$ ):  $\delta$  7.57 – 7.55 (br m, 24H,  $\text{OCH}_2\text{-Ar}$ ), 7.18 – 7.16 (br m, 24H,  $\text{OCH}_2\text{-Ar}$ ), 5.67 – 5.62 (br m, 24H,  $\text{OCH}_2$ ), 3.72 (t, 24H,  $\text{SCH}_2\text{CH}_2$ ), 3.64 – 3.51 (m, 744H,  $\text{SCH}_2\text{CH}_2\text{O}(\text{CH}_2\text{CH}_2\text{O})_{15}$ ), 3.33 (m, 36H,  $(\text{CH}_2\text{CH}_2\text{O})_{15}\text{CH}_3$ ), 3.19 – 3.16 (t, 24H,  $\text{SCH}_2$ ).  $^{11}\text{B}$  NMR (128 MHz,  $\text{CD}_3\text{OD}$ ):  $\delta$  -15.3.  $^{19}\text{F}$  NMR (376 MHz,  $\text{CD}_3\text{OD}$ ):  $\delta$  -136.1 – -136.4 (m, 24F, *-meta*), -145.1 (m, 24F, *-ortho*).

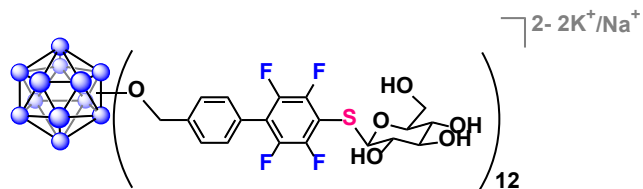
### Synthesis of **3k**



**3** (10.0 mg, 0.0029 mmol) and  $\text{K}_3\text{PO}_4$  (27.0 mg, 0.127 mmol) were added along with a flea micro stir bar to a 4-mL glass vial, which was then sealed with a PTFE/silicone cap under ambient conditions. The vial was then purged and backfilled with  $\text{N}_2$  three times before being transferred into the glovebox. In the glovebox, the vial was opened and 300  $\mu\text{L}$  anhydrous DMF was added, followed by mPEGthiol<sub>2000</sub> (85.0 mg, 0.043 mmol). The vial was sealed again and set to stir at 400

rpm for 20 hours. The vial was transferred out of the glovebox, and its contents were transferred into an NMR tube for *in situ*  $^{19}\text{F}$  NMR spectroscopy to ensure nearly quantitative conversion and *in situ*  $^{11}\text{B}$  NMR spectroscopy to ensure structural integrity of the cluster. The crude mixture was then transferred into a 20-mL glass vial and lyophilized for solvent removal. A 1.25 cm x 35 cm glass column was packed with Sephadex G50 medium in water (23 cm packed height), and the crude product mixture containing **3k** was loaded onto the column with water. 15 1-2 mL fractions were collected, dried *via* lyophilization, and subjected to characterization *via*  $^1\text{H}$ ,  $^{11}\text{B}$ , and  $^{19}\text{F}$  NMR spectroscopy. The pure product fractions as indicated by NMR spectroscopy were combined and dried *via* lyophilization to obtain an isolated yield of 43.2 mg (54 %).  $^1\text{H}$  NMR (400 MHz,  $\text{CD}_3\text{OD}$ ):  $\delta$  7.64 – 7.47 (br m, 24H,  $\text{OCH}_2\text{-Ar}$ ), 7.20 (br m, 24H,  $\text{OCH}_2\text{-Ar}$ ), 5.66 (br m, 24H,  $\text{OCH}_2$ ), 3.92 – 3.44 (m, 2100H,  $\text{SCH}_2\text{CH}_2(\text{CONH})\text{CH}_2\text{CH}_2\text{O}(\text{CH}_2\text{CH}_2\text{O})_{42}$ ), 3.35 (s, 36H,  $(\text{CH}_2\text{CH}_2\text{O})_{42}\text{CH}_3$ ), 3.19 (t, 24H,  $\text{SCH}_2\text{-CH}_2$ ).  $^{11}\text{B}$  NMR (128 MHz,  $\text{CD}_3\text{OD}$ ):  $\delta$  -15.4.  $^{19}\text{F}$  NMR (376 MHz,  $\text{CD}_3\text{OD}$ ):  $\delta$  -136.2 – -137.3 (m, 24F, *-meta*), -145.0 – -145.5 (m, 24F, *-ortho*). GPC trace of **3k** measured in water with 0.02%  $\text{NaN}_3$  at 12 °C gives a  $\text{Đ}$  (polydispersity index) of 1.081 (see Figure 2.3c in main text).

### Synthesis of **3l**



**3** (10.0 mg, 0.0029 mmol) and  $\text{K}_3\text{PO}_4$  (18.7 mg, 0.088 mmol) were added along with a flea micro stir bar to a 4-mL glass vial, which was then sealed with a PTFE/silicone cap under ambient conditions. The vial was then purged and backfilled with  $\text{N}_2$  three times before being transferred

into the glovebox. In the glovebox, the vial was opened and 300  $\mu$ L anhydrous DMF was added, followed by 1-thio- $\beta$ -D-glucose tetraacetate (16.4 mg, 0.045 mmol). The vial was sealed again and set to stir at 400 rpm for 5 hours. The vial was transferred out of the glovebox, and its contents were transferred into an NMR tube for *in situ*  $^{19}\text{F}$  NMR spectroscopy to ensure nearly quantitative conversion and *in situ*  $^{11}\text{B}$  NMR spectroscopy to ensure structural integrity of the cluster. The crude mixture was then transferred into a 20-mL glass vial and lyophilized for solvent removal. The resulting residue was treated with NaOMe (3.8 mg, 0.07 mmol) in 1 mL MeOH for 2 hours. The volatiles were removed *via* rotary evaporation. The crude product mixture containing **31** was dissolved in water and adjusted to pH 7.3 using 3M HCl. This mixture was then centrifuged 5 times – after each of the first 4 centrifugation periods, the supernatant was removed by pipet and more water was added, after the 5<sup>th</sup> centrifugation period, the supernatant was removed and the precipitate was dried *via* lyophilization, and subjected to characterization *via*  $^1\text{H}$ ,  $^{11}\text{B}$ , and  $^{19}\text{F}$  NMR spectroscopy. This pure product as indicated by NMR spectroscopy was dried *via* lyophilization to obtain an isolated yield of 5.3 mg (32 %).  $^1\text{H}$  NMR (400 MHz,  $\text{CD}_3\text{OD}$ ):  $\delta$  7.62 – 7.46 (br m, 24H,  $\text{OCH}_2\text{-Ar}$ ), 7.27 – 7.17 (br m, 24H,  $\text{OCH}_2\text{-Ar}$ ), 5.65 – 5.56 (br m, 24H,  $\text{OCH}_2$ ), 3.77 – 3.33, 3.28 (m, 84H,  $\text{SCH}_2\text{CH}_2\text{OH}(\text{CHOH})_3\text{CHO}$ ).  $^{11}\text{B}$  NMR (128 MHz,  $\text{CD}_3\text{OD}$ ):  $\delta$  -15.4.  $^{19}\text{F}$  NMR (376 MHz,  $\text{CD}_3\text{OD}$ ):  $\delta$  -135.4 – -135.5 (m, 24F, *-meta*), -145.5 – -145.6 (m, 24F, *-ortho*). HRMS (Q-Exactive Plus): *m/z* calculated for  $\text{C}_{228}\text{H}_{204}\text{B}_{12}\text{F}_{48}\text{O}_{72}\text{S}_{12}$  ( $\text{M}^{3-}$ ), 1840.3100 Da; found, 1840.3178 Da.

### **Stability studies of 2i under biologically relevant conditions**

**Cell culture media/fetal bovine serum:** 14.8 mg of **2i** was dissolved in 500  $\mu\text{L}$  of Milli-Q water. 100  $\mu\text{L}$  of this solution was added to 500  $\mu\text{L}$  of serum media (440  $\mu\text{L}$  cell culture media and 60  $\mu\text{L}$  fetal bovine serum). This mixture was vortexed and then transferred to an NMR tube and monitored over 5 days at room temperature by  $^{11}\text{B}$  and  $^{19}\text{F}$  NMR spectroscopy. This sample was then incubated at 37  $^{\circ}\text{C}$  for an additional 5 days and subjected to analysis *via*  $^{11}\text{B}$  and  $^{19}\text{F}$  NMR spectroscopy. No significant change was observed by NMR spectroscopy.

**pH 5:** 14.8 mg of **2i** was dissolved in 500  $\mu\text{L}$  of Milli-Q water. 100  $\mu\text{L}$  of this solution was added to 500  $\mu\text{L}$  of a 0.1 M citric acid/sodium citrate buffer at pH 5.0. This mixture was vortexed and then transferred to an NMR tube and monitored over 5 days at room temperature by  $^{11}\text{B}$  and  $^{19}\text{F}$  NMR spectroscopy. NMR spectroscopy suggests that the structural integrity is maintained. We note that we observed small impurities corresponding to boric acid and borates by  $^{11}\text{B}$  NMR spectroscopy as well as some peak broadening in  $^{11}\text{B}$  and  $^{19}\text{F}$  NMR spectra due to the oxidation of **2i** from the 2- to the 1- oxidation state over time.

**pH 7:** 14.8 mg of **2i** was dissolved in 500  $\mu\text{L}$  of Milli-Q water. 100  $\mu\text{L}$  of this solution was added to 500  $\mu\text{L}$  of a 0.1 M Tris/HCl buffer at pH 7.0. This mixture was vortexed and then transferred to an NMR tube and monitored over 5 days at room temperature by  $^{11}\text{B}$  and  $^{19}\text{F}$  NMR spectroscopy. NMR spectroscopy suggests that the structural integrity is maintained. We note that we observed small impurities corresponding to boric acid and borates by  $^{11}\text{B}$  NMR spectroscopy as well as some peak broadening in  $^{11}\text{B}$  and  $^{19}\text{F}$  NMR spectra due to the oxidation of **2i** from the 2- to the 1- oxidation state over time.

**pH 9:** 14.8 mg of **2i** was dissolved in 500  $\mu\text{L}$  of Milli-Q water. 100  $\mu\text{L}$  of this solution was added to 500  $\mu\text{L}$  of a 0.1 M Tris/HCl buffer at pH 9.0. This mixture was vortexed and then transferred to an NMR tube and monitored over 5 days at room temperature by  $^{11}\text{B}$  and  $^{19}\text{F}$  NMR spectroscopy. NMR spectroscopy suggests that the structural integrity is maintained. We note that we observed small impurities corresponding to borates by  $^{11}\text{B}$  NMR spectroscopy as well as some peak broadening in  $^{11}\text{B}$  and  $^{19}\text{F}$  NMR spectra due to the oxidation of **2i** from the 2- to the 1- oxidation state over time.

**2-Mercaptoethanol:** 16.9 mg of **2i** was dissolve in 2.82 mL of  $\text{D}_2\text{O}$ . 500  $\mu\text{L}$  of this solution was added to 100  $\mu\text{L}$  of a 120 mM 2-mercaptoethanol  $\text{D}_2\text{O}$  solution. This mixture was vortexed and then transferred to an NMR tube and monitored over 11 days at room temperature by  $^1\text{H}$ ,  $^{11}\text{B}$  and  $^{19}\text{F}$  NMR spectroscopy. After 11 days, this sample was subjected to mass spectrometry analysis. Both NMR spectroscopy and mass spectrometry suggest that the structural integrity is maintained. We note that we observed a small boric acid impurity by  $^{11}\text{B}$  NMR spectroscopy.

**Glutathione:** 16.9 mg of **2i** was dissolve in 2.82 mL of  $\text{D}_2\text{O}$ . 500  $\mu\text{L}$  of this solution was added to 100  $\mu\text{L}$  of a 12 mM glutathione  $\text{D}_2\text{O}$  solution. This mixture was vortexed and then transferred to an NMR tube and monitored over 11 days at room temperature by  $^1\text{H}$ ,  $^{11}\text{B}$  and  $^{19}\text{F}$  NMR spectroscopy. After 11 days, this sample was subjected to mass spectrometry analysis. Both NMR spectroscopy and mass spectrometry suggest that the structural integrity is maintained. We note that we observed a small boric acid impurity by  $^{11}\text{B}$  NMR spectroscopy as well as some peak broadening in  $^{11}\text{B}$  and  $^{19}\text{F}$  NMR spectra due to the oxidation of **2i** from the 2- to the 1- oxidation state over time.



## Computational work

### A. PEGylated OCNs

PEGylated nanoparticles (NPs) **2i-k** and **3i-k** (Table S2.3) were modeled using molecular dynamics (MD) simulations in: *i*) water with counter ions and *ii*) a buffer solution of  $\text{HPO}_4^{2-}$  and  $\text{H}_2\text{PO}_4^-$  at a total 0.08 M concentration, where the ratio of the two ions was used matched pH 7.4. The MD simulations were performed with NAMD,<sup>107</sup> using the CHARMM force field.<sup>108-113</sup> *Ab initio* calculations were done with Gaussian09<sup>114</sup> to determine unknown parameters for the dodecaborate cluster center and the non-PEGylated (**2** or **3** type ligand) section of the ligand. The boron center was optimized using a HF/6-31g level of theory, with partial charges derived with a ChelpG algorithm.<sup>115</sup> Bonds, angles, and dihedrals force constants containing boron atoms were chosen to have relatively large values, approximately equal to those of double bonded or aromatic carbons, so that the boron center would be rigid. The type **2** and **3** ligands had their bond and angle parameters determined at the MP2/6-31g(d)//HF/6-31g level of theory with VMD Force Field Toolkit plugin.<sup>116</sup> Unknown dihedral parameters were chosen based on similar atom types in the CHARMM force field.<sup>108-113</sup> Partial charges were determined through the ChelpG algorithm.<sup>115</sup> Amide and PEGylated geometries, parameters, and charges were taken from the CHARMM force field.<sup>108-113</sup>

Each of the 6 NPs was separately simulated in water and ionic solutions. Each system is first minimized for 10,000 steps. Afterwards it is heated to 310 K, with 1 K increments per 20 steps until the system reaches a temperature of 310 K, when a pre-equilibration is done. Simulations are performed in an NPT ensemble, at 310 K and a pressure of 1 atm, with Langevin dynamics and a damping constant of  $0.01 \text{ ps}^{-1}$ . Langevin piston is used with a period of 200 fs and decay of 100 fs. Particle Mesh Ewald<sup>117</sup> is used for long range electrostatic interactions with a grid

spacing of 1.0. Short range interactions are performed with the 12-6 Lennard-Jones potential, using a switching function. Velocity Verlet integration is used with the SHAKE algorithm and a time step of 2 fs. Data and snapshots are recorded every 10 ps or 5,000 steps. Simulation times of 25 ns for the water solution and 30 ns for the salt system were used, respectively. Figures S2.1 and S2.2 show snapshots of PEGylated NPs in water (21 ns) and in the ionic solution (31 ns), respectively. Notice that as the chain length increases, the chains are fluctuating significantly to the extent that the chain distributions become asymmetric. In the following, we describe some characteristics of these systems.

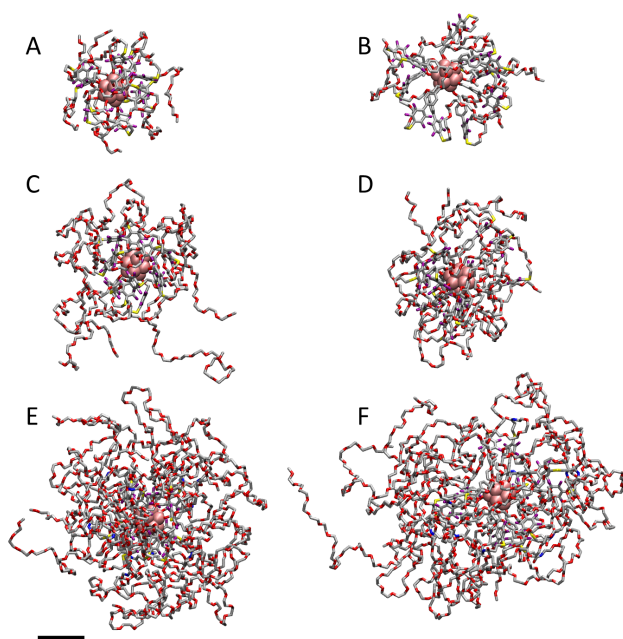


**Figure S2.1.** Nanoparticles snapshots in water after 21 ns of simulations. Scale bar is 1 nm. A) **2i** B) **3i** C) **2j** D) **3j** E) **2k** F) **3k**.

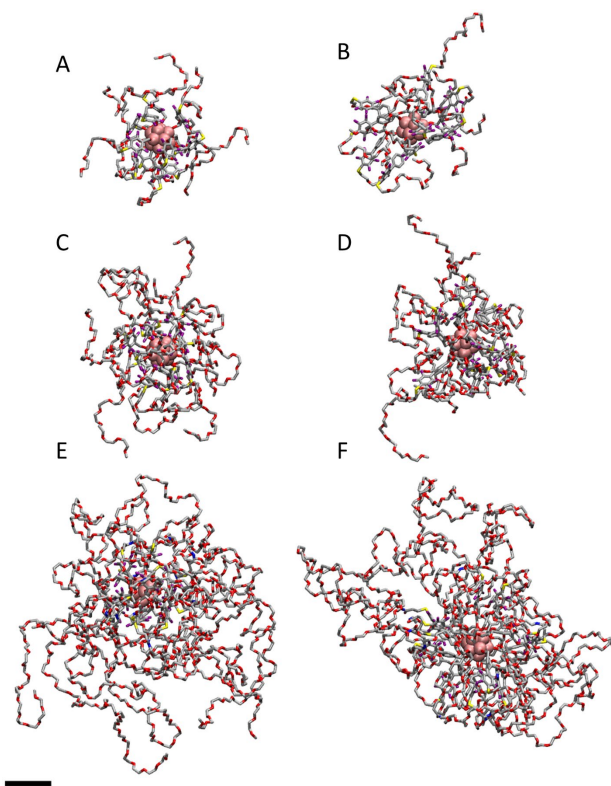


**Figure S2.2.** Nanoparticles snapshots in 0.08 M buffer solution at pH=7.4 (salt) after 31 ns of simulations. Scale bar is 1 nm. A) **2i** B) **3i** C) **2j** D) **3j** E) **2k** F) **3k**.

We use the simulated trajectories of the NPs to calculate the radial distribution functions (RDF),  $g(r)$ , from Eqn. 1. It gives the relative probability of finding the  $j^{\text{th}}$  atom at a distance  $r$  from the  $i^{\text{th}}$  atom with respect to the bulk density:

$$g(r) = \frac{1}{V\rho_N} \sum \delta(r - r_{ij}) . \quad (1)$$

In Eqn. 1,  $\delta$  is a delta function,  $r_{ij}$  is the distance of  $i^{\text{th}}$  and  $j^{\text{th}}$  atoms, and  $V$  is a volume,  $\int 4\pi r^2 dr$ , used in a normalization, and  $\rho_N$  is the number density of the used species (the number of atoms  $N_0$  used in Eqn. 1 divided by the volume of the simulation box). We use Eqn. 1 when we analyze the distribution of C terminal atoms, which are fixed for a given number of ligands (12). When, we consider the distribution of all PEG-chain oxygens (varying number), we remove  $N_0$  (equal the total number of PEG chain oxygens) from  $\rho_N$ , by multiplying Eqn.1 by  $N_0$ , to get  $g'(r)$ , where we

account for the growing distributions for longer PEG chains (more oxygens; system volume is fixed).

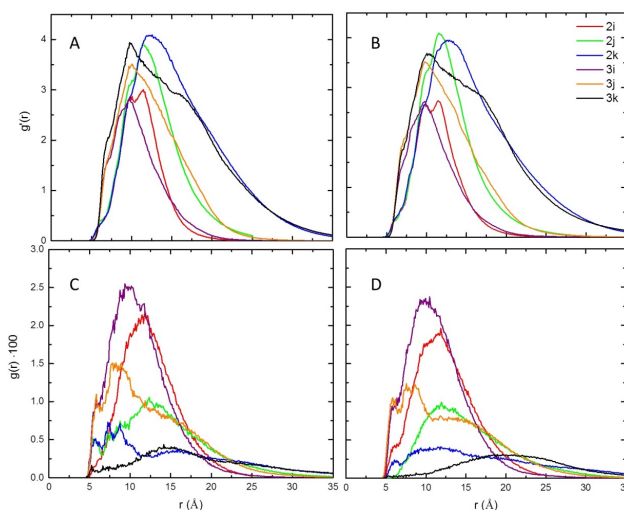


**Figure S2.3.** RDFs of  $2i-k$  and  $3i-k$  NPs.  $g'(r)$  calculated for A) boron-PEG oxygen atoms in water and B) boron-PEG oxygen atoms in ionic solution.  $g(r)$  calculated for C) boron-terminal C atoms in water and D) boron-terminal C atoms in ionic solutions.

In Figure S2.3, we have calculated  $g'(r)$  for (A, B) all the oxygens in PEGylated chains and  $g(r)$  for (C, D) terminal carbon atoms of the PEGylated chains. All the cases were calculated with respect to all the boron atoms. We can clearly see that as the chain becomes longer, the oxygen (A, B) distributions become wider and their peaks,  $r_{\max}$ , become slightly shifted to higher values. Steric effects prevent longer PEGylated chains from folding and wrapping close to the B core, therefore, preventing them from significantly affecting  $r_{\max}$ . The systems present in water and ionic solutions have almost the same PEG-oxygens distributions. On the contrary, in the terminal carbon (CD) distributions, the peaks maxima,  $r_{\max}$ , are significantly shifted to higher values with the chain lengths, since the terminal C atoms are further away from the NPs cores, which they cannot reach. In these distributions, we can also see some differences between water and ionic solution cases, revealing that the terminal atoms in long PEGylated chains are slightly more outstretched in ionic solutions.

The  $g'(r)$  distributions (Figure S2.3A,B) are similar for the **2** and **3** types of ligands, except of some deformations present in the **3** types. These deformations slightly shift the **3** type peaks ( $r_{\max}$ ) to smaller values. For all but **2k** and **3k** terminal carbon RDFs, **3** type ligands have consistently smaller  $r_{\max}$  values than their **2** type counterparts (Figure S2.3), even though **3** has an extra aromatic group, slightly increasing the maximum possible ligand length. The extra aromatic group in **3** ligands enhances  $\pi$ - $\pi$  stacking interactions between the ligands, thus causing the net length to decrease. The split peak in **2i** could be related to the fact that the B shell front and back sides can contribute by separate peaks.

The hydrodynamic radii of the studied NPs were estimated from the regions of decaying  $g'(r)$  (half value compared to  $r_{\max}$ ) for the cases (A–B) (all oxygens). In water, the hydrodynamic radii of **2i** and **3i** are 12 Å; **2j** and **3j** are 15 Å; **2k** and **3k** are 20 Å. In the ionic solution, **2i**, **3i**, **2j**, and **3j** have very similar sizes as in water. At certain times, there are some chains on **2k** or **3k** that extend outwards, but most of the other chains are folded (Figures S2.1E,F and 2.2E,F). Interestingly, the maxima of distributions for the terminal C atoms in Figure 2.3C,D match relatively well to the hydrodynamic radii. One can assume that the terminal C atoms are distributed at the surface of the NPs, revealing thus their radii.

To confirm the previous results, next, the radii of gyration,  $\langle r_{\text{gyr}} \rangle$ , are also calculated for NPs using Eqn. 2:

$$r_{\text{gyr}} = \sqrt{\frac{I}{m}} = \sqrt{\frac{\sum_{i=\text{atoms}} m_i (\vec{r}_i - \vec{r}_{\text{com}})^2}{\sum_{i=\text{atoms}} m_i}} . \quad (2)$$

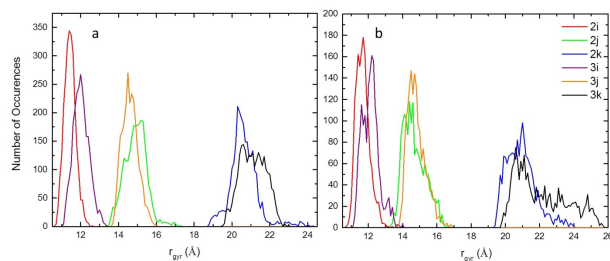
Here,  $I$  is the moment of inertia of the molecule,  $m$  is the total mass of the molecule formed by individual contributions,  $m_i$ , of atoms shifted with respect to a molecular center of mass,  $r_i - r_{\text{com}}$ . Time averaged  $\langle r_{\text{gyr}} \rangle$  was calculated by using equation 2 every 10 ps over 26 ns trajectory (water)

or 34 ns trajectory (salt solution) and then averaged. Standard deviations and confidence intervals were also computed.

**Table S2.3.** Radii of gyration,  $\langle r_{\text{gyr}} \rangle$ , and their confidence intervals for PEGylated species in water and salt solutions

Molecule	Solvent	$\langle r_{\text{gyr}} \rangle$ (Å)
<b>2i</b>	water	11.5 ± 0.9
<b>2j</b>	water	15.0 ± 1.7
<b>2k</b>	water	20.7 ± 2.2
<b>3i</b>	water	12.1 ± 1.2
<b>3j</b>	water	14.7 ± 1.3
<b>3k</b>	water	21.1 ± 2.0
<b>2i</b>	ionic solution	11.7 ± 1.0
<b>2j</b>	ionic solution	14.7 ± 2.0
<b>2k</b>	ionic solution	21.0 ± 2.5
<b>3i</b>	ionic solution	12.2 ± 1.5
<b>3j</b>	ionic solution	14.8 ± 1.6
<b>3k</b>	ionic solution	22.1 ± 4.5

Table S2.3 shows the radii of gyration,  $\langle r_{\text{gyr}} \rangle$  and their >99.5 % confidence intervals for PEGylated species in water and salt solutions. As expected, **2i** and **3i** molecules have the smallest diameters, whereas **2k** and **3k** have the largest diameters in both environments. **2i** and **3i** molecules, with 7 PEGylated oxygens per ligand have diameters of more than 2 nm; **2j** and **3j**, with 16 PEGylated oxygens per ligand, less than 3 nm; **2k** and **3k**, with 43 oxygens per ligand, more than 4 nm. NPs with the type **3** ligands tend to have a slightly larger diameter than those with the type **2** ligands. This size increase could be due to the extra aromatic group in type **3** ligands, which is absent in the **2** type ligands.  $\langle r_{\text{gyr}} \rangle$  does not change appreciably between the two environments. However, **2k** and **3k** ligands are slightly more outstretched in the ionic solutions.



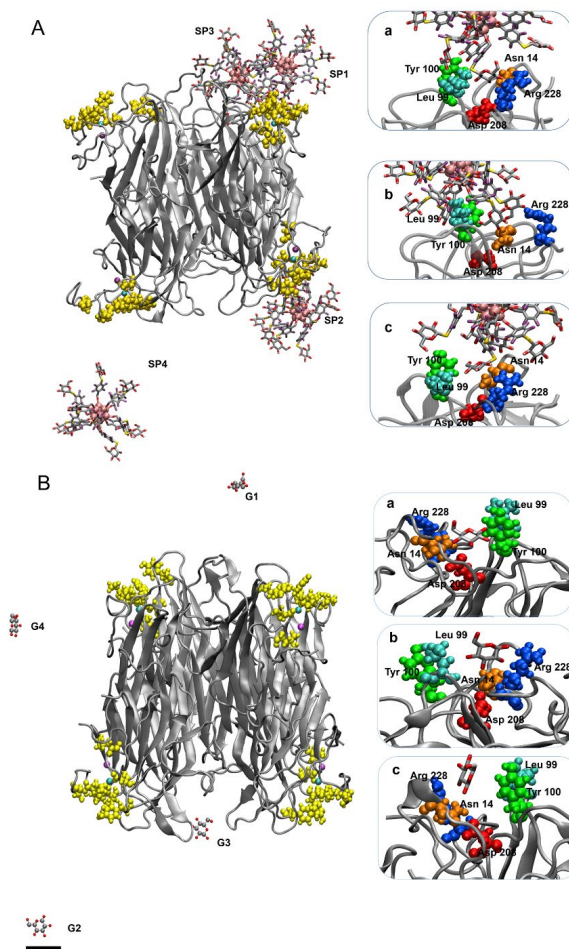
**Figure S2.4.** Distributions of  $r_{\text{gyr}}$  in a) water and b) ionic solutions.

Figure S2.4a and S2.4b show the distributions of  $r_{\text{gyr}}$  in water and salt solutions, respectively. The distributions are asymmetrically broadened at higher values for all molecules, especially for long chains. This reflects that a few chains could extend and then fold back. Comparing the radii of gyration,  $\langle r_{\text{gyr}} \rangle$ , from Table S2.3 and Figure S2.4 with the above hydrodynamic radii and the most likely positions of terminal C atoms, we can see that all these parameters are in good agreement.

## B. Sugar-coated nanoparticles – protein binding

MD simulations were also performed to investigate multivalent binding of sugar-coated nanoparticles and proteins. Concanavalin A (Con A) was chosen as the target protein to bind with multivalent sugar-coated particles (SP) and monovalent  $\beta$ -D glucose (G), respectively. Con A forms quaternary structures, giving at pH 7 a tetramer, having four carbohydrates binding sites (hydrogen bonds).<sup>118</sup> In each Con A, up to 15 amino acids can be involved in the carbohydrate binding, while for the monosaccharide binding only five amino acids are involved, including Asn 14, Leu 99, Tyr 100, Asp 208, Arg 228.<sup>119</sup> In our simulations, the tetramer structure of Con A used was based on X-ray diffraction data (PDB code 1ONA).<sup>119</sup> Figures S2.5A and S2.5B show the structures of tetramer of Con A with SPs and  $\beta$ -D glucose after 20 ns simulation, respectively. The metals manganese (magenta ball) and calcium (cyan ball) were added in Con A according to its metal binding sites.<sup>119</sup> The monosaccharide binding sites are distinguished from the backbone of Con A by different colors (Figure S2.5). The Con A tetramer has four binding positions. We name the top right position as binding position 1 (B1), bottom right as B2, top left as B3, and bottom left as B4.





**Figure S2.5.** A) Tetramer of Con A and sugar-coated particles. B) Tetramer of Con A and  $\beta$ -D glucoses. Details of glucose binding shown in both cases.

For the NPs binding, three SPs (SP1, SP2 and SP4) were initially put near the binding sites of chosen monomers. The last SP (SP3) was placed in the cavity between the B1 and B3 binding positions. For the  $\beta$ -D glucose binding, three glucose molecules (G1, G2 and G3) are separately placed at the binding B1, B2 and B3 positions, while the last glucose molecule (G4) was placed between the B3 and B4 binding position. The two systems were immersed in water together with the counter-ions and the simulations were performed with NAMD.<sup>107</sup>

The bond, angle and dihedral parameters of protein, SPs (nanoparticle **2I**) and  $\beta$ -D glucose were implemented from the CHARMM force field.<sup>108–113</sup> The parameters for the boron core and

ligands were used the same as in the PEGylated calculations. The nonbonding parameters of  $\text{Mn}^{2+}$  ions were based on the calculations of Babu *et al.*<sup>120</sup> Nonbonding interactions of SPs were calculated using a cut-off distance of 10 Å, whereas long-range electrostatic interactions were calculated by the PME method<sup>117</sup> in the presence of periodic boundary conditions. The systems were simulated in the NPT ensemble, using a Langevin dynamics with a damping constant of 0.01  $\text{ps}^{-1}$  and a time step of 1 fs.

First, we modeled the coupling between SPs and the Con A tetramer. At each simulation time, we have calculated a distance between each sugar binding site and its nearest ligand in the SP. Figure S2.6 shows a time-dependent distance between the nearest SPs ligand and the Con A tetramer. During the 20 ns simulations, SP1 and SP2 have an average distance of 4 Å, while SP3 and SP4 have an average distance of about 10 Å. Because the initial position of SP3 is far from any binding site, it can't bind during the short simulations. From Figure S2.5A, we can see that SP3 competes with SP1 for the B1 position, while SP4 shows a different trend. Within 1 ns, SP4 comes near to the Con A tetramer and binds to it. Then, it leaves away and binds again at 4 ns, when the binding lasts for about 4 ns. After 12 ns, SP4 binds to the Con A tetramer again.

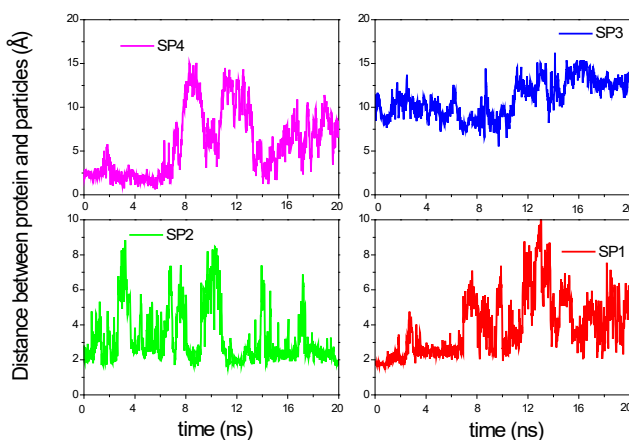


**Figure S2.6.** Nearest distances between SPs ligands and the Con A tetramer.

Figure S2.6 reveals that when SPs bind to the Con A tetramer their binding distance is about 1.8-2 Å. SPs occasionally gain and preserve for significant time periods these small binding distances. Figure S2.5A(a–c) show details of SP1, SP2 and SP4 binding to their binding sites. We can see that in all the cases only one of the SPs ligands binds to the nearby binding site, composed of Asn 14, Leu 99, Tyr 100, Asp 208, Arg 228, which is the monosaccharide binding site shown in different color in Figure S2.5A(a–c). Therefore, there is always one ligand of SPs which performs like a monosaccharide when binding to the Con A tetramer. Because the SPs have several ligands, when one ligand leaves, another nearby ligand comes and binds, which increases the binding probability of SPs. In this way, SPs act like multivalent binders.

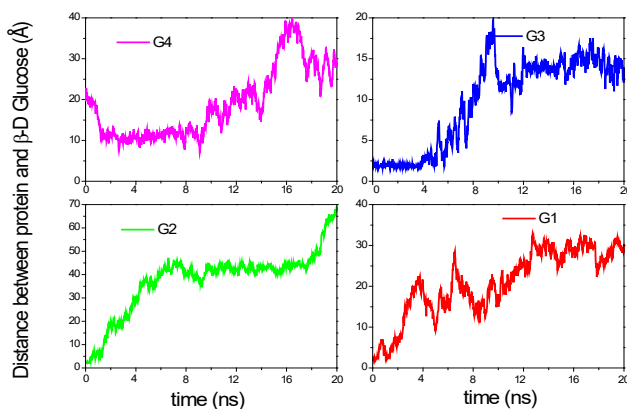


**Figure S2.7.** Nearest distances between  $\beta$ -D glucose molecules and the Con A tetramer.

In order to compare the binding ability of SPs and  $\beta$ -D glucose systems, we simulated binding of  $\beta$ -D glucose and the Con A tetramer. Figure S2.7 shows the nearest distance between  $\beta$ -D glucose and Con A as a function of time. Figure S2.7 shows that G1 only binds to Con A at the first 1 ns and then leaves. G2 only binds at the very beginning and it doesn't bind later; G3 binds to Con A for about 4 ns at the beginning and after that it leaves away; G4 shows weak binding during the first 4 ns. The average distance between all the  $\beta$ -D glucose molecules and the Con A tetramer is more than 20 Å, except G3 whose average distance is about 12 Å. Figure

S2.5B(a-c) shows details of  $\beta$ -D glucose and the Con A tetramer binding. When  $\beta$ -D glucose binds to Con A, it binds to the typical monosaccharide binding sites. Because  $\beta$ -D glucose is monovalent, when one  $\beta$ -D glucose leaves, another  $\beta$ -D glucose from the surrounding solution might come nearby and bind. Overall, monovalent  $\beta$ -D glucose molecules show shorter binding times and longer binding distances than SPs.

## CHAPTER THREE

### **Multivalent Cluster Nanomolecules for Inhibiting Protein-Protein Interactions**

Elaine A. Qian, Yanxiao Han, Marco S. Messina, Heather D. Maynard,

Petr Král, and Alexander M. Spokoyny.

*Bioconjugate Chem.* **2019**, *30*, 2594–2603.

#### **Abstract**

Multivalent protein-protein interactions serve central roles in many essential biological processes, ranging from cell signaling and adhesion to pathogen recognition. Uncovering the rules that govern these intricate interactions is important not only to basic biology and chemistry, but also to the applied sciences where researchers are interested in developing molecules to promote or inhibit these interactions. Here we report the synthesis and application of atomically precise inorganic cluster nanomolecules consisting of an inorganic core and a covalently linked densely-packed layer of saccharides. These hybrid agents are stable under biologically relevant conditions and exhibit multivalent binding capabilities, which enable us to study the complex interactions between glycosylated structures and a dendritic cell lectin receptor. Importantly, we find that subtle changes in the molecular structure lead to significant differences in the nanomolecule's protein-binding properties. Furthermore, we demonstrate an example of using these hybrid nanomolecules to effectively inhibit protein-protein interactions in a human cell line. Ultimately, this work reveals an intricate interplay between the structural design of multivalent agents and their biological activities toward protein surfaces.

## Introduction

Multivalency is a prevalent phenomenon that facilitates many important biological processes in nature.<sup>49</sup> Some of the most fascinating examples are found in our own immune system, where multivalency plays a crucial role in modulating several central functions of the immune cells, including cell signaling, cell-cell interaction, and pathogen recognition.<sup>84,121–123</sup> A notable example of these intricate interactions takes place between glycoproteins and lectins, whose specificity and affinity toward each other are greatly amplified through multivalency. The important role multivalency plays in nature has fascinated both biologists and chemists alike, who are mutually interested in understanding the fundamental mechanisms behind these supramolecular recognition events as well as developing abiotic tools that are inspired by natural phenomena.<sup>95,97,98,123,124</sup>

An important biological target for studying multivalency is a C-type lectin receptor called dendritic cell-specific intercellular adhesion molecule-3-grabbing nonintegrin (DC-SIGN).<sup>125</sup> Predominately expressed on the surface of dendritic cells, it organizes into a homotetrameric structure that is critical for the multivalent recognition of pathogens.<sup>126,127</sup> In particular, DC-SIGN is able to bind specific high-mannose glycoproteins and glycolipids on pathogens with high avidity, which activates a sequence of downstream responses including pathogen uptake and degradation as well as subsequent antigen processing and presentation.<sup>128</sup> However, various pathogens such as HIV-1 have been observed to escape the intracellular degradation pathway following DC-SIGN-facilitated uptake.<sup>129</sup> While the mechanism behind this unusual behavior is not well understood, it is clear that DC-SIGN plays an instrumental role in transmitting HIV-1 to the T cells and enhancing the infection in its early stages.<sup>129–131</sup> Therefore, there is significant interest in 1) uncovering the rules that govern the multivalent interactions between DC-SIGN and

high-mannose glycoconjugates and 2) inhibiting the DC-SIGN-dependent attachment and uptake of certain pathogens. One of the most promising approaches that can potentially tackle both challenges is centered around building molecules that can mimic the dense multivalent display of carbohydrates on the pathogen surface.<sup>97,98,101,132,133</sup>

Previously, several promising classes of glycomimetic ligands for DC-SIGN have been designed and synthesized, which include but are not limited to small molecules,<sup>134,135</sup> peptides,<sup>136,137</sup> linear and dendritic polymers,<sup>138–144</sup> fullerenes,<sup>96,145</sup> supramolecular assemblies,<sup>146–148</sup> and hybrid nanoparticles.<sup>149–151</sup> These constructs are capable of engaging DC-SIGN with high avidities ( $K_D$  spanning nM– $\mu$ M), which allowed several of these systems to inhibit viral entry and infection. In particular, rigid three-dimensional (3D) architectures such as thiol-capped gold nanoparticles (AuNPs) are attractive glycomimetic platforms due to the ease of generating tunable and well-defined multivalent agents. Nevertheless, due to the weak bonding interactions between gold and thiol-based ligands, the surface morphology of these systems is poorly defined and highly dynamic, especially under biologically relevant conditions.<sup>58,67,69,70</sup> This ultimately hinders researchers' ability to understand the precise structure-activity relationships of these systems with respect to biomolecular recognition and binding events.

Here we report the synthesis of a family of atomically precise glycosylated cluster nanomolecules featuring robust inorganic cluster scaffolds as nanoparticle core templates. Specifically, we developed conditions that allow the rapid functionalization of perfluoroaryl-based moieties covalently grafted onto a rigid dodecaborate core *via* “click”-like nucleophilic aromatic substitution ( $S_NAr$ ) chemistry, thus leading to fully covalent nanomolecules with a densely packed layer of saccharides.<sup>6,87</sup> This chemistry mimics the operational simplicity with which thiol-capped AuNPs are synthesized, yet produces well-defined assemblies that are stable under biologically

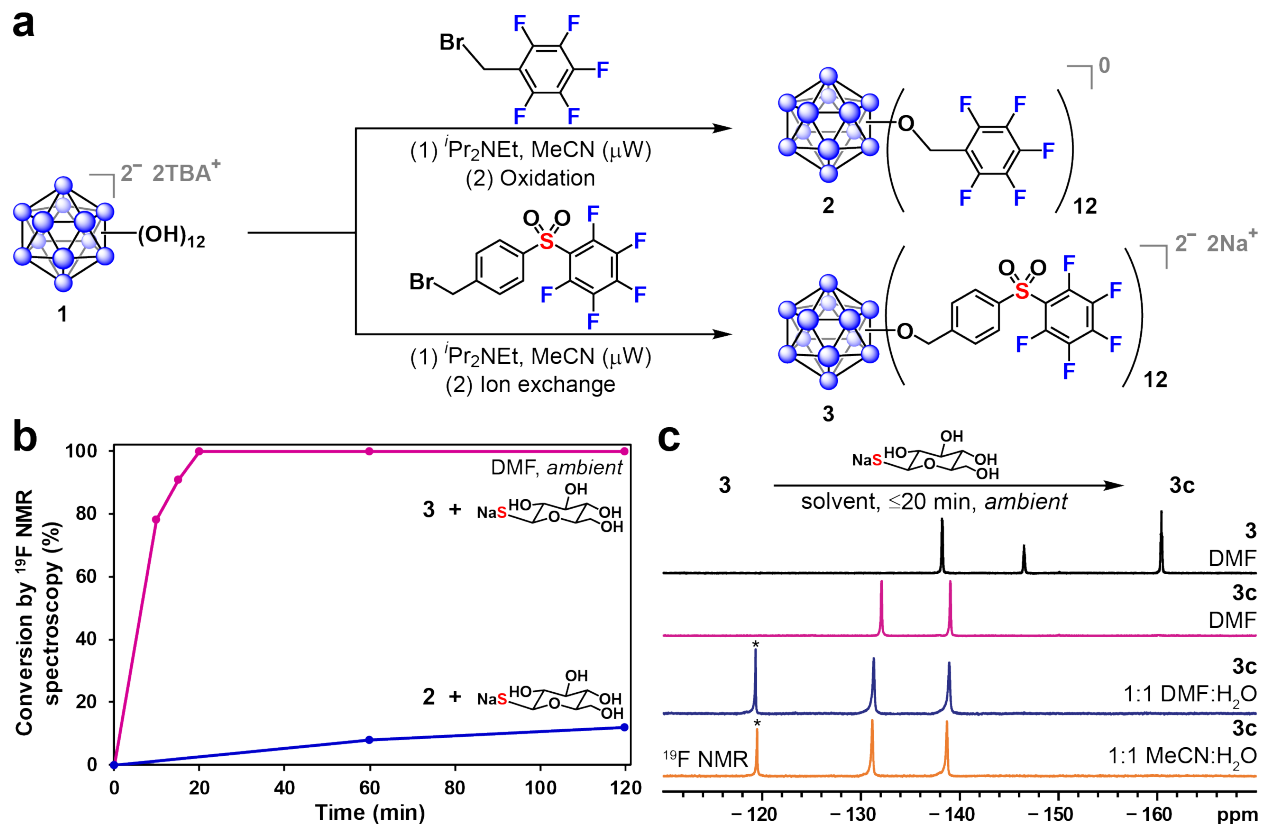
relevant conditions.<sup>6</sup> Importantly, direct binding studies between these hybrid assemblies and DC-SIGN reveal the multivalency-enhanced avidity in addition to the carbohydrate specificity of the lectin and the structural requirements for the multivalent ligands. Furthermore, competitive binding data suggest the mannose-coated nanomolecules can inhibit the protein-protein interactions between DC-SIGN and an HIV-1 envelope glycoprotein, gp120. Moreover, we found that the nanomolecules exhibit no apparent toxicity to a human lymphoblast-like cell line at 0.5–50  $\mu\text{M}$  concentrations. This allowed us to perform cellular experiments, which revealed that the mannose-functionalized clusters are capable of preventing the cell uptake of gp120 by blocking cell-surface DC-SIGN. Therefore, we demonstrate that easily accessible, precisely engineered hybrid cluster-based nanomolecules can be utilized to not only study the rules governing multivalent recognition, but also inhibit protein-protein interactions in cells.

## Results and Discussion

Given our success in installing a wide scope of thiols onto the perfluoroaryl-perfunctionalized clusters using  $\text{S}_{\text{N}}\text{Ar}$  chemistry,<sup>6</sup> we hypothesized that this strategy could be applied to generate a library of atomically precise nanomolecules featuring a variety of saccharides densely packed on the rigid 3D surface. Using the perfluoroaryl-perfunctionalized cluster **2** (Figure 3.1a) and 1-thio- $\beta$ -D-mannose tetraacetate,<sup>6,82,152,153</sup> we performed  $\text{S}_{\text{N}}\text{Ar}$  reactions in the presence of base in dimethylformamide (DMF), stirring under a  $\text{N}_2$  atmosphere. These test conjugation reactions revealed significant conversions, as determined by  $^{19}\text{F}$  NMR spectroscopy. Following efficient optimization facilitated by *in situ*  $^{19}\text{F}$  NMR spectroscopy, we found that employing an excess of the thiol and potassium phosphate ( $\text{K}_3\text{PO}_4$ ) allowed the nearly quantitative ( $\geq 99\%$ ) substitution of **2** with the substrate within 48 hours. The product was briefly treated with sodium



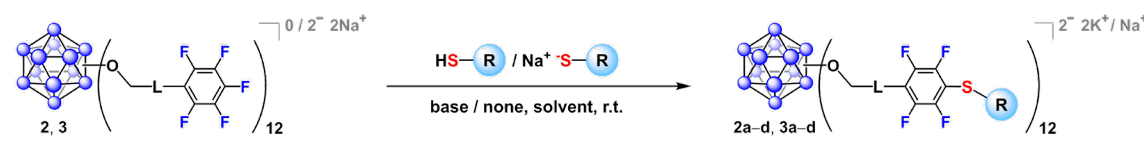
methoxide (NaOMe) to remove all the acetyl groups, then purified by a desalting centrifugal filter to yield the mannose-coated nanomolecule **2a** (Table 3.1, entry 1) in 80% isolated yield (see the Supporting Information for experimental details). The purified **2a** was subsequently subjected to characterization *via*  $^1\text{H}$ ,  $^{11}\text{B}$ , and  $^{19}\text{F}$  NMR spectroscopy and electrospray ionization-high resolution mass spectrometry (ESI-HRMS), which support the proposed structure and composition (see the Supporting Information for characterization data). Furthermore, we found that a similar strategy could be used to perfunctionalize **2** with 1-thio- $\beta$ -D-galactose tetraacetate within 48 hours,<sup>153,154</sup> giving rise to the purified nanomolecule **2b** (Table 3.1, entry 2), after isolation in 84% yield (see the Supporting Information for experimental details and characterization data). Additionally, we prepared previously reported glucose- and poly(ethylene glycol) (PEG)-coated structures **2c** and **2d** (Table 3.1, entries 3 and 4),<sup>6</sup> and notably the isolated yield for **2c** was significantly improved (17% to 65%) through the new purification strategy (see the Supporting Information for experimental details). Overall, these results demonstrate that perfluoroaryl-thiol  $\text{S}_{\text{N}}\text{Ar}$  chemistry can be utilized to assemble a panel of well-defined, multivalent hybrid nanomolecules functionalized with various saccharides including mannose, galactose, and glucose. Moreover, both the glycosylated and PEGylated nanomolecules can be easily purified using desalting centrifugal filters, which streamlines access to the pure materials. Ultimately, these nanomolecules provide us with the ability to evaluate the biological activities of multivalent assemblies as a function of the molecular structure precisely displayed in 3D space.

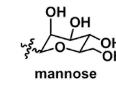
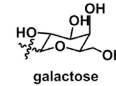
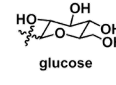
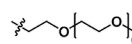
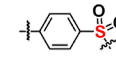
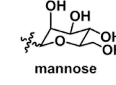
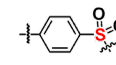
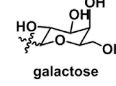
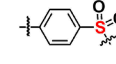
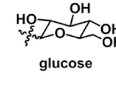
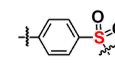
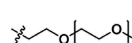


**Figure 3.1.** Synthesis of perfluoroaryl-perfunctionalized clusters and their reactivities toward an unprotected thiolated saccharide. (a) Clusters **2** and **3** are readily prepared from **1** with the assistance of a microwave reactor. (b) Conversion rates of  $S_NAr$  reactions between **2/3** and 1-thio- $\beta$ -D-glucose sodium salt, as monitored by  $^{19}\text{F}$  NMR spectroscopy, reveal the significantly enhanced reactivity of **3** over **2**. (c)  $^{19}\text{F}$  NMR spectra of **3** in DMF and **3c** after conjugation with 1-thio- $\beta$ -D-glucose sodium salt in DMF or mixed aqueous/organic media. \*NaF signal.

With the successful synthesis of glycosylated nanomolecules **2a–c**, we sought to build a new generation of multivalent architectures that share the precision and rigidity of the first-generation assemblies, but feature a rationally designed linker that will modularly extend the cluster scaffold. We envisioned that the new class of larger-sized glycosylated nanomolecules featuring a distinct multivalent display of saccharides, when studied alongside **2a–c**, will allow us to further investigate the complex relationship between molecular structure and activity in the multivalent constructs. Keeping the downstream biological applications in mind, we set out to find

a rigid linker that could ideally lead to water-soluble glycosylated nanomolecules. After testing multiple linker designs, we found a sulfone-bridged biphenyl derivative (Figure 3.1a) to be the most suitable candidate. The rationale behind choosing this linker was two-fold – not only could the polar sulfone group promote the overall water solubility of the nanomolecule (our attempt to use a biphenyl motif resulted in a poorly water-soluble glycosylated cluster), but also a similar molecule, decafluoro-biphenylsulfone, was recently found to exhibit remarkably fast  $S_NAr$  reactivity toward cysteine residues on peptides under aqueous conditions.<sup>155</sup> Therefore, we hypothesized that perfunctionalization of **1** (Figure 3.1a) with the sulfone-bridged linker could enhance the  $S_NAr$  reaction kinetics and impart aqueous compatibility to the cluster conjugation, resulting in a water-soluble glycosylated species. The target benzyl bromide linker containing a terminal  $SO_2C_6F_5$  functional group was synthesized in three steps (see the Supporting Information for experimental details and characterization data). Using a microwave-assisted synthesis method,<sup>81</sup> we observed nearly quantitative conversion of **1** to the perfunctionalized cluster within 30 minutes, based on  $^{11}B$  NMR spectroscopy and ESI-HRMS. The cluster species was isolated from the residual organic-based starting materials *via* silica gel chromatography in 94% yield. After subjecting the compound to a sodium ion exchange column, **3** (Figure 3.1a) was isolated as a light salmon-colored solid (see the Supporting Information for experimental details).  $^1H$ ,  $^{11}B$ , and  $^{19}F$  NMR spectroscopy (Figure 3.1c) and ESI-HRMS results of **3** are consistent with the proposed structure and composition of the dodeca-functionalized  $B_{12}$ -based cluster (see the Supporting Information for characterization data).

**Table 3.1.** Glycosylation and PEGylation of clusters **2** and **3**


Entry	Compound	L	R	Time (h)	<i>In situ</i> yield <sup>a</sup> (%)	Isolated yield <sup>b</sup> (%)
1	<b>2a</b>	none	 mannose	48	≥99	80
2	<b>2b</b>	none	 galactose	48	≥99	84
3	<b>2c*</b>	none	 glucose	24	≥99	65
4	<b>2d*</b>	none		24	≥99	76
5	<b>3a</b>		 mannose	0.3	≥99	83
6	<b>3b</b>		 galactose	0.3	≥99	67
7	<b>3c</b>		 glucose	0.3	≥99	77
8	<b>3d</b>			1.5	≥99	84

<sup>a</sup>Yield determined by <sup>19</sup>F NMR spectroscopy; <sup>b</sup>Isolated yield after purification; \*Previously reported compounds. r.t., room temperature.

To test whether cluster **3** exhibits enhanced S<sub>N</sub>Ar reactivity toward thiols, we exposed **3** dissolved in DMF to a stoichiometric amount of an unprotected thiolated saccharide, 1-thio-β-D-glucose sodium salt, and observed by <sup>19</sup>F NMR spectroscopy a nearly quantitative (≥99%) conversion to **3c** (Table 3.1, entry 7) within 20 minutes (Figure 3.1b, c). The purified water-soluble **3c** was obtained *via* a desalting centrifugal filter, and was subjected to analysis *via* <sup>1</sup>H, <sup>11</sup>B, and <sup>19</sup>F NMR spectroscopy and ESI-HRMS, which support the proposed structure and composition (see the Supporting Information for experimental details and characterization data). Notably, due

to the rapid kinetics, this reaction did not require a N<sub>2</sub> atmosphere in order to proceed to completion, therefore all subsequent conjugation reactions of **3** were performed under ambient conditions. Parallel experiments monitoring the S<sub>N</sub>Ar reaction conversion over time of **2** and **3** by <sup>19</sup>F NMR spectroscopy revealed the significantly improved conversion rates of **3** over **2** (Figure 3.1b), which is consistent with our hypothesis. We then proceeded to test whether **3** tolerates water in the conjugation reaction by subjecting **3** to a stoichiometric amount of 1-thio-β-D-glucose sodium salt in 1:1 DMF:water and 1:1 acetonitrile (MeCN):water mixtures, and in both cases observed nearly quantitative (≥99%) conversion to **3c** within 15 minutes (Figure 3.1c) (see the Supporting Information for experimental details). These remarkably fast reaction kinetics in mixed aqueous/organic media are consistent with the observations by Kalhor-Monfared *et al.* and furthermore may be facilitated by the enhanced solubility of 1-thio-β-D-glucose sodium salt in water.<sup>155</sup> Overall, these studies demonstrate that by employing rational linker design, the S<sub>N</sub>Ar reaction characteristics including kinetics and aqueous compatibility can be dramatically enhanced, allowing for the rapid assembly of atomically precise, densely glycosylated nanomolecules.

Based on the successful glycosylation of **2** to yield functionalized nanomolecules **2a–c**, we hypothesized that **3** could likewise be glycosylated by mannose and galactose in addition to glucose (*vide supra*). Treatment of **3** with the sodium salts of 1-thio-α-D-mannose and 1-thio-β-D-galactose in 1:1 DMF:water mixtures resulted in nearly quantitative (≥99%) conversions within 15 minutes to **3a** and **3b** (Table 3.1, entries 5 and 6), respectively. Following purification, **3a** and **3b** were subjected to characterization *via* <sup>1</sup>H, <sup>11</sup>B, and <sup>19</sup>F NMR spectroscopy and ESI-HRMS, which support the proposed structures and compositions (see the Supporting Information for experimental details and characterization data). Furthermore, we were able to fully PEGylate **3**

within 90 minutes, giving rise to purified **3d** (Table 3.1, entry 8) after isolation in 84% yield (see the Supporting Information for experimental details and characterization data). These experiments demonstrate that cluster **3** can rapidly lead to a library of multivalent hybrid entities featuring diverse functional groups, which allows us to study how the specific surface chemistry affects the protein-binding properties. Ultimately, the family of precisely engineered multivalent nanomolecules (**2a–3** and **3a–d**, *vide supra*) creates a framework which can potentially enable us to study the fundamental rules that govern multivalent biological recognition events.

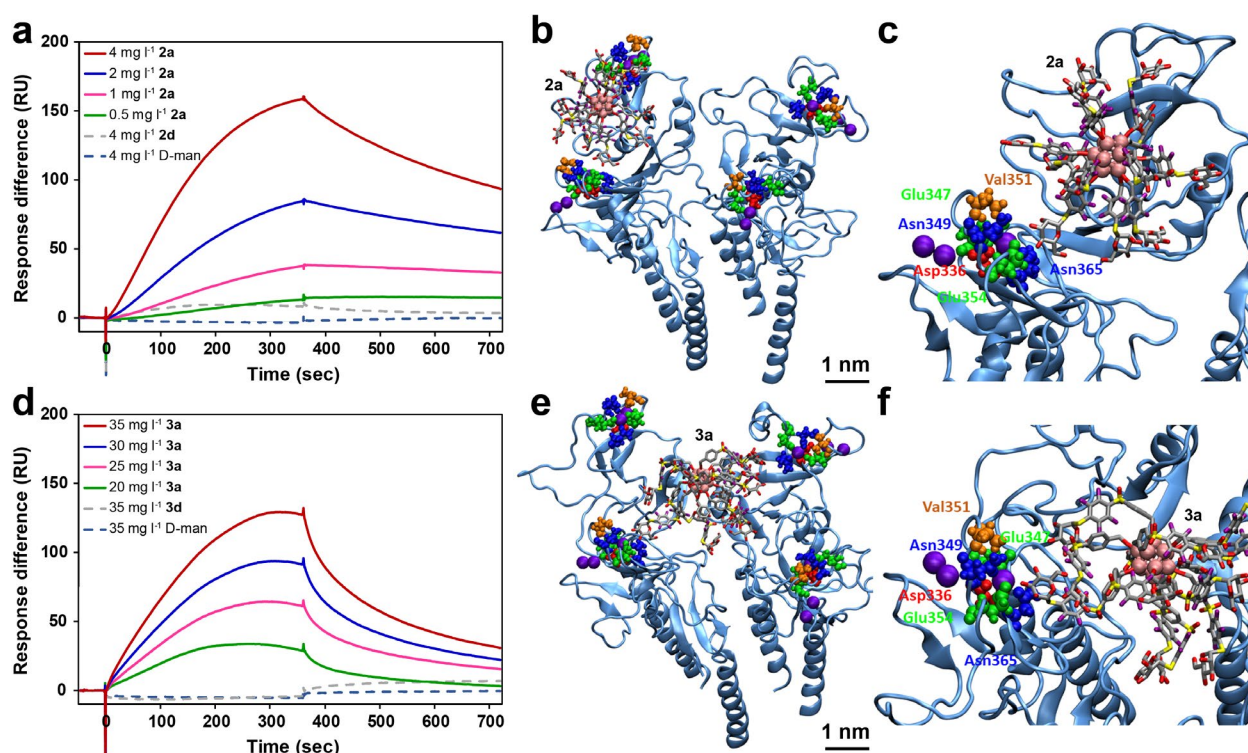


**Figure 3.2.** Multivalent binding interactions between mannose-functionalized nanomolecules and DC-SIGN. (a, d) SPR sensorgrams reveal dose-dependent multivalent binding of **2a** and **3a** to DC-SIGN, respectively, while the controls PEGylated clusters (**2d** and **3d**) and D-mannose exhibit minimal to no binding to DC-SIGN. In all SPR experiments, the flow rate is 5  $\mu\text{L}/\text{min}$ , and the analytes are injected for 6 minutes, followed by buffer flow. (b, e) Snapshots after 40 ns of MD simulations of the binding interactions between **2a/3a** and DC-SIGN. (c, f) Zoomed-in snapshots reveal each nanomolecule binding to the carbohydrate recognition sites of DC-SIGN.

Following the assembly and isolation of the glycosylated and PEGylated clusters, we proceeded to uncover the binding characteristics of the various nanomolecules toward an important dendritic cell receptor, DC-SIGN. Among the existing techniques that can experimentally elucidate the binding affinities between complex molecules and biomolecular targets, the surface plasmon resonance (SPR) technology represents a “gold standard” used by researchers in both academic and biotechnology communities.<sup>156,157</sup> Given the ability of the SPR technology to perform real-time, label-free detection of biomolecular interactions with high sensitivity,<sup>157</sup> we decided to use it for studying the binding interactions between the multivalent cluster nanomolecules and DC-SIGN. In the first set of SPR-based direct binding experiments, the tetrameric DC-SIGN extracellular domain (ECD) was immobilized on a commercial sensor chip *via* standard amide coupling, and the mannose-functionalized nanomolecules **2a** and **3a** were injected over the protein surface for real-time visualization of their respective binding interactions with DC-SIGN (see the Supporting Information for experimental details). The resulting sensorgrams (Figure 3.2a, d) reflect changes in the refractive index as molecules interact with the lectin surface, and reveal the dose-dependent binding response of **2a** and **3a**, respectively, toward DC-SIGN. By fitting the Langmuir 1:1 binding model to the binding curves of the mannose-coated clusters, we estimated  $K_D$  values of 0.11  $\mu\text{M}$  for **2a** and 5.0  $\mu\text{M}$  for **3a**. Compared to D-mannose (low mM affinity),<sup>126</sup> these multivalent systems exhibit avidities three to four orders of magnitude higher for DC-SIGN through the cluster glycoside effect.<sup>84</sup> To further understand the dynamics of the multivalent interactions, we performed computational studies using a tetrameric model derived from an X-ray structure of DC-SIGN (see the Supporting Information for experimental details).<sup>127,158</sup> Molecular dynamics (MD) simulations of the interactions between the DC-SIGN model and **2a/3a** over 40 ns were conducted, and snapshots were taken at the end of both

simulations (Figure 3.2b–c/e–f, respectively; see the Supporting Information for experimental details). The MD data suggest that consistent with previous reports using monosaccharides and oligosaccharides,<sup>126,127</sup> the equatorial 3-OH and 4-OH groups on the cluster-linked mannose residues engage in Ca<sup>2+</sup>-mediated binding in the carbohydrate recognition sites. Furthermore, **2a** was observed to stay longer than **3a** near the binding site of the protein model (Figure S3.16), which agrees with the lower  $K_D$  value of **2a** determined from the SPR experiments. A possible explanation for the observed difference in avidity is the flexibility of the linker – while the extended linker in **3a** is still rigid, it allows more flexibility compared to the benzylic linker in **2a**. Although a more flexible linker can relax the requirements for the precise positioning of ligands on a multivalent scaffold, it can also lower the overall affinity for a target protein.<sup>123</sup>

After analyzing the binding interactions of mannose-coated cluster nanomolecules toward DC-SIGN, we hypothesized that the clusters grafted with other saccharides would exhibit different protein-binding behaviors. Therefore, we conducted another set of SPR-based direct binding studies with the glucose-coated nanomolecules (**2c** and **3c**) (Figures S3.1 and S3.2), which yielded  $K_D$  values of 0.18 and 30  $\mu\text{M}$ , respectively. These similar but slightly higher  $K_D$  values compared to the mannose-coated analogs agree with results from previous reports using monosaccharides,<sup>126,159</sup> which suggest the equatorial 3- and 4-OH groups on glucose allow a similar binding interaction with DC-SIGN. In contrast, the galactose-coated species (**2b** and **3b**) were unable to engage DC-SIGN with similar avidities (the estimated  $K_D$  values were 0.87 and 96  $\mu\text{M}$ , respectively; Figures S3.3 and S3.4). This finding is also consistent with prior reports with monosaccharides and glycopolymers,<sup>126,138,159</sup> since the axial 4-OH group on galactose prevents proper recognition by the carbohydrate-binding sites on DC-SIGN. In contrast, the controls – PEGylated clusters (**2d** and **3d**) and D-mannose – exhibit minimal to no binding to the protein



surface when injected at the highest mass concentrations with respect to **2a** and **3a** (Figure 3.2a, d). Overall, these experiments reveal the dramatically enhanced binding avidities of the glycosylated cluster nanomolecules as a result of multivalency and highlight a potentially intricate relationship between the scaffold flexibility and the binding affinity. Nevertheless, in nature DC-SIGN is known to be a very flexible transmembrane receptor that can reposition its carbohydrate recognition domains to adapt to the ligands,<sup>160</sup> and this dynamic behavior is not fully captured by the immobilized protein setup in the *in vitro* SPR and *in silico* MD experiments.

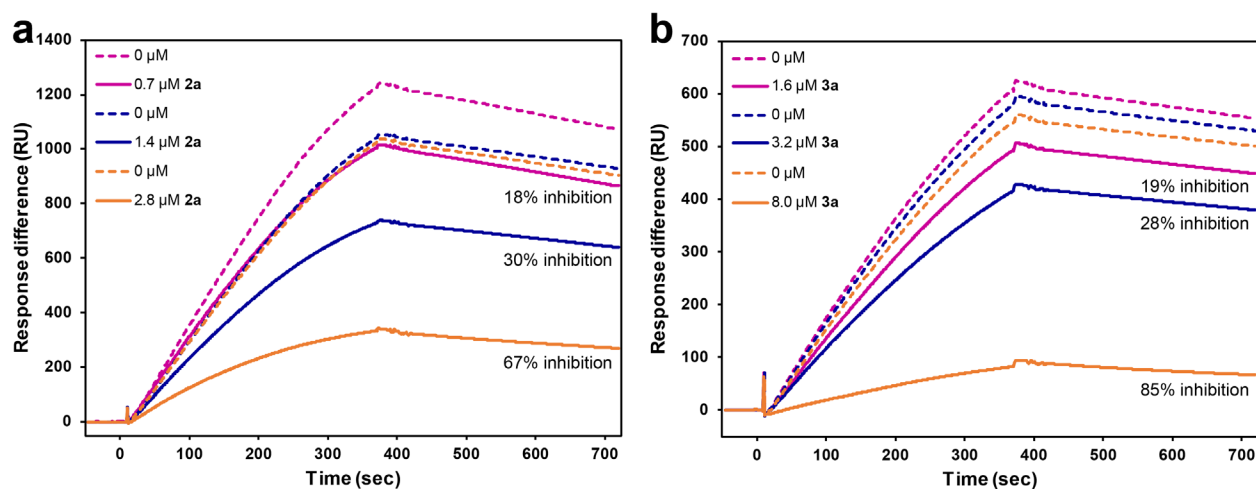


**Figure 3.3.** Mannose-functionalized clusters are capable of inhibiting protein-protein interactions. (a, b) SPR-based competitive binding studies suggest that **2a** and **3a** effectively compete against immobilized gp120 to bind free DC-SIGN, which leads to reduced binding responses.

Therefore, we turned to SPR-based competitive binding assays in order to test 1) whether free (vs immobilized) DC-SIGN exhibits different binding characteristics to the cluster nanomolecules and 2) whether the mannose-coated species can inhibit the protein-protein interactions between DC-SIGN and a sub-nM binder, HIV-1 gp120.<sup>138,161</sup> In these competition experiments, 100 nM DC-SIGN and various concentrations of the nanomolecules were co-injected over the surface-immobilized gp120, and the binding response of each injection was compared to

that of each preceding injection of DC-SIGN alone for an estimation of the % inhibition of the DC-SIGN–gp120 interaction. As shown in Figure 3.3, **2a** and **3a** can both inhibit free DC-SIGN from attaching to gp120, with  $IC_{50}$  values of 2.0 and 5.2  $\mu$ M, respectively. These values are over three orders of magnitude lower than the reported  $IC_{50}$  of monovalent D-mannose (6–9 mM),<sup>159,162</sup> indicating dramatically enhanced inhibition. Notably, compared with the  $IC_{50}$  values from a similar SPR-based competition assay using a multivalent third-generation dendrimer (50  $\mu$ M, 32 mannose residues),<sup>141</sup> these values are an order of magnitude lower. These results suggest that rigid inorganic cluster-based nanomolecules featuring significantly fewer (12) saccharides can serve as more potent inhibitors of this protein-protein interaction. Furthermore, in agreement with the direct binding data, the galactose-coated (**2b**, **3b**) and PEGylated (**2d**, **3d**) nanomolecules as well as D-mannose were less successful at inhibiting this interaction (Figures S3.5 and S3.6). Overall, these competition studies demonstrate for the first time the ability of multivalent glycosylated cluster nanomolecules to effectively compete against a sub-nM-binding viral glycoprotein for DC-SIGN. This suggests that a rigid cluster scaffold-based multivalent display of carbohydrates that mimics the natural highly glycosylated proteins on the surface of pathogens can be engineered to inhibit the interactions between a cell-based lectin receptor and a viral glycoprotein. Moreover, the similarity in  $IC_{50}$  values for **2a** and **3a** in contrast to their different  $K_D$  values could be due to a combination of the free (vs immobilized) DC-SIGN better adapting to the more flexible nanomolecule **3a** and the greater receptor surface coverage by the larger nanomolecule **3a**.

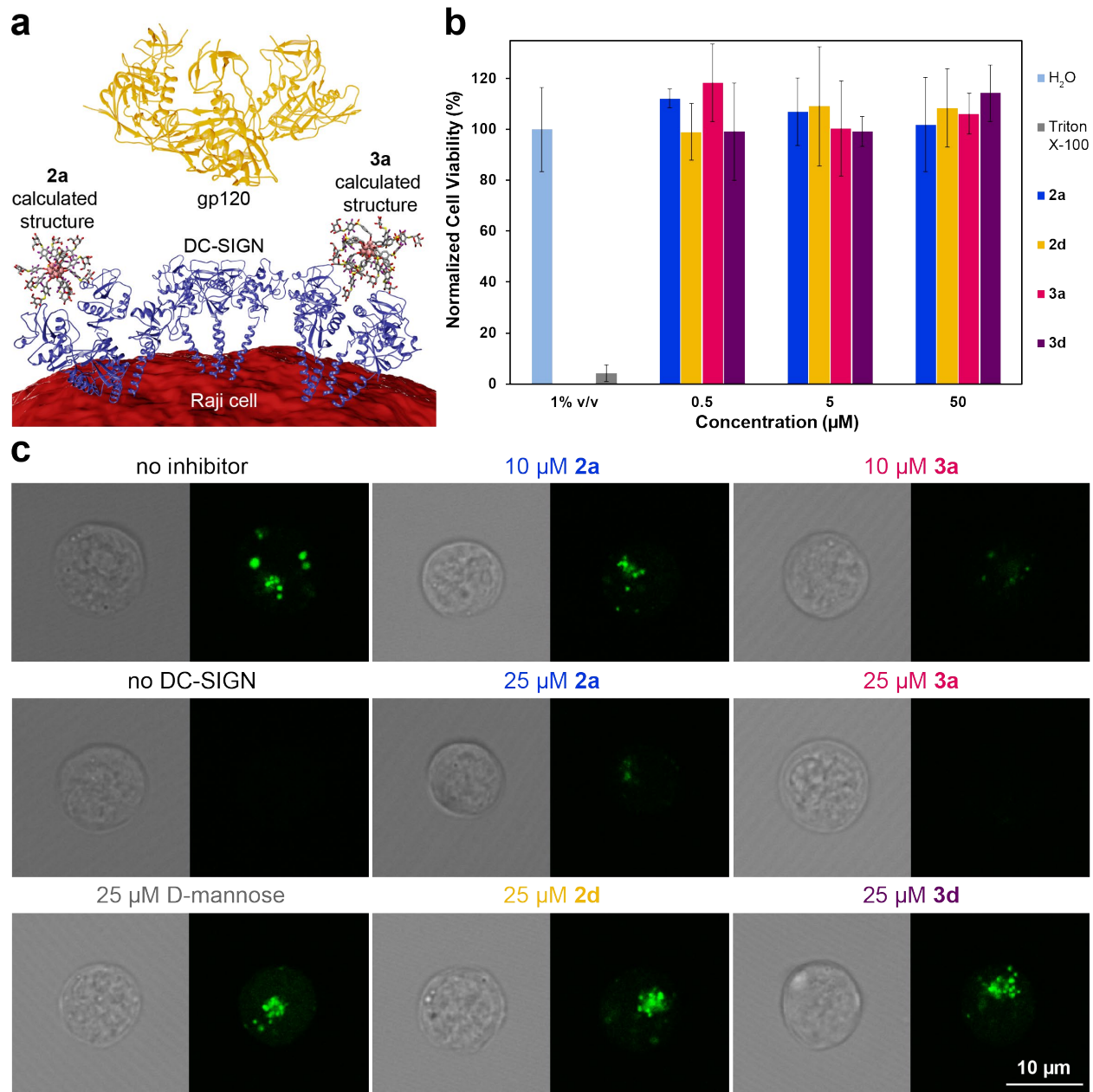


**Figure 3.4.** Biocompatible mannose-coated cluster nanomolecules can serve as multivalent inhibitors to prevent the DC-SIGN-mediated cell uptake of gp120. (a) Glycosylated clusters can potentially inhibit the uptake of viral glycoproteins such as gp120 by blocking cell-surface DC-SIGN. Figure is not drawn to scale. (b) Mannose-coated and PEGylated clusters exhibit no apparent toxicity toward Raji DC-SIGN<sup>+</sup> cells at least up to 50 μM, as assessed by an MTS assay. (c) DC-SIGN-dependent cell uptake of gp120-FITC is inhibited by mannose-coated clusters (**2a** and **3a**), as indicated by confocal microscopy analysis. However, the controls PEGylated clusters (**2d** and **3d**) and D-mannose do not affect the uptake of gp120-FITC.

To further investigate the ability of the mannose-functionalized cluster nanomolecules to inhibit the protein-protein interactions between DC-SIGN and gp120 in an experimental setup more reminiscent of natural systems, we moved to cell-based studies using a DC-SIGN-expressing human lymphoblast-like cell line (Raji DC-SIGN+ cells) and HIV-1 gp120 (Figure 3.4a).<sup>163,164</sup> First, in order to gain a better understanding of the biocompatibility of the cluster nanomolecules, we conducted an MTS-based cell proliferation assay (see the Supporting Information for experimental details), and observed no apparent cytotoxic effects of the mannose-coated (**2a**, **3a**) and PEGylated (**2d**, **3d**) clusters toward Raji DC-SIGN+ cells at 0.5–50  $\mu$ M concentrations (Figure 3.4b). This finding allowed the evaluation of the nanomolecules' potential biological function in inhibiting the attachment of gp120 to cell-surface DC-SIGN. Fluorescein isothiocyanate-labeled gp120 (gp120-FITC) undergoes significant uptake by Raji DC-SIGN+ cells (Figure 3.4c), as observed by a confocal laser scanning microscopy-based assay (see the Supporting Information for experimental details and Figures S3.7–S3.15). This internalization is DC-SIGN-dependent since no gp120-FITC uptake was observed in a Raji cell line not expressing DC-SIGN (Figure 3.4c).<sup>165,166</sup> In order to test competitive inhibition, we introduced mixtures of gp120-FITC and mannose-coated clusters **2a/3a** to Raji DC-SIGN+ cells, and observed reduced gp120-FITC uptake as a function of the cluster concentration (10 to 25  $\mu$ M) (Figure 3.4c). Notably, at the same concentrations, **3a** was more effective than **2a** at preventing the binding and uptake of gp120-FITC. This result suggests that **3a** can bind DC-SIGN in its natural transmembrane conformation better, which could be due to its higher flexibility and larger size. Furthermore, these cell-based studies capture important information about the dynamic receptor-mediated antigen internalization process,<sup>167</sup> thus enabling us to assess both the nanomolecules' binding to DC-SIGN and the inhibition of antigen uptake. Consistent with the presented SPR-based direct and competitive

binding data, the control molecules – PEGylated clusters (**2d** and **3d**) and D-mannose – were not able to bind to DC-SIGN and inhibit gp120 uptake at 25  $\mu$ M (Figure 3.4c). Overall, the biological studies in cells reveal that biocompatible mannose-functionalized cluster nanomolecules are capable of competing against HIV-1 gp120 for cell-surface DC-SIGN and thereby preventing the receptor-mediated internalization of a viral envelope component.

## Conclusions

We have demonstrated the rapid assembly of multivalent glycosylated inorganic cluster nanomolecules capable of inhibiting protein-protein interactions. Specifically, a dense layer of thiolated saccharides can be grafted on a rigid perfluoroaryl-perfunctionalized B<sub>12</sub> cluster within 15 minutes in mixed aqueous/organic media using S<sub>N</sub>Ar chemistry. The resulting fully covalent glycosylated assemblies can serve as multivalent binders with dramatically enhanced affinity compared to monovalent saccharides toward target lectins. We showed an example of using these hybrid agents for engendering ligand-specific, multivalent recognition with a biologically important dendritic cell receptor, DC-SIGN. Importantly, we demonstrated the ability of the cluster nanomolecules to inhibit protein-protein interactions between DC-SIGN and a sub-nM-binding HIV-1 envelope glycoprotein in a competitive binding study. We further found these clusters to be biocompatible in a human cell line and capable of preventing the internalization of gp120 by DC-SIGN-expressing cells. Notably, we uncovered an intricate interplay between the structural designs of multivalent binders and their biological activities. Ultimately, this work showcases a rare example of the application of tunable, stable inorganic cluster-based nanomolecules as valuable tools for studying the rules that govern multivalent interactions and disrupting protein-protein interactions.<sup>168–170</sup>

## Experimental Section

### General considerations

Microwave synthesis reactions and all post-microwave work-up and characterization were performed under ambient conditions. For the purposes of this manuscript, “ambient conditions” refer to room temperature (20 - 28 °C) and uncontrolled laboratory air.

### Materials

Deuterated solvents were purchased from Cambridge Isotope Laboratories. MilliQ water described in this manuscript refers to purified water with a resistivity at 25 °C of  $\leq 18.2$  M $\Omega$ -cm. [NEt<sub>3</sub>H]<sub>2</sub>[B<sub>12</sub>H<sub>12</sub>] was purchased from Boron Specialties. EtOH (200 proof) was purchased from Decon Labs. *N*-bromosuccinimide (NBS, 99%) was purchased from Oakwood Chemical. 1-thio- $\alpha$ -D-mannose sodium salt ( $\geq 98\%$ ) was purchased from Carbosynth.  $\beta$ -D-galactose pentaacetate ( $\geq 98\%$ ) and 1-thio- $\beta$ -D-galactose sodium salt ( $\geq 95\%$ ) was purchased from Chem-Impex. 1-thio- $\beta$ -D-glucose sodium salt (97%), D-(+)-mannose ( $\geq 99\%$ ), NaCl ( $\geq 99\%$ ), MgSO<sub>4</sub> (anhydrous), *meta*-chloroperoxybenzoic acid (mCPBA, 70–75%), CHCl<sub>3</sub> ( $\geq 99.8\%$ ), Na<sub>3</sub>PO<sub>4</sub> ( $\geq 96\%$ ), CaCl<sub>2</sub>·2 H<sub>2</sub>O ( $\geq 99\%$ ), Tween 20, Triton X-100 (98%), D-PBS, RPMI 1640 medium with L-glutamine (no phenol red), bovine serum albumin (BSA), Dowex 50WX8-400 ion exchange resin, and Nunc 96-well polystyrene flat-bottom plates were purchased from Fisher Scientific. 1-thio- $\beta$ -D-glucose tetraacetate (97%), *O*-(2-mercaptoethyl)-*O*'-methyl-hexa(ethylene glycol) (average M<sub>n</sub> 356.48 Da,  $\geq 95\%$ ), HCl (37%), *N,N*-diisopropylethylamine (DIEA,  $\geq 99\%$ ), K<sub>3</sub>PO<sub>4</sub> ( $\geq 98\%$ ), sodium methoxide (NaOMe, 95%), triethylamine ( $\geq 99\%$ ), 2,2'-azobis(2-methylpropionitrile) (AIBN,

98%), *N,N*-dimethylformamide (DMF,  $\geq 99.8\%$ ; anhydrous, 99.8%), acetonitrile (MeCN,  $\geq 99.9\%$ ),  $\text{CH}_2\text{Cl}_2$  ( $\geq 99.5\%$ ), ethyl acetate ( $\geq 99.5\%$ ), hexanes ( $\geq 98.5\%$ ), MeOH ( $\geq 99.8\%$ ), 1,2-dichloroethane ( $\geq 99\%$ ), RPMI 1640 medium with L-glutamine, fetal bovine serum (FBS), penicillin-streptomycin, and trypan blue solution were purchased from Sigma-Aldrich. MTS assay kit, Fluoroshield mounting medium, and anti-DC-SIGN-PE were purchased from Abcam. HIV-1 gp120-FITC was purchased from ImmunoDX. Human BD Fc block was purchased from BD Biosciences.

The following reagents were obtained through the NIH AIDS Reagent Program, Division of AIDS, NIAID, NIH: pcDNA3-DC-SIGN from Drs. S. Pöhlmann, F. Baribaud, F. Kirchhoff, and R.W. Doms,<sup>171</sup> HIV-1 CM235 gp120 recombinant protein from NIAID, DAIDS, and both Raji and Raji DC-SIGN+ cells from Drs. Li Wu and Vineet N. KewalRamani.<sup>163</sup> DC-SIGN expression in the cell lines was monitored with immunofluorescence assays using anti-DC-SIGN-PE.

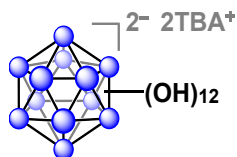
Synthetic procedures for 1-thio- $\beta$ -D-mannose tetraacetate were adapted from previous reports.<sup>152,153</sup> Synthetic procedures for 1-thio- $\beta$ -D-galactose tetraacetate were also adapted from previous reports.<sup>153,154</sup> Soluble recombinant DC-SIGN Extracellular Domain (ECD) was produced in *E. coli* and purified *via* affinity chromatography and refolded as described previously,<sup>159</sup> then further purified *via* size exclusion chromatography.

## Instruments

A CEM Discover SP microwave synthesis reactor was used for microwave reactions. Bruker AV300 and AV400 spectrometers were used to obtain  $^1\text{H}$ ,  $^{11}\text{B}$ ,  $^{13}\text{C}\{^1\text{H}\}$ , and  $^{19}\text{F}$  NMR spectra, and Bruker Topspin software was used to process the NMR data.  $^1\text{H}$  and  $^{13}\text{C}\{^1\text{H}\}$  NMR spectra

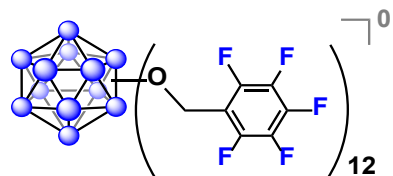
were referenced to residual solvent resonances in deuterated solvents (due to high humidity, H<sub>2</sub>O resonances are often present). <sup>11</sup>B and <sup>19</sup>F NMR spectra were referenced to BF<sub>3</sub>·Et<sub>2</sub>O external standard. *In situ* <sup>11</sup>B and <sup>19</sup>F NMR spectroscopy experiments were run unlocked and unshimmed. <sup>11</sup>B and <sup>19</sup>F NMR spectra were baseline-corrected using the cubic spline correction tool within the Bruker Topspin software. ESI-HRMS data were acquired with a Thermo Scientific Q-Exactive Plus instrument with a quadrupole mass filter and Orbitrap mass analyzer. GC-MS data were collected on an Agilent 7890B GC-MS equipped with an HP-5 column with He carrier gas and a 7250 Accurate-Mass Q-TOF. Surface plasmon resonance (SPR) experiments were run on a GE Healthcare Life Sciences Biacore T200 instrument. MTS assay absorbance measurements were taken with a BioTek Instruments ELx800 plate reader. Confocal microscopy images were acquired with a Leica TCS SPE confocal microscope.

### Synthesis of 1



The [N<sup>n</sup>Bu<sub>4</sub>]<sub>2</sub> salt of [B<sub>12</sub>(OH)<sub>12</sub>]<sup>2-</sup> was prepared according to previous report.<sup>81</sup>

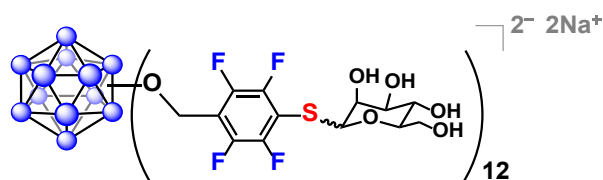
### Synthesis of 2





A previously reported protocol<sup>82</sup> for **2** was adapted as follows: **1** (2.00 g, 2.44 mmol) was transferred out of a N<sub>2</sub>-filled glovebox, opened to air, and dissolved in 20 mL acetonitrile in a 80 mL glass microwave vial. DIEA (8.0 mL, 46 mmol) and 2,3,4,5,6-pentafluorobenzyl bromide (12.0 mL, 79.5 mmol) were added along with an oval rare earth stir bar, the vial was sealed with a Teflon/silicone cap, and the mixture was heated at 140 °C with stirring in the microwave for 45 minutes. The volatiles were removed *via* rotary evaporation, and the excess linker was eluted first through a slurry-packed silica gel column with 65/35 hexanes/ethyl acetate, and the cluster (pink/purple) was eluted with acetone. The volatiles were removed *via* rotary evaporation, and the remaining 1-/2- charged product mixture was dissolved in 30 mL acetonitrile, to which NOBF<sub>4</sub> (0.67 g, 5.7 mmol) was added and the mixture was left to stir for 48 hours. Following oxidation, the mixture was filtered and washed three times with cold acetonitrile on a glass frit, and the product was collected and dried under high vacuum to obtain a yellow-orange solid (5.22 g, 86%). The characterization data of this compound are consistent with those reported previously.

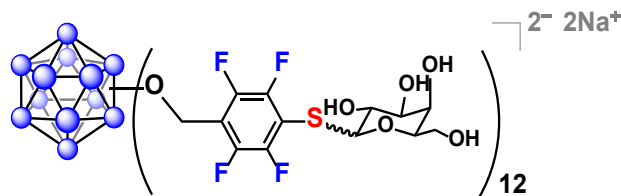
### Synthesis of 2a



**2** (2.0 mg, 0.00080 mmol), 1-thio- $\beta$ -D-mannose tetraacetate (15.5 mg, 0.0425 mmol), and K<sub>3</sub>PO<sub>4</sub> (14.3 mg, 0.0673 mmol) were added along with a flea micro stir bar to a 4 mL glass vial, which was then sealed with a PTFE/silicone cap under ambient conditions. The vial was then purged and backfilled with N<sub>2</sub> three times before being transferred into the glovebox. In the glovebox, the vial was opened and 90  $\mu$ L anhydrous DMF was added. The vial was sealed again and the reaction

mixture was allowed to stir at room temperature for 48 hours. Then, the vial was transferred out of the glovebox, and its contents were diluted and transferred into an NMR tube for *in situ*  $^{19}\text{F}$  NMR spectroscopy to ensure nearly quantitative conversion and *in situ*  $^{11}\text{B}$  NMR spectroscopy to ensure structural integrity of the cluster. The mixture was then transferred to a 15 mL conical polypropylene tube and lyophilized for solvent removal. The resulting residue was treated with NaOMe (2.8 mg, 0.052 mmol) in 0.6 mL 2:1 MeOH:CHCl<sub>3</sub> and allowed to stir for 40 minutes. The volatiles were removed *via* rotary evaporation. The mixture was then redissolved in water and adjusted to pH 7 with 1 M HCl. This solution was filtered through a 1K MWCO Microsep Advance centrifugal device (Pall Life Sciences) three times for the removal of base and excess reagent. The purified material was dried and subjected to characterization *via*  $^1\text{H}$ ,  $^{11}\text{B}$ , and  $^{19}\text{F}$  NMR spectroscopy and ESI-HRMS. This pure product as indicated by NMR spectroscopy and mass spectrometry was dried to obtain an isolated yield of 3.0 mg (80%).  $^1\text{H}$  NMR (400 MHz, MeOD):  $\delta$  5.53 – 5.46 (br m, 24H, OCH<sub>2</sub>), 4.97, 4.08 – 3.47, 3.15 – 3.13 (m, 84H, SCHCH<sub>2</sub>OH(CHOH)<sub>3</sub>CHO).  $^{11}\text{B}$  NMR (128 MHz, MeOD):  $\delta$  -15.7.  $^{19}\text{F}$  NMR (376 MHz, MeOD):  $\delta$  -136.6 – -137.0 (m, 24F, *-meta*), -144.6 – -144.9 (m, 24F, *-ortho*). ESI-HRMS (-): m/z calculated for C<sub>156</sub>H<sub>156</sub>B<sub>12</sub>F<sub>48</sub>O<sub>72</sub>S<sub>12</sub> (M<sup>2-</sup>), 2304.2772 Da; found, 2304.2776 Da.

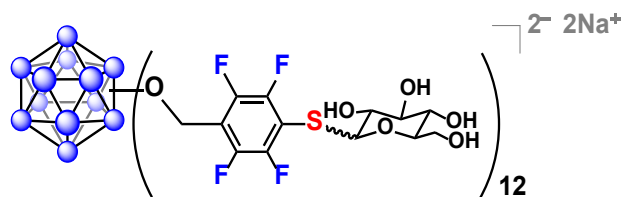
### Synthesis of 2b



**2** (2.0 mg, 0.00080 mmol), 1-thio-β-D-galactose tetraacetate (11.7 mg, 0.0321 mmol), and K<sub>3</sub>PO<sub>4</sub> (7.7 mg, 0.036 mmol) were added along with a flea micro stir bar to a 4 mL glass vial, which was

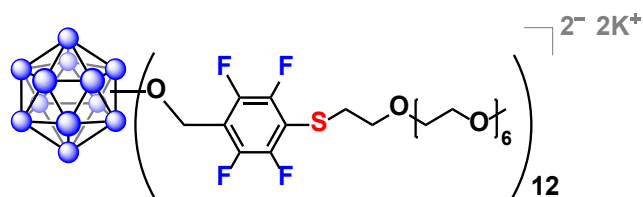
then sealed with a PTFE/silicone cap under ambient conditions. The vial was then purged and backfilled with N<sub>2</sub> three times before being transferred into the glovebox. In the glovebox, the vial was opened and 90 μL anhydrous DMF was added. The vial was sealed again and the reaction mixture was allowed to stir at room temperature for 48 hours. Then, the vial was transferred out of the glovebox, and its contents were diluted and transferred into an NMR tube for *in situ* <sup>19</sup>F NMR spectroscopy to ensure nearly quantitative conversion and *in situ* <sup>11</sup>B NMR spectroscopy to ensure structural integrity of the cluster. The mixture was then transferred to a 15 mL conical polypropylene tube and lyophilized for solvent removal. The resulting residue was treated with NaOMe (2.1 mg, 0.039 mmol) in 0.6 mL 2:1 MeOH:CHCl<sub>3</sub> and allowed to stir for 40 minutes. The volatiles were removed *via* rotary evaporation. The mixture was then redissolved in water and adjusted to pH 7 with 1 M HCl. This solution was filtered through a 1K MWCO Microsep Advance centrifugal device three times for the removal of base and excess reagent. The purified material was dried and subjected to characterization *via* <sup>1</sup>H, <sup>11</sup>B, and <sup>19</sup>F NMR spectroscopy and ESI-HRMS. This pure product as indicated by NMR spectroscopy and mass spectrometry was dried to obtain an isolated yield of 3.1 mg (84%). <sup>1</sup>H NMR (400 MHz, MeOD): δ 5.54 – 5.48 (br m, 24H, OCH<sub>2</sub>), 5.75 – 5.74, 4.69 – 4.66, 4.17 – 3.44 (m, 84H, SCH<sub>2</sub>CH<sub>2</sub>OH(CHOH)<sub>3</sub>CHO). <sup>11</sup>B NMR (128 MHz, MeOD): δ -15.7. <sup>19</sup>F NMR (376 MHz, MeOD): δ -136.3 – -137.0 (m, 24F, *-meta*), -145.0 (br m, 24F, *-ortho*). ESI-HRMS (-): m/z calculated for C<sub>156</sub>H<sub>156</sub>B<sub>12</sub>F<sub>48</sub>O<sub>72</sub>S<sub>12</sub> (M<sup>2-</sup>), 2304.2772 Da; found, 2304.3096 Da.

## Synthesis of 2c



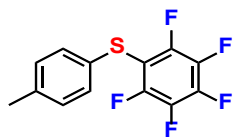
A previously reported protocol<sup>6</sup> was adapted as follows: **2** (2.0 mg, 0.00080 mmol), 1-thio-β-D-glucose tetraacetate (9.0 mg, 0.025 mmol), and K<sub>3</sub>PO<sub>4</sub> (8.0 mg, 0.038 mmol) were added along with a flea micro stir bar to a 4 mL glass vial, which was then sealed with a PTFE/silicone cap under ambient conditions. The vial was then purged and backfilled with N<sub>2</sub> three times before being transferred into the glovebox. In the glovebox, the vial was opened and 90 μL anhydrous DMF was added. The vial was sealed again and the reaction mixture was allowed to stir at room temperature for 24 hours. Then, the vial was transferred out of the glovebox, and its contents were diluted and transferred into an NMR tube for *in situ* <sup>19</sup>F NMR spectroscopy to ensure nearly quantitative conversion and *in situ* <sup>11</sup>B NMR spectroscopy to ensure structural integrity of the cluster. The mixture was then transferred to a 15 mL conical polypropylene tube and lyophilized for solvent removal. The resulting residue was treated with NaOMe (1.6 mg, 0.030 mmol) in 0.6 mL 2:1 MeOH:CHCl<sub>3</sub> and allowed to stir for 40 minutes. The volatiles were removed *via* rotary evaporation. The mixture was then redissolved in water and adjusted to pH 7 with 1 M HCl. This solution was filtered through a 1K MWCO Microsep Advance centrifugal device three times for the removal of base and excess reagent. The purified material was dried and subjected to characterization *via* <sup>1</sup>H, <sup>11</sup>B, and <sup>19</sup>F NMR spectroscopy and ESI-HRMS. This pure product as indicated by NMR spectroscopy and mass spectrometry was dried to obtain an isolated yield of 2.4 mg (65%). The characterization data of this compound are consistent with those reported previously.

## Synthesis of 2d

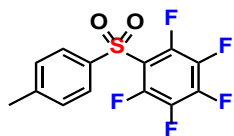


A previously reported protocol<sup>6</sup> was adapted as follows: **2** (2.0 mg, 0.00080 mmol) and K<sub>3</sub>PO<sub>4</sub> (3.4 mg, 0.016 mmol) were added along with a flea micro stir bar to a 4 mL glass vial, which was then sealed with a PTFE/silicone cap under ambient conditions. The vial was then purged and backfilled with N<sub>2</sub> three times before being transferred into the glovebox. In the glovebox, the vial was opened and 100  $\mu$ L anhydrous DMF was added, followed by mPEGthiol<sub>356</sub> (5.25  $\mu$ L, 0.0163 mmol). The vial was sealed again and the reaction mixture was allowed to stir at room temperature for 24 hours. The vial was transferred out of the glovebox, and its contents were diluted and transferred into an NMR tube for *in situ* <sup>19</sup>F NMR spectroscopy to ensure nearly quantitative conversion and *in situ* <sup>11</sup>B NMR spectroscopy to ensure structural integrity of the cluster. The mixture was then transferred to a 15 mL conical polypropylene tube and lyophilized for solvent removal. The resulting residue was redissolved in water and filtered through a 1K MWCO Microsep Advance centrifugal device three times for the removal of base and excess reagent. The purified material was dried and subjected to characterization *via* <sup>1</sup>H, <sup>11</sup>B, and <sup>19</sup>F NMR spectroscopy and ESI-HRMS. This pure product as indicated by NMR spectroscopy and mass spectrometry was dried to obtain an isolated yield of 4.0 mg (76%). The characterization data of this compound are consistent with those reported previously.

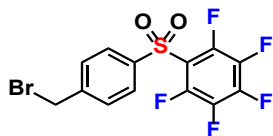
## Synthesis of sulfone-bridged linker



A synthetic procedure for perfluorophenyl *p*-tolyl sulfide was derived from a previously reported protocol for perfluorophenyl phenyl sulfide.<sup>172</sup> Specifically, *p*-bromotoluene (0.47 mL, 3.8 mmol) was dissolved in 7 mL N<sub>2</sub>-purged anhydrous DMF, placed under a positive N<sub>2</sub> flow, and heated at 140 °C while stirring for 15 minutes. Then, CuSC<sub>6</sub>F<sub>5</sub> (1.5 g, 5.7 mmol) was added to the solution, and the reaction mixture was stirred and heated for 7 hours. The reaction mixture was then cooled down and quenched with 40 mL 10% HCl solution. This mixture was extracted with ether, and the organic layer was washed three times with saturated NaCl solution. The organic layer was then dried over MgSO<sub>4</sub> and filtered through Celite on a glass frit. The volatiles were removed *via* rotary evaporation, and the residue was subjected to silica gel column chromatography in hexanes, using UV light for TLC plate visualization. The fractions corresponding to the product were combined, and the volatiles were removed *via* rotary evaporation. The product was dried under high vacuum to afford a clear colorless oil (445 mg, 40%). <sup>1</sup>H NMR (400 MHz, CDCl<sub>3</sub>): δ 7.33 (d, 2H, C<sub>6</sub>H<sub>2</sub>H<sub>2</sub>), 7.13 (d, 2H, C<sub>6</sub>H<sub>2</sub>H<sub>2</sub>), 2.35 (s, 3H, C<sub>6</sub>H<sub>4</sub>CH<sub>3</sub>). <sup>13</sup>C{<sup>1</sup>H} NMR (400 MHz, CDCl<sub>3</sub>): δ 147.6, 142.0, 138.7, 137.9, 131.6, 130.3, 129.4, 110.0, 21.1. <sup>19</sup>F NMR (376 MHz, CDCl<sub>3</sub>): δ -132.3 – -132.4 (q, 2F, -ortho), -152.2 – -152.3 (t, 1F, -para), -160.9 – -161.0 (m, 2F, -meta). GC-MS: m/z calculated for C<sub>13</sub>H<sub>7</sub>F<sub>5</sub>S, 290.0189 Da; found, 290.0175 Da.



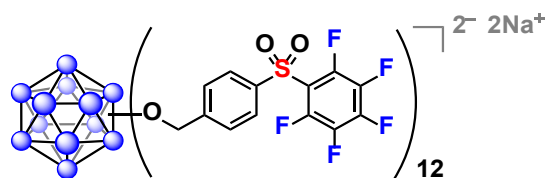
Perfluorophenyl *p*-tolyl sulfide (923 mg, 3.18 mmol) was dissolved in 20 mL CHCl<sub>3</sub>, and the solution was cooled to 0 °C while stirring. mCPBA (2.47 g, 14.3 mmol) was slowly added to solution, and the reaction mixture was stirred at 0 °C to room temperature for 18 hours. Then, the reaction mixture was dried and subjected to a silica plug in CH<sub>2</sub>Cl<sub>2</sub>. The resulting solution was dried *via* rotary evaporation followed by high vacuum, providing perfluorophenyl *p*-tolyl sulfone as a white solid (976 mg, 95%). <sup>1</sup>H NMR (400 MHz, CDCl<sub>3</sub>): δ 7.92 (d, 2H, C<sub>6</sub>H<sub>2</sub>H<sub>2</sub>), 7.38 (d, 2H, C<sub>6</sub>H<sub>2</sub>H<sub>2</sub>), 2.45 (s, 3H, C<sub>6</sub>H<sub>4</sub>CH<sub>3</sub>). <sup>13</sup>C {<sup>1</sup>H} NMR (400 MHz, CDCl<sub>3</sub>): δ 146.5, 144.8, 138.0, 137.9, 130.4, 128.0, 117.9, 21.8. <sup>19</sup>F NMR (376 MHz, CDCl<sub>3</sub>): δ -136.0 – -136.1 (m, 2F, -ortho), -144.8 – -144.9 (m, 1F, -para), -158.7 – -158.8 (m, 2F, -meta). GC-MS: m/z calculated for C<sub>13</sub>H<sub>7</sub>F<sub>5</sub>SO<sub>2</sub>, 322.0087 Da; found, 322.0071 Da.



A flask containing perfluorophenyl *p*-tolyl sulfone (945 mg, 2.93 mmol) and AIBN (48 mg, 0.29 mmol) was purged with N<sub>2</sub>, then 15 mL 1,2-dichloroethane was added. This mixture was heated at 83 °C with stirring for 30 minutes. Then, NBS (574 mg, 3.23 mmol) dissolved in 20 mL 1,2-dichloroethane was slowly added over 30 minutes. The reaction mixture was stirred and heated for 1.5 hours, then it was cooled and dried. The residue was taken up in CH<sub>2</sub>Cl<sub>2</sub> and washed three times with saturated NaCl solution. The organic layer was then dried over MgSO<sub>4</sub> and filtered through Celite on a glass frit. The volatiles were removed *via* rotary evaporation, and the residue was dried under high vacuum to afford a white solid (1.00 g) consisting of the product and a small

amount of the tolyl precursor, which does not affect cluster synthesis.  $^1\text{H}$  NMR (400 MHz,  $\text{CDCl}_3$ ):  $\delta$  8.03 (d, 2H,  $\text{C}_6\text{H}_2\text{H}_2$ ), 7.61 (d, 2H,  $\text{C}_6\text{H}_2\text{H}_2$ ), 4.50 (s, 2H,  $\text{C}_6\text{H}_4\text{CH}_2\text{Br}$ ).  $^{13}\text{C}\{^1\text{H}\}$  NMR (400 MHz,  $\text{CDCl}_3$ ):  $\delta$  145.2, 140.5, 138.1, 130.3, 128.5, 117.3, 31.1.  $^{19}\text{F}$  NMR (376 MHz,  $\text{CDCl}_3$ ):  $\delta$  -135.5 – -135.6 (m, 2F, -ortho), -143.7 – -143.9 (m, 1F, -para), -158.1 – -158.3 (m, 2F, -meta). GC-MS:  $m/z$  calculated for  $\text{C}_{13}\text{H}_6\text{F}_5\text{SO}_2\text{Br}$ , 399.9192 Da; found ( $\text{C}_{13}\text{H}_6\text{F}_5\text{SO}_2$ ), 320.9985 Da.

### Synthesis of 3

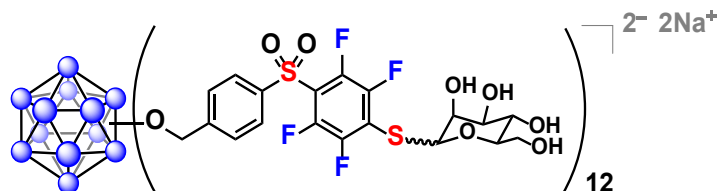


**1** (62 mg, 0.076 mmol) was transferred out of a  $\text{N}_2$ -filled glovebox, opened to air, and dissolved in 1.2 mL acetonitrile in a 10 mL glass microwave vial. DIEA (0.25 mL, 1.4 mmol) and linker (928 mg) were added along with a flea micro stir bar, the vial was sealed with a PTFE/silicone cap, and the mixture was heated at 140  $^\circ\text{C}$  with stirring in the microwave for 30 minutes. The volatiles were removed *via* rotary evaporation, and the excess linker was eluted first through a triethylamine-pretreated slurry-packed silica gel column with 65/35 hexanes/ethyl acetate, and the cluster (orange) was eluted with acetone. The volatiles were removed *via* rotary evaporation, and the product was dried under high vacuum to obtain an orange solid (320 mg, 94% isolated yield). 200 mg of this compound was dissolved in 5 mL acetonitrile first, then diluted with 50 mL 50/50 acetonitrile/water, and ion exchanged with  $\text{Na}^+$ -loaded Dowex 50WX8-400 resin slurry-packed into a 2 x 46 cm column (21 cm packed height). The ion-exchanged product was dried under high vacuum to obtain a light salmon-colored solid (180 mg, 96% isolated yield).  $^1\text{H}$  NMR (400 MHz,  $(\text{CD}_3)_2\text{CO}$ ):  $\delta$  7.71 (d, 24H,  $\text{C}_6\text{H}_2\text{H}_2$ ), 7.56 (d, 24H,  $\text{C}_6\text{H}_2\text{H}_2$ ), 5.52 (s, 24H,  $\text{OCH}_2$ ).  $^{11}\text{B}$  NMR (128



MHz, (CD<sub>3</sub>)<sub>2</sub>CO):  $\delta$  -14.5. <sup>19</sup>F NMR (376 MHz, (CD<sub>3</sub>)<sub>2</sub>CO):  $\delta$  -137.8 – -137.9 (m, 24F, -ortho), -146.7 – -146.8 (m, 12F, -para), -160.4 – -160.6 (m, 24F, -meta). ESI-HRMS (-): m/z calculated for C<sub>156</sub>H<sub>72</sub>B<sub>12</sub>F<sub>60</sub>O<sub>36</sub>S<sub>12</sub> (M<sup>2-</sup>), 2088.0305 Da; found, 2088.0291 Da.

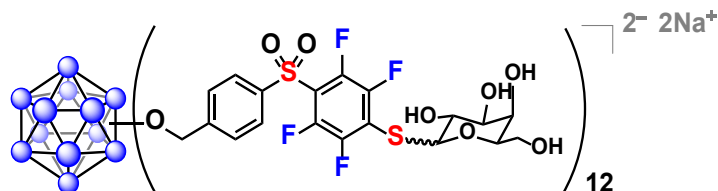
### Synthesis of 3a



Under ambient conditions, 1-thio- $\alpha$ -D-mannose sodium salt (1.3 mg, 0.0058 mmol) dissolved in 50  $\mu$ L MilliQ water was added to a 4 mL glass vial containing **3** (2.0 mg, 0.00047 mmol) dissolved in 50  $\mu$ L DMF and a flea micro stir bar. The vial was sealed with a PTFE/silicone cap and the reaction mixture was allowed to stir at room temperature for 10 minutes. Then, the vial was opened and its contents were diluted and transferred into an NMR tube for *in situ* <sup>19</sup>F NMR spectroscopy to ensure nearly quantitative conversion and *in situ* <sup>11</sup>B NMR spectroscopy to ensure structural integrity of the cluster. The mixture was then transferred to a 15 mL conical polypropylene tube and lyophilized for solvent removal. The mixture was then redissolved in water and filtered through a 1K MWCO Microsep Advance centrifugal device (Pall Life Sciences) three times for the removal of salt and excess reagent. The purified material was dried and subjected to characterization *via* <sup>1</sup>H, <sup>11</sup>B, and <sup>19</sup>F NMR spectroscopy and ESI-HRMS. This pure product as indicated by NMR spectroscopy and mass spectrometry was dried to obtain an isolated yield of 2.5 mg (83%). <sup>1</sup>H NMR (400 MHz, MeOD):  $\delta$  7.61 (d, 24H, C<sub>6</sub>H<sub>2</sub>H<sub>2</sub>), 7.44 (d, 24H, C<sub>6</sub>H<sub>2</sub>H<sub>2</sub>),  $\delta$  5.37 (br s, 24H, OCH<sub>2</sub>), 5.62, 4.11 – 4.10, 3.90 – 3.63 (m, 84H, SCH<sub>2</sub>CH<sub>2</sub>OH(CH<sub>2</sub>OH)<sub>3</sub>CHO). <sup>11</sup>B

NMR (128 MHz, MeOD):  $\delta$  -15.5.  $^{19}\text{F}$  NMR (376 MHz, MeOD):  $\delta$  -132.0 – -132.1 (m, 24F, -*meta*), -138.9 – -138.9 (m, 24F, -*ortho*). ESI-HRMS (-): m/z calculated for  $\text{C}_{228}\text{H}_{204}\text{B}_{12}\text{F}_{48}\text{O}_{96}\text{S}_{24}$  ( $\text{M}^{2-}$ ), 3145.7430 Da; found, 3145.7223 Da.

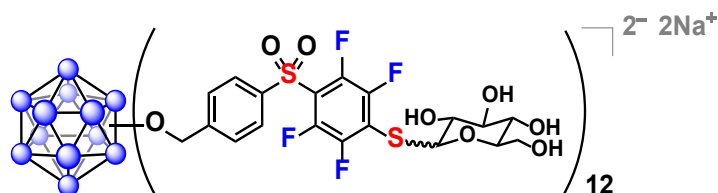
### Synthesis of 3b



Under ambient conditions, 1-thio- $\beta$ -D-galactose sodium salt (1.3 mg, 0.0058 mmol) dissolved in 50  $\mu\text{L}$  MilliQ water was added to a 4 mL glass vial containing **3** (2.0 mg, 0.00047 mmol) dissolved in 50  $\mu\text{L}$  DMF and a flea micro stir bar. The vial was sealed with a PTFE/silicone cap and the reaction mixture was allowed to stir at room temperature for 10 minutes. Then, the vial was opened and its contents were diluted and transferred into an NMR tube for *in situ*  $^{19}\text{F}$  NMR spectroscopy to ensure nearly quantitative conversion and *in situ*  $^{11}\text{B}$  NMR spectroscopy to ensure structural integrity of the cluster. The mixture was then transferred to a 15 mL conical polypropylene tube and lyophilized for solvent removal. The mixture was then redissolved in water and filtered through a 1K MWCO Microsep Advance centrifugal device (Pall Life Sciences) three times for the removal of salt and excess reagent. The purified material was dried and subjected to characterization *via*  $^1\text{H}$ ,  $^{11}\text{B}$ , and  $^{19}\text{F}$  NMR spectroscopy and ESI-HRMS. This pure product as indicated by NMR spectroscopy and mass spectrometry was dried to obtain an isolated yield of 2.0 mg (67%).  $^1\text{H}$  NMR (400 MHz, MeOD):  $\delta$  7.62 (d, 24H,  $\text{C}_6\text{H}_2\text{H}_2$ ), 7.44 (d, 24H,  $\text{C}_6\text{H}_2\text{H}_2$ ),  $\delta$  5.39 (br s, 24H,  $\text{OCH}_2$ ), 3.87 – 3.87, 3.63 – 3.49 (m, 84H,  $\text{SCHCH}_2\text{OH}(\text{CHOH})_3\text{CHO}$ ).  $^{11}\text{B}$  NMR (128 MHz, MeOD):  $\delta$  -15.5.  $^{19}\text{F}$  NMR (376 MHz, MeOD):  $\delta$  -132.5 – -132.6 (m, 24F, -*meta*), -

139.7 – -139.7 (m, 24F, *-ortho*). ESI-HRMS (-):  $m/z$  calculated for  $C_{228}H_{204}B_{12}F_{48}O_{96}S_{24}$  ( $M^{2-}$ ), 3145.7430 Da; found, 3145.7164 Da.

### Synthesis of 3c



#### Procedure using organic solvent

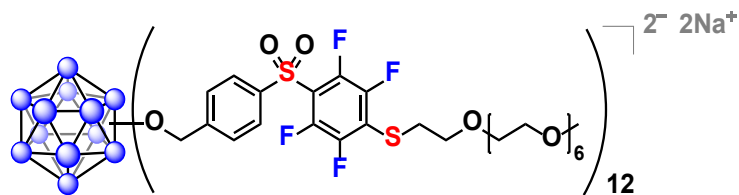
Under ambient conditions, **3** (2.0 mg, 0.00047 mmol) and 1-thio- $\beta$ -D-glucose sodium salt (1.3 mg, 0.0058 mmol) were added along with a flea micro stir bar to a 4 mL glass vial. Then, 100  $\mu$ L DMF was added, and the vial was sealed with a PTFE/silicone cap. The reaction mixture was allowed to stir at room temperature for 20 minutes. Then, the vial was opened and its contents were diluted and transferred into an NMR tube for *in situ*  $^{19}\text{F}$  NMR spectroscopy to ensure nearly quantitative conversion and *in situ*  $^{11}\text{B}$  NMR spectroscopy to ensure structural integrity of the cluster. The mixture was then transferred to a 15 mL conical polypropylene tube and lyophilized for solvent removal. The mixture was then redissolved in water and filtered through a 1K MWCO Microsep Advance centrifugal device (Pall Life Sciences) three times for the removal of salt and excess reagent. The purified material was dried and subjected to characterization *via*  $^1\text{H}$ ,  $^{11}\text{B}$ , and  $^{19}\text{F}$  NMR spectroscopy and ESI-HRMS. This pure product as indicated by NMR spectroscopy and mass spectrometry was dried to obtain an isolated yield of 2.3 mg (77%).

#### Procedure using mixed aqueous/organic media

Under ambient conditions, 1-thio- $\beta$ -D-glucose sodium salt (1.3 mg, 0.0058 mmol) dissolved in 50  $\mu$ L MilliQ water was added to a 4 mL glass vial containing **3** (2.0 mg, 0.00047 mmol) dissolved in 50  $\mu$ L DMF (or 50  $\mu$ L MeCN) and a flea micro stir bar. The vial was sealed with a PTFE/silicone cap and the reaction mixture was allowed to stir at room temperature for 10 minutes. Then, the vial was opened and its contents were diluted and transferred into an NMR tube for *in situ*  $^{19}\text{F}$  NMR spectroscopy to ensure nearly quantitative conversion and *in situ*  $^{11}\text{B}$  NMR spectroscopy to ensure structural integrity of the cluster.

$^1\text{H}$  NMR (400 MHz, MeOD):  $\delta$  7.61 (d, 24H, C<sub>6</sub>H<sub>2</sub>H<sub>2</sub>), 7.43 (d, 24H, C<sub>6</sub>H<sub>2</sub>H<sub>2</sub>),  $\delta$  5.38 (br s, 24H, OCH<sub>2</sub>), 3.72 – 3.54, 3.41 – 3.33, 3.27 – 3.25 (m, 84H, SCHCH<sub>2</sub>OH(CHOH)<sub>3</sub>CHO).  $^{11}\text{B}$  NMR (128 MHz, MeOD):  $\delta$  -15.4.  $^{19}\text{F}$  NMR (376 MHz, MeOD):  $\delta$  -132.7 (br m, 24F, *-meta*), -139.6 (br m, 24F, *-ortho*). ESI-HRMS (-): m/z calculated for C<sub>228</sub>H<sub>204</sub>B<sub>12</sub>F<sub>48</sub>O<sub>96</sub>S<sub>24</sub> (M<sup>2-</sup>), 3145.7430 Da; found, 3145.7291 Da.

### Synthesis of **3d**



**3** (2.0 mg, 0.00047 mmol) and Na<sub>3</sub>PO<sub>4</sub> (1.4 mg, 0.0085 mmol) were added along with a flea micro stir bar to a 4 mL glass vial, which was then sealed with a PTFE/silicone cap under ambient conditions. The vial was then purged and backfilled with N<sub>2</sub> three times before being transferred into the glovebox. In the glovebox, the vial was opened and 100  $\mu$ L anhydrous DMF was added, followed by mPEGthiol<sub>356</sub> (2.2  $\mu$ L, 0.0067 mmol). The vial was sealed again and the reaction

mixture was allowed to stir at room temperature for 1.5 hours. The vial was transferred out of the glovebox, and its contents were diluted and transferred into an NMR tube for *in situ*  $^{19}\text{F}$  NMR spectroscopy to ensure nearly quantitative conversion and *in situ*  $^{11}\text{B}$  NMR spectroscopy to ensure structural integrity of the cluster. The mixture was then transferred to a 15 mL conical polypropylene tube and lyophilized for solvent removal. The resulting residue was redissolved in water and filtered through a 1K MWCO Microsep Advance centrifugal device three times for the removal of base and excess reagent. The purified material was dried and subjected to characterization *via*  $^1\text{H}$ ,  $^{11}\text{B}$ , and  $^{19}\text{F}$  NMR spectroscopy and ESI-HRMS. This pure product as indicated by NMR spectroscopy and mass spectrometry was dried to obtain an isolated yield of 3.2 mg (84%).  $^1\text{H}$  NMR (400 MHz, MeOD):  $\delta$  7.66 – 7.64 (br m, 24H,  $\text{C}_6\text{H}_2\text{H}_2$ ), 7.47 (br m, 24H,  $\text{C}_6\text{H}_2\text{H}_2$ ),  $\delta$  5.39 (br s, 24H,  $\text{OCH}_2$ ), 3.67 – 3.39 (m, 336H,  $\text{SCH}_2\text{CH}_2\text{O}(\text{CH}_2\text{CH}_2\text{O})_6$ ), 3.24 (br m, 36H,  $(\text{CH}_2\text{CH}_2\text{O})_6\text{CH}_3$ ).  $^{11}\text{B}$  NMR (128 MHz, MeOD):  $\delta$  -15.5.  $^{19}\text{F}$  NMR (376 MHz, MeOD):  $\delta$  -133.6 (br m, 24F, *-meta*), -139.7 (br m, 24F, *-ortho*). ESI-HRMS (-):  $m/z$  calculated for  $\text{C}_{336}\text{H}_{444}\text{B}_{12}\text{F}_{48}\text{O}_{120}\text{S}_{24}$  ( $\text{M}^{2-}$ ), 4107.1227 Da; found, 4107.1042 Da.

### **SPR procedure and supplementary data**

All experiments were performed on Series S CM5 chips (GE Healthcare Life Sciences) at a flow rate of 5  $\mu\text{L}/\text{min}$ . The Langmuir 1:1 binding model was fitted to the binding curves on the Biacore T200 evaluation software for an estimation of the binding constants.

#### DC-SIGN ECD direct binding experiments

The running buffer was composed of 10 mM HEPES buffer (pH 7.4) with 150 mM NaCl, 5 mM  $\text{CaCl}_2$ , and 0.005% Tween 20. First, the surface of flow cell #2 was activated with a 0.1 M EDC

and 0.1 M NHS (1:1 v/v) mixture over 5 minutes, followed by 0.01 mg/mL DC-SIGN ECD in the running buffer over 45 minutes and then 1 M ethanolamine HCl (pH 8.5) over 10 minutes. Then, flow cell #1 was prepared as a reference channel by activating its surface with a 0.1 M EDC and 0.1 M NHS (1:1 v/v) mixture over 5 minutes, followed by injection of 1 M ethanolamine HCl (pH 8.5) over 10 minutes. The response difference between cells stabilized around 5,000 RU. Analyte samples at various concentrations in the running buffer were injected in tandem over both cells for 6 minutes, then allowed to dissociate with buffer flow for 6 minutes. Surfaces were regenerated by injecting 10 mM HEPES buffer (pH 7.4) with 150 mM NaCl, 0.005% Tween P20, and 10 mM EDTA over 2 minutes. A flow rate of 5  $\mu$ L/min was used in all steps.

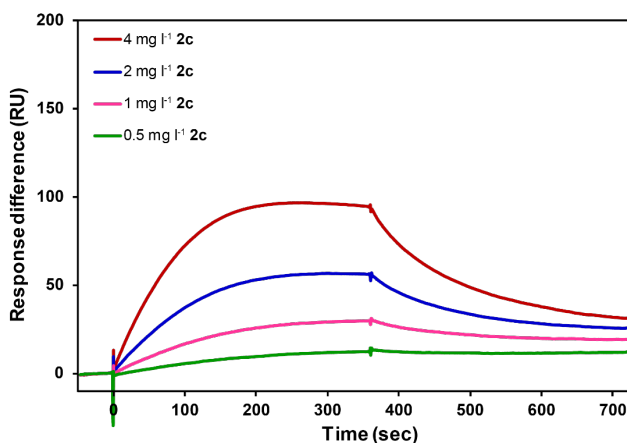


**Figure S3.1.** SPR sensorgrams of **2c** injected over DC-SIGN ECD.

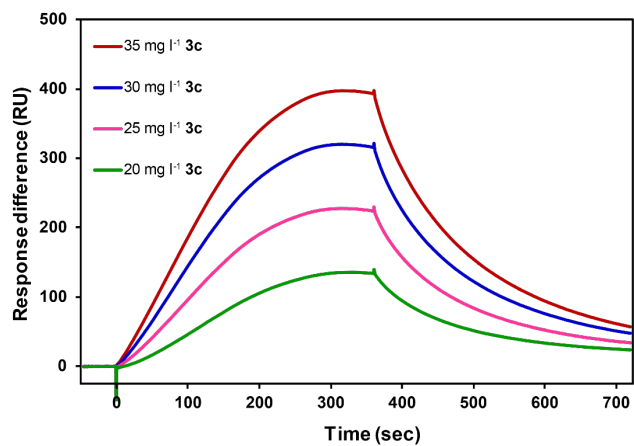


Figure S3.2. SPR sensorgrams of **3c** injected over DC-SIGN ECD.

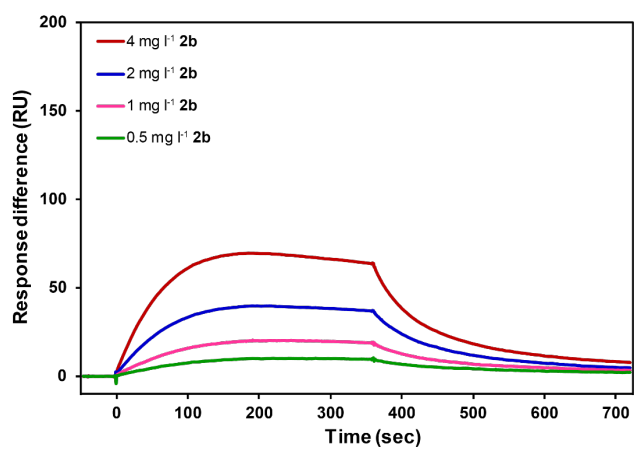


Figure S3.3. SPR sensorgrams of **2b** injected over DC-SIGN ECD.

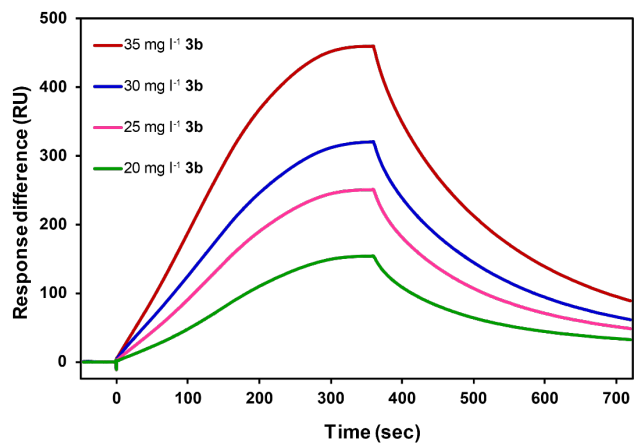
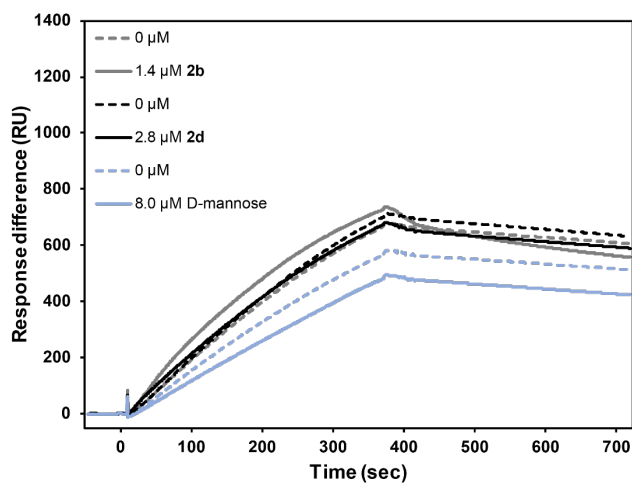


Figure S3.4. SPR sensorgrams of **3b** injected over DC-SIGN ECD.

### DC-SIGN ECD–gp120 competitive binding experiments

The running buffer was composed of 10 mM HEPES buffer (pH 7.4) with 150 mM NaCl, 5 mM CaCl<sub>2</sub>, and 0.005% Tween 20. First, the surface of flow cell #2 was activated with a 0.4 M EDC and 0.1 M NHS (1:1 v/v) mixture over 30 minutes, followed by 0.075 mg/mL gp120 in 10 mM sodium acetate buffer (pH 5.2) over 30 minutes and then 1 M ethanolamine HCl (pH 8.5) over 10 minutes. Then, flow cell #1 was prepared as a reference channel by activating its surface with a 0.4 M EDC and 0.1 M NHS (1:1 v/v) mixture over 30 minutes, followed by injection of 1 M ethanolamine HCl (pH 8.5) over 10 minutes. The response difference between cells stabilized around 7,000 RU. 200 nM DC-SIGN ECD and analyte samples at various concentrations (1:1 v/v) were mixed and vortexed for 60 seconds before being injected in tandem over both cells for 6 minutes, then allowed to dissociate with buffer flow for 6 minutes. Surfaces were regenerated by injecting 10 mM HEPES buffer (pH 7.4) with 150 mM NaCl, 0.005% Tween P20, and 10 mM EDTA over 2 minutes. A flow rate of 5  $\mu$ L/min was used in all steps.



**Figure S3.5.** SPR sensorgrams of DC-SIGN ECD and **2b**, **2d**, or D-mannose co-injected over gp120.



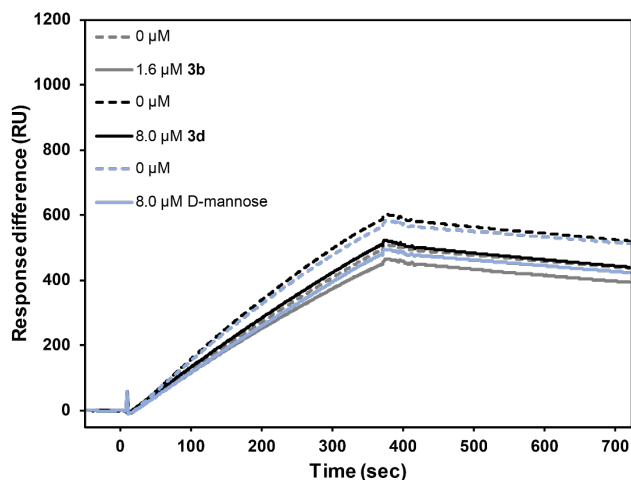


**Figure S3.6.** SPR sensorgrams of DC-SIGN ECD and **3b**, **3d**, or D-mannose co-injected over gp120.

### Cell proliferation assay

Raji DC-SIGN<sup>+</sup> cells (NIH AIDS Reagent Program) were harvested and resuspended in RPMI 1640 medium with L-glutamine (no phenol red) supplemented with 10% v/v FBS and 50 IU mL<sup>-1</sup> penicillin-streptomycin for a density of 1 x 10<sup>5</sup> cells/mL. This cell suspension was added to a polystyrene 96-well plate at a volume of 100 μL/well. Stock solutions of the clusters and controls were added to the cells at 1% v/v in triplicate. The plate was then incubated at 37 °C in a humidified chamber with 5% CO<sub>2</sub> for 24 hours. Following the incubation, 20 μL MTS reagent was added per well and the plate was incubated in the same chamber for 1.5 hour. Then, the plate was shaken briefly, and the absorbance in each well was measured at 490 nm.

### Confocal microscopy procedure and supplementary data

Raji or Raji DC-SIGN<sup>+</sup> cells (both from the NIH AIDS Reagent Program) were harvested and resuspended in D-PBS supplemented with 1% BSA and 2 mM CaCl<sub>2</sub> for a density of 2 x 10<sup>6</sup>

cells/mL, then aliquoted into populations of  $2 \times 10^5$  cells. After 30 minutes of incubation at room temperature, 1.5  $\mu$ L Human BD Fc Block was added to each cell population and incubated for 10 minutes at room temperature. 1  $\mu$ L of either autoclaved MilliQ water or a 2 or 5 mM aqueous stock solution of a compound was mixed with 1  $\mu$ L 1 mg/mL gp120-FITC and quickly added to the cells. The mixtures were incubated for 30 minutes at 37 °C, after which the cells were washed 3 times with 1 mL D-PBS. Fluoroshield mounting medium was added to each sample and mixed, then cells were transferred to clean microscope slides. After 5 minutes, a coverslip was applied to each slide. The slide edges were then sealed with clear nail polish after 20 minutes. The slides were then taken to a confocal microscope, where images from several parts of the slides were acquired in z-stacks (25 sections, 20  $\mu$ m) in both fluorescence and brightfield modes with a 40x lens and 30% excitation laser intensity.

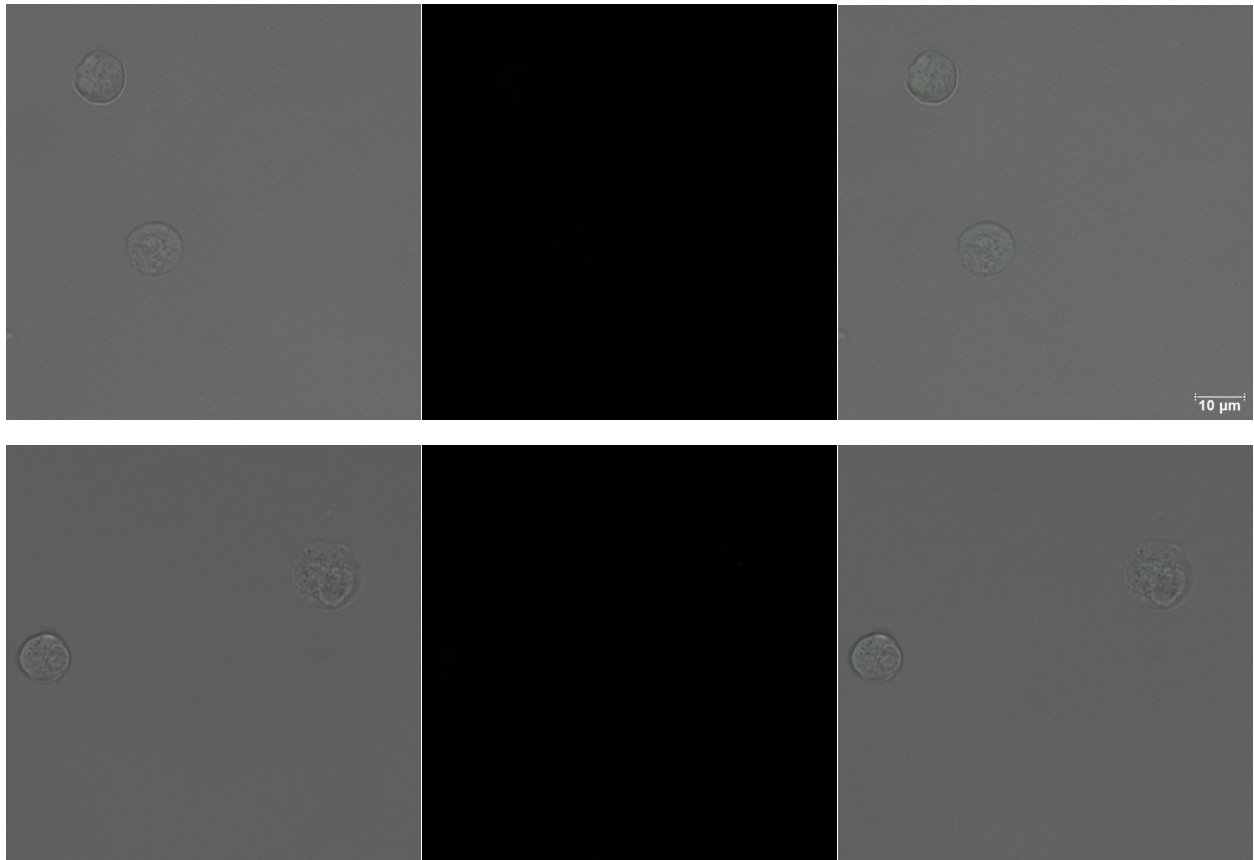


**Figure S3.7.** Confocal microscopy images of Raji cells exposed to gp120-FITC and water (brightfield, green, overlay).

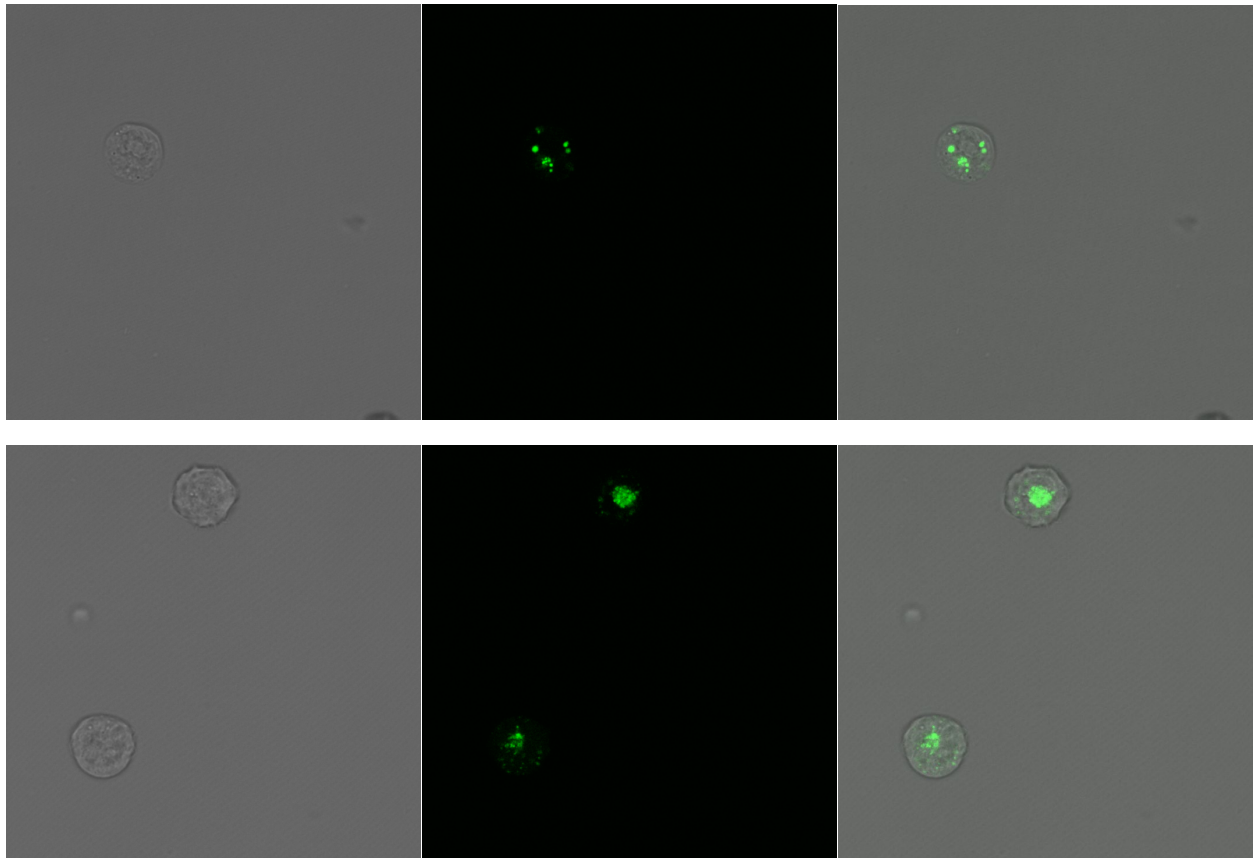


**Figure S3.8.** Confocal microscopy images of Raji DC-SIGN<sup>+</sup> cells exposed to gp120-FITC and water (brightfield, green, overlay).

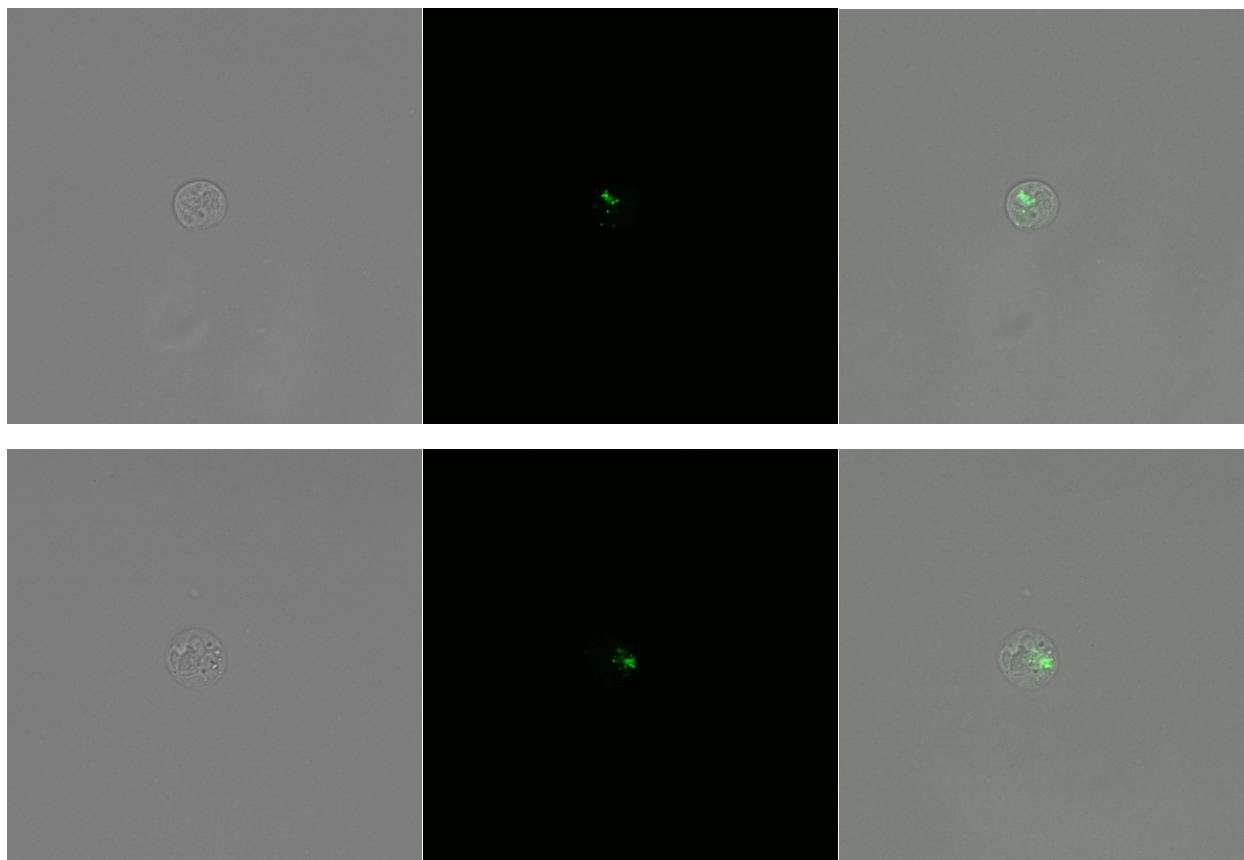


**Figure S3.9.** Confocal microscopy images of Raji DC-SIGN<sup>+</sup> cells exposed to gp120-FITC and 10  $\mu$ M **2a** (brightfield, green, overlay).



**Figure S3.10.** Confocal microscopy images of Raji DC-SIGN<sup>+</sup> cells exposed to gp120-FITC and 25  $\mu$ M **2a** (brightfield, green, overlay).

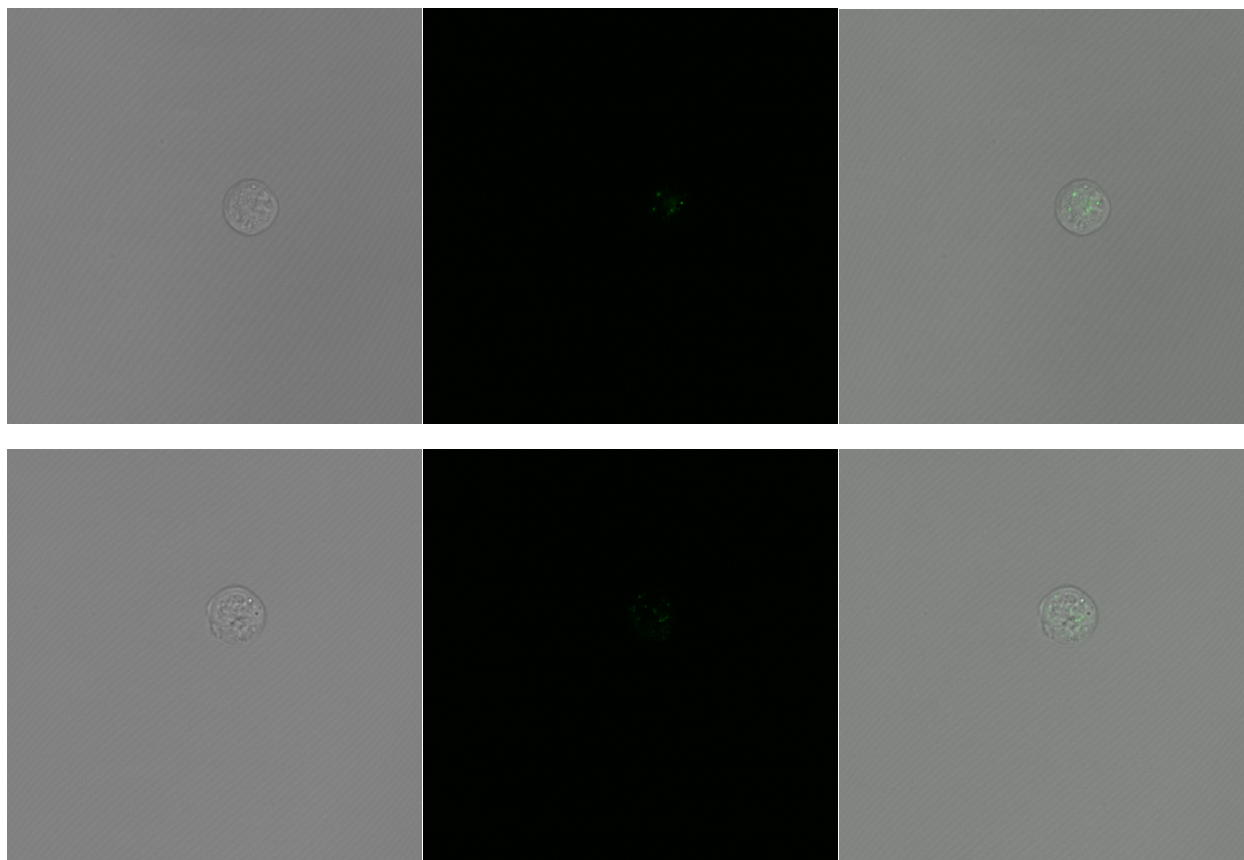


**Figure S3.11.** Confocal microscopy images of Raji DC-SIGN<sup>+</sup> cells exposed to gp120-FITC and 10 μM **3a** (brightfield, green, overlay).

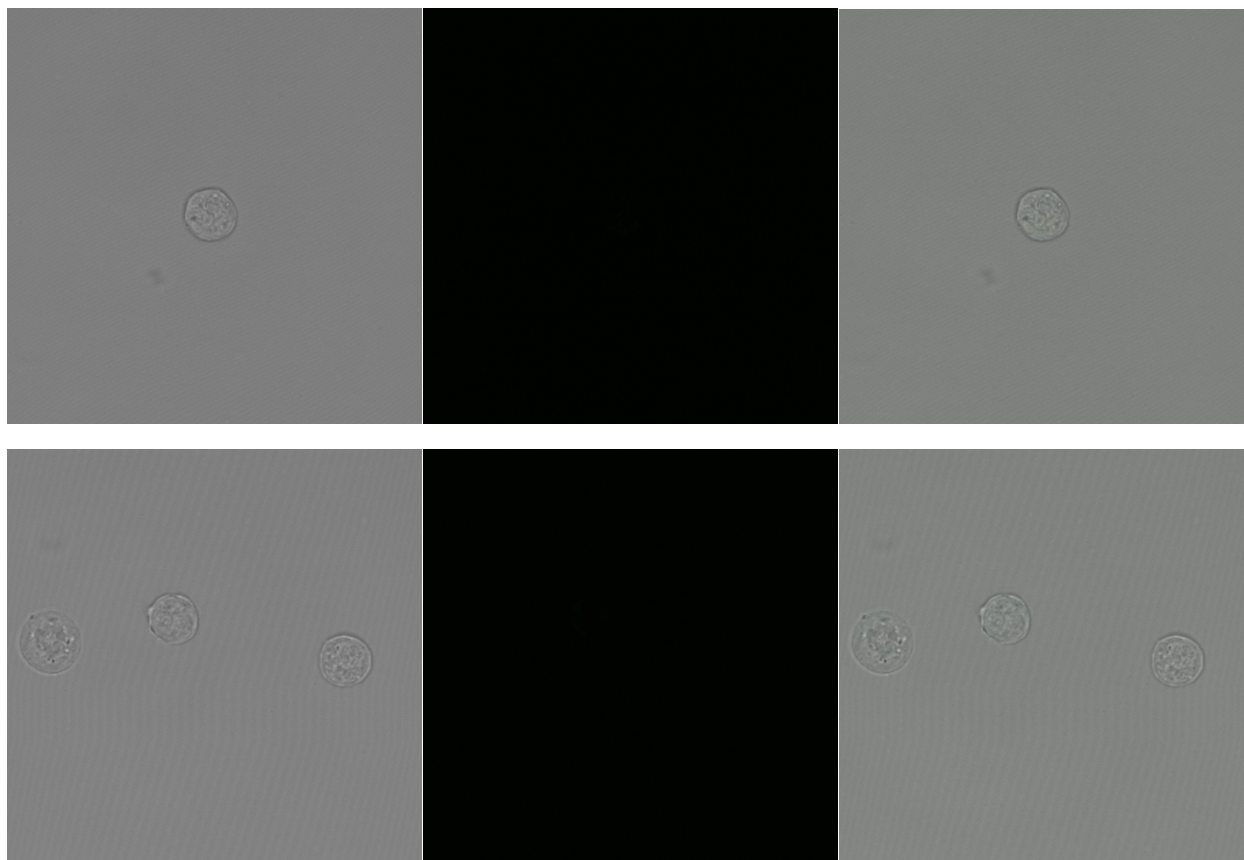


**Figure S3.12.** Confocal microscopy images of Raji DC-SIGN<sup>+</sup> cells exposed to gp120-FITC and 25  $\mu$ M **3a** (brightfield, green, overlay).



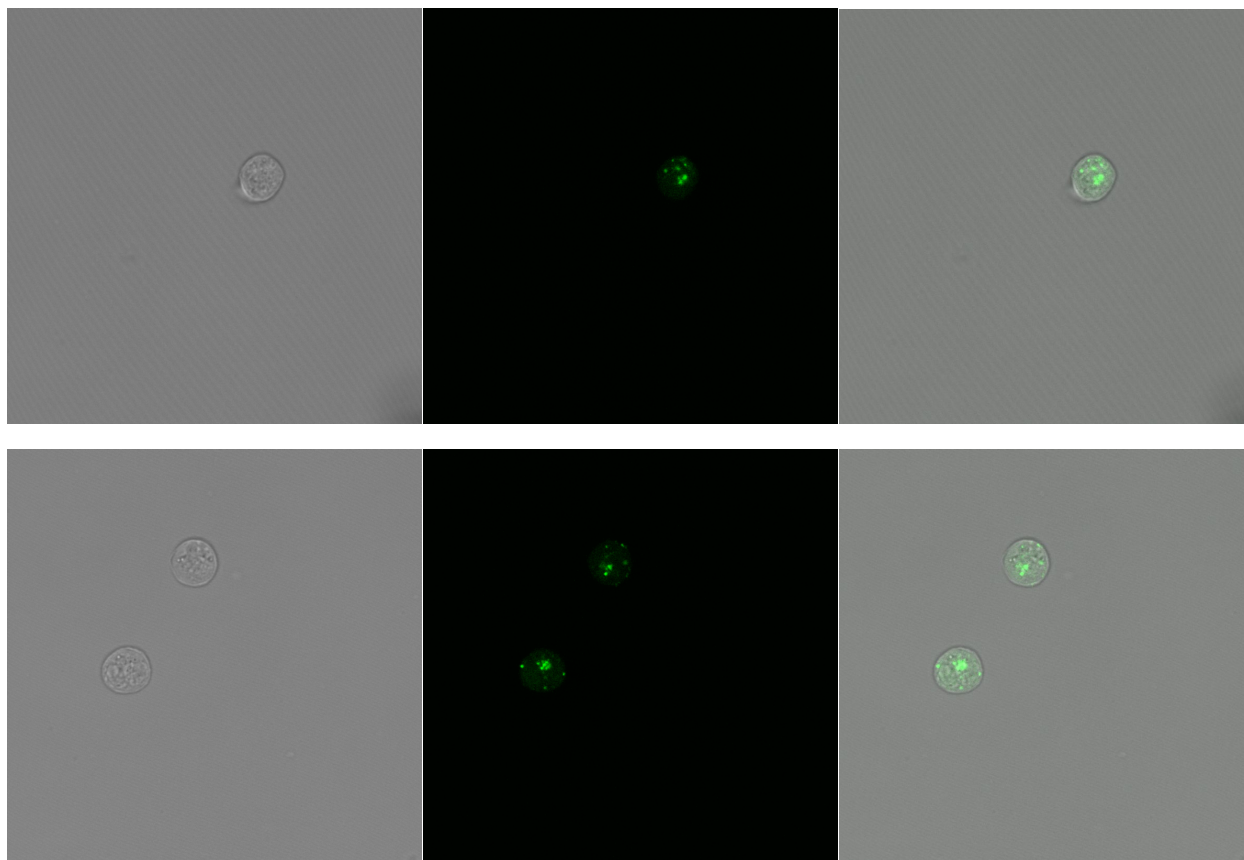


**Figure S3.13.** Confocal microscopy images of Raji DC-SIGN<sup>+</sup> cells exposed to gp120-FITC and 25  $\mu$ M **2d** (brightfield, green, overlay).

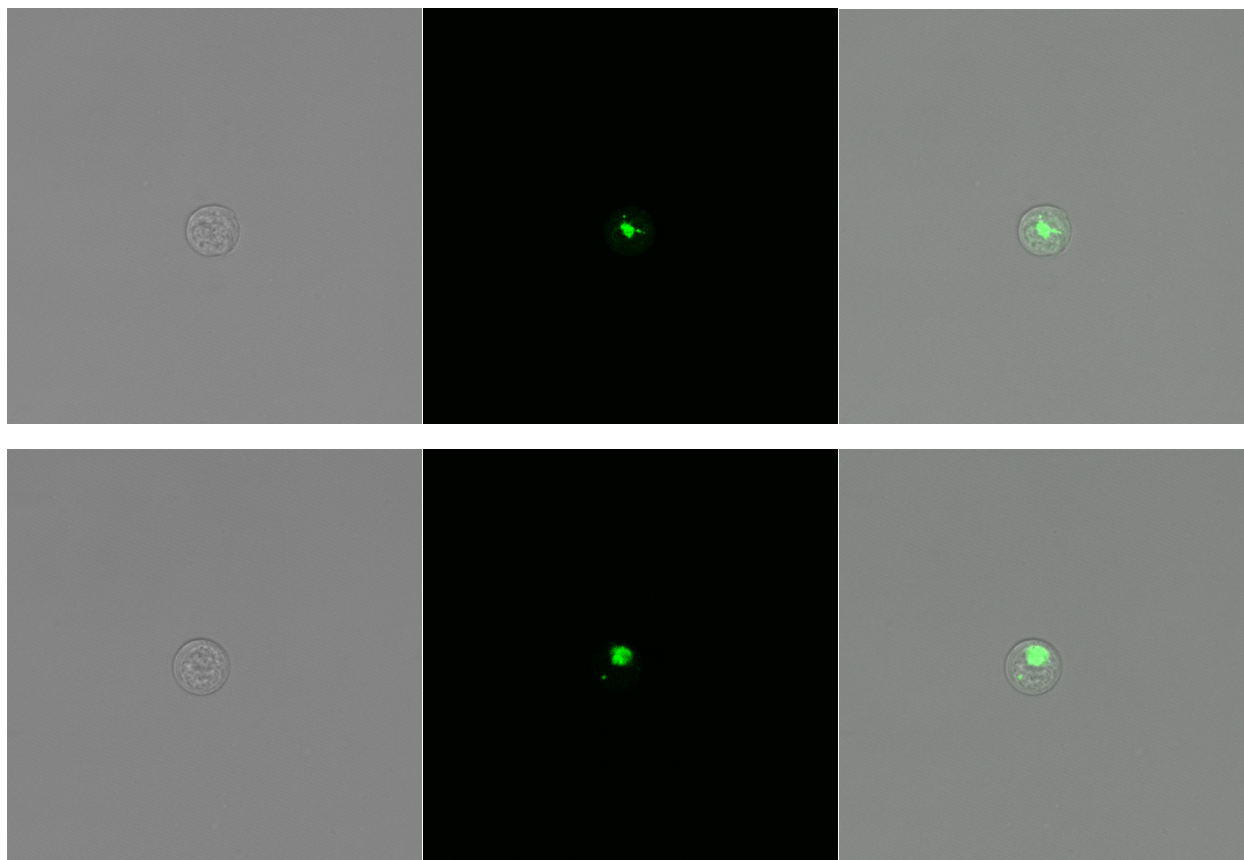


**Figure S3.14.** Confocal microscopy images of Raji DC-SIGN<sup>+</sup> cells exposed to gp120-FITC and 25  $\mu$ M **3d** (brightfield, green, overlay).

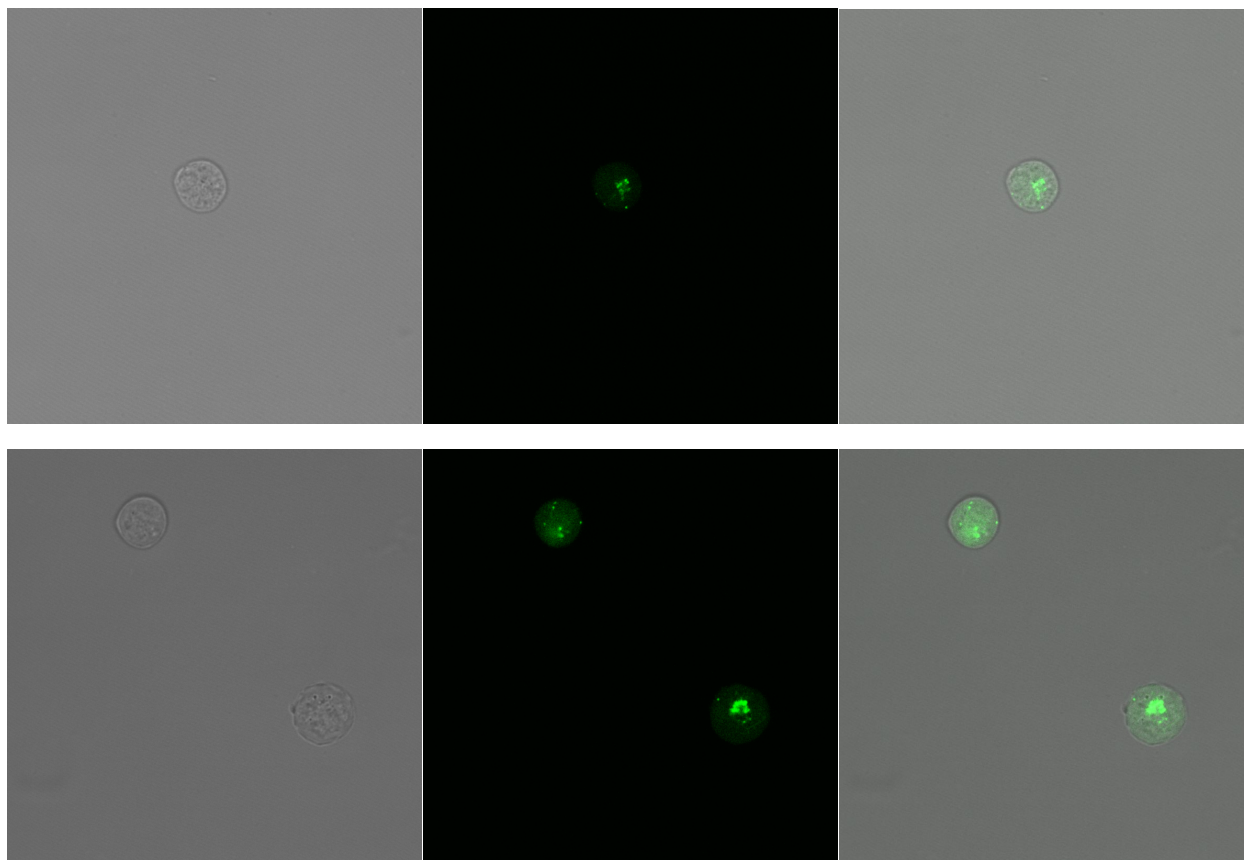


**Figure S3.15.** Confocal microscopy images of Raji DC-SIGN<sup>+</sup> cells exposed to gp120-FITC and 25  $\mu$ M D-mannose (brightfield, green, overlay).

## Computational work

### General systems and methods

In order to check the binding between glycosylated clusters (G1 – **2a** and G2 – **3a**) and DC-SIGN, atomistic molecular dynamics (MD) simulations were performed by NAMD.<sup>107</sup> DC-SIGN (PDB 1K9I) is a tetramer, having four carbohydrates binding sites consisting of residues Val, Asn, Glu and Asp.<sup>127,158,173</sup> Two simulations were set up: G1 with DC-SIGN and G2 with DC-SIGN. Both systems were immersed in 150 mM NaCl solutions.

### Methods

The DC-SIGN protein was described by a CHARMM36 force field,<sup>108</sup> while the clusters were described by a CHARMM general force field.<sup>109</sup> The Particle Mesh Ewald (PME) method<sup>117</sup> was used for the evaluation of long-range Coulombic interactions. The time step was set to 2.0 fs. The simulations were performed in the NPT ensemble ( $p = 1$  bar and  $T = 300$  K), using the Langevin dynamics ( $\gamma_{\text{Lang}} = 1 \text{ ps}^{-1}$ ). After 2,000 steps of minimization, ions and water molecules were equilibrated for 2 ns around protein and clusters, which were restrained using harmonic forces with a spring constant of  $1 \text{ kcal}/(\text{mol } \text{Å}^2)$ . The last frames of restrained equilibration were used to start simulations of free clusters and partial constrained protein (stalks).

### Binding of G1/G2 to DC-SIGN

To quantify the difference between the two binding systems, we monitored the number of hydroxy groups (3-OH and 4-OH) within  $5 \text{ Å}$  of the calcium ion. The results are plotted in Figure S1, where "2" means both 3-OH and 4-OH bind, "1" means one hydroxy binds, and "0" means neither binds. G2 shows rapid switching among "2", "1", and "0" with a longest "1" state of 2 ns, while G1 stays with "2" for a longer time with a longest "2" state of 4 ns after switching between "0" and "1". The

rapid switching of G2 may be induced by the stronger hydrophobic interaction between linkers which can lead to a higher dissociation constant.

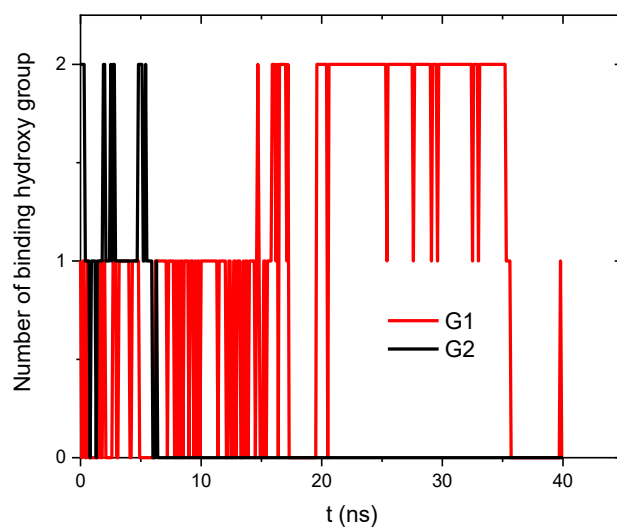


**Figure S3.16.** Changes in the number of hydroxy groups (3-OH and 4-OH) on mannose binding to DC-SIGN over 40 ns.

## CHAPTER FOUR

### **An Organometallic Strategy for Assembling Atomically Precise Hybrid Nanomaterials**

Julia M. Stauber, Elaine A. Qian, Yanxiao Han, Arnold L. Rheingold,

Petr Král, Daishi Fujita, and Alexander M. Spokoyny.

*Submitted.*

#### **Abstract**

For decades, chemists have striven to mimic the intricate design and diverse functions of naturally occurring systems through the bioinspired synthesis of programmable inorganic nanomaterials. The development of thiol-capped gold nanoparticles (AuNPs) has driven advancement in this area; however, although versatile and readily accessible, hybrid AuNPs are rarely atomically precise, which limits control over their surface topology and therefore the study of complex structure-function relationships. Here, we present a bottom-up approach to the systematic assembly of atomically precise hybrid nanoclusters employing a strategy that mimics the synthetic ease with which thiol-capped AuNPs are normally constructed, while producing well-defined covalent nanoscale assemblies with diverse surface topologies. For the first time, using a structurally characterized cluster-based organometallic building block, we demonstrate the systematic synthesis of nanoclusters with multivalent binding capabilities to complex protein targets.

## Introduction

The rational design of surface-modified nanoscale materials using well-defined building block constituents is a powerful strategy for the bottom-up assembly of functional synthetic architectures. Drawing inspiration from nature, chemists have explored a range of platforms with programmable surface chemistry that are designed to interrogate and mimic complex biological interactions.<sup>174</sup> These structural classes include dendrimers,<sup>99,175,176</sup> polymers,<sup>177,178</sup> coordination and supramolecular-based assemblies,<sup>101,124,179</sup> and other nanoscale structures.<sup>50,180,181</sup> In particular, thiol-capped gold nanoparticles (AuNPs) represent a category of surface-functionalized materials that continue to receive considerable attention in this area for probing biological interactions of interest as they are easily accessible and tunable in terms of size and topology.<sup>58,59</sup> Despite these attractive properties, such systems suffer from several fundamental limitations that stem from the relatively weak nature of the gold-thiolate bond (40-50 kcal mol<sup>-1</sup>).<sup>67</sup> For example, thiol-capped AuNPs are known to undergo ligand-exchange processes with other surfactants in solution over short periods of time,<sup>69,182</sup> contributing to limited stability profiles in biologically relevant media.<sup>71</sup> Additionally, hybrid nanoparticle assemblies are seldom atomically precise and therefore typically possess non-uniform composition, size, and surface morphology. These drawbacks present significant challenges in rationally addressing hybrid AuNP structure-function properties on an atomic level, especially within the context of mechanistic exploration for biological applications. Such challenges have led to constant evolution of the nanochemistry field, with current efforts dedicated to addressing the areas of biological stability, atomic precision, and control over the surface topology of programmable nanostructures.<sup>183-185</sup> Specifically, these areas include work dedicated to improving the binding of ligands to noble metal surfaces,<sup>186-188</sup> and the

development of synthetic methods that lead to the formation of gold-based nanoclusters with well-defined metal cores.<sup>189–191</sup>

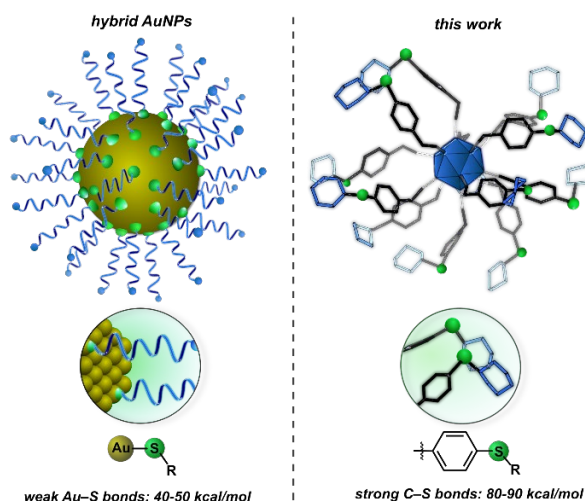


**Figure 4.1.** (Left) Hybrid thiol-capped AuNPs feature non-covalent, weak Au–S bonds (40–50 kcal/mol). (Right) This work presents a class of atomically precise nanoclusters built upon robust and comparatively stronger C–S linkages (80–90 kcal/mol).

Here, we present a conceptually new approach that mimics the chemistry of thiol-capped AuNP assembly processes, while producing a new method of controlling the architecture of complex abiotic molecules on an atomic scale in the context of manipulating biomolecular interactions. The presented approach incorporates, for the first time, the use of robust organometallic-based building blocks as structurally well-defined and tunable templates for assembling atomically precise and biocompatible hybrid nanoclusters. Organometallic gold-based systems have sparked interest in recent years for their use in both catalytic<sup>192,193</sup> and stoichiometric<sup>194</sup> transformations due in part to the reluctance of Au(I) to undergo oxidative addition.<sup>195,196</sup> This reactivity contributes to the high stability and chemoselectivity observed for gold-based reagents, while minimizing the propensity for background reactivity with the variety of species present in complex reaction mixtures. Leveraging these properties, we have developed



a new class of molecules that contain a rigid cluster core functionalized with a dense layer of robust organometallic gold(III) sites that undergo rapid diversification with thiol-based nucleophiles *via* “click”-like C–S bond-forming reductive elimination. The thiol conjugation chemistry is selective and efficient, proceeding at ambient temperature under mild conditions to generate clusters with precisely controlled morphologies. This approach mimics the synthetic ease with which thiol-capped AuNPs are normally constructed,<sup>58–60</sup> while providing functional advantages such as full covalency and atomic precision, which are properties typically associated with dendrimers and molecular systems. We investigated these hybrid nanoclusters as a new class of agents to inhibit important protein-protein and protein-sugar interactions in biological systems and report the binding affinity of saccharide-grafted clusters with plant-based concanavalin A (ConA), bacterial Shiga toxin 1, B subunit (Stx1B), and human-based DC-SIGN (Dendritic Cell-Specific Intercellular adhesion molecule-3-Grabbing Non-integrin) targets, showcasing how this strategy allows for the rapid generation of complex, yet precise multivalency for enhancing molecular recognition.

## Results and Discussion

Our approach to the programmable synthesis of hybrid nanomolecules is based upon a boron cluster core, which serves as a well-defined platform that enables atomic-level precision and control of size and surface morphology upon derivatization. Icosahedral dodecaborane clusters ( $[B_{12}R_{12}]$ ) are excellent building blocks for the assembly of biologically-relevant nanoscale molecules due to their topological rigidity, appropriate size domain, low toxicity, stability under harsh biological conditions, and potential for dense surface polyfunctionalization.<sup>6,79,197</sup> We

envisioned access to such a class of hybrid nanoclusters would be possible through the rational evolution of synthetic handles on the cluster periphery that would ultimately lead to the incorporation of surface organometallic sites capable of facile reaction with thiol-containing substrates.

Accordingly, synthesis of the  $B_{12}(OCH_2C_6H_4I)_{12}$  precursor was achieved through per-O-benylation of  $closo-[B_{12}(OH)_{12}]^{2-}$  with *para*-iodobenzyl bromide in the presence of diisopropylethylamine employing a microwave-assisted synthetic procedure.<sup>197</sup> Following sequential two-electron chemical oxidation with Fe(III), the neutral, air-stable *hypercloso*- $B_{12}(OCH_2C_6H_4I)_{12}$  cluster was isolated in 76% yield as a crystalline solid, and characterized by multinuclear NMR spectroscopy ( $^1H$ ,  $^{13}C$ ,  $^{11}B$ ), high-resolution electrospray ionization mass spectrometry (HR-ESI-MS(-)), cyclic voltammetry, UV-vis spectroscopy, and single crystal X-ray diffraction (see the Supporting Information for experimental details and characterization data).

Bourissou *et al.* recently reported the oxidative addition of simple aryl iodides to Au(I) sites supported by bulky aminophosphine ligands under mild conditions.<sup>198</sup> We envisioned that utilization of the same Au(I) precursor  $((Me-DalPhos)AuCl)^{199}$  with  $B_{12}(OCH_2C_6H_4I)_{12}$  under appropriate synthetic conditions could lead to the conversion of all twelve C–I sites on the cluster periphery to the corresponding C–Au(Me-DalPhos) congeners. Although conceptually simple, this strategy is far more challenging from a synthetic perspective given that successful permetalation of the cluster requires simultaneous and quantitative conversion efficiency for all twelve organometallic transformations. Furthermore, it is well documented that organometallic-based reactions have the propensity to undergo decomposition pathways as well as generate undesired side products. These factors present additional challenges that could potentially complicate purification processes associated with assembling complex systems such as the present one.

Despite these challenges, however, treatment of  $B_{12}(OCH_2C_6H_4I)_{12}$  with excess (Me-DalPhos)AuCl in refluxing DCM (dichloromethane) in the presence of the halide scavenger, AgSbF<sub>6</sub>, resulted in unprecedented 12-fold exhaustive metalation of the cluster *via* oxidative addition of Au(I) into each of the twelve aryl C–I bonds (Figure 4.2A). The permetalated product,  $[B_{12}(OCH_2C_6H_4(Me-DalPhos)AuCl)_{12}][SbF_6]_{11}$  (**[1]** $[SbF_6]_{11}$ ), precipitated directly from the crude reaction mixture over the course of 16 h, and was isolated as a pink solid after purification. Notably, the synthetic and purification procedures proceed cleanly when carried out under open-atmosphere conditions using unpurified solvents. The  $^{31}P\{^1H\}$  NMR spectrum of **[1]** $[SbF_6]_{11}$  features a single resonance located at  $\delta$  75.8 ppm, which is consistent with the isolation of one, well-defined species. Since we were unable to observe the intact **[1]**<sup>11+</sup> complex using mass spectrometry, X-ray crystallographic analysis was the only alternative method available to directly confirm the identity of this product. Fortunately, crystallization of **[1]** $[SbF_6]_{11}$  from an acetonitrile/dimethoxyethane/diethylether solution afforded single, pink crystals of suitable quality for X-ray diffraction analysis, which enabled structural determination of **[1]**<sup>11+</sup> and confirmation of its identity. As displayed in the solid-state structure of **[1]**<sup>11+</sup> (Figure 4.2B), the cluster framework spans a 3 nm distance from end to end, and contains a dense layer of organometallic (Me-DalPhos)AuCl groups, representing an extremely rare example of a structurally characterized atomically precise nanocluster featuring well-defined organometallic fragments.<sup>200,201</sup>

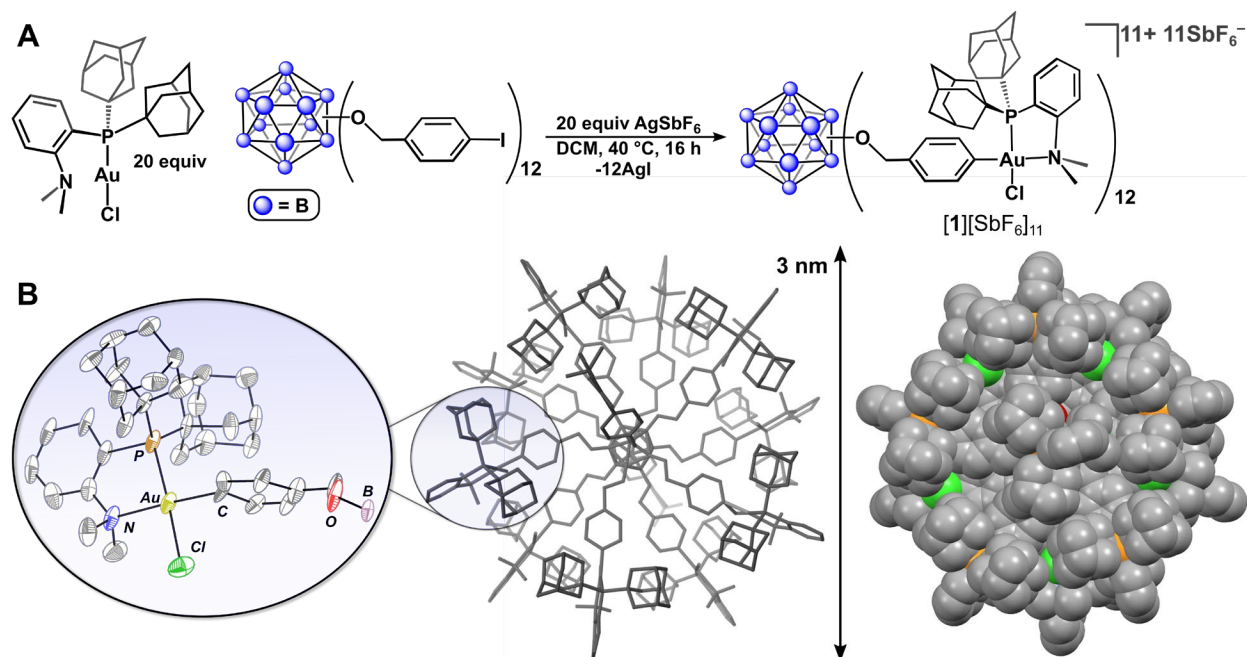


**Figure 4.2.** (A) Synthetic protocol for the preparation of  $[1][SbF_6]_{11}$ . (B) Solid-state structure of  $[1][SbF_6]_{11}$  (center), and zoomed-in image of a single Au(III) organometallic fragment (left) with thermal ellipsoids rendered at the 30% probability level and with hydrogen atoms and counteranions omitted, and space-filling diagram (right). For crystallographic details see the Supporting Information.

We next evaluated the ability of  $[1][SbF_6]_{11}$  to serve as a building block for the construction of hybrid nanocluster thio conjugates. Optimization of conjugation reaction conditions were carried out employing thiophenol as the model substrate. For a typical conjugation reaction, the  $[1][SbF_6]_{11}$  species was generated according to the synthetic procedure described (*vide supra*) and then used *in situ* without its isolation as a solid. The  $[1][SbF_6]_{11}$  complex was subsequently treated with thiophenol (30 equiv) in DMF (dimethylformamide) solution in the presence of potassium phosphate (30 equiv) according to the scheme displayed in Figure 4.3A. Addition of thiophenol immediately elicited a color change from deep purple to colorless due to reduction of the cluster core to the 2- charge state, which was confirmed by the presence of a singlet located at  $\delta$  -15.6 ppm in the  $^{11}B$  NMR spectrum of the reaction mixture. The location of this resonance is

characteristic of reduced clusters in the 2<sup>-</sup> charge state,<sup>6</sup> and is consistent with the reducing capacity of the thiolate species. These reaction conditions afforded the twelve-fold thio-ether substituted conjugate, [K<sub>2</sub>][B<sub>12</sub>(OCH<sub>2</sub>C<sub>6</sub>H<sub>4</sub>SPh)<sub>12</sub>] ([K<sub>2</sub>][**2**]), within minutes (< 15) at 25 °C, as assayed by HR-ESI-MS(-) analysis of the crude mixture. The product was purified *via* silica gel column chromatography and isolated as an air-stable solid in 70% yield. The well-resolved resonances in the <sup>1</sup>H and <sup>11</sup>B NMR spectra in addition to the ESI-MS(-) characterization of the [K<sub>2</sub>][**2**] salt are consistent with its formulation as the fully functionalized thio-ether conjugate and the isolation of one discrete molecular species (see the Supporting Information for experimental details and characterization data). It is important to note that the full covalency of the nanocluster conjugate enables observation of the intact species by ESI-MS, whereas even gentle ionization techniques frequently result in fragmentation of ligands from the gold core of thiol-capped hybrid AuNPs due to cleavage of the Au-S bonds.<sup>202</sup>

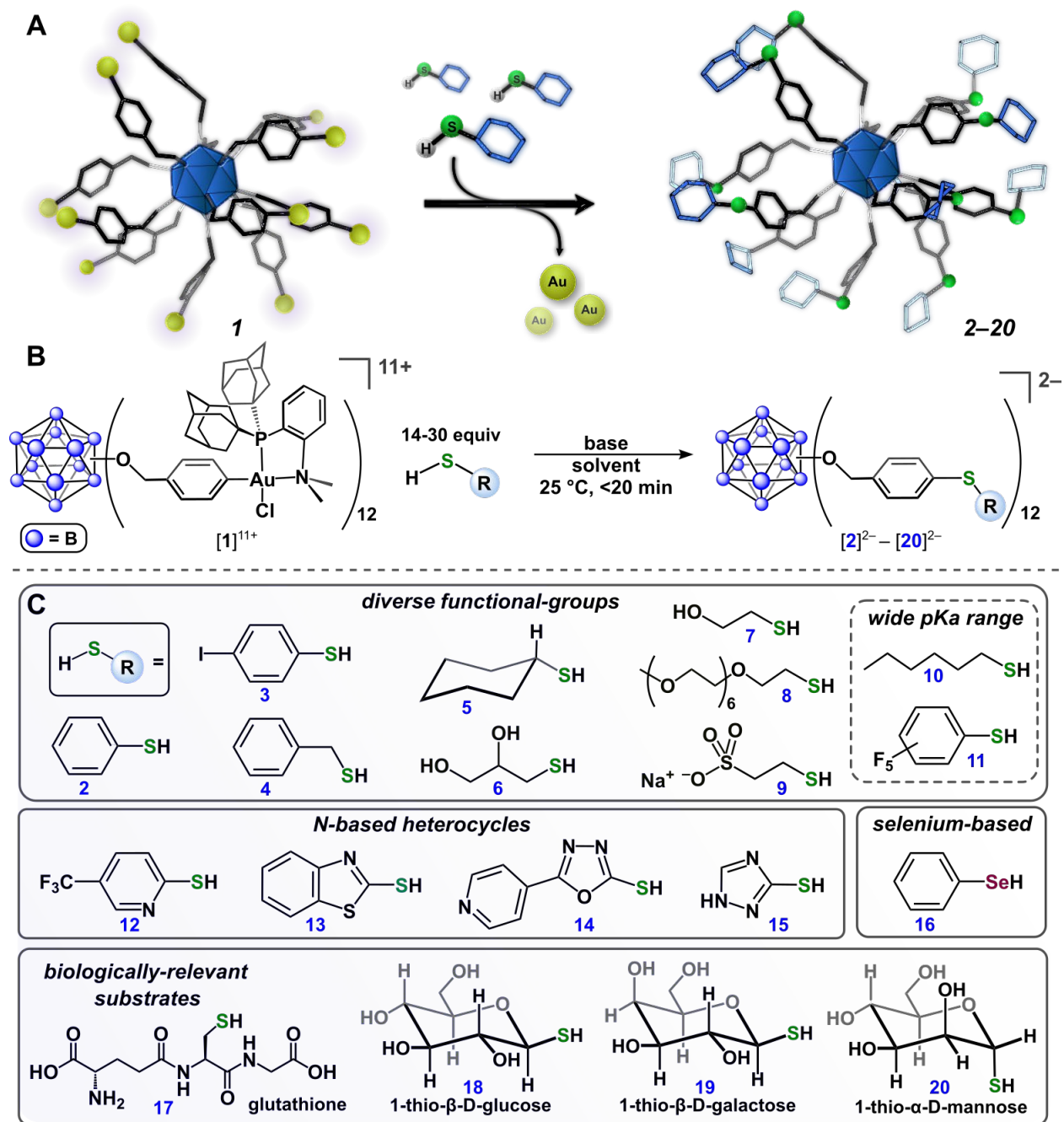


**Figure 4.3.** (A, B) Scheme for reactions of  $[1][\text{SbF}_6]_{11}$  with thiol-containing substrates. (C) Substrate scope for conjugation reactions. All cluster conjugates were isolated and characterized ( $^1\text{H}$  and  $^{11}\text{B}$  NMR spectroscopy, HR-ESI-MS(-)) after purification (see the Supporting Information for experimental details and characterization data).

Extending this approach, we further developed a comprehensive scope of densely functionalized nanocluster thio conjugates. The versatility of this conjugation strategy was first probed by examining the chemoselectivity of the developed chemistry through treatment of [1][SbF<sub>6</sub>]<sub>11</sub> with thiol substrates featuring a variety of functional groups (**2-11**, Figure 4.3C). Thiol-based nucleophiles bearing aryl (**2, 3, 4, 11**), alkyl (**5, 10**), and alcohol-based (**6, 7**) groups cleanly generated the corresponding cluster conjugates as confirmed by ESI-MS(–) and multinuclear NMR spectroscopic analyses of the isolated products. This chemistry is also compatible with thiol nucleophiles featuring a bulky cyclohexyl group (**5**), a poly(ethyleneglycol) (**8**) polymer, and an anionic sulfonate moiety (**9**); this wide ranging functional-group tolerance contributes to a scope of cluster conjugates with highly diverse solubility properties, surface morphologies, and electronic profiles. The conjugation chemistry is also operational with thiol-based reagents that span a broad window of nucleophilicity, as evidenced by the clean reactivity with both electron-rich (*e.g.* hexanethiol, **10**) and electron deficient (*e.g.* pentafluorothiophenol, **11**) substrates with *pK<sub>a</sub>* values ranging from ca. 3-11.<sup>203,204</sup> Importantly, this finding expands the generality of the thiol substrate *pK<sub>a</sub>* scope from the previously developed organometallic-based reagents (palladium and gold) used for cysteine *S*-arylation.<sup>205</sup> While *N*-based heterocycles are challenging coupling partners in transition-metal-mediated organic transformations due to their ability to serve as sigma-donating ligands that can coordinate to and poison the active metal species, cluster conjugates featuring a variety of *N*-based heterocycles (**12-15**) were prepared and characterized, further establishing the chemoselectivity and utility of the present approach. This conjugation strategy was even extended to include a selenium-based nucleophile (phenylselenol, **16**), which further expands the versatility of the described chemistry. Finally, we extended this platform to include a variety of densely functionalized clusters bearing biologically relevant substrates such as a short

peptide (**17**, glutathione) and three different thiol-based saccharides (**18**, **19**, **20**, *vide infra*). The presented organometallic-mediated approach provides a unique method of cluster-based hybrid nanomolecule synthesis,<sup>6</sup> in which the assembly process exhibits extremely fast reaction kinetics (<15 min) under operationally simple and mild conditions and can even be conducted in mixed organic/aqueous media as necessitated by the solubility properties of the thiol substrate.

With a strategy for successful perfunctionalization of **[1]**<sup>11+</sup> (*vide supra*), we envisioned we could establish a new generation of atomically precise nanoclusters that are modularly extended in size through systematic extension of the linker unit. This method was accomplished by employing the radially extended, iodo-aryl thio-ether conjugate, **[3]**<sup>2-</sup>, as the cluster-based precursor. Complete metalation of **[3]**<sup>2-</sup> to afford **[B<sub>12</sub>(OCH<sub>2</sub>C<sub>6</sub>H<sub>4</sub>SC<sub>6</sub>H<sub>4</sub>(Me-DalPhos)AuCl)<sub>12</sub>][SbF<sub>6</sub>]<sub>10</sub>** (**[21]****[SbF<sub>6</sub>]<sub>10</sub>**) was accomplished using conditions similar to those described for the preparation of **[1][SbF<sub>6</sub>]<sub>11</sub>**. The **[21][SbF<sub>6</sub>]<sub>10</sub>** cluster was characterized by <sup>1</sup>H, <sup>11</sup>B and <sup>31</sup>P NMR (Figure 4.4B) spectroscopy, which are all consistent with the formulation of **[21]**<sup>10+</sup> as the fully-functionalized species (see the Supporting Information for experimental details and characterization data). Complex **[21][SbF<sub>6</sub>]<sub>10</sub>** undergoes facile conjugation chemistry with thiol-containing nucleophiles to generate species **[22]**<sup>2-</sup>-**[28]**<sup>2-</sup> under the same reaction conditions employed for the conjugation chemistry of **[1]**<sup>11+</sup>. This template-based approach to the construction of hybrid nanoclusters that are systematically extended in size is reminiscent of the layer-by-layer assembly process of building composite core-shell nanomaterials in which multiple films are layered onto colloidal particles followed by selective template removal.<sup>206,207</sup> This method allows for rational engineering and precise control over the size, shape, composition, and surface topology of the resulting nanoclusters. Notably, we can easily recycle the (Me-DalPhos)AuCl complex that is generated as the byproduct from the conjugation reactions through purification on silica gel (see



the Supporting Information for experimental details and data). This recovered material can then be reused in the preparation of  $[1][SbF_6]_{11}$  and  $[21][SbF_6]_{10}$ , thereby demonstrating the efficiency of the present approach.

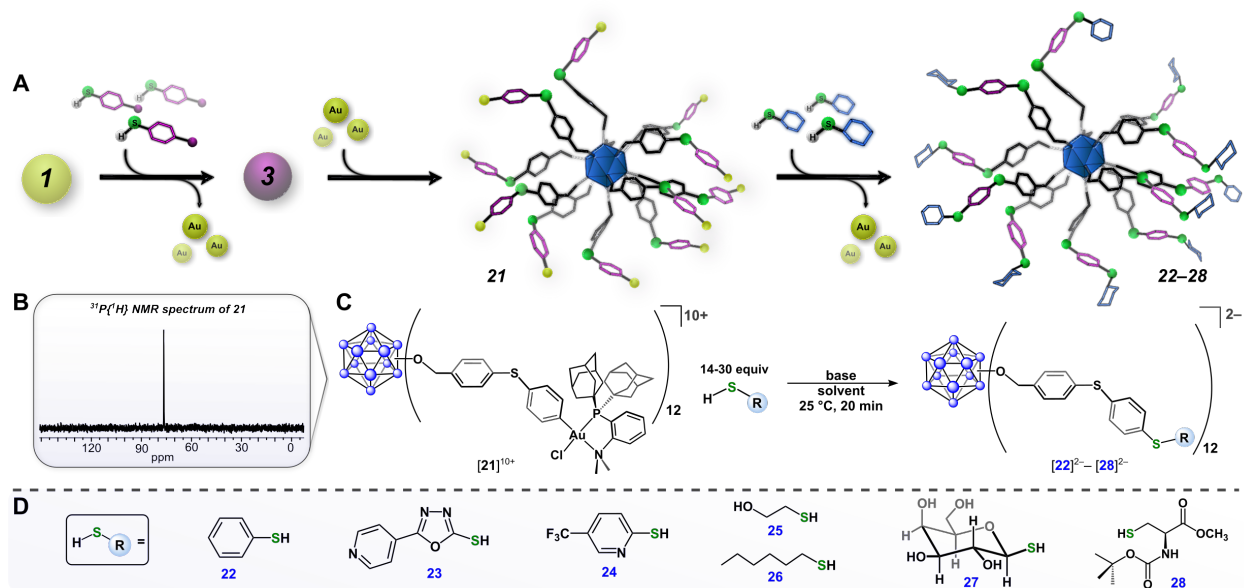


**Figure 4.4.** (A) “Layer-by-layer” assembly strategy for building nanoclusters that are modularly extended in size. (B)  $^{31}P\{^1H\}$  NMR spectrum of  $[21][SbF_6]_{10}$ . (C) Synthetic scheme for reactions of  $[21][SbF_6]_{10}$  and thiol-containing substrates. (D) Substrate scope for conjugation reactions. All cluster conjugates were observed *in situ* by ESI-MS(–) (see the Supporting Information for experimental details and characterization data).

We next focused on evolving the present method to rationally build a class of hybrid nanoclusters that contain specific recognition moieties capable of engaging in multivalent binding interactions with complex protein targets. Multivalency plays a vital role in numerous biological processes and especially in those involving pathogen-host relationships based on protein-glycan recognition.<sup>50,84</sup> Naturally occurring multivalent glycoconjugates such as glycoproteins and glycolipids can bind lectins with affinities that surpass the weak binding association of the corresponding monosaccharides, making the design of high-affinity, synthetic analogues with

controlled spatial and topology parameters an area of growing interest for preventing or treating pathogen-based diseases.<sup>175,179</sup>

Using commercial thiolate precursors, we prepared the glucose- ([Na<sub>2</sub>][**18**]), galactose- ([Na<sub>2</sub>][**19**]), and mannose-grafted ([Na<sub>2</sub>][**20**]) nanoclusters (Figure 4.3C) that feature precise spatial arrangements of the twelve appended saccharides on the cluster periphery. All three water-soluble glycosylated clusters were isolated after purification *via* size-exclusion chromatography, and characterized by heteronuclear NMR spectroscopy (<sup>1</sup>H and <sup>11</sup>B) and HR-ESI-MS(-). We next evaluated the stability of the glycoconjugates in biologically relevant media using the glucose-functionalized cluster, [**18**]<sup>2-</sup>, as a model. Species [Na<sub>2</sub>][**18**] was exposed to fetal bovine serum cell-culture media as well as solutions of various pH environments (pH = 5 and 10) for extended periods of time (≥ 7 days) without any observable degradation as assayed by spectroscopic analyses (<sup>11</sup>B NMR, Figure 4.5B; ESI-MS(-), see the Supporting Information for experimental details and data). The excellent stability profile of [Na<sub>2</sub>][**18**] in biologically relevant media is a direct consequence of its full covalency, further demonstrating the advantage of using systems built upon robust C–S linkages as opposed to the significantly weaker Au–S bonds characteristic of thiol-capped AuNPs.<sup>71,182</sup> The excellent stability profile of [Na<sub>2</sub>][**18**] further motivated us to probe the use of glycosylated nanoclusters as functional agents to interrogate multivalent binding interactions with protein targets.

Accordingly, we evaluated and quantified the binding affinity of glycosylated clusters, [Na<sub>2</sub>][**18**], [Na<sub>2</sub>][**19**], and [Na<sub>2</sub>][**20**] with protein targets from three biological kingdoms (ConA, Stx1B, and DC-SIGN, respectively) by surface plasmon resonance (SPR). The PEGylated conjugate, [K<sub>2</sub>][**8**], was used in each case as a control to assess the extent of non-specific binding

interactions for each target, and the corresponding monosaccharide was used in each case as a monovalent reference.

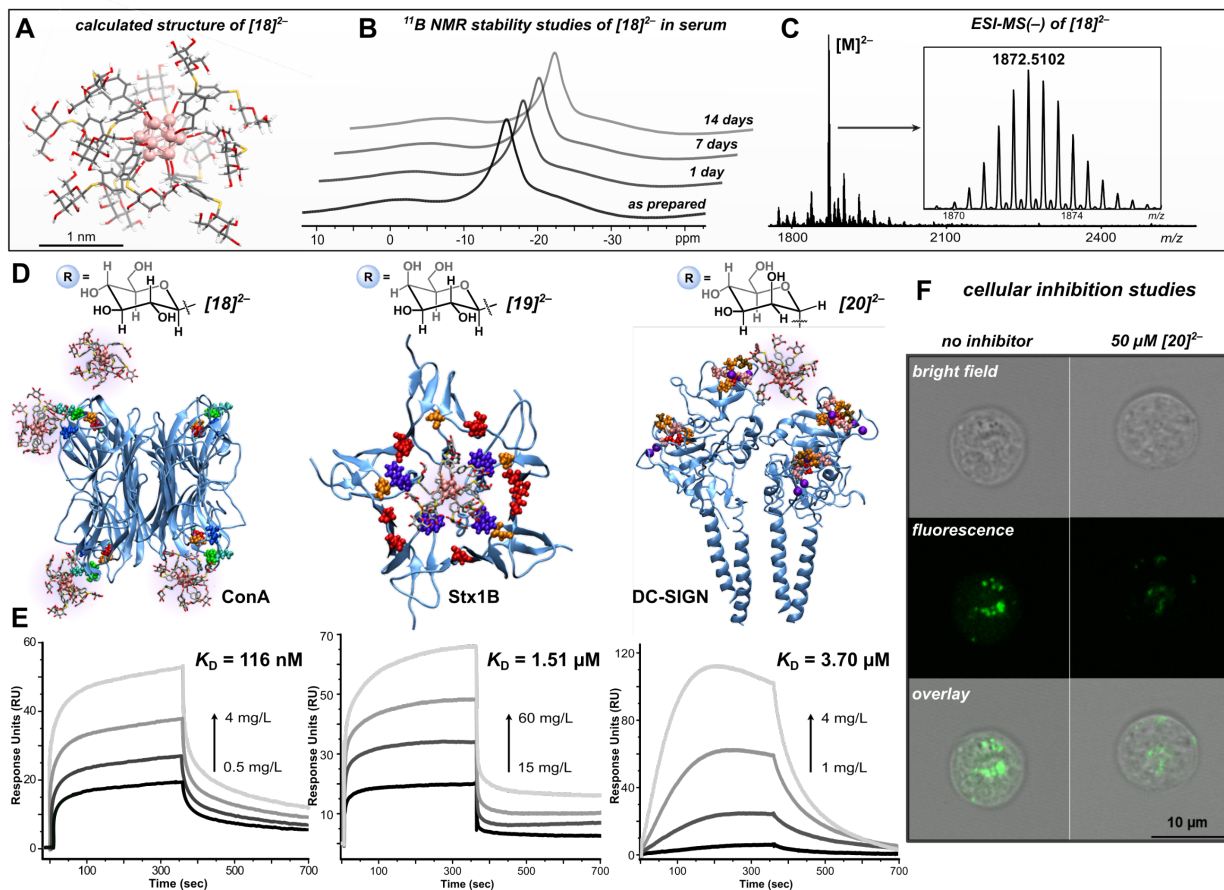


**Figure 4.5.** (A) Calculated structure of  $[18]^{2-}$ . (B)  $^{11}\text{B}$  NMR stability studies of  $[18]^{2-}$  in fetal bovine serum monitored over the course of 14 days indicating the cluster maintains its structural integrity under these conditions. (C) ESI-MS(-) of  $[18]^{2-}$ . (D) Snapshots of MD simulations (after 20 ns) depicting the multivalent binding interactions between  $[18]^{2-}$  (one molecule per binding site) and ConA (left),  $[19]^{2-}$  and Stx1B (middle), and  $[20]^{2-}$  and DC-SIGN (right). (E) SPR sensorgrams with calculated  $K_D$  values for direct binding measurements of each nanocluster and its respective protein target depicted in (D). (F) Confocal microscopy images of Raji DC-SIGN+ cells incubated with FITC-tagged gp120 and DMSO (control, left) and with  $[\text{Na}_2][20]$  (right, 50  $\mu\text{M}$ ), showing significant inhibition of DC-SIGN mediated cellular entry of gp-120 in the presence of the  $[\text{Na}_2][20]$  inhibitor.

ConA, a protein specific for manno- and glucopyranosides,<sup>181</sup> was initially investigated as a model target. The binding affinity ( $K_D$ ) of the glucose-functionalized conjugate,  $[\text{Na}_2][18]$ , with

ConA was determined to be 116 nM at pH 7.4 based on SPR binding experiments (Figure 4.5E). This  $K_D$  value agrees well with the equilibrium constant determined for the previously developed dodecaborate perfluoroaryl analogue (54 nM)<sup>6</sup> with ConA under similar experimental conditions. When the PEGylated ( $[K_2][\mathbf{8}]$ ) cluster control was injected at the highest mass concentration of  $[Na_2][\mathbf{18}]$  evaluated ( $4 \text{ mgL}^{-1}$ ,  $1 \text{ }\mu\text{M}$ ), only minimal binding was observed (see the Supporting Information for experimental details and SPR data), indicating that ConA binds  $[\mathbf{18}]^{2-}$  with a high degree of specificity. Similarly, a negligible response was observed when a solution of the D-glucose monomer was injected at a significantly higher concentration ( $40 \text{ mgL}^{-1}$ ,  $200 \text{ }\mu\text{M}$ ) over the protein surface, suggesting that the multivalent nature of  $[\mathbf{18}]^{2-}$  results in a dramatically enhanced binding profile per mole of saccharide. In fact, the  $K_D$  value of  $[Na_2][\mathbf{18}]$  with ConA displays a nearly 3,000-fold enhancement (250-fold increase per saccharide) when compared with the  $K_D$  value reported for methyl D-glucopyranoside and ConA.<sup>99</sup> The determined binding affinity is consistent with the reported  $K_D$  value (15.8 nM) for the binding between ConA and a glycodendrimer that features over twice the number of D-glucose residues<sup>99</sup> when compared with the functionalization of  $[\mathbf{18}]^{2-}$ . The comparable  $K_D$  values highlight the advantages provided by the present system such as dense functionalization and core-scaffold rigidity when binding affinity is compared on a per-carbohydrate basis. To gain a better understanding of the cluster-target binding process, we performed a molecular dynamics (MD) simulation to model the dynamic nature of the multivalent interactions between  $[\mathbf{18}]^{2-}$  and each of the four binding sites of ConA (see the Supporting Information for experimental details and MD data), and a snapshot of the simulation is displayed in Figure 4.5D.

We next probed the binding interactions of the multivalent ligand-carrier,  $[B_{12}(OCH_2C_6H_4-1\text{-thio-D-galactose})]^{2-}$  ( $[Na_2][\mathbf{19}]$ ), with the B subunit of Shiga toxin 1 (Stx1B). Shiga toxin is an

AB<sub>5</sub>-type cytotoxin expressed by the *S. dysenteriae* strain of *E. coli* that contains one enzymatically active A subunit, and a radially-symmetric B subunit pentamer, and represents one of the most potent bacterial poisons known.<sup>208</sup> The B subunit features multiple sites that engage in multivalent binding interactions with the cellular receptor, globotriaosylceramide (Gb<sub>3</sub>), which is a galactose-containing glycolipid responsible for bacterial uptake into cells.<sup>208</sup> Since cell-surface binding is a critical first step in the cytotoxicity pathway of the pathogen, building multivalent agents that block the B pentamer from binding to Gb<sub>3</sub> is a potential method for protecting host cells from attack by the toxin.<sup>176</sup> A  $K_D$  value of 1.51  $\mu$ M was determined for the binding of [19]<sup>2-</sup> with Stx1B by direct SPR studies (Figure 4.5E). Even at high concentrations, the free D-galactose monomer does not bind to Stx1B (100 mg/L), and a phenylene-bridged disaccharide control (gal-C<sub>6</sub>H<sub>4</sub>-gal, 100 mg/L) fails to engage in significant binding with Stx1B as displayed by its minimal SPR response. These data suggest the multivalent binding properties of [19]<sup>2-</sup> are responsible for the enhancement in its binding capacity when compared with that of its mono- and divalent controls. The proposed multivalent nature of the binding process between [19]<sup>2-</sup> and Stx1B agrees well with the MD simulation performed for this cluster-protein system (see the Supporting Information for experimental details and MD data), and a snapshot of this dynamic interaction is displayed in Figure 4.5D.

Expanding our study, we investigated the multivalent binding properties of the mannosylated cluster, [20]<sup>2-</sup>, with the DC-SIGN receptor. DC-SIGN is a tetrameric receptor expressed in dendritic cells that recognizes mannose-rich glycoproteins, including the viral envelope glycoprotein of HIV-1 (gp-120) through multivalent carbohydrate-lectin interactions that facilitate receptor-mediated endocytosis.<sup>150</sup> We envisioned [20]<sup>2-</sup> could mimic the high surface density of mannose units on gp120 and therefore potentially serve as a multivalent inhibitor of the

DC-SIGN-mediated cellular uptake of the viral glycoprotein. SPR binding data reveal that  $[20]^{2-}$  exhibits an enhanced dose-dependent avidity ( $K_D = 3.7 \mu\text{M}$ , Figure 4.5E) toward DC-SIGN when compared with the negligible responses observed for the D-mannose monosaccharide and PEGylated controls ( $[8]^{2-}$ ) at significantly higher mass concentrations (see the Supporting Information for experimental details and SPR data). These findings support the multivalent nature of the binding interaction between  $[20]^{2-}$  and DC-SIGN and agree well with the MD simulation performed for this system (see the Supporting Information for experimental details and MD data), which displays the specific binding in atomic detail. The calculated  $K_D$  value is also in good agreement with the avidity of a related mannose-coated multivalent gold nanoparticle bearing 25 surface sugars that binds DC-SIGN with high affinity ( $K_D = 0.974 \mu\text{M}$ ).<sup>150</sup>

Given the strong affinity of  $[20]^{2-}$  towards DC-SIGN, we next conducted cell-based inhibition studies to probe the capacity of  $[20]^{2-}$  to prevent DC-SIGN-dependent cell recognition of gp120. An assay was conducted in which Raji DC-SIGN+ cells were incubated with FITC-tagged gp120 (FITC = fluorescein isothiocyanate) and either  $[20]^{2-}$ ,  $[8]^{2-}$ , free D-mannose, or DMSO as a control. Confocal fluorescence microscopy was used to image the cells and assess the cellular uptake of gp120, and thus the extent of glycoprotein binding inhibition. As shown in Figure 4.5F (left), in the absence of  $[20]^{2-}$ , gp120-FITC readily undergoes endocytosis by DC-SIGN-expressing Raji cells. In contrast, there was a significant reduction in the gp120-FITC cellular uptake in the presence of  $[20]^{2-}$  (Figure 4.5F, right), therefore indicating that the mannose-functionalized cluster can prevent the binding and cellular uptake of the gp120 viral envelope glycoprotein by blocking the extracellular receptor DC-SIGN. Consistent with the negligible binding response observed for  $[8]^{2-}$  and free D-mannose from the SPR binding studies, there was no detectable reduction in the gp120-FITC cellular uptake when experiments were conducted in

the presence of these control molecules (see the Supporting Information for experimental details and microscopy data). These results highlight the excellent selectivity of the present system and the critical role the multivalent nature of the binding interactions play in effective inhibition of DC-SIGN-dependent cellular uptake of gp120.

## **Conclusions**

With this work, we have introduced a new platform that allows for the rapid generation of a library of well-defined and functional abiotic nanoclusters with protein binding capabilities. This approach is operationally reminiscent of the chemoselective assembly process associated with thiol-capped AuNP synthesis, while providing access to molecules with enhanced properties such as atomic precision, and full covalency. Furthermore, this strategy provides exceptional control over multivalency and topological rigidity of the resulting nanoclusters, thereby expanding the underlying design principles governing the development of agents capable of engaging in the specific inhibition of complex protein targets. For the first time, combining elements of inorganic cluster chemistry, organometallic synthesis, and bio-nanotechnology, we have provided a basis for the generation of robust and programmable hybrid nanoclusters with unique applications targeting molecular recognition.

## Experimental Section

### General considerations

All manipulations were performed under open atmosphere conditions in a fume hood unless otherwise indicated.

### Materials

All reagents were purchased from Sigma Aldrich, Strem Chemicals, ChemImpex, Oakwood Chemicals, TCI, Fisher Scientific, Carbosynth, Combi-Blocks, or Alfa Aesar, and used as received unless otherwise noted. Solvents (EtOH (ethanol), dichloromethane (DCM), methanol (MeOH), acetone, acetonitrile (MeCN), dimethoxyethane (DME), diethyl ether (Et<sub>2</sub>O), *N,N*-dimethylformamide (DMF), ethyl acetate (EtOAc), hexanes, and dimethyl sulfoxide (DMSO)) were used as received without further purification unless otherwise specified. *Para*-iodo thiophenol,<sup>209</sup> Me-DalPhos,<sup>210</sup>  $[(\text{Me-DalPhos})\text{AuCl}]_2\text{C}_6\text{H}_4[\text{SbF}_6]_2$ ,<sup>194</sup> and  $[\text{TBA}]_2[\text{B}_{12}(\text{OH})_{12}]$ <sup>81</sup> were prepared following previously reported procedures. The (Me-DalPhos)AuCl complex was either used as received (Sigma Aldrich) or prepared according to a procedure adapted from the literature.<sup>199</sup> Glutathione (reduced), concanavalin A (ConA), and Shiga toxin 1, B subunit were purchased from Sigma Aldrich and stored at -20 °C prior to use. Na[1-thio-β-D-glucose] (Sigma Aldrich), Na[1-thio-β-D-galactose] (ChemImpex), and Na[1-thio-α-D-mannose] (Carbosynth) were purchased from commercial sources and used as received. AgSbF<sub>6</sub> and  $[\text{TBA}]_2[\text{B}_{12}(\text{OH})_{12}]$  were stored under an atmosphere of purified N<sub>2</sub> in a Vacuum Atmospheres NexGen glovebox prior to use. Deuterated solvents (CD<sub>3</sub>CN, CD<sub>3</sub>OD, acetone-*d*<sub>6</sub>, CD<sub>2</sub>Cl<sub>2</sub>, CDCl<sub>3</sub>, and D<sub>2</sub>O) were obtained



from Cambridge Isotope Laboratories and used as received. Aqueous solutions of TRIS (tris(hydroxymethyl)aminomethane) buffer were prepared by dissolution of TRIS•HCl (Sigma Aldrich) in Milli-Q water and adjustment to the appropriate pH with NaOH. TRIS buffer solutions in DMF were prepared by dissolution of the free Trizma base (Sigma Aldrich) in DMF.

Soluble recombinant DC-SIGN Extracellular Domain (ECD) was produced in *E. coli* and purified *via* affinity chromatography and refolded as described previously,<sup>159</sup> then further purified *via* size exclusion chromatography.

### **Instruments and methods**

All NMR spectra were obtained on Bruker Avance 400 or 300 MHz broad band FT NMR spectrometers. <sup>1</sup>H NMR and <sup>13</sup>C{<sup>1</sup>H} NMR spectra were referenced to residual protio-solvent signals, <sup>31</sup>P{<sup>1</sup>H} NMR chemical shifts are reported with respect to an external reference (85% H<sub>3</sub>PO<sub>4</sub> in H<sub>2</sub>O, δ 0.0 ppm), <sup>19</sup>F NMR spectra were referenced to freon-113 (1% in C<sub>6</sub>D<sub>6</sub>, δ -68.22 and -72.50 ppm relative to CFCl<sub>3</sub>), and <sup>11</sup>B{<sup>1</sup>H} chemical shifts were referenced to BF<sub>3</sub>•Et<sub>2</sub>O (15% in CDCl<sub>3</sub>, δ 0.0 ppm). ESI-MS data were collected on a Thermo Instruments Q-Exactive Plus Hybrid Quadrupole-Orbitrap instrument operating in ESI-negative mode for all detections. Full mass scan (1000 to 5000 *m/z*) was used at 70,000 resolution, with automatic gain control (AGC) target of 1 x 10<sup>6</sup> ions, electrospray ionization operating at a 1.5 kV spray voltage, and a capillary temperature of 250 °C. LC-MS data were collected on an Agilent 1260 Infinity 6530 Q-TOF ESI instrument using an Agilent ZORBAX 300SB-C18 column (2.1 × 150 mm, 5 μm). Elemental analyses (C, H, N) were performed by Atlantic Microlab Inc. EPR measurements were carried out using an X-band ADANI SPINSCAN X instrument with a microwave frequency of 9.42 GHz and

cavity temperature of 32 °C, and the data were processed using ADANI e-SPINOZA software. UV-vis measurements were conducted using an Ocean Optics Flame-S-UV-VIS-ES miniature spectrometer equipped with a DH-2000 UV-vis NIR light source. All measurements were carried out using quartz cuvettes (1 cm path length) and conducted at 25 °C with solution samples ranging in concentration from 0.1–0.06 mM. Cyclic voltammetry measurements were performed with a CH Instruments CHI630D potentiostat using a glassy carbon working electrode, platinum counter electrode and Ag/AgCl pseudo-reference electrode. Measurements were conducted at a scan rate of 100 mV/s with [TBA][PF<sub>6</sub>] (0.1 M, DCM) supporting electrolyte under an inert atmosphere of N<sub>2</sub> and referenced vs. Fc/Fc<sup>+</sup>. High performance liquid chromatography (HPLC) purification was performed on an Agilent Technologies 1260 Infinity II HPLC instrument equipped with a Variable Wavelength Detector (VWD, 254, 214 nm) and using an Agilent ZORBAX SB-C18 (9.4 × 250 mm, 5 μm) reversed-phase column.

Microwave reactions were performed using a CEM Discover SP microwave synthesis reactor. All reactions were performed in 10 mL glass microwave reactor vials purchased from CEM with silicone/PTFE caps. Teflon coated stir bars were used in the vials with magnetic stirring set to high with 15 s of premixing prior to the temperature ramping. All microwave reactions were carried out at 140 °C with the pressure release limit set to 250 psi and the maximum wattage set to 250 W. The power applied was dynamically controlled by the microwave instrument and did not exceed this limit for any reactions.

### Synthesis of Me-DalPhos

The Me-DalPhos ligand was prepared as previously reported by Stradiotto *et al.*<sup>210</sup>

The  $^1\text{H}$  and  $^{31}\text{P}\{^1\text{H}\}$  NMR spectra match the reported data.  $^1\text{H}$  NMR (400 MHz, 25 °C,  $\text{CDCl}_3$ )  $\delta$ : 7.71 (m, 1H, Ar-*H*), 7.32 (m, 1H, Ar-*H*), 7.20 (m, 1H, Ar-*H*), 7.05 (m, 1H, Ar-*H*), 2.71 (s, 6H,  $\text{N}(\text{CH}_3)_2$ ), 2.01–1.89 (m, 18H, 1-Ad), 1.67 (s, 12H, 1-Ad) ppm.  $^{31}\text{P}\{^1\text{H}\}$  NMR (162 MHz, 25 °C,  $\text{CDCl}_3$ )  $\delta$ : 20.1 ppm.

### Synthesis of (Me-DalPhos)AuCl

The preparation of (Me-DalPhos)AuCl was adapted from a similar procedure reported by Stradiotto *et al.*<sup>199</sup>

To a stirring solution of  $\text{HAuCl}_4 \cdot 3\text{H}_2\text{O}$  (165 mg, 0.419 mmol, 1.00 equiv) in  $\text{H}_2\text{O}$  (1 mL) was added 2,2'-thiodiethanol (126  $\mu\text{L}$ , 1.22 mmol, 3.00 equiv) over the course of 30 min during which time the color of the reaction mixture changed from yellow to colorless. To this mixture was added solid Me-DalPhos (177 mg, 0.420 mmol, 1.00 equiv) all at once followed by EtOH (3 mL), and the resulting colorless suspension was allowed to stir at 25 °C for an additional 3 h. The suspension was then filtered, and the colorless solids were washed with MeOH ( $4 \times 2$  mL), and dried under reduced pressure to afford (Me-DalPhos)AuCl as a colorless powder (184 mg, 0.280 mmol, 67%).  $^1\text{H}$  NMR (400 MHz, 25 °C,  $\text{CD}_2\text{Cl}_2$ )  $\delta$ : 7.77 (m, 1H, Ar-*H*), 7.60–7.52 (m, 2H, Ar-*H*), 7.31 (m, 1H, Ar-*H*), 2.57 (s, 6H,  $\text{N}(\text{CH}_3)_2$ ), 2.25–2.21 (m, 6H, 1-Ad), 2.11–2.07 (m, 6H, 1-Ad), 1.99 (m, 6H, 1-Ad), 1.69 (s, 12H, 1-Ad) ppm.  $^{31}\text{P}\{^1\text{H}\}$  NMR (162 MHz, 25 °C,  $\text{CD}_2\text{Cl}_2$ )  $\delta$ : 56.8 ppm.

### Synthesis of $\text{B}_{12}(\text{OCH}_2\text{C}_6\text{H}_4)_{12}$

$[\text{TBA}]_2[\text{B}_{12}(\text{OH})_{12}]$  (100 mg, 0.122 mmol, 1.00 equiv) was removed from a nitrogen-filled glovebox and transferred to a 10 mL microwave reaction tube equipped with a Teflon-coated stir

bar. To this tube was added 4-iodobenzylbromide (1.090 g, 3.671 mmol, 30.00 equiv) and *N,N*-diisopropylethylamine (400  $\mu$ L, 2.30 mmol, 18.8 equiv), followed by MeCN (2 mL). The reaction tube was capped with a PTFE/silicone cap and the mixture was heated to 140  $^{\circ}$ C with stirring in the microwave for 1 h. The reaction mixture was then removed from the microwave, and the resulting bright magenta reaction mixture was evaporated to dryness, and the residue was suspended in a mixture of 35/65 EtOAc/hexanes (4 mL) and acetone (1 mL), and then loaded into a silica-packed column. The excess 4-iodobenzyl bromide was eluted first using a 35:65 EtOAc:hexanes mixture, followed by elution of the magenta band consisting of a mixture of the [TBA][B<sub>12</sub>(OCH<sub>2</sub>C<sub>6</sub>H<sub>4</sub>I)<sub>12</sub>]/[TBA]<sub>2</sub>[B<sub>12</sub>(OCH<sub>2</sub>C<sub>6</sub>H<sub>4</sub>I)<sub>12</sub>] species with acetone. The acetone solution was evaporated to dryness and then the resulting magenta residue was suspended in a 90:10 EtOH:MeCN mixture (5 mL). To this suspension was added FeCl<sub>3</sub>•6H<sub>2</sub>O (300 mg, 1.11 mmol, 9.10 equiv) as a solid, resulting in an immediate darkening of the color of the reaction mixture. The suspension was allowed to stir at 25  $^{\circ}$ C for a total of 20 h, at which point all volatiles were removed *in vacuo*. The resulting dark red residue was dissolved in DCM (4 mL) and eluted through a silica plug with DCM. A dark red band was recovered, and all volatiles were removed from the solution under reduced pressure, resulting in isolation of the neutral B<sub>12</sub>(OCH<sub>2</sub>C<sub>6</sub>H<sub>4</sub>I)<sub>12</sub> product as a dark red, crystalline solid in 76% yield (273 mg, 0.0933 mmol). Single dark red crystals of suitable quality for an X-ray diffraction study were grown by vapor diffusion of Et<sub>2</sub>O into a saturated DCM solution of B<sub>12</sub>(OCH<sub>2</sub>C<sub>6</sub>H<sub>4</sub>I)<sub>12</sub> at 25  $^{\circ}$ C over the course of 24 h. Elem. Anal. found for C<sub>84</sub>H<sub>72</sub>O<sub>12</sub>B<sub>12</sub>I<sub>12</sub> (calc'd): C: 34.70 (34.43); H: 2.46 (2.48). UV-vis (DCM, 25  $^{\circ}$ C, 0.1 mM) [ $\epsilon$ ]: 451 nm [15,500 M<sup>-1</sup>cm<sup>-1</sup>]. <sup>1</sup>H NMR (400 MHz, 25  $^{\circ}$ C, CDCl<sub>3</sub>)  $\delta$ : 7.51 (d, 24H, Ar-H, <sup>3</sup>J = 8 Hz), 6.71 (d, 24H, Ar-H, <sup>3</sup>J = 8 Hz), 5.03 (s, 24H, -CH<sub>2</sub>-) ppm. <sup>13</sup>C {<sup>1</sup>H} NMR (101 MHz, 25  $^{\circ}$ C, CDCl<sub>3</sub>)  $\delta$ : 139.3 (C<sub>Ar</sub>-O), 137.7 (C<sub>Ar</sub>H), 128.8 (C<sub>Ar</sub>H), 93.2 (C<sub>Ar</sub>-I), 72.8 (-CH<sub>2</sub>-) ppm. <sup>11</sup>B {<sup>1</sup>H}

NMR (128 MHz, 25 °C, CDCl<sub>3</sub>) δ: 41.5 ppm. ESI-MS(-) (MeCN): 2926.4649 (calc'd, 2926.4778) *m/z*. The dianionic species is observed under ESI-MS conditions in MeCN.

### Synthesis of [B<sub>12</sub>(OCH<sub>2</sub>C<sub>6</sub>H<sub>4</sub>((Me-DalPhos)AuCl)<sub>12</sub>][SbF<sub>6</sub>]<sub>11</sub> (**1**)[SbF<sub>6</sub>]<sub>11</sub>)

To a cooled (-4 °C) solution of AgSbF<sub>6</sub> (10 mg, 0.029 mmol, 20 equiv) in DCM (1 mL) was added a cooled (-4 °C) solution of B<sub>12</sub>(OCH<sub>2</sub>C<sub>6</sub>H<sub>4</sub>I)<sub>12</sub> (4 mg, 0.001 mmol, 1 equiv) and (Me-DalPhos)AuCl (19 mg, 0.029 mmol, 20 equiv) in DCM (1 mL) under protection from light. The reaction mixture was sealed and placed in a preheated oil bath set to 45 °C and allowed to stir for a total of 16 h under protection from light. The maroon suspension was then filtered through a pad of Celite, resulting in a pale-yellow filtrate and dark red filter cake containing the product. The filter cake was washed with DCM (3 × 2 mL) to remove unreacted (Me-DalPhos)AuCl, and then the product was extracted with DMF (1.5 mL) and filtered through the pad of Celite to give a purple/red filtrate. To the filtrate was added Et<sub>2</sub>O (20 mL) with stirring, resulting in the precipitation of [B<sub>12</sub>(OCH<sub>2</sub>C<sub>6</sub>H<sub>4</sub>((Me-DalPhos)AuCl)<sub>12</sub>][SbF<sub>6</sub>]<sub>11</sub> as a dark pink powder.\* The precipitate was collected by filtration, washed with Et<sub>2</sub>O (2 × 3 mL), and dried under reduced pressure to afford a pink solid (7 mg, 40%, 0.6 μmol). The resulting solids were dissolved in MeCN (0.5 mL) and then the solution was filtered through a piece of glass microfiber filter paper. DME (0.5 mL) was carefully layered on top of the resulting dark pink solution followed by careful layering of Et<sub>2</sub>O (1 mL). This solution was allowed to stand at 25 °C for 18 h to afford a crop of dark pink crystals of suitable quality for an X-ray diffraction study (5 mg, 30%, 0.4 μmol). The crystalline material obtained following the described procedure was used for structural determination and all subsequent characterization of [**1**][SbF<sub>6</sub>]<sub>11</sub>. Elem. Anal. found for [B<sub>12</sub>(OCH<sub>2</sub>C<sub>6</sub>H<sub>4</sub>((Me-DalPhos)AuCl)<sub>12</sub>][SbF<sub>6</sub>]<sub>11</sub> (C<sub>420</sub>H<sub>552</sub>N<sub>12</sub>O<sub>12</sub>Au<sub>12</sub>B<sub>12</sub>Cl<sub>12</sub>Sb<sub>11</sub>F<sub>66</sub>) (calc'd): C:

42.47 (42.56); H: 4.85 (4.70); N: 1.44 (1.42). UV-vis (MeCN, 25 °C, 0.06 mM) [ $\epsilon$ ]: 350 [25,200 M<sup>-1</sup>cm<sup>-1</sup>], 543 [15,900 M<sup>-1</sup>cm<sup>-1</sup>] nm. <sup>1</sup>H NMR (400 MHz, 25 °C, CD<sub>3</sub>CN)  $\delta$ : 8.02 (m, 12H, Me-DalPhos Ar-*H*), 7.96 (m, 24h, Me-DalPhos Ar-*H*), 7.70 (t, 12H, Me-DalPhos Ar-*H*, <sup>3</sup>*J* = 6 Hz), 7.51 (br s, 48H, Ar-*H*), 3.42 (s, 72H, N(CH<sub>3</sub>)<sub>2</sub>), 2.23 (m, 72H, 1-Ad), 2.01 (m, 144H, 1-Ad, signals overlapping with CD<sub>3</sub>CN residual solvent signal), 1.67 (m, 144H, 1-Ad) ppm. The signals attributed to the aryl and methylene protons of the –OCH<sub>2</sub>C<sub>6</sub>H<sub>4</sub>– spacer are broadened due to their proximity to the paramagnetic [B<sub>12</sub>]<sup>-</sup> core.\* <sup>31</sup>P{<sup>1</sup>H} NMR (162 MHz, 25 °C, CD<sub>3</sub>CN)  $\delta$ : 75.8 ppm. <sup>11</sup>B{<sup>1</sup>H} NMR (128 MHz, 25 °C, CD<sub>3</sub>CN)  $\delta$ : A silent <sup>11</sup>B{<sup>1</sup>H} NMR spectrum was observed for [1][SbF<sub>6</sub>]<sub>11</sub> due to the paramagnetic dodecaborate [B<sub>12</sub>]<sup>-</sup> core.\*

\*It is noted that during the course of this reaction/workup procedure, the [B<sub>12</sub>] cluster core undergoes a one-electron reduction from the neutral ([B<sub>12</sub>]<sup>0</sup>) to monoanionic charge state ([B<sub>12</sub>]<sup>-</sup>). This redox chemistry corresponds to an overall charge for the permetalated complex, **1**, of 11+ as opposed to the expected 12+ charge, which would be the case in the absence of any cluster-based reduction (each (Me-DalPhos)Au<sup>III</sup>ClAr fragment carries a 1+ charge together with a charge compensating [SbF<sub>6</sub>]<sup>-</sup> anion). It has been reported by our group and others that perfunctionalized dodecaborate clusters undergo rich redox chemistry,<sup>81,197,211,212</sup> and it is likely that the DMF used in the described workup procedure serves as the reducing agent<sup>213</sup> to result in the formation of the [1][SbF<sub>6</sub>]<sub>11</sub> species.

## General procedure for conjugation reactions with [1][SbF<sub>6</sub>]<sub>11</sub>

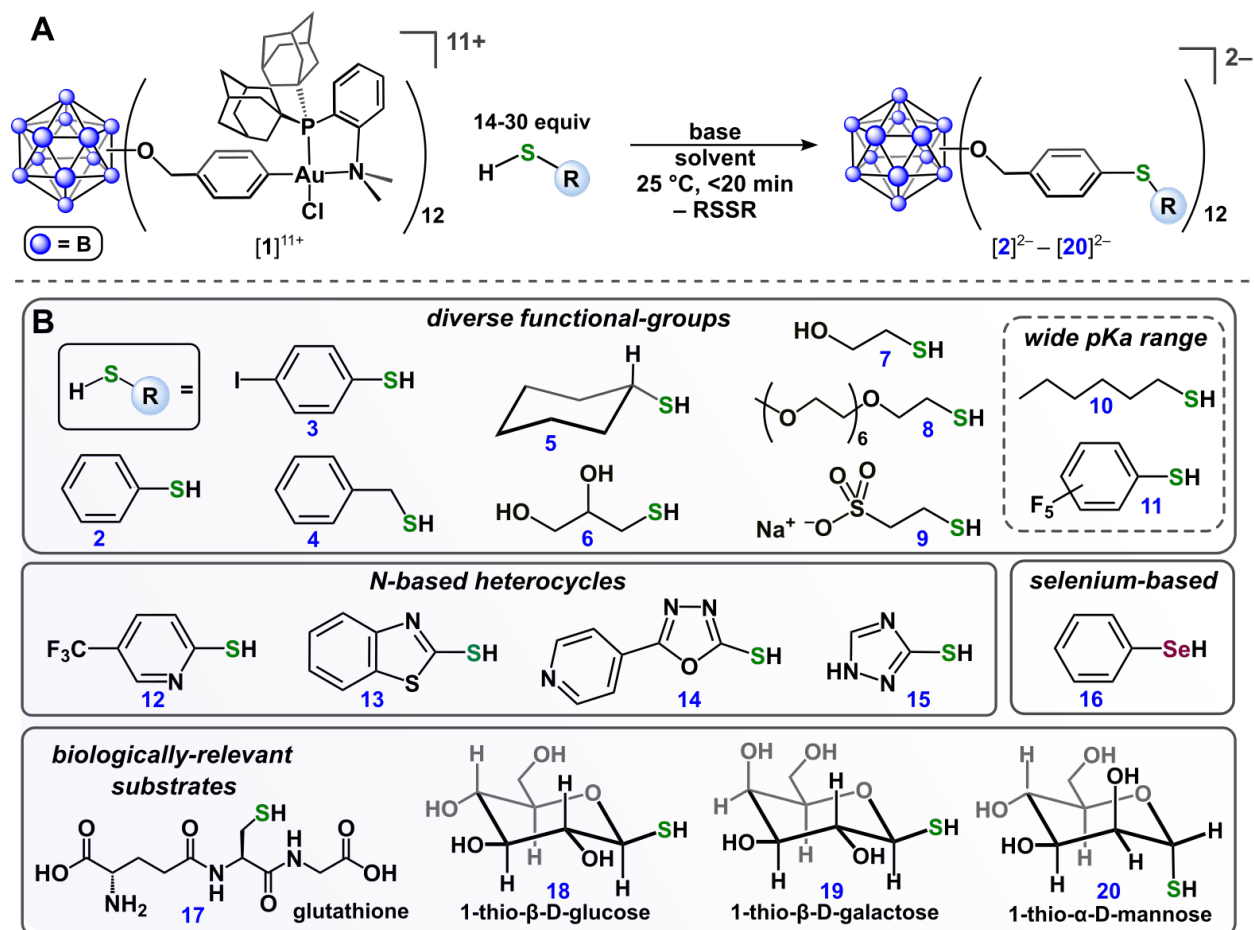


**Figure S4.1.** (A) General scheme for conjugation reactions of [1][SbF<sub>6</sub>]<sub>11</sub> with thiol-containing substrates. (B) Scope of nanocluster thio-conjugates.

To a cooled (-4 °C) solution of AgSbF<sub>6</sub> (10 mg, 0.029 mmol, 20 equiv) in DCM (1 mL) was added a cooled (-4 °C) solution of B<sub>12</sub>(OCH<sub>2</sub>C<sub>6</sub>H<sub>4</sub>I)<sub>12</sub> (4 mg, 0.001 mmol, 1 equiv) and (Me-DalPhos)AuCl (19 mg, 0.029 mmol, 20 equiv) in DCM (1 mL) under protection from light. The reaction mixture was sealed and placed in a preheated oil bath set to 45 °C and allowed to stir for a total of 16 h under protection from light. The maroon suspension was then filtered through a pad of Celite, resulting in a pale-yellow filtrate and dark red filter cake containing the product. The filter cake was then washed with DCM (3 × 2 mL), at which point the product was extracted with

DMF (1 mL) and filtered through the pad of Celite to give a purple/red filtrate. The  $[\mathbf{1}][\text{SbF}_6]_{11}$  complex was used in this DMF solution for all conjugation reactions and without further purification. This solution was treated with the corresponding thiol substrate and base as described in the following sections.

### Synthesis of $[\text{K}_2][\text{B}_{12}(\text{OCH}_2\text{C}_6\text{H}_4\text{SPh})_{12}]$ ( $[\text{K}_2][\mathbf{2}]$ )

The general reaction procedure to generate  $[\mathbf{1}][\text{SbF}_6]_{11}$  was followed. The DMF solution containing  $[\mathbf{1}][\text{SbF}_6]_{11}$  (0.0014 mmol, 1 mL) was transferred to a vial containing solid  $\text{K}_3\text{PO}_4$  (9 mg, 0.04 mmol, 30 equiv), and a Teflon-coated stir bar. To this solution was added a solution of thiophenol (35  $\mu\text{L}$  of a 0.97 M solution in MeCN, 0.034 mmol, 24 equiv) with stirring. The color of the reaction mixture gradually changed from dark purple to colorless over the course of 15 min, at which point all volatiles were removed under reduced pressure with gentle heating (35  $^\circ\text{C}$ ). The resulting colorless residue was suspended in a 65:35 hexanes:EtOAc mixture and loaded into a silica-packed pipette column. Using a 65:35 hexanes:EtOAc solvent combination, unreacted thiophenol and the (Me-DalPhos)AuCl byproduct were eluted first, followed by elution of the  $[\text{K}_2][\text{B}_{12}(\text{OCH}_2\text{C}_6\text{H}_4\text{SPh})_{12}]$  product with DCM. The product fractions were combined, and all volatiles were removed under reduced pressure to afford  $[\text{K}_2][\text{B}_{12}(\text{OCH}_2\text{C}_6\text{H}_4\text{SPh})_{12}]$  in 70% yield (3 mg, 0.001 mmol) as a pale pink, oily solid.  $^1\text{H}$  NMR (400 MHz, 25  $^\circ\text{C}$ ,  $\text{CD}_2\text{Cl}_2$ )  $\delta$ : 7.24-7.14 (m, 108H, Ar-*H*, all aromatic signals overlapping), 5.29 (s, 24H,  $-\text{CH}_2-$ ) ppm.  $^{11}\text{B}\{^1\text{H}\}$  NMR (128 MHz, 25  $^\circ\text{C}$ ,  $\text{CD}_2\text{Cl}_2$ )  $\delta$ : -15.6 ppm. ESI-MS(-): 1356.3758 (calc'd, 1356.3772) *m/z*.



### Synthesis of $[\text{K}_2][\text{B}_{12}(\text{OCH}_2\text{C}_6\text{H}_4\text{SC}_6\text{H}_4\text{I})_{12}]$ ( $[\text{K}_2][\mathbf{3}]$ )

The general reaction procedure to generate  $[\mathbf{1}][\text{SbF}_6]_{11}$  was followed. The DMF solution containing  $[\mathbf{1}][\text{SbF}_6]_{11}$  (0.0014 mmol, 1 mL) was transferred to a vial containing solid  $\text{K}_3\text{PO}_4$  (9 mg, 0.04 mmol, 30 equiv), *p*-iodothiophenol<sup>209</sup> (10 mg, 0.042 mmol, 30 equiv), and a Teflon-coated stir bar. The reaction mixture was allowed to stir at 25 °C for 15 min, during which time the color of the reaction mixture gradually changed from dark purple to colorless. All volatiles were then removed from the reaction mixture under reduced pressure with gentle heating (35 °C). The resulting colorless residue was suspended in a 65:35 hexanes:EtOAc mixture and loaded into a silica-packed pipette column. Using a 65:35 hexanes:EtOAc solvent combination, unreacted *p*-iodothiophenol and the (Me-DalPhos)AuCl byproduct were eluted first, followed by elution of the  $[\text{K}_2][\text{B}_{12}(\text{OCH}_2\text{C}_6\text{H}_4\text{SC}_6\text{H}_4\text{I})_{12}]$  product with DCM. The product fractions were combined, and all volatiles were removed *in vacuo* to afford  $[\text{K}_2][\text{B}_{12}(\text{OCH}_2\text{C}_6\text{H}_4\text{SC}_6\text{H}_4\text{I})_{12}]$  in 80% yield (5 mg, 0.001 mmol) as a colorless solid.  $^1\text{H}$  NMR (400 MHz, 25 °C, acetone-*d*<sub>6</sub>)  $\delta$ : 7.55 (d, 24H, Ar-*H*,  $^3J = 8$  Hz), 7.41 (d, 24H, Ar-*H*,  $^3J = 8$  Hz), 7.16 (d, 24H, Ar-*H*,  $^3J = 8$  Hz), 6.92 (d, 24H, Ar-*H*,  $^3J = 8$  Hz), 5.52 (s, 24H,  $-\text{CH}_2-$ ) ppm.  $^{11}\text{B}\{^1\text{H}\}$  NMR (128 MHz, 25 °C, acetone-*d*<sub>6</sub>)  $\delta$ : -16.1 ppm. ESI-MS(-): 2111.7569 (calc'd, 2111.7606) *m/z*.

### Synthesis of $[\text{K}_2][\text{B}_{12}(\text{OCH}_2\text{C}_6\text{H}_4\text{SCH}_2\text{C}_6\text{H}_5)_{12}]$ ( $[\text{K}_2][\mathbf{4}]$ )

The general reaction procedure to generate  $[\mathbf{1}][\text{SbF}_6]_{11}$  was followed. The DMF solution containing  $[\mathbf{1}][\text{SbF}_6]_{11}$  (0.0014 mmol, 1 mL) was transferred to a vial containing solid  $\text{K}_3\text{PO}_4$  (9 mg, 0.04 mmol, 30 equiv) and a Teflon-coated stir bar. To this solution was added a solution of benzylmercaptan (33  $\mu\text{L}$  of a 0.85 M solution in MeCN, 0.028 mmol, 20 equiv) with stirring. The color of the reaction mixture gradually changed from dark purple to colorless over the course of

15 min, at which point all volatiles were removed under reduced pressure with gentle heating (35 °C). The resulting colorless residue was suspended in a 65:35 hexanes:EtOAc mixture and loaded into a silica-packed pipette column. Using a 65:35 hexanes:EtOAc solvent combination, unreacted benzylmercaptan and the (Me-DalPhos)AuCl byproduct were eluted first, followed by elution of the  $[K_2][B_{12}(OCH_2C_6H_4SCH_2C_6H_5)_{12}]$  product with DCM. The product fractions were combined, and all volatiles were removed *in vacuo* to afford  $[K_2][B_{12}(OCH_2C_6H_4SCH_2C_6H_5)_{12}]$  as a pale-pink residue in 70% yield (3 mg, 0.9  $\mu$ mol).  $^1H$  NMR (400 MHz, 25 °C,  $CD_2Cl_2$ )  $\delta$ : 7.27–7.15 (m, 108H, Ar-H, all aromatic resonances overlapping), one  $CH_2$  resonance overlapping with residual DCM solvent peak, 4.08 (s, 24H,  $-CH_2-$ ) ppm.  $^{11}B\{^1H\}$  NMR (128 MHz, 25 °C,  $CD_2Cl_2$ )  $\delta$ : -15.7 ppm. ESI-MS(-): 1440.4703 (calc'd, 1440.4749) *m/z*.

#### **Synthesis of $[K_2][B_{12}(OCH_2C_6H_4(\text{cyclohexanethiol}))_{12}]$ ( $[K_2][5]$ )**

The general reaction procedure to generate  $[1][SbF_6]_{11}$  was followed. The DMF solution containing  $[1][SbF_6]_{11}$  (0.0014 mmol, 1 mL) was transferred to a vial containing solid  $K_3PO_4$  (9 mg, 0.04 mmol, 30 equiv), and a Teflon-coated stir bar. To this solution was added a solution of cyclohexanethiol (50  $\mu$ L of a 0.83 M solution in MeCN, 0.042 mmol, 30 equiv) with stirring. The color of the reaction mixture gradually changed from dark purple to colorless over the course of 15 min, at which point all volatiles were removed under reduced pressure with gentle heating (35 °C). The resulting colorless residue was suspended in an 80:20 hexanes:EtOAc mixture and loaded into a silica-packed pipette column. Using an 80:20 hexanes:EtOAc solvent combination, unreacted cyclohexanethiol and the (Me-DalPhos)AuCl byproduct were eluted first, followed by the  $[K_2][B_{12}(OCH_2C_6H_4(\text{cyclohexanethiol}))_{12}]$  product. The product fractions were combined, and all volatiles were removed under reduced pressure to afford

[K<sub>2</sub>][B<sub>12</sub>(OCH<sub>2</sub>C<sub>6</sub>H<sub>4</sub>(cyclohexanethiol))<sub>12</sub>] as an oily pale-pink residue in 75% yield (3 mg, 0.001 mmol). <sup>1</sup>H NMR (400 MHz, 25 °C, acetone-*d*<sub>6</sub>) δ: 7.29 (d, 24H, Ar-*H*, <sup>3</sup>*J* = 8 Hz), 7.18 (d, 24H, Ar-*H*, <sup>3</sup>*J* = 8 Hz), 5.45 (s, 24H, -CH<sub>2</sub>-), 3.10–3.08 (m, 12H, S-CH cyclohexane), 1.96–1.92 (m, 24H, cyclohexane), 1.77–1.74 (m, 24H, cyclohexane), 1.39–1.22 (m, 72H, cyclohexane) ppm. <sup>11</sup>B{<sup>1</sup>H} NMR (128 MHz, 25 °C, acetone-*d*<sub>6</sub>) δ: -15.1 ppm. ESI-MS(-): 1392.6616 (calc'd, 1392.6625) *m/z*.

### Synthesis of [K<sub>2</sub>][B<sub>12</sub>(OCH<sub>2</sub>C<sub>6</sub>H<sub>4</sub>(1-thioglycerol))<sub>12</sub>] ([K<sub>2</sub>][6])

The general reaction procedure to generate [1][SbF<sub>6</sub>]<sub>11</sub> was followed. The DMF solution containing [1][SbF<sub>6</sub>]<sub>11</sub> (0.0014 mmol, 1 mL) was transferred to a vial containing solid K<sub>3</sub>PO<sub>4</sub> (9 mg, 0.04 mmol, 30 equiv), and a Teflon-coated stir bar. To this solution was added a solution of 1-thioglycerol (36 μL of a 1.2 M solution in MeCN, 0.042 mmol, 30 equiv) with stirring. The color of the reaction mixture gradually changed from dark purple to colorless over the course of 15 min, at which point all volatiles were removed under reduced pressure with gentle heating (35 °C). The resulting colorless residue was suspended in an 65:35 hexanes:EtOAc mixture and loaded into a silica-packed pipette column. Using a 65:35 hexanes:EtOAc solvent combination, the (Me-DalPhos)AuCl byproduct was eluted first, followed by elution of unreacted 1-thioglycerol with acetone. The [K<sub>2</sub>][B<sub>12</sub>(OCH<sub>2</sub>C<sub>6</sub>H<sub>4</sub>(1-thioglycerol))<sub>12</sub>] product was then eluted with MeOH. The fractions containing the product were combined and then all volatiles were removed under reduced pressure to afford [K<sub>2</sub>][B<sub>12</sub>(OCH<sub>2</sub>C<sub>6</sub>H<sub>4</sub>(1-thioglycerol))<sub>12</sub>] in 50% yield (2 mg, 0.7 μmol) as a pale-pink oily solid. <sup>1</sup>H NMR (400 MHz, 25 °C, CD<sub>3</sub>OD) δ: 7.24–7.18 (two sets of doublets overlapping, 48H, Ar-*H*), 5.35 (s, 24H, -CH<sub>2</sub>-), 3.74–3.69 (m, 12H, -CH- glycerol), 3.62–3.53

(m, 24H,  $-CH_2-$  glycerol), 3.08–2.90 (m, 24H,  $-CH_2-$  glycerol) ppm.  $^{11}\text{B}\{^1\text{H}\}$  NMR (128 MHz, 25 °C,  $\text{CD}_3\text{OD}$ )  $\delta$ : -14.6 ppm. ESI-MS(-): 1344.4214 (calc'd, 1344.4129)  $m/z$ .

### Synthesis of $[\text{K}_2][\text{B}_{12}(\text{OCH}_2\text{C}_6\text{H}_4(2\text{-mercaptoethanol}))_{12}]$ ( $[\text{K}_2][7]$ )

The general reaction procedure to generate  $[\mathbf{1}][\text{SbF}_6]_{11}$  was followed. The DMF solution containing  $[\mathbf{1}][\text{SbF}_6]_{11}$  (0.0014 mmol, 1 mL) was transferred to a vial containing solid  $\text{K}_3\text{PO}_4$  (9 mg, 0.04 mmol, 30 equiv), and a Teflon-coated stir bar. To this solution was added a solution of 2-mercaptoethanol (29  $\mu\text{L}$  of a 1.4 M solution in MeCN, 0.042 mmol, 30 equiv) with stirring. The color of the reaction mixture gradually changed from dark purple to colorless over the course of 15 min, at which point all volatiles were removed under reduced pressure with gentle heating (35 °C). The resulting colorless residue was suspended in EtOAc and loaded into a silica-packed pipette column. The unreacted (Me-DalPhos)AuCl byproduct was eluted with EtOAc first, followed by elution of the  $[\text{K}_2][\text{B}_{12}(\text{OCH}_2\text{C}_6\text{H}_4(2\text{-mercaptoethanol}))_{12}]$  product with acetone. The fractions containing the product were combined and then all volatiles were removed under reduced pressure to afford  $[\text{K}_2][\text{B}_{12}(\text{OCH}_2\text{C}_6\text{H}_4(2\text{-mercaptoethanol}))_{12}]$  as a pale pink residue in 60% yield (2 mg, 0.8  $\mu\text{mol}$ ).  $^1\text{H}$  NMR (400 MHz, 25 °C, acetone- $d_6$ )  $\delta$ : 7.29 (d, 24H, Ar-H,  $^3J = 8$  Hz), 7.18 (d, 24H, Ar-H,  $^3J = 8$  Hz), 5.45 (s, 24H,  $-CH_2-$ ), 3.67 (t, 24H,  $\text{CH}_2\text{-OH}$ ,  $^3J = 6$  Hz), 3.02 (t, 24H,  $\text{CH}_2\text{-S}$ ,  $^3J = 6$  Hz) ppm.  $^{11}\text{B}\{^1\text{H}\}$  NMR (128 MHz, 25 °C, acetone- $d_6$ )  $\delta$ : -15.1 ppm. ESI-MS(-): 1164.3479 (calc'd, 1164.3491)  $m/z$ .

### Synthesis of $[\text{K}_2][\text{B}_{12}(\text{OCH}_2\text{C}_6\text{H}_4(m\text{PEG}_{350}\text{ thiol}))_{12}]$ ( $[\text{K}_2][8]$ )

The general reaction procedure to generate  $[\mathbf{1}][\text{SbF}_6]_{11}$  was followed. The DMF solution containing  $[\mathbf{1}][\text{SbF}_6]_{11}$  (0.0014 mmol, 1 mL) was transferred to a vial containing solid  $\text{K}_3\text{PO}_4$  (9

mg, 0.04 mmol, 30 equiv), and a Teflon-coated stir bar. To this solution was added a solution of *m*PEG<sub>350</sub> thiol (*O*-(2-Mercaptoethyl)-*O'*-methyl-hexa(ethylene glycol) purchased from Sigma Aldrich) (15 mg, 0.042 mmol, 30 equiv) in H<sub>2</sub>O (0.5 mL) with stirring. The reaction mixture was allowed to stir at 25 °C for 20 min, during which time the color changed from purple to colorless. All volatiles were then removed under reduced pressure with gentle heating (35 °C). The resulting residue was dissolved in MeOH (0.5 mL) and loaded into a column packed with Sephadex LH20 medium in MeOH. The pure product was eluted as a pale pink band first, followed by elution of fractions containing (Me-DalPhos)AuCl and unreacted *m*PEG<sub>350</sub> thiol. The fractions containing the pure product were combined, and all volatiles were removed under reduced pressure to afford [K<sub>2</sub>][B<sub>12</sub>(OCH<sub>2</sub>C<sub>6</sub>H<sub>4</sub>(*m*PEG<sub>350</sub> thiol))<sub>12</sub>] as an oily pink residue (6 mg, 0.001 mmol, 75%). <sup>1</sup>H NMR (400 MHz, 25 °C, CD<sub>3</sub>OD) δ: 7.25 (d, 24H, Ar-*H*, <sup>3</sup>*J* = 8 Hz), 7.17 (d, 24H, Ar-*H*, <sup>3</sup>*J* = 8 Hz), 5.37 (s, 24H, -CH<sub>2</sub>-), 3.64–3.56 (m, 312H, *m*PEG<sub>350</sub>), 3.48 (m, 36H, *m*PEG<sub>350</sub>), 3.06 (t, 24H, *m*PEG<sub>350</sub>, <sup>3</sup>*J* = 7 Hz) ppm. <sup>11</sup>B {<sup>1</sup>H} NMR (128 MHz, 25 °C, CD<sub>3</sub>OD) δ: -14.4 ppm. ESI-MS(-): 2833.8776 (calc'd, 2833.8900) *m/z*.

### **Synthesis of [Na<sub>14</sub>][B<sub>12</sub>(OCH<sub>2</sub>C<sub>6</sub>H<sub>4</sub>(2-thioethanesulfonate))<sub>12</sub>] ([Na<sub>14</sub>][9])**

The general reaction procedure to generate [1][SbF<sub>6</sub>]<sub>11</sub> was followed. To a stirring solution of [1][SbF<sub>6</sub>]<sub>11</sub> (0.0014 mmol) and Na<sub>3</sub>PO<sub>4</sub> (7 mg, 0.04 mmol, 30 equiv) in DMF (1 mL) was added a solution of sodium 2-mercaptoethanesulfonate (7 mg, 0.04 mmol, 30 equiv) in H<sub>2</sub>O (1 mL). The purple reaction mixture was allowed to stir at 25 °C for a total of 15 min, during which time the solution gradually became colorless. All volatiles were then removed from the reaction mixture under reduced pressure. The resulting pale pink residue was suspended in H<sub>2</sub>O (4 mL), sonicated for 10 min, and then centrifuged (2,200 × g, 5 min). The supernatant was removed and filtered

through a 0.45  $\mu\text{m}$  PTFE syringe filter and into a Pall Microsep™ Advance 1K Omega Centrifugal Filter sample reservoir.\* The device was capped and centrifuged for 75 min at  $7,500 \times g$ . The device was then removed from the centrifuge, the solution in the filtrate receiver tube removed, and  $\text{H}_2\text{O}$  (5 mL) was added to the sample reservoir containing the aqueous solution of the product. This process was repeated twice more for a total of three centrifuge cycles. After the third cycle, the solution in the sample reservoir (ca. 0.5 mL) was removed, transferred to a 15 mL conical tube, and the  $\text{H}_2\text{O}$  was lyophilized overnight to afford  $[\text{Na}_{14}][\text{B}_{12}(\text{OCH}_2\text{C}_6\text{H}_4(2\text{-thioethanesulfonate}))_{12}]$  as a pale-pink powder (3 mg, 0.9  $\mu\text{mol}$ , 60%).  $^1\text{H}$  NMR (400 MHz, 25  $^\circ\text{C}$ ,  $\text{D}_2\text{O}$ )  $\delta$ : 7.24 (two sets of doublets overlapping, 48H, Ar-H), 5.31 (s, 24H,  $-\text{CH}_2-$ ), 3.33–3.26 (m, 24H,  $-\text{CH}_2-$ ), 3.19–3.13 (m, 24H,  $-\text{CH}_2-$ ) ppm.  $^{11}\text{B}\{^1\text{H}\}$  NMR (128 MHz, 25  $^\circ\text{C}$ ,  $\text{D}_2\text{O}$ )  $\delta$ : -15.4 ppm. ESI-MS(-): 537.5129 ( $[\text{B}_{12}(\text{OCH}_2\text{C}_6\text{H}_4(2\text{-thioethanesulfonate}))_{12}]^{14-} + 6\text{Na}^+ + 2\text{H}^+]^{6-}$ ; calc'd, 537.5170)  $m/z$ .

\*It is noted that prior to sample purification, the Pall Microsep™ Advance 1K Omega Centrifugal Filter was pre rinsed by filtering HPLC-grade  $\text{H}_2\text{O}$  (5 mL) through the device at  $7,500 \times g$  for 15 min. The filtrate was discarded prior to use.

### **Synthesis of $[\text{H}_3\text{NC}(\text{CH}_2\text{OH})_3/\text{Na}]_{14}[\text{B}_{12}(\text{OCH}_2\text{C}_6\text{H}_4(2\text{-thioethanesulfonate}))_{12}]$ ( $[\text{H}_3\text{NC}(\text{CH}_2\text{OH})_3/\text{Na}]_{14}[9]$ )**

The general reaction procedure to generate  $[1][\text{SbF}_6]_{11}$  was followed. To a stirring solution of  $[1][\text{SbF}_6]_{11}$  (0.0014 mmol) in DMF (1 mL) was added sodium 2-mercaptoethanesulfonate (7 mg, 0.04 mmol, 30 equiv) in an aqueous solution of TRIS buffer (0.5 mL of a 200 mM solution, pH 8). The purple reaction mixture was allowed to stir at 25  $^\circ\text{C}$  for a total of 15 min, at which point all volatiles were removed under reduced pressure. The resulting purple residue was suspended in  $\text{H}_2\text{O}$  (4 mL), sonicated for 10 min, and then centrifuged ( $2,200 \times g$ , 5 min). The purple supernatant was removed and filtered through a 0.45  $\mu\text{m}$  PTFE filter into a Pall Microsep™ Advance 1K

Omega Centrifugal Filter sample reservoir.\* The device was capped and centrifuged for 75 min at  $7,500 \times g$ . The device was then removed from the centrifuge, the solution in the filtrate receiver tube removed, and H<sub>2</sub>O (5 mL) was added to the sample reservoir containing the aqueous solution of the product. This process was repeated twice more for a total of three centrifuge cycles. After the third cycle, the solution in the sample reservoir (ca. 0.5 mL) was removed, transferred to a 15 mL conical tube, and the H<sub>2</sub>O was lyophilized overnight to afford [H<sub>3</sub>NC(CH<sub>2</sub>OH)<sub>3</sub>/Na]<sub>14</sub>[B<sub>12</sub>(OCH<sub>2</sub>C<sub>6</sub>H<sub>4</sub>(2-thioethanesulfonate))<sub>12</sub>] as a light purple powder (4 mg). <sup>1</sup>H NMR (400 MHz, 25 °C, D<sub>2</sub>O) δ: 7.24 (two sets of doublets overlapping, 48H, Ar-*H*), 5.32 (s, 24H, -CH<sub>2</sub>-), 3.68 (s, 60H, [H<sub>3</sub>NC(CH<sub>2</sub>OH)<sub>3</sub>]), 3.30–3.26 (m, 24H, -CH<sub>2</sub>-), 3.19–3.16 (m, 24H, -CH<sub>2</sub>-) ppm. <sup>11</sup>B {<sup>1</sup>H} NMR (128 MHz, 25 °C, D<sub>2</sub>O) δ: -15.4 ppm.

\*It is noted that prior to sample purification, the Pall Microsep™ Advance 1K Omega Centrifugal Filter was pre rinsed by filtering HPLC-grade H<sub>2</sub>O (5 mL) through the device at  $7,500 \times g$  for 15 min. The filtrate was discarded prior to use.

\*\*This reaction can be conducted using TRIS buffer as the base to generate the mixed cation species described above, or with Na<sub>3</sub>PO<sub>4</sub> as the base to prepare the [Na]<sub>14</sub>[B<sub>12</sub>(OCH<sub>2</sub>C<sub>6</sub>H<sub>4</sub>(2-thioethanesulfonate))<sub>12</sub>] salt.

### **Synthesis of [K<sub>2</sub>][B<sub>12</sub>(OCH<sub>2</sub>C<sub>6</sub>H<sub>4</sub>S(CH<sub>2</sub>)<sub>5</sub>CH<sub>3</sub>)<sub>12</sub>] ([K<sub>2</sub>][10])**

The general reaction procedure to generate [1][SbF<sub>6</sub>]<sub>11</sub> was followed. The DMF solution containing [1][SbF<sub>6</sub>]<sub>11</sub> (0.0014 mmol, 1 mL) was transferred to a vial containing solid K<sub>3</sub>PO<sub>4</sub> (9 mg, 0.04 mmol, 30 equiv), and a Teflon-coated stir bar. To this solution was added a solution of hexanethiol (60 μL of a 0.70 M solution in MeCN, 0.042 mmol, 30 equiv) with stirring. The color of the reaction mixture gradually changed from dark purple to colorless over the course of 20 min,

at which point all volatiles were removed under reduced pressure with gentle heating (35 °C). The resulting colorless residue was suspended in an 80:20 hexanes:EtOAc mixture and loaded into a silica-packed pipette column. Using an 80:20 hexanes:EtOAc solvent combination, unreacted hexanethiol and the (Me-DalPhos)AuCl byproduct were eluted first, followed by elution of the  $[\text{K}_2][\text{B}_{12}(\text{OCH}_2\text{C}_6\text{H}_4\text{S}(\text{CH}_2)_5\text{CH}_3)_{12}]$  product. The product fractions were combined, and all volatiles were removed under reduced pressure to afford  $[\text{K}_2][\text{B}_{12}(\text{OCH}_2\text{C}_6\text{H}_4\text{S}(\text{CH}_2)_5\text{CH}_3)_{12}]$  as a pale-pink oily residue in 80% yield (3 mg, 0.001 mmol).  $^1\text{H}$  NMR (400 MHz, 25 °C, acetone- $d_6$ )  $\delta$ : 7.29 (d, 24H, Ar-H,  $^3J = 8$  Hz), 7.13 (d, 24H, Ar-H,  $^3J = 8$  Hz), 5.44 (s, 24H,  $-\text{CH}_2-$ ), 2.89 (t, 24H, S- $\text{CH}_2$ - $\text{CH}_2$ ,  $^3J = 7$  Hz), 1.60 (quin, 24H,  $\text{CH}_2$ - $\text{CH}_2$ - $\text{CH}_2$ ,  $^3J = 7$  Hz), 1.44 (quin, 24H,  $\text{CH}_2$ - $\text{CH}_2$ - $\text{CH}_2$ ,  $^3J = 7$  Hz), 1.29 (m, 48H,  $\text{CH}_2$ - $(\text{CH}_2)_2$ - $\text{CH}_3$ ), 0.88 (t, 24H,  $\text{CH}_2$ - $\text{CH}_3$ ,  $^3J = 7$  Hz) ppm.  $^{11}\text{B}\{^1\text{H}\}$  NMR (128 MHz, 25 °C, acetone- $d_6$ )  $\delta$ : -15.3 ppm. ESI-MS(-): 1404.7557 (calc'd, 1404.7564)  $m/z$ .

### Synthesis of $[\text{K}_2][\text{B}_{12}(\text{OCH}_2\text{C}_6\text{H}_4\text{SC}_6\text{F}_5)_{12}]$ ( $[\text{K}_2][\mathbf{11}]$ )

The general reaction procedure to generate  $[\mathbf{1}][\text{SbF}_6]_{11}$  was followed. The DMF solution containing  $[\mathbf{1}][\text{SbF}_6]_{11}$  (0.0014 mmol, 1 mL) was transferred to a vial containing solid  $\text{K}_3\text{PO}_4$  (9 mg, 0.04 mmol, 30 equiv), and a Teflon-coated stir bar. To this solution was added pentafluorothiophenol (6  $\mu\text{L}$ , 0.04 mmol, 30 equiv) with stirring. The color of the reaction mixture gradually changed from dark purple to colorless over the course of 15 min, at which point all volatiles were removed under reduced pressure with gentle heating (35 °C). The resulting colorless residue was suspended in an 85:15 hexanes:EtOAc mixture and loaded into a silica-packed pipette column. Using an 85:15 hexanes:EtOAc solvent combination, unreacted pentafluorothiophenol and the (Me-DalPhos)AuCl byproduct were eluted first, followed by elution of the



[K<sub>2</sub>][B<sub>12</sub>(OCH<sub>2</sub>C<sub>6</sub>H<sub>4</sub>SC<sub>6</sub>F<sub>5</sub>)<sub>12</sub>] product with acetone. The product fractions were combined, and all volatiles were removed *in vacuo* to afford [K<sub>2</sub>][B<sub>12</sub>(OCH<sub>2</sub>C<sub>6</sub>H<sub>4</sub>SC<sub>6</sub>F<sub>5</sub>)<sub>12</sub>] as a colorless residue in 80% yield (4 mg, 0.001 mmol). <sup>1</sup>H NMR (400 MHz, 25 °C, CD<sub>2</sub>Cl<sub>2</sub>) δ: 7.14–7.06 (two sets of doublets overlapping, 48H, Ar-*H*), 5.18 (s, 24H, –CH<sub>2</sub>–) ppm. <sup>19</sup>F{<sup>1</sup>H} NMR (376 MHz, 25 °C, CD<sub>2</sub>Cl<sub>2</sub>) δ: -132.86 (d, 24F, *ortho*-F), -152.21 (t, 12F, *para*-F), -161.30 (m, 24F, *meta*-F) ppm. <sup>11</sup>B{<sup>1</sup>H} NMR (128 MHz, 25 °C, CD<sub>2</sub>Cl<sub>2</sub>) δ: -15.7 ppm. ESI-MS(–): 1896.0961 (calc'd, 1896.0981) *m/z*.

**Synthesis of [H<sub>3</sub>NC(CH<sub>2</sub>OH)<sub>3</sub>]<sub>2</sub>[B<sub>12</sub>(OCH<sub>2</sub>C<sub>6</sub>H<sub>4</sub>(2-thio-5-trifluoromethylpyridine))<sub>12</sub>] ([H<sub>3</sub>NC(CH<sub>2</sub>OH)<sub>3</sub>]<sub>2</sub>[12])**

The general reaction procedure to generate [1][SbF<sub>6</sub>]<sub>11</sub> was followed. The DMF solution (1 mL) containing [1][SbF<sub>6</sub>]<sub>11</sub> (0.0014 mmol) was transferred to a vial containing solid 2-mercapto-5-trifluoromethylpyridine (5 mg, 0.03 mmol, 20 equiv), and a Teflon-coated stir bar. To this stirring solution was added a solution of TRIS buffer in DMF (50 mM, 0.5 mL). The reaction mixture was allowed to stir at 25 °C for a total of 15 min, during which time the color of the solution changed to colorless. All volatiles were removed from the reaction mixture under reduced pressure, and the resulting colorless residue was dissolved in MeOH (0.5 mL) and loaded into a column packed with Sephadex LH20 medium in MeOH. The pure product was eluted first, followed by elution of fractions containing (Me-DalPhos)AuCl and unreacted 2-mercapto-5-trifluoromethylpyridine. The fractions containing the pure product were combined, and all volatiles were removed under reduced pressure to afford [H<sub>3</sub>NC(CH<sub>2</sub>OH)<sub>3</sub>]<sub>2</sub>[B<sub>12</sub>(OCH<sub>2</sub>C<sub>6</sub>H<sub>4</sub>(2-thio-5-trifluoromethylpyridine))<sub>12</sub>] as a colorless solid in 60% yield (3 mg, 8 μmol). <sup>1</sup>H NMR (400 MHz, 25 °C, CD<sub>3</sub>OD) δ: 8.49 (m, 12H, pyr H6), 7.61–7.59 (m, 36H, two resonances overlapping), 7.32 (d, 24H, Ar-*H*, <sup>3</sup>*J* = 8 Hz), 6.81 (d, 12H, pyr H3, <sup>3</sup>*J* = 9 Hz), 5.61 (br s, 24H, –CH<sub>2</sub>–, this signal is

broadened due to slow oxidation of the diamagnetic dianionic species to the paramagnetic monoanion in solution in the presence of air), 3.61 (s, 12H,  $[\text{H}_3\text{NC}(\text{CH}_2\text{OH})_3]^+$ ) ppm.  $^{19}\text{F}\{^1\text{H}\}$  NMR (376 MHz, 25 °C,  $\text{CD}_3\text{OD}$ )  $\delta$ : -63.70 ppm.  $^{11}\text{B}\{^1\text{H}\}$  NMR (128 MHz, 25 °C,  $\text{CD}_3\text{OD}$ )  $\delta$ : -14.5 ppm. ESI-MS(-): 1770.2774 (calc'd, 1770.2765) *m/z*.

### Synthesis of $[\text{K}_2][\text{B}_{12}(\text{OCH}_2\text{C}_6\text{H}_4(2\text{-mercaptobenzothiazole}))_{12}]$ ( $[\text{K}_2][\mathbf{13}]$ )

The general reaction procedure to generate  $[\mathbf{1}][\text{SbF}_6]_{11}$  was followed. The DMF solution (1 mL) containing  $[\mathbf{1}][\text{SbF}_6]_{11}$  (0.0014 mmol) was transferred to a vial containing solid  $\text{K}_3\text{PO}_4$  (9 mg, 0.04 mmol, 30 equiv), and 2-mercaptobenzothiazole (7 mg, 0.04 mmol, 30 equiv). The purple solution was allowed to stir at 25 °C for a total of 15 min, during which time the color of the reaction mixture changed to colorless. All volatiles were removed from the reaction mixture under reduced pressure, and the resulting colorless residue was suspended in EtOAc (0.5 mL) and loaded into a silica-packed pipette column. The unreacted 2-mercaptobenzothiazole and the (Me-DalPhos)AuCl byproduct were eluted first using EtOAc, followed by elution of the  $[\text{K}_2][\text{B}_{12}(\text{OCH}_2\text{C}_6\text{H}_4(2\text{-mercaptobenzothiazole}))_{12}]$  product with acetone. The product fractions were combined, and all volatiles were removed *in vacuo* to afford  $[\text{K}_2][\text{B}_{12}(\text{OCH}_2\text{C}_6\text{H}_4(2\text{-mercaptobenzothiazole}))_{12}]$  as a colorless solid in 80% yield (4 mg, 0.001 mmol).  $^1\text{H}$  NMR (400 MHz, 25 °C, acetone- $d_6$ )  $\delta$ : 7.71 (d, 24H, Ar-*H*,  $^3J = 8$  Hz), 7.69 (d, 12H, Ar-*H*,  $^3J = 8$  Hz), 7.63 (d, 12H, Ar-*H*,  $^3J = 8$  Hz), 7.56 (d, 24H, Ar-*H*,  $^3J = 8$  Hz), 7.31 (t, 12H, Ar-*H*,  $^3J = 8$  Hz), 7.11 (t, 12H, Ar-*H*,  $^3J = 8$  Hz), 5.80 (s, 24H, -*CH*<sub>2</sub>-) ppm.  $^{11}\text{B}\{^1\text{H}\}$  NMR (128 MHz, 25 °C, acetone- $d_6$ )  $\delta$ : -15.0 ppm. ESI-MS(-): 1698.6726 (calc'd, 1698.6840) *m/z*.

### Synthesis of $[\text{K}_2][\text{B}_{12}(\text{OCH}_2\text{C}_6\text{H}_4(2\text{-thio-5-(4\text{-pyridyl)}\text{-1,3,4\text{-oxadiazole}))}_{12}]$ ( $[\text{K}_2][14]$ )

The general reaction procedure to generate  $[\mathbf{1}][\text{SbF}_6]_{11}$  was followed. The DMF solution (1 mL) containing  $[\mathbf{1}][\text{SbF}_6]_{11}$  (0.0014 mmol) was transferred to a vial containing solid  $\text{K}_3\text{PO}_4$  (9 mg, 0.04 mmol, 30 equiv), and 2-thiol-5-(4-pyridyl)-1,3,4-oxadiazole (5 mg, 0.03 mmol, 20 equiv). The purple solution was allowed to stir at 25 °C for a total of 15 min, during which time the color of the reaction mixture changed to colorless. All volatiles were then removed from the reaction mixture under reduced pressure, and the resulting colorless residue was dissolved in MeOH (0.5 mL) and loaded into a column packed with Sephadex LH-20 medium in MeOH. The pure product was eluted first, followed by elution of fractions containing (Me-DalPhos)AuCl and unreacted 2-thiol-5-(4-pyridyl)-1,3,4-oxadiazole. The fractions containing the pure product were combined, and all volatiles were removed *in vacuo* to afford  $[\text{K}_2][\text{B}_{12}(\text{OCH}_2\text{C}_6\text{H}_4(2\text{-thio-5-(4\text{-pyridyl)}\text{-1,3,4\text{-oxadiazole}))}_{12}]$  as a colorless residue in 60% yield (3 mg, 0.8  $\mu\text{mol}$ ).  $^1\text{H}$  NMR (400 MHz, 25 °C,  $\text{CD}_2\text{Cl}_2$ )  $\delta$ : 8.67 (d, 24H, pyr-*H*,  $^3J = 6$  Hz), 7.69 (d, 24H, pyr-*H*,  $^3J = 6$  Hz), 7.59–7.53 (two sets of doublets overlapping, 48H, Ar-*H*), 5.63 (s, 24H,  $-\text{CH}_2-$ ) ppm.  $^{11}\text{B}\{^1\text{H}\}$  NMR (128 MHz, 25 °C,  $\text{CD}_2\text{Cl}_2$ )  $\delta$ : -15.3 ppm. ESI-MS(-): 1770.3601 (calc'd, 1770.3588) *m/z*.

### Synthesis of $[\text{K}_2][\text{B}_{12}(\text{OCH}_2\text{C}_6\text{H}_4(3\text{-thio-1,2,4\text{-triazole}))}_{12}]$ ( $[\text{K}_2][15]$ )

The general reaction procedure to generate  $[\mathbf{1}][\text{SbF}_6]_{11}$  was followed. The DMF solution (1 mL) containing  $[\mathbf{1}][\text{SbF}_6]_{11}$  (0.0014 mmol) was transferred to a vial containing solid  $\text{K}_3\text{PO}_4$  (9 mg, 0.04 mmol, 30 equiv) and 3-thiol-1,2,4-triazole (4 mg, 0.04 mmol, 30 equiv). The purple solution was allowed to stir at 25 °C for a total of 15 min, during which time the color of the reaction mixture changed to colorless. All volatiles were then removed from the reaction mixture under reduced pressure, and the resulting colorless residue was suspended in EtOAc (0.5 mL) and loaded into a

silica-packed pipette column. The unreacted 3-thiol-1,2,4-triazole and the (Me-DalPhos)AuCl byproduct were eluted first using EtOAc, followed by elution of the  $[\text{K}_2][\text{B}_{12}(\text{OCH}_2\text{C}_6\text{H}_4(3\text{-thio-1,2,4-triazole}))_{12}]$  product with MeOH. The product fractions were combined and all volatiles were removed under reduced pressure to afford  $[\text{K}_2][\text{B}_{12}(\text{OCH}_2\text{C}_6\text{H}_4(3\text{-thio-1,2,4-triazole}))_{12}]$  in 80% yield (3 mg, 0.001 mmol).  $^1\text{H}$  NMR (400 MHz, 25 °C,  $\text{CD}_3\text{OD}$ )  $\delta$ : 8.29 (s, 12H, CH, triazole), 7.22–7.17 (two sets of doublets overlapping, 24H, Ar-H), 5.31 (s, 24H,  $-\text{CH}_2-$ ) ppm.  $^{11}\text{B}\{^1\text{H}\}$  NMR (128 MHz, 25 °C,  $\text{CD}_3\text{OD}$ )  $\delta$ : -15.3 ppm. ESI-MS(-): 1301.7943 (calc'd, 1301.7900)  $m/z$ .

### Synthesis of $[\text{K}_2][\text{B}_{12}(\text{OCH}_2\text{C}_6\text{H}_4\text{SePh})_{12}]$ ( $[\text{K}_2][\mathbf{16}]$ )

The general reaction procedure to generate  $[\mathbf{1}][\text{SbF}_6]_{11}$  was followed. The DMF solution containing  $[\mathbf{1}][\text{SbF}_6]_{11}$  (0.0014 mmol, 1 mL) was transferred to a vial containing solid  $\text{K}_3\text{PO}_4$  (9 mg, 0.04 mmol, 30 equiv) and a Teflon-coated stir bar. To this solution was added phenylselenol (3  $\mu\text{L}$ , 0.03 mmol, 20 equiv) with stirring. The reaction mixture was allowed to stir at 25 °C for 15 min, during which time the color of the reaction mixture gradually changed from dark purple to colorless. All volatiles were then removed from the reaction mixture under reduced pressure with gentle heating (35 °C). The resulting colorless residue was suspended in an 85:15 hexanes:EtOAc mixture and loaded onto a silica-packed pipette column. Using an 85:15 hexanes:EtOAc solvent combination, unreacted phenylselenol and the (Me-DalPhos)AuCl byproduct were eluted first, followed by elution of the  $[\text{K}_2][\text{B}_{12}(\text{OCH}_2\text{C}_6\text{H}_4\text{SePh})_{12}]$  product with DCM. The product fractions were combined, and all volatiles were removed *in vacuo* to afford  $[\text{K}_2][\text{B}_{12}(\text{OCH}_2\text{C}_6\text{H}_4\text{SePh})_{12}]$  as a pale-pink residue in 60% yield (3 mg, 0.9  $\mu\text{mol}$ ).  $^1\text{H}$  NMR (400 MHz, 25 °C, acetone- $d_6$ )  $\delta$ : 7.35–7.18 (all aromatic resonances overlapping, m, 108H, Ar-H), 5.46 (s, 24H,  $-\text{CH}_2-$ ) ppm. It is noted that there is ca. 13% of (Me-DalPhos)AuCl present as an impurity

in the isolated material due to difficulty in its separation on silica gel.  $^{11}\text{B}\{^1\text{H}\}$  NMR (128 MHz, 25 °C, acetone- $d_6$ )  $\delta$ : -15.3 ppm. ESI-MS(-): 1638.0519 (calc'd, 1638.0528)  $m/z$ .

### Synthesis of $[\text{H}_3\text{NC}(\text{CH}_2\text{OH})_3][\text{B}_{12}(\text{OCH}_2\text{C}_6\text{H}_4(\text{glutathione}))_{12}]$ ( $[\text{H}_3\text{NC}(\text{CH}_2\text{OH})_3][17]$ )

The general reaction procedure to generate  $[\mathbf{1}][\text{SbF}_6]_{11}$  was followed. To a stirring solution of  $[\mathbf{1}][\text{SbF}_6]_{11}$  (0.0014 mmol) in DMF (1 mL) was added L-glutathione (6 mg, 0.02 mmol, 14 equiv) in an aqueous solution of TRIS buffer (1 mL of a 200 mM solution, pH 8). The purple reaction mixture was allowed to stir at 25 °C for a total of 15 min, at which point all volatiles were removed under reduced pressure. The resulting purple residue was suspended in H<sub>2</sub>O spiked with 0.1% TFA (1.5 mL), sonicated for 10 min, and then centrifuged (2,200 × g, 5 min). The purple supernatant was removed and filtered through a 0.22 μm PTFE filter, resulting in a homogeneous purple solution containing the product. The product was purified by reversed-phase HPLC with an Agilent Technologies 1260 Infinity II HPLC instrument equipped with a Variable Wavelength Detector (VWD, 254, 214 nm) and using an Agilent ZORBAX SB-C18 reversed-phase column (9.4 × 250 mm, 5 μm) with the following method (solvent A: H<sub>2</sub>O spiked with 0.1% TFA; solvent B: MeCN spiked with 0.1% TFA): 0–5 min, A (100%) : B (0%); 5–60 min, A (100–45%) : B (0–55%); 60–75 min, A (45–0%) : B (55–100%); 75–90 min, A (0%) : B (100%) and with a flow rate of 3 mL/min. The fractions containing the pure product were combined and the solvent was lyophilized to afford  $[\text{H}_3\text{NC}(\text{CH}_2\text{OH})_3][\text{B}_{12}(\text{OCH}_2\text{C}_6\text{H}_4(\text{glutathione}))_{12}]$  as a purple solid in 70% yield (5 mg, 0.001 mmol).  $^1\text{H}$  NMR (400 MHz, 25 °C, D<sub>2</sub>O spiked with CD<sub>3</sub>CN)  $\delta$ : 7.23 (br s, Ar-*H*), 4.59 (br s, glutathione), 3.82 (br s, glutathione), 3.37–3.23 (br m, glutathione), 2.45 (br s, glutathione) ppm. The signals observed in the  $^1\text{H}$  NMR spectrum are paramagnetically broadened due to the monoanionic dodecaborate  $[\text{B}_{12}]^-$  core.  $^{11}\text{B}\{^1\text{H}\}$  NMR (128 MHz, 25 °C, D<sub>2</sub>O spiked

with CD<sub>3</sub>CN)  $\delta$ : A silent <sup>11</sup>B{<sup>1</sup>H} NMR spectrum was observed due to the paramagnetic [B<sub>12</sub>]<sup>-</sup> core. ESI-MS(-): 847.6064 (calc'd, 847.6001 for [[B<sub>12</sub>(OCH<sub>2</sub>C<sub>6</sub>H<sub>4</sub>(glutathione))<sub>12</sub>]<sup>2-</sup> + 8H<sup>+</sup>]<sup>6+</sup>) *m/z*. UV-vis (H<sub>2</sub>O, 25 °C):  $\lambda_{\text{max}}$  549 nm.

### Synthesis of [Na<sub>2</sub>][B<sub>12</sub>(OCH<sub>2</sub>C<sub>6</sub>H<sub>4</sub>(1-thio- $\beta$ -D-glucose))<sub>12</sub>] ([Na<sub>2</sub>][18])

The general reaction procedure to generate [1][SbF<sub>6</sub>]<sub>11</sub> was followed. To a stirring solution of [1][SbF<sub>6</sub>]<sub>11</sub> (0.0014 mmol) in DMF (1 mL) was added a solution of Na[1-thio- $\beta$ -D-glucose] (9 mg, 0.04 mmol, 30 equiv) in H<sub>2</sub>O (0.5 mL). The resulting mixture was allowed to stir at 25 °C for 15 min, during which time the color of the solution changed from dark purple to colorless. All volatiles were then removed from the reaction mixture under reduced pressure, resulting in a colorless residue. To the solid residue was added H<sub>2</sub>O (4.5 mL), resulting in a colorless suspension. The suspension was sonicated (5 min), and then centrifuged (2,200  $\times$  g, 5 min). The supernatant was then removed and filtered through a 0.45  $\mu$ m PTFE filter into a Pall Microsep™ Advance 1K Omega Centrifugal Filter sample reservoir.\* The device was capped and centrifuged for 75 min at 7,500  $\times$  g. The device was then removed from the centrifuge, the solution in the filtrate receiver tube removed, and H<sub>2</sub>O (5 mL) was added to the sample reservoir containing the aqueous solution of the product. This process was repeated twice more for a total of three centrifuge cycles. After the third cycle, the solution in the sample reservoir (ca. 0.5 mL) was removed, transferred to a 15 mL conical tube, and the H<sub>2</sub>O was lyophilized overnight to afford [Na<sub>2</sub>][B<sub>12</sub>(OCH<sub>2</sub>C<sub>6</sub>H<sub>4</sub>(1-thio- $\beta$ -D-glucose))<sub>12</sub>] as a pale-pink powder (3 mg, 0.8  $\mu$ mol, 60%). <sup>1</sup>H NMR (400 MHz, 25 °C, D<sub>2</sub>O)  $\delta$ : 7.38 (d, 24H, Ar-*H*, <sup>3</sup>*J* = 7 Hz), 7.24 (br d, 24H, Ar-*H*), 5.25 (br s, 24H, -CH<sub>2</sub>-), 4.65 (d, 12H, *J* = 10 Hz, glc H1), 3.76 (d, 12H, *J* = 12 Hz, glc H6), 3.67–3.63 (dd, 12H, *J* = 5, 12 Hz, glc H6), 3.52 (t, 12H, *J* = 9 Hz, glc H3), 3.40 (t, 12H, *J* = 9 Hz, glc H5), 3.32 (t, 24H, *J* = 9 Hz, glc H4 and H2

signals overlapping) ppm (broadening of the aryl and methylene  $^1\text{H}$  NMR signals is due to slow oxidation of the diamagnetic dianionic species to the paramagnetic monoanion in  $\text{H}_2\text{O}$  in the presence of air).  $^{11}\text{B}\{^1\text{H}\}$  NMR (128 MHz, 25 °C,  $\text{D}_2\text{O}$ )  $\delta$ : -16.0 ppm. ESI-MS(-): 1878.5102 (calc'd, 1872.5103)  $m/z$ .

$^1\text{H}$  NMR (400 MHz, 25 °C,  $\text{CD}_3\text{OD}$ )  $\delta$ : 7.38 (d, 24H, Ar-H,  $^3J = 8$  Hz), 7.26 (d, 24H, Ar-H,  $^3J = 8$  Hz), 5.39 (s, 24H,  $-\text{CH}_2-$ ), 4.55 (d, 12H,  $J = 10$  Hz, glc H1), 3.84 (dd, 12H,  $J = 2, 12$  Hz, glc H6), 3.67 (dd, 12H,  $J = 5, 12$  Hz, glc H6), 3.42 (t, 12H,  $J = 9$  Hz, glc H4), 3.29 (glc H3 and H5 resonances overlapping with  $\text{CD}_3\text{OD}$  solvent, 24H), 3.19 (dd, 12H,  $J = 9, 10$  Hz, glc H2) ppm.  $^{11}\text{B}\{^1\text{H}\}$  NMR (128 MHz, 25 °C,  $\text{CD}_3\text{OD}$ )  $\delta$ : -14.9 ppm.

\*It is noted that prior to sample purification, the Pall Microsep™ Advance 1K Omega Centrifugal Filter was pre rinsed by filtering HPLC-grade  $\text{H}_2\text{O}$  (5 mL) through the device at  $7,500 \times g$  for 15 min. The filtrate was discarded prior to use.

### **Synthesis of $[\text{Na}_2][\text{B}_{12}(\text{OCH}_2\text{C}_6\text{H}_4(1\text{-thio-}\beta\text{-D-galactose))}_{12}]$ ( $[\text{Na}_2][\mathbf{19}]$ )**

The general reaction procedure to generate  $[\mathbf{1}][\text{SbF}_6]_{11}$  was followed. To a stirring solution of  $[\mathbf{1}][\text{SbF}_6]_{11}$  (0.0014 mmol) in DMF (1 mL) was added a solution of Na[1-thio- $\beta$ -D-galactose] (9 mg, 0.04 mmol, 30 equiv) in  $\text{H}_2\text{O}$  (0.5 mL). The resulting mixture was allowed to stir at 25 °C for 15 min, during which time the color of the solution changed from dark purple to colorless. All volatiles were then removed from the reaction mixture under reduced pressure, resulting in a colorless residue. To the solid residue was added  $\text{H}_2\text{O}$  (4.5 mL), resulting in a colorless suspension. The suspension was sonicated (5 min), and then centrifuged ( $2,200 \times g$ , 5 min). The supernatant was then removed and filtered through a 0.45  $\mu\text{m}$  PTFE filter into a Pall Microsep™ Advance 1K Omega Centrifugal Filter sample reservoir.\* The device was capped and centrifuged for 75 min at

7,500 × g. The device was then removed from the centrifuge, the solution in the filtrate receiver tube removed, and H<sub>2</sub>O (5 mL) was added to the sample reservoir containing the aqueous solution of the product. This process was repeated twice more for a total of three centrifuge cycles. After the third cycle, the solution in the sample reservoir (ca. 0.5 mL) was removed, transferred to a 15 mL conical tube, and the H<sub>2</sub>O was lyophilized overnight to afford [Na<sub>2</sub>][B<sub>12</sub>(OCH<sub>2</sub>C<sub>6</sub>H<sub>4</sub>(1-thio-β-D-galactose))<sub>12</sub>] as a pale-pink powder (3 mg, 0.8 μmol, 60%). <sup>1</sup>H NMR (400 MHz, 25 °C, D<sub>2</sub>O) δ: 7.39 (d, 24H, Ar-H, <sup>3</sup>J = 8 Hz), 7.23 (d, 24H, Ar-H, <sup>3</sup>J = 8 Hz), 5.26 (br s, 24H, -CH<sub>2</sub>-), 4.63 (d, 12H, J = 10 Hz, gal H1), 3.98 (d, 12H, J = 3 Hz, gal H4), 3.70–3.56 (m, 60H, gal H6, H5, H3, and H2 resonances overlapping) ppm (broadening of the aryl and methylene <sup>1</sup>H NMR signals is due to slow oxidation of the diamagnetic dianionic species to the paramagnetic monoanion in H<sub>2</sub>O in the presence of air). <sup>11</sup>B{<sup>1</sup>H} NMR (128 MHz, 25 °C, D<sub>2</sub>O) δ: -15.8 ppm. ESI-MS(-): 1878.5051 (calc'd, 1872.5103) m/z.

<sup>1</sup>H NMR (400 MHz, 25 °C, CD<sub>3</sub>OD spiked with D<sub>2</sub>O) δ: 7.35 (d, 24H, Ar-H, <sup>3</sup>J = 8 Hz), 7.23 (d, 24H, Ar-H, <sup>3</sup>J = 8 Hz), 5.35 (s, 24H, -CH<sub>2</sub>-), 4.57 (dd, 12H, J = 5, 10 Hz, gal H1), 3.94 (br m, 12H, gal H4), 3.77–3.67 (m, 24H, gal H6), 3.59 (m, 36H, gal H2 H3 and H5 resonances overlapping) ppm. <sup>11</sup>B{<sup>1</sup>H} NMR (128 MHz, 25 °C, CD<sub>3</sub>OD spiked with D<sub>2</sub>O) δ: -15.6 ppm.

\*It is noted that prior to sample purification, the Pall Microsep™ Advance 1K Omega Centrifugal Filter was pre rinsed by filtering HPLC-grade H<sub>2</sub>O (5 mL) through the device at 7,500 × g for 15 min. The filtrate was discarded prior to use.

### Synthesis of [Na<sub>2</sub>][B<sub>12</sub>(OCH<sub>2</sub>C<sub>6</sub>H<sub>4</sub>(1-thio-α-D-mannose))<sub>12</sub>] ([Na<sub>2</sub>][20])

The general reaction procedure to generate [1][SbF<sub>6</sub>]<sub>11</sub> was followed. To a stirring solution of [1][SbF<sub>6</sub>]<sub>11</sub> (0.0014 mmol) in DMF (1 mL) was added a solution of Na[1-thio-α-D-mannose] (9



mg, 0.04 mmol, 30 equiv) in H<sub>2</sub>O (0.5 mL). The resulting mixture was allowed to stir at 25 °C for 15 min, during which time the color of the solution changed from dark purple to colorless. All volatiles were then removed from the reaction mixture under reduced pressure, resulting in a colorless residue. To the solid residue was added H<sub>2</sub>O (4.5 mL), resulting in a colorless suspension. The suspension was sonicated (5 min), and then centrifuged (2,200 × g, 5 min). The supernatant was then removed and filtered through a 0.45 μm PTFE filter into a Pall Microsep™ Advance 1K Omega Centrifugal Filter sample reservoir.\* The device was capped and centrifuged for 75 min at 7,500 × g. The device was then removed from the centrifuge, the solution in the filtrate receiver tube removed, and H<sub>2</sub>O (5 mL) was added to the reservoir containing the aqueous solution of the product. This process was repeated twice more for a total of three centrifuge cycles. After the third cycle, the solution in the sample reservoir (ca. 0.5 mL) was removed, transferred to a 15 mL conical tube, and the H<sub>2</sub>O was lyophilized overnight to afford [Na<sub>2</sub>][B<sub>12</sub>(OCH<sub>2</sub>C<sub>6</sub>H<sub>4</sub>(1-thio- $\alpha$ -D-mannose))<sub>12</sub>] as a pale-pink powder (2 mg, 5 μmol, 40%). <sup>1</sup>H NMR (400 MHz, 25 °C, D<sub>2</sub>O spiked with CD<sub>3</sub>OD)  $\delta$ : 7.12–7.06 (two sets of doublets overlapping, 48H, Ar-*H*), 5.41 (s, 12H, man H1), 5.18 (br s, 24H, -CH<sub>2</sub>-), 4.24–4.08 (m, 48H, gal resonances overlapping), 3.88–3.72 (m, 72H, gal resonances overlapping) ppm (broadening of the aryl and methylene <sup>1</sup>H NMR signals is due to slow oxidation of the diamagnetic dianionic species to the paramagnetic monoanion in H<sub>2</sub>O in the presence of air). <sup>11</sup>B{<sup>1</sup>H} NMR (128 MHz, 25 °C, D<sub>2</sub>O spiked with CD<sub>3</sub>OD)  $\delta$ : -15.3 ppm. ESI-MS(-): 1248.0036 (calc'd, 1248.0046 for ([B<sub>12</sub>(OCH<sub>2</sub>C<sub>6</sub>H<sub>4</sub>(1-thio- $\alpha$ -D-mannose))<sub>12</sub> - H<sup>+</sup>]<sup>3-</sup>) *m/z*.

\*It is noted that prior to sample purification, the Pall Microsep™ Advance 1K Omega Centrifugal Filter was pre rinsed by filtering HPLC-grade H<sub>2</sub>O (5 mL) through the device at 7,500 × g for 15 min. The filtrate was discarded prior to use.

### Synthesis of $[B_{12}(OCH_2C_6H_4SC_6H_4(Me-DalPhos)AuCl)_{12}][SbF_6]_{10}$ (**[21]**)[ $SbF_6$ ]<sub>10</sub>)

To a cooled (-4 °C) solution of  $AgSbF_6$  (9 mg, 0.026 mmol, 16 equiv) in DCM (1 mL) was added a cooled solution (-4 °C) of  $[K_2][\mathbf{3}]$  (7 mg, 0.002 mmol, 1 equiv) and  $(Me-DalPhos)AuCl$  (17 mg, 0.026 mmol, 16 equiv) in DCM (1 mL) under protection from light. The reaction mixture was allowed to warm to 25 °C and then transferred to a pre-heated oil bath set to 45 °C and allowed to stir for a total of 20 h under protection from light. Throughout the course of the reaction, a color change from colorless to brick red was observed concomitant with the formation of gray precipitate. The red reaction mixture was then filtered through a pad of Celite, and the filtrate was dried under reduced pressure. The red residue was then dissolved in MeCN (1.5 mL), and this solution was filtered again through a pad of Celite. To the red filtrate was added  $Et_2O$  (20 mL) with vigorous stirring, resulting in the precipitation of pink solids from solution. The solids were isolated by filtration and dried under reduced pressure to afford  $[B_{12}(OCH_2C_6H_4SC_6H_4(Me-DalPhos)AuCl)_{12}][SbF_6]_{10}$  as a bright pink solid (11 mg, 0.84  $\mu$ mol, 42%). UV-vis (MeCN, 25 °C, 0.06 mM)  $[\epsilon]$ : 389 [8,300  $M^{-1}cm^{-1}$ ], 541 [8,170  $M^{-1}cm^{-1}$ ] nm.  $^1H$  NMR (400 MHz, 25 °C,  $CD_3CN$ )  $\delta$ : 8.02 (m, 12H, Ar-*H* Me-DalPhos), 7.95 (m, 24H, Ar-*H* Me-DalPhos), 7.69 (m, 12H, Ar-*H* Me-DalPhos), 7.45 (br m, 48H, Ar-*H*), 7.11 (br m, 48H, Ar-*H*), 3.44 (s, 72H,  $N(CH_3)_2$ ), 2.22 (m, 72H, 1-Ad), 1.99 (m, 144H, 1-Ad, signals overlapping with  $CD_3CN$  residual solvent signal), 1.61 (m, 144H, 1-Ad) ppm. The aromatic and methylene protons resonances of the benzyl linker are broadened due to partial oxidation of the dianionic  $[B_{12}]^{2-}$  cluster core to the paramagnetic, monoanionic  $[B_{12}]^-$  core in air.  $^{31}P\{^1H\}$  (162 MHz, 25 °C,  $CD_3CN$ )  $\delta$ : 76.6 ppm.  $^{11}B\{^1H\}$  NMR (128 MHz, 25 °C,  $CD_3CN$ )  $\delta$ : -14.9 ppm.

## General procedure for conjugation reactions with [21][SbF<sub>6</sub>]<sub>10</sub>

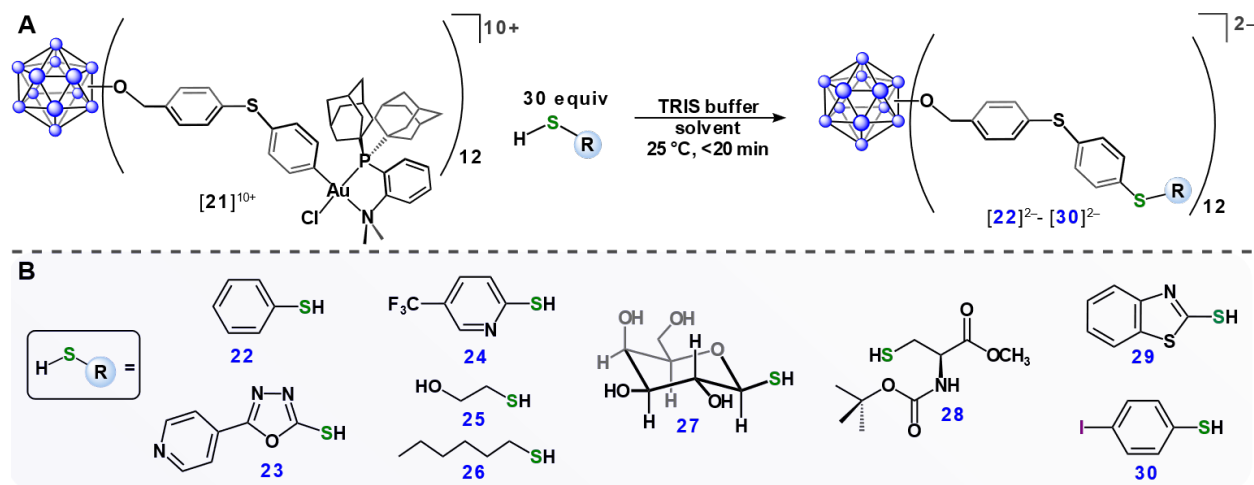


**Figure S4.2.** (A) General scheme for conjugation reactions of [21][SbF<sub>6</sub>]<sub>10</sub> with thiol-containing substrates. (B) Scope of nanocluster thio-conjugates. All species were observed *in situ* by ESI-MS(-).

To a cooled (-4 °C) solution of AgSbF<sub>6</sub> (7 mg, 0.02 mmol, 16 equiv) in DCM (1 mL) was added a cooled solution (-4 °C) of [K<sub>2</sub>][3] (5 mg, 0.001 mmol, 1 equiv) and (Me-DalPhos)AuCl (13 mg, 0.019 mmol, 16 equiv) in DCM (1 mL) under protection from light. The reaction mixture was allowed to warm to 25 °C and then transferred to a pre-heated oil bath set to 45 °C and allowed to stir for a total of 20 h under protection from light. Throughout the course of the reaction, a color change from colorless to brick red was observed concomitant with the formation of gray precipitate. The red reaction mixture was then filtered through a pad of Celite, and the filtrate was dried under reduced pressure. The red residue was then dissolved in MeCN (1 mL), and this solution was filtered again through a pad of Celite. This MeCN solution (1 mM) was used in subsequent conjugation reactions described in this section.

**Synthesis of  $[\text{H}_3\text{NC}(\text{CH}_2\text{OH})_3]_2[\text{B}_{12}(\text{OCH}_2\text{C}_6\text{H}_4\text{SC}_6\text{H}_4\text{SPh})_{12}]$  ( $[\text{H}_3\text{NC}(\text{CH}_2\text{OH})_3]_2[\mathbf{22}]$ )**

The general procedure to generate a solution of  $[\mathbf{21}][\text{SbF}_6]_{10}$  in MeCN (1 mM) was followed. A 50  $\mu\text{L}$  (0.07  $\mu\text{mol}$ , 1 equiv) aliquot of this solution was removed and treated with a solution of thiophenol in MeCN (18  $\mu\text{L}$  of a 0.1 M solution, 1.8  $\mu\text{mol}$ , 30 equiv) followed by a solution of TRIS buffer in DMF (50  $\mu\text{L}$  of a 50 mM solution) while stirring. The reaction mixture changed from purple to colorless after ca. 5 min of stirring, at which point an aliquot was removed, diluted with MeCN, and analyzed by ESI-MS(-), which confirmed the formation and identity of the  $[\text{B}_{12}(\text{OCH}_2\text{C}_6\text{H}_4\text{SC}_6\text{H}_4\text{SPh})_{12}]^{2-}$  species. ESI-MS(-): 2005.3916 (calc'd, 2005.4015) *m/z*.

**Synthesis of  $[\text{H}_3\text{NC}(\text{CH}_2\text{OH})_3]_2[\text{B}_{12}(\text{OCH}_2\text{C}_6\text{H}_4\text{SC}_6\text{H}_4(5-(4\text{-pyridyl})\text{-oxadiazole-2-thiol}))_{12}]$  ( $[\text{H}_3\text{NC}(\text{CH}_2\text{OH})_3]_2[\mathbf{23}]$ )**

The general procedure to generate a solution of  $[\mathbf{21}][\text{SbF}_6]_{10}$  in MeCN (1 mM) was followed. A 50  $\mu\text{L}$  (0.07  $\mu\text{mol}$ , 1 equiv) aliquot of this solution was removed and treated with a solution of 5-(4-pyridyl)-oxadiazole-2-thiol in DMF (106  $\mu\text{L}$  of a 17 mM solution, 1.8  $\mu\text{mol}$ , 30 equiv) followed by a solution of TRIS buffer in DMF (100  $\mu\text{L}$  of a 50 mM solution) while stirring. The reaction mixture changed from purple to colorless after ca. 5 min of stirring, at which point an aliquot was removed, diluted with MeCN, and analyzed by ESI-MS(-), which confirmed the formation and identity of the  $[\text{B}_{12}(\text{OCH}_2\text{C}_6\text{H}_4\text{SC}_6\text{H}_4(5-(4\text{-pyridyl})\text{-oxadiazole-2-thiol}))_{12}]^{2-}$  species. ESI-MS(-): 2419.2896 (calc'd, 2419.3796) *m/z*.

**Synthesis of  $[\text{H}_3\text{NC}(\text{CH}_2\text{OH})_3]_2[\text{B}_{12}(\text{OCH}_2\text{C}_6\text{H}_4\text{SC}_6\text{H}_4(2\text{-thio-5-trifluoromethylpyridine}))_{12}]$  ( $[\text{H}_3\text{NC}(\text{CH}_2\text{OH})_3]_2[\mathbf{24}]$ )**

The general procedure to generate a solution of  $[\mathbf{21}][\text{SbF}_6]_{10}$  in MeCN (1 mM) was followed. A 50  $\mu\text{L}$  (0.07  $\mu\text{mol}$ , 1 equiv) aliquot of this solution was removed and treated with a solution of 2-thio-5-trifluoromethylpyridine in DMF (108  $\mu\text{L}$  of a 17 mM solution, 1.8  $\mu\text{mol}$ , 30 equiv) followed

by a solution of TRIS buffer in DMF (50  $\mu$ L of a 50 mM solution) while stirring. The reaction mixture changed from purple to colorless after ca. 5 min of stirring, at which point an aliquot was removed, diluted with MeCN, and analyzed by ESI-MS(-), which confirmed the formation and identity of the  $[\text{B}_{12}(\text{OCH}_2\text{C}_6\text{H}_4\text{SC}_6\text{H}_4(2\text{-thio-5-trifluoromethylpyridine}))_{12}]^{2-}$  species. ESI-MS(-): 2419.2898 (calc'd, 2419.2794) *m/z*.

**Synthesis of  $[\text{H}_3\text{NC}(\text{CH}_2\text{OH})_3]_2[\text{B}_{12}(\text{OCH}_2\text{C}_6\text{H}_4\text{SC}_6\text{H}_4(2\text{-mercaptoethanol}))_{12}]$  ( $[\text{H}_3\text{NC}(\text{CH}_2\text{OH})_3]_2[\text{25}]$ )**

The general procedure to generate a solution of  $[\text{21}][\text{SbF}_6]_{10}$  in MeCN (1 mM) was followed. A 50  $\mu$ L (0.07  $\mu$ mol, 1 equiv) aliquot of this solution was removed and treated with a solution of 2-mercaptoethanol in MeCN (18  $\mu$ L of a 0.10 M solution, 1.8  $\mu$ mol, 30 equiv) followed by a solution of TRIS buffer in DMF (50  $\mu$ L of a 50 mM solution) while stirring. The reaction mixture changed from purple to colorless after ca. 5 min of stirring, at which point an aliquot was removed, diluted with MeCN, and analyzed by ESI-MS(-), which confirmed the formation and identity of the  $[\text{B}_{12}(\text{OCH}_2\text{C}_6\text{H}_4\text{SC}_6\text{H}_4(2\text{-mercaptoethanol}))_{12}]^{2-}$  species. ESI-MS(-): 1812.8703 (calc'd, 1812.8702) *m/z*.

**Synthesis of  $[\text{H}_3\text{NC}(\text{CH}_2\text{OH})_3]_2[\text{B}_{12}(\text{OCH}_2\text{C}_6\text{H}_4\text{SC}_6\text{H}_4\text{S}(\text{CH}_2)_5\text{CH}_3)_{12}]$  ( $[\text{H}_3\text{NC}(\text{CH}_2\text{OH})_3]_2[\text{26}]$ )**

The general procedure to generate a solution of  $[\text{21}][\text{SbF}_6]_{10}$  in MeCN (1 mM) was followed. A 50  $\mu$ L (0.07  $\mu$ mol, 1 equiv) aliquot of this solution was removed and treated with a solution of hexanethiol in MeCN (18  $\mu$ L of a 0.10 M solution, 1.8  $\mu$ mol, 30 equiv) followed by a solution of TRIS buffer in DMF (50  $\mu$ L of a 50 mM solution) while stirring. The reaction mixture changed from purple to colorless after ca. 5 min of stirring, at which point an aliquot was removed, diluted

with MeCN, and analyzed by ESI-MS(-), which confirmed the formation and identity of the  $[\text{B}_{12}(\text{OCH}_2\text{C}_6\text{H}_4\text{SC}_6\text{H}_4\text{S}(\text{CH}_2)_5\text{CH}_3)_{12}]^{2-}$  species. ESI-MS(-): 2053.7671 (calc'd, 2053.7772) *m/z*.

#### **Synthesis of $[\text{Na}_2][\text{B}_{12}(\text{OCH}_2\text{C}_6\text{H}_4\text{SC}_6\text{H}_4(1\text{-thio-}\beta\text{-D-galactose}))_{12}]$ ( $[\text{Na}_2][27]$ )**

The general procedure to generate a solution of  $[\mathbf{21}][\text{SbF}_6]_{10}$  in MeCN (1 mM) was followed. A 50  $\mu\text{L}$  (0.07  $\mu\text{mol}$ , 1 equiv) aliquot of this solution was removed and treated with a solution of Na[1-thio- $\beta$ -D-galactose] in H<sub>2</sub>O (36  $\mu\text{L}$  of a 30 mM solution, 1.8  $\mu\text{mol}$ , 30 equiv) followed by dilution with DMF (30  $\mu\text{L}$ ) while stirring. The reaction mixture changed from purple to colorless after ca. 5 min of stirring, at which point an aliquot was removed, diluted with MeOH, and analyzed by ESI-MS(-), which confirmed the formation and identity of the  $[\text{B}_{12}(\text{OCH}_2\text{C}_6\text{H}_4\text{SC}_6\text{H}_4(1\text{-thio-}\beta\text{-D-galactose}))_{12}]^{2-}$  species. ESI-MS(-): 1680.6948 (calc'd, 1680.6848 for  $[\text{M}^{2-}\text{-H}^+]^{3-}$ ) *m/z*.

#### **Synthesis of $[\text{H}_3\text{NC}(\text{CH}_2\text{OH})_3]_2[\text{B}_{12}(\text{OCH}_2\text{C}_6\text{H}_4\text{SC}_6\text{H}_4(N\text{-}(tert\text{-butoxycarbonyl})\text{-L-cysteine methyl ester}))_{12}]$ ( $[\text{H}_3\text{NC}(\text{CH}_2\text{OH})_3]_2[28]$ )**

The general procedure to generate a solution of  $[\mathbf{21}][\text{SbF}_6]_{10}$  in MeCN (1 mM) was followed. A 50  $\mu\text{L}$  (0.07  $\mu\text{mol}$ , 1 equiv) aliquot of this solution was removed and treated with a solution of *N*-(*tert*-butoxycarbonyl)-L-cysteine methyl ester in MeCN (18  $\mu\text{L}$  of a 0.10 M solution, 1.8  $\mu\text{mol}$ , 30 equiv) followed by a solution of TRIS buffer in DMF (50  $\mu\text{L}$  of a 50 mM solution) while stirring. The reaction mixture changed from purple to colorless after ca. 5 min of stirring, at which point an aliquot was removed, diluted with MeCN, and analyzed by ESI-MS(-), which confirmed the formation and identity of the  $[\text{B}_{12}(\text{OCH}_2\text{C}_6\text{H}_4\text{SC}_6\text{H}_4(N\text{-}(tert\text{-butoxycarbonyl})\text{-L-cysteine methyl ester}))_{12}]^{2-}$  species. ESI-MS(-): 2755.7974 (calc'd, 2755.8152) *m/z*.

**Synthesis of  $[\text{H}_3\text{NC}(\text{CH}_2\text{OH})_3]_2[\text{B}_{12}(\text{OCH}_2\text{C}_6\text{H}_4\text{SC}_6\text{H}_4(2\text{-mercaptobenzothiazole}))_{12}]$  ( $[\text{H}_3\text{NC}(\text{CH}_2\text{OH})_3]_2[\mathbf{29}]$ )**

The general procedure to generate a solution of  $[\mathbf{21}][\text{SbF}_6]_{10}$  in MeCN (1 mM) was followed. A 50  $\mu\text{L}$  (0.07  $\mu\text{mol}$ , 1 equiv) aliquot of this solution was removed and treated with a solution of 2-mercaptobenzothiazole in DMF (60  $\mu\text{L}$  of a 30 mM solution, 1.8  $\mu\text{mol}$ , 30 equiv) followed by a solution of TRIS buffer in DMF (50  $\mu\text{L}$  of a 50 mM solution) while stirring. The reaction mixture changed from purple to colorless after ca. 5 min of stirring, at which point an aliquot was removed, diluted with MeCN, and analyzed by ESI-MS(-), which confirmed the formation and identity of the  $[\text{B}_{12}(\text{OCH}_2\text{C}_6\text{H}_4\text{SC}_6\text{H}_4(2\text{-mercaptobenzothiazole}))_{12}]^{2-}$  species. ESI-MS(-): 2347.6916 (calc'd, 2347.7046) *m/z*.

**Synthesis of  $[\text{H}_3\text{NC}(\text{CH}_2\text{OH})_3]_2[\text{B}_{12}(\text{OCH}_2\text{C}_6\text{H}_4\text{SC}_6\text{H}_4\text{SC}_6\text{H}_4\text{I})_{12}]$  ( $[\text{H}_3\text{NC}(\text{CH}_2\text{OH})_3]_2[\mathbf{30}]$ )**

The general procedure to generate a solution of  $[\mathbf{21}][\text{SbF}_6]_{10}$  in MeCN (1 mM) was followed. A 50  $\mu\text{L}$  (0.07  $\mu\text{mol}$ , 1 equiv) aliquot of this solution was removed and treated with a solution of *para*-iodothiophenol in DMF (138  $\mu\text{L}$  of a 13 mM solution, 1.8  $\mu\text{mol}$ , 30 equiv) followed by a solution of TRIS buffer in DMF (50  $\mu\text{L}$  of a 50 mM solution) while stirring. The reaction mixture changed from purple to colorless after ca. 5 min of stirring, at which point an aliquot was removed, diluted with MeCN, and analyzed by ESI-MS(-), which confirmed the formation and identity of the  $[\text{B}_{12}(\text{OCH}_2\text{C}_6\text{H}_4\text{SC}_6\text{H}_4\text{SC}_6\text{H}_4\text{I})_{12}]^{2-}$  species. ESI-MS(-): 2760.7586 (calc'd, 2760.7814) *m/z*.

### Synthesis of (1-thio-β-D-galactose)<sub>2</sub>C<sub>6</sub>H<sub>4</sub>

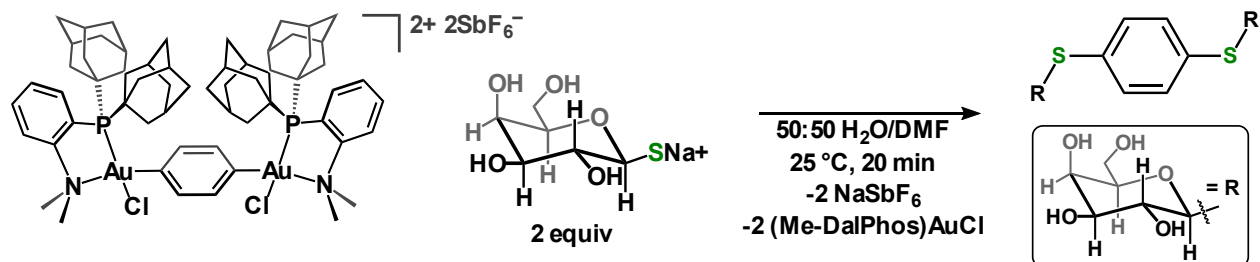


**Figure S4.3.** Reaction scheme for the preparation of (1-thio-β-D-galactose)<sub>2</sub>C<sub>6</sub>H<sub>4</sub>.

The [((Me-DalPhos)AuCl)<sub>2</sub>C<sub>6</sub>H<sub>4</sub>][SbF<sub>6</sub>]<sub>2</sub> complex was prepared following a previously reported procedure.<sup>194</sup>

To a stirring solution of Na[1-thio-β-D-galactose] (6 mg, 0.03 mmol, 2 equiv) in H<sub>2</sub>O (1 mL) was added a solution of [((Me-DalPhos)AuCl)<sub>2</sub>C<sub>6</sub>H<sub>4</sub>][SbF<sub>6</sub>]<sub>2</sub> (24 mg, 0.013 mmol, 1.0 equiv) in DMF (1.5 mL). The color of the reaction mixture gradually changed from yellow to colorless over the course of 15 min, at which point all volatiles were removed under reduced pressure. The resulting colorless residue was suspended in H<sub>2</sub>O (2 mL). The resulting suspension was sonicated (5 min), and then centrifuged (2,200 × g, 5 min). The supernatant was removed and filtered through a 0.22 μm PTFE membrane syringe filter to remove any insoluble (Me-DalPhos)AuCl remaining in the solution. The filtrate was then lyophilized to afford (1-thio-β-D-galactose)<sub>2</sub>C<sub>6</sub>H<sub>4</sub> as a colorless solid (5 mg, 0.01 mmol, 80%). <sup>1</sup>H NMR (400 MHz, 25 °C, D<sub>2</sub>O) δ: 7.55 (s, 4H, Ar-*H*), 4.01 (d, 2H, gal), 4.01–3.64 (m, 12H, gal) ppm.



## **Stability studies of $[\text{Na}_2][\text{B}_{12}(\text{OCH}_2\text{C}_6\text{H}_4(1\text{-thio-}\beta\text{-D-glucose}))_{12}]$ under biologically relevant conditions**

The  $[\text{Na}_2][\text{B}_{12}(\text{OCH}_2\text{C}_6\text{H}_4(1\text{-thio-}\beta\text{-D-glucose}))_{12}]$  cluster was prepared according to the procedure described and used in the stability studies described in the following subsections.

**Fetal bovine serum cell culture medium:** A sample of  $[\text{Na}_2][\text{B}_{12}(\text{OCH}_2\text{C}_6\text{H}_4(1\text{-thio-}\beta\text{-D-glucose}))_{12}]$  (2 mg) was dissolved in fetal bovine serum RPMI 1640 cell medium (0.5 mL, Sigma Aldrich). The solution was transferred to an NMR tube, and an initial  $^{11}\text{B}\{^1\text{H}\}$  NMR spectrum of the sample was collected immediately. A second  $^{11}\text{B}\{^1\text{H}\}$  NMR spectrum was collected after allowing the sample to stand for 24 h at 25 °C.  $^{11}\text{B}\{^1\text{H}\}$  NMR spectra of the sample were collected every 24 h for a total of seven days without any observable cluster degradation. After monitoring the solution for one week at 25 °C, the same sample was heated at 37 °C and monitored by  $^{11}\text{B}\{^1\text{H}\}$  NMR spectroscopy every 24 h for an additional seven days. The  $^{11}\text{B}\{^1\text{H}\}$  NMR spectra collected during the course of this study show that the cluster maintains its structural integrity under these conditions. The sample was also analyzed by ESI-MS(–) after the two week stability study, confirming the presence of the intact cluster.

**pH 10:** A sample of  $[\text{Na}_2][\text{B}_{12}(\text{OCH}_2\text{C}_6\text{H}_4(1\text{-thio-}\beta\text{-D-glucose}))_{12}]$  (2 mg) was dissolved in an aqueous solution of TRIS buffer (adjusted to pH 10). The solution was transferred to an NMR tube, and an initial  $^{11}\text{B}\{^1\text{H}\}$  NMR spectrum of the sample was collected immediately. A second  $^{11}\text{B}\{^1\text{H}\}$  NMR spectrum was collected after allowing the sample to stand for 24 h at 25 °C.  $^{11}\text{B}\{^1\text{H}\}$  NMR spectra of the sample were collected every 24 h for a total of seven days without any observable cluster degradation. The sample was also analyzed by ESI-MS(–) after the one week stability study, confirming the presence of the intact cluster.

**pH 5:** A sample of  $[\text{Na}_2][\text{B}_{12}(\text{OCH}_2\text{C}_6\text{H}_4(1\text{-thio-}\beta\text{-D-glucose}))_{12}]$  (2 mg) was dissolved in an aqueous solution of acetate buffer (pH 5 solution prepared by dissolution of NaOAc (7 mL of a 0.2 M solution) and HOAc (3 mL of a 0.2M solution) in 10 mL Milli-Q  $\text{H}_2\text{O}$ ). The solution was transferred to an NMR tube, and an initial  $^{11}\text{B}\{^1\text{H}\}$  NMR spectrum of the sample was collected immediately. A second  $^{11}\text{B}\{^1\text{H}\}$  NMR spectrum was collected after allowing the sample to stand for 24 h at 25 °C.  $^{11}\text{B}\{^1\text{H}\}$  NMR spectra of the sample were collected every 24 h for a total of seven days without any observable cluster degradation. The sample was also analyzed by ESI-MS(–) after the one week stability study, confirming the presence of the intact cluster.

## Monitoring the conjugation reaction between [1][SbF<sub>6</sub>]<sub>11</sub> and Na[1-thio-β-D-galactose] by <sup>31</sup>P NMR spectroscopy

The general reaction procedure to generate [1][SbF<sub>6</sub>]<sub>11</sub> was followed. The DMF solution containing [1][SbF<sub>6</sub>]<sub>11</sub> (0.0014 mmol, 1 mL) was transferred to an NMR tube containing a solution of OPPh<sub>3</sub> (5 mg, 0.02 mmol) dissolved in DMF (75 μL) in a sealed capillary tube. A <sup>31</sup>P{<sup>1</sup>H} NMR spectrum of the sample was collected (Figure S4.4, top), and then the solution was transferred to a vial equipped with a Teflon-coated stir bar. To this solution was added a solution of Na[1-thio-β-D-galactose] (9 mg, 0.04 mmol, 30 equiv) in water (0.5 ml) with stirring. The reaction mixture was allowed to stir at 25 °C for 15 min, during which time the color of the solution changed from dark purple to colorless. The reaction mixture was then transferred an NMR tube containing the same OPPh<sub>3</sub> internal standard, and a <sup>31</sup>P{<sup>1</sup>H} NMR spectrum of the sample was collected (Figure S4.4, bottom), indicating complete conversion of [1][SbF<sub>6</sub>]<sub>11</sub> to (Me-DalPhos)AuCl. We note that the slight difference in the integration values of [1][SbF<sub>6</sub>]<sub>11</sub> (0.88 compared to OPPh<sub>3</sub>) when compared with the integration value of the (Me-DalPhos)AuCl byproduct (0.78 compared to OPPh<sub>3</sub>) is likely due to loss of sample while transferring the reaction solution.

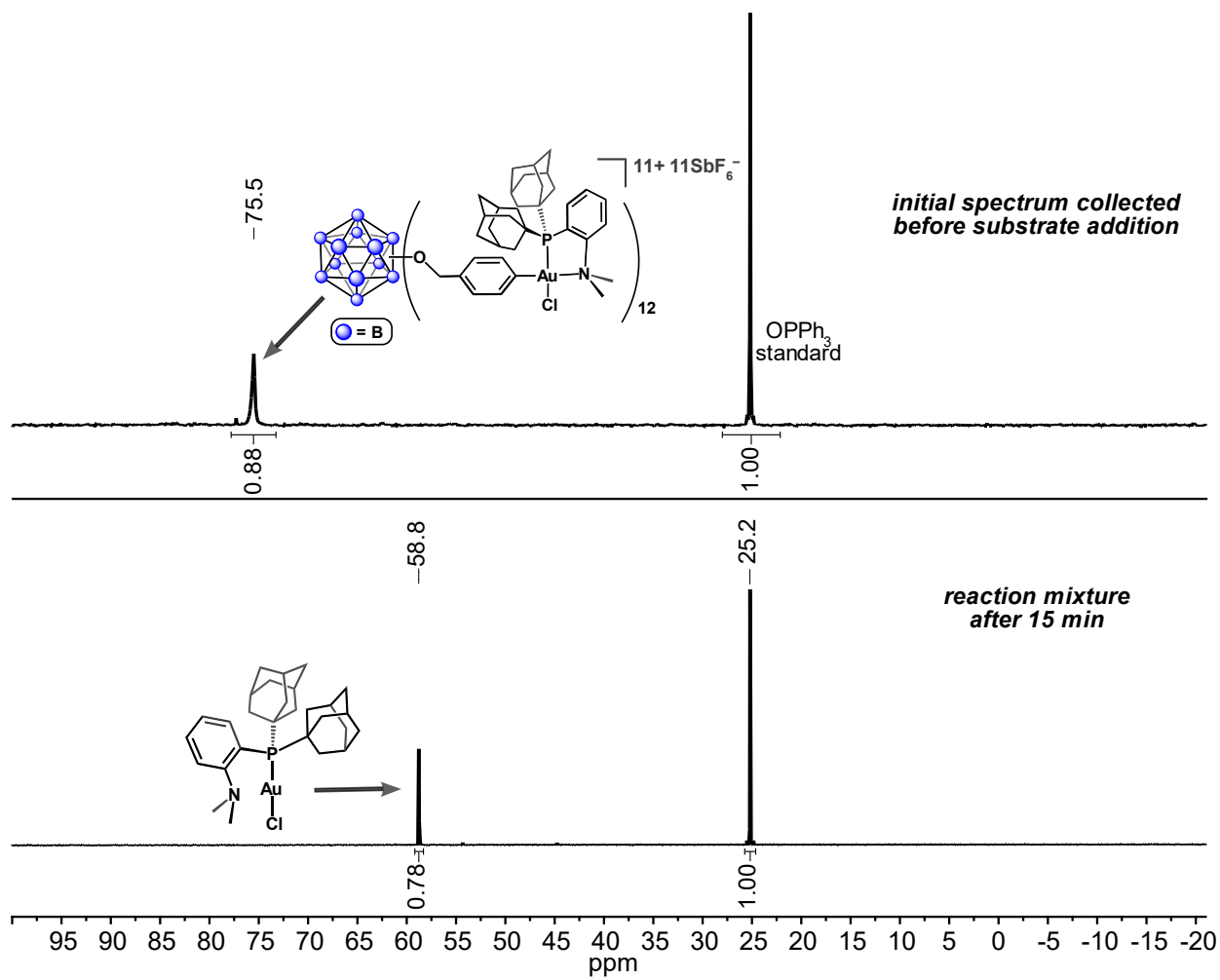


**Figure S4.41.**  $^{31}\text{P}\{^1\text{H}\}$  NMR spectra taken of an initial DMF solution of  $[\mathbf{1}][\text{SbF}_6]_{11}$  before addition of Na[1-thio- $\beta$ -D-galactose] (top), and of the crude reaction mixture 15 min after substrate addition (bottom) (DMF, 162 MHz, 25 °C).

### Procedure for (Me-DalPhos)AuCl recovery after conjugation reactions

The DCM washes from the preparation of  $[1][SbF_6]_{11}$  were combined in addition to all fractions that did not contain the desired  $[K_2/Na_2][B_{12}(OCH_2C_6H_4SR)]$  products from the previously described conjugation reactions. The recovered solutions from 12 independent reactions were used for this procedure. Many of these fractions contained the unreacted thiol substrate, small amounts of the  $[K_2/Na_2][B_{12}(OCH_2Ar)]$  clusters, and the (Me-DalPhos)AuCl complex. All volatiles were removed from the combined fractions under reduced pressure, and a  $^1H$  NMR spectrum (Figure S4.5, top) of the resulting solids was collected. The (Me-DalPhos)AuCl species was purified away from all other byproducts in this complex mixture by column chromatography on silica gel by elution with an 85:15 hexanes:EtOAc mixture. The fractions containing pure (Me-DalPhos)AuCl were combined and dried under reduced pressure to afford the recovered (Me-DalPhos)AuCl material as a colorless solid (62 mg, 0.095 mmol, 30% recovery\*).

\*Calculation based on the amount of (Me-DalPhos)AuCl used for twelve conjugation reactions (0.027 mmol for each reaction = 0.32 mmol for 12 total reactions).

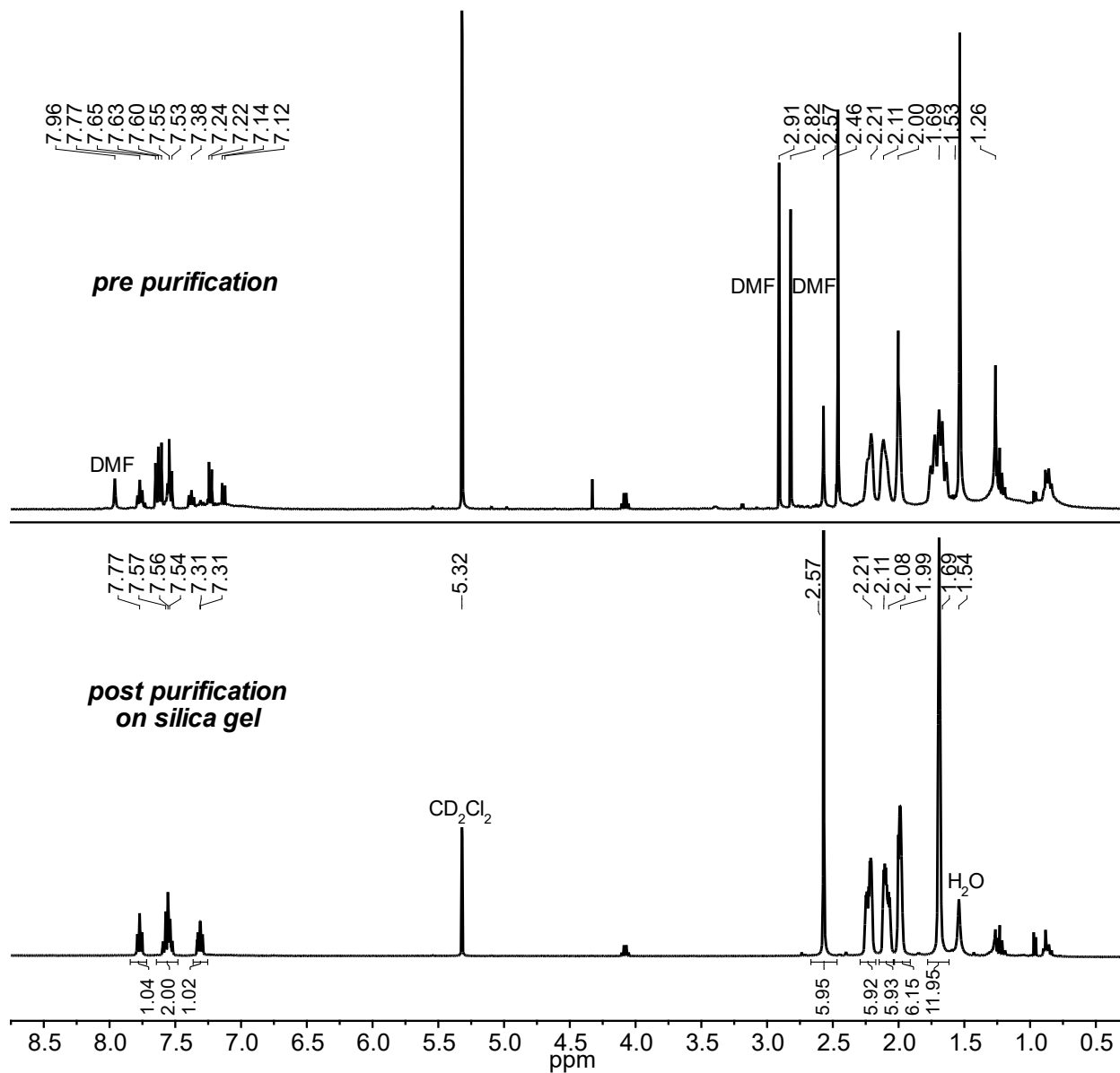


**Figure S4.5.** <sup>1</sup>H NMR spectra of mixture collected from conjugation reactions before purification (*top*) and recovered (Me-DalPhos)AuCl post purification (*bottom*) (CD<sub>2</sub>Cl<sub>2</sub>, 400 MHz, 25 °C).

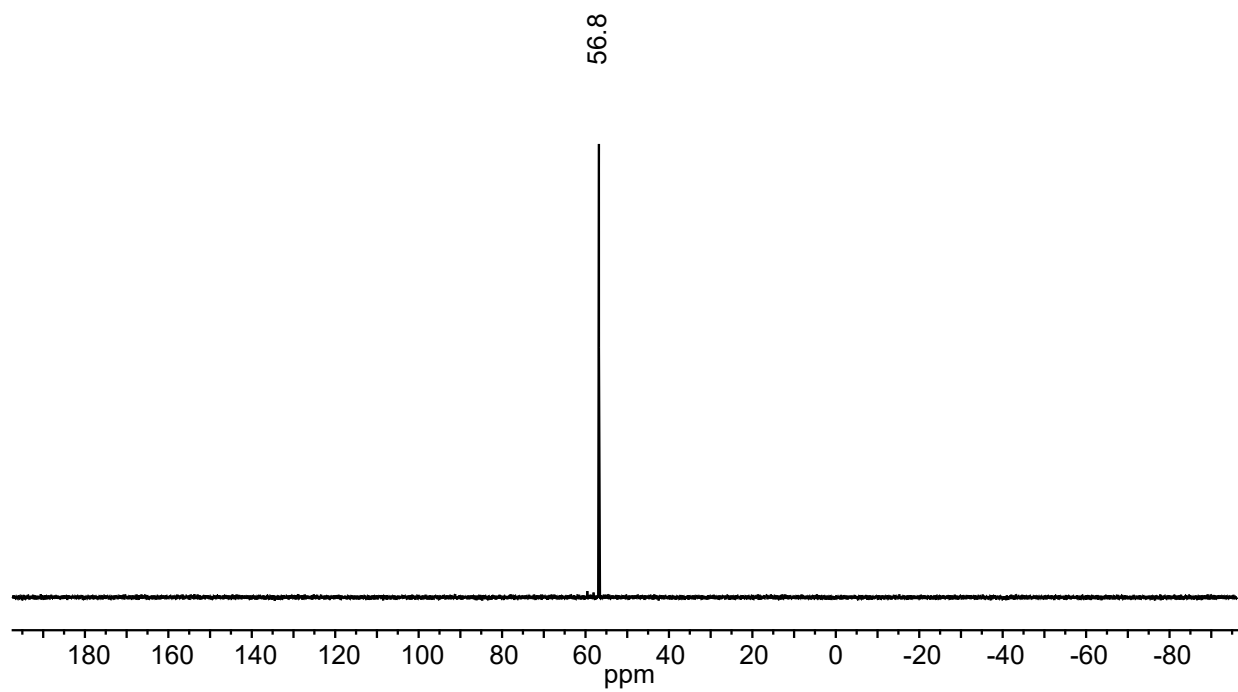


**Figure S4.6.**  $^{31}\text{P}\{^1\text{H}\}$  NMR spectrum of recovered (Me-DalPhos)AuCl after purification ( $\text{CD}_2\text{Cl}_2$ , 162 MHz, 25 °C).

## Surface plasmon resonance (SPR) measurements

All experiments were performed on a Biacore T200 instrument with Series S CM5 chips (GE Healthcare Life Sciences). The binding curves were fitted to the Langmuir 1:1 binding model on the Biacore T200 analysis software for determination of the binding affinity ( $K_D$ ).

### Concanavalin A (ConA)

The running buffer was composed of an aqueous solution of HEPES buffer (10 mM, pH 7.4),  $\text{CaCl}_2$  (1 mM),  $\text{MgCl}_2$  (1 mM),  $\text{MnCl}_2$  (1 mM), and TWEEN® 20 (0.005% by volume). First, the surface of flow cell #2 was activated with a mixture of EDC (0.4 M) and NHS (0.1 M) (1:1 v/v in  $\text{H}_2\text{O}$ ) over 30 min, followed by injection of ConA (0.1 mg/mL) in the running buffer over 40 min and then ethanolamine HCl (1 M in  $\text{H}_2\text{O}$ , pH 8.5) over 30 min. Then, flow cell #1 was prepared as a reference channel by activation of its surface with a mixture of EDC (0.4 M) and NHS (0.1 M) (1:1 v/v in  $\text{H}_2\text{O}$ ) over 30 min, followed by injection of ethanolamine HCl (1 M in  $\text{H}_2\text{O}$ , pH 8.5) over 30 min. Analyte samples ( $[\text{Na}_2][\text{B}_{12}(\text{OCH}_2\text{C}_6\text{H}_4(1\text{-thio-}\beta\text{-D-glucose}))_{12}]$  ( $[\text{Na}_2][\mathbf{18}]$ ), 0.5, 1, 2, 4 mg/L;  $[\text{K}_2][\text{B}_{12}(\text{OCH}_2\text{C}_6\text{H}_4(m\text{PEG}_{350}\text{thiol}))_{12}]$  ( $[\text{K}_2][\mathbf{8}]$ ), 4 mg/L; D-glucose, 30 mg/L (Figure S4.7)) were injected in tandem over both cells for 6 min, followed by a 6 min dissociation period with buffer flow. The surfaces were regenerated by injection of HCl (10 mM) over 2 min, followed by injection of glycine HCl (10 mM in  $\text{H}_2\text{O}$ , pH 2.5) over 2 min. A flow rate of 5  $\mu\text{L}/\text{min}$  was used throughout the experiment.



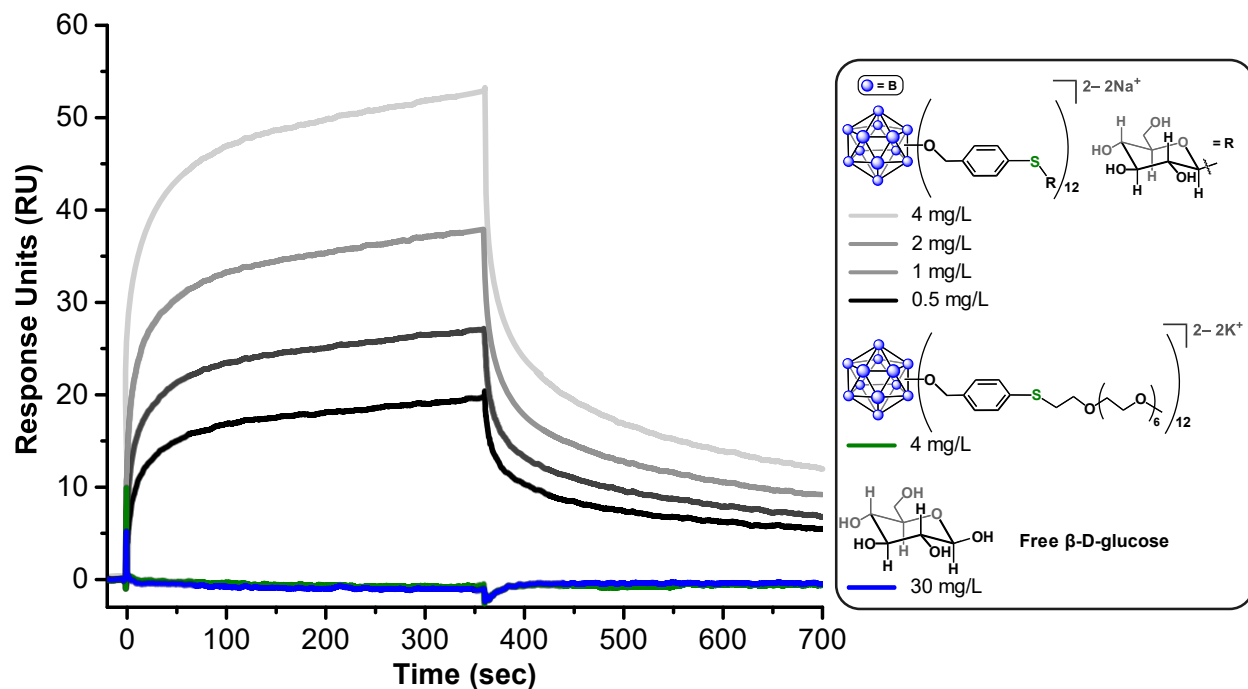


**Figure S4.7.** SPR sensorgram for the binding of  $[\text{Na}_2][\text{B}_{12}(\text{OCH}_2\text{C}_6\text{H}_4(1\text{-thio-}\beta\text{-D-glucose}))_{12}]$  (0.5, 1, 2, 4 mg/L concentrations) to ConA with  $[\text{K}_2][\text{B}_{12}(\text{OCH}_2\text{C}_6\text{H}_4(m\text{PEG}_{350}\text{ thiol}))_{12}]$  (4 mg/L) and free D-glucose (30 mg/L) controls.

$k_a$ :  $2.09 \times 10^4 \text{ M}^{-1}\text{s}^{-1}$ ,  $k_d$ :  $2.35 \times 10^{-3} \text{ s}^{-1}$ ,  $K_D$ : **116 nM**

### Shiga Toxin 1, B Subunit (Stx1B)

The running buffer was composed of an aqueous solution of HEPES buffer (10 mM, pH 7.4), NaCl (150 mM), and TWEEN® 20 (0.005% by volume). First, the surface of flow cell #2 was activated with a mixture of EDC (0.4 M) and NHS (0.1 M) (1:1 v/v in  $\text{H}_2\text{O}$ ) over 30 min at a flow rate of 10  $\mu\text{L}/\text{min}$ , followed by injection of Stx1B (0.05 mg/mL) in a sodium acetate buffer solution (10 mM, pH 5.2) over 8 minutes at a flow rate of 40  $\mu\text{L}/\text{min}$  followed by a solution of ethanolamine HCl (1 M, pH 8.5) over 10 min at a flow rate of 10  $\mu\text{L}/\text{min}$ . Then, flow cell #1 was prepared as a reference channel by activation of its surface with a mixture of EDC (0.4 M) and NHS (0.1 M) (1:1 v/v in  $\text{H}_2\text{O}$ ) over 30 min at a flow rate of 10  $\mu\text{L}/\text{min}$ , followed by injection of ethanolamine HCl (1 M in

H<sub>2</sub>O, pH 8.5) over 10 min at a flow rate of 10  $\mu$ L/min. Analyte samples ([Na<sub>2</sub>][B<sub>12</sub>(OCH<sub>2</sub>C<sub>6</sub>H<sub>4</sub>(1-thio- $\beta$ -D-galactose))<sub>12</sub>] ([Na<sub>2</sub>][**19**]), 15, 30, 45, 60 mg/L; (1-thio- $\beta$ -D-galactose)<sub>2</sub>C<sub>6</sub>H<sub>4</sub>, 100 mg/L; D-galactose, 100 mg/L (Figure S4.8); [K<sub>2</sub>][B<sub>12</sub>(OCH<sub>2</sub>C<sub>6</sub>H<sub>4</sub>(*m*PEG<sub>350</sub>thiol))<sub>12</sub>] ([K<sub>2</sub>][**8**]), 40, 60, 80, 100 mg/L (Figure S4.9)) were injected in tandem over both cells for 6 min, followed by a 6 min dissociation period with buffer flow. Surfaces were regenerated by injection of HCl (10 mM, pH 4.3) over 2 min at a flow rate of 5  $\mu$ L/min.

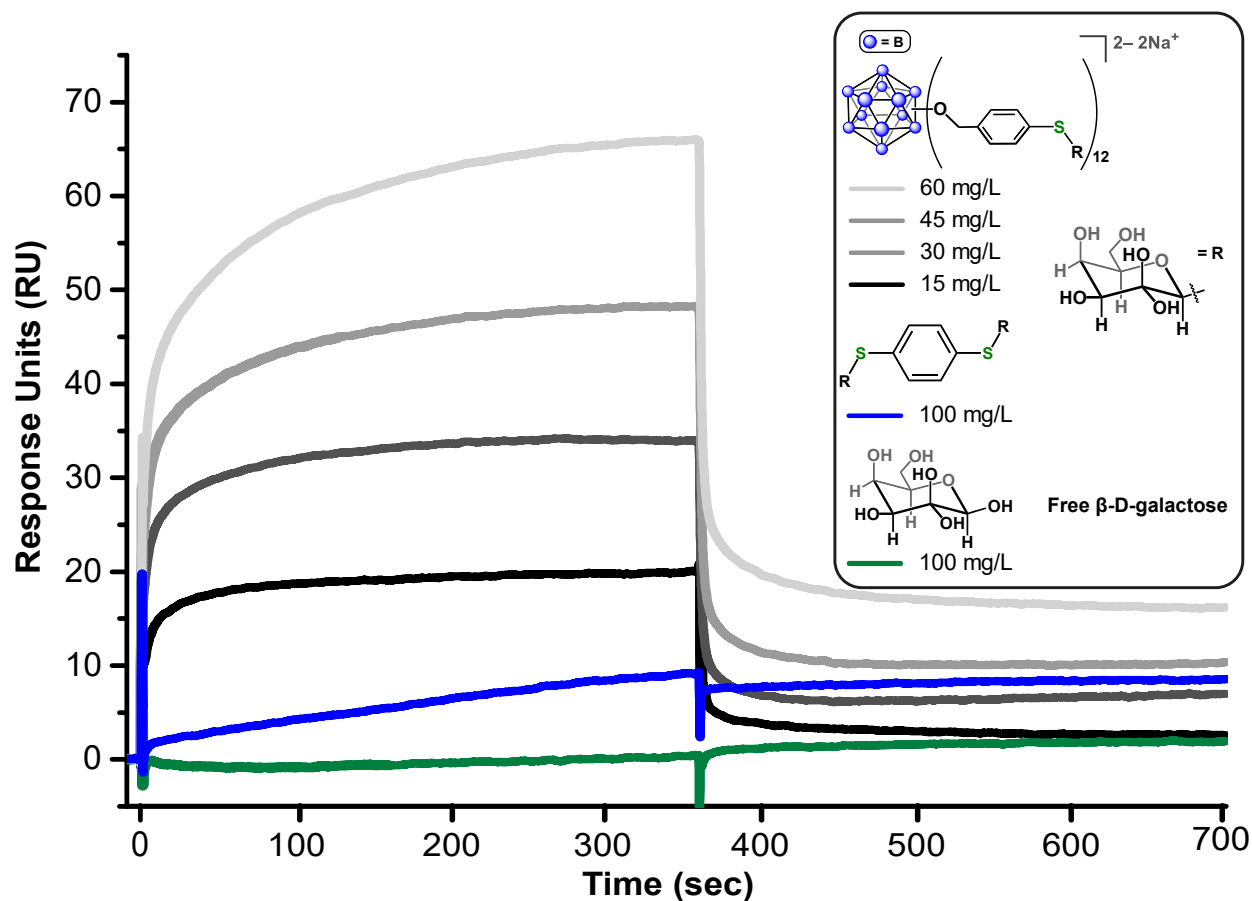


**Figure S4.8.** SPR sensorgram for the binding of [Na<sub>2</sub>][B<sub>12</sub>(OCH<sub>2</sub>C<sub>6</sub>H<sub>4</sub>(1-thio- $\beta$ -D-galactose))<sub>12</sub>] (15, 30, 45, 60 mg/L concentrations) to Stx1B with (1-thio-galactose)<sub>2</sub>C<sub>6</sub>H<sub>4</sub> (100 mg/L) and free D-galactose (100 mg/L) controls.

$$k_a: 7.42 \times 10^2 \text{ M}^{-1}\text{s}^{-1}, k_d: 1.10 \times 10^{-3} \text{ s}^{-1}, K_D: 1.51 \text{ }\mu\text{M}$$

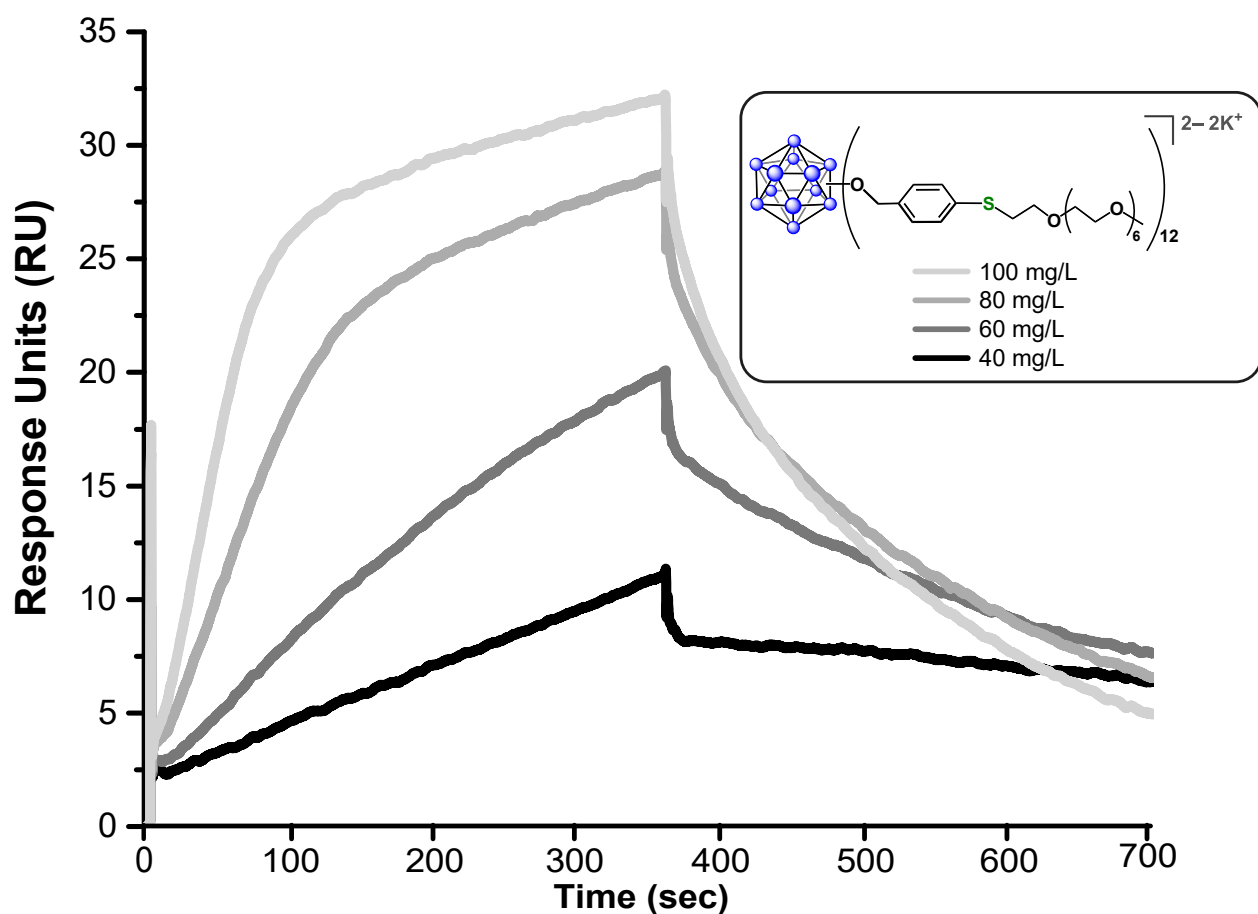


**Figure S4.9.** SPR sensorgram for the binding of  $[K_2][B_{12}(OCH_2C_6H_4(mPEG_{350}thiol))_{12}]$  (40, 60, 80, 100 mg/L concentrations) to Stx1B.

$k_a$ :  $3.59 \times 10^2 \text{ M}^{-1}\text{s}^{-1}$ ,  $k_d$ :  $3.77 \times 10^{-3} \text{ s}^{-1}$ ,  $K_D$ : **10.1  $\mu\text{M}$**

### DC-SIGN ECD

The running buffer was composed of an aqueous solution of HEPES buffer (10 mM, pH 7.4), NaCl (150 mM),  $\text{CaCl}_2$  (5 mM), and TWEEN® 20 (0.005% by volume). First, the surface of flow cell #2 was activated with a mixture of EDC (0.4 M) and NHS (0.1 M) (1:1 v/v in  $\text{H}_2\text{O}$ ) over 5 min, followed by injection of DC-SIGN ECD (0.01 mg/mL) in the running buffer over 45 min and then

ethanolamine HCl (1 M in H<sub>2</sub>O, pH 8.5) over 10 min. Then, flow cell #1 was prepared as a reference channel by activation of its surface with a mixture of EDC (0.4 M) and NHS (0.1 M) (1:1 v/v in H<sub>2</sub>O) over 5 min, followed by injection of ethanolamine HCl (1 M in H<sub>2</sub>O, pH 8.5) over 10 min. Analyte samples ([Na<sub>2</sub>][B<sub>12</sub>(OCH<sub>2</sub>C<sub>6</sub>H<sub>4</sub>(1-thio- $\alpha$ -D-mannose))<sub>12</sub>], 1, 2, 3, 4 mg/L; [K<sub>2</sub>][B<sub>12</sub>(OCH<sub>2</sub>C<sub>6</sub>H<sub>4</sub>(*m*PEG<sub>350</sub>thiol))<sub>12</sub>], 8 mg/L; D-mannose, 20 mg/L (Figure S4.10) were injected in tandem over both cells for 6 min, followed by a 6 min dissociation period with buffer flow. Surfaces were regenerated by injection of an aqueous solution of HEPES buffer (10 mM, pH 7.4), NaCl (150 mM), TWEEN® 20 (0.005% by volume), and EDTA (10 mM) over 2 min. A flow rate of 5  $\mu$ L/min was used throughout the experiment.

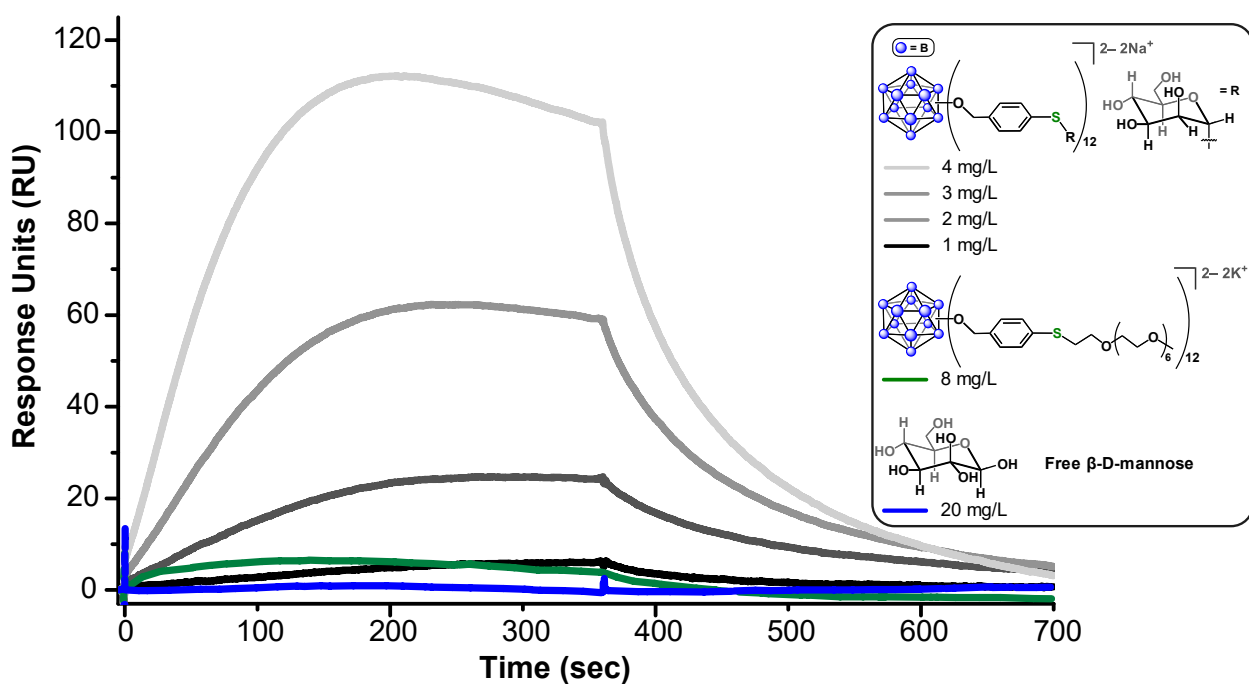


**Figure S4.10.** SPR sensorgram for the binding of [Na<sub>2</sub>][B<sub>12</sub>(OCH<sub>2</sub>C<sub>6</sub>H<sub>4</sub>(1-thio- $\alpha$ -D-mannose))<sub>12</sub>] (1, 2, 3, 4 mg/L concentrations) to DC-SIGN with [K<sub>2</sub>][B<sub>12</sub>(OCH<sub>2</sub>C<sub>6</sub>H<sub>4</sub>(*m*PEG<sub>350</sub> thiol))<sub>12</sub>] (8 mg/L) and free D-mannose (20 mg/L) controls.

$k_a$ :  $2.99 \times 10^3 \text{ M}^{-1}\text{s}^{-1}$ ,  $k_d$ :  $1.11 \times 10^{-2} \text{ s}^{-1}$ ,  $K_D$ : **3.70  $\mu$ M**

## Confocal microscopy studies with DC-SIGN

Raji DC-SIGN<sup>+</sup> cells were harvested and resuspended in D-PBS buffer (Fisher Scientific) supplemented with 1% bovine serum albumin (Fisher Scientific) and CaCl<sub>2</sub> (2 mM, Fisher Scientific) for a density of  $2 \times 10^6$  cells/mL, and then aliquoted into populations of  $2 \times 10^5$  cells. After 30 min of incubation at 25 °C, Human BD Fc Block (1.5 μL, BD Biosciences) was added to each cell population and incubated for 10 min at 25 °C. Solutions of each analyte ([K<sub>2</sub>][**8**], [Na<sub>2</sub>][**20**], and D-mannose) in DMSO (1 μL of a 10 mM stock solution) were independently mixed with a solution of HIV-1 gp120-FITC (ImmunoDX, 1 μL of a 1 mg/mL solution), and then the resulting mixture (2 μL total) was subsequently added to the cell population (100 μL) and mixed. The mixtures were then incubated for 30 min at 37 °C, after which the cells were washed with D-PBS (3 × 1 mL). Fluoroshield mounting medium (Abcam) was added to each sample and mixed, and then the cells were transferred to microscope slides. After 5 min, a coverslip was applied to each slide. After an additional 20 min, the edges were sealed with clear nail polish. The slides were then taken to a Leica TCS SPE confocal microscope, where images were acquired in z-stacks (25 sections, 20 μm) in both fluorescence and brightfield modes with a 40× lens and 30% excitation laser intensity. This procedure was repeated using a DMSO solution in the absence of any added analyte as a control. Figure S4.11A displays side-by-side image comparisons of the described experiments, and the following subsections include additional images.

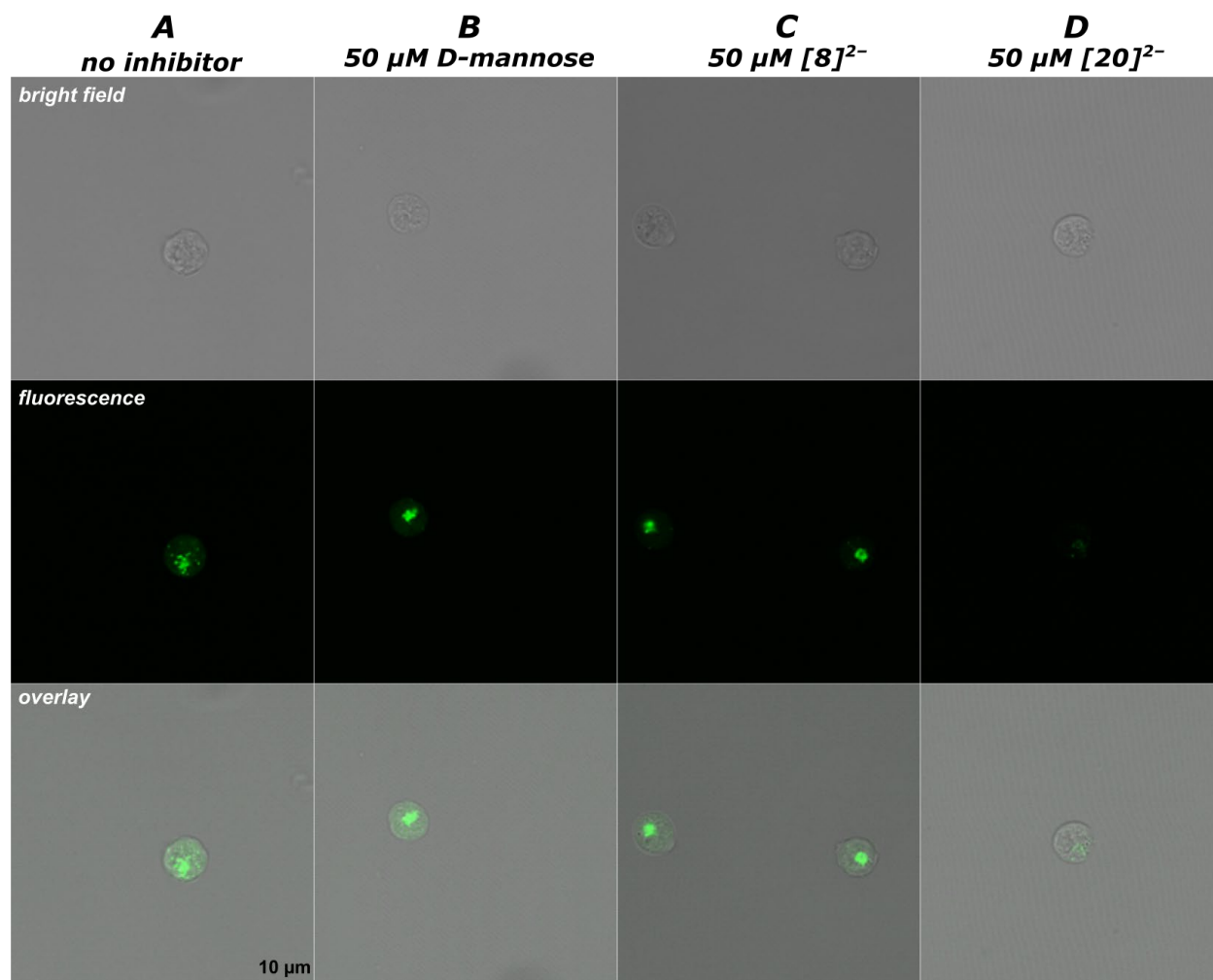


**Figure S4.11.** Confocal laser scanning microscopy images (bright field, fluorescence, and overlay) of Raji DC-SIGN+ cells incubated with gp120-FITC (83 nM) and (A) DMSO as a control; (B) free D-mannose (50 μM solution in DMSO); (C) [K<sub>2</sub>][**8**] (50 μM solution in DMSO); (D) [Na<sub>2</sub>][**20**] (50 μM solution in DMSO), demonstrating significant reduction in cellular uptake of gp120-FITC in the presence of the [Na<sub>2</sub>][**20**] inhibitor, and no observable reduction in gp120-FITC cellular uptake for the control experiments (B, C).

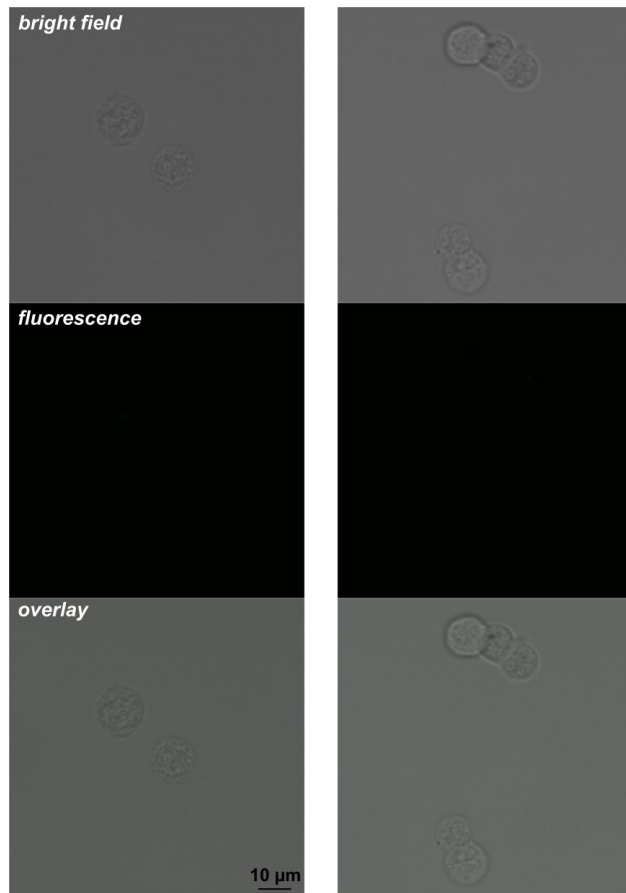


**Figure S4.12.** Two sets of confocal microscopy images of Raji cells (no DC-SIGN) exposed to gp120-FITC and DMSO (bright field, fluorescence, and overlay).

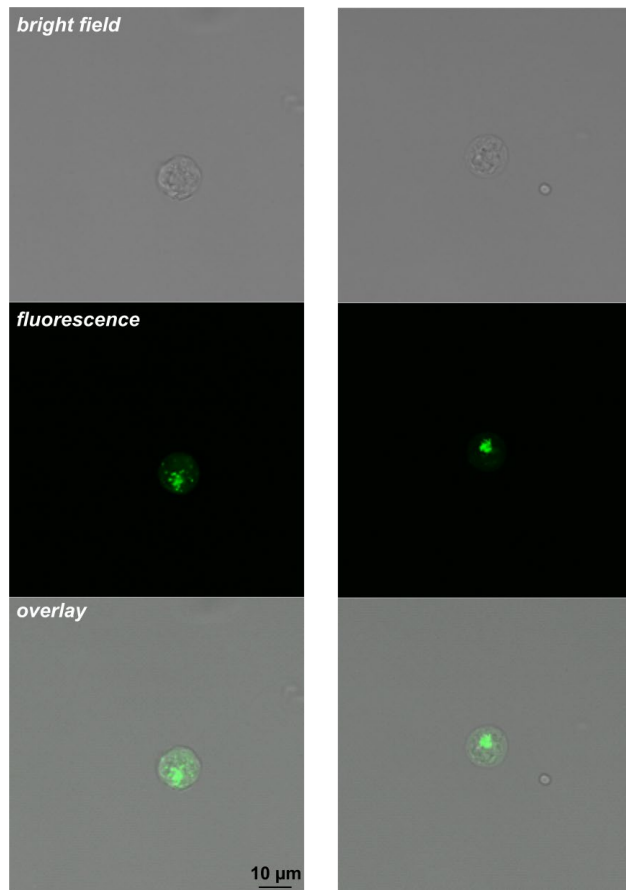


**Figure S4.13.** Two sets of confocal microscopy images of Raji DC-SIGN<sup>+</sup> cells exposed to gp120-FITC and DMSO (bright field, fluorescence, and overlay).



### Free D-mannose control

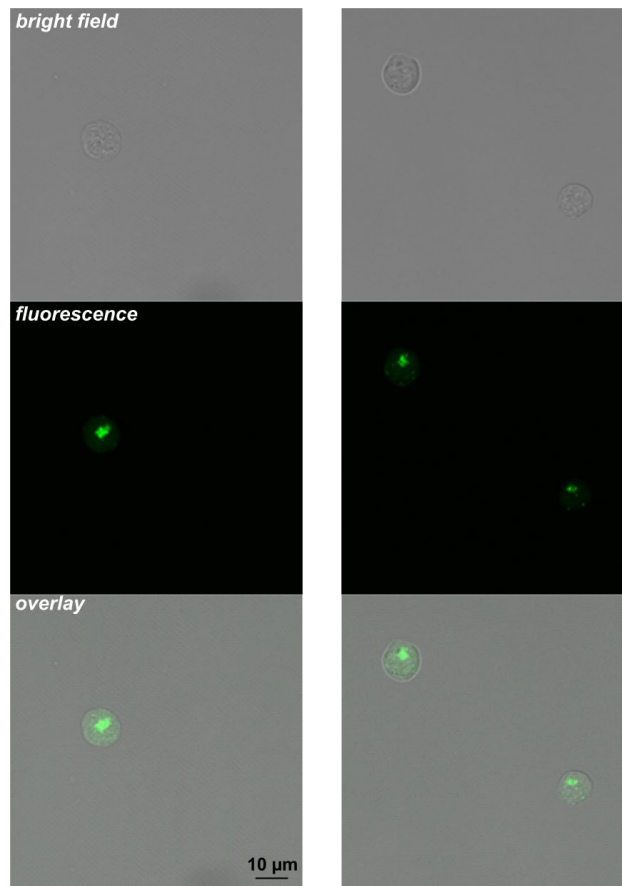


**Figure S4.14.** Two sets of confocal microscopy images of Raji DC-SIGN<sup>+</sup> cells exposed to gp120-FITC and free D-mannose (50 μM) (bright field, fluorescence, and overlay).

**[K<sub>2</sub>][8] control**

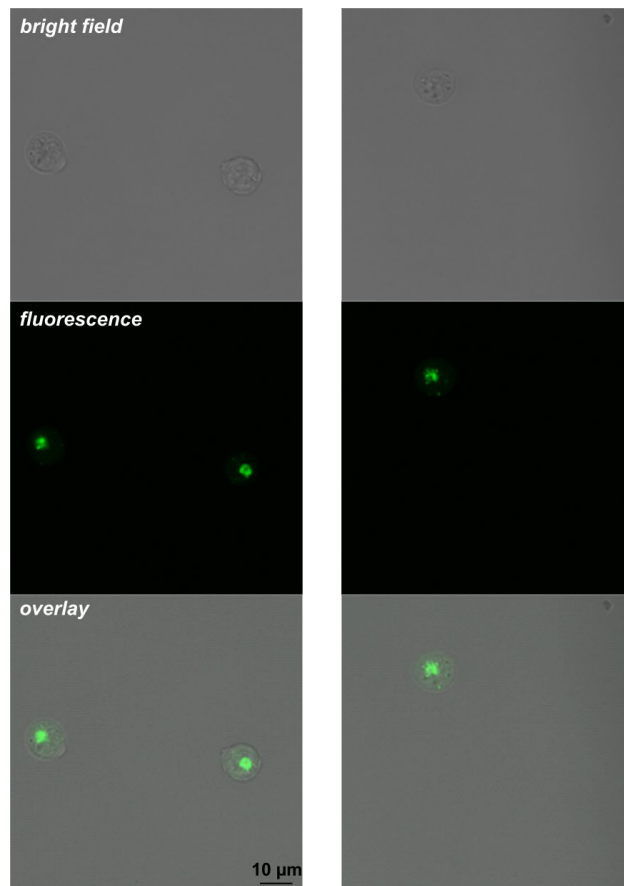


**Figure S4.15.** Two sets of confocal microscopy images of Raji DC-SIGN<sup>+</sup> cells exposed to gp120-FITC and [K<sub>2</sub>][8] (50 μM) (bright field, fluorescence, and overlay).

**[Na<sub>2</sub>][20] inhibitor**

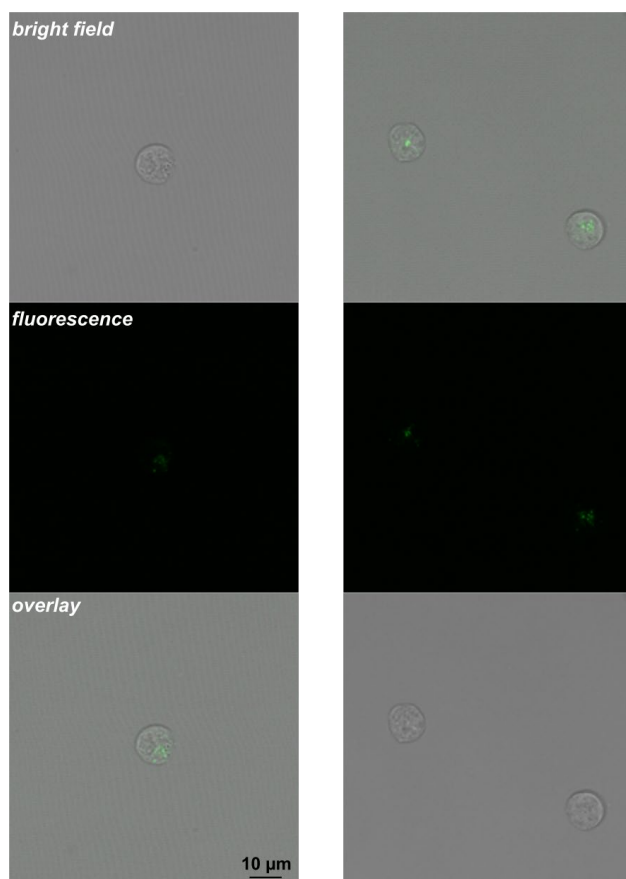


**Figure S4.16.** Two sets of confocal microscopy images of Raji DC-SIGN<sup>+</sup> cells exposed to gp120-FITC and [K<sub>2</sub>][20] (50 μM) (bright field, fluorescence, and overlay).

## Computational studies

### Systems and methods

In order to assess the binding between the saccharide-grafted nanoclusters and their respective protein targets, atomistic molecular dynamics simulations were performed. Concanavalin A (ConA PDB code 1ONA)<sup>119</sup> was used as target protein for the 1-thio-D-glucose-functionalized boron cluster (**[18]**<sup>2-</sup>), Stx1B (PDB code 1CQF)<sup>214</sup> was the target for the boron clusters grafted with either 1-thio-D-galactose (**[19]**<sup>2-</sup>) or PEG<sub>350</sub> (**[8]**<sup>2-</sup>), and DC-SIGN (PDB code 1k9I)<sup>173</sup> was used as the target for the 1-thio-D-mannose-functionalized boron cluster (**[20]**<sup>2-</sup>).

The target proteins were described by a CHARMM36<sup>108</sup> force field, while the clusters were described by a CHARMM general force field.<sup>109</sup> The atomic charges of the boron clusters and their methylbenzene substituents were recalculated by DFT-BLYP<sup>215</sup> with the RESP<sup>216</sup> method. The simulations were performed with NAMD.<sup>107</sup> The Particle Mesh Ewald (PME)<sup>117</sup> method was used for the evaluation of long-range Coulombic interactions. The time step was set to 2.0 fs. The simulations were performed in the NPT ensemble ( $p = 1$  bar and  $T = 300$  K), using the Langevin dynamics ( $\gamma_{\text{Lang}} = 1 \text{ ps}^{-1}$ ). After 2,000 steps of minimization, ions and water molecules were equilibrated for 2 ns around the protein and cluster, which were restrained using harmonic forces with a spring constant of 1 kcal/(mol Å<sup>2</sup>). The last frames of the restrained equilibration were used to start simulations of the free cluster and partial constrained protein.

Figure S4.21, Figure S4.23, Figure S4.25, and Figure S4.27 display snapshots from the four nanocluster/protein binding simulations. The proteins are shown in cartoon representation (light blue), and the appended saccharides of the cluster are in gray, with boron, carbon, oxygen, calcium

and manganese atoms represented in pink, gray, red, purple, and cyan, respectively. The amino acids color scheme is Asn: orange, Trp: purple, Asp: red, Arg: blue, Tyr: green, Leu: light blue, Val: ochre, Ser: yellow, Gly: white, and Glu: pink. The term “ligand” is used in this section to refer to one appended group on the cluster periphery (*i.e.*  $[\mathbf{18}]^{2-}$  contains 12 glucose ligands). Figure S4.22, Figure S4.24, Figure S4.26, and Figure S4.28 display plots that represent the number of ligands of each nanocluster that are within 4 Å of the amino acid residues on the protein binding sites.

### Calculated structures

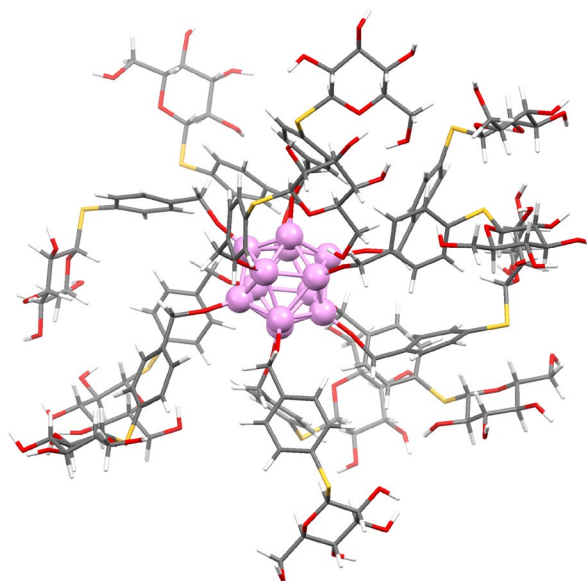


**Figure S4.17.** Calculated structure of  $[\mathbf{18}]^{2-}$ . Gray: C; white: H; red: O; yellow: S; pink: B.

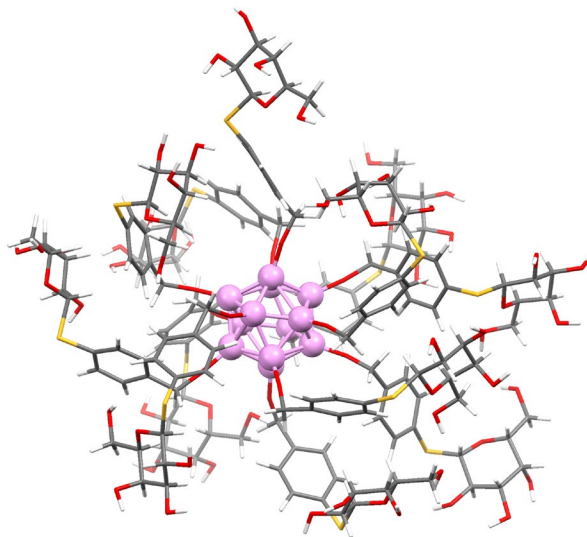


**Figure S4.18.** Calculated structure of  $[19]^{2-}$ . Gray: C; white: H; red: O; yellow: S; pink: B.

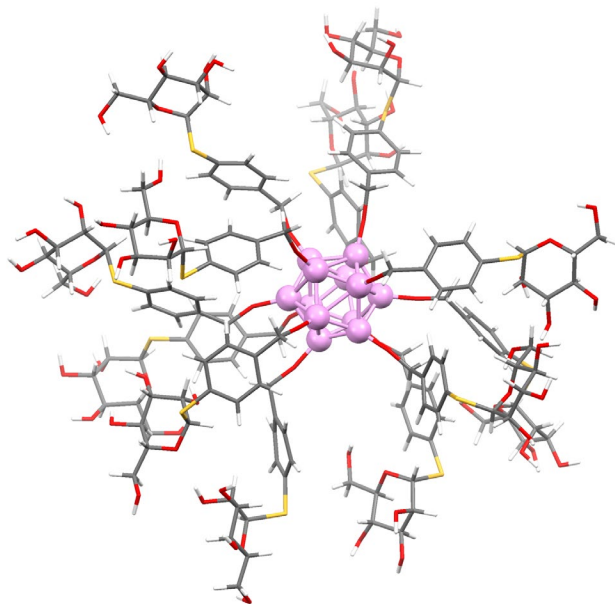


**Figure S4.19.** Calculated structure of  $[20]^{2-}$ . Gray: C; white: H; red: O; yellow: S; pink: B.

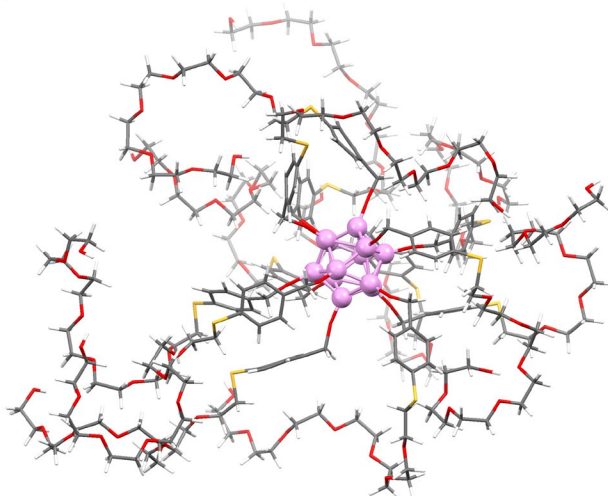


**Figure S4.20.** Calculated structure of  $[8]^{2-}$ . Gray: C; white: H; red: O; yellow: S; pink: B.

### **Binding of $[18]^{2-}$ with ConA**

Four  $[18]^{2-}$  nanoclusters were initially positioned near the typical sugar binding sites of Con A (Tyr 12, Tyr 100, Pro 13, Asn 14, Thr 15, Asp 16, Asp 208, Arg 228, and Leu 229), which are highlighted in Figure S4.21a. After the 20 ns simulation (Figure S4.21b), the  $[18]^{2-}$ -1 nanocluster remains bound to the same binding pocket at which it was originally positioned, as shown in Figure S4.21c. After the 20 ns simulation, the  $[18]^{2-}$ -2 cluster is bound to the surrounding amino acid residues of the binding pocket (Figure S4.21d), while the  $[18]^{2-}$ -3 cluster spans the binding pocket (Figure S4.21e), and the  $[18]^{2-}$ -4 cluster is dissociated from the protein binding site. As shown in Figure S4.22, there are on average two glucose ligands from  $[18]^{2-}$ -1 and two from  $[18]^{2-}$ -2 that interact with the amino acids of the binding pocket, while fewer ligands ( $<2$ ) from the  $[18]^{2-}$ -3 and  $[18]^{2-}$ -4 clusters bind to the surrounding amino acids throughout the simulation. Since the four binding pockets are separated from each other, there are four distinct binding scenarios observed.

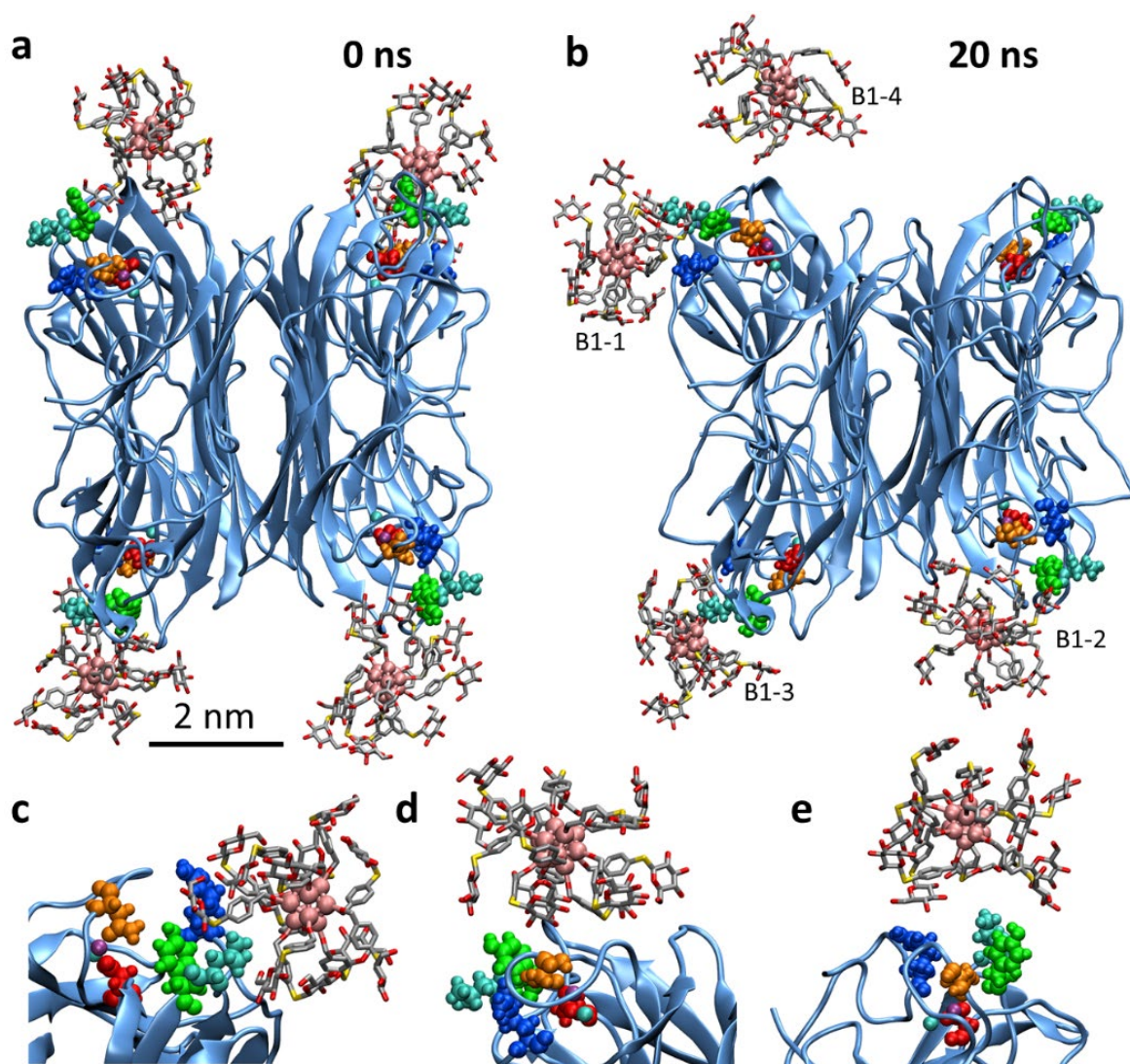


**Figure S4.21.** Binding of four independent  $[18]^{2-}$  molecules to the four distinct binding sites of ConA. (a) Initial configuration of the four  $[18]^{2-}$  clusters with ConA. (b) Final configuration after the 20 ns simulation. (c) Zoomed-in image of  $[18]^{2-}$ -1 interacting with one of the four sugar binding pockets. (d) Zoomed-in image of  $[18]^{2-}$ -2 binding to the surrounding residues of the pocket. (e) Zoomed-in image of  $[18]^{2-}$ -3 showing the glucose ligands spanning the binding pocket.



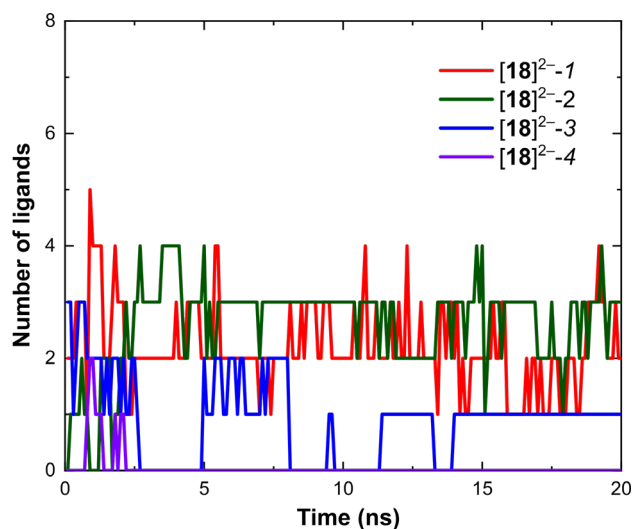


**Figure S4.22.** Plot displaying the number of ligands of the  $[18]^{2-}-1$  -  $[18]^{2-}-4$  clusters that interact with the specific binding pocket of ConA over the course of the 20 ns simulation.

### Binding of $[19]^{2-}$ and $[8]^{2-}$ with Stx1B

The  $[19]^{2-}$  and  $[8]^{2-}$  clusters were initially positioned on the side of Stx1B (sugar binding sites 1 and 2)<sup>217</sup> and above the binding surface of Stx1B (binding site 3) as shown in Figure S4.23 and Figure S4.25. Both  $[19]^{2-}$  and  $[8]^{2-}$  bind to the edge of Stx1B (sites 1 and 2) with a maximum of 7 and 8 binding ligands, respectively. Similarly, both clusters interact with the polar residues on the surface of Stx1B (site 3), with  $[19]^{2-}$  having up to 10 interacting ligands (galactose), while  $[8]^{2-}$  has up to 7 interacting ligands (PEG) during the course of the 20 ns simulation (Figure S4.24 and Figure S4.26). Although  $[19]^{2-}$  has shorter ligands than  $[8]^{2-}$ , it shows stronger multivalent binding towards the broad binding surface of Stx1B. The  $[8]^{2-}$ /Stx1B binding simulation suggests there is an interaction between the PEGylated cluster and the surface of Stx1B. This result is consistent with the binding response observed by SPR studies for this system; however, the  $K_D$  value calculated for the  $[8]^{2-}$  cluster (10.1  $\mu\text{M}$ ) is significantly lower than that of the  $[19]^{2-}$  cluster (1.51  $\mu\text{M}$ ) with Stx1B.

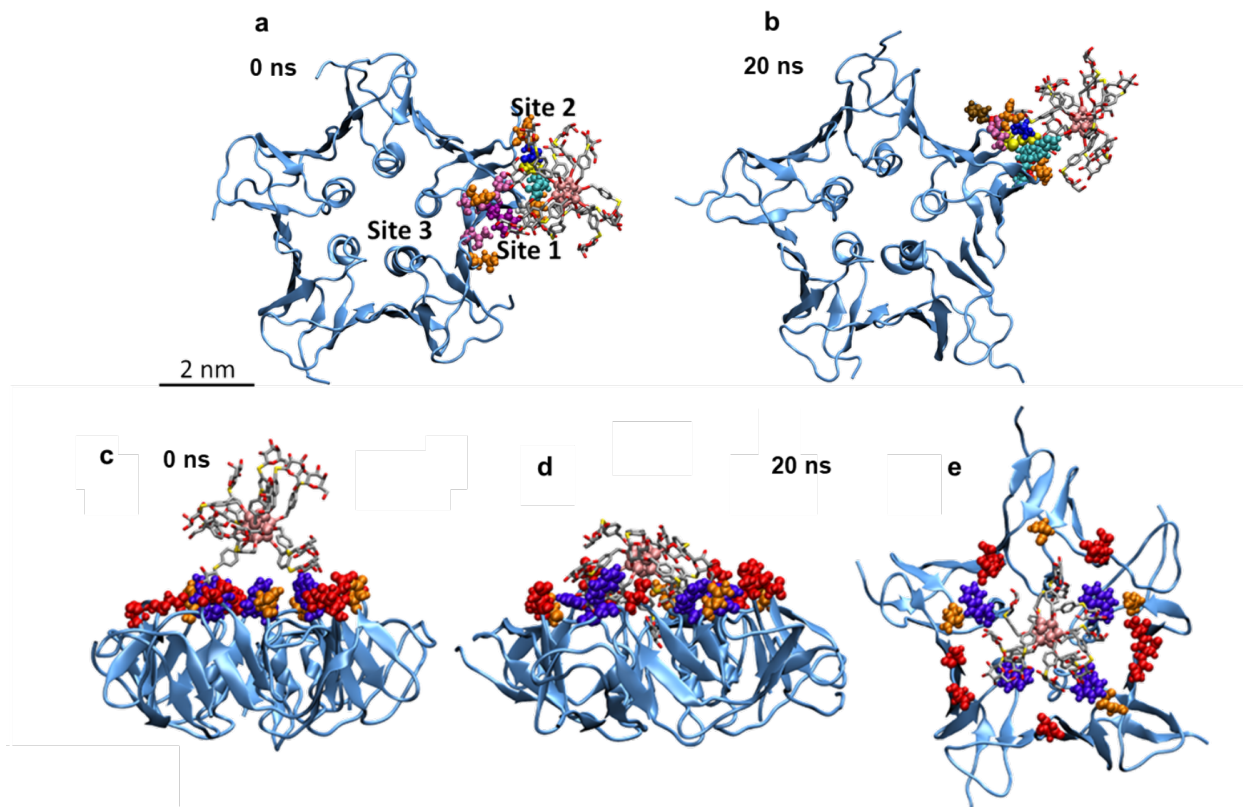


**Figure S4.23.** Binding of  $[19]^{2-}$  to Stx1B. (a) Initial configuration at sites 1 and 2. (b) Final binding configuration at sites 1 and 2 after 20 ns. (c) Initial configuration at site 3. (d, e) Two views of the final binding configuration at site 3 after 20 ns.

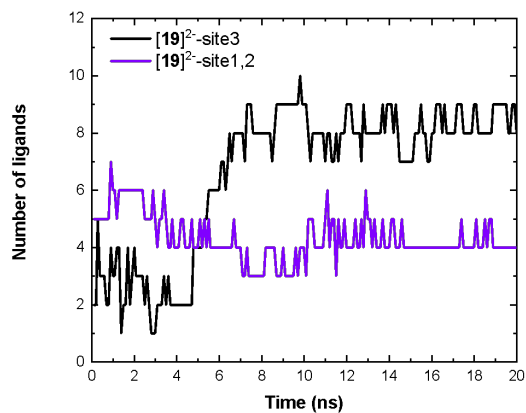


**Figure S4.24.** Plot displaying the number of ligands of the  $[19]^{2-}$  cluster that interact with the specific binding sites of Stx1B over the course of the 20 ns simulation.

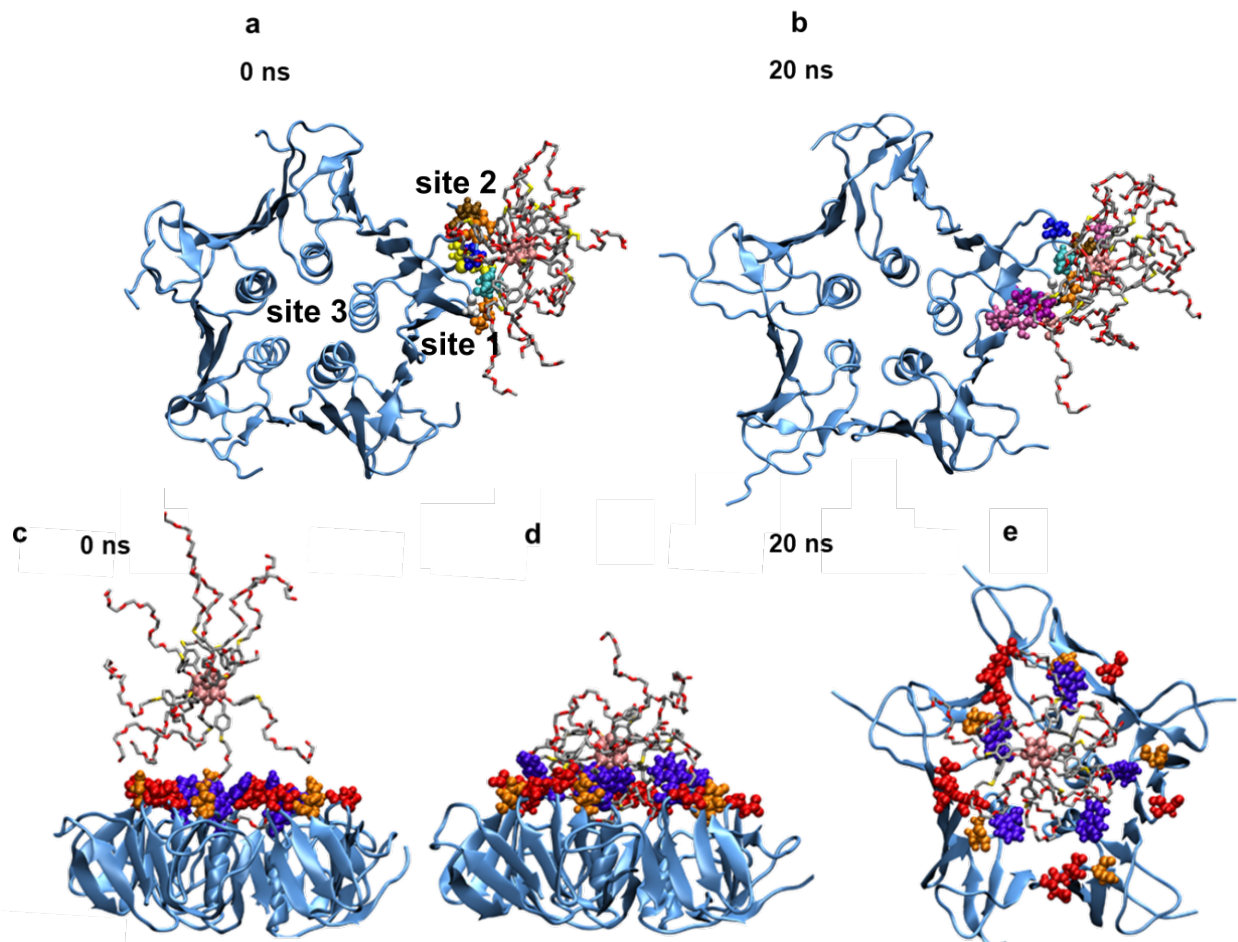


**Figure S4.25.** Binding of  $[8]^{2-}$  to Stx1B. (a) Initial configuration at sites 1 and 2. (b) Final binding configuration at sites 1 and 2 after 20 ns. (c) Initial configuration at site 3. (d, e) Two views of the final binding configuration at site 3 after 20 ns.

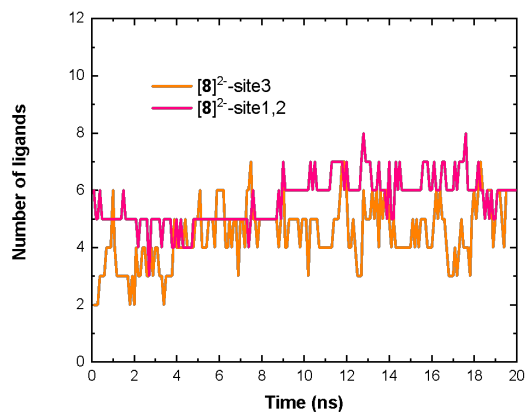


**Figure S4.26.** Plot displaying the number of ligands of the  $[8]^{2-}$  cluster that interact with the specific binding sites of Stx1B over the course of the 20 ns simulation.

## Binding of $[20]^{2-}$ with DC-SIGN

The  $[20]^{2-}$  cluster was initially positioned near one binding pocket of DC-SIGN (Asp 336, Glu 347, Asn 349, Val 351, Glu 354, and Asn 365). During the first 10 ns of the simulation, the cluster binds to the specific sugar binding pockets with a maximum of three ligands interacting with the pocket. It then dissociates from the binding site with only one ligand interacting with the residues of the protein (Figure S4.27 and Figure S4.28).

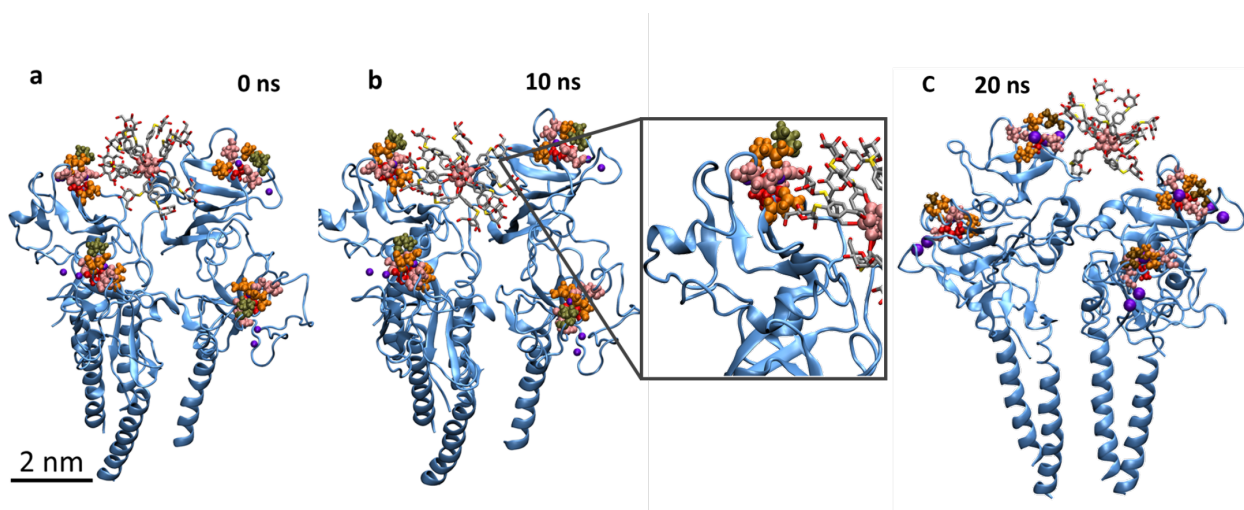


**Figure S4.27.** Binding of  $[20]^{2-}$  to DC-SIGN. (a) Initial configuration. (b) Configuration at 10 ns with zoomed-in image. (c) Final binding configuration after 20 ns.

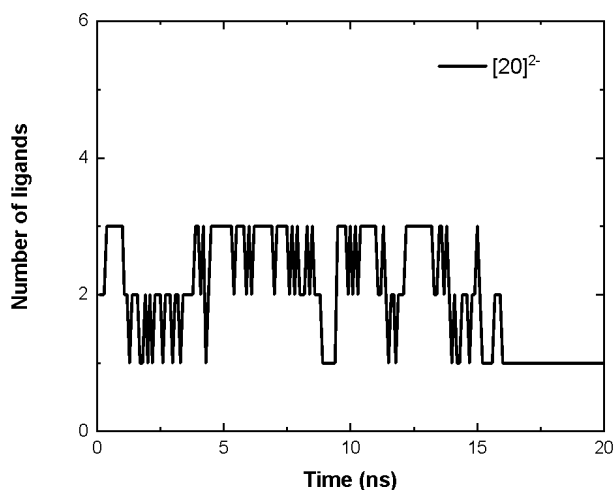


**Figure S4.28.** Plot displaying the number of ligands of the  $[20]^{2-}$  cluster that interact with the specific binding pocket of DC-SIGN over the course of the 20 ns simulation.

## X-ray crystallographic details

### $B_{12}(OCH_2C_6H_4I)_{12}$

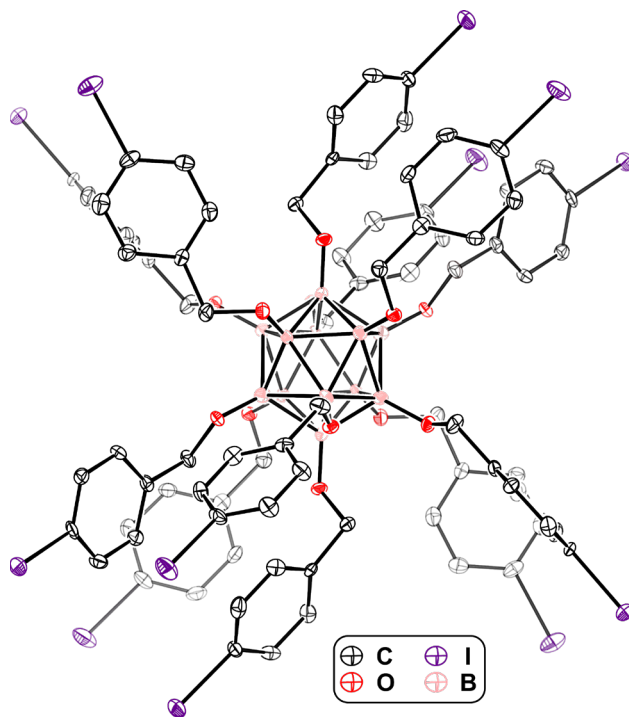


**Figure S4.29.** Solid-state structure of  $B_{12}(OCH_2C_6H_4I)_{12}$  with thermal ellipsoids rendered at the 50% probability level with PLATON<sup>218</sup> and with hydrogen atoms omitted for clarity.

**Table S4.1. Crystallographic and structure refinement information for B<sub>12</sub>(OCH<sub>2</sub>C<sub>6</sub>H<sub>4</sub>I)<sub>12</sub>**

CCDC code	1942748	
Empirical formula	C <sub>84</sub> H <sub>72</sub> B <sub>12</sub> I <sub>12</sub> O <sub>12</sub>	
Formula weight	2925.93	
Temperature	100.0 K	
Wavelength	0.71073 Å	
Crystal system	Triclinic	
Space group	<i>P</i> $\bar{1}$	
Unit cell dimensions	<i>a</i> = 10.6995(10) Å	<i>α</i> = 113.864(3)°
	<i>b</i> = 15.7093(14) Å	<i>β</i> = 90.520(3)°
	<i>c</i> = 16.1872(14) Å	<i>γ</i> = 109.249(3)°
Volume	2316.9(4) Å <sup>3</sup>	
<i>Z</i> , <i>Z'</i>	1, 0.5	
Density (calculated)	2.097 Mg/m <sup>3</sup>	
Absorption coefficient	4.068 mm <sup>-1</sup>	
<i>F</i> (000)	1368	
Crystal size	0.33 x 0.29 x 0.08 mm <sup>3</sup>	
Theta range for data collection	2.056 to 25.405°	
Index ranges	-12 ≤ <i>h</i> ≤ 12, -18 ≤ <i>k</i> ≤ 18, -19 ≤ <i>l</i> ≤ 18	
Reflections collected	25884	
Independent reflections	8477 [ <i>R</i> (int) = 0.0395]	
Completeness to theta = 25.242°	99.8 %	
Absorption correction	Semi-empirical from equivalents	
Max. and min. transmission	0.1480 and 0.0945	
Refinement method	Full-matrix least-squares on <i>F</i> <sup>2</sup>	
Data / restraints / parameters	8477 / 0 / 541	
Goodness-of-fit on <i>F</i> <sup>2</sup>	1.022	
Final <i>R</i> indices [ <i>I</i> > 2σ( <i>I</i> )]	<i>R</i> 1 = 0.0308, w <i>R</i> 2 = 0.0593	
<i>R</i> indices (all data)	<i>R</i> 1 = 0.0462, w <i>R</i> 2 = 0.0640	
Largest diff. peak and hole	1.045 and -0.976 e.Å <sup>-3</sup>	

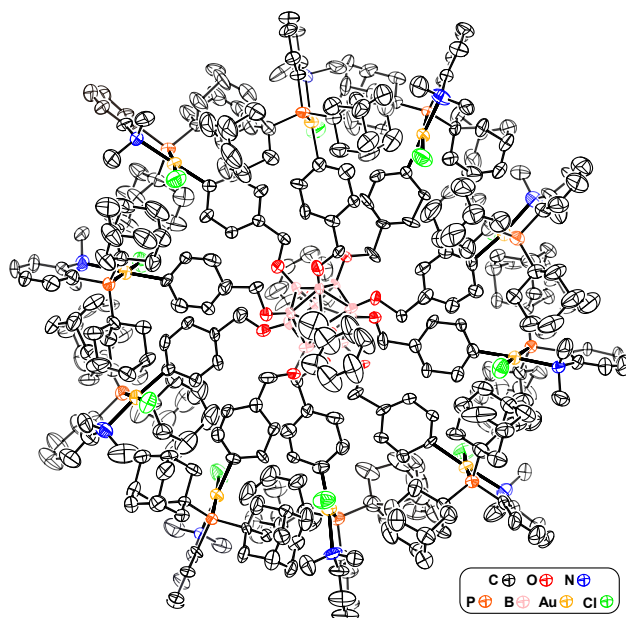


**Figure S4.30.** Solid-state structure of  $[\mathbf{1}]^{11+}$  with thermal ellipsoids rendered at the 50% probability level with PLATON<sup>218</sup> and with hydrogen atoms and  $\text{SbF}_6^-$  anions omitted for clarity.

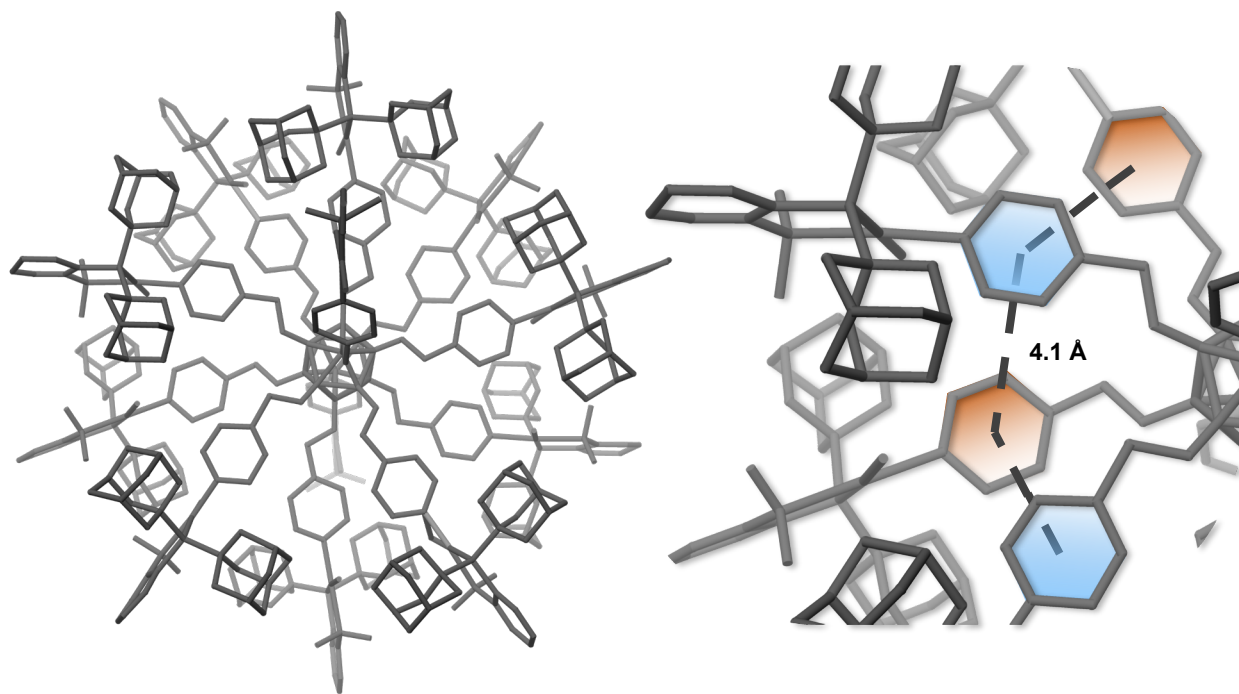


**Figure S4.31.** Solid-state structure of [1]<sup>11+</sup> (left) with zoomed-in image (right) displaying the benzyl group  $\pi$ -stacking interactions.



**Table S4.2. Crystallographic and structure refinement information for [1][SbF<sub>6</sub>]<sub>11</sub>**

CCDC code	1949777	
Empirical formula	C <sub>396.2</sub> H <sub>514</sub> Au <sub>11.2</sub> B <sub>12</sub> Cl <sub>11.2</sub> F <sub>58.3</sub> N <sub>11.2</sub> O <sub>12</sub> P <sub>11.2</sub> Sb <sub>9.7</sub>	
Formula weight	10984.21	
Temperature	298.2 K	
Wavelength	0.4934 Å	
Crystal system	Monoclinic	
Space group	Cc	
Unit cell dimensions	$a = 45.6445(4)$ Å	$\alpha = 90^\circ$
	$b = 29.7686(3)$ Å	$\beta = 93.524(1)^\circ$
	$c = 41.2098(6)$ Å	$\gamma = 90^\circ$
Volume	55888.7(11) Å <sup>3</sup>	
Z, Z'	4, 1	
Density (calculated)	1.305 g/mm <sup>3</sup>	
Absorption coefficient	3.474 mm <sup>-1</sup>	
F(000)	21536	
Crystal size	0.1 x 0.07 x 0.02 mm <sup>3</sup>	
Theta range for data collection	1.458 to 17.291°	
Index ranges	-54 ≤ h ≤ 54, -35 ≤ k ≤ 35, -49 ≤ l ≤ 49	
Reflections collected	338876	
Independent reflections	101864 [R(int) = 0.0622]	
Completeness to theta = 17.29°	99.80 %	
Absorption correction	multi-scan	
Max. and min. transmission	1.00000 and 0.05141	
Refinement method	Full-matrix least-squares on F <sup>2</sup>	
Data / restraints / parameters	101864 / 7952 / 5257	
Goodness-of-fit on F <sup>2</sup>	1.053 *[1.027]	
Final R indices [F <sub>o</sub> >4σ(F <sub>o</sub> )]	R1 = 0.0561, wR2 = 0.1717	
	*[R1 = 0.0697, wR2 = 0.2355]	

*R* indices (all data)

$R1 = 0.0730$  \*[ $R1 = 0.0876$ ]

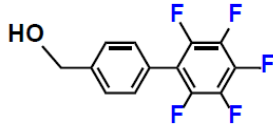
Largest diff. peak and hole

1.37 and -0.86 e.Å<sup>-3</sup> \*[1.92 and -0.91 e.Å<sup>-3</sup>]

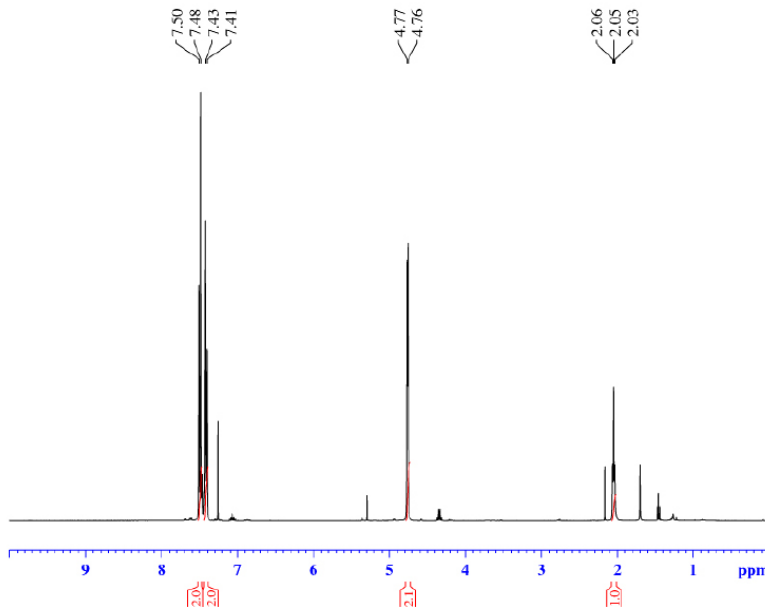
\*indicates values before applying SQUEEZE<sup>218</sup>

# APPENDICES

## Supplementary Data Relevant to Chapter Two



<sup>1</sup>H NMR

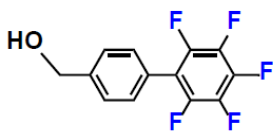


Current Data Parameters  
 NAME G2-CH1  
 EXPNO 80  
 PROCNO 1

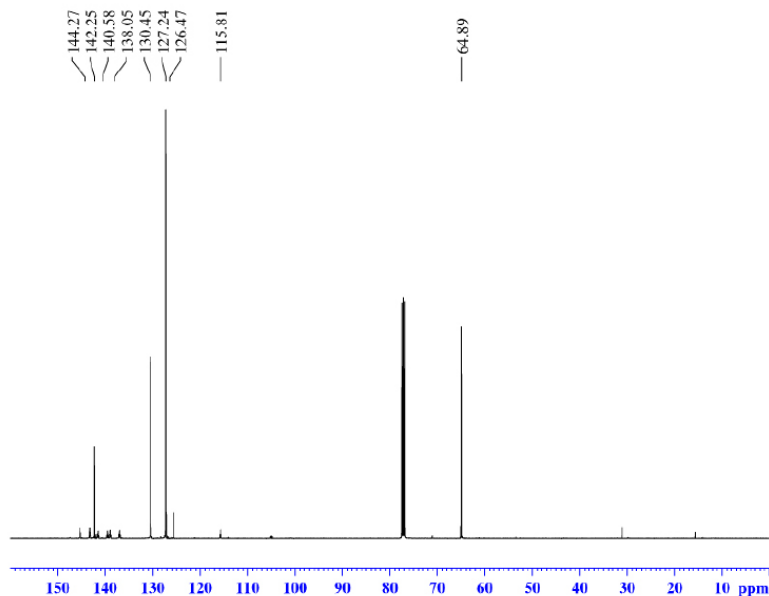
F2 - Acquisition Parameters  
 Date\_ 20160805  
 Time 2.22  
 INSTRUM av400  
 PROBHID 5 mm PABBO BB/  
 PULPROG zg30  
 TD 52882  
 SOLVENT CDCl3  
 NS 80  
 DS 0  
 SWH 8012.820 Hz  
 FIDRES 0.151523 Hz  
 AQ 3.2998369 sec  
 RG 155.85  
 DW 62.400 usec  
 DE 6.50 usec  
 TE 299.0 K  
 D1 2.00000000 sec  
 TDO 1

==== CHANNEL f1 =====  
 SFO1 400.1324008 MHz  
 NUC1 1H  
 P1 15.00 usec  
 PLW1 13.00000000 W

F2 - Processing parameters  
 SI 65556  
 SF 400.1300176 MHz  
 WDW EM  
 SSB 0  
 LB 0.30 Hz  
 GB 0  
 PC 1.60



$^{13}\text{C}\{^1\text{H}\}$  NMR

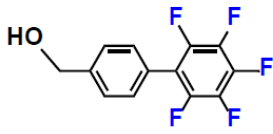


```

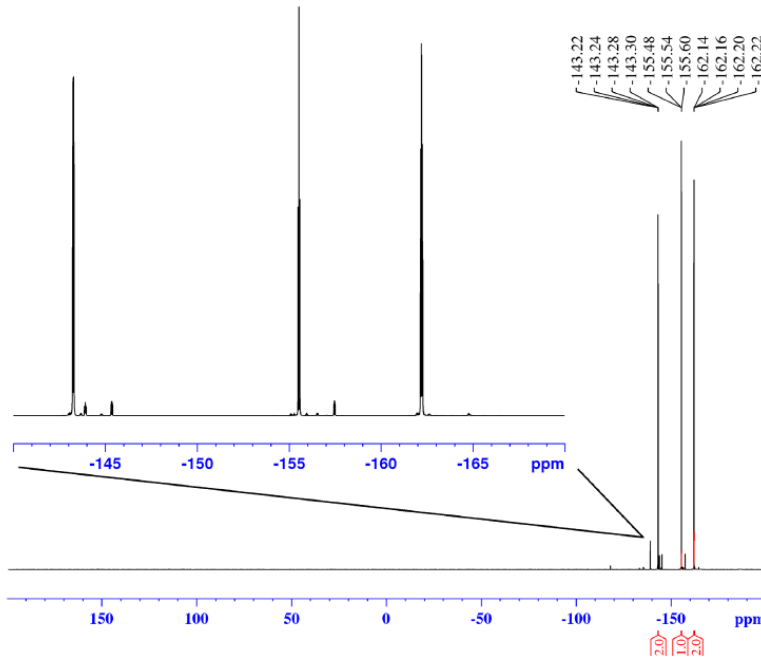
Current Data Parameters
NAME      02_081
EXPNO     10
PROCNO    1

F2 - Acquisition Parameters
Date_     20160805
Time      14:25 h
INSTRUM   av500
PROBHD    Z119248_0002 (
PULPROG   zgpg30
TD         65536
SOLVENT   CDCl3
NS         475
DS         2
SWH        31250.000 Hz
FIDRES     0.853674 Hz
AQ         1.0485760 sec
RG         304.54
DW         16.000 usec
DE         18.00 usec
TE         298.0 K
D1         2.00000000 sec
D11        0.03000000 sec
TD0        1
SFO1       125.7722511 MHz
NUC1       13C
P1         10.30 usec
PLW1       25.00000000 W
SFO2       500.1330008 MHz
NUC2       1H
CPCPD2[1] waltz16
PCPD2      80.00 usec
PLW2       15.50000000 W
PLW12      6.21094000 W
PLW13      0.10610000 W

F2 - Processing parameters
SI         131072
SF         125.7577740 MHz
WDW        EM
SSB        0
LB         1.00 Hz
GB         0
PC         1.40
  
```



<sup>19</sup>F NMR



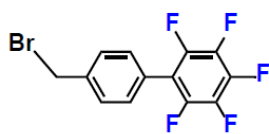
```

Current Data Parameters
NAME      G2-OH
EXPNO     81
PROCNO    1

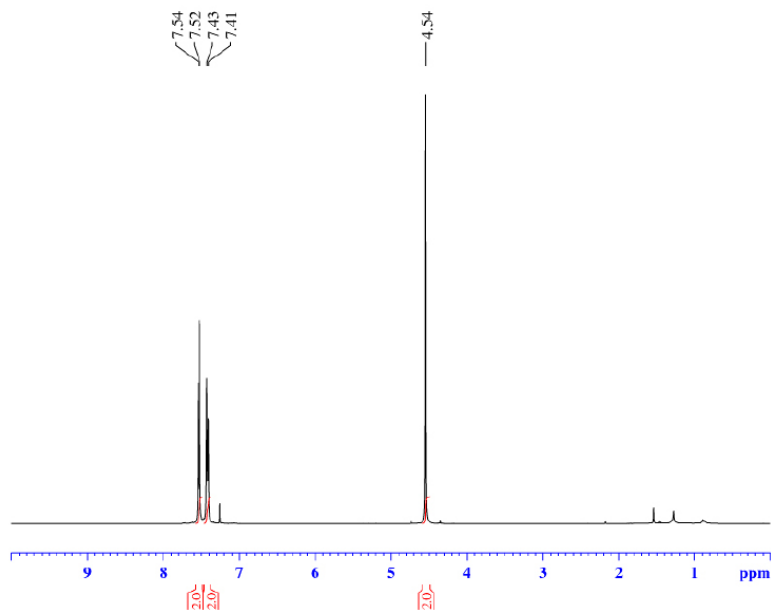
F2 - Acquisition Parameters
Date_     20160805
Time      2.29
INSTRUM   av400
PROBHD    5 mm PABBO BB/
PULPROG   zgpg30
TD         262144
SOLVENT   CDCl3
NS         128
DS         0
SWH        150000.000 Hz
FIDRES     0.572205 Hz
AQ         0.8738133 sec
RG         189.85
DW         3.333 usec
DE         6.50 usec
TE         299.0 K
D1         2.00000000 sec
TDO        1

===== CHANNEL f1 =====
SFO1      376.4983660 MHz
NUC1       19F
P1         14.50 usec
PLW1      17.00000000 W

F2 - Processing parameters
SI         262144
SF         376.4983660 MHz
WDW        EM
SSB        0
LB         1.00 Hz
GB         0
PC         1.00
  
```



<sup>1</sup>H NMR



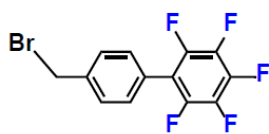
```

Current Data Parameters
NAME      G2-Br
EXPNO    30
PROCNO    1

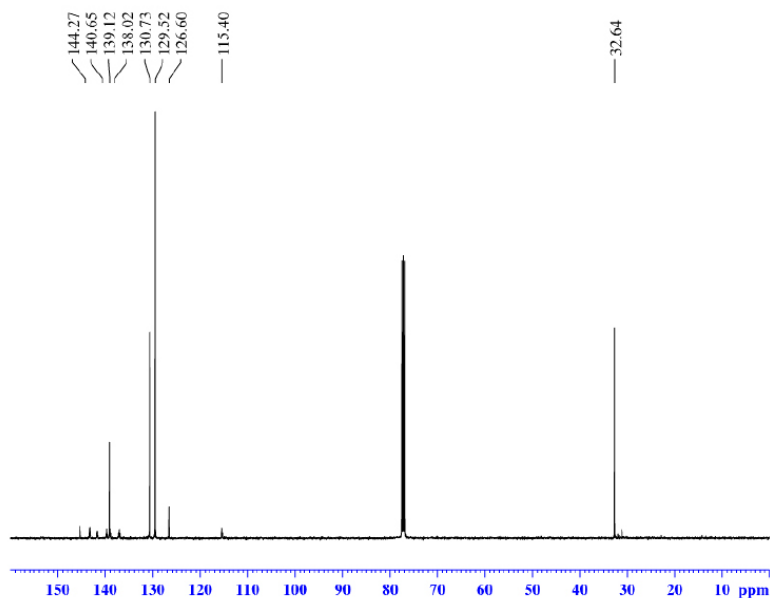
F2 - Acquisition Parameters
Date_    20160523
Time     11.42
INSTRUM  av400
PROBHD   5 mm PABBO BB/
PULPROG  zg30
TD       52882
SOLVENT  CDCl3
NS       48
DS       6
SWH      8012.820 Hz
FIDRES   0.151523 Hz
AQ       3.2998369 sec
RG       73.86
DW       62.400 usec
DE       0.50 usec
TE       299.0 K
D1       2.00000000 sec
TDO      1

===== CHANNEL f1 =====
SFO1    400.1324008 MHz
NUC1    1H
P1      15.00 usec
PLW1    13.00000000 W

F2 - Processing parameters
SI      65536
SF      400.130176 MHz
WDW     EM
SSB     0
LB      0.30 Hz
GB      0
PC      1.00
  
```

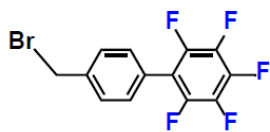


$^{13}\text{C}\{^1\text{H}\}$  NMR

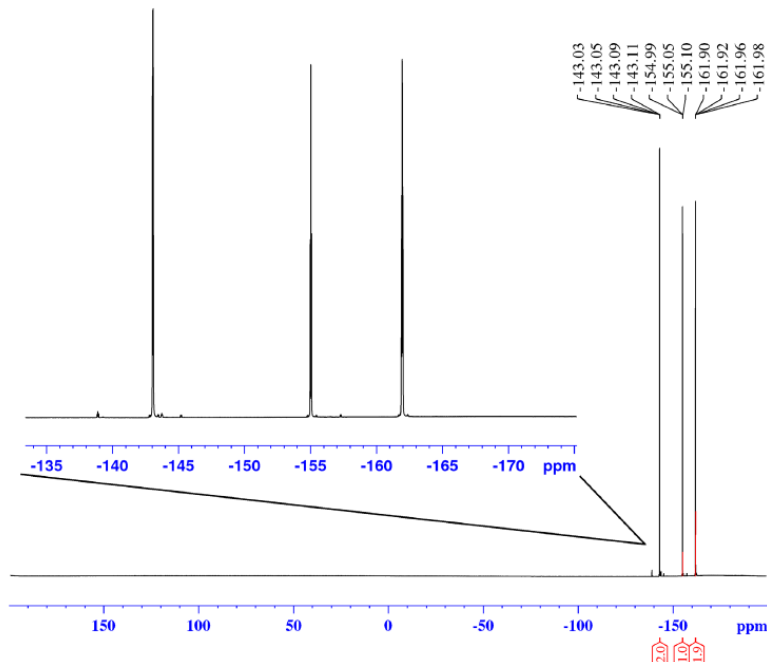


Current Data Parameters  
 NAME: Shift\_C2-Br  
 EXPNO: 2  
 PROCNO: 1  
 Date\_: 2016080  
 Time: 13:00  
 INSTRUM: spect  
 PROBHD: 5 mm bb-ZZ800  
 PULPROG: zgpg30  
 TE: 655.6  
 SOLVENT: CDCl3  
 NS: 1186  
 DS: 4  
 SWH: 32679.738 Hz  
 FIDRES: 0.199853 Hz  
 AQ: 1.002709 sec  
 RG: 14596.5  
 DW: 15.300 usec  
 DE: 6.08 usec  
 TE: 298.1 K  
 D1: 2.0000000 sec  
 d11: 0.0300000 sec  
 TDO: 1

===== CHANNEL f1 =====  
 NUC1:  $^{13}\text{C}$   
 P1: 6.50 usec  
 PL1: 0 dB  
 SFO1: 125.8231939 MHz  
 ===== CHANNEL f2 =====  
 CTDPRG2: waltz16  
 NUC2:  $^1\text{H}$   
 PCPD2: 100.00 usec  
 PL2: 0 dB  
 PL12: 17.32 dB  
 SFO2: 500.3250013 MHz  
 F2 - Processing parameters  
 SI: 65536  
 SF: 125.8080650 MHz  
 WDW: EM  
 SSI: 0  
 LB: 100 Hz  
 GB: 0  
 PC: 1.40



<sup>19</sup>F NMR



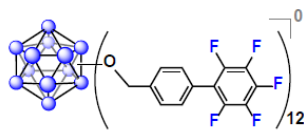
Current Data Parameters  
 NAME G2-Br  
 EXPNO 31  
 PROCNO 1

F2 - Acquisition Parameters  
 Date\_ 20160523  
 Time 11.46  
 INSTRUM av400  
 PROBHD 5 mm PABBO BB/  
 PULPROG zgpg30  
 TD 262144  
 SOLVENT CDCl3  
 NS 64  
 DS 0  
 SWH 150000.000 Hz  
 FIDRES 0.572205 Hz  
 AQ 0.8738133 sec  
 RG 189.85  
 DW 3.333 usec  
 DE 6.50 usec  
 TE 299.0 K  
 D1 2.00000000 sec  
 TDO 1

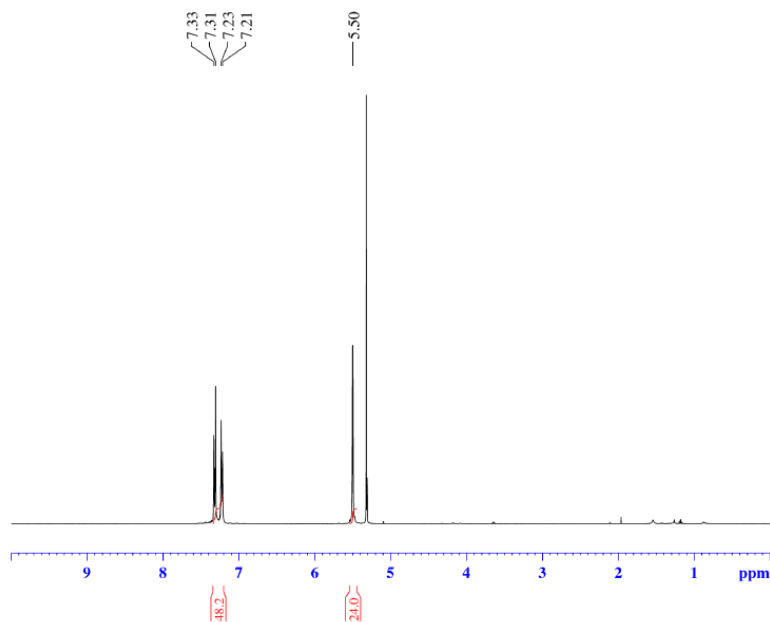
===== CHANNEL f1 =====  
 SFO1 376.4983660 MHz  
 NUC1 19F  
 P1 14.50 usec  
 PLW1 17.00000000 W

F2 - Processing parameters  
 SI 262144  
 SF 376.4983660 MHz  
 WDW EM  
 SSB 0  
 LB 1.00 Hz  
 GB 0  
 PC 1.00





<sup>1</sup>H NMR



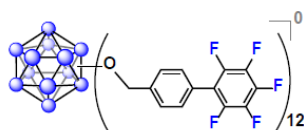
```

Current Data Parameters
NAME      B12(O-PhPF6)n12 aka Gen2
EXPNO    91
PROCNO   1

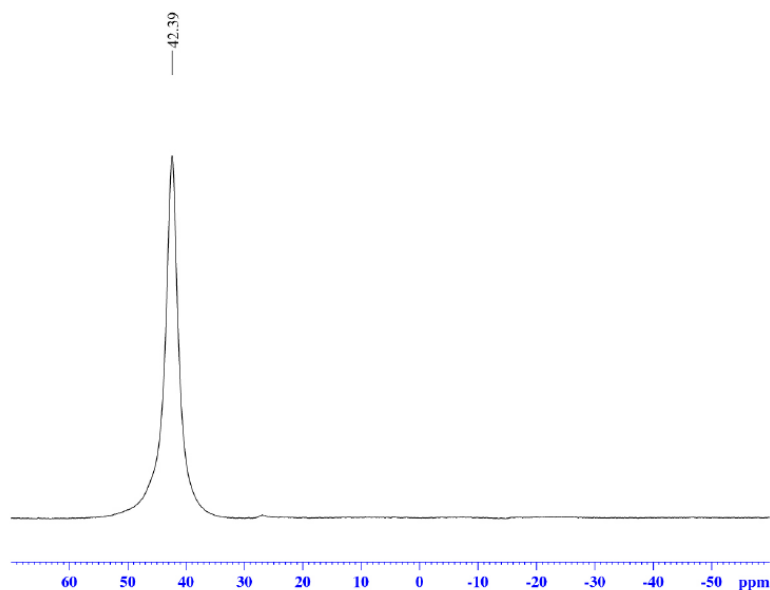
F2 - Acquisition Parameters
Date_    20151220
Time     14.27
INSTRUM  av400
PROBHD   5 mm PABBO BB/
PULPROG  zg30
TD       52882
SOLVENT  CD2Cl2
NS       32
DS       0
SWH      8012.820 Hz
FIDRES   0.151523 Hz
AQ       3.2998369 sec
RG       155.85
DW       62.400 usec
DE       6.50 usec
TE       299.0 K
D1       2.00000000 sec
TDO      1

===== CHANNEL f1 =====
SFO1    400.1324008 MHz
NUC1    1H
P1      15.00 usec
PLW1    13.00000000 W

F2 - Processing parameters
SI      65536
SF      400.1300203 MHz
WDW     EM
SSB     0
LB      0.30 Hz
GB      0
PC      1.00
  
```



$^{11}\text{B}$   $\{^1\text{H}\}$  NMR



```

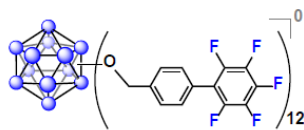
Current Data Parameters
NAME      B12(O-CH2C6H4CF3)12 aka Gen2
EXPNO    90
PROCNO   1

F2 - Acquisition Parameters
Date_    20151220
Time     14.23
INSTRUM  mv400
PROBHD   5 mm PABBO BB/
PULPROG  zgdc.js
TD       5096
SOLVENT  CDCl2
NS       1024
DS       0
SWH      51020.406 Hz
FIDRES   10.011854 Hz
AQ       0.0498405 sec
RG       189.85
DFW      9.850 usec
DE       6.50 usec
TE       299.0 K
D1       0.05000000 sec
D11      0.03000000 sec
TD0      1

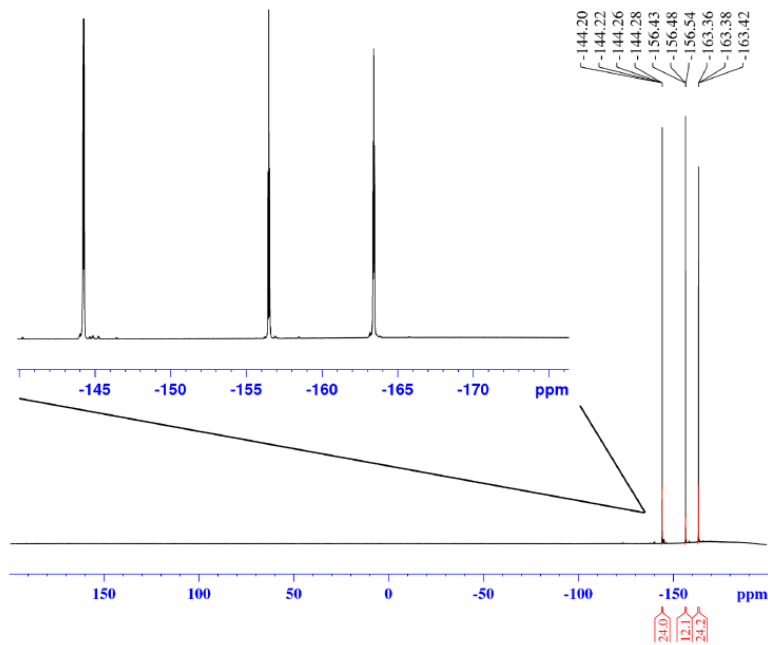
===== CHANNEL f1 =====
SFO1    128.3776161 MHz
NUC1     11B
P1       10.00 usec
PLW1    52.00000000 W

===== CHANNEL f2 =====
SFO2    400.1324008 MHz
NUC2     1H
CPDPRG2  waltz16
PCPD2    90.00 usec
PLW2    13.00000000 W
PLW12   0.36111000 W

F2 - Processing parameters
SI       32768
SF       128.3776161 MHz
WDW      EM
SSB      0
LB       10.00 Hz
GB       0
PC       1.40
  
```



<sup>19</sup>F NMR

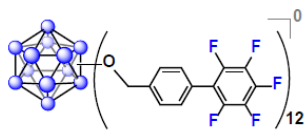


Current Data Parameters  
 NAME B12(O-PhPF6n)12 aka Gen2  
 EXPNO 32  
 PROCNO 1

F2 - Acquisition Parameters  
 Date\_ 20151220  
 Time 14.33  
 INSTRUM av400  
 PROBHD 5 mm PABBO BB/  
 PULPROG zgpg30  
 TD 262144  
 SOLVENT CD2Cl2  
 NS 64  
 DS 0  
 SWH 150000.000 Hz  
 FIDRES 0.572205 Hz  
 AQ 0.8738133 sec  
 RG 189.85  
 DW 3.333 usec  
 DE 6.50 usec  
 TE 299.0 K  
 D1 2.00000000 sec  
 TDO 1

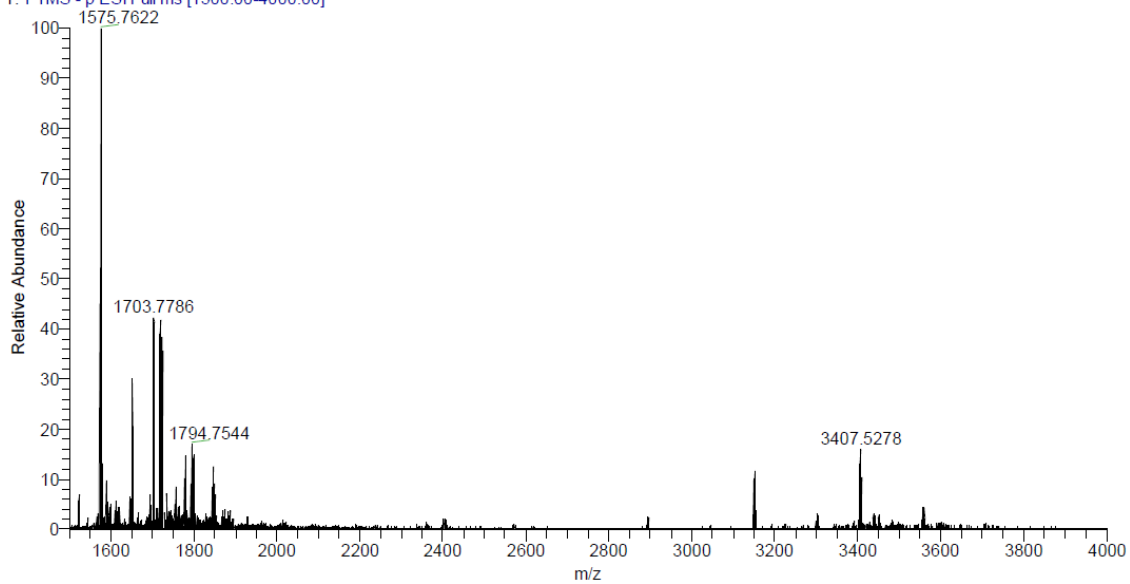
===== CHANNEL f1 =====  
 SFO1 376.4983660 MHz  
 NUC1 19F  
 P1 14.50 usec  
 PLW1 17.00000000 W

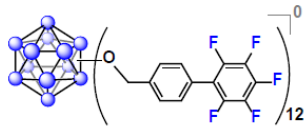
F2 - Processing parameters  
 SI 262144  
 SF 376.4983660 MHz  
 WDW EM  
 SSB 0  
 LB 1.00 Hz  
 GB 0  
 PC 1.00



## Q Exactive High-Res Mass Spec

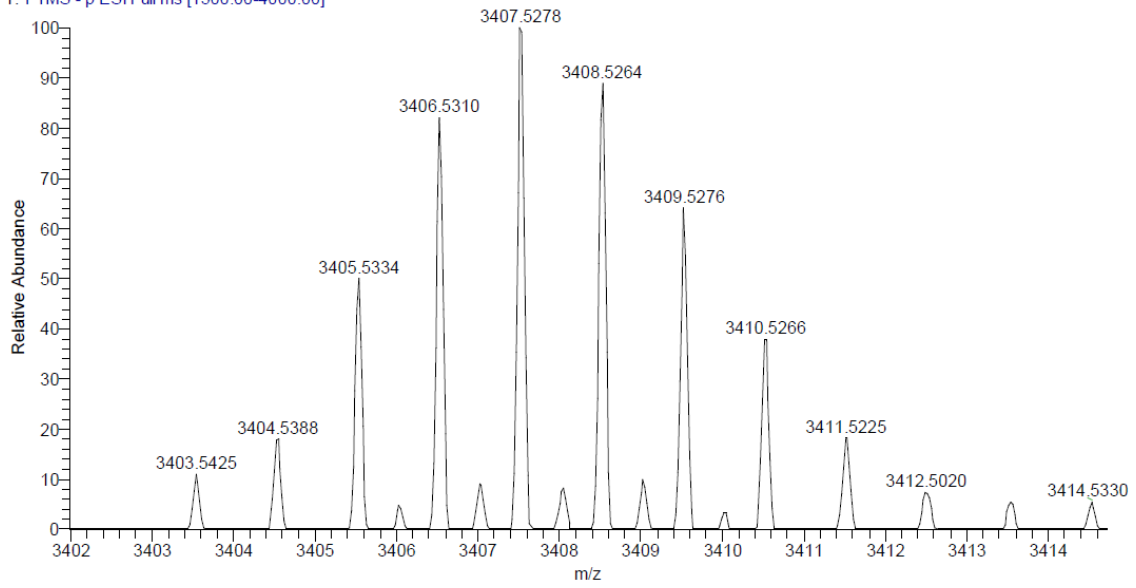
PhPFB #1 RT: 0.01 AV: 1 NL: 3.76E5  
T: FTMS - p ESI Full ms [1500.00-4000.00]

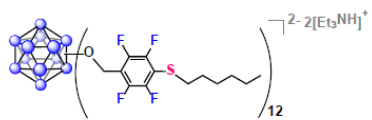




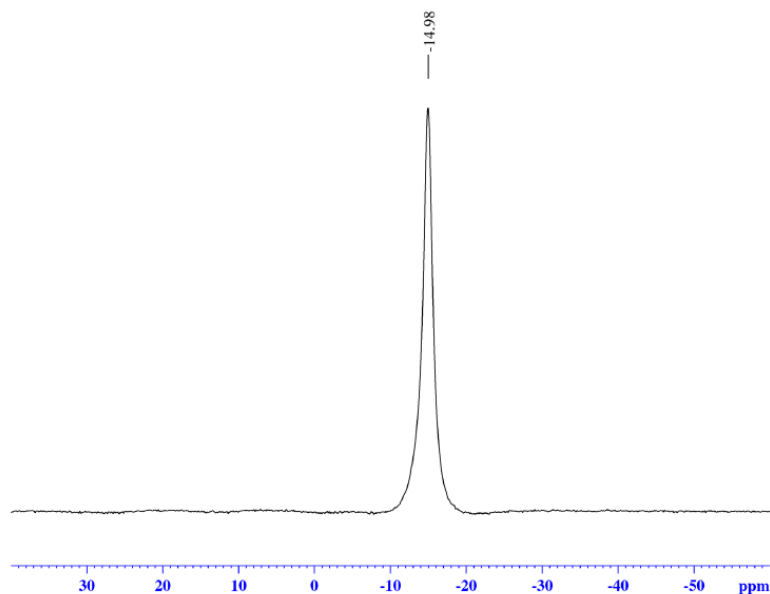
### Q Exactive High-Res Mass Spec

PhPFB #1 RT: 0.01 AV: 1 NL: 6.03E4  
T: FTMS - p ESI Full ms [1500.00-4000.00]





*in situ* <sup>11</sup>B NMR



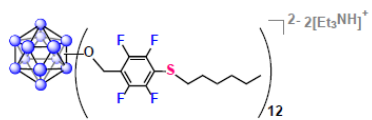
```

Current Data Parameters
NAME      0219
EXPNO    31
PROCNO    1

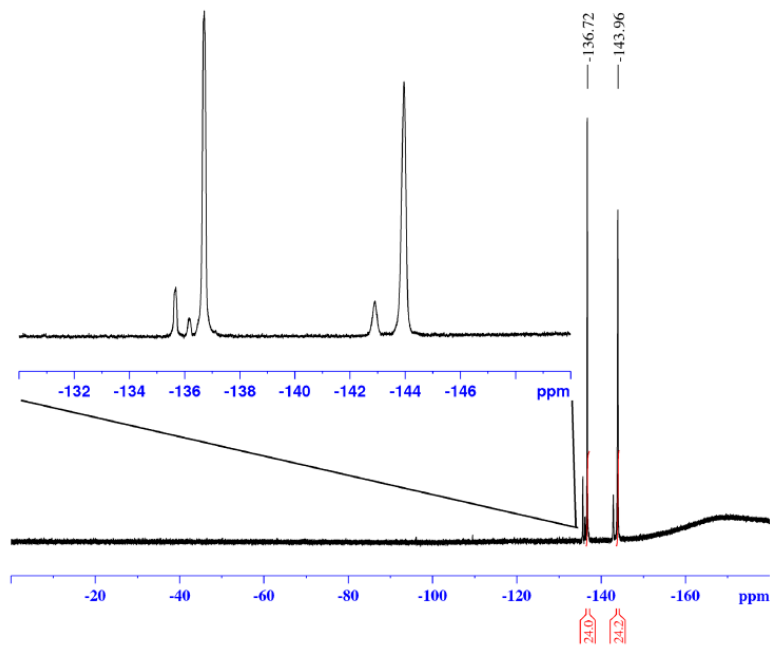
F2 - Acquisition Parameters
Date_     20160219
Time      11.46
INSTRUM   av400
PROBHD    5 mm PABBO BB/
PULPROG   zg
TD         5096
SOLVENT   None
NS         1024
DS         0
SWH        51020.406 Hz
FIDRES     10.011854 Hz
AQ         0.0499408 sec
RG         189.85
DW         9.800 usec
DE         6.50 usec
TE         299.0 K
D1         0.05000000 sec
TDO        1

===== CHANNEL f1 =====
SFO1      128.3776052 MHz
NUC1       11B
P1         10.00 usec
PLW1       52.00000000 W

F2 - Processing parameters
SI         32768
SF         128.3776161 MHz
WDW        EM
SSB        0
LB         10.00 Hz
GB         0
PC         1.40
  
```



*in situ*  $^{19}\text{F}$  NMR



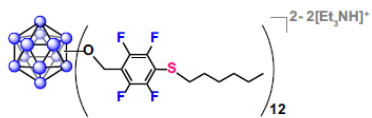
Current Data Parameters  
 NAME 0219  
 EXPNO 30  
 PROCNO 1

F2 - Acquisition Parameters  
 Date\_ 20160219  
 Time 11.42  
 INSTRUM av400  
 PROBHD 5 mm PABBO BB/  
 PULPROG zgpg30  
 TD 262144  
 SOLVENT None  
 NS 64  
 DS 0  
 SWH 150000.000 Hz  
 FIDRES 0.572205 Hz  
 AQ 0.8738133 sec  
 RG 189.85  
 DW 3.333 usec  
 DE 6.50 usec  
 TE 299.0 K  
 D1 2.00000000 sec  
 TDO 1

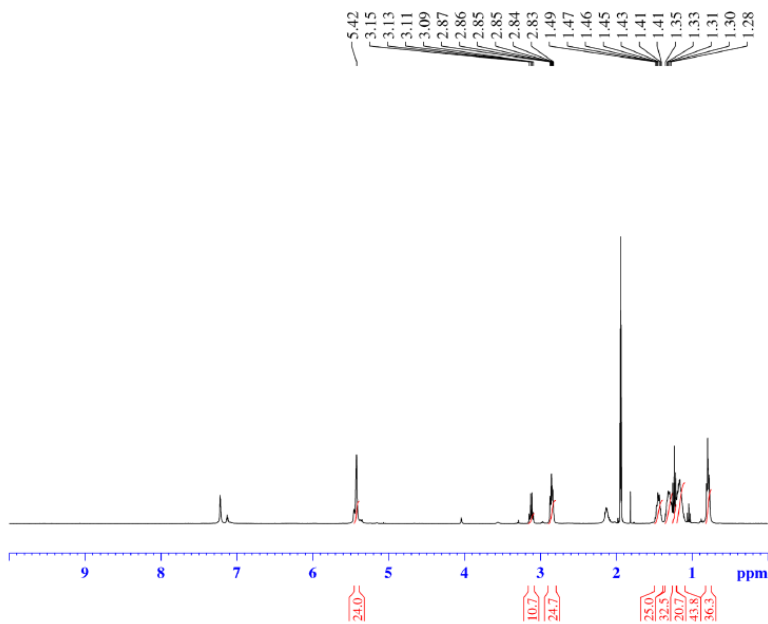
===== CHANNEL f1 =====  
 SFO1 376.4983660 MHz  
 NUC1  $^{19}\text{F}$   
 P1 14.50 usec  
 PLW1 17.00000000 W

F2 - Processing parameters  
 SI 262144  
 SF 376.4983660 MHz  
 WDW EM  
 SSB 0  
 LB 1.00 Hz  
 GB 0  
 PC 1.00

Small impurities are present due to the commercial 1-hexanethiol used (95% pure).



# <sup>1</sup>H NMR



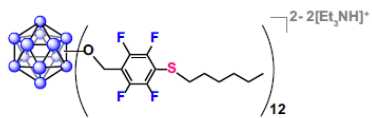
Current Data Parameters  
 NAME Feb23-2016  
 EXPNO 52  
 PROCNO 1

F2 - Acquisition Parameters  
 Date\_ 20160223  
 Time 11.30  
 INSTRUM av400  
 PROBHD 5 mm PABBO BB/  
 PULPROG zg30  
 TD 160254  
 SOLVENT CD3CN  
 NS 32  
 DS 0  
 SWH 8012.820 Hz  
 FIDRES 0.050001 Hz  
 AQ 9.9998493 sec  
 RG 155.85  
 DW 62.400 usec  
 DE 6.50 usec  
 TE 299.0 K  
 D1 10.00000000 sec  
 TDO 1

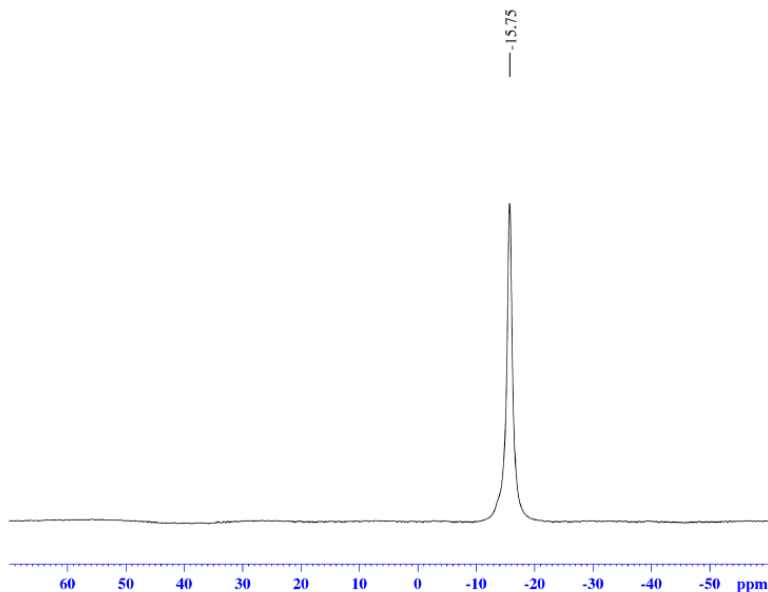
===== CHANNEL f1 =====  
 SFO1 400.1324008 MHz  
 NUC1 1H  
 P1 15.00 usec  
 PLW1 13.00000000 W

F2 - Processing parameters  
 SI 65536  
 SF 400.1300112 MHz  
 WDW EM  
 SSB 0  
 LB 0.30 Hz  
 GB 0  
 PC 1.00





<sup>11</sup>B {<sup>1</sup>H} NMR



```

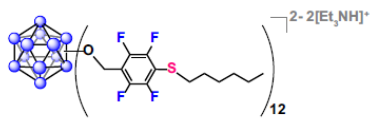
Current Data Parameters
NAME      Feb13_2016
EXPNO    50
PROCNO   1

F2 - Acquisition Parameters
Date_    20160223
Time     11.14
INSTRUM  av400
PROBHD   5 mm PABBO BB/
PULPROG  zgpg30
TD       5096
SOLVENT  CD3CN
NS       1024
DS       0
SWH      51020.406 Hz
FIDRES   10.011834 Hz
AQ       0.0499405 sec
RG       189.85
DF       9.850 usec
DE       6.50 usec
TE       299.1 K
D1       0.0500000 sec
D11      0.0300000 sec
TDO      1

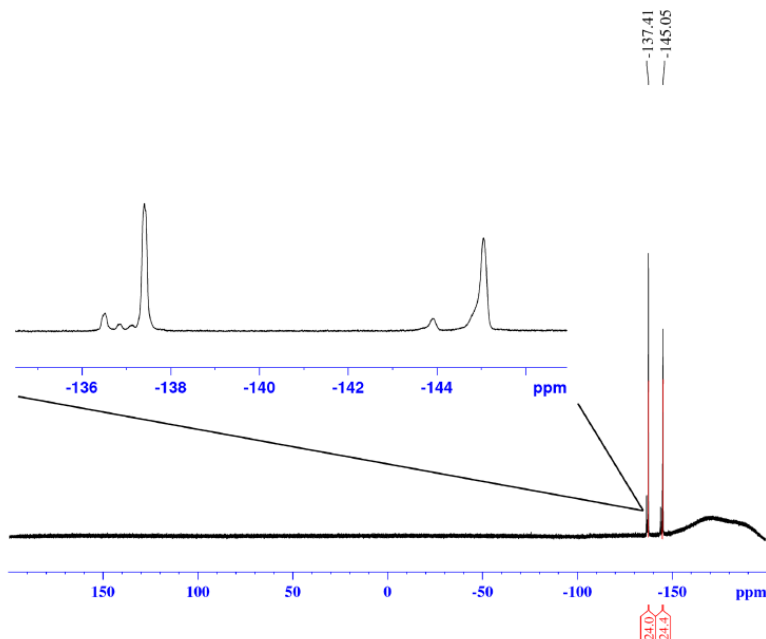
===== CHANNEL f1 =====
SFO1    128.377652 MHz
NUC1     11B
P1       10.00 usec
PLW1    52.00000000 W

===== CHANNEL f2 =====
SFO2    400.1334008 MHz
NUC2     1H
CPDPRG2  waltz16
PCPD2    90.00 usec
PLW2    13.00000000 W
PLW12   0.36111000 W

F2 - Processing parameters
SI       32768
SF       128.3776161 MHz
WDW      EM
SSB      0
LB       10.00 Hz
GB       0
PC       1.40
  
```



<sup>19</sup>F NMR



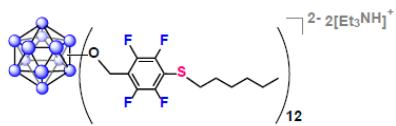
Current Data Parameters  
 NAME Feb23-2016  
 EXPNO 51  
 PROCNO 1

F2 - Acquisition Parameters  
 Date\_ 20160223  
 Time 11.18  
 INSTRUM av400  
 PROBHD 5 mm PABBO BB/  
 PULPROG zgpg30  
 TD 262144  
 SOLVENT CD3CN  
 NS 64  
 DS 0  
 SWH 150000.000 Hz  
 FIDRES 0.572205 Hz  
 AQ 0.8738133 sec  
 RG 189.85  
 DW 3.333 usec  
 DE 6.50 usec  
 TE 299.0 K  
 D1 2.00000000 sec  
 TDO 1

==== CHANNEL f1 =====  
 SFO1 376.4983660 MHz  
 NUC1 19F  
 P1 14.50 usec  
 PLW1 17.00000000 W

F2 - Processing parameters  
 SI 262144  
 SF 376.4983660 MHz  
 WDW EM  
 SSB 0  
 LB 1.00 Hz  
 GB 0  
 PC 1.00

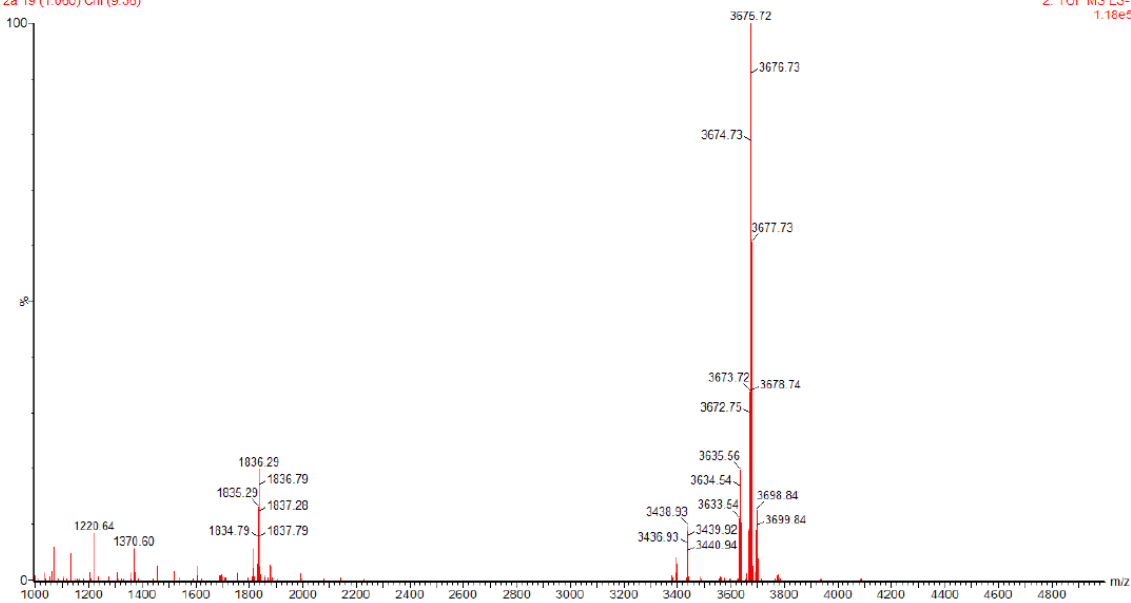
Small impurities are present due to the commercial 1-hexanethiol used (95% pure).

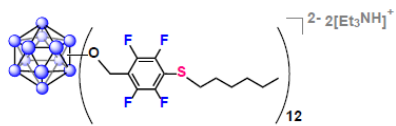


## Waters Mass Spec

high m/z scan  
2a 19 (1.060) Cm (9.36)

2: TOF MS ES-  
1.18e5

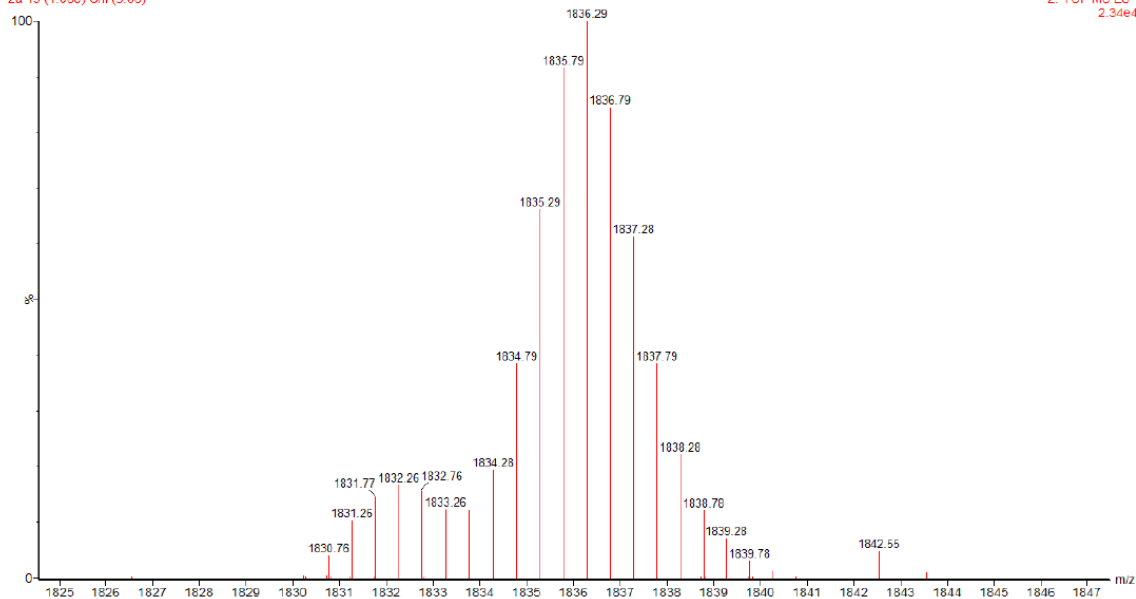


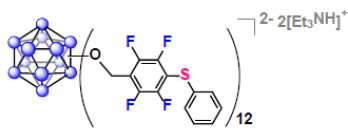


## Waters Mass Spec

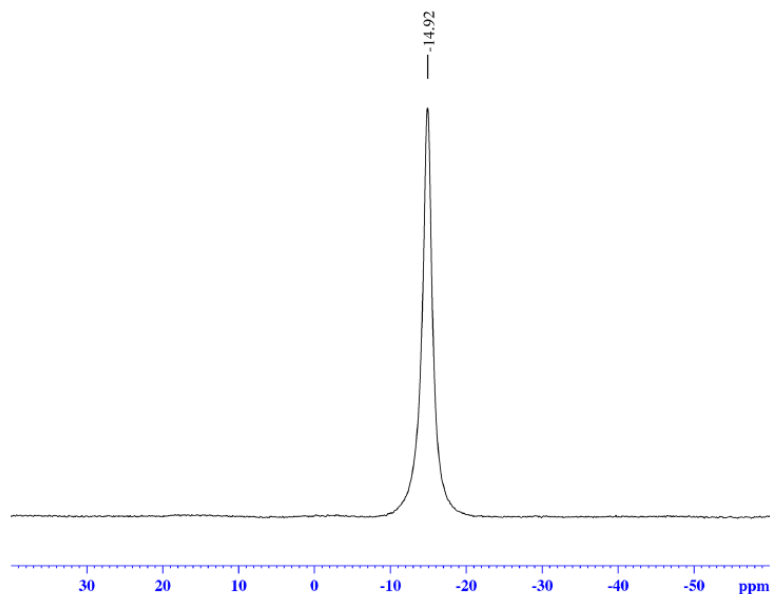
high m/z scan  
2a 19 (1.060) Cm (9.36)

2: TOF MS ES-  
2.34e4





*in situ*  $^{11}\text{B}$  NMR



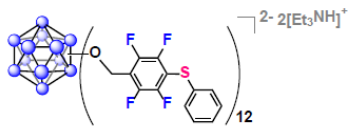
```

Current Data Parameters
NAME          0129
EXPNO         221
PROCNO        1

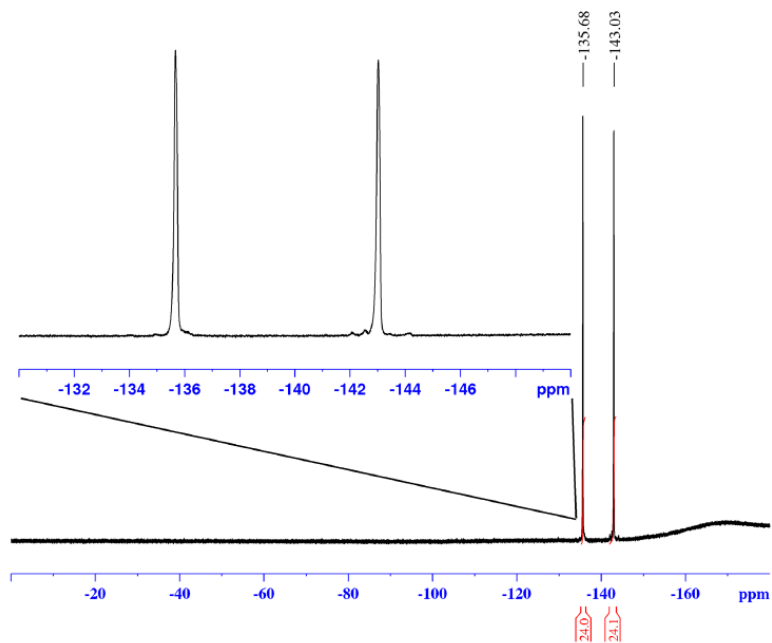
F2 - Acquisition Parameters
Date_         20160129
Time          20.43
INSTRUM       av400
PROBHD        5 mm PABBO BB/
PULPROG       zg
TD            5096
SOLVENT       None
NS            1024
DS            0
SWH           51020.406 Hz
FIDRES        10.011854 Hz
AQ            0.0499408 sec
RG            189.85
DW            9.800 usec
DE            6.50 usec
TE            299.0 K
D1            0.05000000 sec
TDO           1

===== CHANNEL f1 =====
SF01          128.3776052 MHz
NUC1           11B
P1            10.00 usec
PLW1          52.00000000 W

F2 - Processing parameters
SI            32768
SF           128.3776161 MHz
WDW           EM
SSB           0
LB            10.00 Hz
GB            0
PC            1.40
  
```



*in situ*  $^{19}\text{F}$  NMR

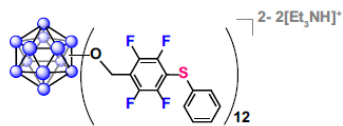


Current Data Parameters  
 NAME 0129  
 EXPNO 220  
 PROCNO 1

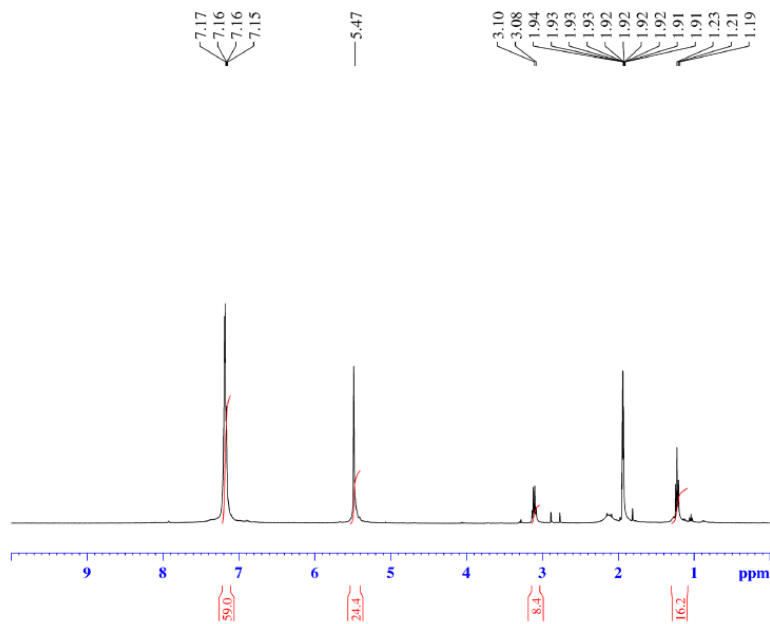
F2 - Acquisition Parameters  
 Date\_ 20160129  
 Time 20.39  
 INSTRUM av400  
 PROBHD 5 mm PABBO BB/  
 PULPROG zgpg30  
 TD 262144  
 SOLVENT None  
 NS 64  
 DS 0  
 SWH 150000.000 Hz  
 FIDRES 0.572205 Hz  
 AQ 0.8738133 sec  
 RG 189.85  
 DW 3.333 usec  
 DE 6.50 usec  
 TE 299.0 K  
 D1 2.00000000 sec  
 TDO 1

===== CHANNEL f1 =====  
 SFO1 376.4983660 MHz  
 NUC1  $^{19}\text{F}$   
 P1 14.50 usec  
 PLW1 17.00000000 W

F2 - Processing parameters  
 SI 262144  
 SF 376.4983660 MHz  
 WDW EM  
 SSB 0  
 LB 1.00 Hz  
 GB 0  
 PC 1.00



# <sup>1</sup>H NMR

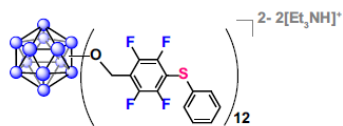


Current Data Parameters  
 NAME F8603-2016  
 EXPNO 102  
 PROCNO 1

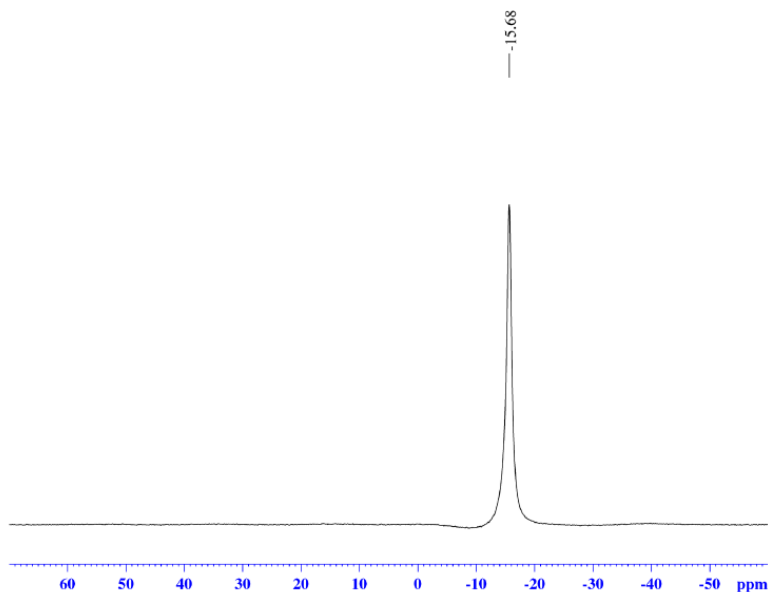
F2 - Acquisition Parameters  
 Date\_ 20160203  
 Time 15.16  
 INSTRUM av400  
 PROBHD 5 mm PABBO BB/  
 PULPROG zg30  
 TD 52882  
 SOLVENT CD3CN  
 NS 32  
 DS 0  
 SWH 8012.820 Hz  
 FIDRES 0.151523 Hz  
 AQ 3.2998369 sec  
 RG 155.85  
 DW 62.400 usec  
 DE 6.50 usec  
 TE 299.0 K  
 D1 5.00000000 sec  
 TDO 1

===== CHANNEL f1 =====  
 SFO1 400.1324008 MHz  
 NUC1 1H  
 P1 15.00 usec  
 PLW1 13.00000000 W

F2 - Processing parameters  
 SI 65536  
 SF 400.1300112 MHz  
 WDW EM  
 SSB 0  
 LB 0.30 Hz  
 GB 0  
 PC 1.00



<sup>11</sup>B {<sup>1</sup>H} NMR



```

Current Data Parameters
NAME      F093-2016
EXPNO     100
PROCNO    1

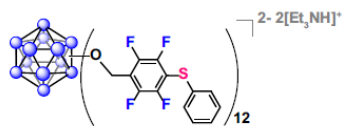
F2 - Acquisition Parameters
Date_     20160203
Time      15.06
INSTRUM   av400
PROBHD    5 mm PABBO BB/
PULPROG   zgdc.js
TD         5096
SOLVENT   CD3CN
NS         1024
DS         0
SWH        51020.406 Hz
FIDRES     10.011854 Hz
AQ         0.0499405 sec
RG         189.85
DW         9.500 usec
DE         6.50 usec
TE         299.0 K
D1         0.0500000 sec
D11        0.0300000 sec
TD0        1

===== CHANNEL f1 =====
SFO1      128.377632 MHz
NUC1      11B
P1         10.00 usec
PLW1      52.00000000 W

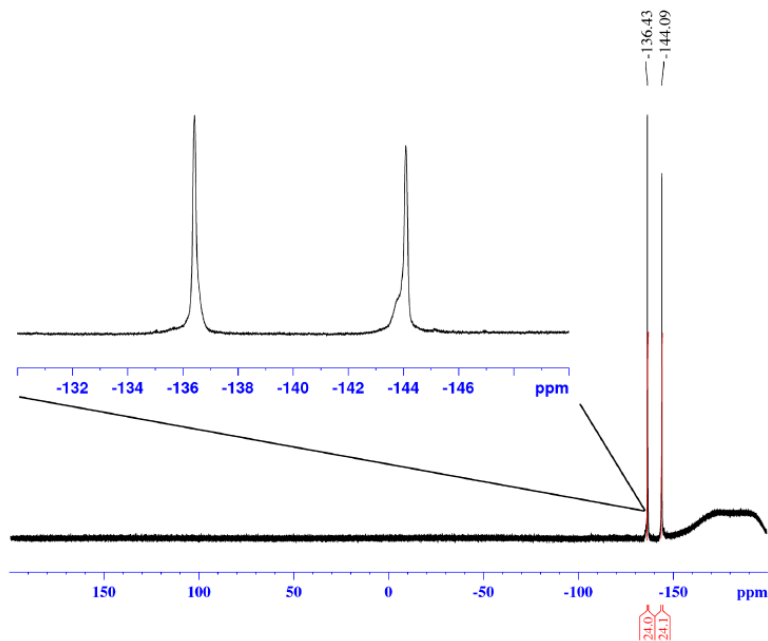
===== CHANNEL f2 =====
SFO2      400.1334068 MHz
NUC2      1H
CPDPRG2   waltz16
PCPD2     90.00 usec
PLW2      13.00000000 W
PLW12     0.36111000 W

F2 - Processing parameters
SI         32768
SF         128.3776161 MHz
WDW        EM
SSB        0
LB         10.00 Hz
GB         0
PC         1.40
  
```





# <sup>19</sup>F NMR

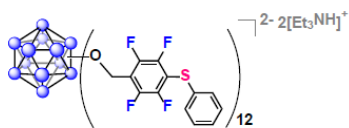


Current Data Parameters  
 NAME Feb03-2016  
 EXPNO 101  
 PROCNO 1

F2 - Acquisition Parameters  
 Date\_ 20160203  
 Time 15.10  
 INSTRUM av400  
 PROBHD 5 mm PABBO BB/  
 PULPROG zgpg30  
 TD 262144  
 SOLVENT CD3CN  
 NS 64  
 DS 0  
 SWH 150000.000 Hz  
 FIDRES 0.572205 Hz  
 AQ 0.8738133 sec  
 RG 189.85  
 DW 3.333 usec  
 DE 6.50 usec  
 TE 299.0 K  
 D1 2.00000000 sec  
 TDO 1

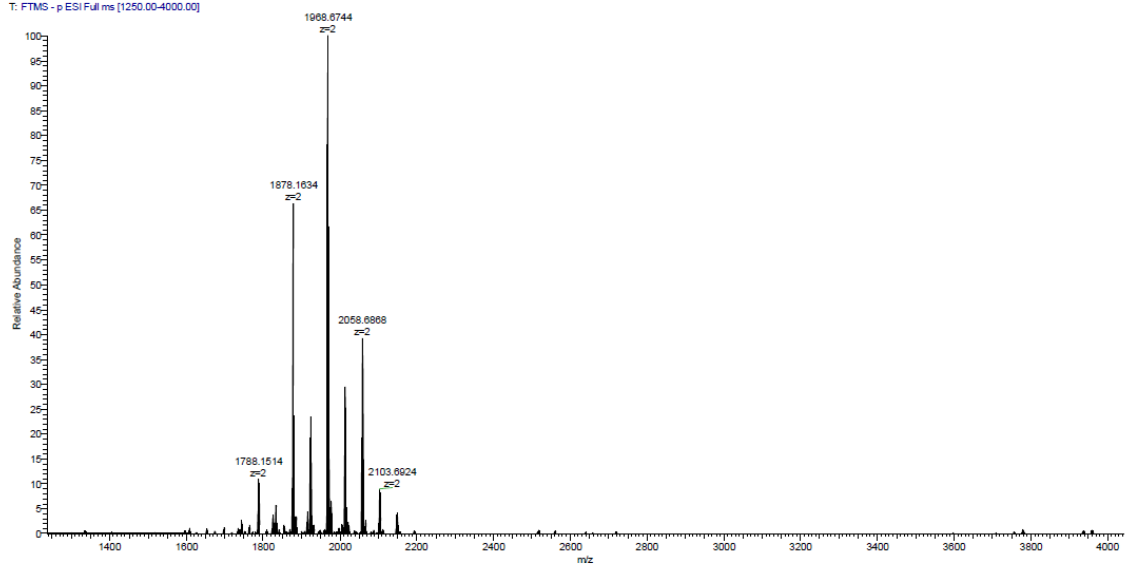
===== CHANNEL f1 =====  
 SFO1 376.4983660 MHz  
 NUC1 19F  
 P1 14.50 usec  
 PLW1 17.00000000 W

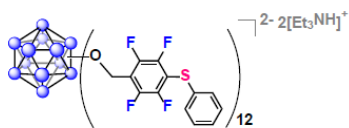
F2 - Processing parameters  
 SI 262144  
 SF 376.4983660 MHz  
 WDW EM  
 SSB 0  
 LB 1.00 Hz  
 GB 0  
 PC 1.00



## Q Exactive High-Res Mass Spec

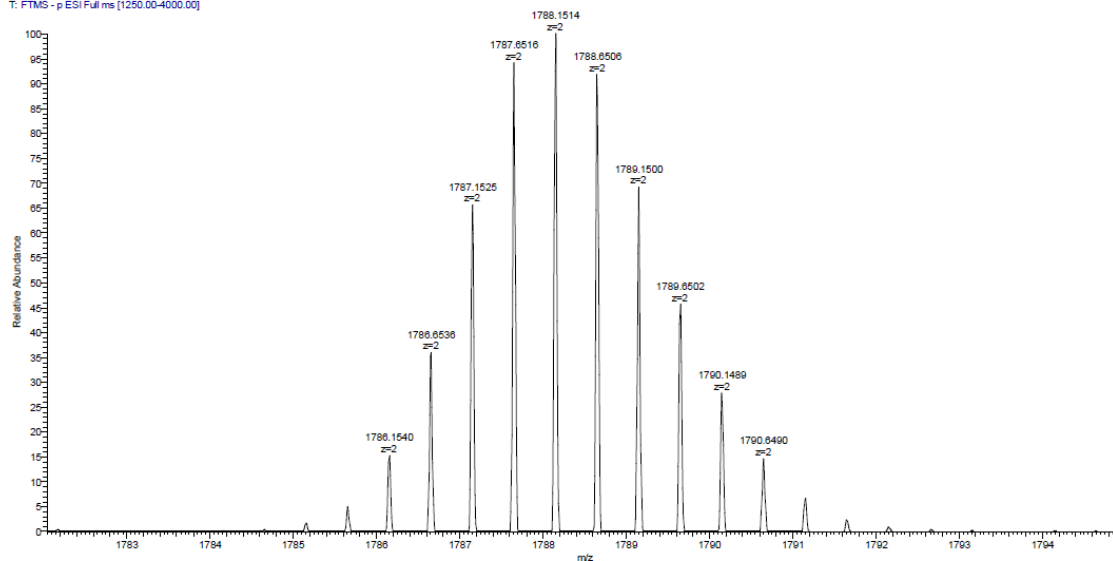
2b 1.25-4k #1-16 RT: 0.01-0.14 AV: 16 NL: 4.27E7  
T: FTMS - p-ESI Full.ms [1250.00-4000.00]

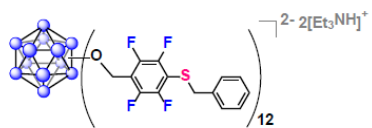




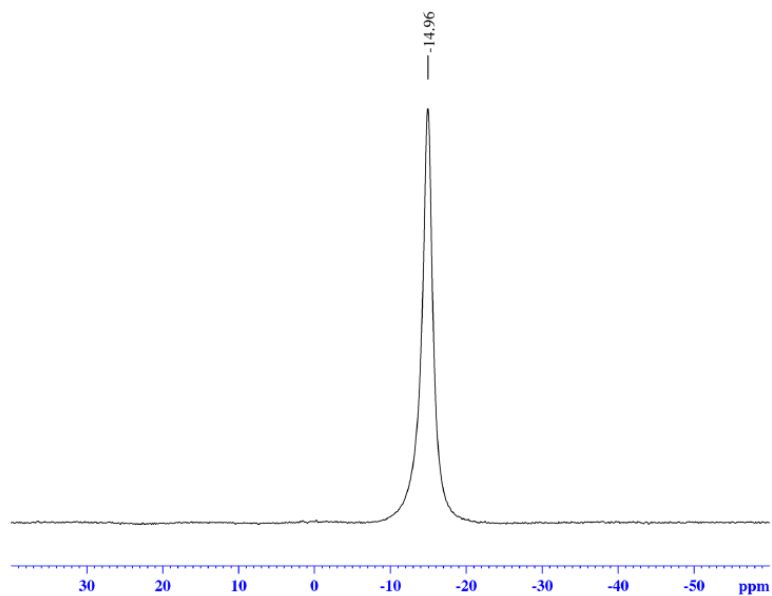
## Q Exactive High-Res Mass Spec

2b 1.25-4k #1-16 RT: 0.01-0.14 AV: 16 NL: 4.68E6  
T: FTMS - p-ESI Full.ms [1250.00-4000.00]





*in situ*  $^{11}\text{B}$  NMR



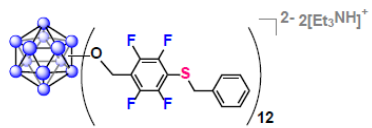
```

Current Data Parameters
NAME      0201
EXPNO    131
PROCNO   1

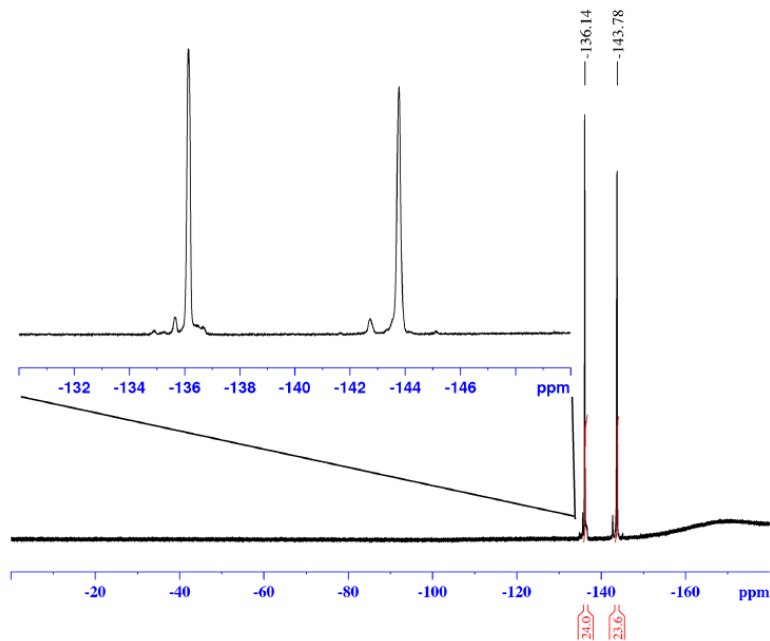
F2 - Acquisition Parameters
Date_    20160201
Time     20.18
INSTRUM  av400
PROBHD   5 mm PABBO BB/
PULPROG  zg
TD        5096
SOLVENT  None
NS        1024
DS        0
SWH       51020.406 Hz
FIDRES    10.011854 Hz
AQ        0.0499408 sec
RG        189.85
DW        9.800 usec
DE        6.50 usec
TE        299.0 K
D1        0.05000000 sec
TD0       1

===== CHANNEL f1 =====
SFO1    128.3776052 MHz
NUC1     11B
P1       10.00 usec
PLW1    52.00000000 W

F2 - Processing parameters
SI       32768
SF       128.3776161 MHz
WDW      EM
SSB      0
LB       10.00 Hz
GB       0
PC       1.40
  
```



*in situ*  $^{19}\text{F}$  NMR



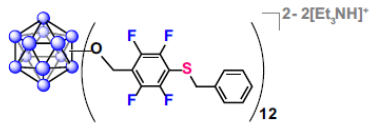
```

Current Data Parameters
NAME          0201
EXPNO         130
PROCNO        1

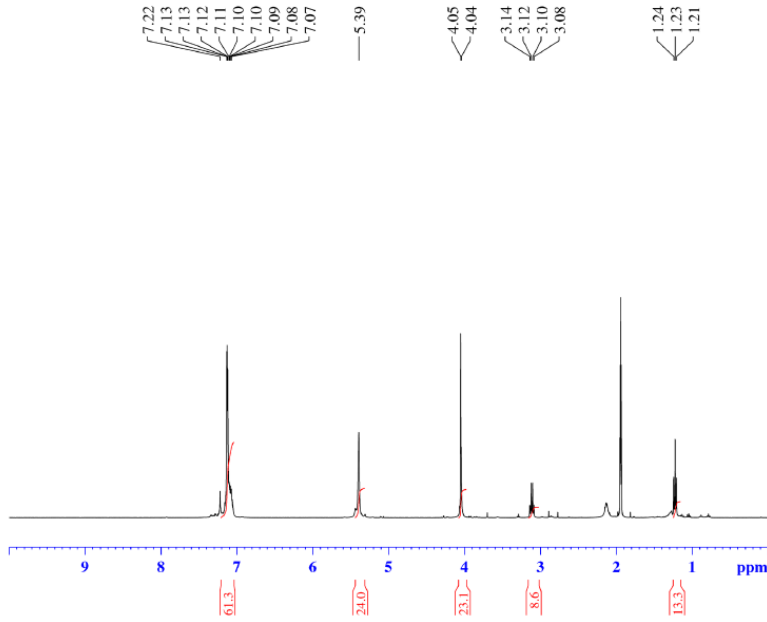
F2 - Acquisition Parameters
Date_         20160201
Time          20.15
INSTRUM       av400
PROBHD        5 mm PABBO BB/
PULPROG       zgpg30
TD            262144
SOLVENT       None
NS            64
DS            0
SWH           150000.000 Hz
FIDRES        0.572205 Hz
AQ            0.8738133 sec
RG            189.85
DW            3.333 usec
DE            6.50 usec
TE            299.0 K
D1            2.00000000 sec
TD0           1

===== CHANNEL f1 =====
SF01          376.4983660 MHz
NUC1          19F
P1            14.50 usec
PLW1          17.00000000 W

F2 - Processing parameters
SI            262144
SF            376.4983660 MHz
WDW           EM
SSB           0
LB            1.00 Hz
GB            0
PC            1.00
  
```



<sup>1</sup>H NMR



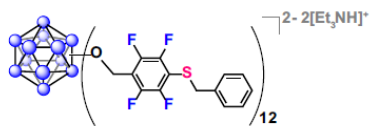
```

Current Data Parameters
NAME      Feb03-2016
EXPNO    92
PROCNO   1

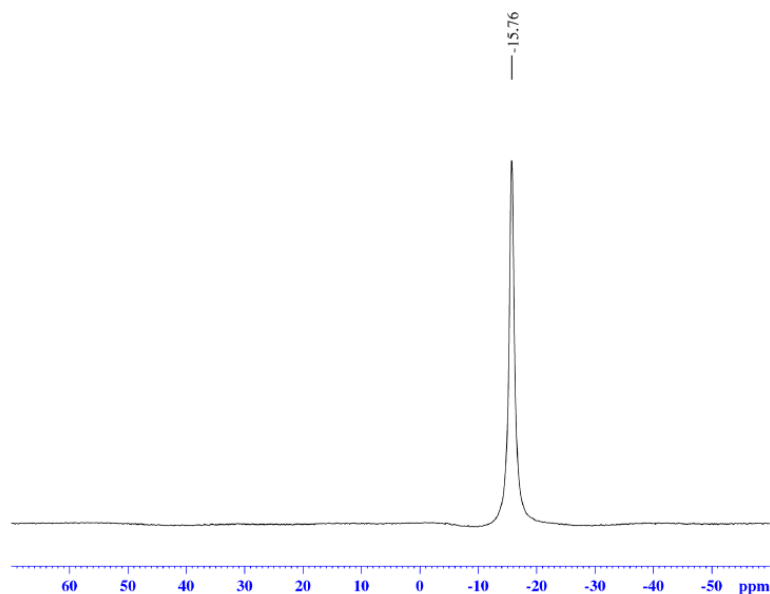
F2 - Acquisition Parameters
Date_    20160203
Time     14.59
INSTRUM  av400
PROBHD   5 mm PABBO BB/
PULPROG  zg30
TD       52882
SOLVENT  CD3CN
NS       32
DS       0
SWH      8012.820 Hz
FIDRES   0.151523 Hz
AQ       3.2998369 sec
RG       155.85
DW       62.400 usec
DE       6.50 usec
TE       299.0 K
D1       5.00000000 sec
TDO      1

===== CHANNEL f1 =====
SFO1    400.1324008 MHz
NUC1    1H
P1      15.00 usec
PLW1    13.00000000 W

F2 - Processing parameters
SI      65536
SF      400.1300113 MHz
WDW     EM
SSB     0
LB      0.30 Hz
GB      0
PC      1.00
  
```



$^{11}\text{B} \{^1\text{H}\}$  NMR



```

Current Data Parameters
NAME: F093-2016
EXPNO: 90
PROCNO: 1

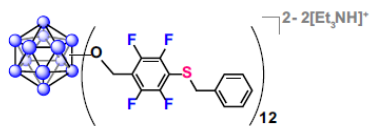
F2 - Acquisition Parameters
Date_: 20160203
Time: 14.49
INSTRUM: av400
PROBHD: 5 mm PABBO BB/
PULPROG: zgpg30
TD: 5096
SOLVENT: CD3CN
NS: 1024
DS: 0
SWH: 51020.406 Hz
FIDRES: 10.011854 Hz
AQ: 0.0499405 sec
RG: 189.85
DW: 9.500 usec
DE: 6.50 usec
TE: 299.0 K
D1: 0.0500000 sec
D11: 0.0300000 sec
TDO: 1

===== CHANNEL f1 =====
SFO1: 128.377632 MHz
NUC1: 11B
P1: 10.00 usec
PLW1: 52.0000000 W

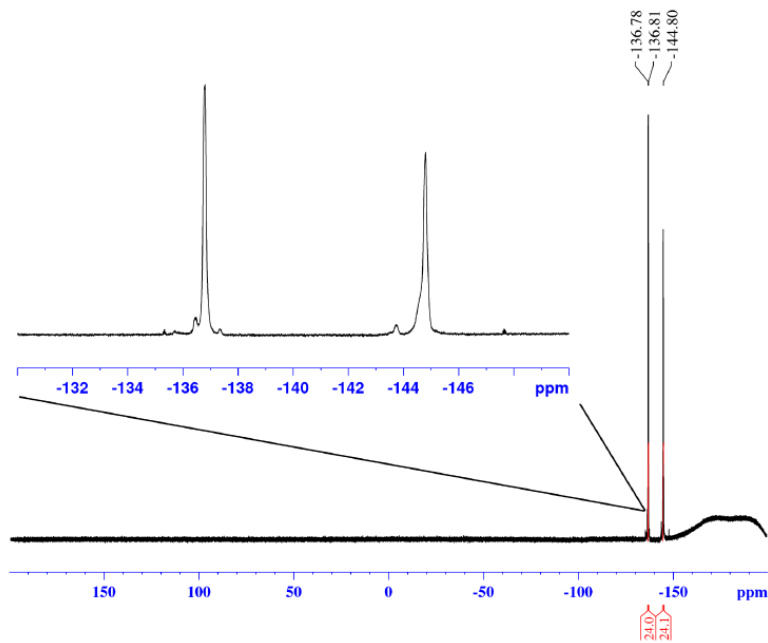
===== CHANNEL f2 =====
SFO2: 400.1334068 MHz
NUC2: 1H
CPDPRG2: waltz16
PCPD2: 90.00 usec
PLW2: 13.0000000 W
PLW12: 0.36111000 W

F2 - Processing parameters
SI: 32768
SF: 128.3776161 MHz
WDW: EM
SSB: 0
LB: 10.00 Hz
GB: 0
PC: 1.40

```



<sup>19</sup>F NMR



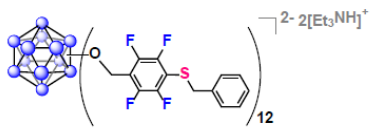
Current Data Parameters  
 NAME Feb03-2016  
 EXPNO 91  
 PROCNO 1

F2 - Acquisition Parameters  
 Date\_ 20160203  
 Time 14.53  
 INSTRUM av400  
 PROBHD 5 mm PABBO BB/  
 PULPROG zgpg30  
 TD 262144  
 SOLVENT CD3CN  
 NS 64  
 DS 0  
 SWH 150000.000 Hz  
 FIDRES 0.572205 Hz  
 AQ 0.8738133 sec  
 RG 189.85  
 DW 3.333 usec  
 DE 6.50 usec  
 TE 299.0 K  
 D1 2.00000000 sec  
 TDO 1

===== CHANNEL f1 =====  
 SFO1 376.4983660 MHz  
 NUC1 19F  
 P1 14.50 usec  
 PLW1 17.00000000 W

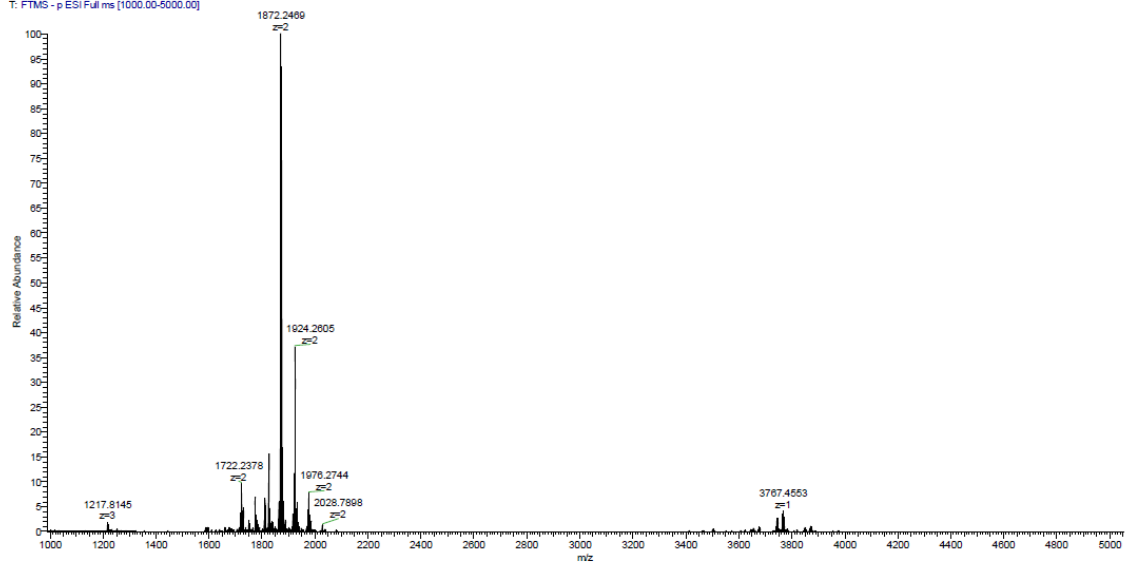
F2 - Processing parameters  
 SI 262144  
 SF 376.4983660 MHz  
 WDW EM  
 SSB 0  
 LB 1.00 Hz  
 GB 0  
 PC 1.00

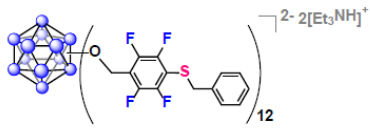




## Q Exactive High-Res Mass Spec

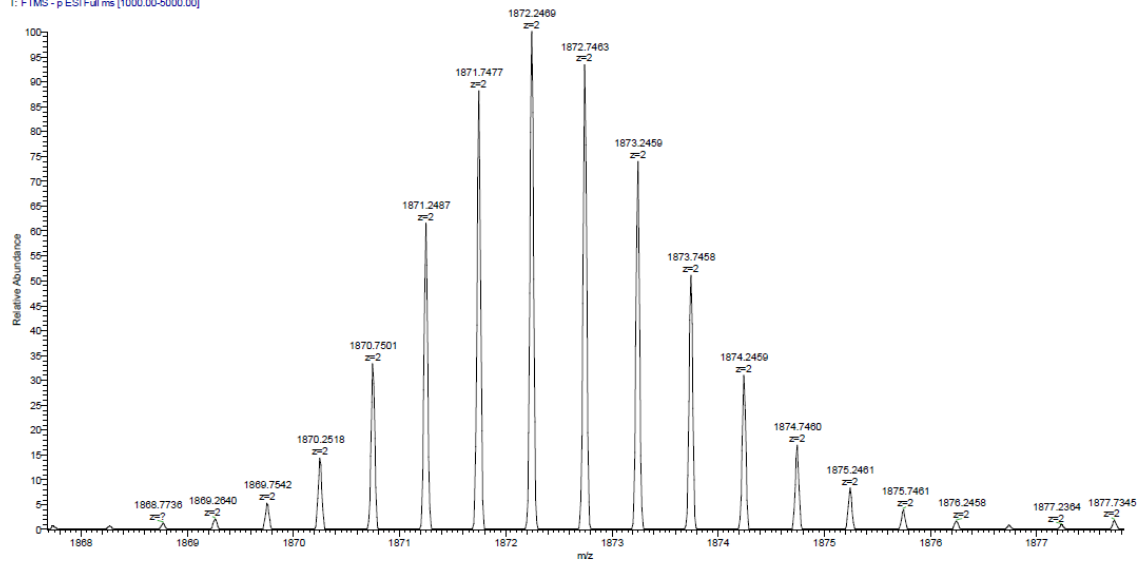
2e 1-5k #1-16 RT: 0.04-0.09 AV: 10 NL: 1.70E7  
T: FTMS - p-ESI Full.ms [1000.00-5000.00]

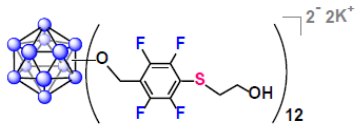




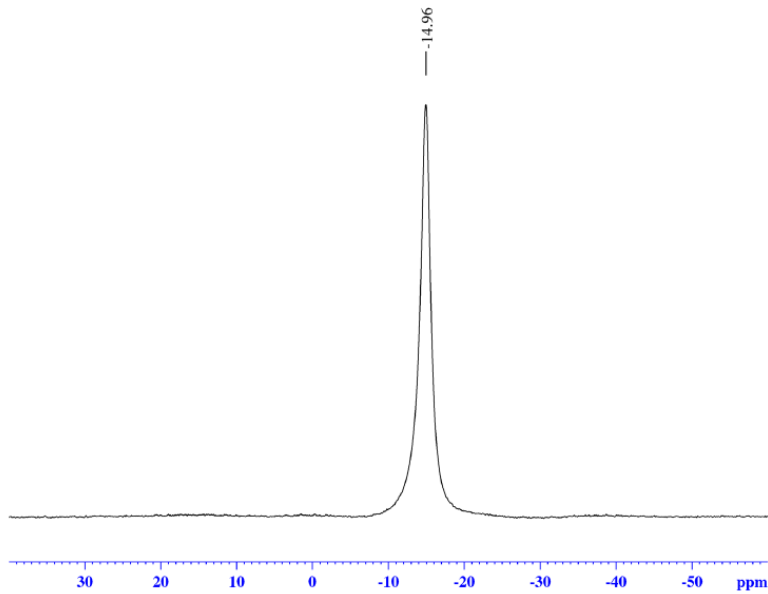
## Q Exactive High-Res Mass Spec

2e 1-5k #1-16 RT: 0.04-0.09 AV: 10 NL: 1.70E7  
T: FTMS - p-ESI Full.ms [1000.00-5000.00]





*in situ*  $^{11}\text{B}$  NMR



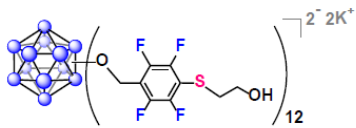
```

Current Data Parameters
NAME      0203
EXPNO    41
PROCNO   1

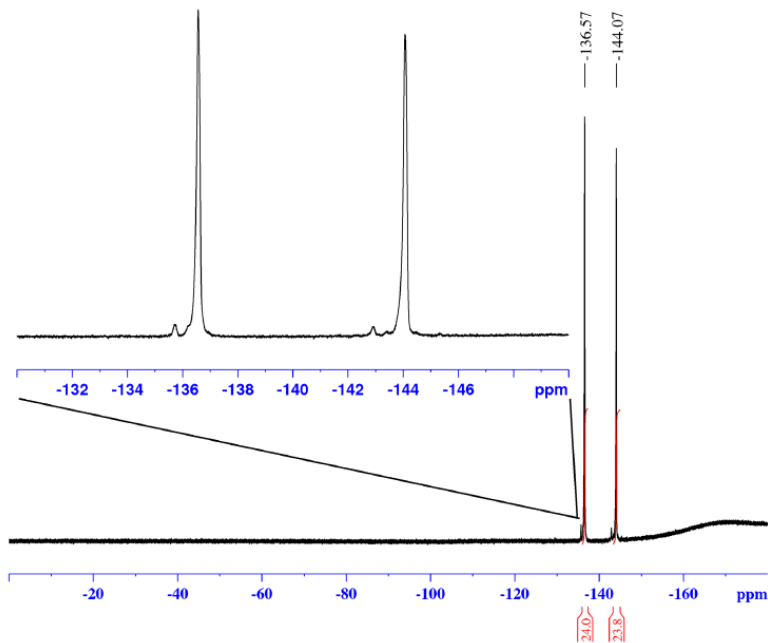
F2 - Acquisition Parameters
Date_    20160203
Time     13.16
INSTRUM  av400
PROBHD   5 mm PABBO BB/
PULPROG  zg
TD        5096
SOLVENT  None
NS        1024
DS        0
SWH       51020.406 Hz
FIDRES    10.011854 Hz
AQ        0.0499408 sec
RG        189.85
DW        9.800 usec
DE        6.50 usec
TE        299.0 K
D1        0.05000000 sec
TDO       1

===== CHANNEL f1 =====
SFO1    128.3776052 MHz
NUC1     11B
P1       10.00 usec
PLW1    52.00000000 W

F2 - Processing parameters
SI       32768
SF       128.3776161 MHz
WDW      EM
SSB      0
LB       10.00 Hz
GB       0
PC       1.40
  
```



*in situ*  $^{19}\text{F}$  NMR



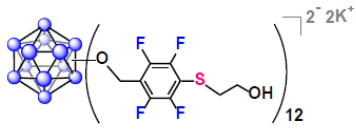
```

Current Data Parameters
NAME      0203
EXPNO    40
PROCNO    1

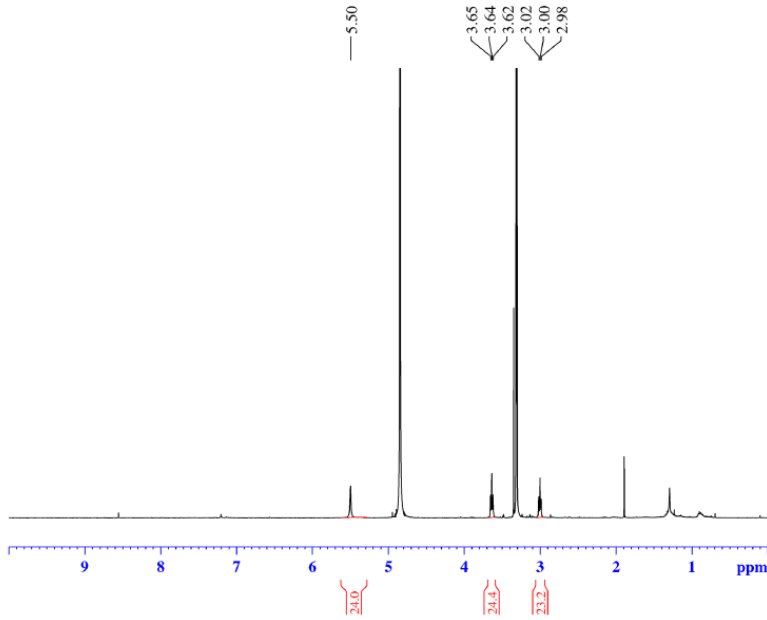
F2 - Acquisition Parameters
Date_     20160203
Time      13.13
INSTRUM   av400
PROBHD    5 mm PABBO BB/
PULPROG   zgpg30
TD        262144
SOLVENT   None
NS        64
DS        0
SWH       150000.000 Hz
FIDRES    0.572205 Hz
AQ        0.8738133 sec
RG        189.85
DW        3.333 usec
DE        6.50 usec
TE        299.0 K
D1        2.00000000 sec
TD0       1

===== CHANNEL f1 =====
SFO1     376.4983660 MHz
NUC1     19F
P1       14.50 usec
PLW1    17.00000000 W

F2 - Processing parameters
SI       262144
SF       376.4983660 MHz
WDW      EM
SSB      0
LB       1.00 Hz
GB       0
PC       1.00
  
```



# <sup>1</sup>H NMR



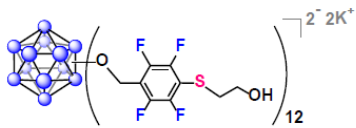
```

Current Data Parameters
NAME      G1 2ME 0204 0202 (MeOD)
EXPNO    250
PROCNO    1

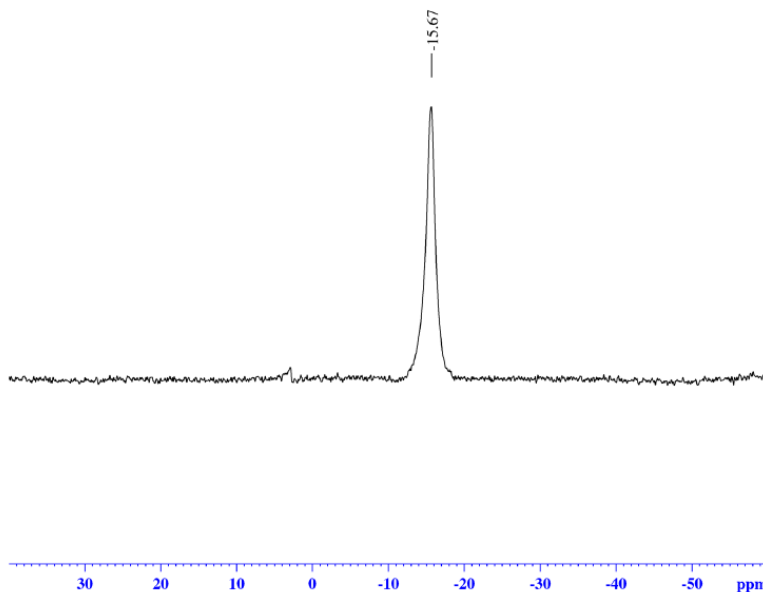
F2 - Acquisition Parameters
Date_    20160208
Time     16.59
INSTRUM  av400
PROBHD   5 mm PABBO BB/
PULPROG  zg30
TD       52882
SOLVENT  MeOD
NS       32
DS       0
SWH      8012.820 Hz
FIDRES   0.151523 Hz
AQ       3.2998369 sec
RG       155.85
DW       62.400 usec
DE       6.50 usec
TE       299.0 K
D1       5.00000000 sec
TDO      1

===== CHANNEL f1 =====
SFO1    400.1324008 MHz
NUC1    1H
P1      15.00 usec
PLW1    13.00000000 W

F2 - Processing parameters
SI      65536
SF      400.1300078 MHz
WDW     EM
SSB     0
LB      0.30 Hz
GB      0
PC      1.00
  
```



<sup>11</sup>B NMR

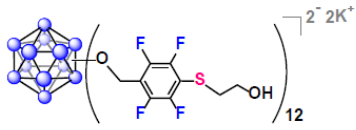


Current Data Parameters  
 NAME G1 2ME 0204 0202 (MeOD)  
 EXPNO 251  
 PROCNO 1

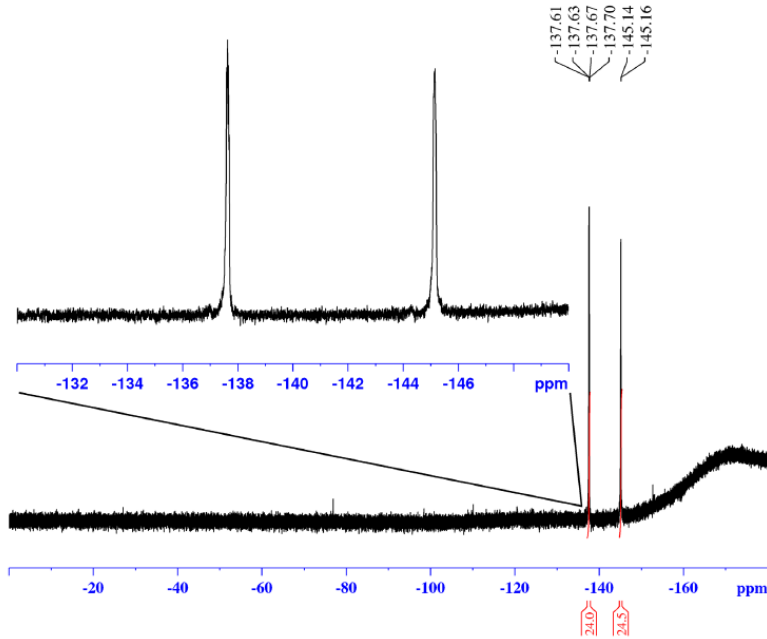
F2 - Acquisition Parameters  
 Date\_ 20160208  
 Time 17.02  
 INSTRUM av400  
 PROBHD 5 mm PABBO BB/  
 PULPROG zg  
 TD 5096  
 SOLVENT MeOD  
 NS 1024  
 DS 0  
 SWH 51020.406 Hz  
 FIDRES 10.011854 Hz  
 AQ 0.0499408 sec  
 RG 189.85  
 DW 9.800 usec  
 DE 6.50 usec  
 TE 299.0 K  
 D1 0.05000000 sec  
 TDO 1

===== CHANNEL f1 =====  
 SFO1 128.3776052 MHz  
 NUC1 11B  
 P1 10.00 usec  
 PLW1 52.00000000 W

F2 - Processing parameters  
 SI 32768  
 SF 128.3776161 MHz  
 WDW EM  
 SSB 0  
 LB 10.00 Hz  
 GB 0  
 PC 1.40



<sup>19</sup>F NMR

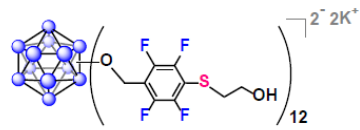


Current Data Parameters  
 NAME G1 2ME 0204 0202 (MeOD)  
 EXPNO 252  
 PROCNO 1

F2 - Acquisition Parameters  
 Date\_ 20160208  
 Time 17.06  
 INSTRUM av400  
 PROBHD 5 mm PABBO BB/  
 PULPROG zgpg30  
 TD 262144  
 SOLVENT MeOD  
 NS 64  
 DS 0  
 SWH 150000.000 Hz  
 FIDRES 0.572205 Hz  
 AQ 0.8738133 sec  
 RG 189.85  
 DW 3.333 usec  
 DE 6.50 usec  
 TE 299.0 K  
 D1 2.00000000 sec  
 TDO 1

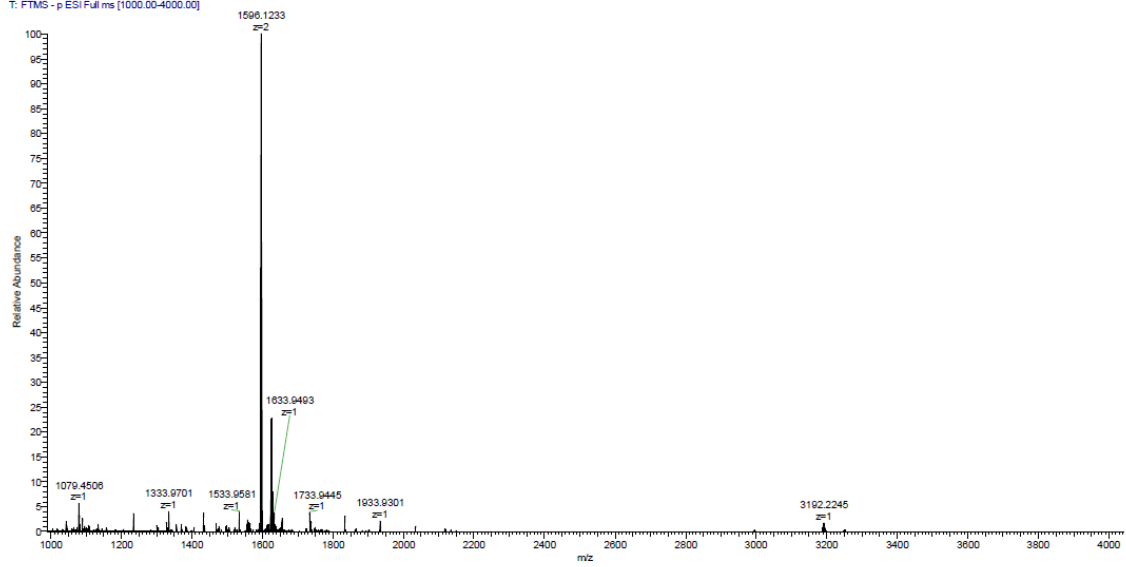
===== CHANNEL f1 =====  
 SF01 376.4983660 MHz  
 NUC1 19F  
 P1 14.50 usec  
 PLW1 17.00000000 W

F2 - Processing parameters  
 SI 262144  
 SF 376.4983660 MHz  
 WDW EM  
 SSB 0  
 LB 1.00 Hz  
 GB 0  
 PC 1.00

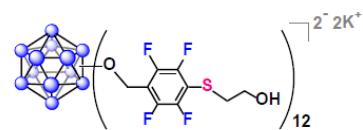


## Q Exactive High-Res Mass Spec

2d 1-4k #1-38 RT: 0.01-0.33 AV: 38 NL: 8.62E8  
T: FTMS - p-ESI Full.ms [1000.00-4000.00]

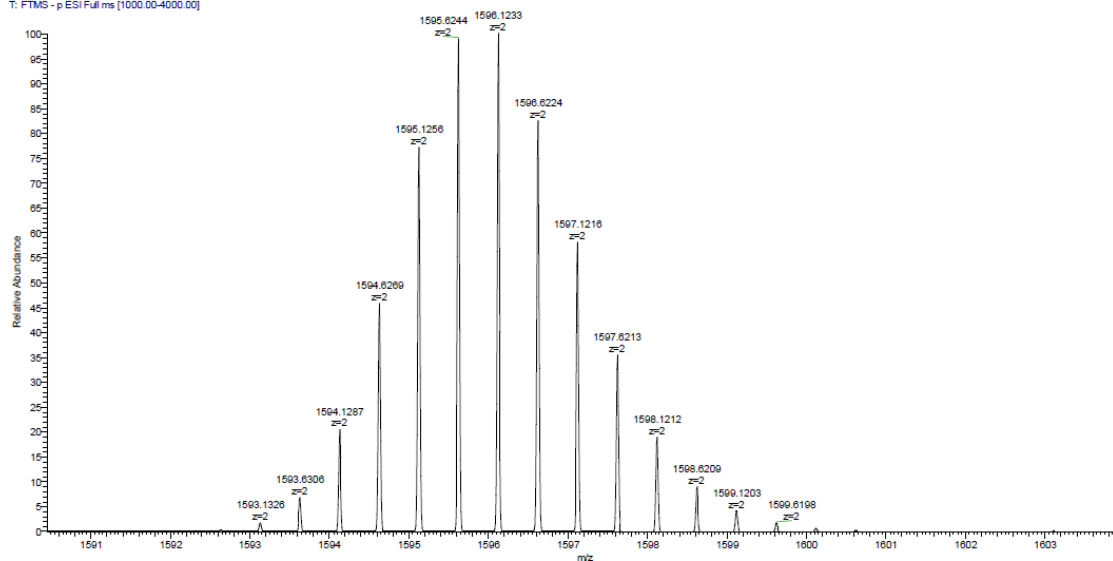


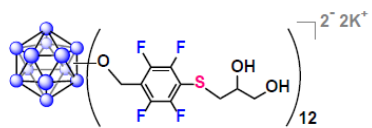




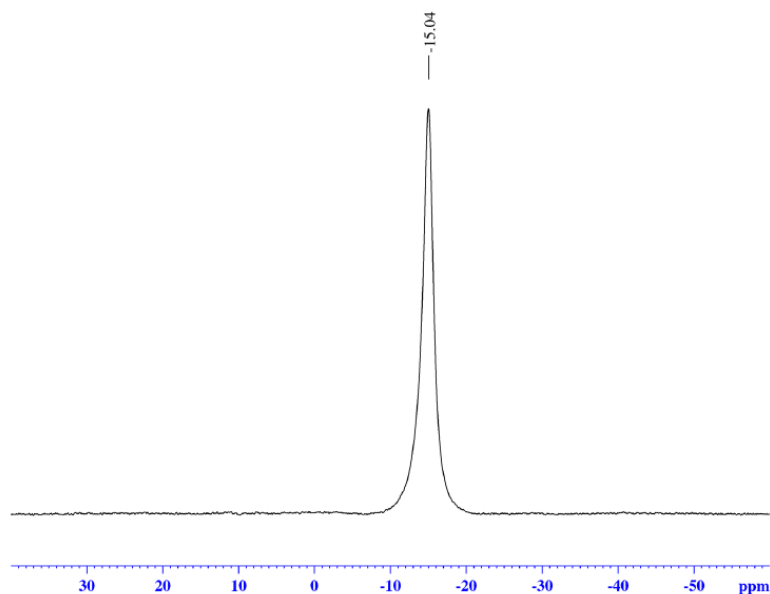
## Q Exactive High-Res Mass Spec

2d 1-4k #1-38 RT: 0.01-0.33 AV: 38 NL: 8.62E9  
T: FTMS - p-ESI Full.ms [1000.00-4000.00]





*in situ*  $^{11}\text{B}$  NMR



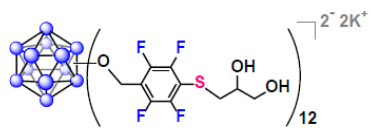
```

Current Data Parameters
NAME      0203
EXPNO    51
PROCNO   1

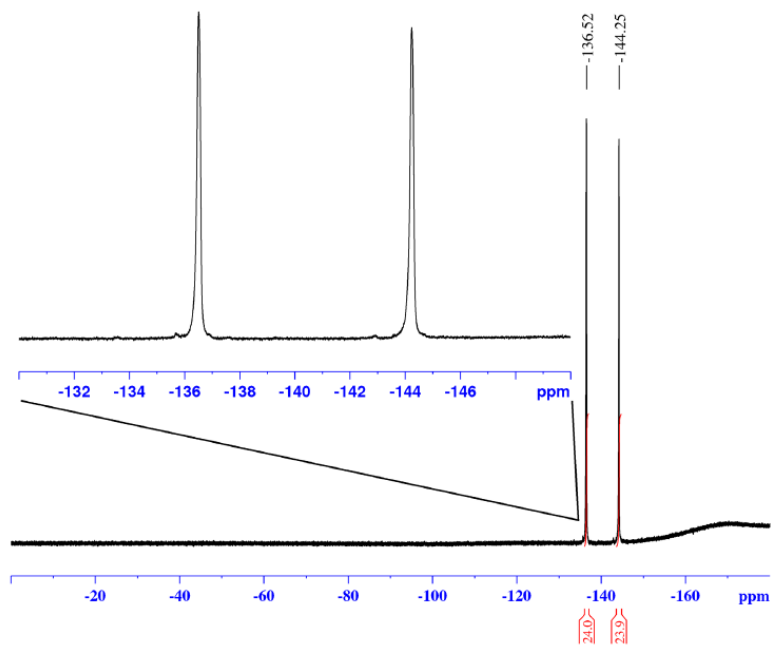
F2 - Acquisition Parameters
Date_    20160203
Time     13.25
INSTRUM  av400
PROBHD   5 mm PABBO BB/
PULPROG  zg
TD       5096
SOLVENT  None
NS       1024
DS       0
SWH      51020.406 Hz
FIDRES   10.011854 Hz
AQ       0.0499408 sec
RG       189.85
DW       9.800 usec
DE       6.50 usec
TE       299.0 K
D1       0.05000000 sec
TDO      1

===== CHANNEL f1 =====
SFO1    128.3776052 MHz
NUC1     11B
P1      10.00 usec
PLW1    52.00000000 W

F2 - Processing parameters
SI      32768
SF      128.3776161 MHz
WDW     EM
SSB     0
LB      10.00 Hz
GB      0
PC      1.40
  
```



*in situ*  $^{19}\text{F}$  NMR



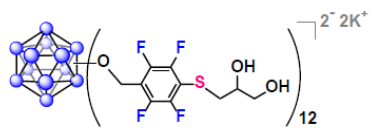
```

Current Data Parameters
NAME          0203
EXPNO         50
PROCNO        1

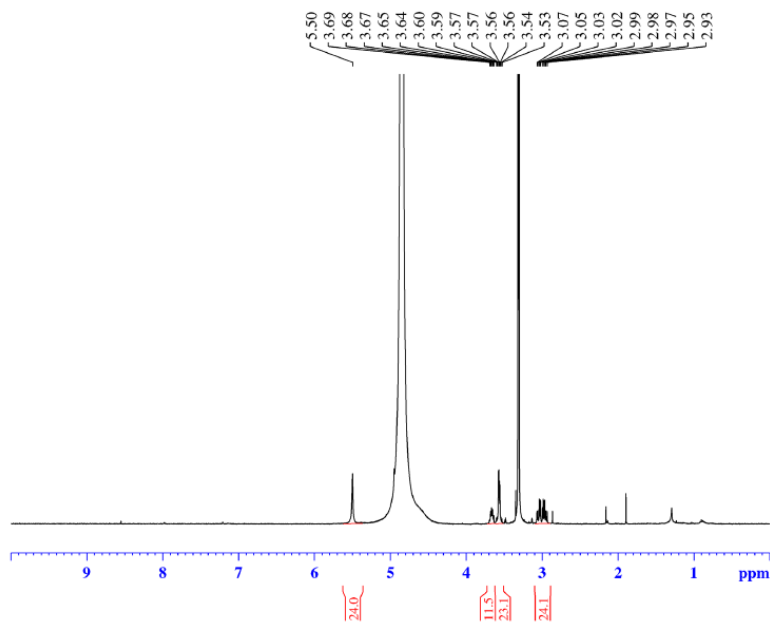
F2 - Acquisition Parameters
Date_         20160203
Time          13.22
INSTRUM       av400
PROBHD        5 mm PABBO BB/
PULPROG       zgpg30
TD            262144
SOLVENT       None
NS            64
DS            0
SWH           150000.000 Hz
FIDRES        0.572205 Hz
AQ            0.8738133 sec
RG            189.85
DW            3.333 usec
DE            6.50 usec
TE            299.0 K
D1            2.00000000 sec
TD0           1

===== CHANNEL f1 =====
SF01          376.4983660 MHz
NUC1           19F
P1            14.50 usec
PLW1          17.00000000 W

F2 - Processing parameters
SI            262144
SF            376.4983660 MHz
WDW           EM
SSB           0
LB            1.00 Hz
GB            0
PC            1.00
  
```



<sup>1</sup>H NMR

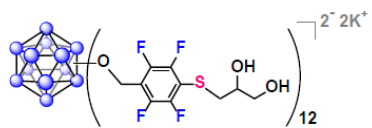


Current Data Parameters  
 NAME G1 Glycerol 0204 0202 (MeOD)  
 EXPNO 90  
 PROCNO 1

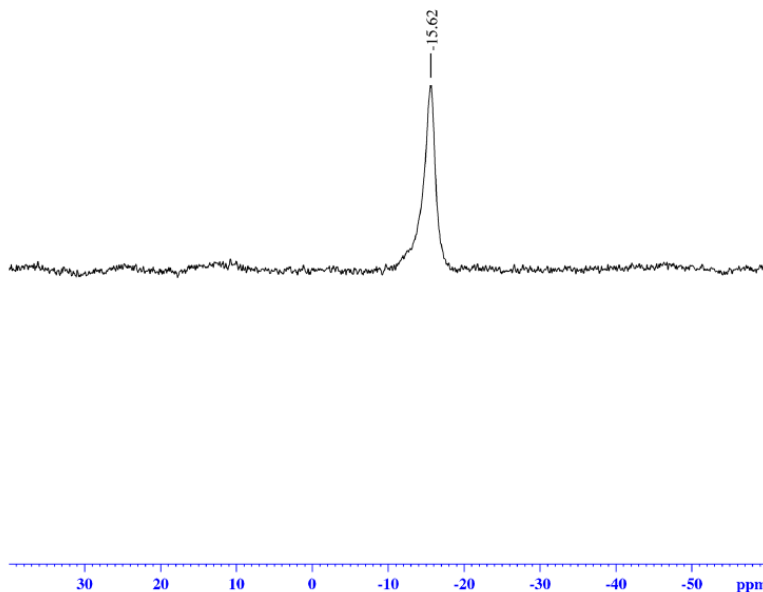
F2 - Acquisition Parameters  
 Date\_ 20160205  
 Time 12.37  
 INSTRUM av400  
 PROBHD 5 mm PABBO BB/  
 PULPROG zg30  
 TD 52882  
 SOLVENT MeOD  
 NS 32  
 DS 0  
 SWH 8012.820 Hz  
 FIDRES 0.151523 Hz  
 AQ 3.2998369 sec  
 RG 155.85  
 DW 62.400 usec  
 DE 6.50 usec  
 TE 299.0 K  
 D1 5.00000000 sec  
 TDO 1

===== CHANNEL f1 =====  
 SFO1 400.1324008 MHz  
 NUC1 1H  
 P1 15.00 usec  
 PLW1 13.00000000 W

F2 - Processing parameters  
 SI 65536  
 SF 400.130078 MHz  
 WDW EM  
 SSB 0  
 LB 0.30 Hz  
 GB 0  
 PC 1.00



<sup>11</sup>B NMR

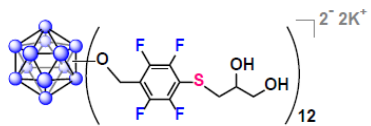


Current Data Parameters  
 NAME G1 Glycerol 0204 0202 (MeOD)  
 EXPNO 91  
 PROCNO 1

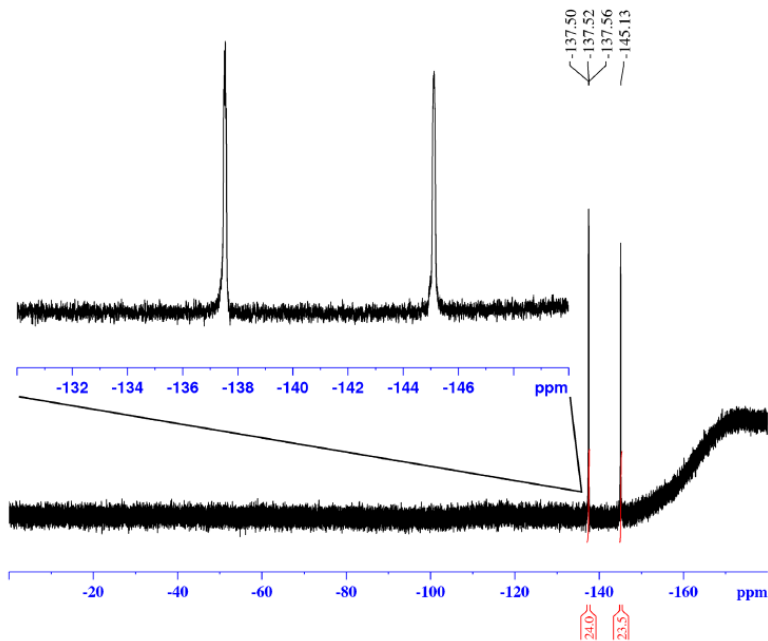
F2 - Acquisition Parameters  
 Date\_ 20160205  
 Time 12.40  
 INSTRUM av400  
 PROBHD 5 mm PABBO BB/  
 PULPROG zg  
 TD 5096  
 SOLVENT MeOD  
 NS 1024  
 DS 0  
 SWH 51020.406 Hz  
 FIDRES 10.011854 Hz  
 AQ 0.0499408 sec  
 RG 189.85  
 DW 9.800 usec  
 DE 6.50 usec  
 TE 299.0 K  
 D1 0.05000000 sec  
 TDO 1

===== CHANNEL f1 =====  
 SFO1 128.3776052 MHz  
 NUC1 11B  
 P1 10.00 usec  
 PLW1 52.00000000 W

F2 - Processing parameters  
 SI 32768  
 SF 128.3776161 MHz  
 WDW EM  
 SSB 0  
 LB 10.00 Hz  
 GB 0  
 PC 1.40



<sup>19</sup>F NMR

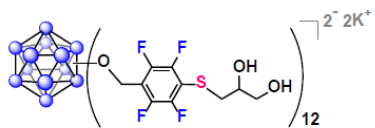


Current Data Parameters  
 NAME G1 Glycerol 0204 0202 (MeOD)  
 EXPNO 92  
 PROCNO 1

F2 - Acquisition Parameters  
 Date\_ 20160205  
 Time 12.45  
 INSTRUM av400  
 PROBHD 5 mm PABBO BB/  
 PULPROG zgpg30  
 TD 262144  
 SOLVENT MeOD  
 NS 64  
 DS 0  
 SWH 150000.000 Hz  
 FIDRES 0.572205 Hz  
 AQ 0.8738133 sec  
 RG 189.85  
 DW 3.333 usec  
 DE 6.50 usec  
 TE 299.0 K  
 D1 2.0000000 sec  
 TDO 1

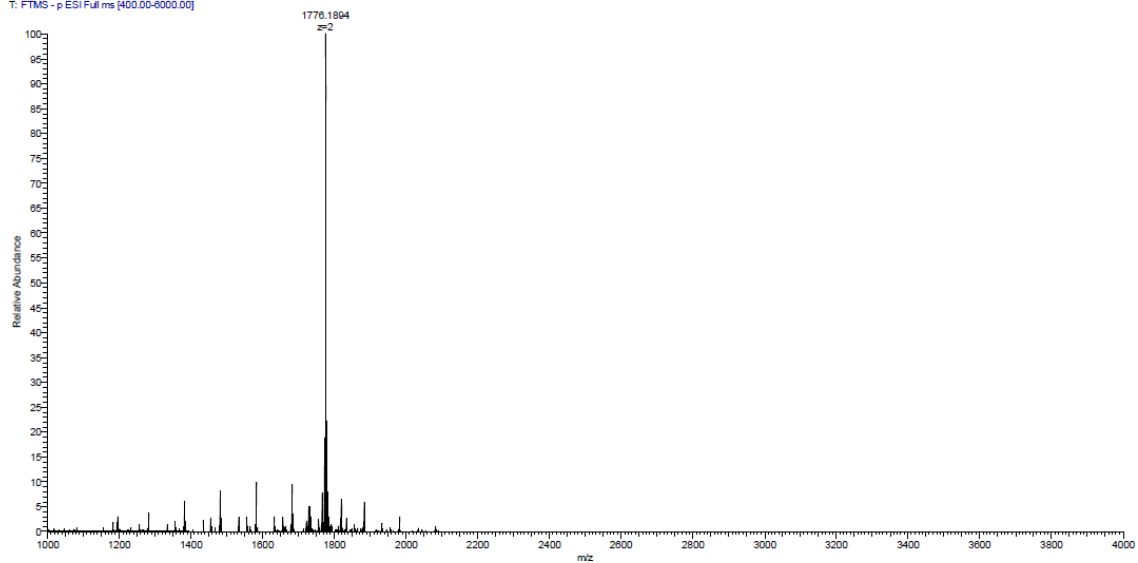
===== CHANNEL f1 =====  
 SFO1 376.4983660 MHz  
 NUC1 19F  
 P1 14.50 usec  
 PLW1 17.00000000 W

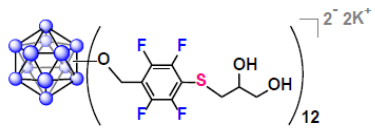
F2 - Processing parameters  
 SI 262144  
 SF 376.4983660 MHz  
 WDW EM  
 SSB 0  
 LB 1.00 Hz  
 GB 0  
 PC 1.00



**Q Exactive  
High-Res Mass Spec**

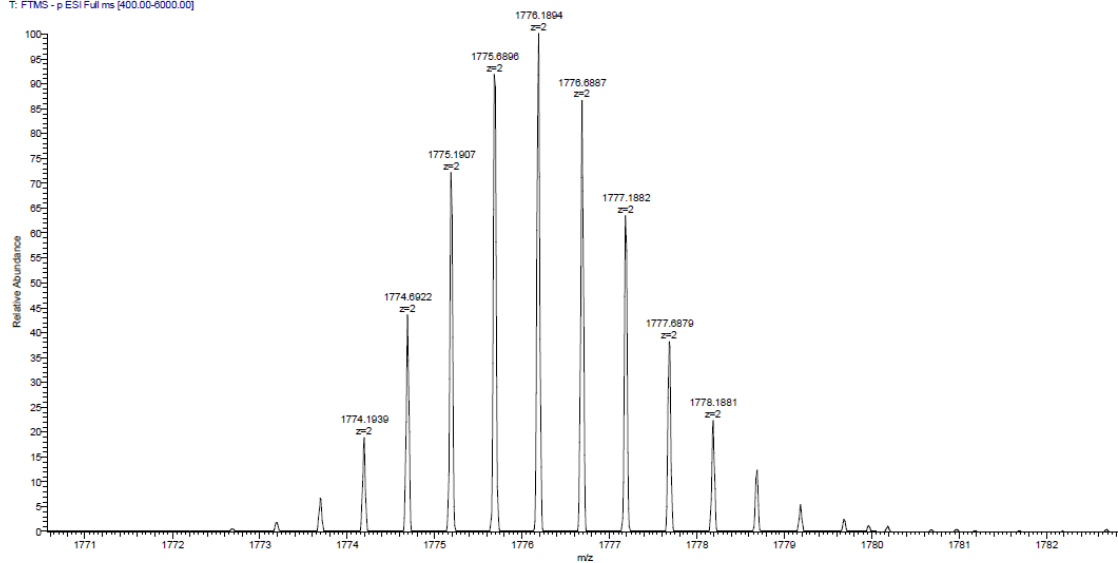
2e #1-10 RT: 0.01-0.09 AV: 10 NL: 1.77E8  
T: FTMS - p-ESI Full ms [400.00-6000.00]



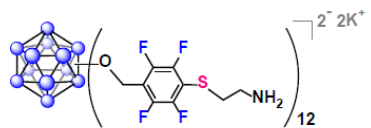


## Q Exactive High-Res Mass Spec

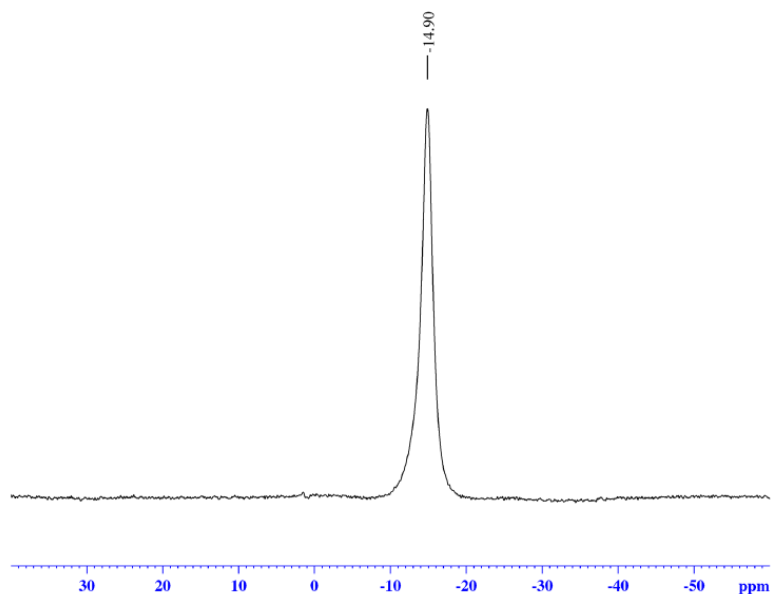
2e #1-10 RT: 0.01-0.09 AV: 10 NL: 1.77E8  
T: FTMS - p-ESI Full.ms [400.00-6000.00]







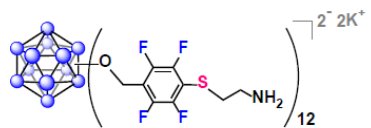
*in situ* <sup>11</sup>B NMR



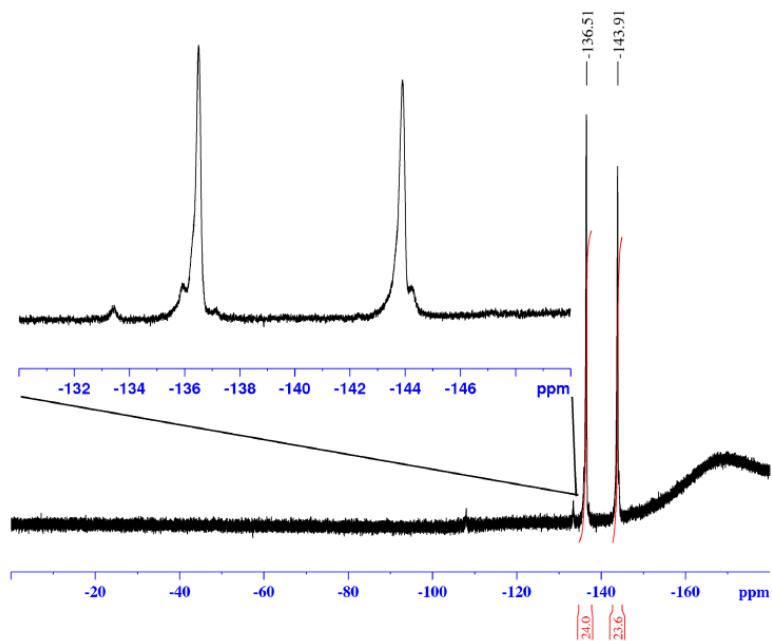
Current Data Parameters  
 NAME 0225  
 EXPNO 71  
 PROCNO 1

F2 - Acquisition Parameters  
 Date\_ 20160225  
 Time 16:57 h  
 INSTRUM av400  
 PROBHD Z108618\_0656 ( )  
 PULPROG zg  
 TD 5096  
 SOLVENT None  
 NS 1024  
 DS 0  
 SWH 51020.406 Hz  
 FIDRES 20.023708 Hz  
 AQ 0.0499408 sec  
 RG 189.85  
 DW 9.800 usec  
 DE 6.50 usec  
 TE 299.0 K  
 D1 0.05000000 sec  
 TDO 1  
 SFO1 128.3776052 MHz  
 NUC1 11B  
 P1 10.00 usec  
 PLW1 52.00000000 W

F2 - Processing parameters  
 SI 32768  
 SF 128.3776161 MHz  
 WDW EM  
 SSB 0  
 LB 10.00 Hz  
 GB 0  
 PC 1.40



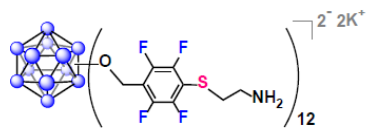
*in situ* <sup>19</sup>F NMR



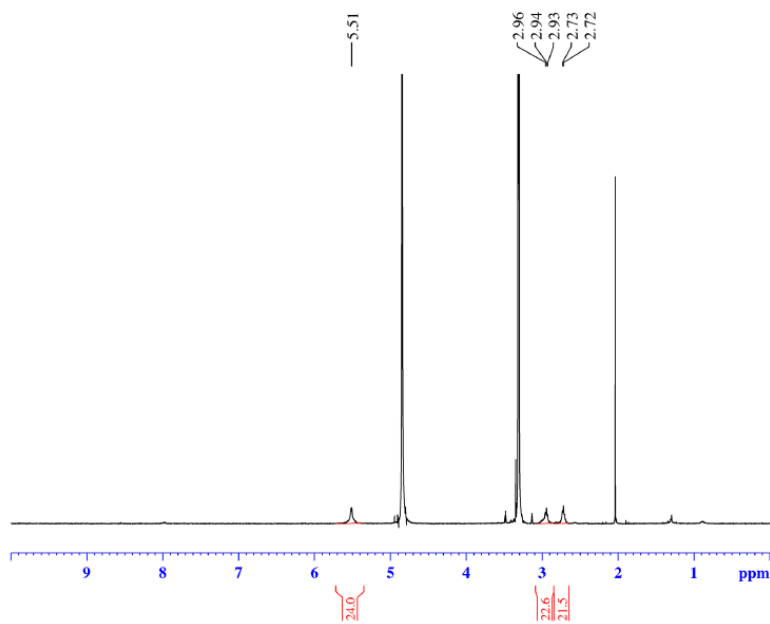
Current Data Parameters  
 NAME 0225  
 EXPNO 70  
 PROCNO 1

F2 - Acquisition Parameters  
 Date\_ 20160225  
 Time 16:54 h  
 INSTRUM av400  
 PROBHD Z108618\_0656 ( )  
 PULPROG zgpg30  
 TD 262144  
 SOLVENT None  
 NS 64  
 DS 0  
 SWH 150000.000 Hz  
 FIDRES 1.144409 Hz  
 AQ 0.8738133 sec  
 RG 189.85  
 DW 3.333 usec  
 DE 6.50 usec  
 TE 299.0 K  
 D1 2.00000000 sec  
 TDO 1  
 SFO1 376.4983660 MHz  
 NUC1 19F  
 P1 14.50 usec  
 PLW1 17.00000000 W

F2 - Processing parameters  
 SI 262144  
 SF 376.4983660 MHz  
 WDW EM  
 SSB 0  
 LB 1.00 Hz  
 GB 0  
 PC 1.00



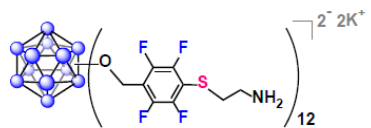
<sup>1</sup>H NMR



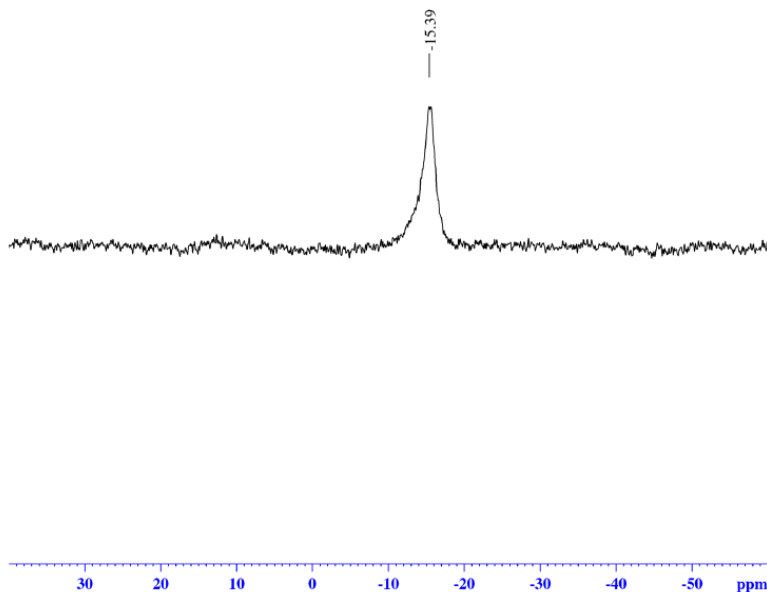
Current Data Parameters  
 NAME G1 CA 0303 0224 (MeOD)  
 EXPNO 80  
 PROCNO 1

F2 - Acquisition Parameters  
 Date\_ 20160303  
 Time 20.06 h  
 INSTRUM av400  
 PROBHD Z108618\_0656 ( )  
 PULPROG zg30  
 TD 52882  
 SOLVENT MeOD  
 NS 32  
 DS 0  
 SWH 8012.820 Hz  
 FIDRES 0.303045 Hz  
 AQ 3.2998369 sec  
 RG 155.85  
 DW 62.400 usec  
 DE 6.50 usec  
 TE 299.0 K  
 D1 5.00000000 sec  
 TDO 1  
 SFO1 400.1324008 MHz  
 NUC1 1H  
 P1 15.00 usec  
 PLW1 13.00000000 W

F2 - Processing parameters  
 SI 65536  
 SF 400.130077 MHz  
 WDW EM  
 SSB 0  
 LB 0.30 Hz  
 GB 0  
 PC 1.00



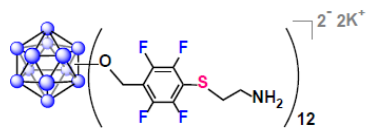
<sup>11</sup>B NMR



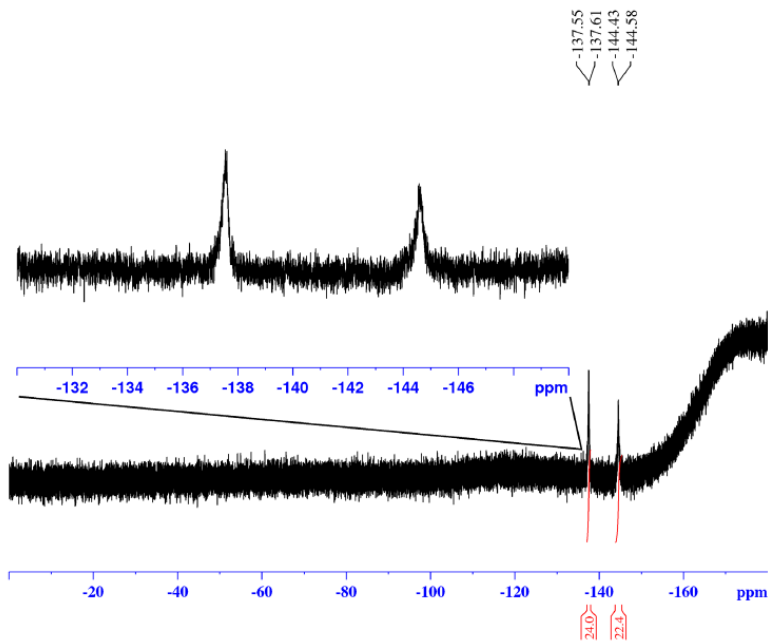
Current Data Parameters  
 NAME G1 CA 0303 0224 (MeOD)  
 EXPNO 81  
 PROCNO 1

F2 - Acquisition Parameters  
 Date\_ 20160303  
 Time 20.09 h  
 INSTRUM av400  
 PROBHD Z108618\_0656 ( )  
 PULPROG zg  
 TD 5096  
 SOLVENT MeOD  
 NS 1024  
 DS 0  
 SWH 51020.406 Hz  
 FIDRES 20.023708 Hz  
 AQ 0.0499408 sec  
 RG 189.85  
 DW 9.800 usec  
 DE 6.50 usec  
 TE 299.0 K  
 D1 0.05000000 sec  
 TDO 1  
 SFO1 128.3776052 MHz  
 NUC1 11B  
 P1 10.00 usec  
 PLW1 52.00000000 W

F2 - Processing parameters  
 SI 32768  
 SF 128.3776161 MHz  
 WDW EM  
 SSB 0  
 LB 10.00 Hz  
 GB 0  
 PC 1.40



<sup>19</sup>F NMR



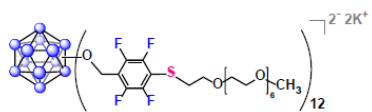
Current Data Parameters  
 NAME G1 CA 0303 0224 (MeOD)  
 EXPNO 82  
 PROCNO 1

F2 - Acquisition Parameters  
 Date\_ 20160303  
 Time 20.14 h  
 INSTRUM av400  
 PROBHD Z108618\_0656 ( )  
 PULPROG zgpg30  
 TD 262144  
 SOLVENT MeOD  
 NS 64  
 DS 0  
 SWH 150000.000 Hz  
 FIDRES 1.144409 Hz  
 AQ 0.8738133 sec  
 RG 189.85  
 DW 3.333 usec  
 DE 6.50 usec  
 TE 299.0 K  
 D1 2.0000000 sec  
 TDO 1  
 SFO1 376.4983660 MHz  
 NUC1 19F  
 P1 14.50 usec  
 PLW1 17.00000000 W

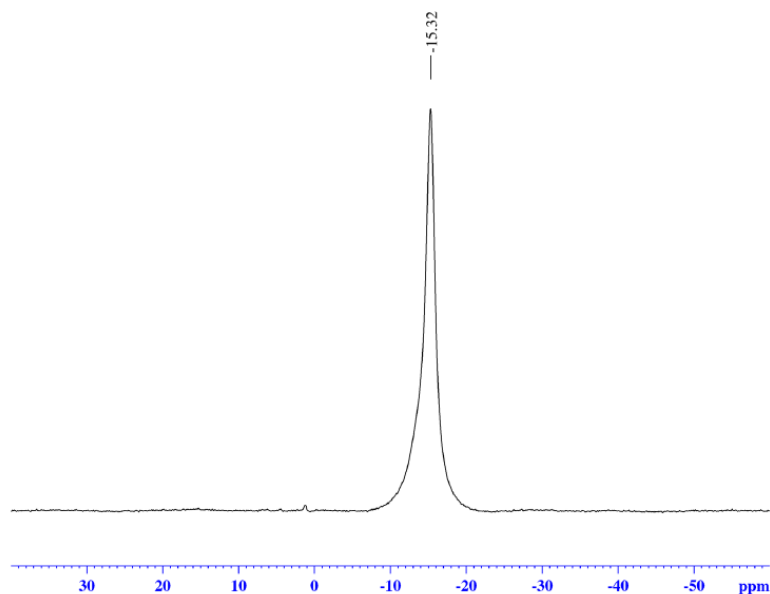
F2 - Processing parameters  
 SI 262144  
 SF 376.4983660 MHz  
 WDW EM  
 SSB 0  
 LB 1.00 Hz  
 GB 0  
 PC 1.00







*in situ*  $^{11}B$  NMR



```

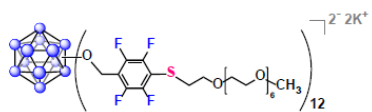
Current Data Parameters
NAME      0711
EXPNO    51
PROCNO   1

F2 - Acquisition Parameters
Date_    20160711
Time     18.26
INSTRUM  av400
PROBHD   5 mm PABBO BB/
PULPROG  zg
TD       5096
SOLVENT  None
NS       1024
DS       0
SWH      51020.406 Hz
FIDRES   10.011854 Hz
AQ       0.0499408 sec
RG       189.85
DW       9.800 usec
DE       6.50 usec
TE       299.0 K
D1       0.05000000 sec
TD0      1

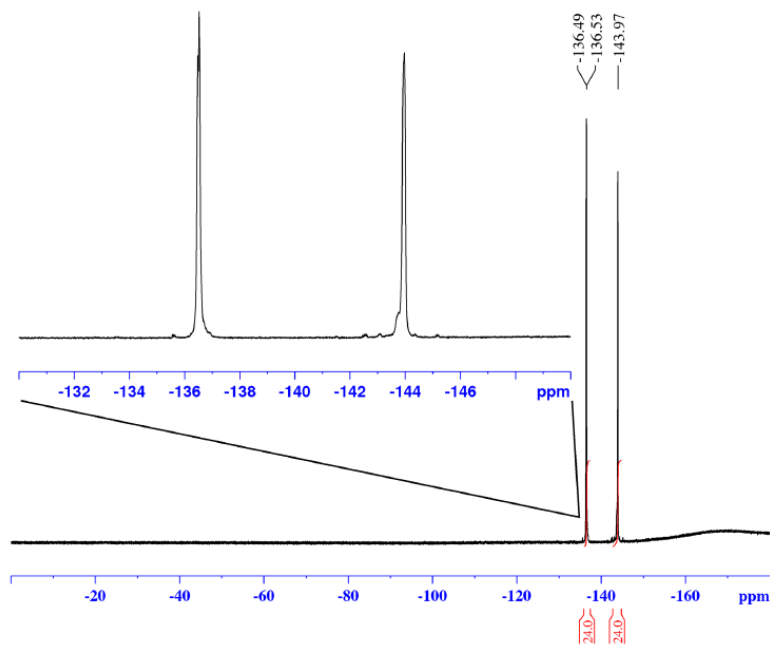
===== CHANNEL f1 =====
SFO1    128.3776052 MHz
NUC1     11B
P1       10.00 usec
PLW1    52.00000000 W

F2 - Processing parameters
SI       32768
SF       128.3776161 MHz
WDW      EM
SSB      0
LB       10.00 Hz
GB       0
PC       1.40
  
```





*in situ*  $^{19}\text{F}$  NMR

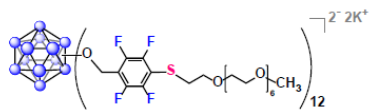


Current Data Parameters  
 NAME 0711  
 EXPNO 50  
 PROCNO 1

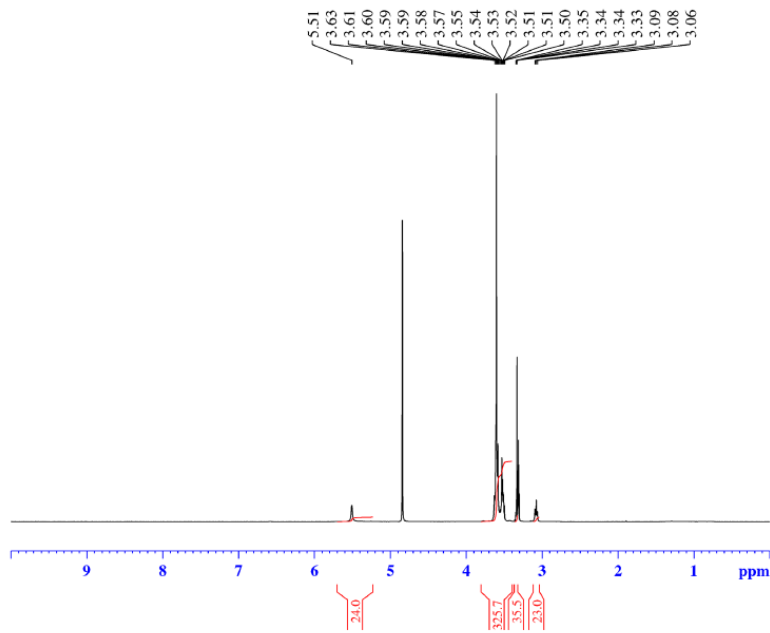
F2 - Acquisition Parameters  
 Date\_ 20160711  
 Time 18.23  
 INSTRUM av400  
 PROBHD 5 mm PABBO BB/  
 PULPROG zgpg30  
 TD 262144  
 SOLVENT None  
 NS 64  
 DS 0  
 SWH 150000.000 Hz  
 FIDRES 0.572205 Hz  
 AQ 0.8738133 sec  
 RG 189.85  
 DW 3.333 usec  
 DE 6.50 usec  
 TE 299.0 K  
 D1 2.00000000 sec  
 TDO 1

===== CHANNEL f1 =====  
 SFO1 376.4983660 MHz  
 NUC1  $^{19}\text{F}$   
 P1 14.50 usec  
 PLW1 17.00000000 W

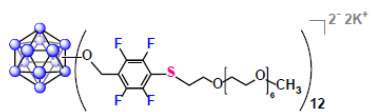
F2 - Processing parameters  
 SI 262144  
 SF 376.4983660 MHz  
 WDW EM  
 SSB 0  
 LB 1.00 Hz  
 GB 0  
 PC 1.00



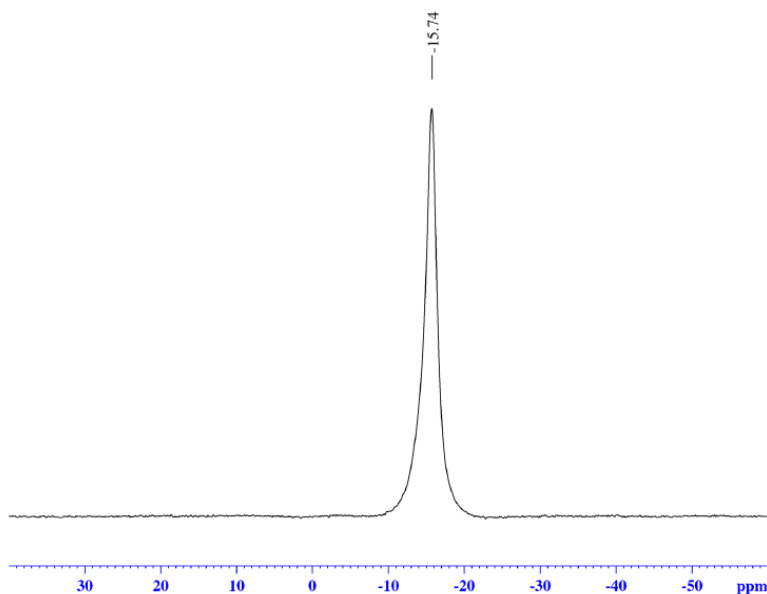
# $^1H$ NMR



Current Data Parameters  
 NAME G1 PEG350 8 mg 0713 0710 (MeOD)  
 EXPNO 32  
 PROCNO 1  
 F2 - Acquisition Parameters  
 Date\_ 20160713  
 Time 15.01  
 INSTRUM 40400  
 PROBHD 5 mm PABBO BB/  
 PULPROG zg30  
 TD 52882  
 SOLVENT MeOD  
 NS 32  
 DS 0  
 SWH 8012.820 Hz  
 FIDRES 0.151523 Hz  
 AQ 3.2998369 sec  
 RG 155.85  
 DW 62.400 usec  
 DE 6.50 usec  
 TE 299.0 K  
 D1 5.0000000 sec  
 TDO 1  
 ===== CHANNEL f1 =====  
 SFO1 400.132408 MHz  
 NUC1  $^1H$   
 P1 15.00 usec  
 PLW1 13.00000000 W  
 F2 - Processing parameters  
 SI 65536  
 SF 400.1300075 MHz  
 WDW EM  
 SSB 0  
 LB 0.30 Hz  
 GB 0  
 PC 1.00



<sup>11</sup>B NMR



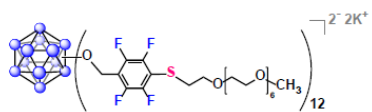
```

Current Data Parameters
NAME      G1 PEG350 8 mg 0713 0710 (MeOD)
EXPNO     30
PROCNO    1

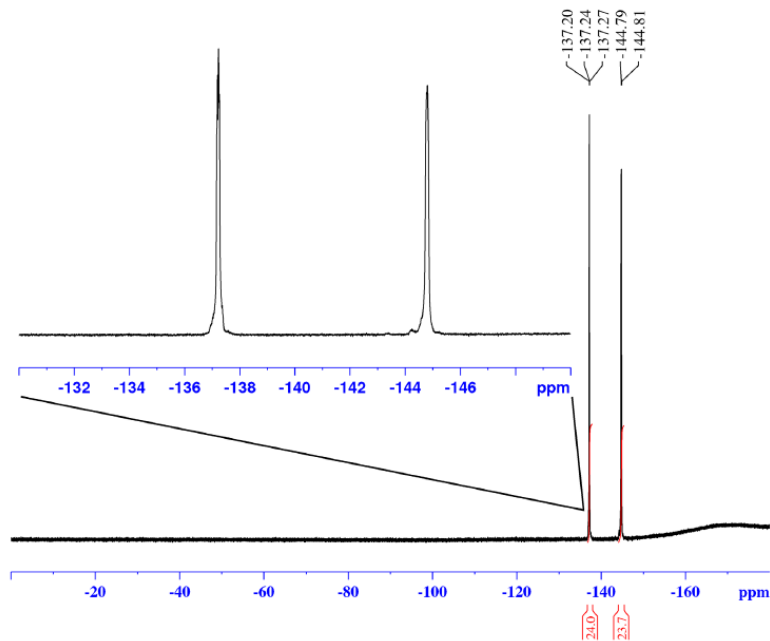
F2 - Acquisition Parameters
Date_     20160713
Time      14.52
INSTRUM   zgpg30
PROBHD    5 mm PABBO BB/
PULPROG   zgpg30
TD         5096
SOLVENT   MeOD
NS         1024
DS         0
SWH        51020.406 Hz
FIDRES     10.011854 Hz
AQ         0.04899408 sec
RG         189.85
DW         9.800 usec
DE         6.50 usec
TE         293.0 K
D1         0.05000000 sec
TDO        1

===== CHANNEL f1 =====
SFO1      128.3776052 MHz
NUC1       11B
P1         10.00 usec
PLW1      52.00000000 W

F2 - Processing parameters
SI         32768
SF         128.3776161 MHz
WDW        EM
SSB        0
LB         10.00 Hz
GB         0
PC         1.40
  
```



<sup>19</sup>F NMR

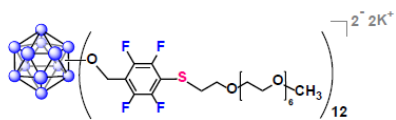


Current Data Parameters  
 NAME G1 PEG350 8 mg 0713 0710 (MeOD)  
 EXPNO 31  
 PROCNO 1

F2 - Acquisition Parameters  
 Date\_ 20160713  
 Time 14.56  
 INSTRUM us400  
 PROBHD 5 mm PABBO BB/  
 PULPROG zgpg30  
 TD 262144  
 SOLVENT MeOD  
 NS 64  
 DS 0  
 SWH 150000.000 Hz  
 FIDRES 0.572205 Hz  
 AQ 0.8738133 sec  
 RG 189.85  
 DW 3.333 usec  
 DE 6.50 usec  
 TE 299.0 K  
 D1 2.0000000 sec  
 TDO 1

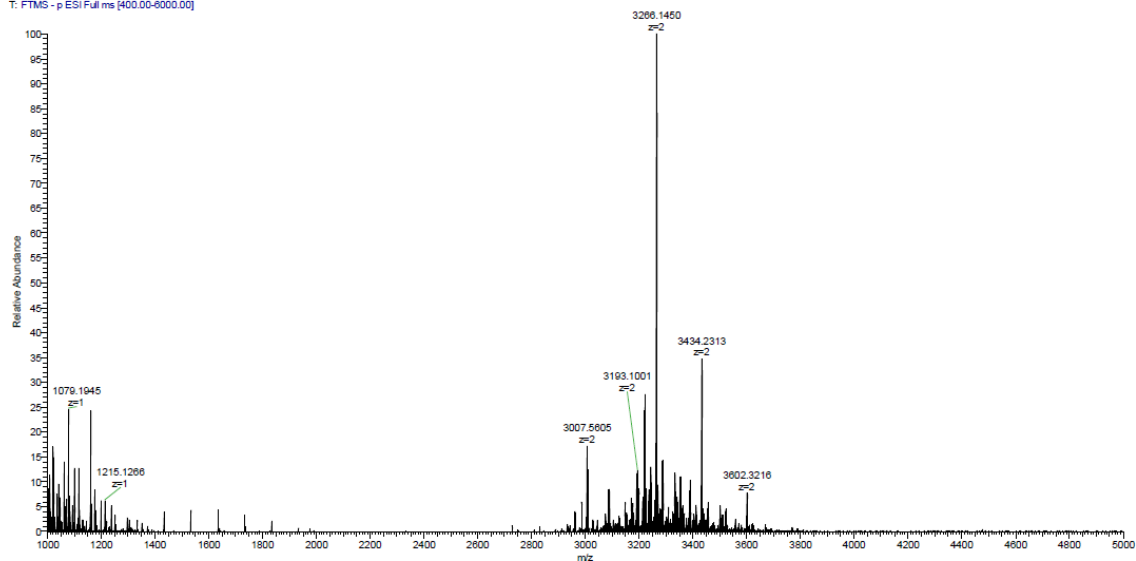
===== CHANNEL f1 =====  
 SFO1 376.4983660 MHz  
 NUC1 19F  
 P1 14.50 usec  
 PLW1 17.00000000 W

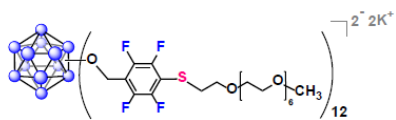
F2 - Processing parameters  
 SI 262144  
 SF 376.4983660 MHz  
 WDW EM  
 SSB 0  
 LB 1.00 Hz  
 GB 0  
 PC 1.00



## Q Exactive High-Res Mass Spec

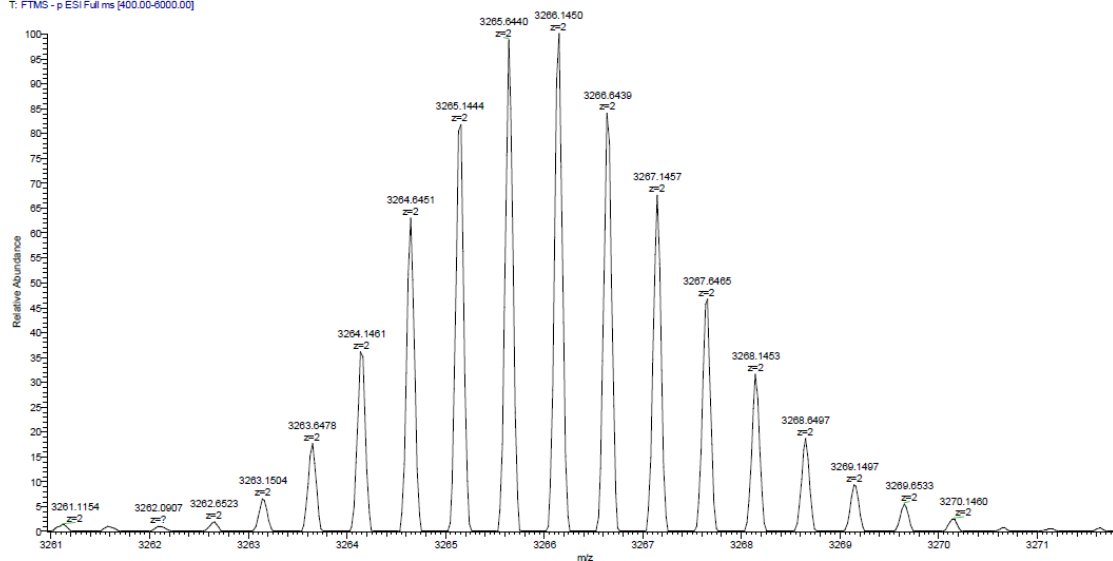
21 #1-16 RT: 0.01-0.14 AV: 16 NL: 2.75E6  
T: FTMS - p-ESI Full.ms [400.00-6000.00]

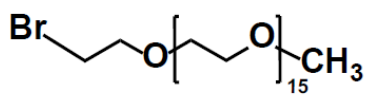




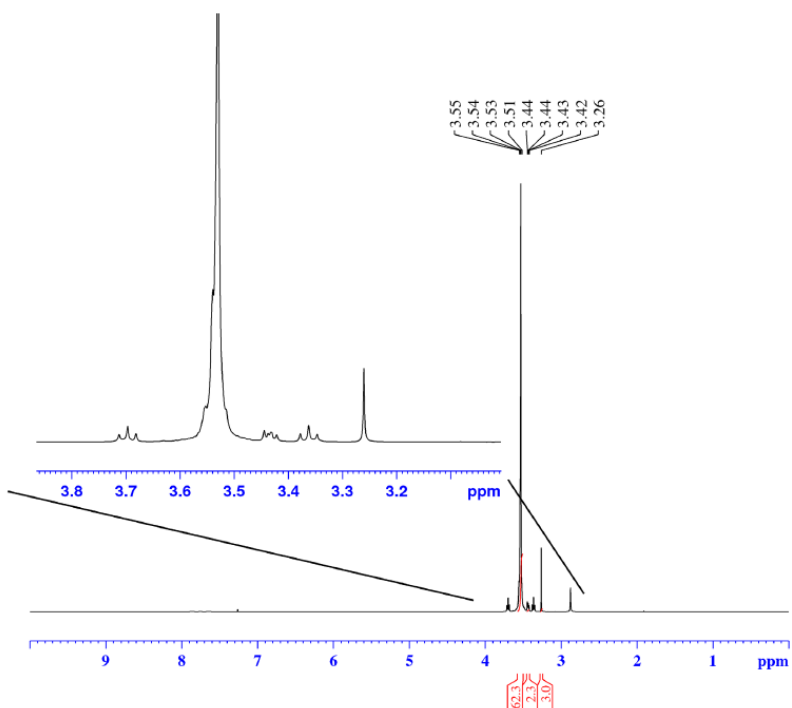
## Q Exactive High-Res Mass Spec

21 #1-16 RT: 0.01-0.14 AV: 16 NL: 2.75E6  
T: FTMS - p-ESI Full.ms [400.00-6000.00]





<sup>1</sup>H NMR



Current Data Parameters  
 NAME mPEG-Br  
 EXPNO 60  
 PROCNO 1

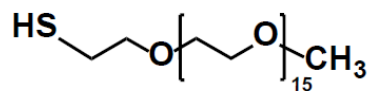
F2 - Acquisition Parameters  
 Date\_ 20151213  
 Time 15.05  
 INSTRUM av400  
 PROBHD 5 mm PABBO BB/  
 PULPROG zg30  
 TD 52882  
 SOLVENT CDCl3  
 NS 64  
 DS 0  
 SWH 8012.820 Hz  
 FIDRES 0.151523 Hz  
 AQ 3.2998369 sec  
 RG 12.23  
 DW 62.400 usec  
 DE 6.50 usec  
 TE 299.0 K  
 D1 2.00000000 sec  
 TDO 1

===== CHANNEL f1 =====  
 SFO1 400.1324008 MHz  
 NUC1 1H  
 P1 15.00 usec  
 PLW1 13.00000000 W

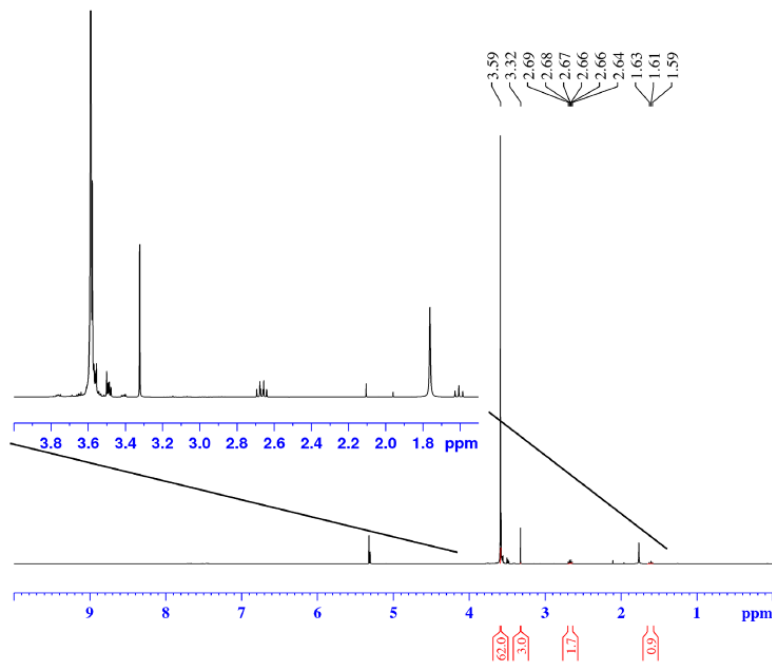
F2 - Processing parameters  
 SI 65536  
 SF 400.1300173 MHz  
 WDW EM  
 SSB 0  
 LB 0.30 Hz  
 GB 0  
 PC 1.00







<sup>1</sup>H NMR



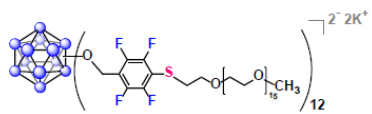
```

Current Data Parameters
NAME      mPEG-SH
EXPNO    80
PROCNO   1

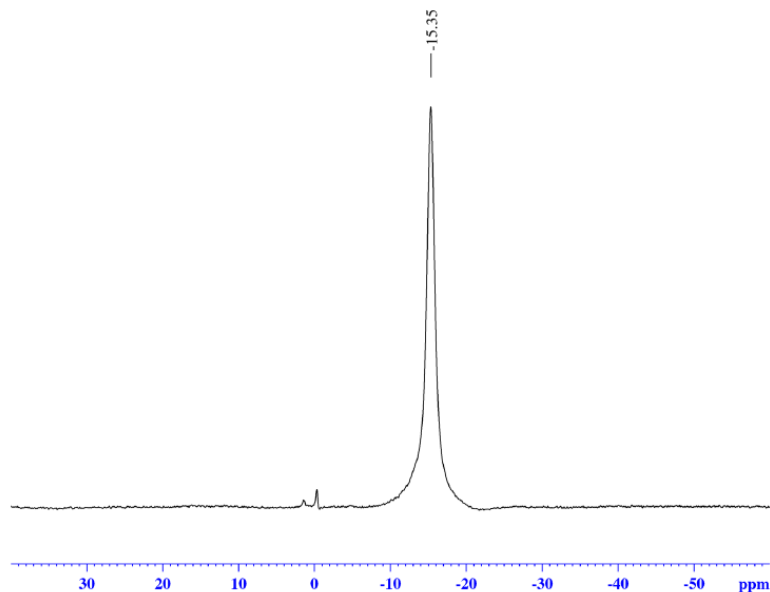
F2 - Acquisition Parameters
Date_    20151216
Time     19.25
INSTRUM  av400
PROBHD   5 mm PABBO BB/
PULPROG  zg30
TD       52882
SOLVENT  CD2Cl2
NS       80
DS       0
SWH      8012.820 Hz
FIDRES   0.151523 Hz
AQ       3.2998369 sec
RG       155.85
DW       62.400 usec
DE       6.50 usec
TE       299.0 K
D1       2.00000000 sec
TD0      1

===== CHANNEL f1 =====
SFO1    400.1324008 MHz
NUC1     1H
P1       15.00 usec
PLW1    13.00000000 W

F2 - Processing parameters
SI       65536
SF       400.1300203 MHz
WDW      EM
SSB      0
LB       0.30 Hz
GB       0
PC       1.00
  
```



*in situ*  $^{11}\text{B}$  NMR



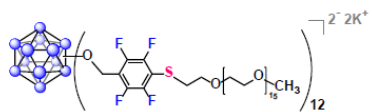
```

Current Data Parameters
NAME      0209
EXPNO    91
PROCNO   1

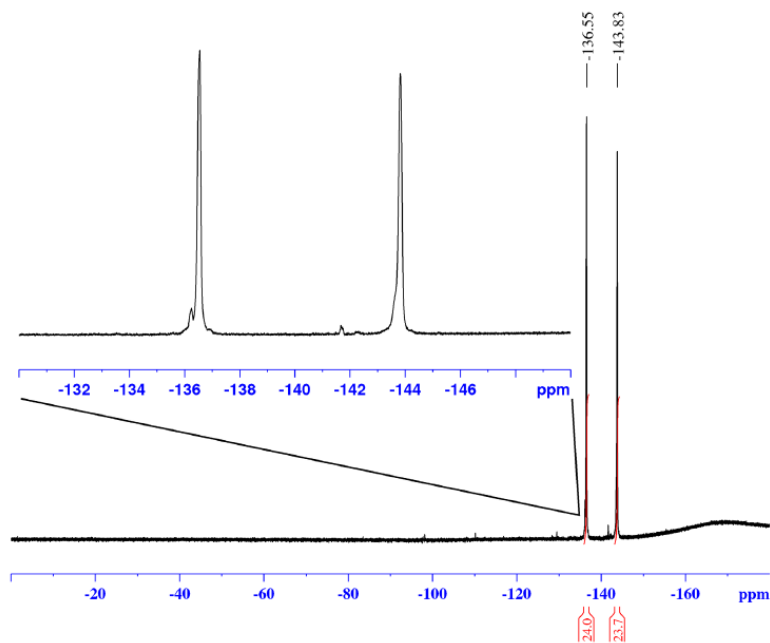
F2 - Acquisition Parameters
Date_    20160209
Time     19.27
INSTRUM  av400
PROBHD   5 mm PABBO BB/
PULPROG  zg
TD        5096
SOLVENT  None
NS        1024
DS         0
SWH       51020.406 Hz
FIDRES    10.011854 Hz
AQ        0.0499408 sec
RG        189.85
DW        9.800 usec
DE        6.50 usec
TE        299.0 K
D1        0.05000000 sec
TDO       1

===== CHANNEL f1 =====
SFO1     128.3776052 MHz
NUC1     11B
P1       10.00 usec
PLW1     52.00000000 W

F2 - Processing parameters
SI       32768
SF       128.3776161 MHz
WDW      EM
SSB      0
LB       10.00 Hz
GB       0
PC       1.40
  
```



*in situ*  $^{19}\text{F}$  NMR



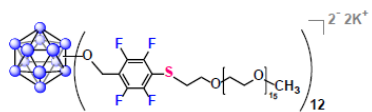
```

Current Data Parameters
NAME          0209
EXPNO         90
PROCNO        1

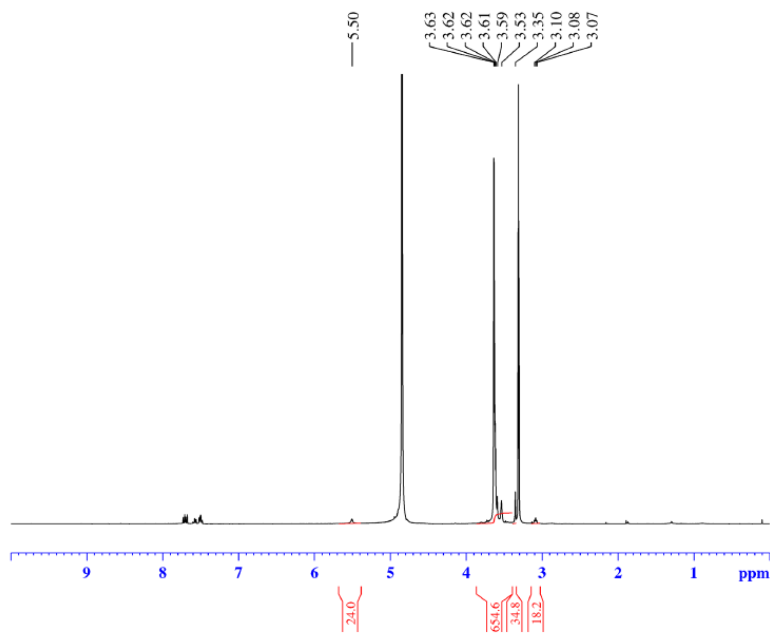
F2 - Acquisition Parameters
Date_         20160209
Time          19.24
INSTRUM       av400
PROBHD        5 mm PABBO BB/
PULPROG       zgpg30
TD            262144
SOLVENT       None
NS            64
DS            0
SWH           150000.000 Hz
FIDRES        0.572205 Hz
AQ            0.8738133 sec
RG            189.85
DW            3.333 usec
DE            6.50 usec
TE            299.0 K
D1            2.00000000 sec
TD0           1

===== CHANNEL f1 =====
SF01          376.4983660 MHz
NUC1          19F
P1            14.50 usec
PLW1          17.00000000 W

F2 - Processing parameters
SI            262144
SF            376.4983660 MHz
WDW           EM
SSB           0
LB            1.00 Hz
GB            0
PC            1.00
  
```



<sup>1</sup>H NMR



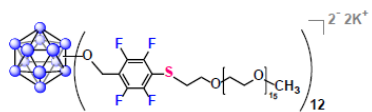
```

Current Data Parameters
NAME      G1 PEG750 0211 0208 MeOD
EXPNO    170
PROCNO   1

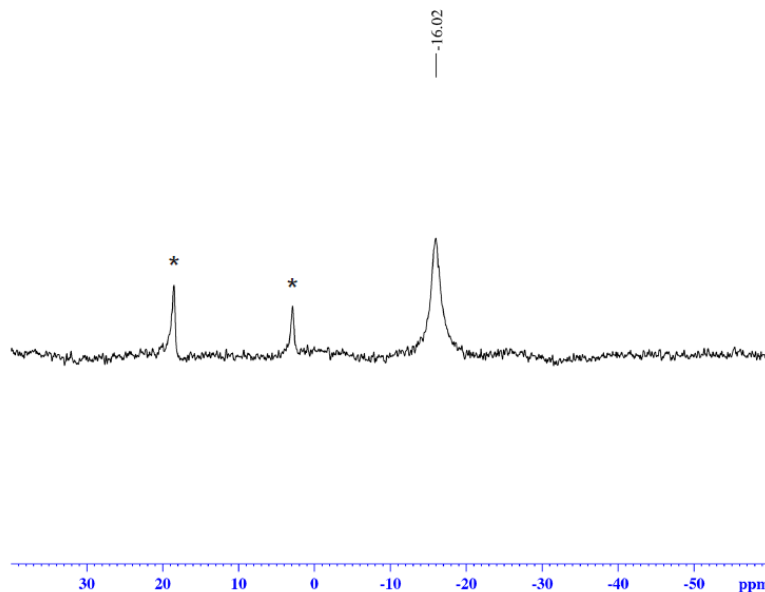
F2 - Acquisition Parameters
Date_    20160213
Time     20.35
INSTRUM  av400
PROBHD   5 mm PABBO BB/
PULPROG  zg30
TD       52882
SOLVENT  MeOD
NS       32
DS       0
SWH      8012.820 Hz
FIDRES   0.151523 Hz
AQ       3.2998369 sec
RG       155.85
DW       62.400 usec
DE       6.50 usec
TE       299.0 K
D1       10.00000000 sec
TDO      1

===== CHANNEL f1 =====
SFO1    400.1324008 MHz
NUC1    1H
P1      15.00 usec
PLW1    13.00000000 W

F2 - Processing parameters
SI      65536
SF      400.1300079 MHz
WDW     EM
SSB     0
LB      0.30 Hz
GB      0
PC      1.00
  
```



$^{11}\text{B}$  NMR



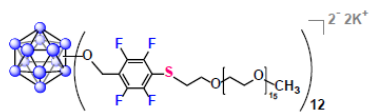
Current Data Parameters  
 NAME G1 PEG750 0211 0208 MeOD  
 EXPNO 171  
 PROCNO 1

F2 - Acquisition Parameters  
 Date\_ 20160213  
 Time 20.38  
 INSTRUM av400  
 PROBHD 5 mm PABBO BB/  
 PULPROG zg  
 TD 5096  
 SOLVENT MeOD  
 NS 1024  
 DS 0  
 SWH 51020.406 Hz  
 FIDRES 10.011854 Hz  
 AQ 0.0499408 sec  
 RG 189.85  
 DW 9.800 usec  
 DE 6.50 usec  
 TE 299.0 K  
 D1 0.05000000 sec  
 TDO 1

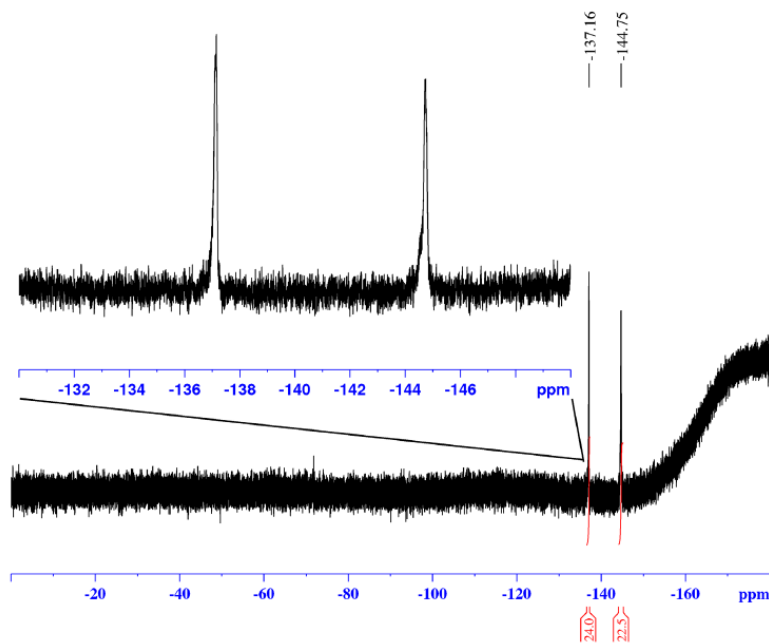
===== CHANNEL f1 =====  
 SFO1 128.3776052 MHz  
 NUC1  $^{11}\text{B}$   
 P1 10.00 usec  
 PLW1 52.00000000 W

F2 - Processing parameters  
 SI 32768  
 SF 128.3776161 MHz  
 WDW EM  
 SSB 0  
 LB 10.00 Hz  
 GB 0  
 PC 1.40

\* These peaks correspond to small impurities - boric acid and borates.



<sup>19</sup>F NMR

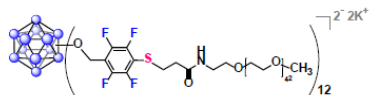


Current Data Parameters  
 NAME G1 PEG750 0211 0208 MeOD  
 EXPNO 172  
 PROCNO 1

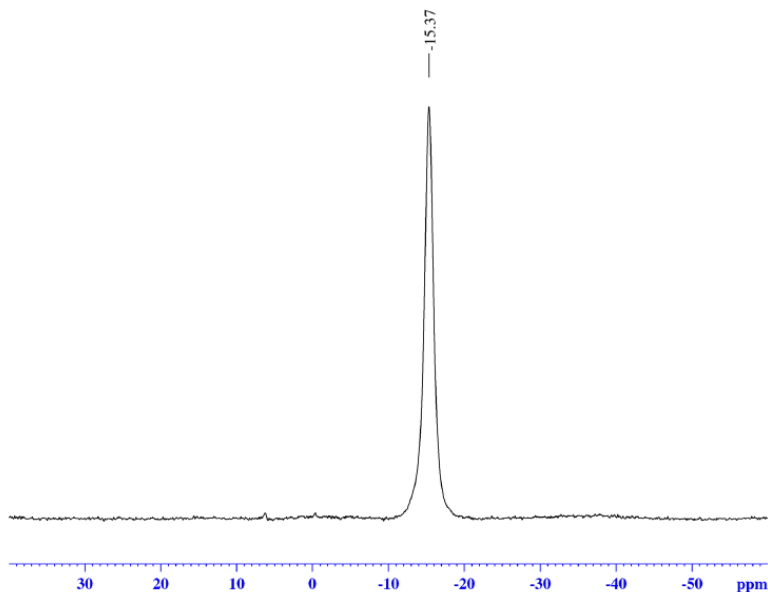
F2 - Acquisition Parameters  
 Date\_ 20160213  
 Time 20.42  
 INSTRUM av400  
 PROBHD 5 mm PABBO BB/  
 PULPROG zgpg30  
 TD 262144  
 SOLVENT MeOD  
 NS 64  
 DS 0  
 SWH 150000.000 Hz  
 FIDRES 0.572205 Hz  
 AQ 0.8738133 sec  
 RG 189.85  
 DW 3.333 usec  
 DE 6.50 usec  
 TE 299.0 K  
 D1 2.00000000 sec  
 TDO 1

===== CHANNEL f1 =====  
 SF01 376.4983660 MHz  
 NUC1 19F  
 P1 14.50 usec  
 PLW1 17.00000000 W

F2 - Processing parameters  
 SI 262144  
 SF 376.4983660 MHz  
 WDW EM  
 SSB 0  
 LB 1.00 Hz  
 GB 0  
 PC 1.00



*in situ*  $^{11}\text{B}$  NMR



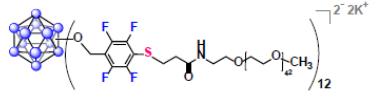
```

Current Data Parameters
NAME          0209
EXPNO         101
PROCNO        1

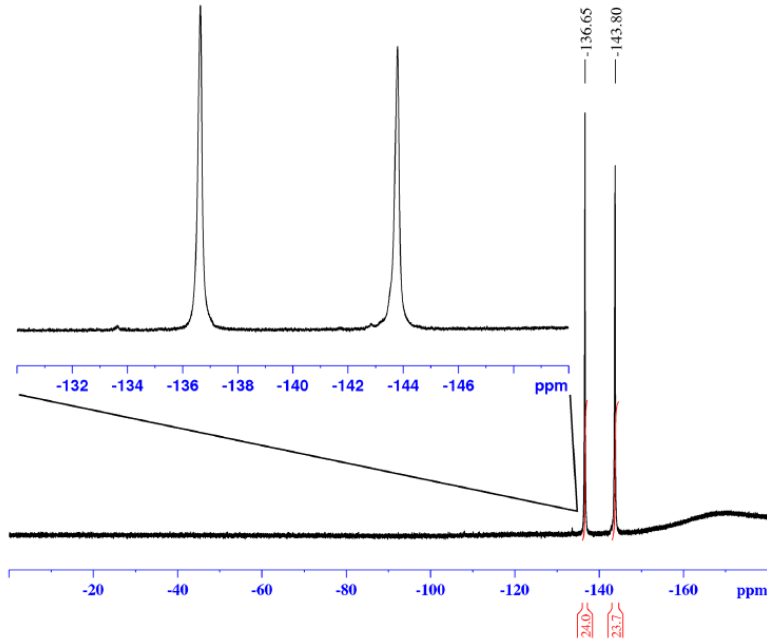
F2 - Acquisition Parameters
Date_         20160209
Time          19.36
INSTRUM       av400
PROBHD        5 mm PABBO BB/
PULPROG       zg
TD            5096
SOLVENT       None
NS            1024
DS            0
SWH           51020.406 Hz
FIDRES        10.011854 Hz
AQ            0.0499408 sec
RG            189.85
DW            9.800 usec
DE            6.50 usec
TE            299.0 K
D1            0.05000000 sec
TDO           1

===== CHANNEL f1 =====
SFO1          128.3776052 MHz
NUC1          11B
P1            10.00 usec
PLW1          52.00000000 W

F2 - Processing parameters
SI            32768
SF            128.3776161 MHz
WDW           EM
SSB           0
LB            10.00 Hz
GB            0
PC            1.40
  
```



*in situ*  $^{19}\text{F}$  NMR

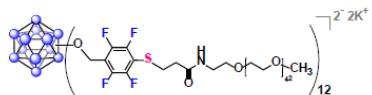


Current Data Parameters  
 NAME 0209  
 EXPNO 100  
 PROCNO 1  
 F2 - Acquisition Parameters  
 Date\_ 20160209  
 Time 19.33  
 INSTRUM av400  
 PROBHD 5 mm PABBO BB/  
 PULPROG zgpg30  
 TD 262144  
 SOLVENT None  
 NS 64  
 DS 0  
 SWH 150000.000 Hz  
 FIDRES 0.572205 Hz  
 AQ 0.8738133 sec  
 RG 189.85  
 DW 3.333 usec  
 DE 6.50 usec  
 TE 299.0 K  
 D1 2.00000000 sec  
 TDO 1

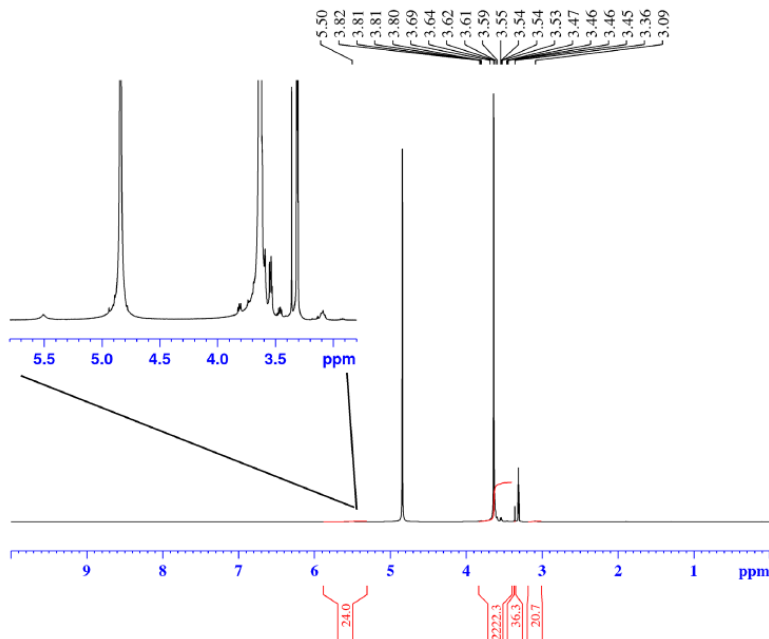
===== CHANNEL f1 =====  
 SFO1 376.4983660 MHz  
 NUC1  $^{19}\text{F}$   
 P1 14.50 usec  
 PLW1 17.00000000 W

F2 - Processing parameters  
 SI 262144  
 SF 376.4983660 MHz  
 WDW EM  
 SSB 0  
 LB 1.00 Hz  
 GB 0  
 PC 1.00





# <sup>1</sup>H NMR

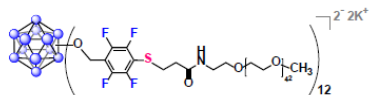


Current Data Parameters  
 NAME G1 PEG2000 0211 0208 MeOD  
 EXPNO 100  
 PROCNO 1

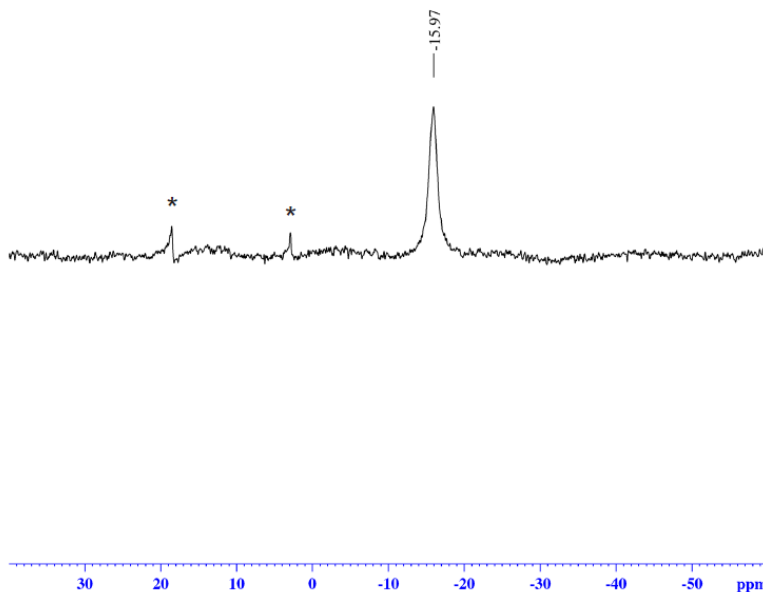
F2 - Acquisition Parameters  
 Date\_ 20160216  
 Time 21.55  
 INSTRUM av400  
 PROBHD 5 mm PABBO BB/  
 PULPROG zg30  
 TD 52882  
 SOLVENT MeOD  
 NS 32  
 DS 0  
 SWH 8012.820 Hz  
 FIDRES 0.151523 Hz  
 AQ 3.2998369 sec  
 RG 155.85  
 DW 62.400 usec  
 DE 6.50 usec  
 TE 299.0 K  
 D1 10.00000000 sec  
 TDO 1

===== CHANNEL f1 =====  
 SFO1 400.1324008 MHz  
 NUC1 1H  
 P1 15.00 usec  
 PLW1 13.00000000 W

F2 - Processing parameters  
 SI 65536  
 SF 400.130076 MHz  
 WDW EM  
 SSB 0  
 LB 0.30 Hz  
 GB 0  
 PC 1.00



<sup>11</sup>B NMR



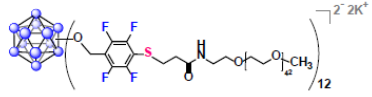
Current Data Parameters  
 NAME G1 PEG2000 0211 0208 MeOD  
 EXPNO 102  
 PROCNO 1

F2 - Acquisition Parameters  
 Date\_ 20160212  
 Time 13.59  
 INSTRUM av400  
 PROBHD 5 mm PABBO BB/  
 PULPROG zg  
 TD 5096  
 SOLVENT MeOD  
 NS 1024  
 DS 0  
 SWH 51020.406 Hz  
 FIDRES 10.011854 Hz  
 AQ 0.0499408 sec  
 RG 189.85  
 DW 9.800 usec  
 DE 6.50 usec  
 TE 299.0 K  
 D1 0.05000000 sec  
 TDO 1

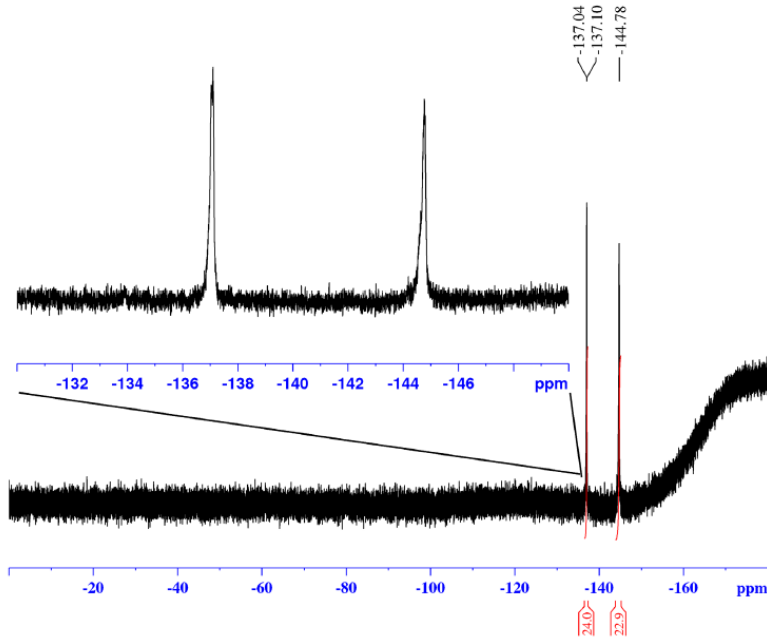
===== CHANNEL f1 =====  
 SFO1 128.3776052 MHz  
 NUC1 11B  
 P1 10.00 usec  
 PLW1 52.00000000 W

F2 - Processing parameters  
 SI 32768  
 SF 128.3776161 MHz  
 WDW EM  
 SSB 0  
 LB 10.00 Hz  
 GB 0  
 PC 1.40

\* These peaks correspond to small impurities - boric acid and borates.



<sup>19</sup>F NMR

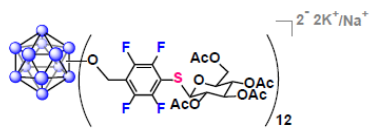


Current Data Parameters  
 NAME G1 PEG2000 0211 0208 MeOD  
 EXPNO 101  
 PROCNO 1

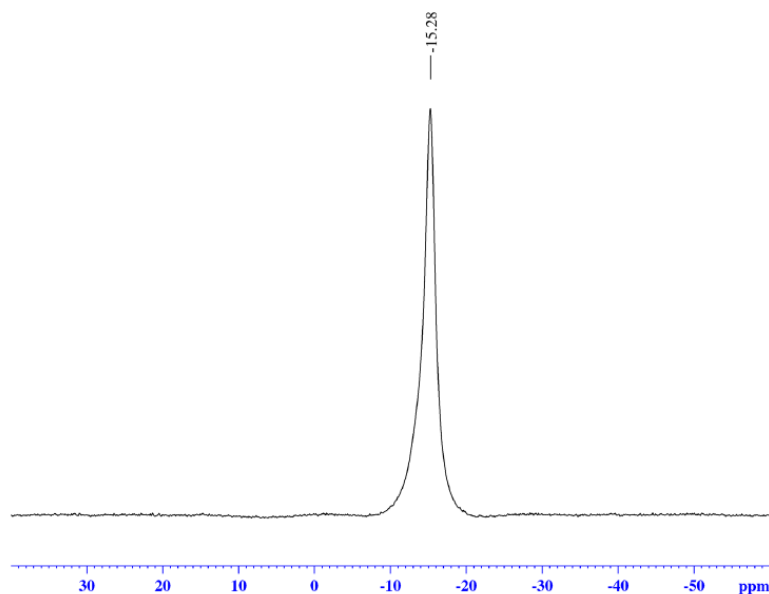
F2 - Acquisition Parameters  
 Date\_ 20160212  
 Time 14.03  
 INSTRUM av400  
 PROBHD 5 mm PABBO BB/  
 PULPROG zgpg30  
 TD 262144  
 SOLVENT MeOD  
 NS 64  
 DS 0  
 SWH 150000.000 Hz  
 FIDRES 0.572205 Hz  
 AQ 0.8738133 sec  
 RG 189.85  
 DW 3.333 usec  
 DE 6.50 usec  
 TE 299.0 K  
 D1 2.0000000 sec  
 TDO 1

===== CHANNEL f1 =====  
 SFO1 376.4983660 MHz  
 NUC1 <sup>19</sup>F  
 P1 14.50 usec  
 PLW1 17.00000000 W

F2 - Processing parameters  
 SI 262144  
 SF 376.4983660 MHz  
 WDW EM  
 SSB 0  
 LB 1.00 Hz  
 GB 0  
 PC 1.00



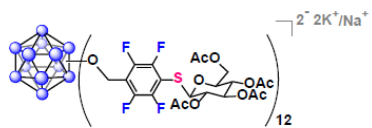
*in situ*  $^{11}\text{B}$  NMR



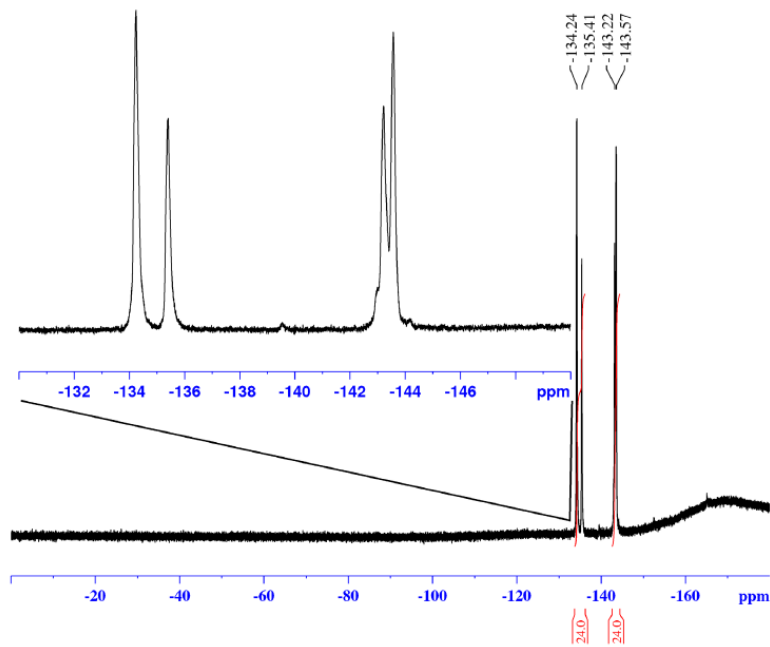
Current Data Parameters  
 NAME 0308  
 EXPNO 71  
 PROCNO 1

F2 - Acquisition Parameters  
 Date\_ 20160308  
 Time 15:42 h  
 INSTRUM av400  
 PROBHD Z108618\_0656 ( )  
 PULPROG zg  
 TD 5096  
 SOLVENT None  
 NS 1024  
 DS 0  
 SWH 51020.406 Hz  
 FIDRES 20.023708 Hz  
 AQ 0.0499408 sec  
 RG 189.85  
 DW 9.800 usec  
 DE 6.50 usec  
 TE 299.0 K  
 D1 0.05000000 sec  
 TDO 1  
 SFO1 128.3776052 MHz  
 NUC1 11B  
 P1 10.00 usec  
 PLW1 52.00000000 W

F2 - Processing parameters  
 SI 32768  
 SF 128.3776161 MHz  
 WDW EM  
 SSB 0  
 LB 10.00 Hz  
 GB 0  
 PC 1.40



*in situ* <sup>19</sup>F NMR

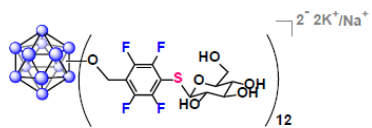


Current Data Parameters  
 NAME 0308  
 EXPNO 70  
 PROCNO 1

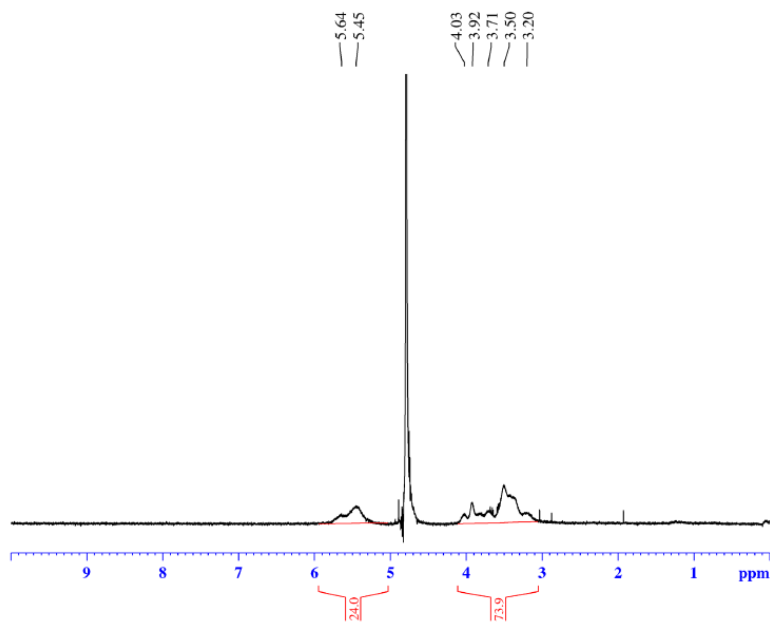
F2 - Acquisition Parameters  
 Date\_ 20160308  
 Time 15.39 h  
 INSTRUM av400  
 PROBHD Z108618\_0656 ( )  
 PULPROG zgpg30  
 TD 262144  
 SOLVENT None  
 NS 64  
 DS 0  
 SWH 150000.000 Hz  
 FIDRES 1.144409 Hz  
 AQ 0.8738133 sec  
 RG 189.85  
 DW 3.333 usec  
 DE 6.50 usec  
 TE 299.0 K  
 D1 2.0000000 sec  
 TDO 1  
 SFO1 376.4983660 MHz  
 NUC1 19F  
 P1 14.50 usec  
 PLW1 17.00000000 W

F2 - Processing parameters  
 SI 262144  
 SF 376.4983660 MHz  
 WDW EM  
 SSB 0  
 LB 1.00 Hz  
 GB 0  
 PC 1.00

Split peaks are due to the restricted rotational conformations of the molecule.



<sup>1</sup>H NMR

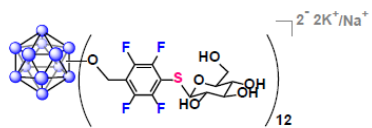


Current Data Parameters  
 NAME G1 Gic 2 0711 0307 D2O  
 EXPNO 202  
 PROCNO 1

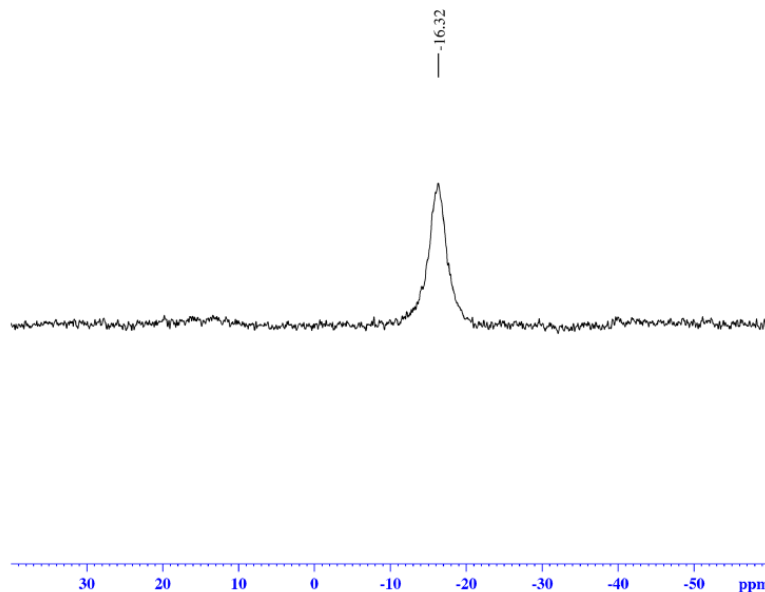
F2 - Acquisition Parameters  
 Date\_ 20160713  
 Time 20.32  
 INSTRUM av400  
 PROBHD 5 mm PABBO BB/  
 PULPROG zg30  
 TD 52882  
 SOLVENT D2O  
 NS 32  
 DS 0  
 SWH 8012.820 Hz  
 FIDRES 0.151523 Hz  
 AQ 3.2998369 sec  
 RG 189.85  
 DW 62.400 usec  
 DE 6.50 usec  
 TE 299.0 K  
 D1 5.00000000 sec  
 TDO 1

===== CHANNEL f1 =====  
 SFO1 400.1324008 MHz  
 NUC1 1H  
 P1 15.00 usec  
 PLW1 13.00000000 W

F2 - Processing parameters  
 SI 65536  
 SF 400.1299638 MHz  
 WDW EM  
 SSB 0  
 LB 0.30 Hz  
 GB 0  
 PC 1.00



<sup>11</sup>B NMR

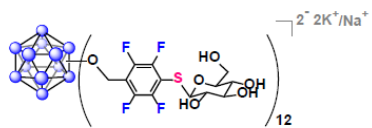


Current Data Parameters  
 NAME G1 G1c 2 0711 0307 D2O  
 EXPNO 200  
 PROCNO 1

F2 - Acquisition Parameters  
 Date\_ 20160713  
 Time 20.23  
 INSTRUM av400  
 PROBHD 5 mm PABBO BB/  
 PULPROG zg  
 TD 5096  
 SOLVENT D2O  
 NS 1024  
 DS 0  
 SWH 51020.406 Hz  
 FIDRES 10.011854 Hz  
 AQ 0.0499408 sec  
 RG 189.85  
 DW 9.800 usec  
 DE 6.50 usec  
 TE 299.0 K  
 D1 0.05000000 sec  
 TDO 1

===== CHANNEL f1 =====  
 SFO1 128.3776052 MHz  
 NUC1 11B  
 P1 10.00 usec  
 PLW1 52.00000000 W

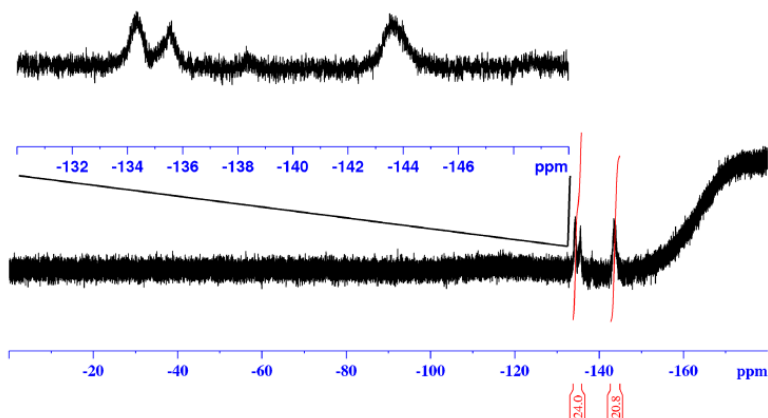
F2 - Processing parameters  
 SI 32768  
 SF 128.3776161 MHz  
 WDW EM  
 SSB 0  
 LB 10.00 Hz  
 GB 0  
 PC 1.40



<sup>19</sup>F NMR



-134.33  
-135.60  
-143.52



Current Data Parameters  
NAME G1 Gic 2 0711 0307 D2O  
EXPNO 201  
PROCNO 1

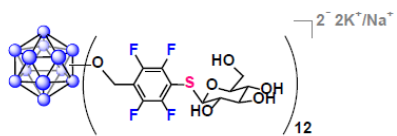
F2 - Acquisition Parameters  
Date\_ 20160713  
Time 20.27  
INSTRUM av400  
PROBHD 5 mm PABBO BB/  
PULPROG zgpg30  
TD 262144  
SOLVENT D2O  
NS 64  
DS 0  
SWH 150000.000 Hz  
FIDRES 0.572205 Hz  
AQ 0.8738133 sec  
RG 189.85  
DW 3.333 usec  
DE 6.50 usec  
TE 299.0 K  
D1 2.00000000 sec  
TDO 1

===== CHANNEL f1 =====  
SF01 376.4983660 MHz  
NUC1 19F  
P1 14.50 usec  
PLW1 17.00000000 W

F2 - Processing parameters  
SI 262144  
SF 376.4983660 MHz  
WDW EM  
SSB 0  
LB 1.00 Hz  
GB 0  
PC 1.00

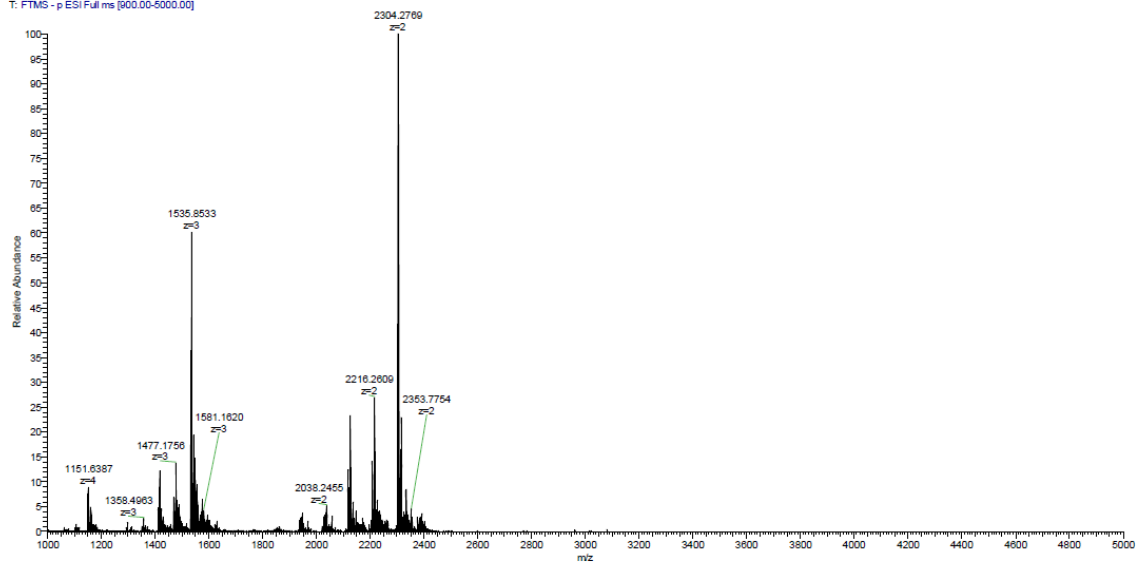
Broad, split peaks are due to the restricted rotational conformations of the molecule.

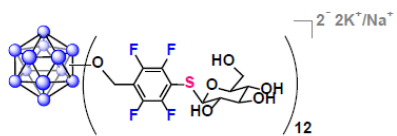




## Q Exactive High-Res Mass Spec

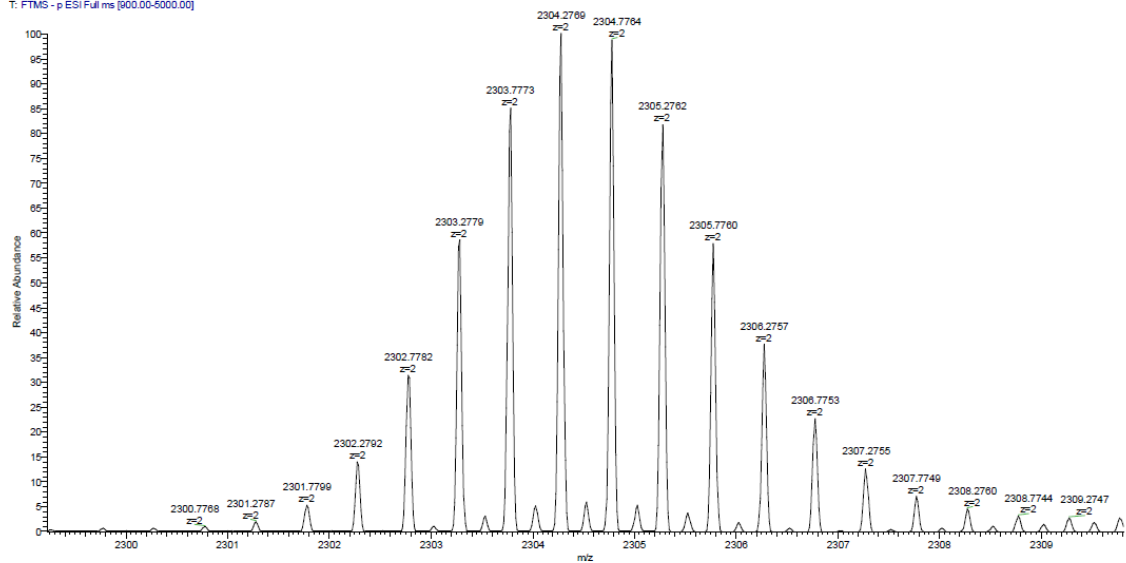
21#1-57 RT: 0.01-0.49 AV: 57 NL: 2.33E7  
T: FTMS - p-ESI Full ms [600.00-5000.00]

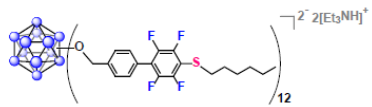




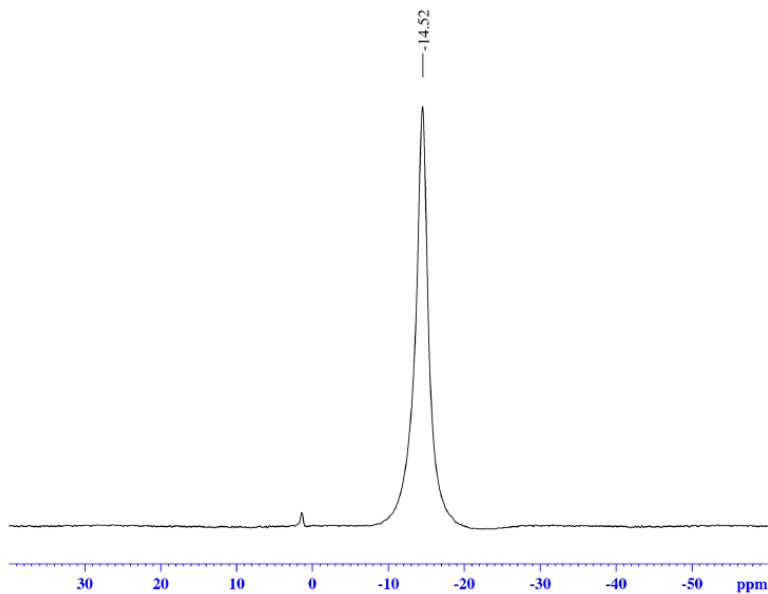
## Q Exactive High-Res Mass Spec

21#1-57 RT: 0.01-0.49 AV: 57 NL: 2.33E7  
T: FTMS - p-ESI Full.ms [600.00-6300.00]





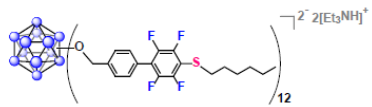
*in situ*  $^{11}\text{B}$  NMR



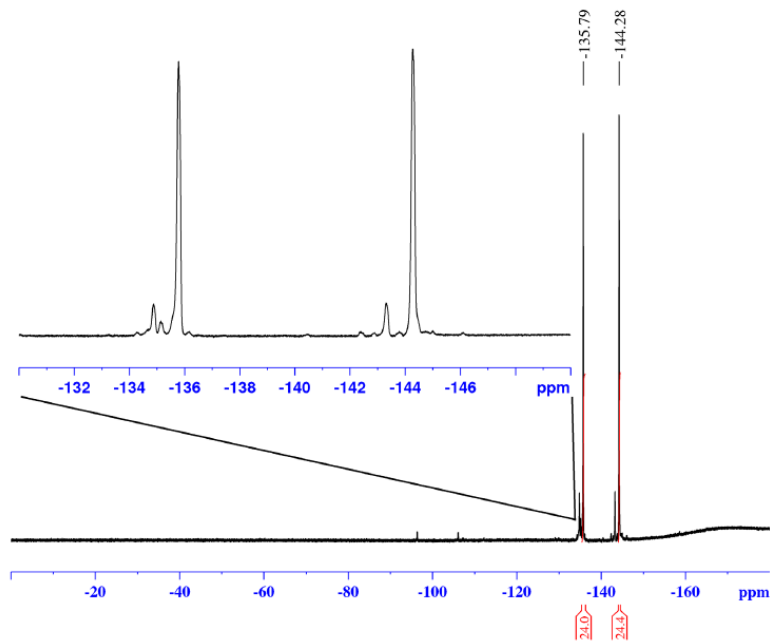
Current Data Parameters  
 NAME 0119  
 EXPNO 151  
 PROCNO 1  
 F2 - Acquisition Parameters  
 Date\_ 20160119  
 Time 19.56  
 INSTRUM av400  
 PROBHD 5 mm PABBO BB/  
 PULPROG zg  
 TD 5096  
 SOLVENT None  
 NS 1024  
 DS 0  
 SWH 51020.406 Hz  
 FIDRES 10.011854 Hz  
 AQ 0.0499408 sec  
 RG 189.85  
 DW 9.800 usec  
 DE 6.50 usec  
 TE 299.0 K  
 D1 0.05000000 sec  
 TDO 1

===== CHANNEL f1 =====  
 SFO1 128.3776052 MHz  
 NUC1 11B  
 P1 10.00 usec  
 PLW1 52.00000000 W

F2 - Processing parameters  
 SI 32768  
 SF 128.3776161 MHz  
 WDW EM  
 SSB 0  
 LB 10.00 Hz  
 GB 0  
 PC 1.40



*in situ* <sup>19</sup>F NMR



```

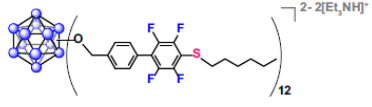
Current Data Parameters
NAME      0119
EXPNO    150
PROCNO    1

F2 - Acquisition Parameters
Date_    20160119
Time     19.53
INSTRUM  av400
PROBHD   5 mm PABBO BB/
PULPROG  zgpg30
TD       262144
SOLVENT  None
NS       64
DS       0
SWH      150000.000 Hz
FIDRES   0.572205 Hz
AQ       0.8738133 sec
RG       189.85
DW       3.333 usec
DE       6.50 usec
TE       299.0 K
D1       2.00000000 sec
TD0      1

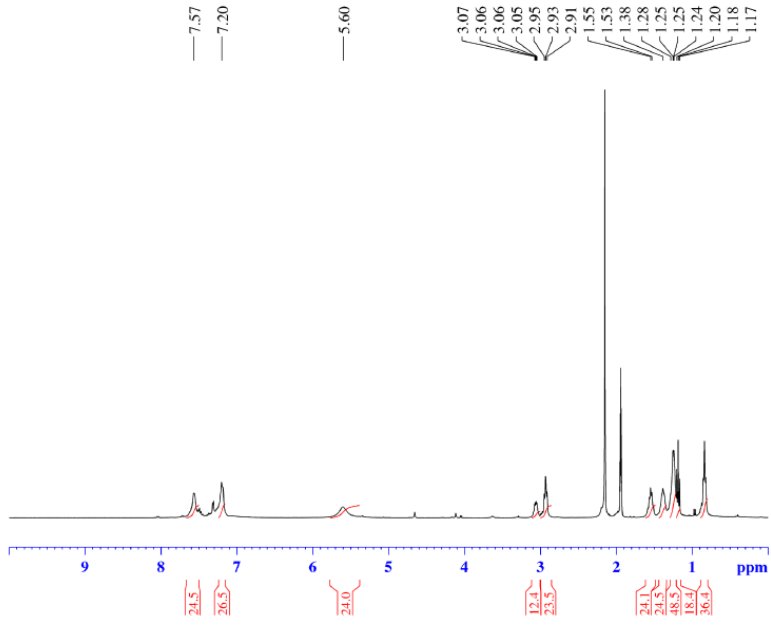
===== CHANNEL f1 =====
SF01    376.4983660 MHz
NUC1     19F
P1       14.50 usec
PLW1    17.00000000 W

F2 - Processing parameters
SI       262144
SF       376.4983660 MHz
WDW      EM
SSB      0
LB       1.00 Hz
GB       0
PC       1.00
  
```

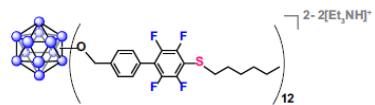
Small impurities are present due to the commercial 1-hexanethiol used (95% pure).



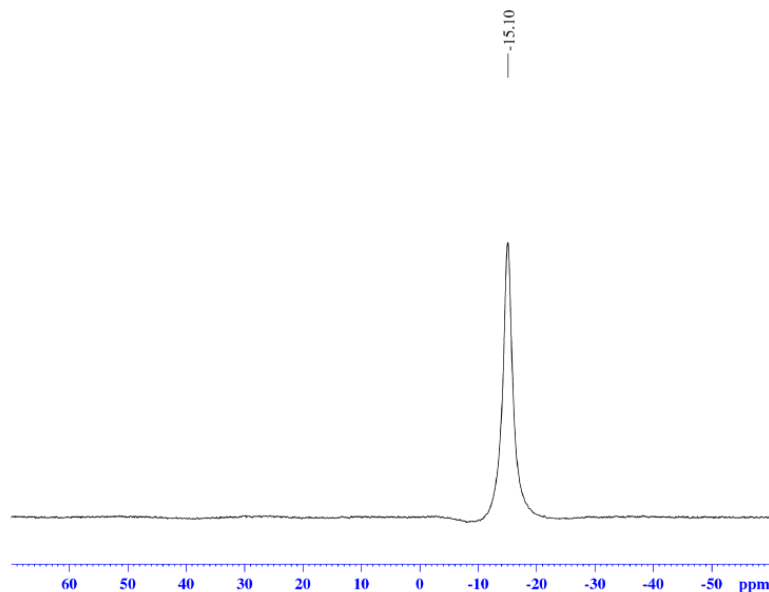
<sup>1</sup>H NMR



Current Data Parameters  
 NAME Jan26-2016  
 EXPNO 41  
 PROCNO 1  
 F2 - Acquisition Parameters  
 Date\_ 20160126  
 Time 13.00  
 INSTRUM av400  
 PROBHD 5 mm PABBO BB/  
 PULPROG zg30  
 TD 128204  
 SOLVENT CD3CN  
 NS 32  
 DS 0  
 SWH 8012.820 Hz  
 FIDRES 0.062501 Hz  
 AQ 7.999294 sec  
 RG 155.85  
 DW 62.400 usec  
 DE 6.50 usec  
 TE 299.0 K  
 D1 5.00000000 sec  
 TDO 1  
 ===== CHANNEL f1 =====  
 SFO1 400.1324008 MHz  
 NUC1 1H  
 P1 15.00 usec  
 PLW1 13.00000000 W  
 F2 - Processing parameters  
 SI 63536  
 SF 400.1300114 MHz  
 WDW EM  
 SSB 0  
 LB 0.30 Hz  
 GB 0  
 PC 1.00



$^{11}\text{B}$   $\{^1\text{H}\}$  NMR



```

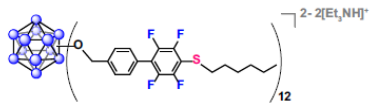
Current Data Parameters
NAME      Jan26-2016
EXPNO    40
PROCNO   1

F2 - Acquisition Parameters
Date_    20160126
Time     12.53
INSTRUM  av400
PROBHD   5 mm PABBO BB/
PULPROG  zgpg30
TD       5096
SOLVENT  CD3CN
NS       1024
DS       0
SWH      51020.406 Hz
FIDRES   10.011854 Hz
AQ       0.0499405 sec
RG       189.85
DW       9.500 usec
DE       6.50 usec
TE       299.1 K
D1       0.0500000 sec
D11      0.0300000 sec
TD0      1

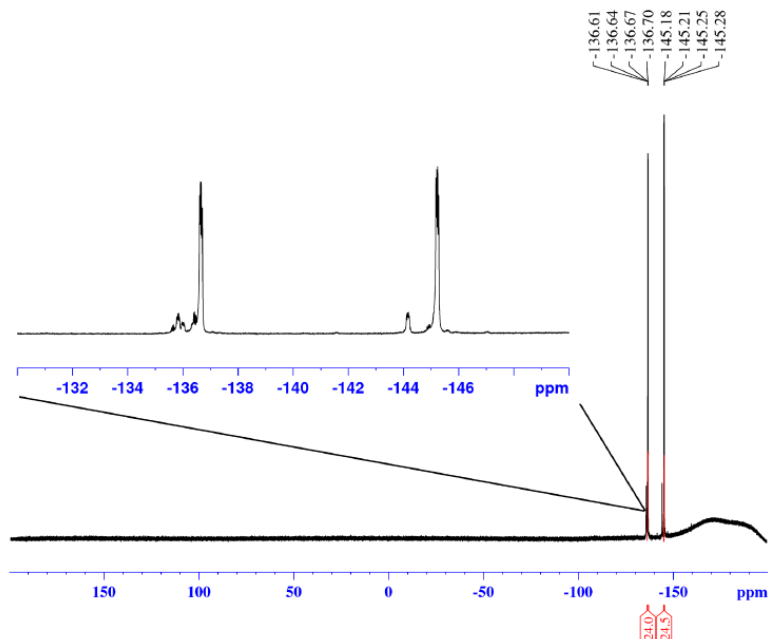
===== CHANNEL f1 =====
SFO1    128.377632 MHz
NUC1    11B
P1      10.00 usec
PLW1    52.00000000 W

===== CHANNEL f2 =====
SFO2    400.1334008 MHz
NUC2    1H
CPDPRG2 waltz16
PCPD2   90.00 usec
PLW2    13.00000000 W
PLW12   0.36111000 W

F2 - Processing parameters
SI      32768
SF      128.3776161 MHz
WDW     EM
SSB     0
LB      10.00 Hz
GB      0
PC      1.40
  
```

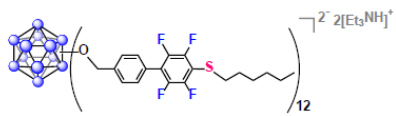


<sup>19</sup>F NMR



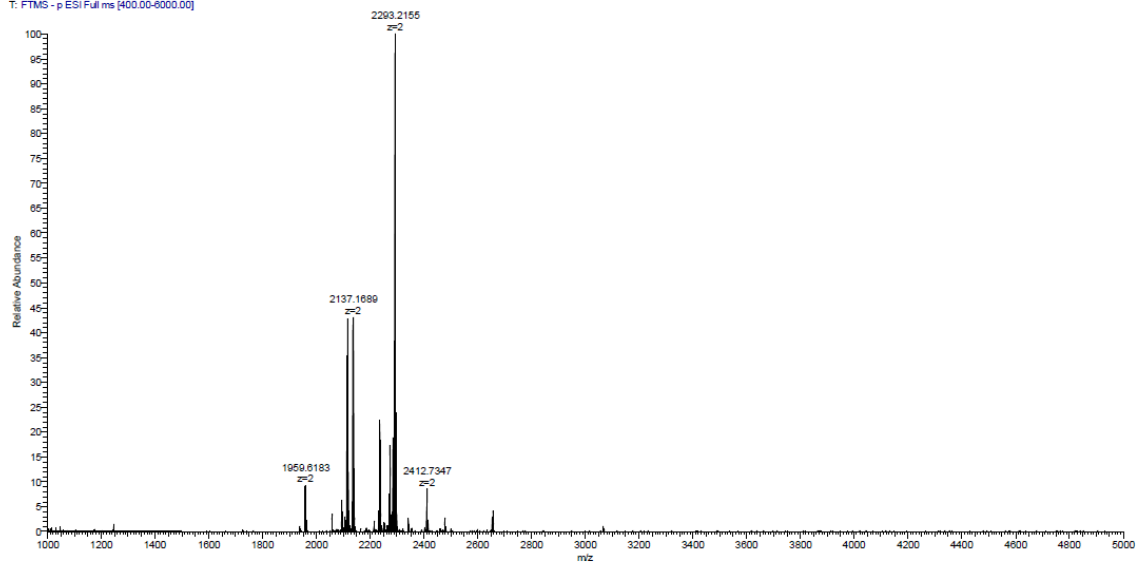
Current Data Parameters  
 NAME Jan26-2016  
 EXPNO 42  
 PROCNO 1  
 F2 - Acquisition Parameters  
 Date\_ 20160126  
 Time 13.05  
 INSTRUM av400  
 PROBHD 5 mm PABBO BB/  
 PULPROG zgpg30  
 TD 262144  
 SOLVENT CD3CN  
 NS 64  
 DS 0  
 SWH 150000.000 Hz  
 FIDRES 0.572205 Hz  
 AQ 0.8738133 sec  
 RG 189.85  
 DW 3.333 usec  
 DE 6.50 usec  
 TE 299.0 K  
 D1 2.00000000 sec  
 TDO 1  
 ===== CHANNEL f1 =====  
 SFO1 376.4983660 MHz  
 NUC1 19F  
 P1 14.50 usec  
 PLW1 17.00000000 W  
 F2 - Processing parameters  
 SI 262144  
 SF 376.4983660 MHz  
 WDW EM  
 SSB 0  
 LB 1.00 Hz  
 GB 0  
 PC 1.00

Small impurities are present due to the commercial 1-hexanethiol used (95% pure).

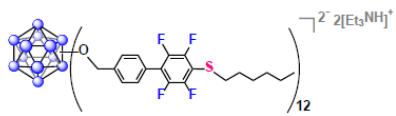


## Q Exactive High-Res Mass Spec

3a #1-26 RT: 0.01-0.22 AV: 26 NL: 6.99E8  
T: FTMS - p-ESI Full ms [400.00-6000.00]

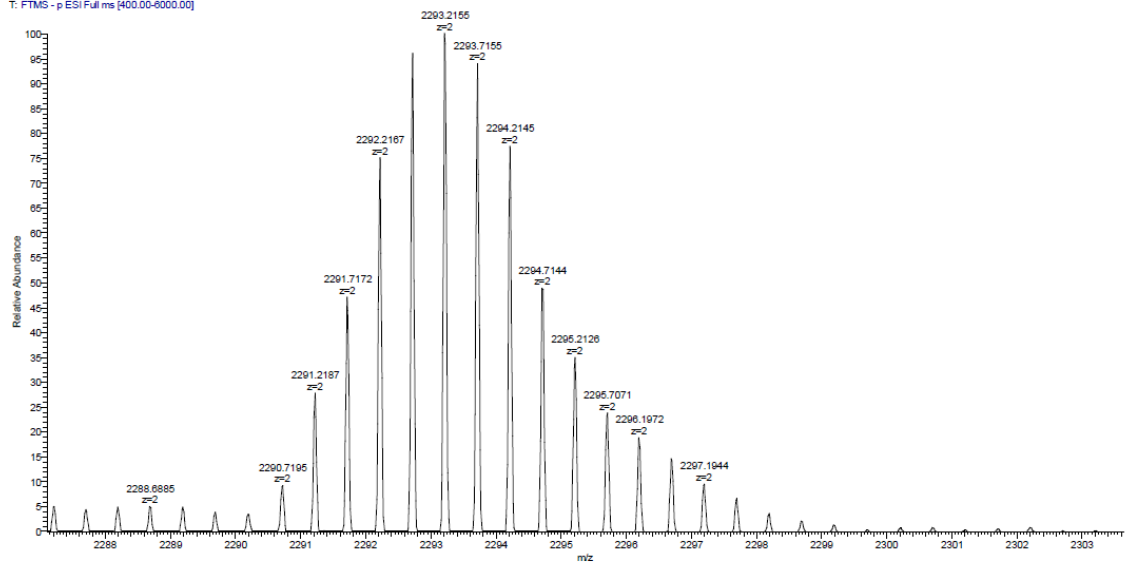


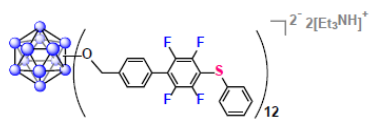




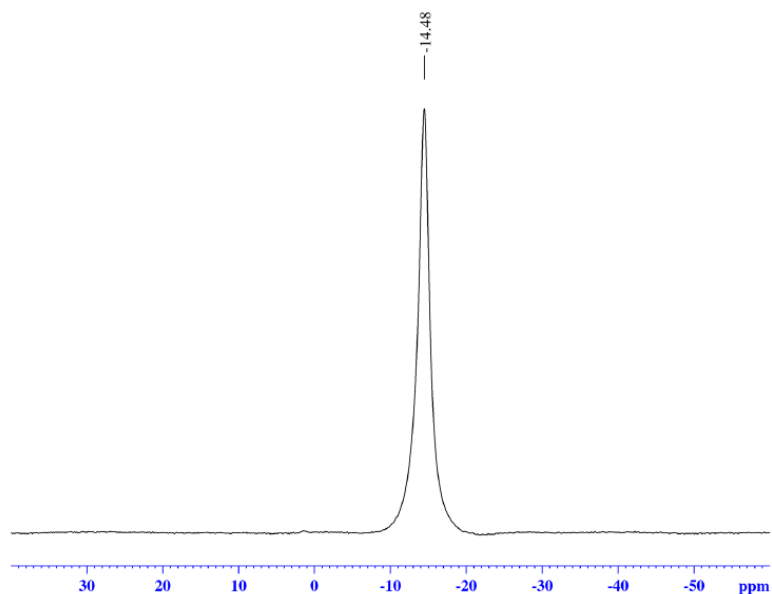
## Q Exactive High-Res Mass Spec

3a #1-26 RT: 0.01-0.22 AV: 26 NL: 6.99E8  
T: FTMS - p-ESI Full ms [400.00-6000.00]





*in situ*  $^{11}\text{B}$  NMR



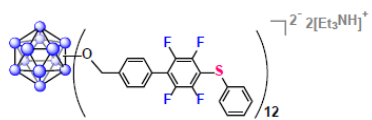
```

Current Data Parameters
NAME      0119
EXPNO    131
PROCNO   1

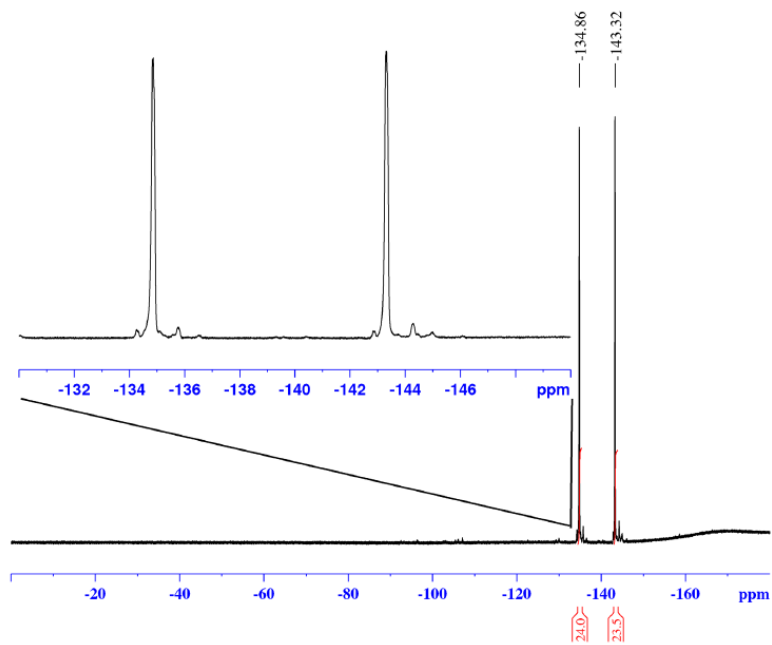
F2 - Acquisition Parameters
Date_    20160119
Time     19.39
INSTRUM  av400
PROBHD   5 mm PABBO BB/
PULPROG  zg
TD        5096
SOLVENT  None
NS        1024
DS        0
SWH       51020.406 Hz
FIDRES    10.011854 Hz
AQ        0.0499408 sec
RG        189.85
DW        9.800 usec
DE        6.50 usec
TE        299.0 K
D1        0.05000000 sec
TDO       1

===== CHANNEL f1 =====
SFO1     128.3776052 MHz
NUC1     11B
P1       10.00 usec
PLW1     52.00000000 W

F2 - Processing parameters
SI       32768
SF       128.3776161 MHz
WDW      EM
SSB      0
LB       10.00 Hz
GB       0
PC       1.40
  
```



*in situ*  $^{19}\text{F}$  NMR



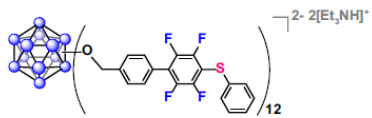
```

Current Data Parameters
NAME          0119
EXPNO         130
PROCNO        1

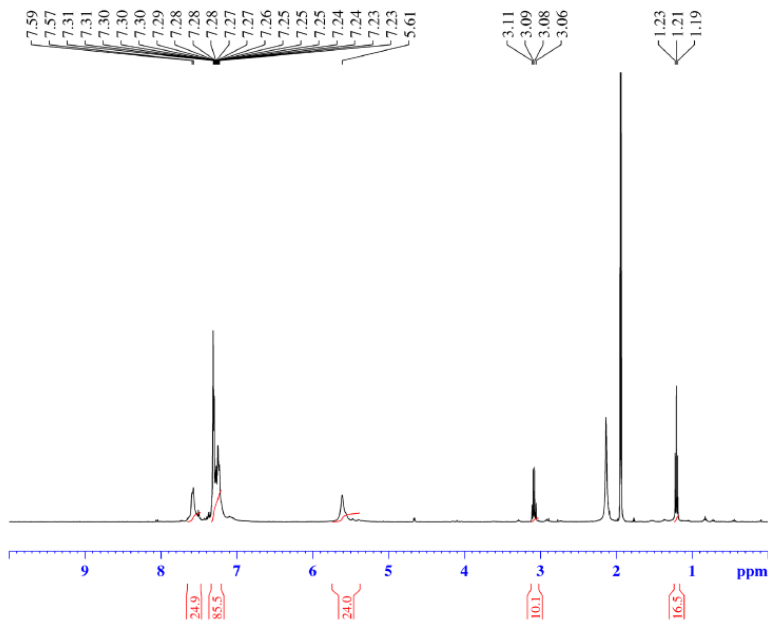
F2 - Acquisition Parameters
Date_         20160119
Time          19.35
INSTRUM       av400
PROBHD        5 mm PABBO BB/
PULPROG       zgpg30
TD            262144
SOLVENT       None
NS            64
DS            0
SWH           150000.000 Hz
FIDRES        0.572205 Hz
AQ            0.8738133 sec
RG            189.85
DW            3.333 usec
DE            6.50 usec
TE            299.0 K
D1            2.00000000 sec
TD0           1

===== CHANNEL f1 =====
SFO1          376.4983660 MHz
NUC1          19F
P1            14.50 usec
PLW1          17.00000000 W

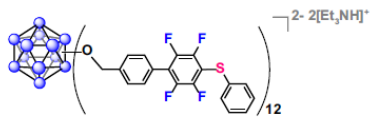
F2 - Processing parameters
SI            262144
SF            376.4983660 MHz
WDW           EM
SSB           0
LB            1.00 Hz
GB            0
PC            1.00
  
```



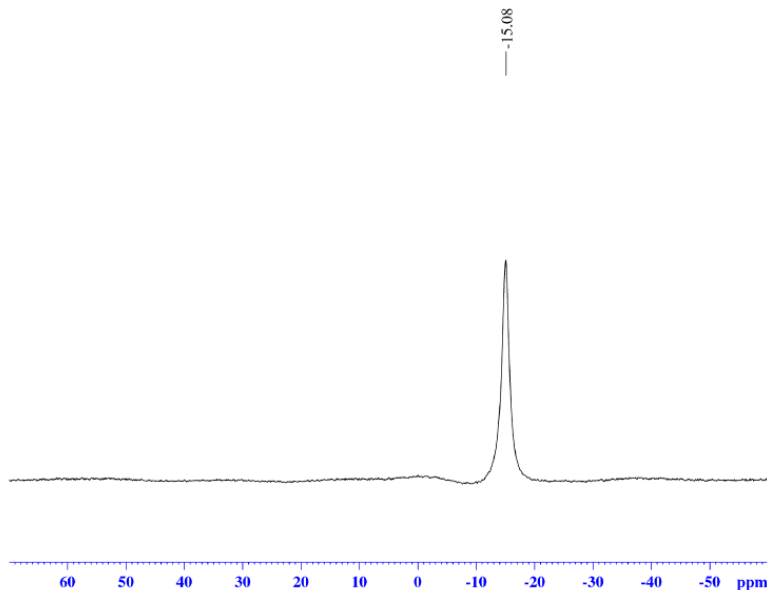
<sup>1</sup>H NMR



Current Data Parameters  
 NAME Jan22-2016  
 EXPNO 71  
 PROCNO 1  
 F2 - Acquisition Parameters  
 Date\_ 20160122  
 Time 15.13  
 INSTRUM av400  
 PROBHD 5 mm PABBO BB/  
 PULPROG zg30  
 TD 128204  
 SOLVENT CD3CN  
 NS 32  
 DS 0  
 SWH 8012.820 Hz  
 FIDRES 0.062501 Hz  
 AQ 7.9999294 sec  
 RG 189.85  
 DW 62.400 usec  
 DE 6.50 usec  
 TE 299.0 K  
 D1 5.00000000 sec  
 TDO 1  
 ===== CHANNEL f1 =====  
 SFO1 400.1324008 MHz  
 NUC1 1H  
 P1 15.00 usec  
 PLW1 13.00000000 W  
 F2 - Processing parameters  
 SI 65536  
 SF 400.1300114 MHz  
 WDW EM  
 SSB 0  
 LB 0.30 Hz  
 GB 0  
 PC 1.00



<sup>11</sup>B {<sup>1</sup>H} NMR



```

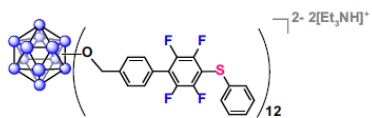
Current Data Parameters
NAME      Jan23-2016
EXPNO    70
PROCNO   1

F2 - Acquisition Parameters
Date_    20160122
Time     15.05
INSTRUM  av400
PROBHD   5 mm PABBO BB/
PULPROG  zgpg30
TD       5096
SOLVENT  CD3CN
NS       1024
DS       0
SWH      51020.406 Hz
FIDRES   10.011854 Hz
AQ       0.0499405 sec
RG       189.85
DW       9.500 usec
DE       6.50 usec
TE       299.0 K
D1       0.0500000 sec
D11      0.0300000 sec
TDO      1

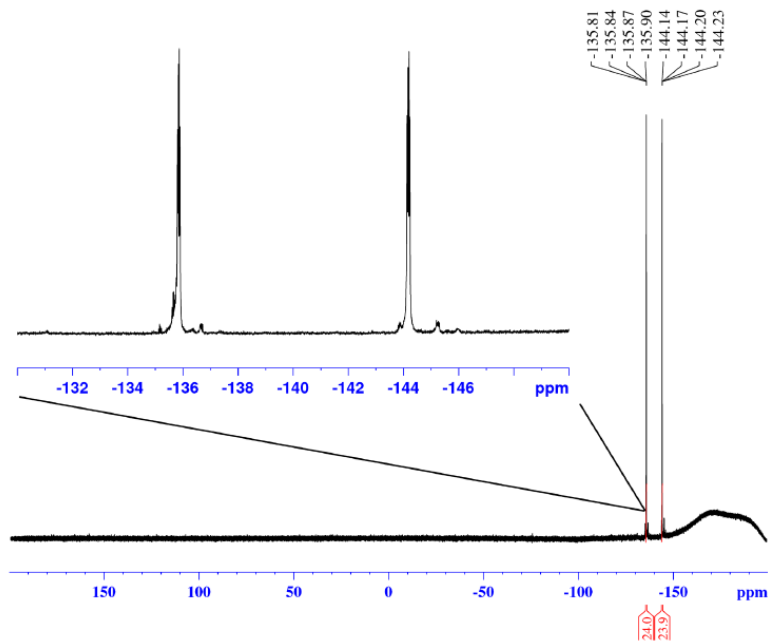
===== CHANNEL f1 =====
SFO1    128.377632 MHz
NUC1     11B
P1       10.00 usec
PLW1    52.00000000 W

===== CHANNEL f2 =====
SFO2    400.1334008 MHz
NUC2     1H
CPDPRG2  waltz16
PCPD2    90.00 usec
PLW2    13.00000000 W
PLW12   0.36111000 W

F2 - Processing parameters
SI       32768
SF       128.3776161 MHz
WDW      EM
SSB      0
LB       10.00 Hz
GB       0
PC       1.40
  
```

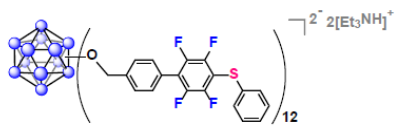


<sup>19</sup>F NMR



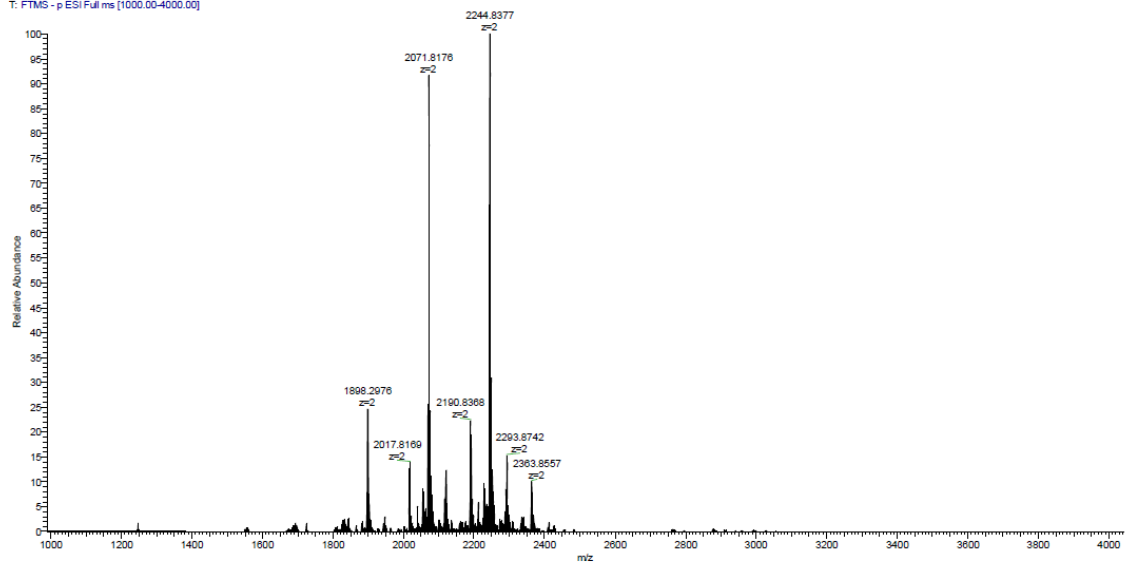
-135.81  
-135.84  
-135.87  
-135.90  
-144.14  
-144.17  
-144.20  
-144.23

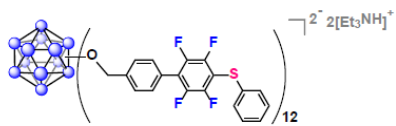
Current Data Parameters  
 NAME Jan22-2016  
 EXPNO 72  
 PROCNO 1  
 F2 - Acquisition Parameters  
 Date\_ 20160122  
 Time 15.17  
 INSTRUM av400  
 PROBHD 5 mm PABBO BB/  
 PULPROG zgpg30  
 TD 262144  
 SOLVENT CD3CN  
 NS 64  
 DS 0  
 SWH 150000.000 Hz  
 FIDRES 0.572205 Hz  
 AQ 0.8738133 sec  
 RG 189.85  
 DW 3.333 usec  
 DE 6.50 usec  
 TE 299.0 K  
 D1 2.00000000 sec  
 TDO 1  
 ===== CHANNEL f1 =====  
 SFO1 376.4983660 MHz  
 NUC1 19F  
 P1 14.50 usec  
 PLW1 17.00000000 W  
 F2 - Processing parameters  
 SI 262144  
 SF 376.4983660 MHz  
 WDW EM  
 SSB 0  
 LB 1.00 Hz  
 GB 0  
 PC 1.00



## Q Exactive High-Res Mass Spec

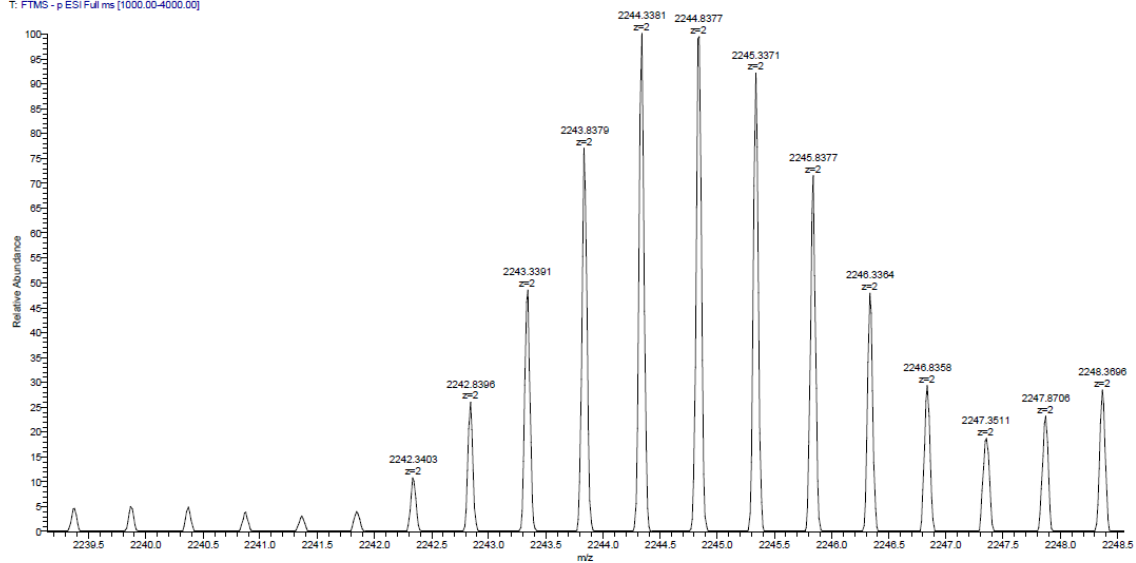
3b 1-4k #1-19 RT: 0.01-0.16 AV: 19 NL: 1.40E7  
T: FTMS - p-ESI Full.ms [1000.00-4000.00]



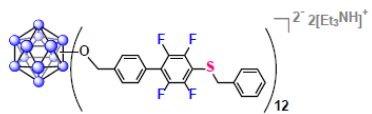


## Q Exactive High-Res Mass Spec

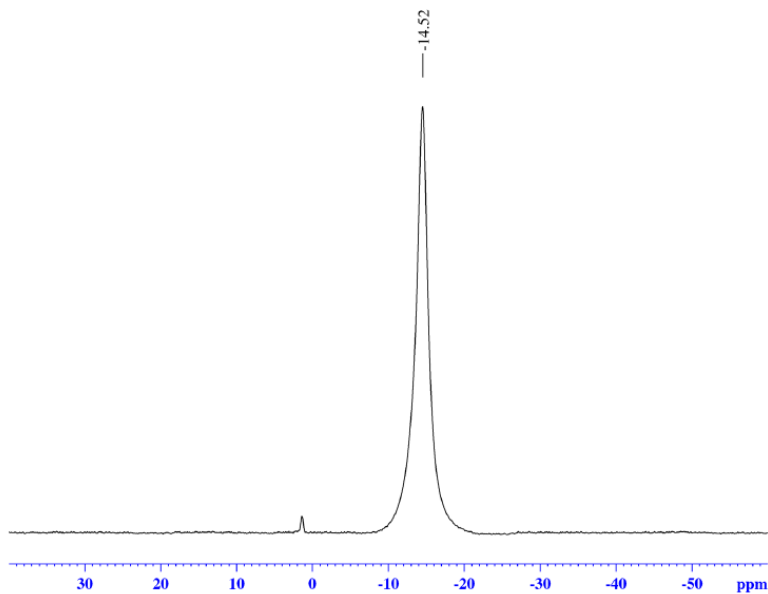
3b 1-4k #1-19 RT: 0.01-0.16 AV: 19 NL: 1.40E7  
T: FTMS - p-ESI Full.ms [1000.00-4000.00]







*in situ*  $^{11}B$  NMR



```

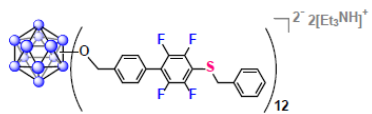
Current Data Parameters
NAME      0120
EXPNO    71
PROCNO    1

F2 - Acquisition Parameters
Date_    20160120
Time     18.53
INSTRUM  av400
PROBHD   5 mm PABBO BB/
PULPROG  zg
TD       5096
SOLVENT  None
NS       1024
DS       0
SWH      51020.406 Hz
FIDRES   10.011854 Hz
AQ       0.0499408 sec
RG       189.85
DW       9.800 usec
DE       6.50 usec
TE       299.0 K
D1       0.05000000 sec
TDO      1

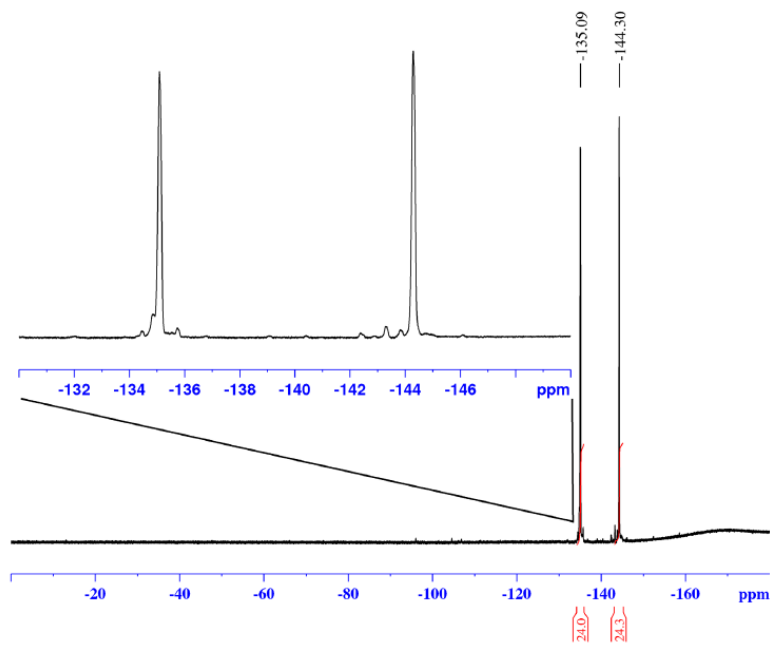
===== CHANNEL f1 =====
SFO1    128.3776052 MHz
NUC1     11B
P1       10.00 usec
PLW1    52.00000000 W

F2 - Processing parameters
SI       32768
SF       128.3776161 MHz
WDW      EM
SSB      0
LB       10.00 Hz
GB       0
PC       1.40

```



*in situ*  $^{19}\text{F}$  NMR



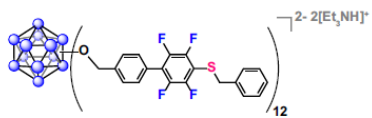
```

Current Data Parameters
NAME          0120
EXPNO         70
PROCNO        1

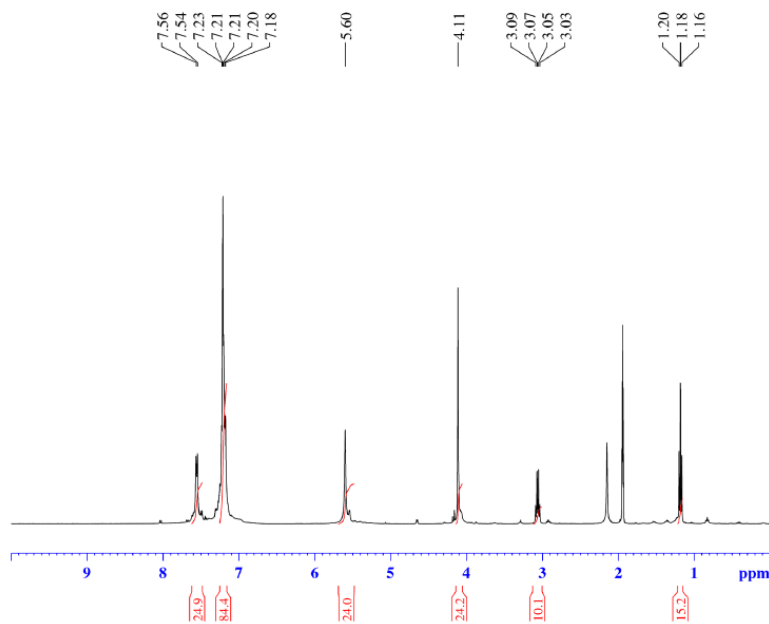
F2 - Acquisition Parameters
Date_         20160120
Time          18.50
INSTRUM       av400
PROBHD        5 mm PABBO BB/
PULPROG       zgpg30
TD            262144
SOLVENT       None
NS            64
DS            0
SWH           150000.000 Hz
FIDRES        0.572205 Hz
AQ            0.8738133 sec
RG            189.85
DW            3.333 usec
DE            6.50 usec
TE            299.0 K
D1            2.00000000 sec
TD0           1

===== CHANNEL f1 =====
SF01          376.4983660 MHz
NUC1          19F
P1            14.50 usec
PLW1          17.00000000 W

F2 - Processing parameters
SI            262144
SF            376.4983660 MHz
WDW           EM
SSB           0
LB            1.00 Hz
GB            0
PC            1.00
  
```



<sup>1</sup>H NMR

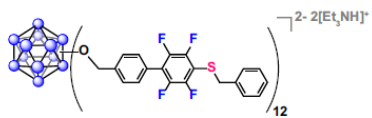


Current Data Parameters  
 NAME Jan26-2016  
 EXPNO 31  
 PROCNO 1

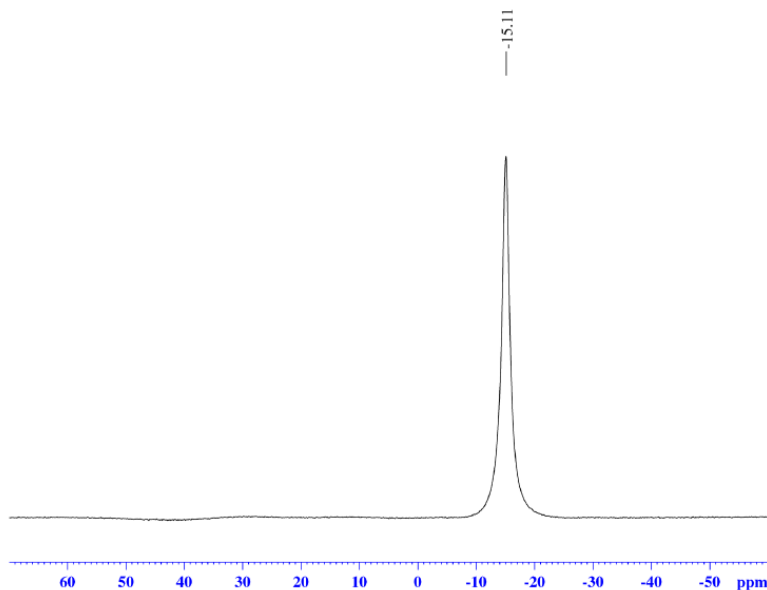
F2 - Acquisition Parameters  
 Date\_ 20160126  
 Time 12.36  
 INSTRUM av400  
 PROBHD 5 mm PABBO BB/  
 PULPROG zg30  
 TD 128204  
 SOLVENT CD3CN  
 NS 32  
 DS 0  
 SWH 8012.820 Hz  
 FIDRES 0.062501 Hz  
 AQ 7.999294 sec  
 RG 155.85  
 DW 62.400 usec  
 DE 6.50 usec  
 TE 299.0 K  
 D1 5.00000000 sec  
 TDO 1

===== CHANNEL f1 =====  
 SFO1 400.1324008 MHz  
 NUC1 1H  
 P1 15.00 usec  
 PLW1 13.00000000 W

F2 - Processing parameters  
 SI 63536  
 SF 400.1300113 MHz  
 WDW EM  
 SSB 0  
 LB 0.30 Hz  
 GB 0  
 PC 1.00



$^{11}\text{B}$   $\{^1\text{H}\}$  NMR



```

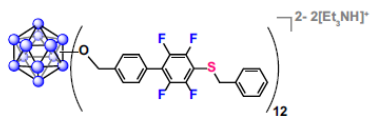
Current Data Parameters
NAME      Jan26-2016
EXPNO    30
PROCNO   1

F2 - Acquisition Parameters
Date_    20160126
Time     12.28
INSTRUM  av400
PROBHD   5 mm PABBO BB/
PULPROG  zgpg30
TD       5096
SOLVENT  CD3CN
NS       1024
DS       0
SWH      51020.406 Hz
FIDRES   10.011854 Hz
AQ       0.0499405 sec
RG       189.85
DW       9.500 usec
DE       6.50 usec
TE       299.0 K
D1       0.0500000 sec
D11      0.0300000 sec
TDO      1

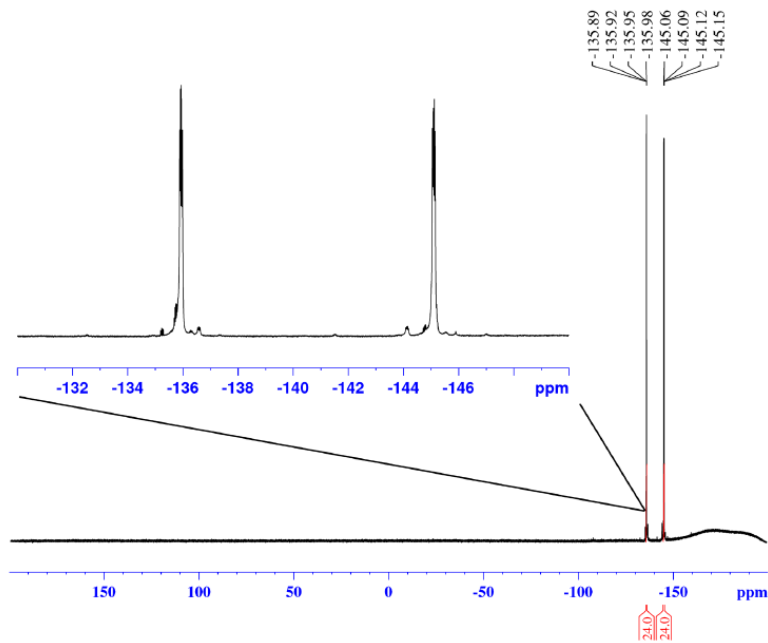
===== CHANNEL f1 =====
SFO1    128.377632 MHz
NUC1     11B
P1       10.00 usec
PLW1    52.00000000 W

===== CHANNEL f2 =====
SFO2    400.1334068 MHz
NUC2     1H
CPDPRG2  waltz16
PCPD2    90.00 usec
PLW2    13.00000000 W
PLW12   0.36111000 W

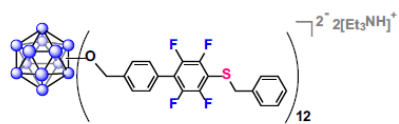
F2 - Processing parameters
SI       32768
SF       128.3776161 MHz
WDW      EM
SSB      0
LB       10.00 Hz
GB       0
PC       1.40
  
```



<sup>19</sup>F NMR

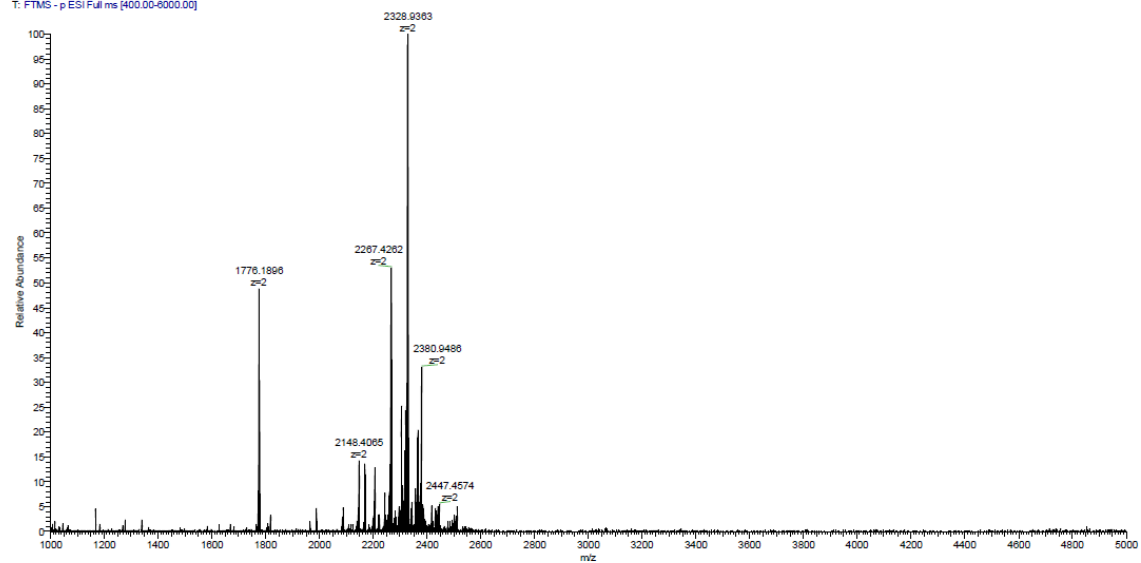


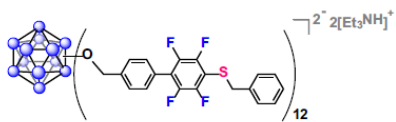
Current Data Parameters  
 NAME Jan26-2016  
 EXPNO 32  
 PROCNO 1  
 F2 - Acquisition Parameters  
 Date\_ 20160126  
 Time 12.40  
 INSTRUM av400  
 PROBHD 5 mm PABBO BB/  
 PULPROG zgpg30  
 TD 262144  
 SOLVENT CD3CN  
 NS 64  
 DS 0  
 SWH 150000.000 Hz  
 FIDRES 0.572205 Hz  
 AQ 0.8738133 sec  
 RG 189.85  
 DW 3.333 usec  
 DE 6.50 usec  
 TE 299.0 K  
 D1 2.00000000 sec  
 TDO 1  
 ===== CHANNEL f1 =====  
 SFO1 376.4983660 MHz  
 NUC1 19F  
 P1 14.50 usec  
 PLW1 17.00000000 W  
 F2 - Processing parameters  
 SI 262144  
 SF 376.4983660 MHz  
 WDW EM  
 SSB 0  
 LB 1.00 Hz  
 GB 0  
 PC 1.00



## Q Exactive High-Res Mass Spec

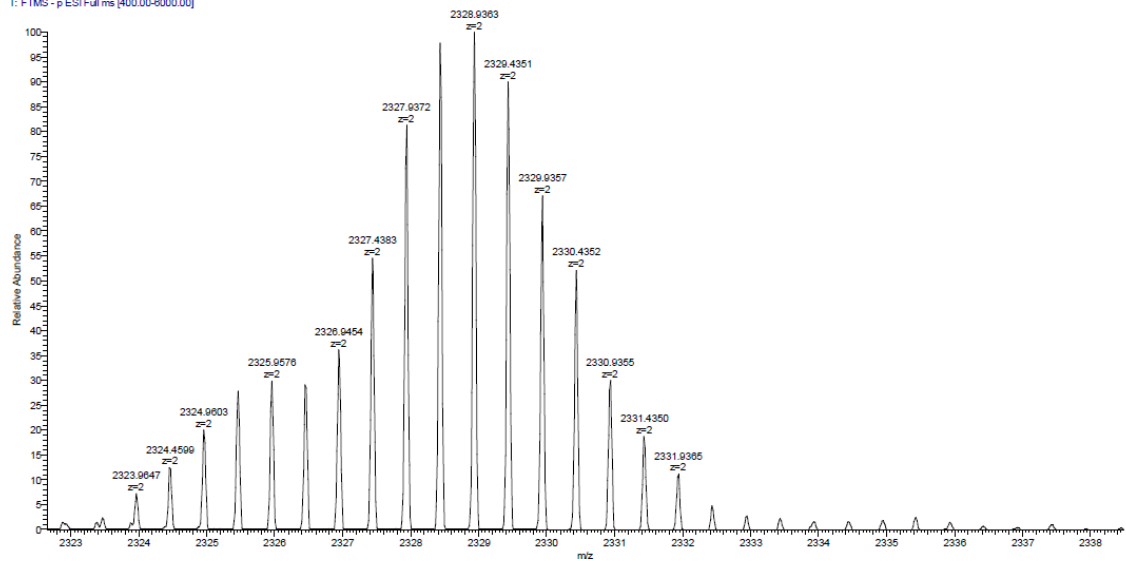
3e #1-16 RT: 0.01-0.14 AV: 16 NL: 1.92E6  
T: FTMS - p-ESI Full.ms [400.00-6000.00]

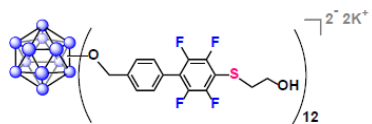




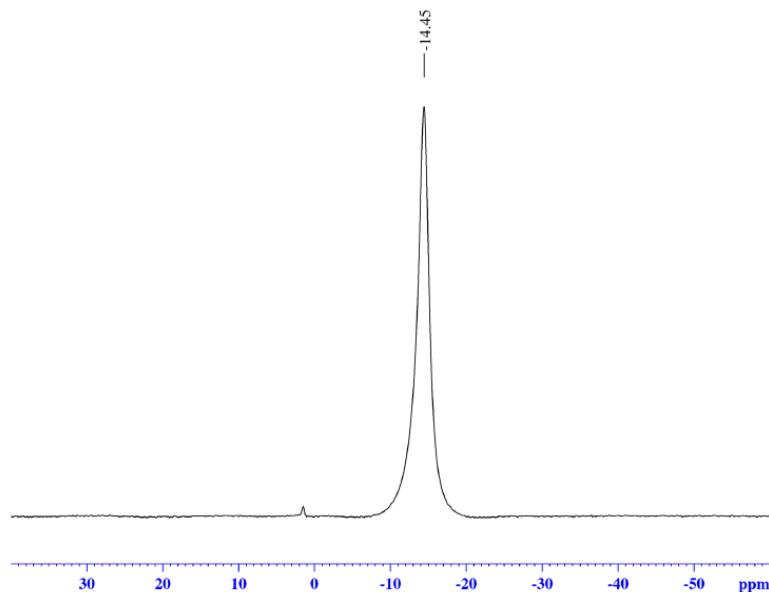
## Q Exactive High-Res Mass Spec

3e #1-16 RT: 0.01-0.14 AV: 16 NL: 1.92E6  
T: FTMS - p-ESI Full ms [400.00-6000.00]





*in situ* <sup>11</sup>B NMR



```

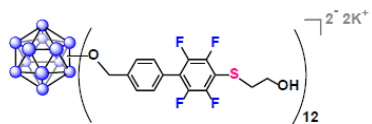
Current Data Parameters
NAME      0110
EXPNO    41
PROCNO   1

F2 - Acquisition Parameters
Date_    20160110
Time     20.38
INSTRUM  av400
PROBHD   5 mm PABBO BB/
PULPROG  zg
TD        5096
SOLVENT  None
NS        1024
DS         0
SWH       51020.406 Hz
FIDRES    10.011854 Hz
AQ        0.0499408 sec
RG         189.85
DW         9.800 usec
DE         6.50 usec
TE         299.0 K
D1         0.05000000 sec
TD0        1

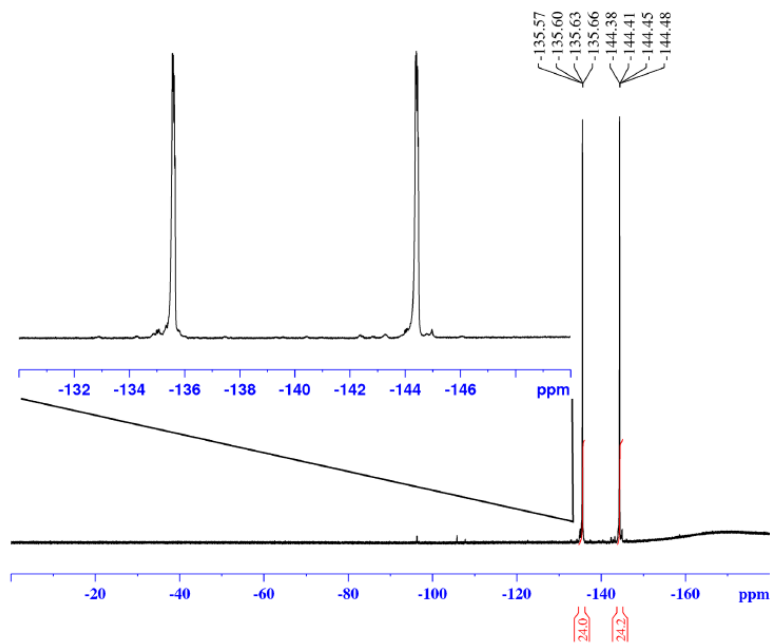
===== CHANNEL f1 =====
SFO1    128.3776052 MHz
NUC1     11B
P1       10.00 usec
PLW1    52.00000000 W

F2 - Processing parameters
SI       32768
SF       128.3776161 MHz
WDW      EM
SSB      0
LB       10.00 Hz
GB       0
PC       1.40
  
```





*in situ*  $^{19}\text{F}$  NMR

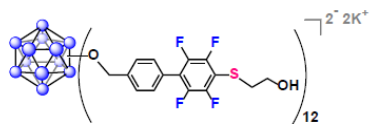


Current Data Parameters  
 NAME 0110  
 EXPNO 40  
 PROCNO 1

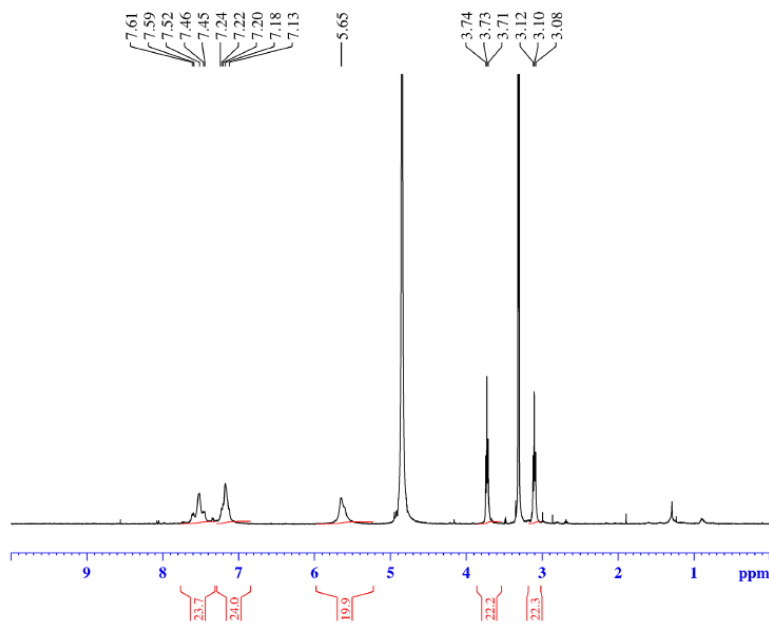
F2 - Acquisition Parameters  
 Date\_ 20160110  
 Time 20.34  
 INSTRUM av400  
 PROBHD 5 mm PABBO BB/  
 PULPROG zgpg30  
 TD 262144  
 SOLVENT None  
 NS 64  
 DS 0  
 SWH 150000.000 Hz  
 FIDRES 0.572205 Hz  
 AQ 0.8738133 sec  
 RG 189.85  
 DW 3.333 usec  
 DE 6.50 usec  
 TE 299.0 K  
 D1 2.00000000 sec  
 TDO 1

===== CHANNEL f1 =====  
 SFO1 376.4983660 MHz  
 NUC1  $^{19}\text{F}$   
 P1 14.50 usec  
 PLW1 17.00000000 W

F2 - Processing parameters  
 SI 262144  
 SF 376.4983660 MHz  
 WDW EM  
 SSB 0  
 LB 1.00 Hz  
 GB 0  
 PC 1.00



<sup>1</sup>H NMR



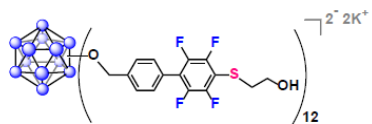
```

Current Data Parameters
NAME      G2 2ME 0111 0110 (MeOD)
EXPNO    1160
PROCNO   1

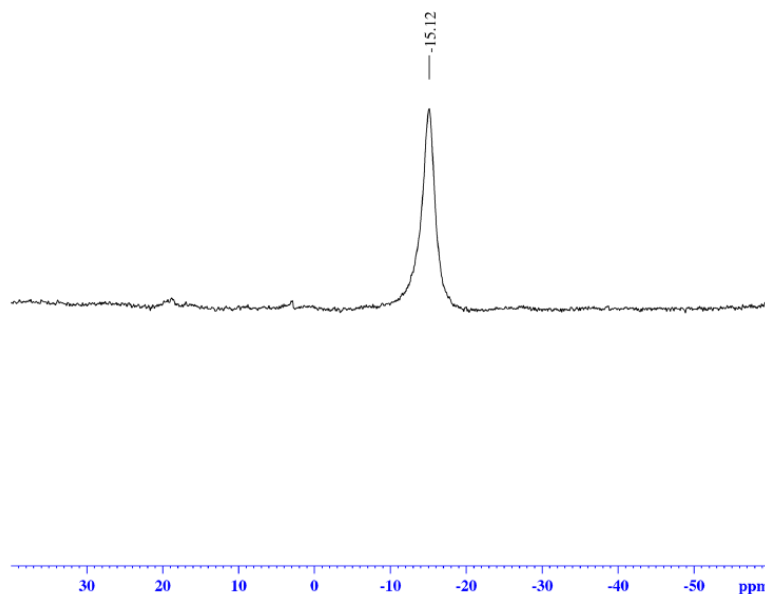
F2 - Acquisition Parameters
Date_    20160112
Time     16.27
INSTRUM  av400
PROBHD   5 mm PABBO BB/
PULPROG  zg30
TD       52882
SOLVENT  MeOD
NS       32
DS       0
SWH      8012.820 Hz
FIDRES   0.151523 Hz
AQ       3.2998369 sec
RG       155.85
DW       62.400 usec
DE       6.50 usec
TE       299.0 K
D1       2.00000000 sec
TDO     1

===== CHANNEL f1 =====
SFO1    400.1324008 MHz
NUC1     1H
P1      15.00 usec
PLW1    13.00000000 W

F2 - Processing parameters
SI      65536
SF      400.1300078 MHz
WDW     EM
SSB     0
LB      0.30 Hz
GB      0
PC      1.00
  
```



$^{11}\text{B}$  NMR

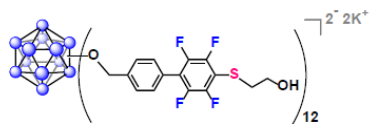


Current Data Parameters  
 NAME G2 2ME 0111 0110 (MeOD)  
 EXPNO 1162  
 PROCNO 1

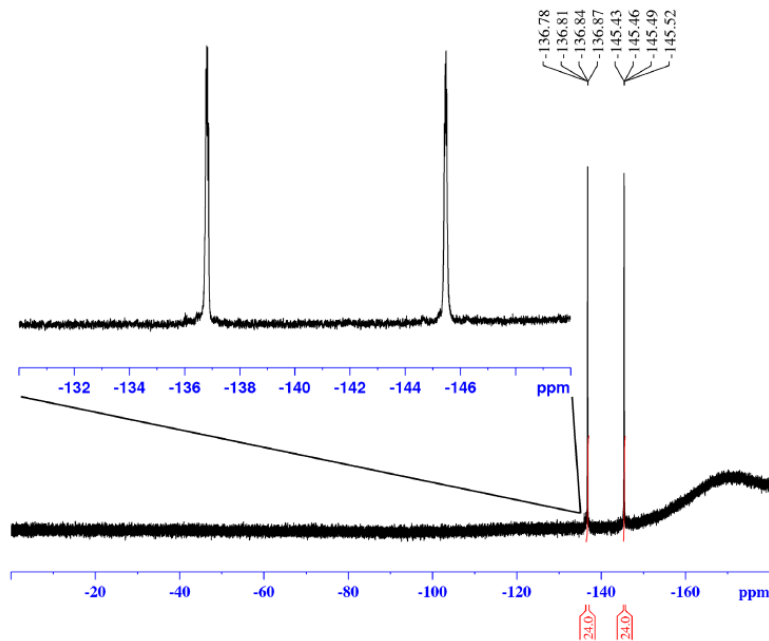
F2 - Acquisition Parameters  
 Date\_ 20160112  
 Time 16.35  
 INSTRUM av400  
 PROBHD 5 mm PABBO BB/  
 PULPROG zg  
 TD 5096  
 SOLVENT MeOD  
 NS 1024  
 DS 0  
 SWH 51020.406 Hz  
 FIDRES 10.011854 Hz  
 AQ 0.0499408 sec  
 RG 189.85  
 DW 9.800 usec  
 DE 6.50 usec  
 TE 299.0 K  
 D1 0.05000000 sec  
 TDO 1

===== CHANNEL f1 =====  
 SFO1 128.3776052 MHz  
 NUC1  $^{11}\text{B}$   
 P1 10.00 usec  
 PLW1 52.00000000 W

F2 - Processing parameters  
 SI 32768  
 SF 128.3776161 MHz  
 WDW EM  
 SSB 0  
 LB 10.00 Hz  
 GB 0  
 PC 1.40



<sup>19</sup>F NMR

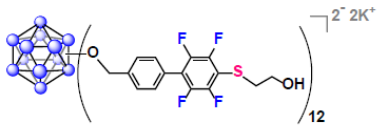


Current Data Parameters  
 NAME G2 2ME 0111 0110 (MeOD)  
 EXPNO 1161  
 PROCNO 1

F2 - Acquisition Parameters  
 Date\_ 20160112  
 Time 16.32  
 INSTRUM av400  
 PROBHD 5 mm PABBO BB/  
 PULPROG zgpg30  
 TD 262144  
 SOLVENT MeOD  
 NS 64  
 DS 0  
 SWH 150000.000 Hz  
 FIDRES 0.572205 Hz  
 AQ 0.8738133 sec  
 RG 189.85  
 DW 3.333 usec  
 DE 6.50 usec  
 TE 299.0 K  
 D1 2.00000000 sec  
 TDO 1

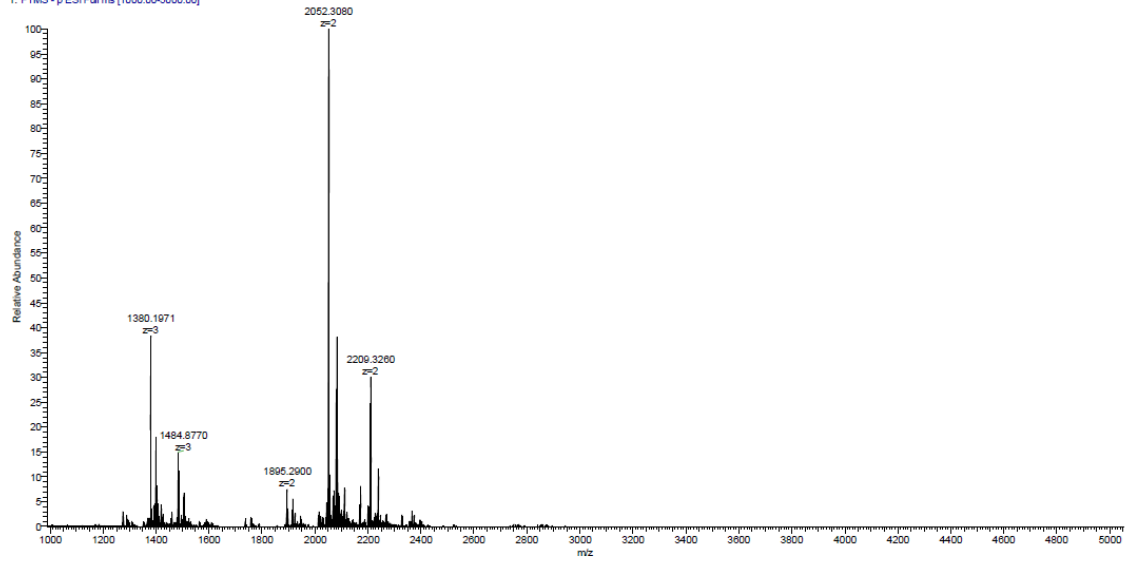
===== CHANNEL f1 =====  
 SF01 376.4983660 MHz  
 NUC1 19F  
 P1 14.50 usec  
 PLW1 17.00000000 W

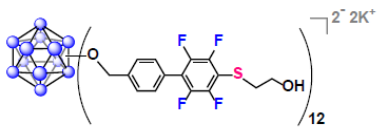
F2 - Processing parameters  
 SI 262144  
 SF 376.4983660 MHz  
 WDW EM  
 SSB 0  
 LB 1.00 Hz  
 GB 0  
 PC 1.00



## Q Exactive High-Res Mass Spec

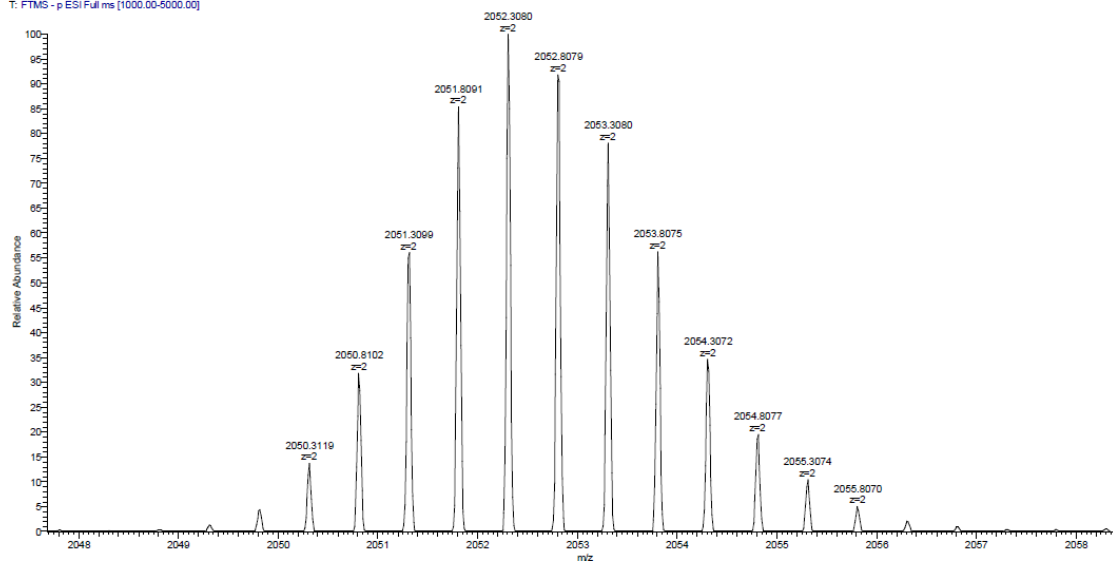
3d 1-6k #1-16 RT: 0.04-0.09 AV: 16 NL: 5.34E9  
T: FTMS - p-ESI Full.ms [1000.00-5000.00]

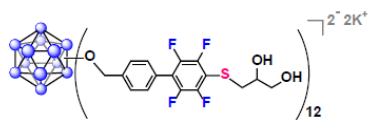




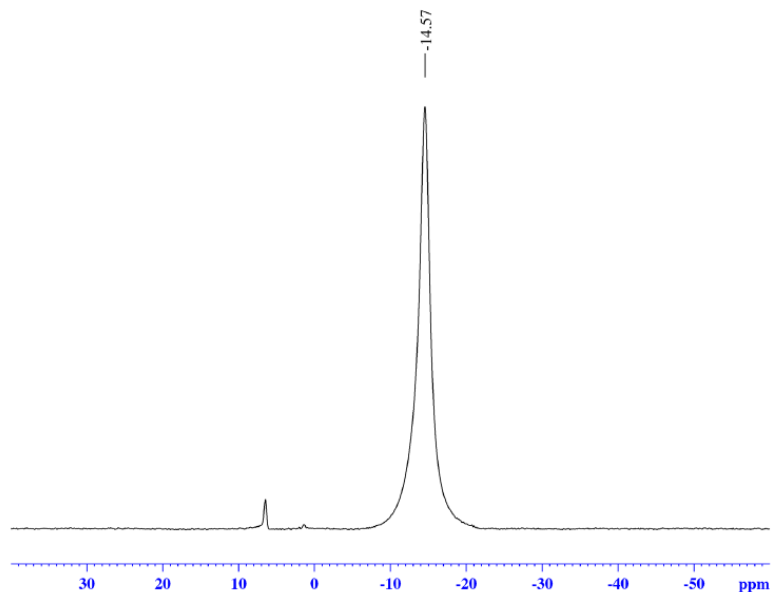
## Q Exactive High-Res Mass Spec

3d 1-6k #1-16 RT: 0.04-0.09 AV: 10 NL: 5.34E9  
T: FTMS - p-ESI Full.ms [1000.00-5000.00]





*in situ*  $^{11}\text{B}$  NMR



```

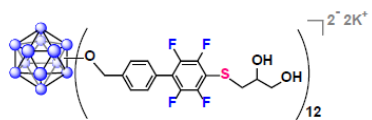
Current Data Parameters
NAME      0110
EXPNO    61
PROCNO    1

F2 - Acquisition Parameters
Date_    20160110
Time     20.56
INSTRUM  av400
PROBHD   5 mm PABBO BB/
PULPROG  zg
TD       5096
SOLVENT  None
NS       1024
DS       0
SWH      51020.406 Hz
FIDRES   10.011854 Hz
AQ       0.0499408 sec
RG       189.85
DW       9.800 usec
DE       6.50 usec
TE       299.0 K
D1       0.05000000 sec
TDO      1

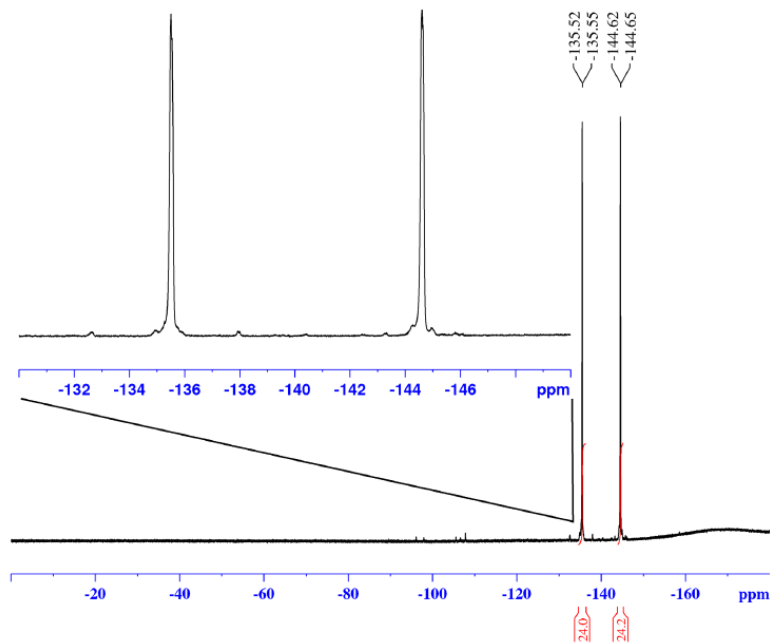
===== CHANNEL f1 =====
SFO1    128.3776052 MHz
NUC1     11B
P1      10.00 usec
PLW1    52.00000000 W

F2 - Processing parameters
SI      32768
SF      128.3776161 MHz
WDW     EM
SSB     0
LB      10.00 Hz
GB      0
PC      1.40

```



*in situ*  $^{19}\text{F}$  NMR



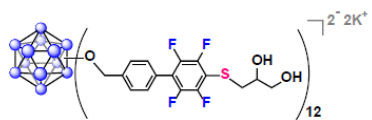
Current Data Parameters  
 NAME 0110  
 EXPNO 60  
 PROCNO 1

F2 - Acquisition Parameters  
 Date\_ 20160110  
 Time 20.53  
 INSTRUM av400  
 PROBHD 5 mm PABBO BB/  
 PULPROG zgpg30  
 TD 262144  
 SOLVENT None  
 NS 64  
 DS 0  
 SWH 150000.000 Hz  
 FIDRES 0.572205 Hz  
 AQ 0.8738133 sec  
 RG 189.85  
 DW 3.333 usec  
 DE 6.50 usec  
 TE 299.0 K  
 D1 2.0000000 sec  
 TDO 1

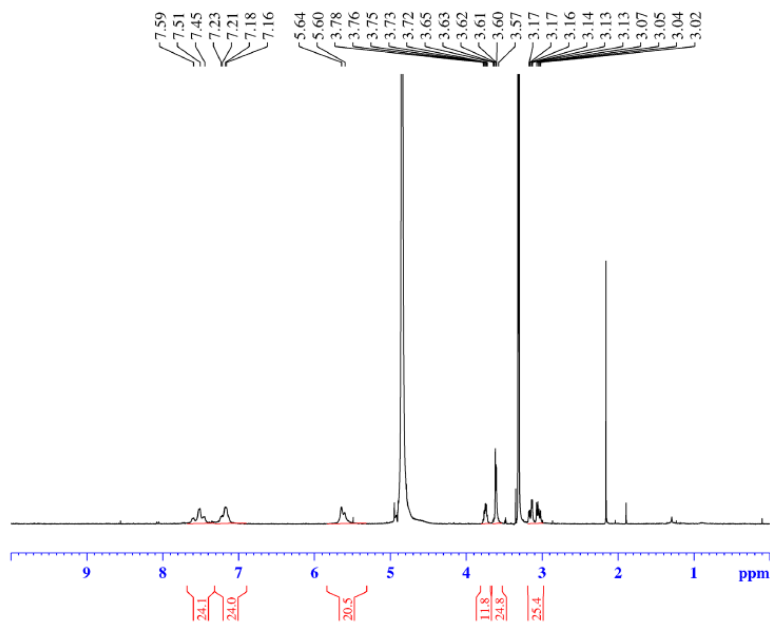
===== CHANNEL f1 =====  
 SFO1 376.4983660 MHz  
 NUC1  $^{19}\text{F}$   
 P1 14.50 usec  
 PLW1 17.00000000 W

F2 - Processing parameters  
 SI 262144  
 SF 376.4983660 MHz  
 WDW EM  
 SSB 0  
 LB 1.00 Hz  
 GB 0  
 PC 1.00





<sup>1</sup>H NMR

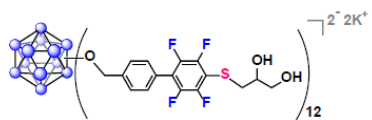


Current Data Parameters  
 NAME G2 Glycerol 0111 0110 (MeOD)  
 EXPNO 250  
 PROCNO 1

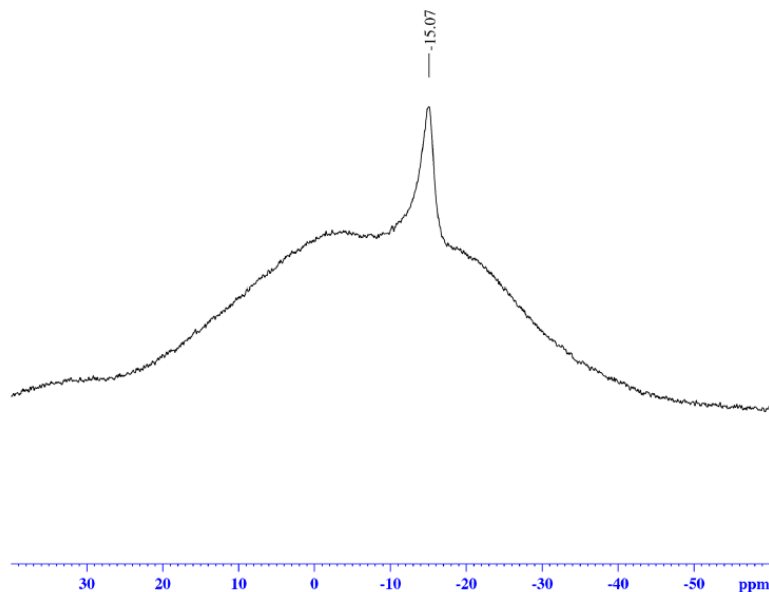
F2 - Acquisition Parameters  
 Date\_ 20160112  
 Time 22.11  
 INSTRUM av400  
 PROBHD 5 mm PABBO BB/  
 PULPROG zg30  
 TD 52882  
 SOLVENT MeOD  
 NS 32  
 DS 0  
 SWH 8012.820 Hz  
 FIDRES 0.151523 Hz  
 AQ 3.2998369 sec  
 RG 155.85  
 DW 62.400 usec  
 DE 6.50 usec  
 TE 299.0 K  
 D1 2.00000000 sec  
 TDO 1

===== CHANNEL f1 =====  
 SFO1 400.1324008 MHz  
 NUC1 1H  
 P1 15.00 usec  
 PLW1 13.00000000 W

F2 - Processing parameters  
 SI 65536  
 SF 400.1300077 MHz  
 WDW EM  
 SSB 0  
 LB 0.30 Hz  
 GB 0  
 PC 1.00



<sup>11</sup>B NMR

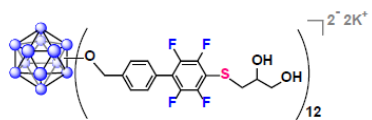


Current Data Parameters  
 NAME G2 Glycerol 0111 0110 (MeOD)  
 EXPNO 252  
 PROCNO 1

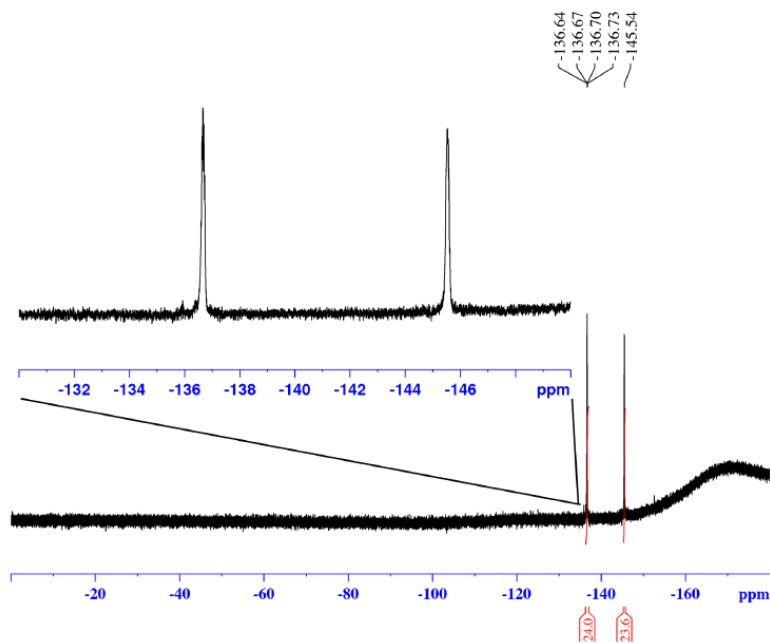
F2 - Acquisition Parameters  
 Date\_ 20160112  
 Time 22.18  
 INSTRUM av400  
 PROBHD 5 mm PABBO BB/  
 PULPROG zg  
 TD 5096  
 SOLVENT MeOD  
 NS 1024  
 DS 0  
 SWH 51020.406 Hz  
 FIDRES 10.011854 Hz  
 AQ 0.0499408 sec  
 RG 189.85  
 DW 9.800 usec  
 DE 6.50 usec  
 TE 299.0 K  
 D1 0.05000000 sec  
 TDO 1

===== CHANNEL f1 =====  
 SFO1 128.3776052 MHz  
 NUC1 11B  
 P1 10.00 usec  
 PLW1 52.00000000 W

F2 - Processing parameters  
 SI 32768  
 SF 128.3776161 MHz  
 WDW EM  
 SSB 0  
 LB 10.00 Hz  
 GB 0  
 PC 1.40



<sup>19</sup>F NMR

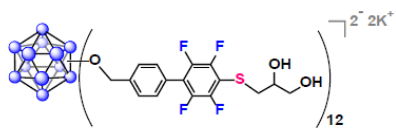


Current Data Parameters  
 NAME G2 Glycerol 0111 0110 (MeOD)  
 EXPNO 251  
 PROCNO 1

F2 - Acquisition Parameters  
 Date\_ 20160112  
 Time 22.15  
 INSTRUM av400  
 PROBHD 5 mm PABBO BB/  
 PULPROG zgpg30  
 TD 262144  
 SOLVENT MeOD  
 NS 64  
 DS 0  
 SWH 150000.000 Hz  
 FIDRES 0.572205 Hz  
 AQ 0.8738133 sec  
 RG 189.85  
 DW 3.333 usec  
 DE 6.50 usec  
 TE 299.0 K  
 D1 2.0000000 sec  
 TDO 1

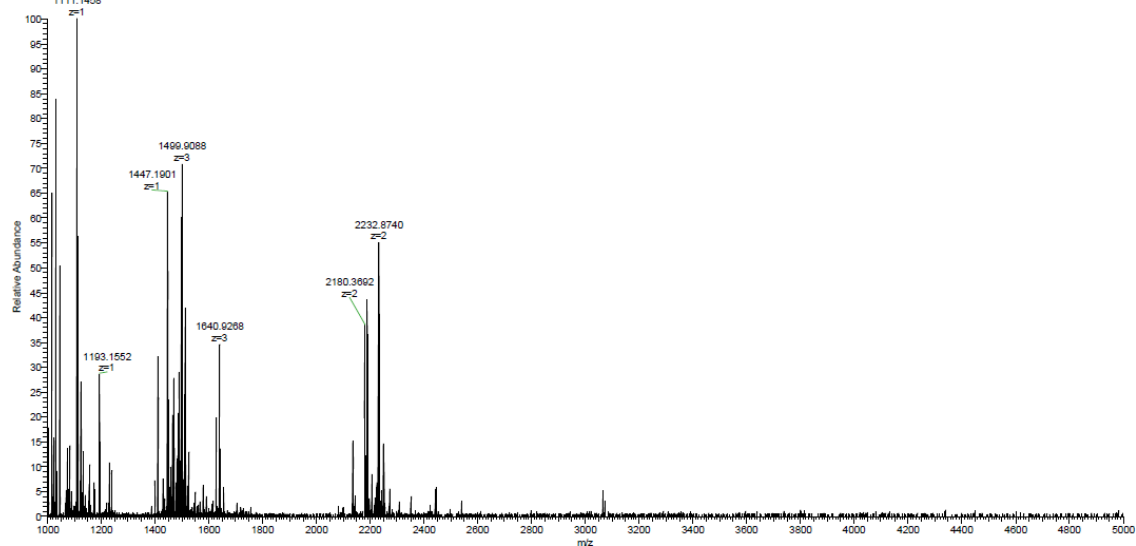
===== CHANNEL f1 =====  
 SFO1 376.4983660 MHz  
 NUC1 19F  
 P1 14.50 usec  
 PLW1 17.00000000 W

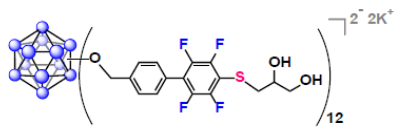
F2 - Processing parameters  
 SI 262144  
 SF 376.4983660 MHz  
 WDW EM  
 SSB 0  
 LB 1.00 Hz  
 GB 0  
 PC 1.00



## Q Exactive High-Res Mass Spec

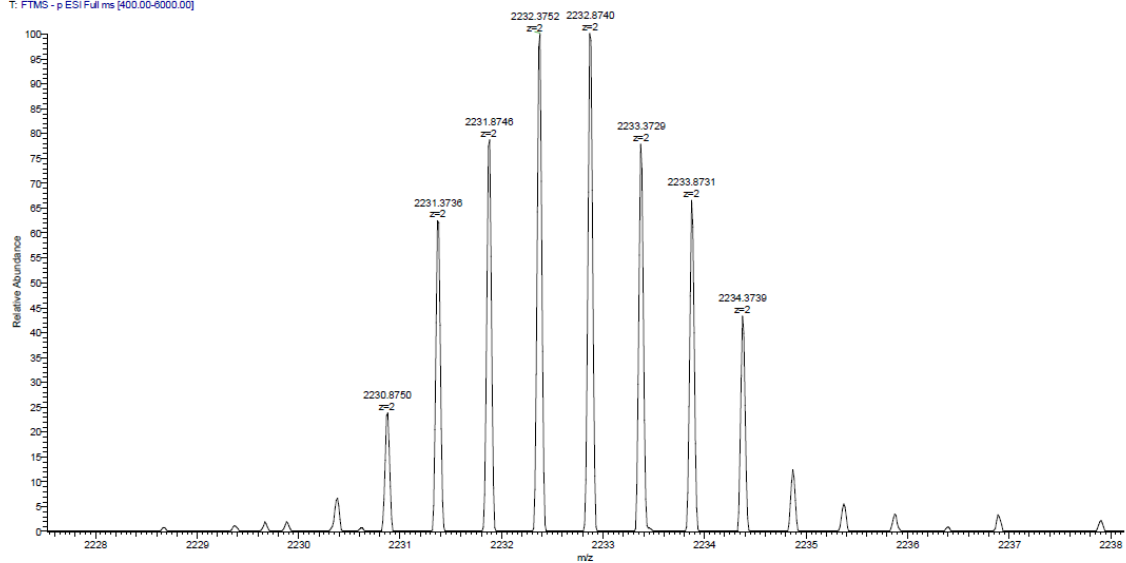
3e 0.4-6k #1-18 RT: 0.01-0.16 AV: 18 NL: 1.79E6  
T: FTMS - p-ESI Full ms [400.00-6000.00]  
1111.1458

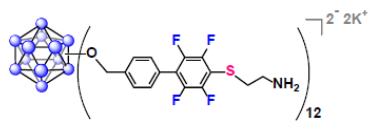




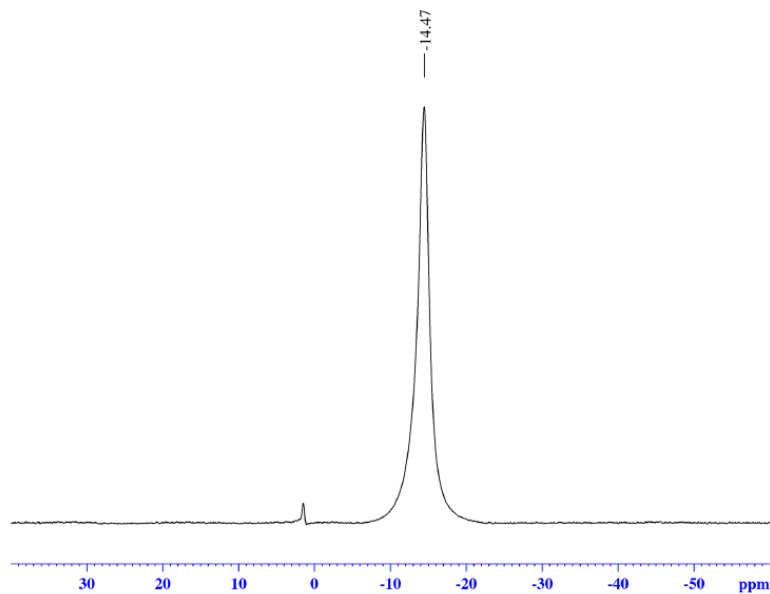
### Q Exactive High-Res Mass Spec

3e 0.4-0k #1-18 RT: 0.01-0.16 AV: 18 NL: 9.85E5  
T: FTMS - p-ESI Full ms [400.00-6000.00]





*in situ*  $^{11}\text{B}$  NMR



```

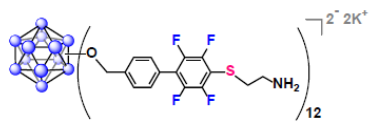
Current Data Parameters
NAME      0110
EXPNO     51
PROCNO    1

F2 - Acquisition Parameters
Date_     20160110
Time      20.47
INSTRUM   av400
PROBHD    5 mm PABBO BB/
PULPROG   zg
TD         5096
SOLVENT   None
NS         1024
DS         0
SWH        51020.406 Hz
FIDRES     10.011854 Hz
AQ         0.0499408 sec
RG         189.85
DW         9.800 usec
DE         6.50 usec
TE         299.0 K
D1         0.05000000 sec
TDO        1

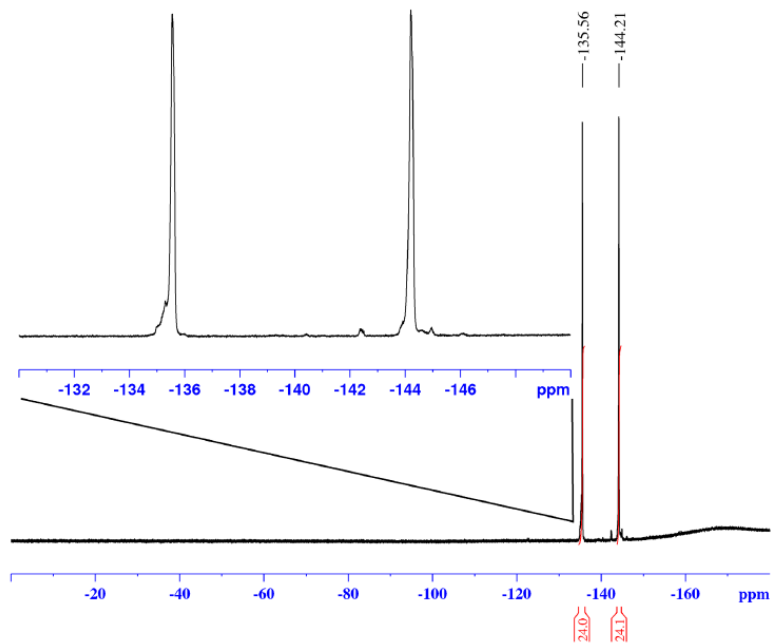
===== CHANNEL f1 =====
SFO1      128.3776052 MHz
NUC1       11B
P1         10.00 usec
PLW1      52.00000000 W

F2 - Processing parameters
SI         32768
SF         128.3776161 MHz
WDW        EM
SSB        0
LB         10.00 Hz
GB         0
PC         1.40

```



*in situ* <sup>19</sup>F NMR

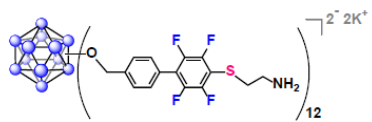


Current Data Parameters  
 NAME 0110  
 EXPNO 50  
 PROCNO 1

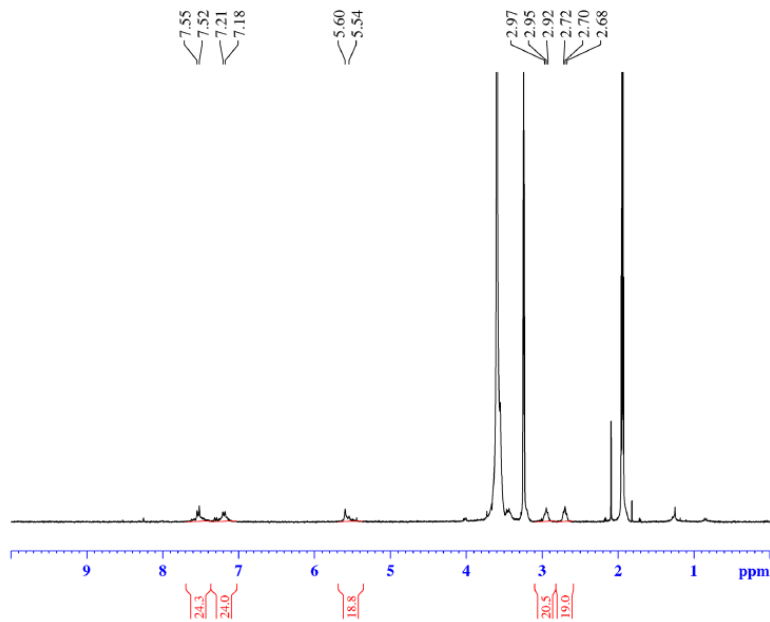
F2 - Acquisition Parameters  
 Date\_ 20160110  
 Time 20.44  
 INSTRUM av400  
 PROBHD 5 mm PABBO BB/  
 PULPROG zgpg30  
 TD 262144  
 SOLVENT None  
 NS 64  
 DS 0  
 SWH 150000.000 Hz  
 FIDRES 0.572205 Hz  
 AQ 0.8738133 sec  
 RG 189.85  
 DW 3.333 usec  
 DE 6.50 usec  
 TE 299.0 K  
 D1 2.00000000 sec  
 TDO 1

===== CHANNEL f1 =====  
 SFO1 376.4983660 MHz  
 NUC1 <sup>19</sup>F  
 P1 14.50 usec  
 PLW1 17.00000000 W

F2 - Processing parameters  
 SI 262144  
 SF 376.4983660 MHz  
 WDW EM  
 SSB 0  
 LB 1.00 Hz  
 GB 0  
 PC 1.00



<sup>1</sup>H NMR



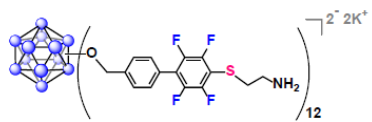
Current Data Parameters  
 NAME G2 CA 0112 0110 (ACN & MeOD)  
 EXPNO 3  
 PROCNO 1

F2 - Acquisition Parameters  
 Date\_ 20160113  
 Time 19.32  
 INSTRUM av300  
 PROBHD 5 mm PA1BBO BB-  
 PULPROG zg30  
 TD 65536  
 SOLVENT CD3CN  
 NS 32  
 DS 0  
 SWH 5995.204 Hz  
 FIDRES 0.071480 Hz  
 AQ 5.4657025 sec  
 RG 574.7  
 DW 83.400 usec  
 DE 6.00 usec  
 TE 297.8 K  
 D1 2.00000000 sec  
 TDO 1

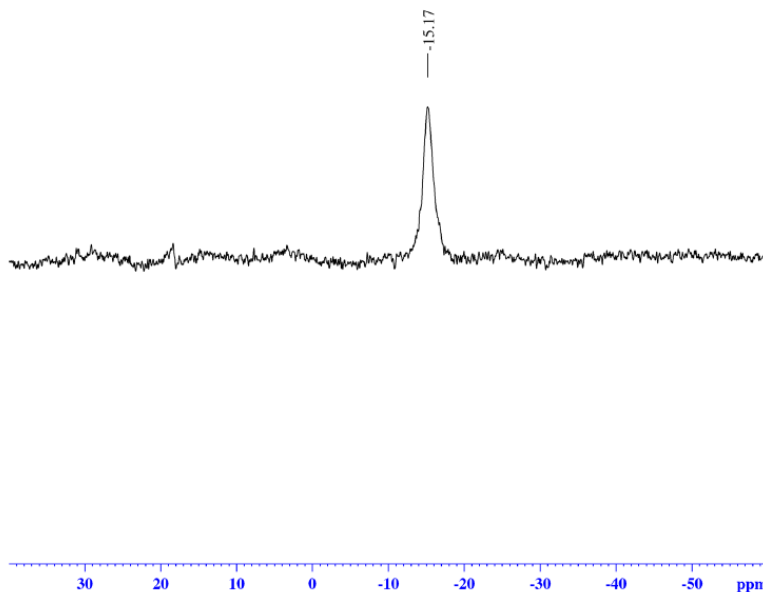
===== CHANNEL f1 =====  
 NUC1 1H  
 P1 14.75 usec  
 PL1 0 dB  
 PL1W 9.31909847 W  
 SFO1 300.1318008 MHz

F2 - Processing parameters  
 SI 65536  
 SF 300.1300074 MHz  
 WDW EM  
 SSB 0  
 LB 0.30 Hz  
 GB 0  
 PC 1.40





# <sup>11</sup>B NMR



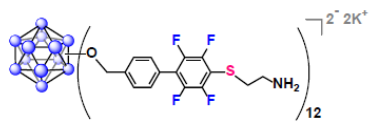
```

Current Data Parameters
NAME      G2 CA 0112 0110 (ACN & MeOD)
EXPNO     100
PROCNO    1

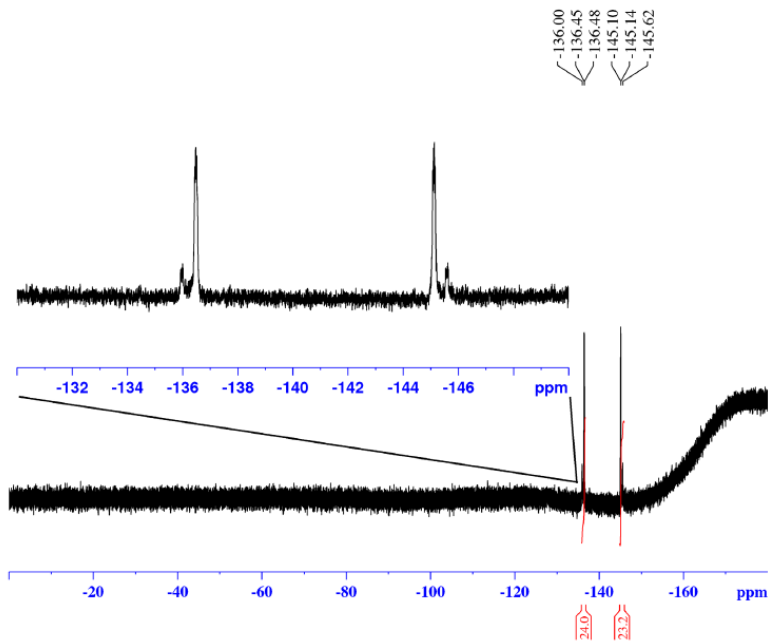
F2 - Acquisition Parameters
Date_     20160113
Time      18.51
INSTRUM   av400
PROBHD    5 mm PABBO BB/
PULPROG   zg
TD         5096
SOLVENT   CD3CN
NS         1024
DS         0
SWH        51020.406 Hz
FIDRES     10.011854 Hz
AQ         0.04099408 sec
RG         189.85
DW         9.800 usec
DE         6.50 usec
TE         299.0 K
D1         0.05000000 sec
TDO        1

===== CHANNEL f1 =====
SFO1      128.3776052 MHz
NUC1       11B
P1         10.00 usec
PLW1       52.00000000 W

F2 - Processing parameters
SI         32768
SF         128.3776161 MHz
WDW        EM
SSB        0
LB         10.00 Hz
GB         0
PC         1.40
  
```



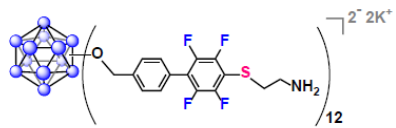
<sup>19</sup>F NMR



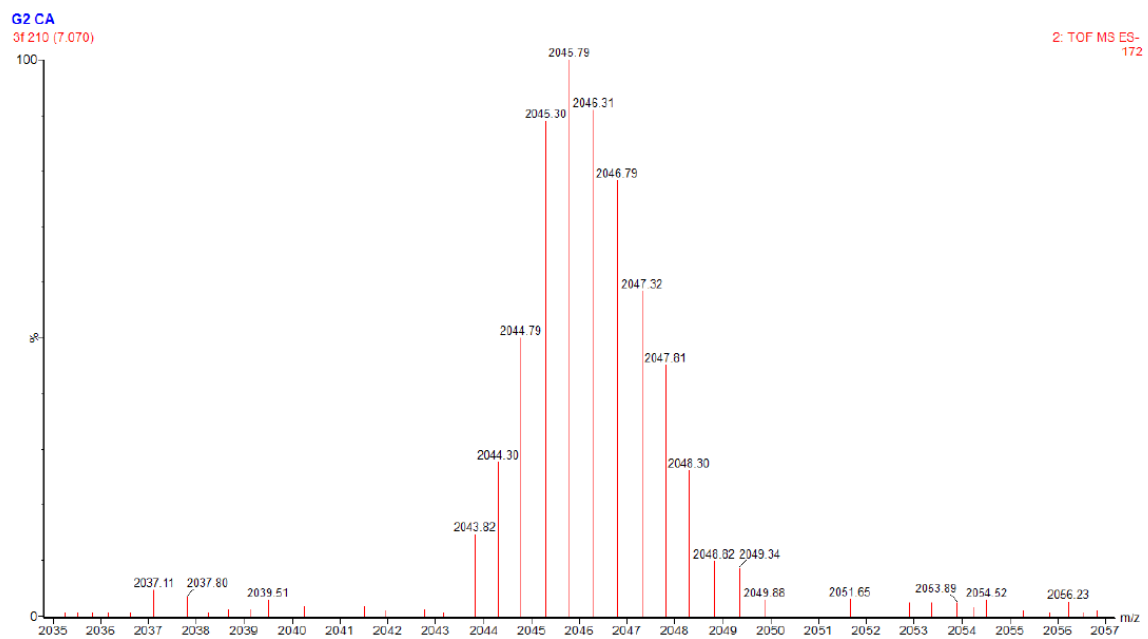
-136.00  
-136.45  
-136.48  
-145.10  
-145.14  
-145.62

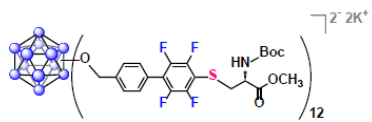
Current Data Parameters  
 NAME G2 CA 0112 0110 (ACN & MeOD)  
 EXPNO 101  
 PROCNO 1  
 F2 - Acquisition Parameters  
 Date\_ 20160113  
 Time 18.55  
 INSTRUM av400  
 PROBHD 5 mm PABBO BB/  
 PULPROG zgpg30  
 TD 262144  
 SOLVENT CD3CN  
 NS 64  
 DS 0  
 SWH 150000.000 Hz  
 FIDRES 0.572205 Hz  
 AQ 0.8738133 sec  
 RG 189.85  
 DW 3.333 usec  
 DE 6.50 usec  
 TE 299.0 K  
 D1 2.0000000 sec  
 TDO 1  
 ===== CHANNEL f1 =====  
 SFO1 376.4983660 MHz  
 NUC1 19F  
 P1 14.50 usec  
 PLW1 17.0000000 W  
 F2 - Processing parameters  
 SI 262144  
 SF 376.4983660 MHz  
 WDW EM  
 SSB 0  
 LB 1.00 Hz  
 GB 0  
 PC 1.00



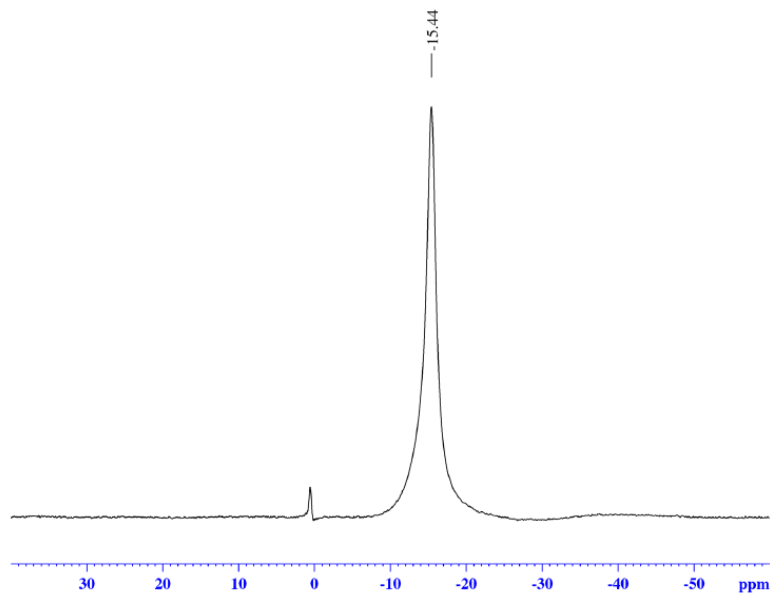


## Waters Mass Spec





*in situ*  $^{11}\text{B}$  NMR

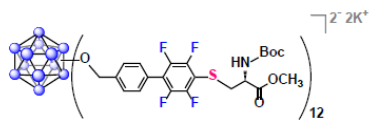


Current Data Parameters  
 NAME 0623  
 EXPNO 91  
 PROCNO 1

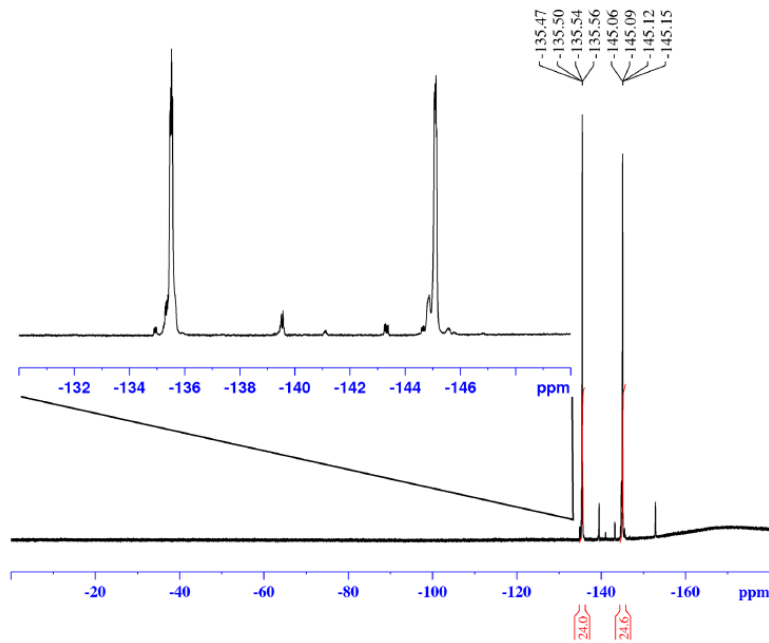
F2 - Acquisition Parameters  
 Date\_ 20160623  
 Time 19.12  
 INSTRUM av400  
 PROBHD 5 mm PABBO BB/  
 PULPROG zg  
 TD 5096  
 SOLVENT None  
 NS 1024  
 DS 0  
 SWH 51020.406 Hz  
 FIDRES 10.011854 Hz  
 AQ 0.0499408 sec  
 RG 189.85  
 DW 9.800 usec  
 DE 6.50 usec  
 TE 299.0 K  
 D1 0.05000000 sec  
 TDO 1

===== CHANNEL f1 =====  
 SF01 128.3776052 MHz  
 NUC1  $^{11}\text{B}$   
 P1 10.00 usec  
 PLW1 52.00000000 W

F2 - Processing parameters  
 SI 32768  
 SF 128.3776161 MHz  
 WDW EM  
 SSB 0  
 LB 10.00 Hz  
 GB 0  
 PC 1.40



*in situ* <sup>19</sup>F NMR

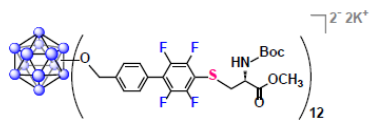


Current Data Parameters  
 NAME 0623  
 EXPNO 90  
 PROCNO 1

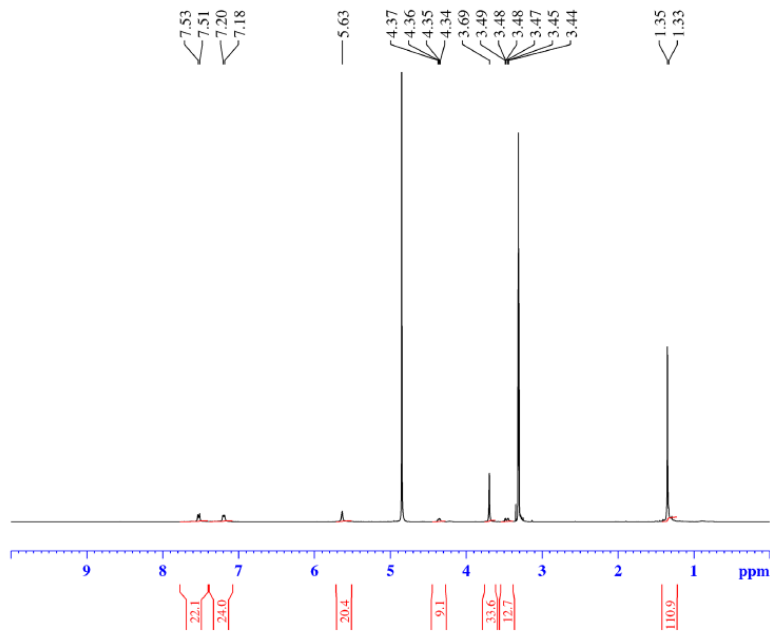
F2 - Acquisition Parameters  
 Date\_ 20160623  
 Time 19.08  
 INSTRUM av400  
 PROBHD 5 mm PABBO BB/  
 PULPROG zgpg30  
 TD 262144  
 SOLVENT None  
 NS 64  
 DS 0  
 SWH 150000.000 Hz  
 FIDRES 0.572205 Hz  
 AQ 0.8738133 sec  
 RG 189.85  
 DW 3.333 usec  
 DE 6.50 usec  
 TE 299.0 K  
 D1 2.0000000 sec  
 TDO 1

===== CHANNEL f1 =====  
 SFO1 376.4983660 MHz  
 NUC1 19F  
 P1 14.50 usec  
 PLW1 17.00000000 W

F2 - Processing parameters  
 SI 262144  
 SF 376.4983660 MHz  
 WDW EM  
 SSB 0  
 LB 1.00 Hz  
 GB 0  
 PC 1.00



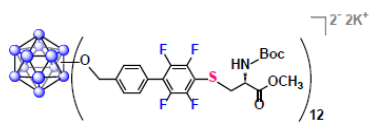
# <sup>1</sup>H NMR



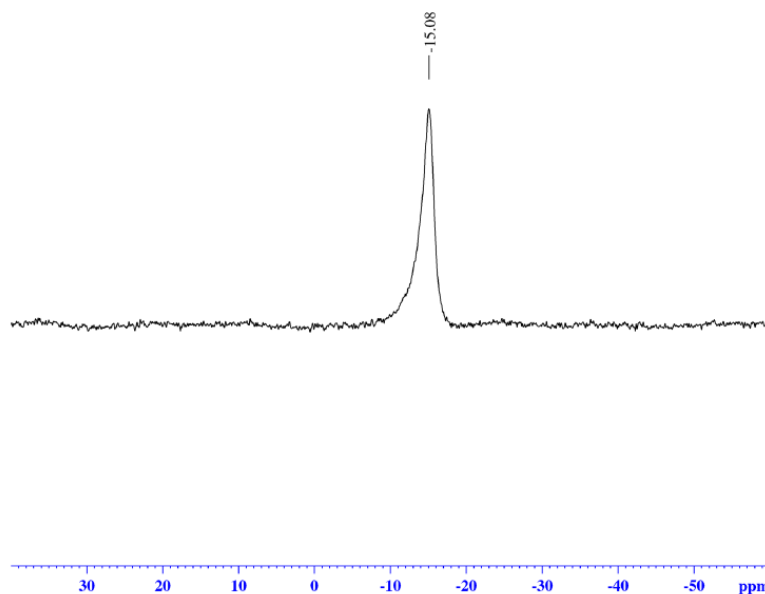
Current Data Parameters  
 NAME G2 BC 0630 0623 (MeOD)  
 EXPNO 50  
 PROCNO 1  
 F2 - Acquisition Parameters  
 Date\_ 20160630  
 Time 19.48  
 INSTRUM av400  
 PROBHD 5 mm PABBO BB/  
 PULPROG zg30  
 TD 52882  
 SOLVENT MeOD  
 NS 32  
 DS 0  
 SWH 8012.820 Hz  
 FIDRES 0.151523 Hz  
 AQ 3.2998369 sec  
 RG 189.85  
 DW 62.400 usec  
 DE 6.50 usec  
 TE 299.0 K  
 D1 5.00000000 sec  
 TDO 1

==== CHANNEL f1 =====  
 SFO1 400.1324008 MHz  
 NUC1 1H  
 P1 15.00 usec  
 PLW1 13.00000000 W

F2 - Processing parameters  
 SI 65536  
 SF 400.1300077 MHz  
 WDW EM  
 SSB 0  
 LB 0.30 Hz  
 GB 0  
 PC 1.00



<sup>11</sup>B NMR



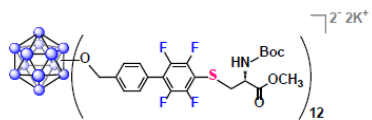
Current Data Parameters  
 NAME G2 BC 0630 0623 (MeOD)  
 EXPNO 52  
 PROCNO 1

F2 - Acquisition Parameters  
 Date\_ 20160630  
 Time 19.54  
 INSTRUM av400  
 PROBHD 5 mm PABBO BB/  
 PULPROG zg  
 TD 5096  
 SOLVENT MeOD  
 NS 1024  
 DS 0  
 SWH 51020.406 Hz  
 FIDRES 10.011854 Hz  
 AQ 0.0499408 sec  
 RG 189.85  
 DW 9.800 usec  
 DE 6.50 usec  
 TE 299.0 K  
 D1 0.05000000 sec  
 TDO 1

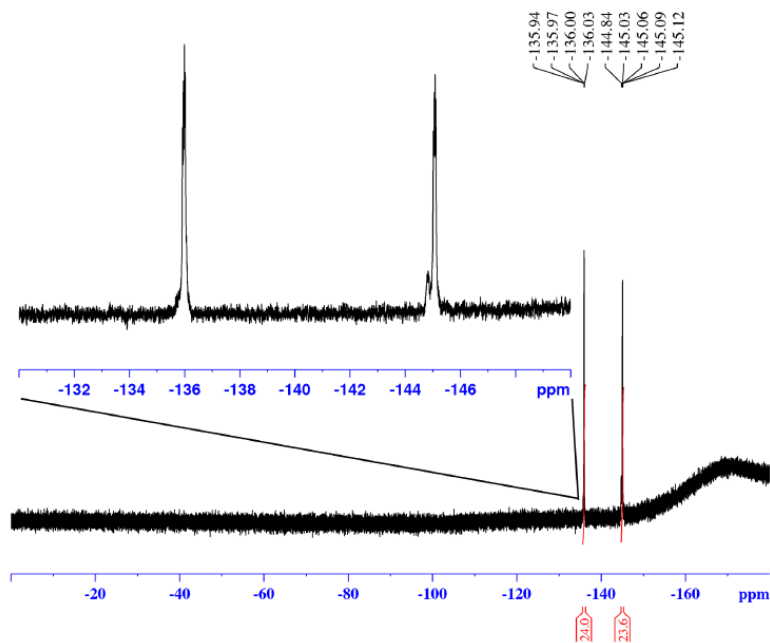
===== CHANNEL f1 =====  
 SFO1 128.3776052 MHz  
 NUC1 11B  
 P1 10.00 usec  
 PLW1 52.00000000 W

F2 - Processing parameters  
 SI 32768  
 SF 128.3776161 MHz  
 WDW EM  
 SSB 0  
 LB 10.00 Hz  
 GB 0  
 PC 1.40





<sup>19</sup>F NMR

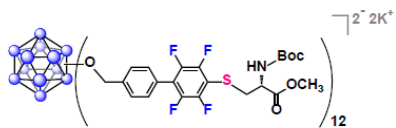


Current Data Parameters  
 NAME G2 BC 0630 0623 (MeOD)  
 EXPNO 51  
 PROCNO 1

F2 - Acquisition Parameters  
 Date\_ 20160630  
 Time 19.50  
 INSTRUM av400  
 PROBHD 5 mm PABBO BB/  
 PULPROG zgpg30  
 TD 262144  
 SOLVENT MeOD  
 NS 32  
 DS 0  
 SWH 150000.000 Hz  
 FIDRES 0.572205 Hz  
 AQ 0.8738133 sec  
 RG 189.85  
 DW 3.333 usec  
 DE 6.50 usec  
 TE 299.0 K  
 D1 2.00000000 sec  
 TDO 1

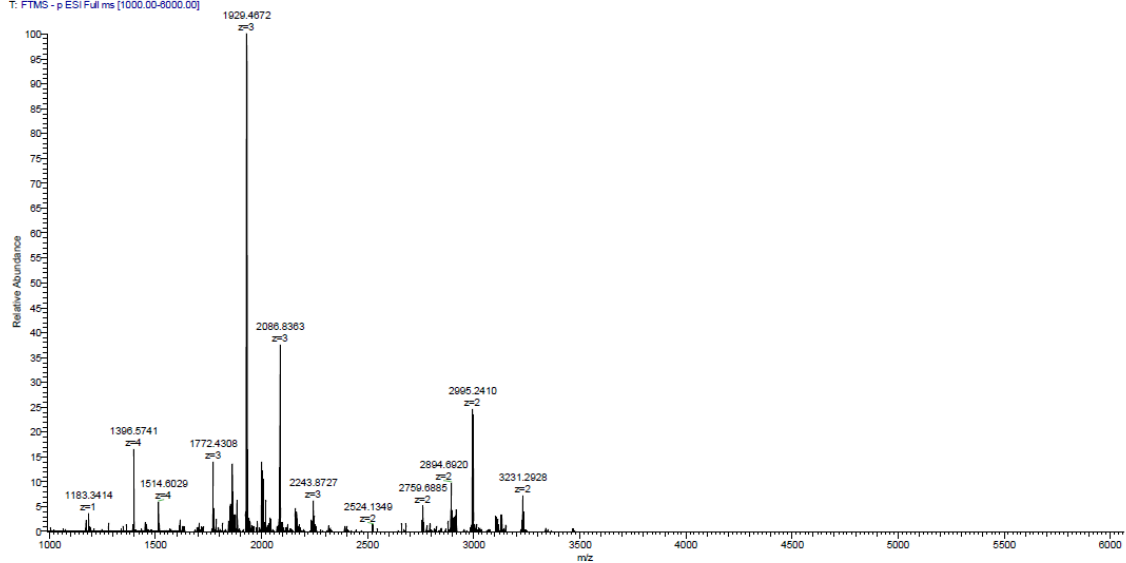
===== CHANNEL f1 =====  
 SFO1 376.4983660 MHz  
 NUC1 19F  
 P1 14.50 usec  
 PLW1 17.00000000 W

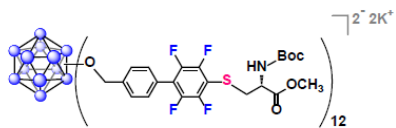
F2 - Processing parameters  
 SI 262144  
 SF 376.4983660 MHz  
 WDW EM  
 SSB 0  
 LB 1.00 Hz  
 GB 0  
 PC 1.00



## Q Exactive High-Res Mass Spec

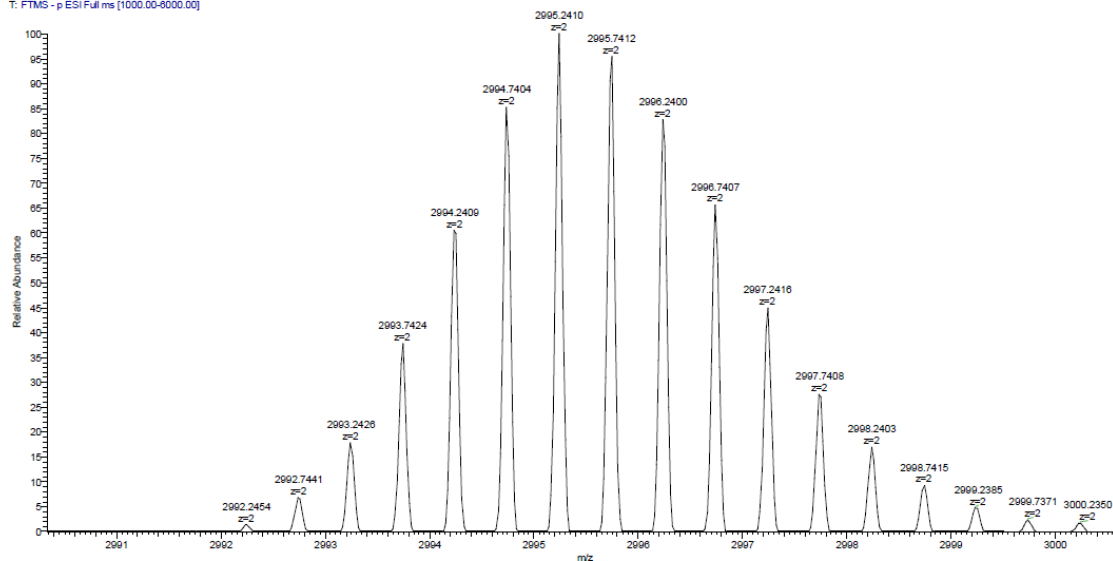
3g #1-152 RT: 0.01-1.31 AV: 152 NL: 8.01E6  
T: FTMS - p-ESI Full.ms [1000.00-6000.00]

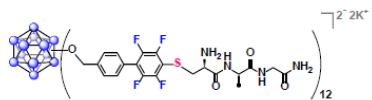




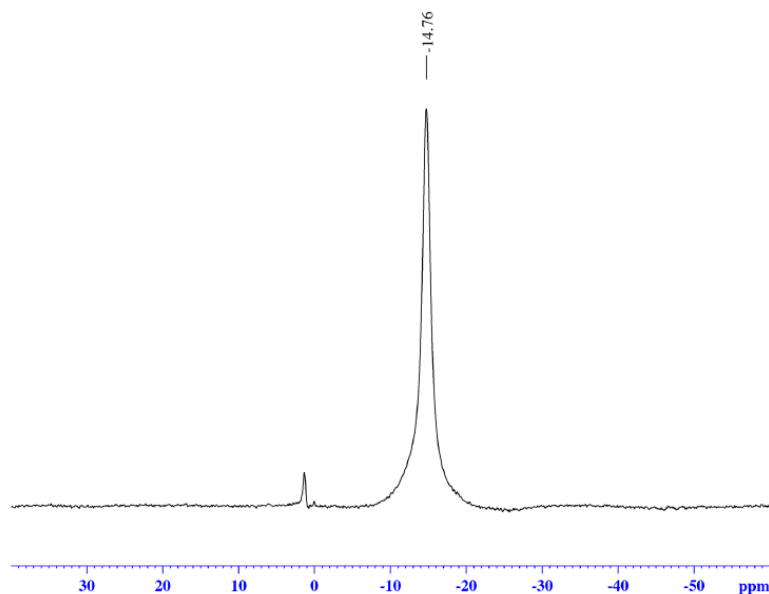
## Q Exactive High-Res Mass Spec

3g #1-152 RT: 0.01-1.31 AV: 152 NL: 1.97E6  
T: FTMS - p-ESI Full.ms [1000.00-9000.00]





*in situ*  $^{11}\text{B}$  NMR



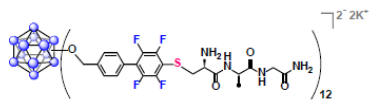
```

Current Data Parameters
NAME      0520
EXPNO    131
PROCNO   1

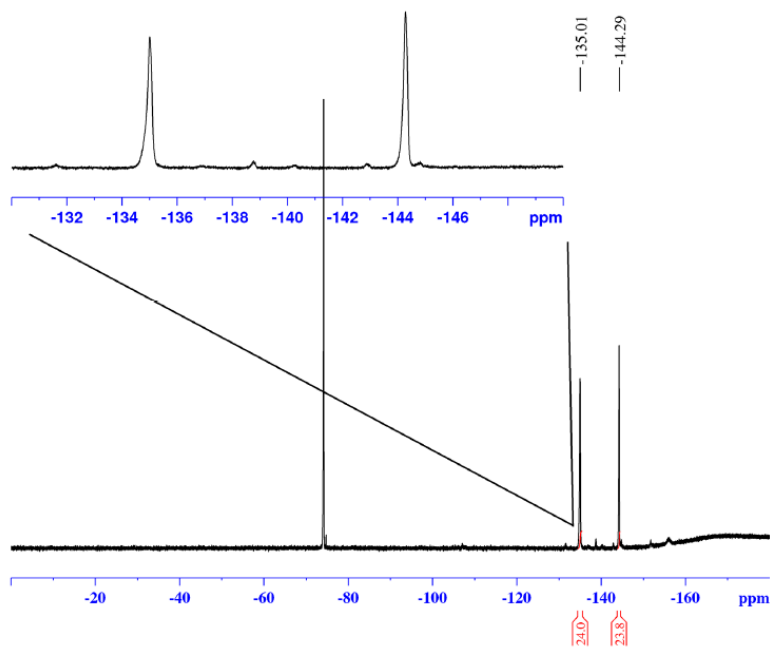
F2 - Acquisition Parameters
Date_    20160530
Time     21.13
INSTRUM  av400
PROBHD   5 mm PABBO BB/
PULPROG  zg
TD        5096
SOLVENT  None
NS        1024
DS         0
SWH       51020.406 Hz
FIDRES    10.011854 Hz
AQ        0.0499408 sec
RG        189.85
DW        9.800 usec
DE        6.50 usec
TE        299.0 K
D1        0.05000000 sec
TDO       1

===== CHANNEL f1 =====
SFO1    128.3776052 MHz
NUC1     11B
P1       10.00 usec
PLW1    52.00000000 W

F2 - Processing parameters
SI       32768
SF       128.3776161 MHz
WDW      EM
SSB      0
LB       10.00 Hz
GB       0
PC       1.40
  
```



*in situ*  $^{19}\text{F}$  NMR

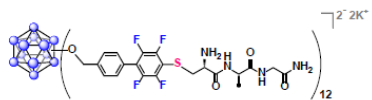


Current Data Parameters  
 NAME 0520  
 EXPNO 130  
 PROCNO 1

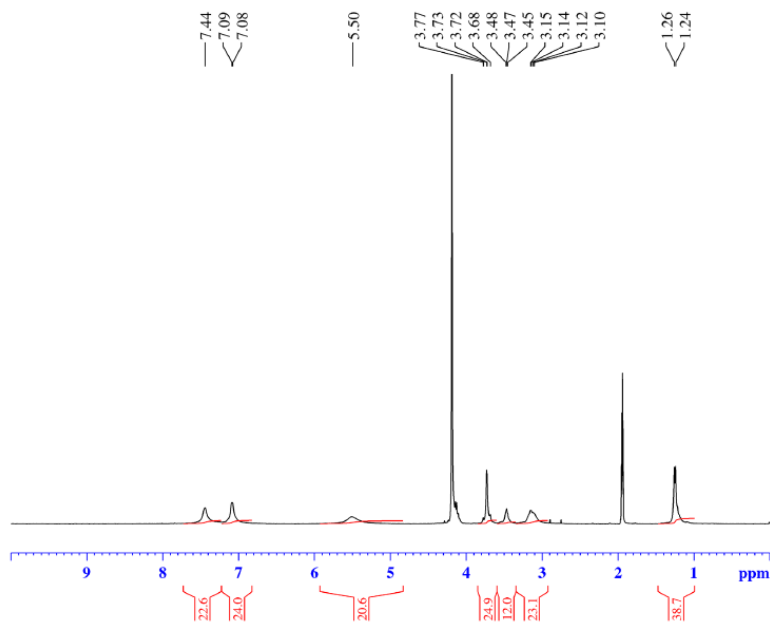
F2 - Acquisition Parameters  
 Date\_ 20160530  
 Time 21.10  
 INSTRUM av400  
 PROBHD 5 mm PABBO BB/  
 PULPROG zgpg30  
 TD 262144  
 SOLVENT None  
 NS 64  
 DS 0  
 SWH 150000.000 Hz  
 FIDRES 0.572205 Hz  
 AQ 0.8738133 sec  
 RG 189.85  
 DW 3.333 usec  
 DE 6.50 usec  
 TE 299.0 K  
 D1 2.00000000 sec  
 TDO 1

===== CHANNEL f1 =====  
 SF01 376.4983660 MHz  
 NUC1  $^{19}\text{F}$   
 P1 14.50 usec  
 PLW1 17.00000000 W

F2 - Processing parameters  
 SI 262144  
 SF 376.4983660 MHz  
 WDW EM  
 SSB 0  
 LB 1.00 Hz  
 GB 0  
 PC 1.00



# <sup>1</sup>H NMR

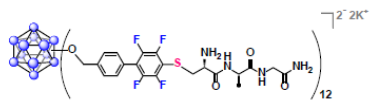


Current Data Parameters  
 NAME G2 CAG 0620 0520 (ACN & D2O)  
 EXPNO 80  
 PROCNO 1

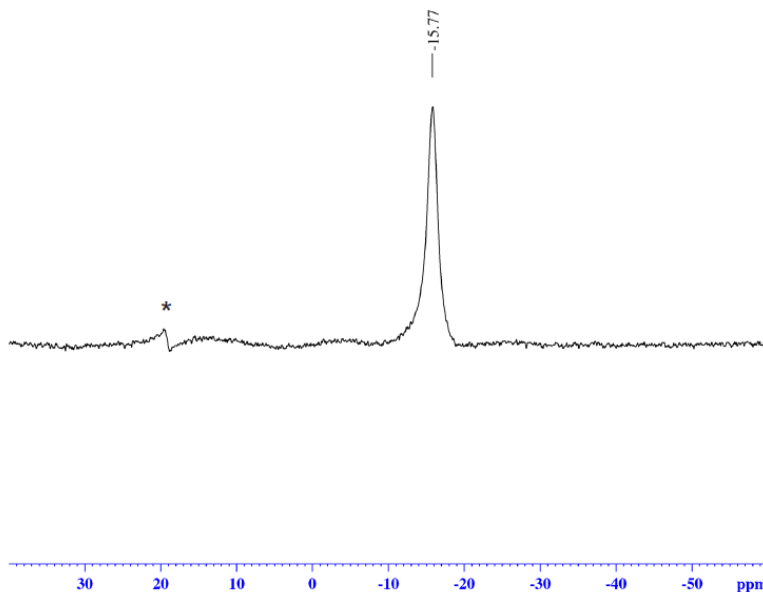
F2 - Acquisition Parameters  
 Date\_ 20160622  
 Time 16.18  
 INSTRUM av400  
 PROBHD 5 mm PABBO BB/  
 PULPROG zg30  
 TD 52882  
 SOLVENT CD3CN  
 NS 64  
 DS 0  
 SWH 8012.820 Hz  
 FIDRES 0.131523 Hz  
 AQ 3.2998369 sec  
 RG 155.85  
 DW 62.400 usec  
 DE 6.50 usec  
 TE 299.0 K  
 D1 5.0000000 sec  
 TDO 1

===== CHANNEL f1 =====  
 SFO1 400.1324008 MHz  
 NUC1 1H  
 P1 15.00 usec  
 PLW1 13.00000000 W

F2 - Processing parameters  
 SI 65536  
 SF 400.1290946 MHz  
 WDW EM  
 SSB 0  
 LB 0.30 Hz  
 GB 0  
 PC 1.00



<sup>11</sup>B NMR



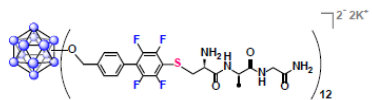
Current Data Parameters  
 NAME G2 CAG 0620 0520 (ACN & D2O)  
 EXPNO 82  
 PROCNO 1

F2 - Acquisition Parameters  
 Date\_ 20160622  
 Time 16.25  
 INSTRUM av400  
 PROBHD 5 mm PABBO BB/  
 PULPROG zg  
 TD 5096  
 SOLVENT CD3CN  
 NS 1024  
 DS 0  
 SWH 51020.406 Hz  
 FIDRES 10.011854 Hz  
 AQ 0.0099408 sec  
 RG 189.85  
 DW 9.800 usec  
 DE 6.50 usec  
 TE 299.0 K  
 D1 0.05000000 sec  
 TDO 1

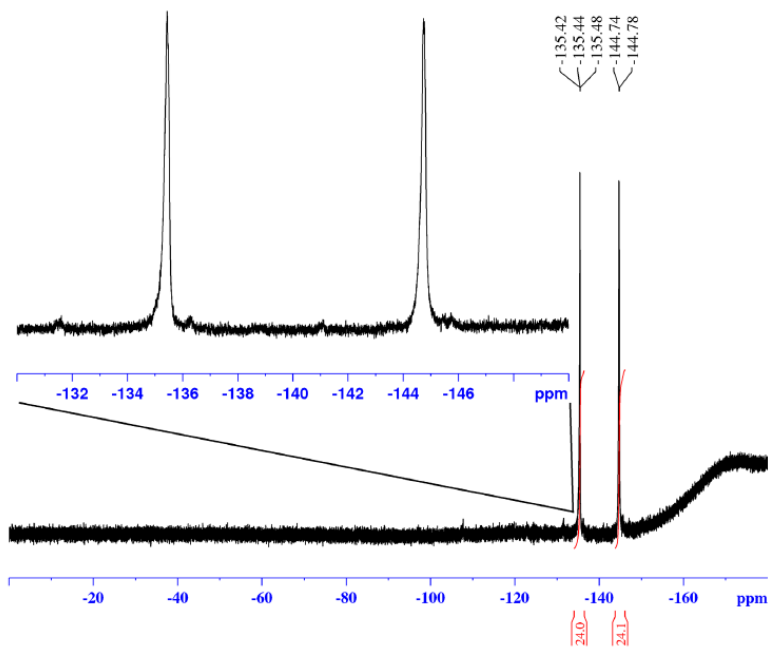
===== CHANNEL f1 =====  
 SFO1 128.3776052 MHz  
 NUC1 11B  
 P1 10.00 usec  
 PLW1 52.00000000 W

F2 - Processing parameters  
 SI 32768  
 SF 128.3773553 MHz  
 WDW EM  
 SSB 0  
 LB 10.00 Hz  
 GB 0  
 PC 1.40

\* This peak corresponds to a small boric acid impurity.



<sup>19</sup>F NMR



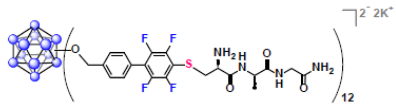
Current Data Parameters  
 NAME G2 CAG 0620 0520 (ACN & D2O)  
 EXPNO 81  
 PROCNO 1

F2 - Acquisition Parameters  
 Date\_ 20160622  
 Time 16.22  
 INSTRUM av400  
 PROBHD 5 mm PABBO BB/  
 PULPROG zgpg30  
 TD 262144  
 SOLVENT CD3CN  
 NS 64  
 DS 0  
 SWH 150000.000 Hz  
 FIDRES 0.572205 Hz  
 AQ 0.8738133 sec  
 RG 189.85  
 DW 3.333 usec  
 DE 6.50 usec  
 TE 299.0 K  
 D1 2.0000000 sec  
 TD0 1

===== CHANNEL f1 =====  
 SFO1 376.4983660 MHz  
 NUC1 19F  
 P1 14.50 usec  
 PLW1 17.00000000 W

F2 - Processing parameters  
 SI 262144  
 SF 376.4975772 MHz  
 WDW EM  
 SSB 0  
 LB 1.00 Hz  
 GB 0  
 PC 1.00

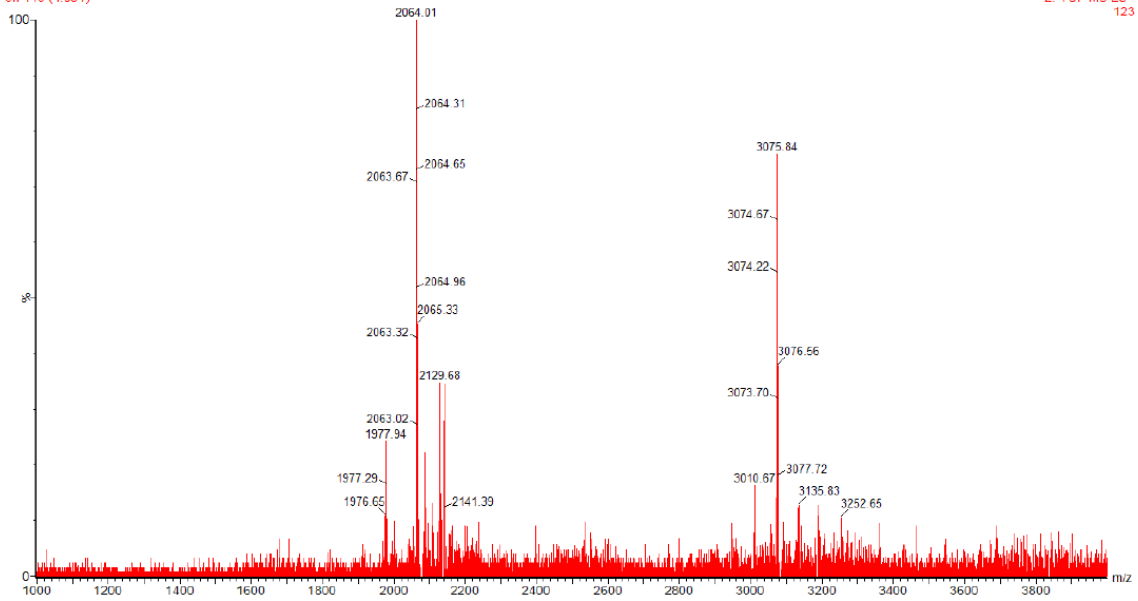


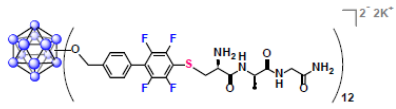


## Waters Mass Spec

G2 CAG 5 mg/mL, 4:1 H<sub>2</sub>O:MeCN  
3h 145 (4.891)

2: TOF MS ES-  
123

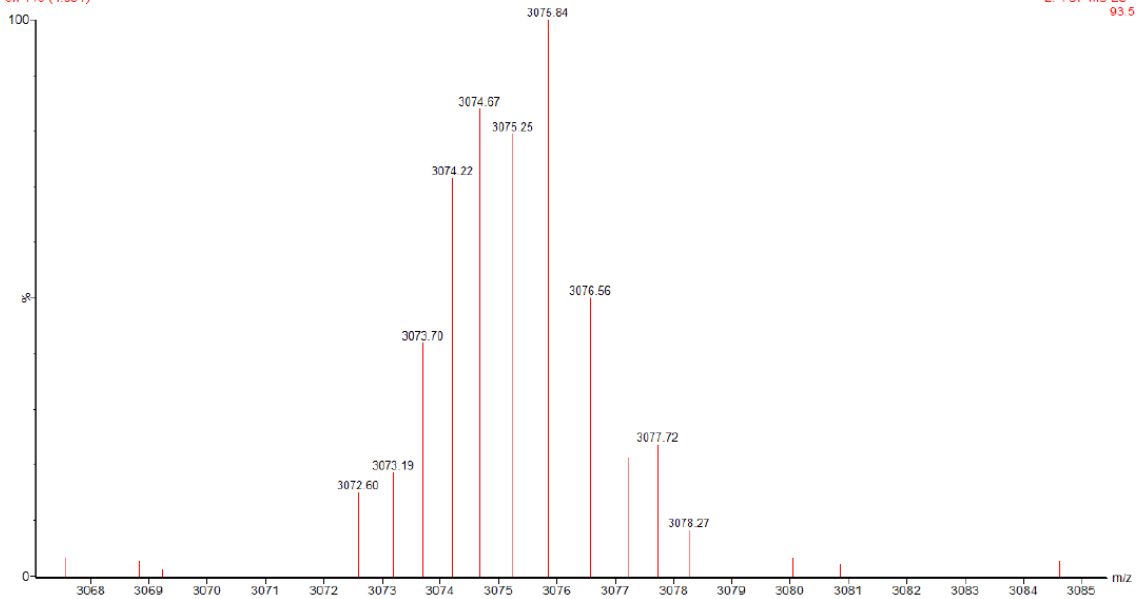


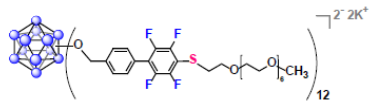


## Waters Mass Spec

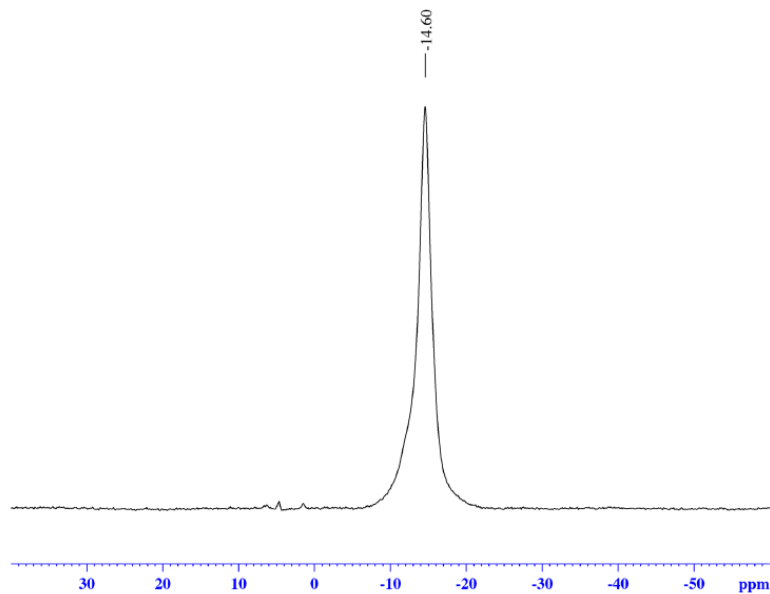
G2 CAG 5 mg/mL, 4:1 H<sub>2</sub>O:MeCN  
3h 145 (4.891)

2: TOF MS ES-  
93.5





*in situ*  $^{11}\text{B}$  NMR



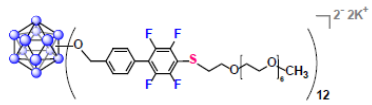
```

Current Data Parameters
NAME      1209
EXPNO    111
PROCNO   1

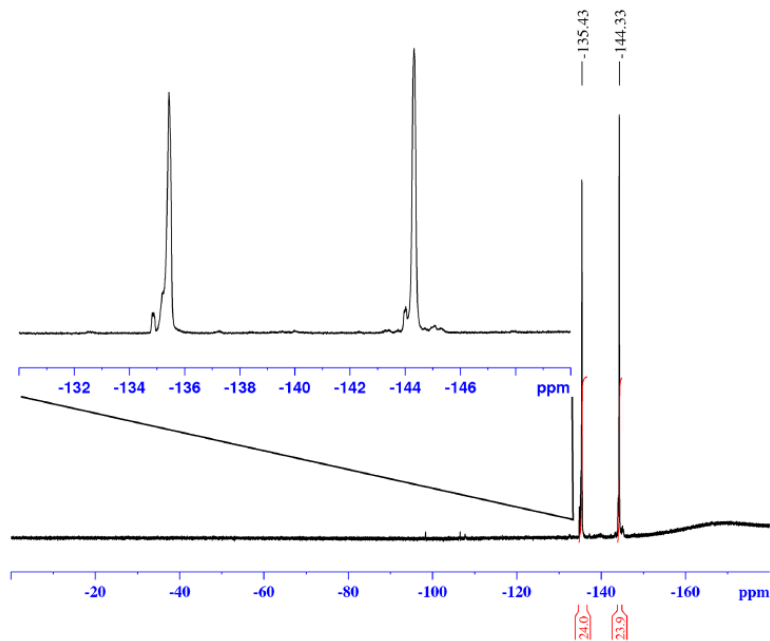
F2 - Acquisition Parameters
Date_    20151209
Time     20.03
INSTRUM  av400
PROBHD   5 mm PABBO BB/
PULPROG  zg
TD       5096
SOLVENT  None
NS       1024
DS       0
SWH      51020.406 Hz
FIDRES   10.011854 Hz
AQ       0.0499408 sec
RG       189.85
DW       9.800 usec
DE       6.50 usec
TE       299.0 K
D1       0.05000000 sec
TDO      1

===== CHANNEL f1 =====
SFO1    128.3776052 MHz
NUC1     11B
P1       10.00 usec
PLW1    52.00000000 W

F2 - Processing parameters
SI       32768
SF       128.3776161 MHz
WDW      EM
SSB      0
LB       10.00 Hz
GB       0
PC       1.40
  
```



*in situ*  $^{19}\text{F}$  NMR

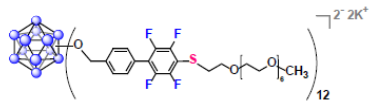


Current Data Parameters  
 NAME 1209  
 EXPNO 110  
 PROCNO 1

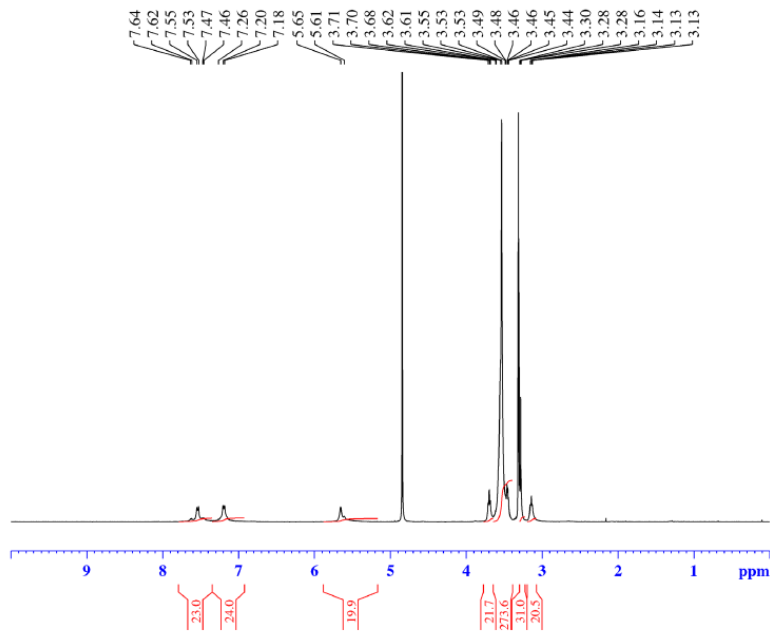
F2 - Acquisition Parameters  
 Date\_ 20151209  
 Time 20.00  
 INSTRUM av400  
 PROBHD 5 mm PABBO BB/  
 PULPROG zgpg30  
 TD 262144  
 SOLVENT None  
 NS 64  
 DS 0  
 SWH 150000.000 Hz  
 FIDRES 0.572205 Hz  
 AQ 0.8738133 sec  
 RG 189.85  
 DW 3.333 usec  
 DE 6.50 usec  
 TE 299.0 K  
 D1 2.00000000 sec  
 TDO 1

===== CHANNEL f1 =====  
 SF01 376.4983660 MHz  
 NUC1  $^{19}\text{F}$   
 P1 14.50 usec  
 PLW1 17.00000000 W

F2 - Processing parameters  
 SI 262144  
 SF 376.4983660 MHz  
 WDW EM  
 SSB 0  
 LB 1.00 Hz  
 GB 0  
 PC 1.00



<sup>1</sup>H NMR

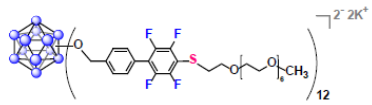


Current Data Parameters  
 NAME G2 PEG350 1217 1209 (MeOD)  
 EXPNO 2  
 PROCNO 1

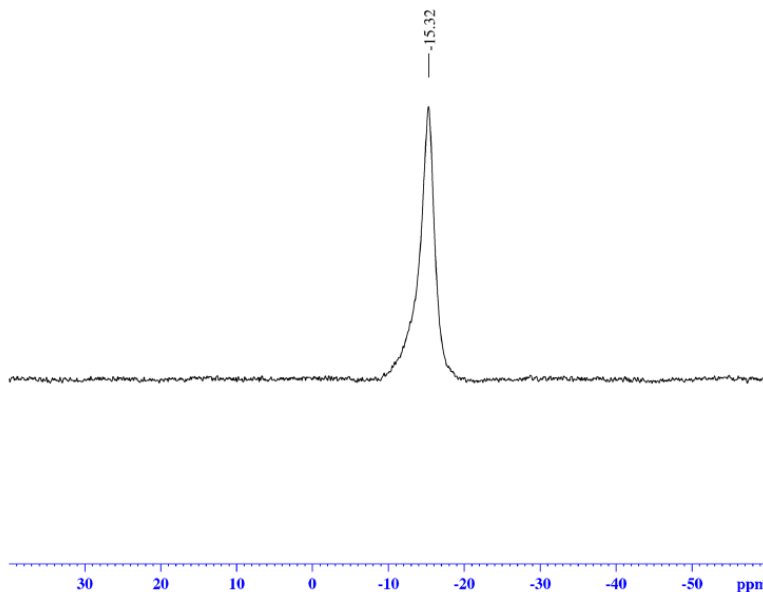
F2 - Acquisition Parameters  
 Date\_ 20151220  
 Time 13.12  
 INSTRUM av400  
 PROBHD 5 mm PABBO BB/  
 PULPROG zg30  
 TD 52882  
 SOLVENT MeOD  
 NS 32  
 DS 0  
 SWH 8012.820 Hz  
 FIDRES 0.151523 Hz  
 AQ 3.2998369 sec  
 RG 155.85  
 DW 62.400 usec  
 DE 6.50 usec  
 TE 299.0 K  
 D1 2.00000000 sec  
 TDO 1

==== CHANNEL f1 =====  
 SF01 400.1324008 MHz  
 NUC1 1H  
 P1 15.00 usec  
 PLW1 13.00000000 W

F2 - Processing parameters  
 SI 65536  
 SF 400.1300078 MHz  
 WDW EM  
 SSB 0  
 LB 0.30 Hz  
 GB 0  
 PC 1.00



<sup>11</sup>B NMR



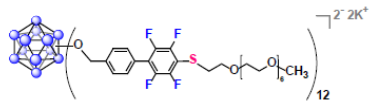
```

Current Data Parameters
NAME      G2 PEG350 1217 1209 (MeOD)
EXPNO    3
PROCNO   1

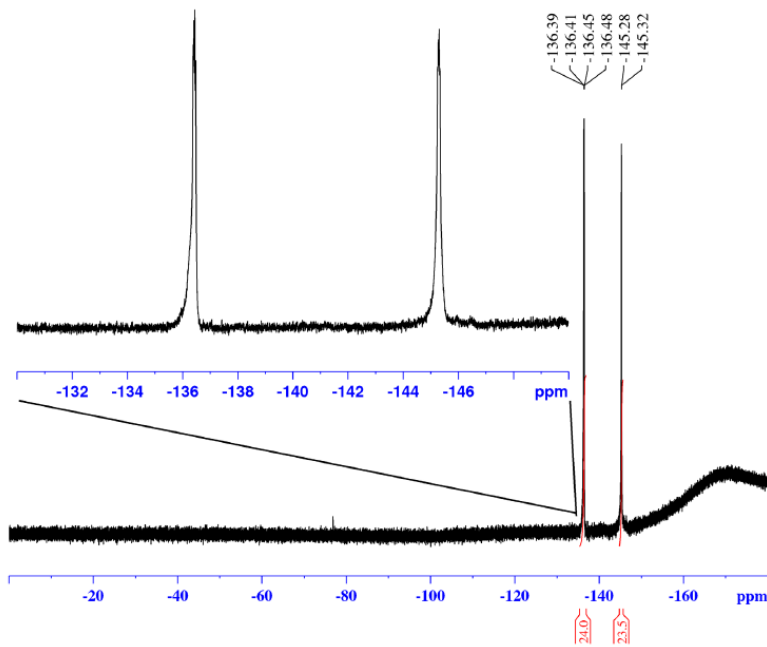
F2 - Acquisition Parameters
Date_    20151220
Time     13.15
INSTRUM  av400
PROBHD   5 mm PABBO BB/
PULPROG  zg
TD       5096
SOLVENT  MeOD
NS       1024
DS       0
SWH      51020.406 Hz
FIDRES   10.011854 Hz
AQ       0.0499408 sec
RG       189.85
DW       9.800 usec
DE       6.50 usec
TE       299.0 K
D1       0.05000000 sec
TD0      1

===== CHANNEL f1 =====
SFO1    128.3776052 MHz
NUC1    11B
P1      10.00 usec
PLW1    52.00000000 W

F2 - Processing parameters
SI      32768
SF      128.3776161 MHz
WDW     EM
SSB     0
LB      10.00 Hz
GB      0
PC      1.40
  
```



<sup>19</sup>F NMR

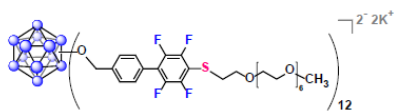


Current Data Parameters  
 NAME G2 PEG350 1217 1209 (MeOD)  
 EXPNO 4  
 PROCNO 1

F2 - Acquisition Parameters  
 Date\_ 20151220  
 Time 13.19  
 INSTRUM av400  
 PROBHD 5 mm PABBO BB/  
 PULPROG zgpg30  
 TD 262144  
 SOLVENT MeOD  
 NS 64  
 DS 0  
 SWH 150000.000 Hz  
 FIDRES 0.572205 Hz  
 AQ 0.8738133 sec  
 RG 189.85  
 DW 3.333 usec  
 DE 6.50 usec  
 TE 299.0 K  
 D1 2.0000000 sec  
 TDO 1

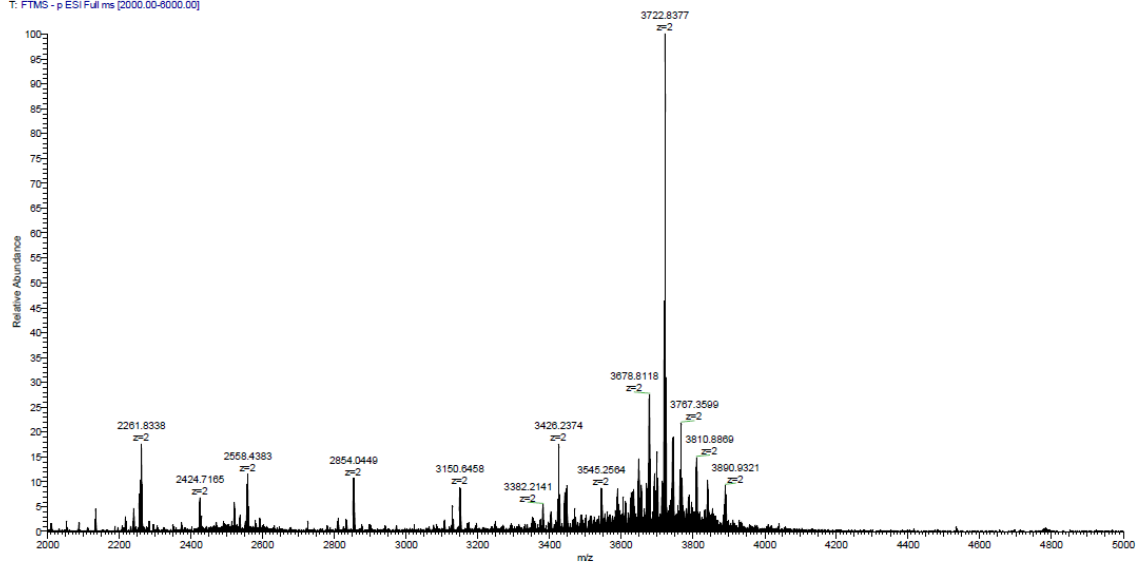
===== CHANNEL f1 =====  
 SFO1 376.4983660 MHz  
 NUC1 19F  
 P1 14.50 usec  
 PLW1 17.00000000 W

F2 - Processing parameters  
 SI 262144  
 SF 376.4983660 MHz  
 WDW EM  
 SSB 0  
 LB 1.00 Hz  
 GB 0  
 PC 1.00

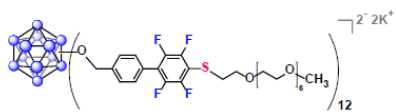


## Q Exactive High-Res Mass Spec

312 #1-20 RT: 0.01-0.17 AV: 20 NL: 2.87E5  
T: FTMS - p-ESI Full ms (2000.00-6000.00)

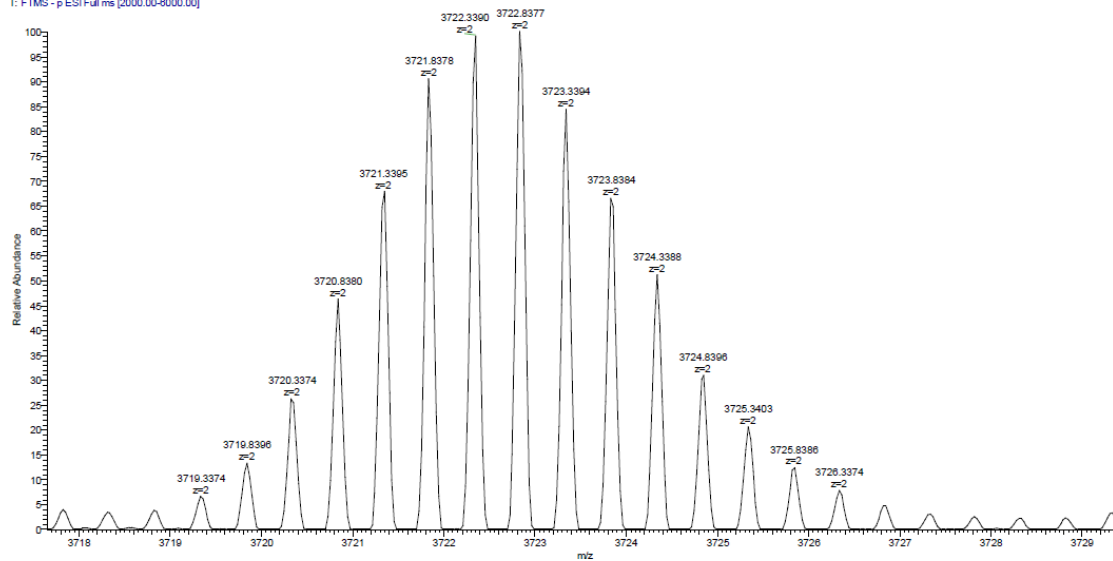


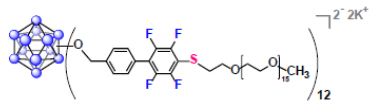




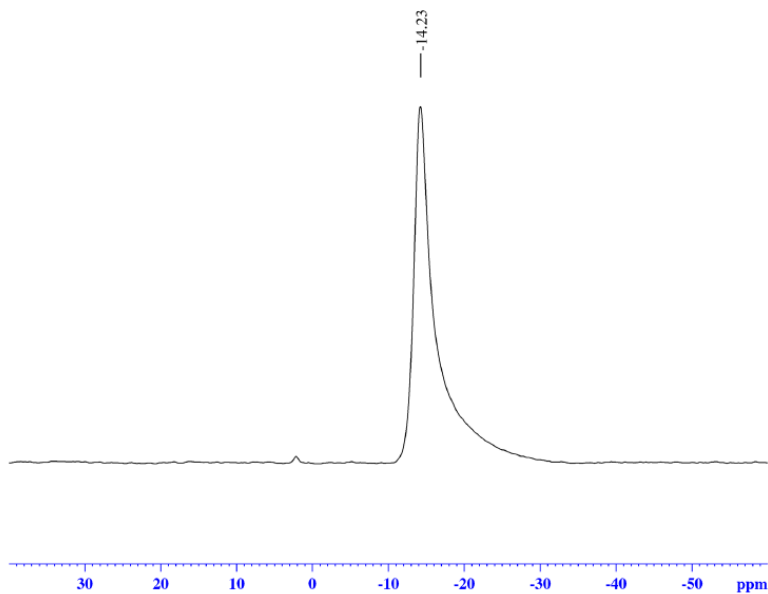
### Q Exactive High-Res Mass Spec

31.2 #1-20 RT: 0.01-0.17 AV: 20 NL: 2.87E5  
T: FTMS - p-ESI Full.ms [2000.00-6000.00]





*in situ*  $^{11}\text{B}$  NMR



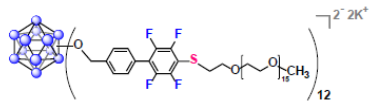
```

Current Data Parameters
NAME      0115
EXPNO     2
PROCNO    1

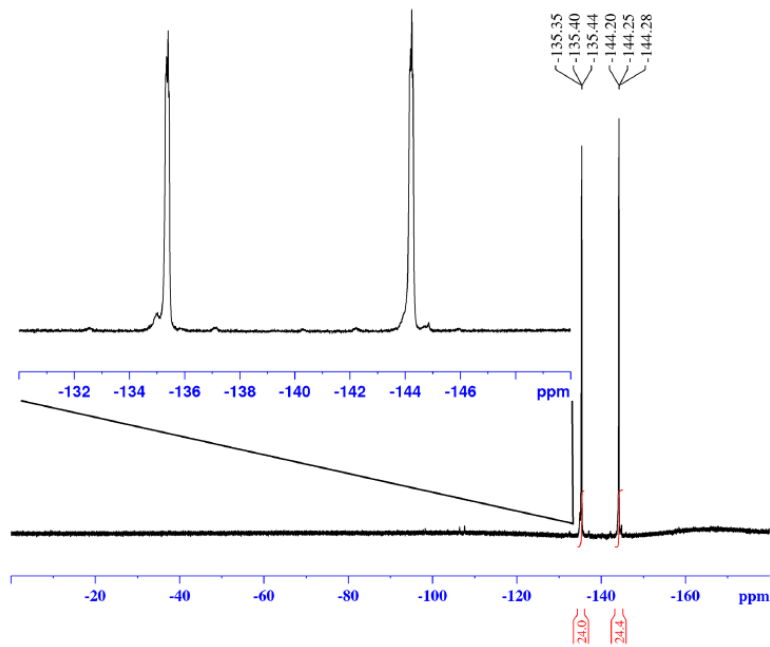
F2 - Acquisition Parameters
Date_     20160115
Time      20.01
INSTRUM   av300
PROBHD    5 mm PABBO BB-
PULPROG   zg
TD         3848
SOLVENT   C6D6
NS         1024
DS         0
SWH        38335.645 Hz
FIDRES     10.014461 Hz
AQ         0.0499278 sec
RG         114
DW         12.975 usec
DE         6.00 usec
TE         297.7 K
D1         0.00000400 sec
TDO        1

===== CHANNEL f1 =====
NUC1      11B
P1        5.00 usec
PL1       -2.00 dB
SFO1      96.2936310 MHz

F2 - Processing parameters
SI         32768
SF         96.2935644 MHz
WDW        EM
SSB        0
LB         50.00 Hz
GB         0
PC         1.40
  
```



*in situ*  $^{19}\text{F}$  NMR

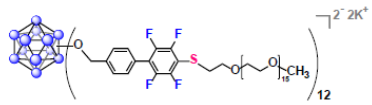


Current Data Parameters  
 NAME 0115  
 EXPNO 1  
 PROCNO 1

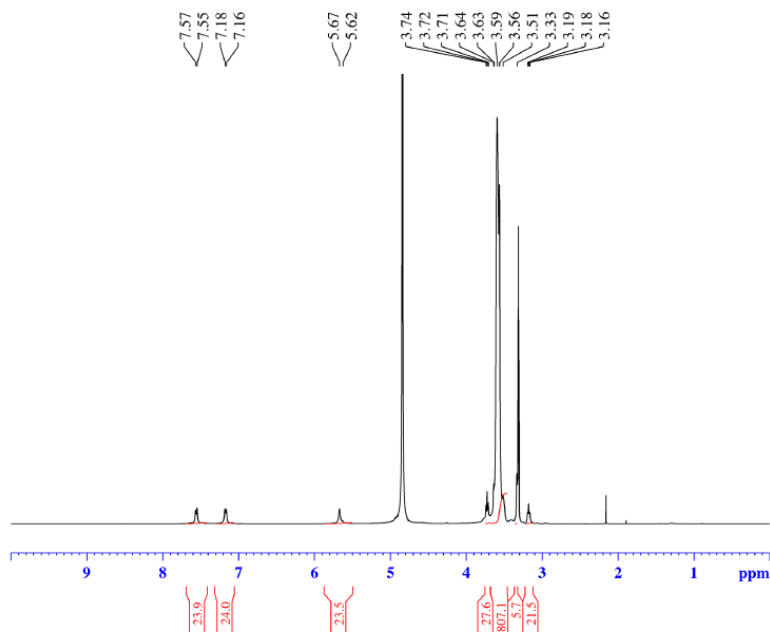
F2 - Acquisition Parameters  
 Date\_ 20160115  
 Time 19.55  
 INSTRUM av300  
 PROBHD 5 mm PABBO BB-  
 PULPROG zg30  
 TD 131072  
 SOLVENT C6D6  
 NS 64  
 DS 0  
 SWH 75187.969 Hz  
 FIDRES 0.573639 Hz  
 AQ 0.8716288 sec  
 RG 2398.8  
 DW 6.650 usec  
 DE 6.00 usec  
 TE 297.7 K  
 D1 2.00000000 sec  
 TD0 1

===== CHANNEL f1 =====  
 NUC1  $^{19}\text{F}$   
 P1 13.75 usec  
 PL1 -2.00 dB  
 PL1W 19.90535927 W  
 SFO1 282.3761146 MHz

F2 - Processing parameters  
 SI 65536  
 SF 282.4043550 MHz  
 WDW EM  
 SSB 0  
 LB 0.30 Hz  
 GB 0  
 PC 1.00



# <sup>1</sup>H NMR

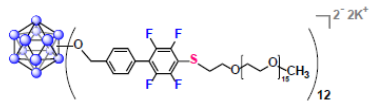


Current Data Parameters  
 NAME G2 PEG750 (MeOD)  
 EXPNO 160  
 PROCNO 1

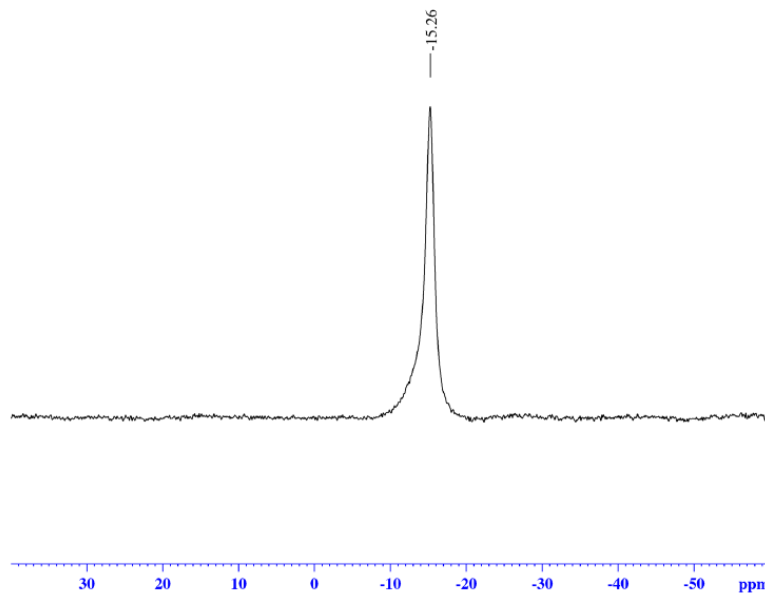
F2 - Acquisition Parameters  
 Date\_ 20160119  
 Time 20.06  
 INSTRUM av400  
 PROBHD 5 mm PABBO BB/  
 PULPROG zg30  
 TD 52882  
 SOLVENT MeOD  
 NS 32  
 DS 0  
 SWH 8012.820 Hz  
 FIDRES 0.151523 Hz  
 AQ 3.2998369 sec  
 RG 83.63  
 DW 62.400 usec  
 DE 6.50 usec  
 TE 299.0 K  
 D1 4.00000000 sec  
 TDO 1

===== CHANNEL f1 =====  
 SFO1 400.1324008 MHz  
 NUC1 1H  
 P1 15.00 usec  
 PLW1 13.00000000 W

F2 - Processing parameters  
 SI 65536  
 SF 400.1300080 MHz  
 WDW EM  
 SSB 0  
 LB 0.30 Hz  
 GB 0  
 PC 1.00



<sup>11</sup>B NMR

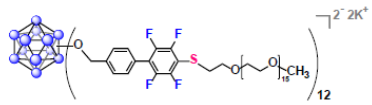


Current Data Parameters  
 NAME G2 PEG750 (MeOD)  
 EXPNO 161  
 PROCNO 1

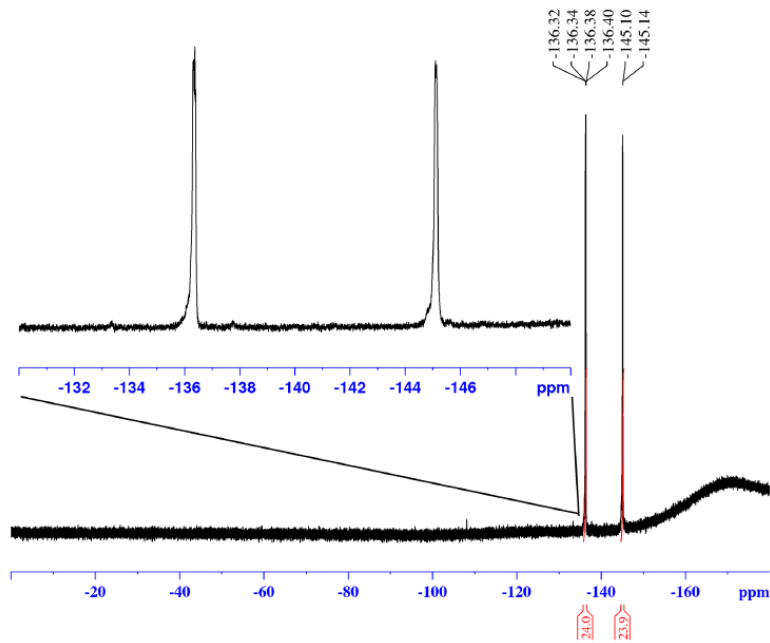
F2 - Acquisition Parameters  
 Date\_ 20160119  
 Time 20.09  
 INSTRUM av400  
 PROBHD 5 mm PABBO BB/  
 PULPROG zg  
 TD 5096  
 SOLVENT MeOD  
 NS 1024  
 DS 0  
 SWH 51020.406 Hz  
 FIDRES 10.011854 Hz  
 AQ 0.0499408 sec  
 RG 189.85  
 DW 9.800 usec  
 DE 6.50 usec  
 TE 299.0 K  
 D1 0.05000000 sec  
 TDO 1

===== CHANNEL f1 =====  
 SFO1 128.3776052 MHz  
 NUC1 11B  
 P1 10.00 usec  
 PLW1 52.00000000 W

F2 - Processing parameters  
 SI 32768  
 SF 128.3776161 MHz  
 WDW EM  
 SSB 0  
 LB 10.00 Hz  
 GB 0  
 PC 1.40



<sup>19</sup>F NMR

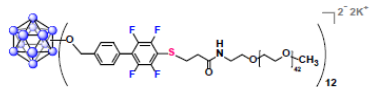


Current Data Parameters  
 NAME G2 PEG750 (MeOD)  
 EXPNO 162  
 PROCNO 1

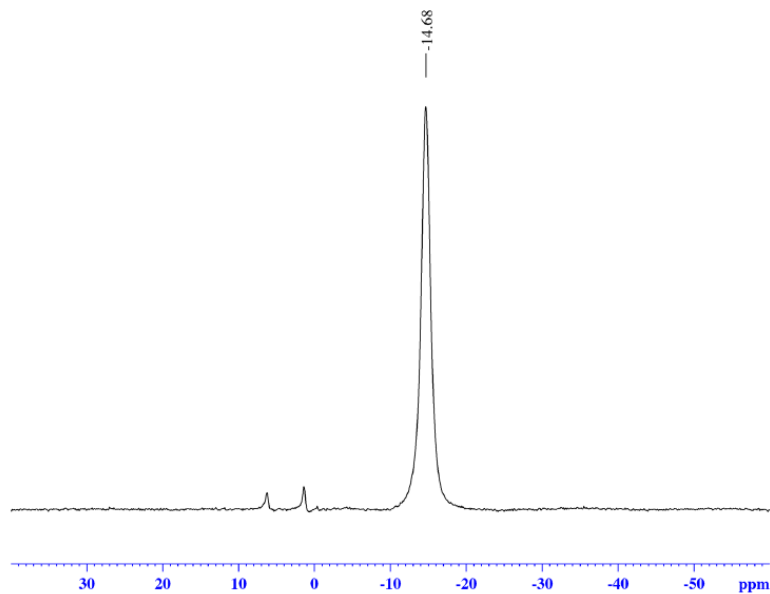
F2 - Acquisition Parameters  
 Date\_ 20160119  
 Time 20.13  
 INSTRUM av400  
 PROBHD 5 mm PABBO BB/  
 PULPROG zgpg30  
 TD 262144  
 SOLVENT MeOD  
 NS 64  
 DS 0  
 SWH 150000.000 Hz  
 FIDRES 0.572205 Hz  
 AQ 0.8738133 sec  
 RG 189.85  
 DW 3.333 usec  
 DE 6.50 usec  
 TE 299.0 K  
 D1 2.0000000 sec  
 TDO 1

===== CHANNEL f1 =====  
 SFO1 376.4983660 MHz  
 NUC1 <sup>19</sup>F  
 P1 14.50 usec  
 PLW1 17.00000000 W

F2 - Processing parameters  
 SI 262144  
 SF 376.4983660 MHz  
 WDW EM  
 SSB 0  
 LB 1.00 Hz  
 GB 0  
 PC 1.00



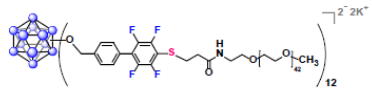
*in situ*  $^{11}\text{B}$  NMR



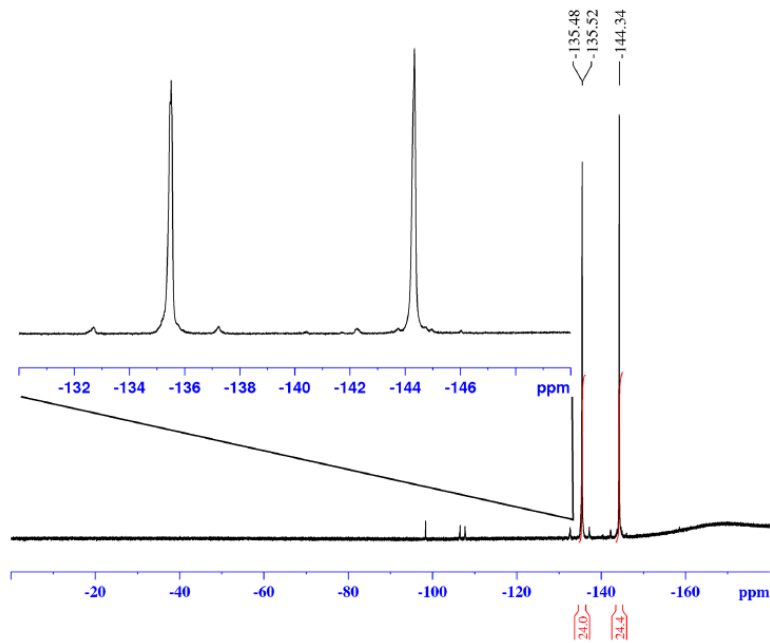
Current Data Parameters  
 NAME 0126  
 EXPNO 81  
 PROCNO 1  
 F2 - Acquisition Parameters  
 Date\_ 20160126  
 Time 16.30  
 INSTRUM av400  
 PROBHD 5 mm PABBO BB/  
 PULPROG zg  
 TD 5096  
 SOLVENT None  
 NS 1024  
 DS 0  
 SWH 51020.406 Hz  
 FIDRES 10.011854 Hz  
 AQ 0.0499408 sec  
 RG 189.85  
 DW 9.800 usec  
 DE 6.50 usec  
 TE 299.0 K  
 D1 0.05000000 sec  
 TDO 1

===== CHANNEL f1 =====  
 SFO1 128.3776052 MHz  
 NUC1 11B  
 P1 10.00 usec  
 PLW1 52.00000000 W

F2 - Processing parameters  
 SI 32768  
 SF 128.3776161 MHz  
 WDW EM  
 SSB 0  
 LB 10.00 Hz  
 GB 0  
 PC 1.40



*in situ*  $^{19}\text{F}$  NMR



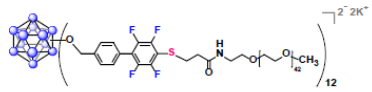
Current Data Parameters  
 NAME 0126  
 EXPNO 80  
 PROCNO 1

F2 - Acquisition Parameters  
 Date\_ 20160126  
 Time 16.27  
 INSTRUM av400  
 PROBHD 5 mm PABBO BB/  
 PULPROG zgpg30  
 TD 262144  
 SOLVENT None  
 NS 64  
 DS 0  
 SWH 150000.000 Hz  
 FIDRES 0.572205 Hz  
 AQ 0.8738133 sec  
 RG 189.85  
 DW 3.333 usec  
 DE 6.50 usec  
 TE 299.0 K  
 D1 2.00000000 sec  
 TDO 1

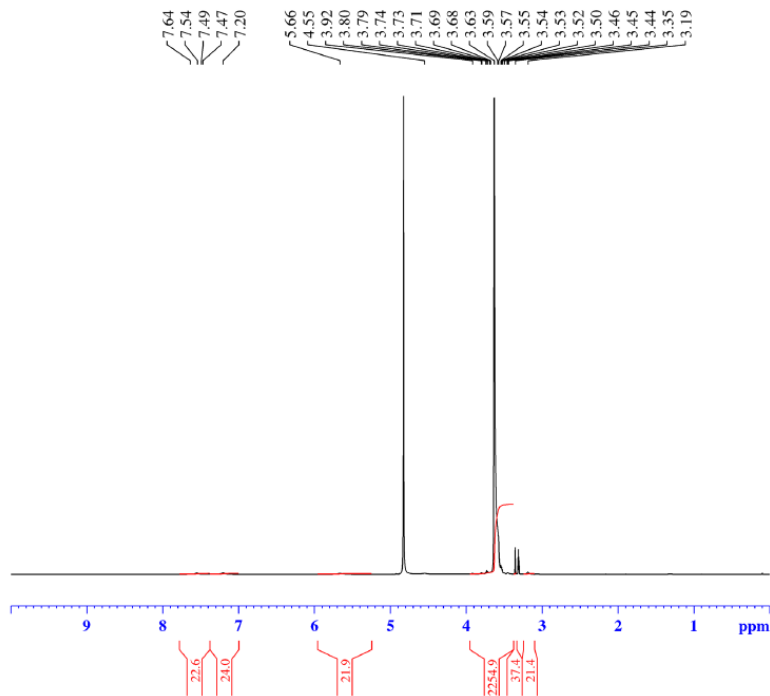
===== CHANNEL f1 =====  
 SF01 376.4983660 MHz  
 NUC1  $^{19}\text{F}$   
 P1 14.50 usec  
 PLW1 17.00000000 W

F2 - Processing parameters  
 SI 262144  
 SF 376.4983660 MHz  
 WDW EM  
 SSB 0  
 LB 1.00 Hz  
 GB 0  
 PC 1.00





<sup>1</sup>H NMR

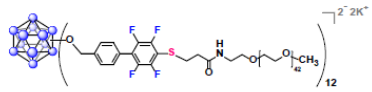


Current Data Parameters  
 NAME G2 PEG2000 0203 0125 MeOD  
 EXPNO 12  
 PROCNO 1

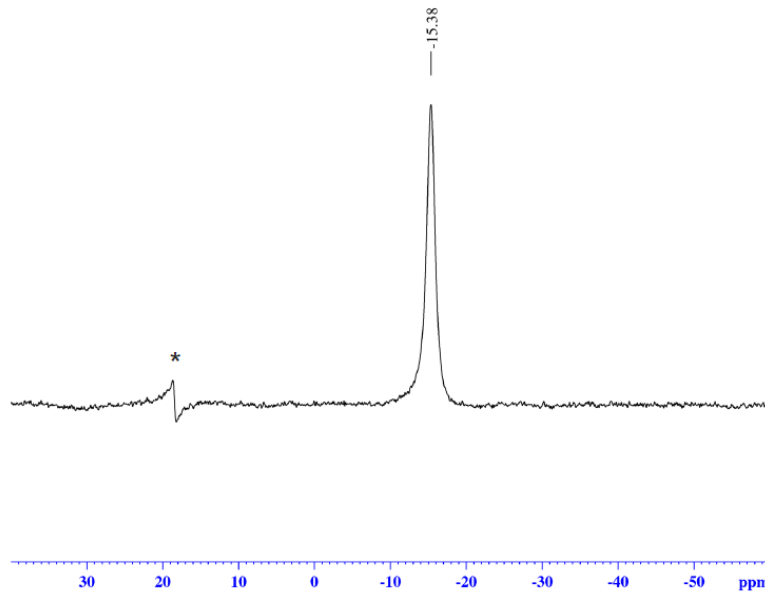
F2 - Acquisition Parameters  
 Date\_ 20160204  
 Time 17.21  
 INSTRUM av400  
 PROBHD 5 mm PABBO BB/  
 PULPROG zg30  
 TD 52882  
 SOLVENT MeOD  
 NS 32  
 DS 0  
 SWH 8012.820 Hz  
 FIDRES 0.151523 Hz  
 AQ 3.2998369 sec  
 RG 48.1  
 DW 62.400 usec  
 DE 6.50 usec  
 TE 299.0 K  
 D1 5.00000000 sec  
 TDO 1

===== CHANNEL f1 =====  
 SFO1 400.1324008 MHz  
 NUC1 1H  
 P1 15.00 usec  
 PLW1 13.00000000 W

F2 - Processing parameters  
 SI 65536  
 SF 400.1300074 MHz  
 WDW EM  
 SSB 0  
 LB 0.30 Hz  
 GB 0  
 PC 1.00



<sup>11</sup>B NMR



```

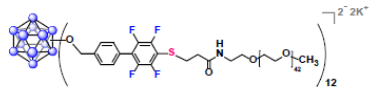
Current Data Parameters
NAME      G2 PEG2000 0203 0125 MeOD
EXPNO     10
PROCNO    1

F2 - Acquisition Parameters
Date_     20160204
Time      17.11
INSTRUM   av400
PROBHD    5 mm PABBO BB/
PULPROG   zg
TD         5096
SOLVENT   MeOD
NS         1024
DS         0
SWH        51020.406 Hz
FIDRES     10.011854 Hz
AQ         0.0499408 sec
RG         189.85
DW         9.800 usec
DE         6.50 usec
TE         299.0 K
D1         0.05000000 sec
TDO        1

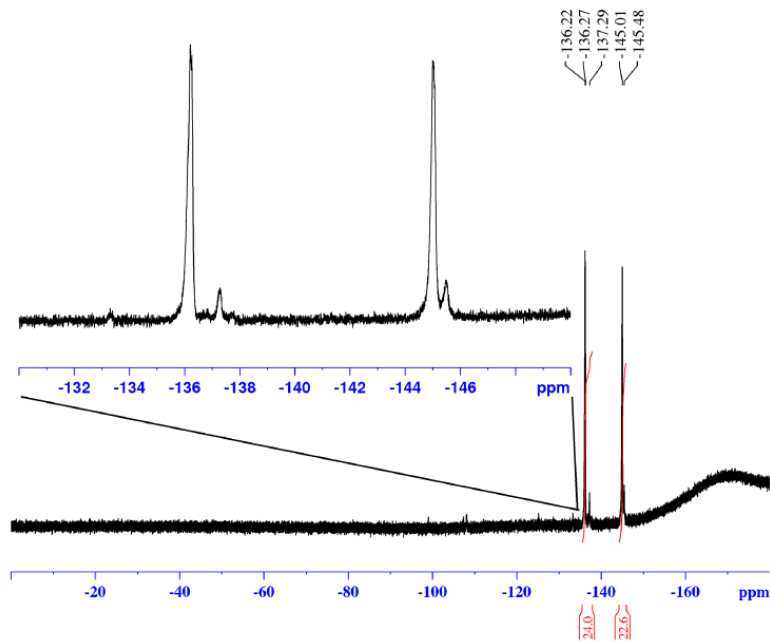
===== CHANNEL f1 =====
SFO1      128.376052 MHz
NUC1       11B
P1         10.00 usec
PLW1      52.00000000 W

F2 - Processing parameters
SI         32768
SF         128.3776161 MHz
WDW        EM
SSB        0
LB         10.00 Hz
GB         0
PC         1.40
  
```

\* This peak corresponds to a small boric acid impurity.



<sup>19</sup>F NMR

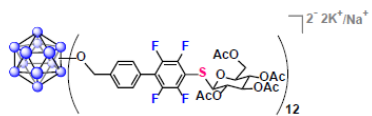


Current Data Parameters  
 NAME G2 PEG2000 0203 0125 MeOD  
 EXPNO 11  
 PROCNO 1

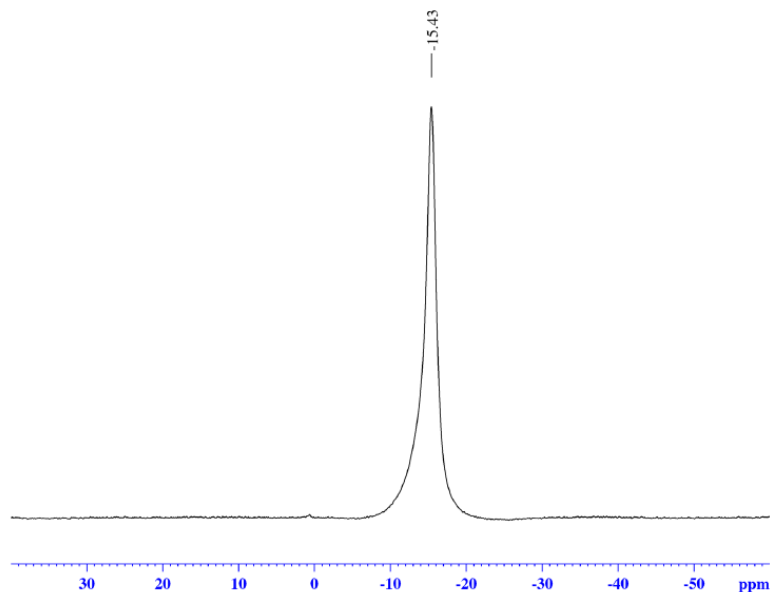
F2 - Acquisition Parameters  
 Date\_ 20160204  
 Time 17.15  
 INSTRUM av400  
 PROBHD 5 mm PABBO BB/  
 PULPROG zgpg30  
 TD 262144  
 SOLVENT MeOD  
 NS 64  
 DS 0  
 SWH 150000.000 Hz  
 FIDRES 0.572205 Hz  
 AQ 0.8738133 sec  
 RG 189.85  
 DW 3.333 usec  
 DE 6.50 usec  
 TE 299.0 K  
 D1 2.00000000 sec  
 TDO 1

===== CHANNEL f1 =====  
 SFO1 376.4983660 MHz  
 NUC1 19F  
 P1 14.50 usec  
 PLW1 17.00000000 W

F2 - Processing parameters  
 SI 262144  
 SF 376.4983660 MHz  
 WDW EM  
 SSB 0  
 LB 1.00 Hz  
 GB 0  
 PC 1.00



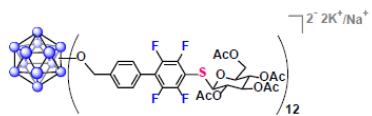
*in situ*  $^{11}\text{B}$  NMR



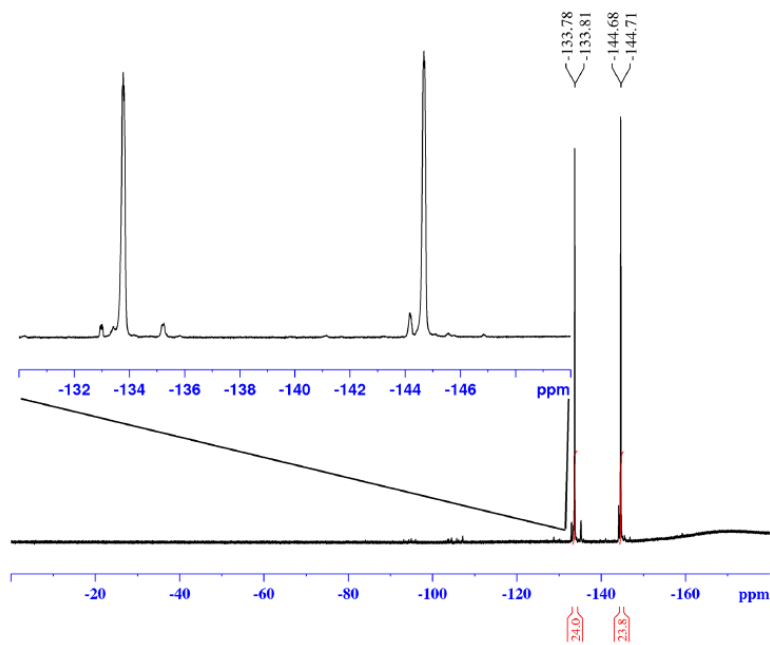
Current Data Parameters  
 NAME 0303  
 EXPNO 91  
 PROCNO 1

F2 - Acquisition Parameters  
 Date\_ 20160303  
 Time 20.25 h  
 INSTRUM av400  
 PROBHD Z108618\_0656 ( )  
 PULPROG zg  
 TD 5096  
 SOLVENT None  
 NS 1024  
 DS 0  
 SWH 51020.406 Hz  
 FIDRES 20.023708 Hz  
 AQ 0.0499408 sec  
 RG 189.85  
 DW 9.800 usec  
 DE 6.50 usec  
 TE 299.0 K  
 D1 0.05000000 sec  
 TDO 1  
 SFO1 128.3776052 MHz  
 NUC1 11B  
 P1 10.00 usec  
 PLW1 52.00000000 W

F2 - Processing parameters  
 SI 32768  
 SF 128.3776161 MHz  
 WDW EM  
 SSB 0  
 LB 10.00 Hz  
 GB 0  
 PC 1.40



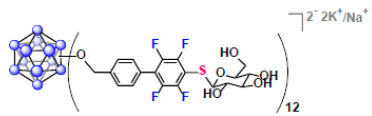
*in situ*  $^{19}\text{F}$  NMR



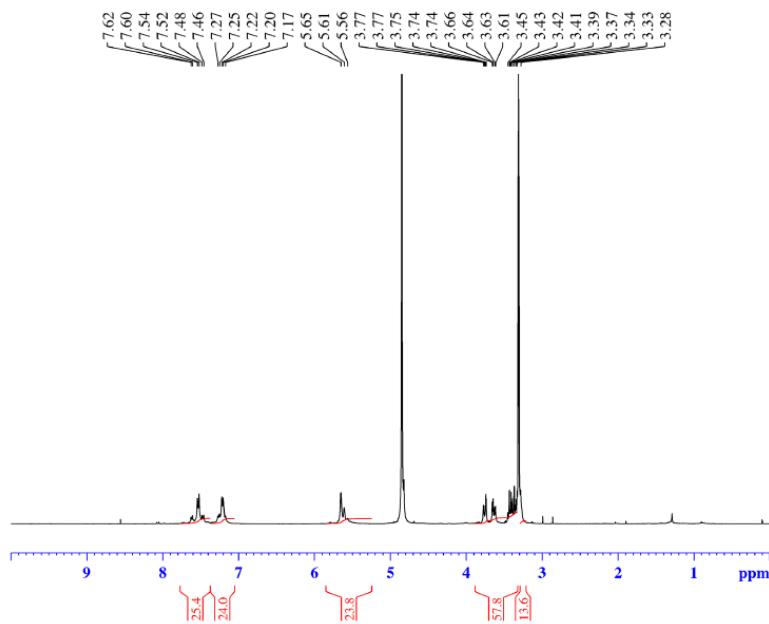
Current Data Parameters  
 NAME 0303  
 EXPNO 90  
 PROCNO 1

F2 - Acquisition Parameters  
 Date\_ 20160303  
 Time 20.20 h  
 INSTRUM av400  
 PROBHD Z108618\_0656 ( )  
 PULPROG zgpg30  
 TD 262144  
 SOLVENT None  
 NS 64  
 DS 0  
 SWH 150000.000 Hz  
 FIDRES 1.144409 Hz  
 AQ 0.8738133 sec  
 RG 189.85  
 DW 3.333 usec  
 DE 6.50 usec  
 TE 299.0 K  
 D1 2.00000000 sec  
 TDO 1  
 SFO1 376.4983660 MHz  
 NUC1  $^{19}\text{F}$   
 P1 14.50 usec  
 PLW1 17.00000000 W

F2 - Processing parameters  
 SI 262144  
 SF 376.4983660 MHz  
 WDW EM  
 SSB 0  
 LB 1.00 Hz  
 GB 0  
 PC 1.00



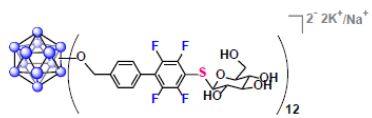
<sup>1</sup>H NMR



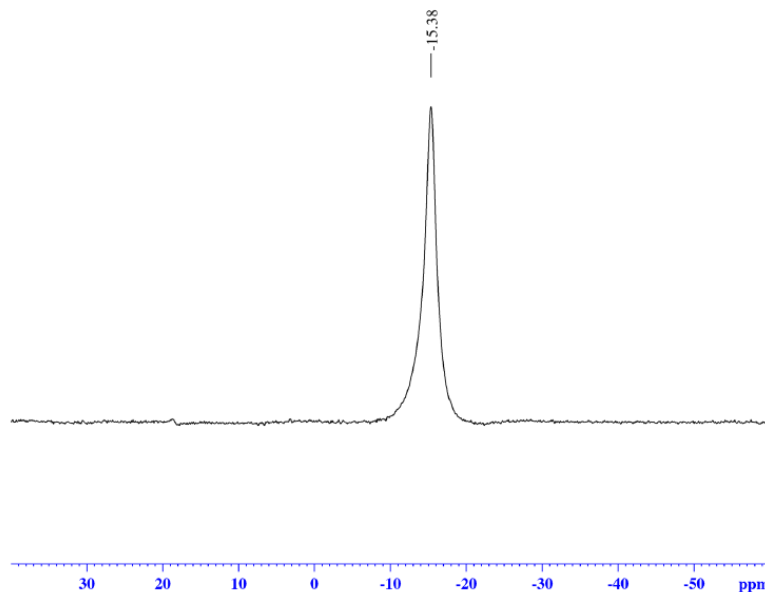
Current Data Parameters  
 NAME G2 Glc 0307 0303 (MeOD)  
 EXPNO 82  
 PROCNO 1

F2 - Acquisition Parameters  
 Date\_ 20160308  
 Time 15:59 h  
 INSTRUM av400  
 PROBHD Z108618\_0656 ( )  
 PULPROG zg30  
 TD 52882  
 SOLVENT MeOD  
 NS 32  
 DS 0  
 SWH 8012.820 Hz  
 FIDRES 0.303045 Hz  
 AQ 3.2998369 sec  
 RG 155.85  
 DW 62.400 usec  
 DE 6.50 usec  
 TE 299.0 K  
 D1 5.00000000 sec  
 TDO 1  
 SFO1 400.1324008 MHz  
 NUC1 1H  
 P1 15.00 usec  
 PLW1 13.00000000 W

F2 - Processing parameters  
 SI 65536  
 SF 400.130077 MHz  
 WDW EM  
 SSB 0  
 LB 0.30 Hz  
 GB 0  
 PC 1.00



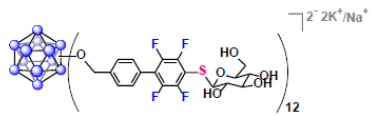
# $^{11}\text{B}$ NMR



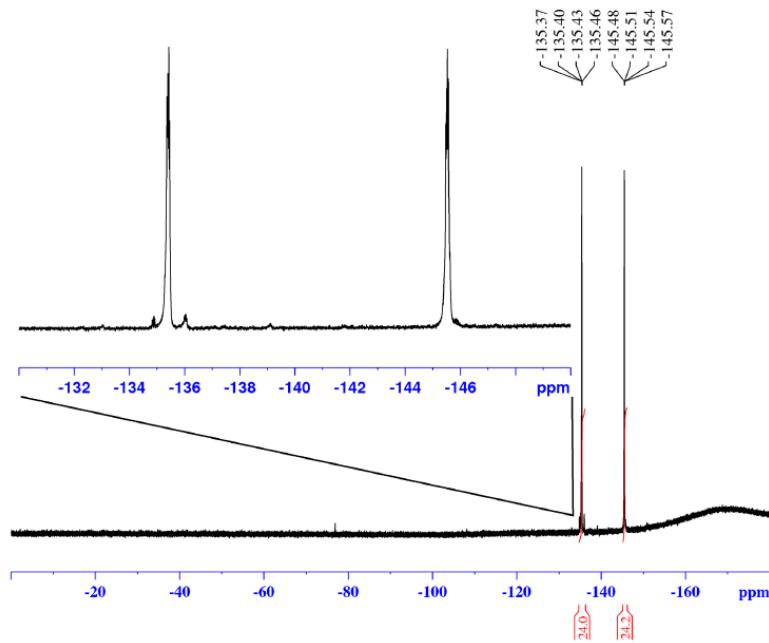
Current Data Parameters  
 NAME G2 Glc 0307 0303 (MeOD)  
 EXPNO 81  
 PROCNO 1

F2 - Acquisition Parameters  
 Date\_ 20160308  
 Time 15.54 h  
 INSTRUM av400  
 PROBHD Z108618\_0656 (z)  
 PULPROG zg  
 TD 5096  
 SOLVENT MeOD  
 NS 1024  
 DS 0  
 SWH 51020.406 Hz  
 FIDRES 20.023708 Hz  
 AQ 0.0499408 sec  
 RG 189.85  
 DW 9.800 usec  
 DE 6.50 usec  
 TE 299.0 K  
 D1 0.05000000 sec  
 TDO 1  
 SFO1 128.3776052 MHz  
 NUC1  $^{11}\text{B}$   
 P1 10.00 usec  
 PLW1 52.00000000 W

F2 - Processing parameters  
 SI 32768  
 SF 128.3776161 MHz  
 WDW EM  
 SSB 0  
 LB 10.00 Hz  
 GB 0  
 PC 1.40



$^{19}F$  NMR



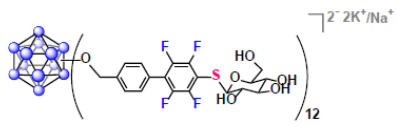
Current Data Parameters  
 NAME G2 Glc 0307 0303 (MeOD)  
 EXPNO 80  
 PROCNO 1

F2 - Acquisition Parameters  
 Date\_ 20160308  
 Time 15.51 h  
 INSTRUM av400  
 PROBHD Z108618\_0656 ( )  
 PULPROG zgpg30  
 TD 262144  
 SOLVENT MeOD  
 NS 64  
 DS 0  
 SWH 150000.000 Hz  
 FIDRES 1.144409 Hz  
 AQ 0.8738133 sec  
 RG 189.85  
 DW 3.333 usec  
 DE 6.50 usec  
 TE 299.0 K  
 D1 2.00000000 sec  
 TDO 1  
 SFO1 376.4983660 MHz  
 NUC1  $^{19}F$   
 P1 14.50 usec  
 PLW1 17.00000000 W

F2 - Processing parameters  
 SI 262144  
 SF 376.4983660 MHz  
 WDW EM  
 SSB 0  
 LB 1.00 Hz  
 GB 0  
 PC 1.00

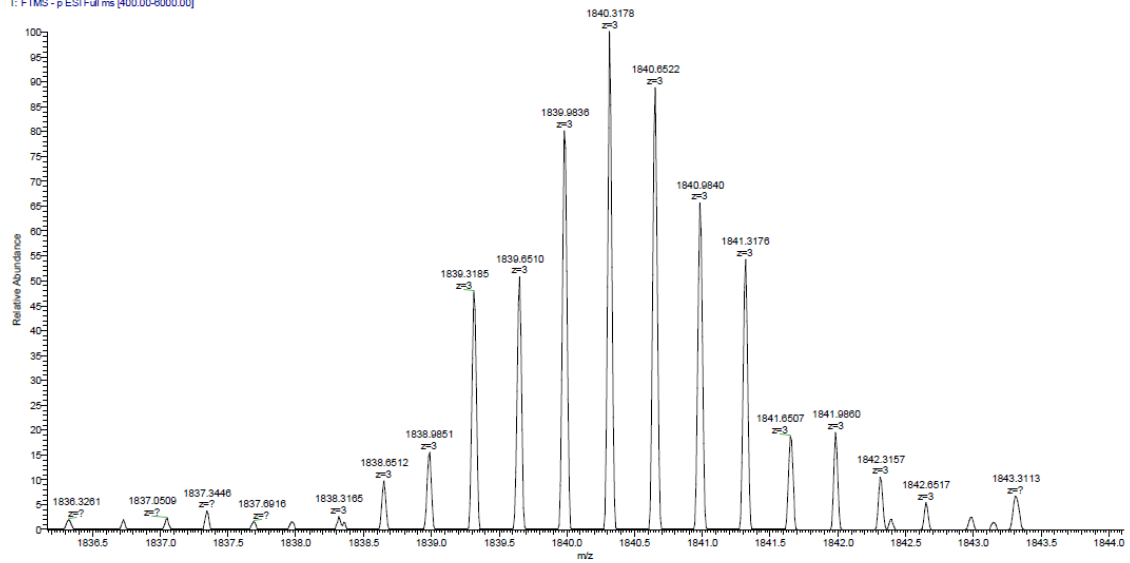


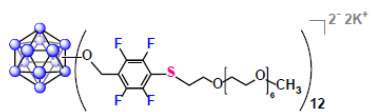




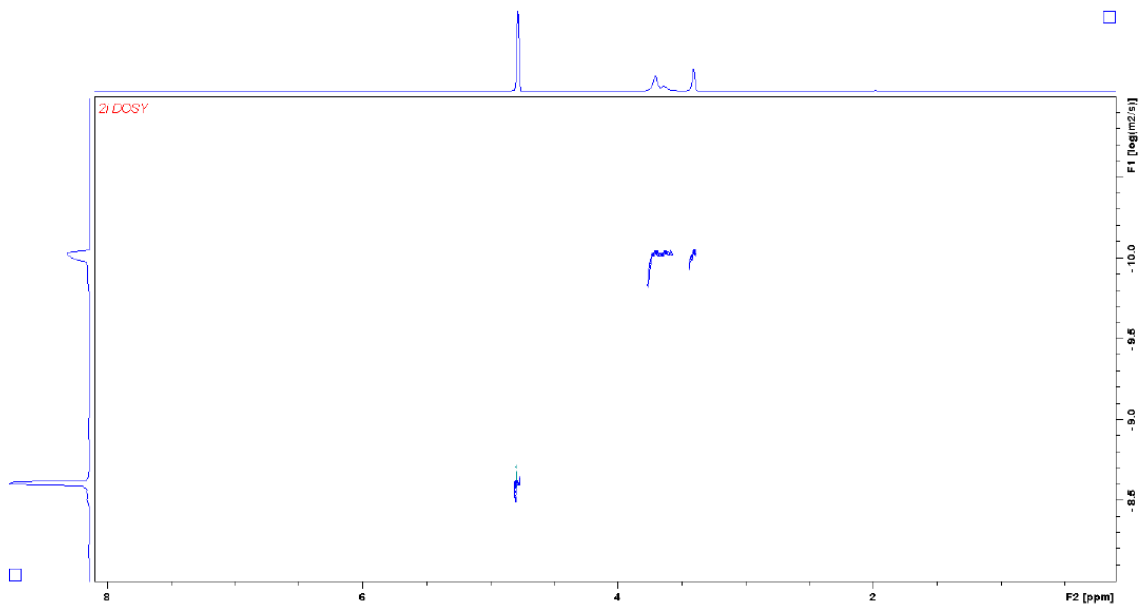
## Q Exactive High-Res Mass Spec

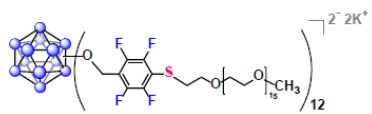
31#1-16 RT: 0.01-0.14 AV: 16 NL: 1.10E5  
T: FTMS - p-ESI Full ms [400.00-6000.00]



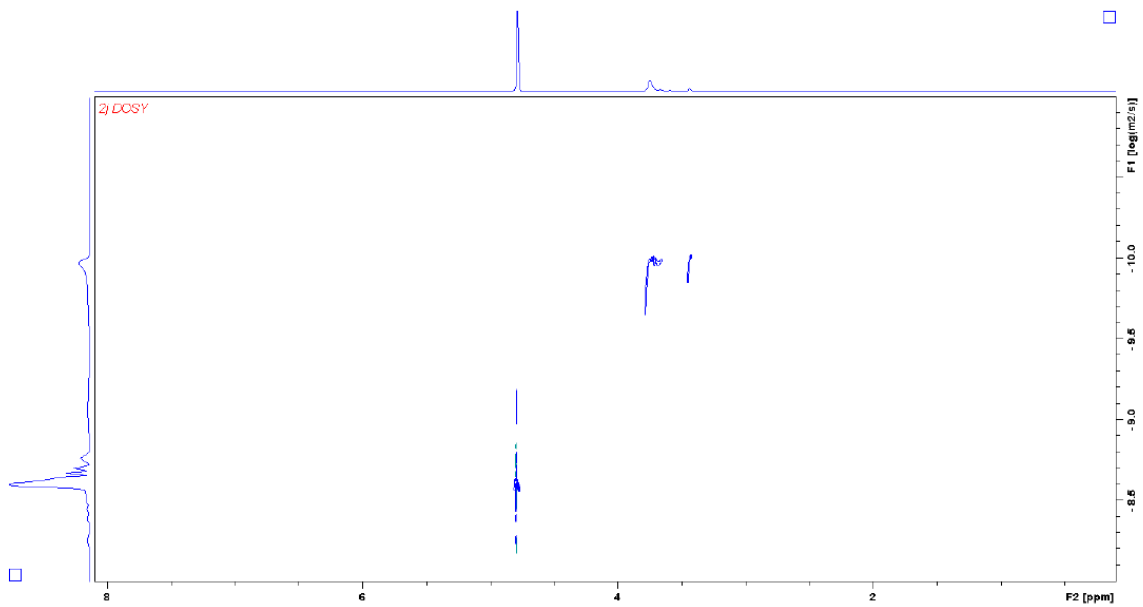


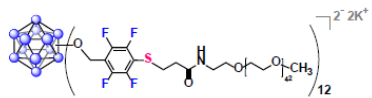
## 2D DOSY $^1H$ NMR



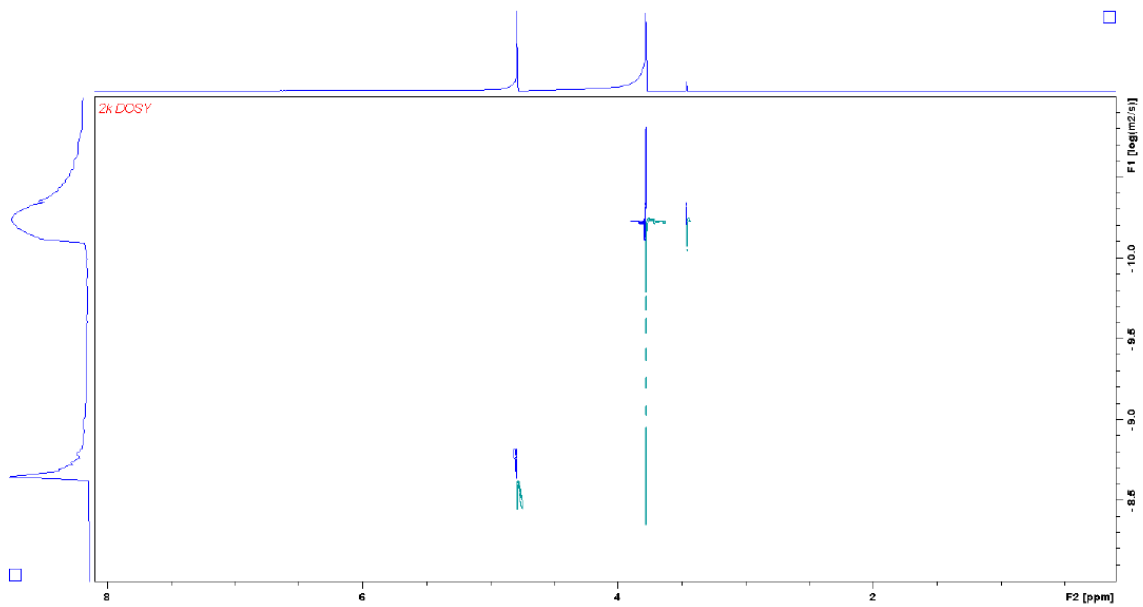


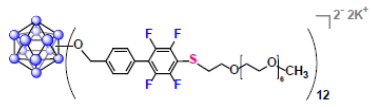
2D DOSY <sup>1</sup>H NMR



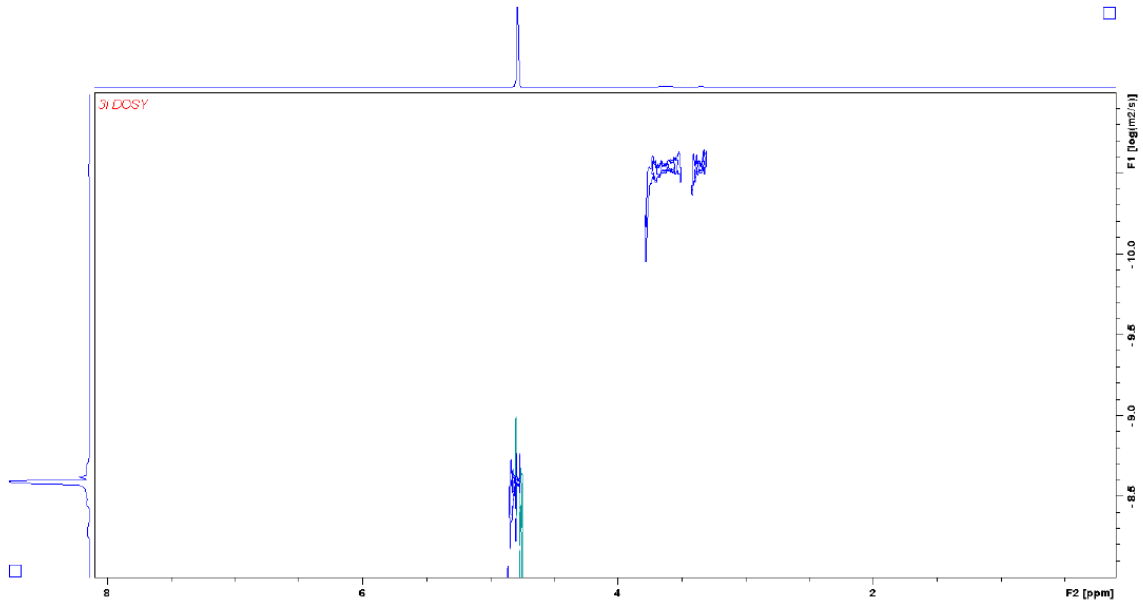


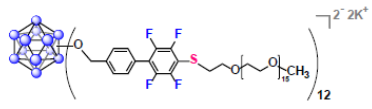
2D DOSY <sup>1</sup>H NMR



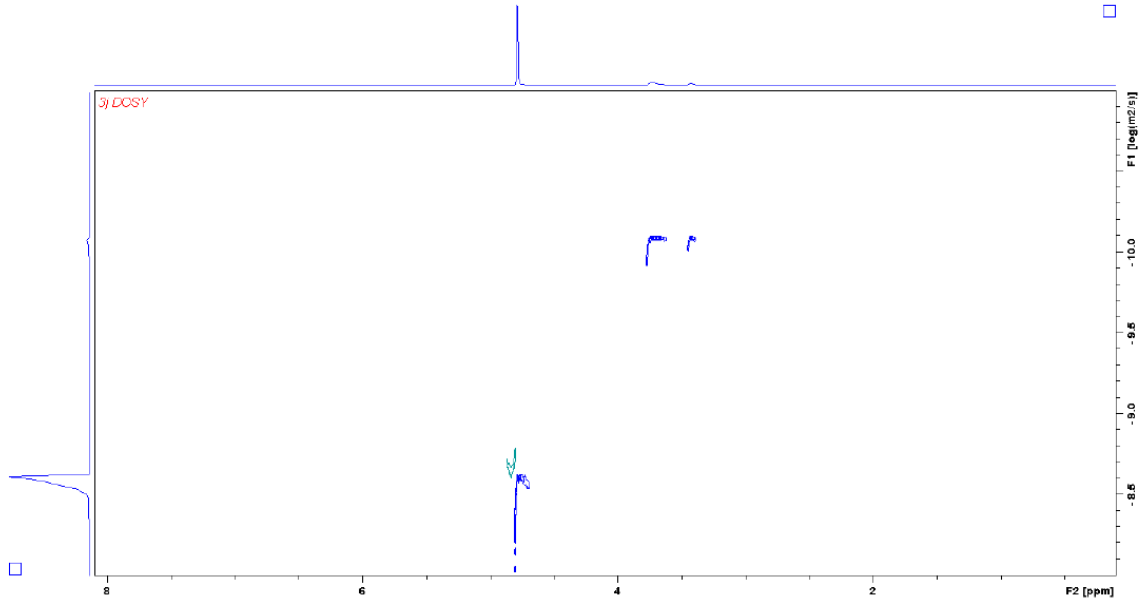


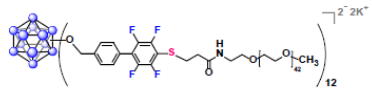
## 2D DOSY $^1\text{H}$ NMR



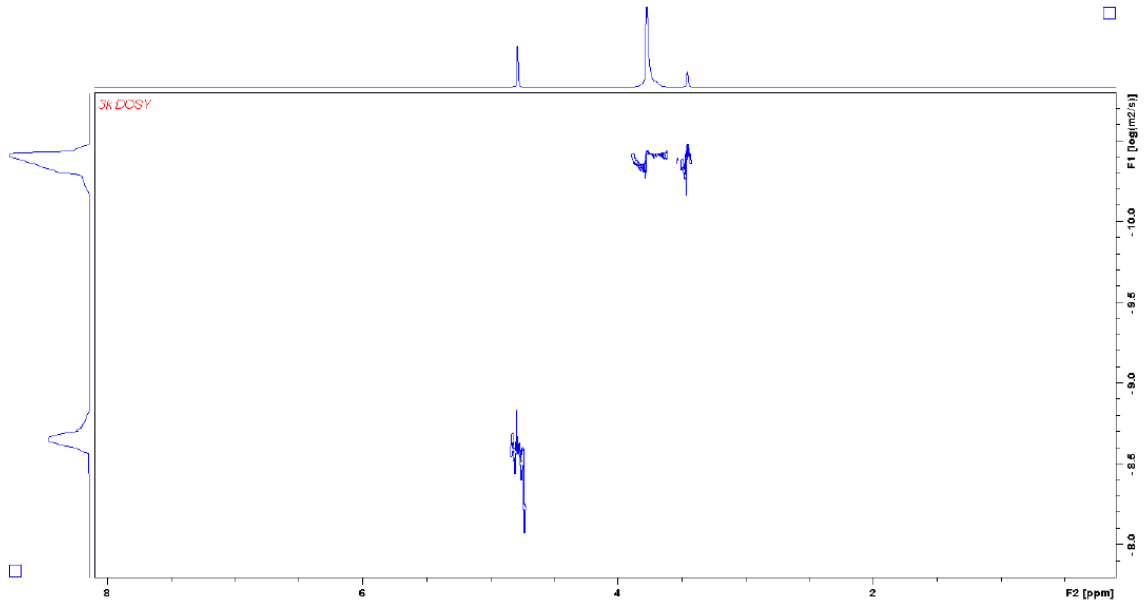


### 2D DOSY <sup>1</sup>H NMR

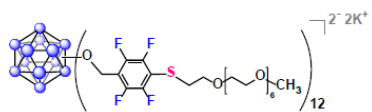




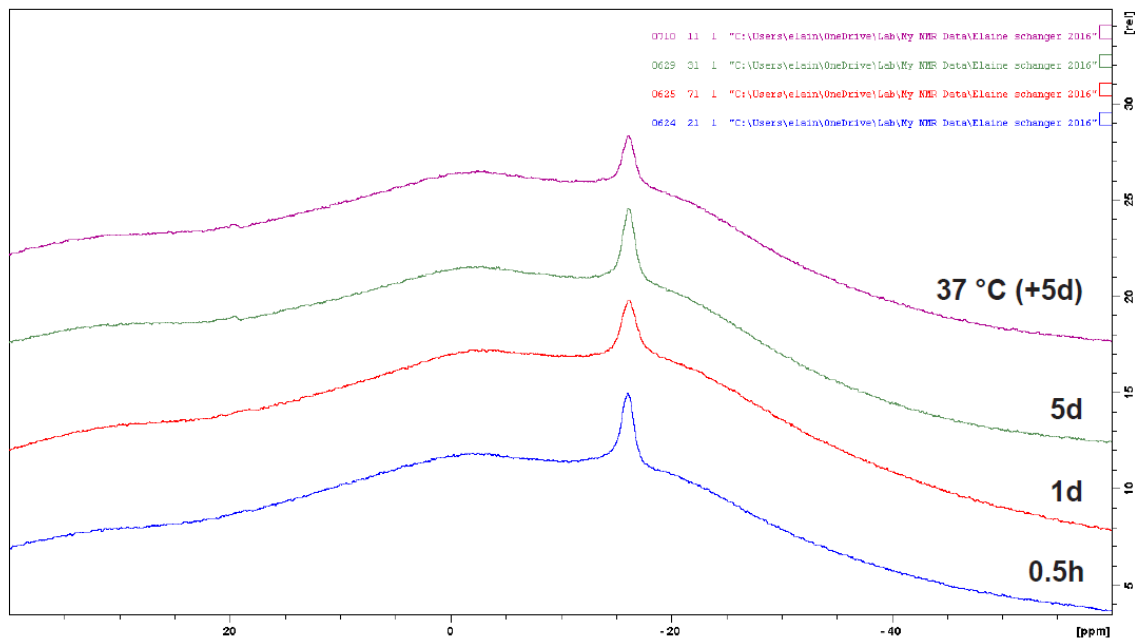
## 2D DOSY $^1\text{H}$ NMR

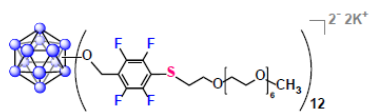




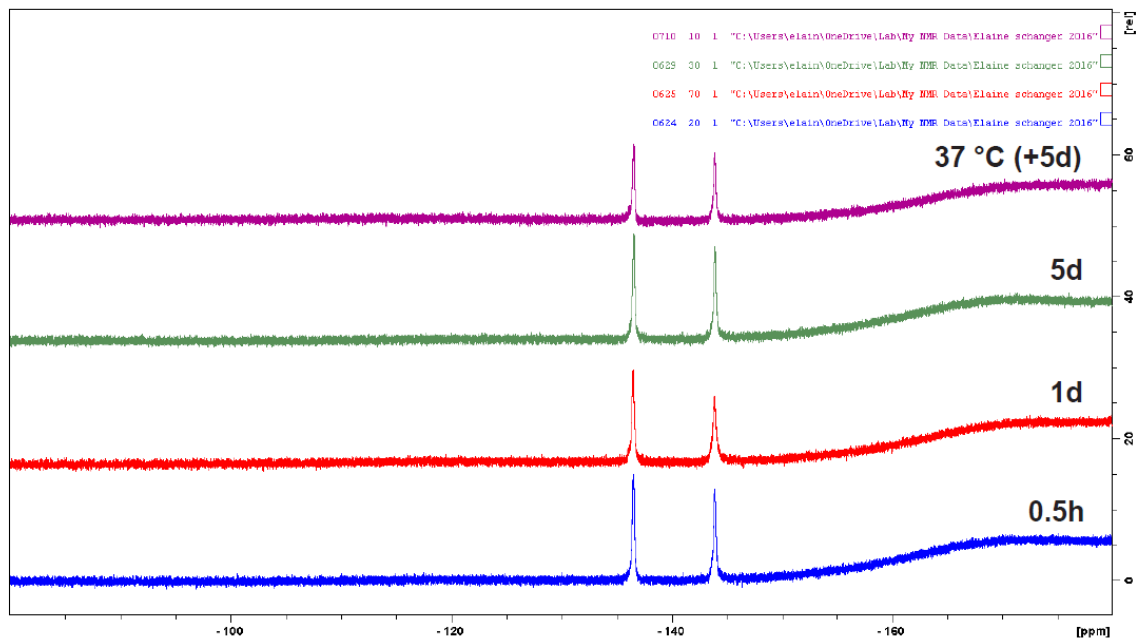


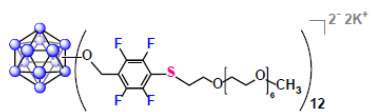
### Stability of 2i in Serum <sup>11</sup>B NMR



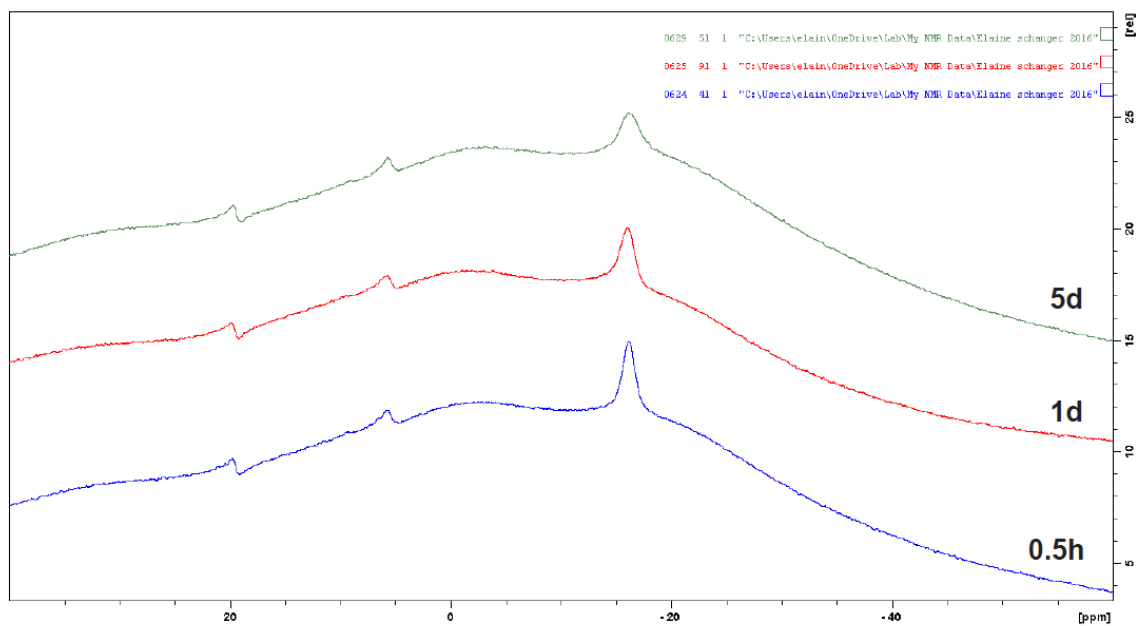


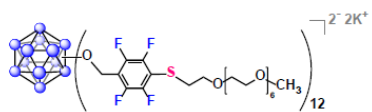
### Stability of 2i in Serum <sup>19</sup>F NMR



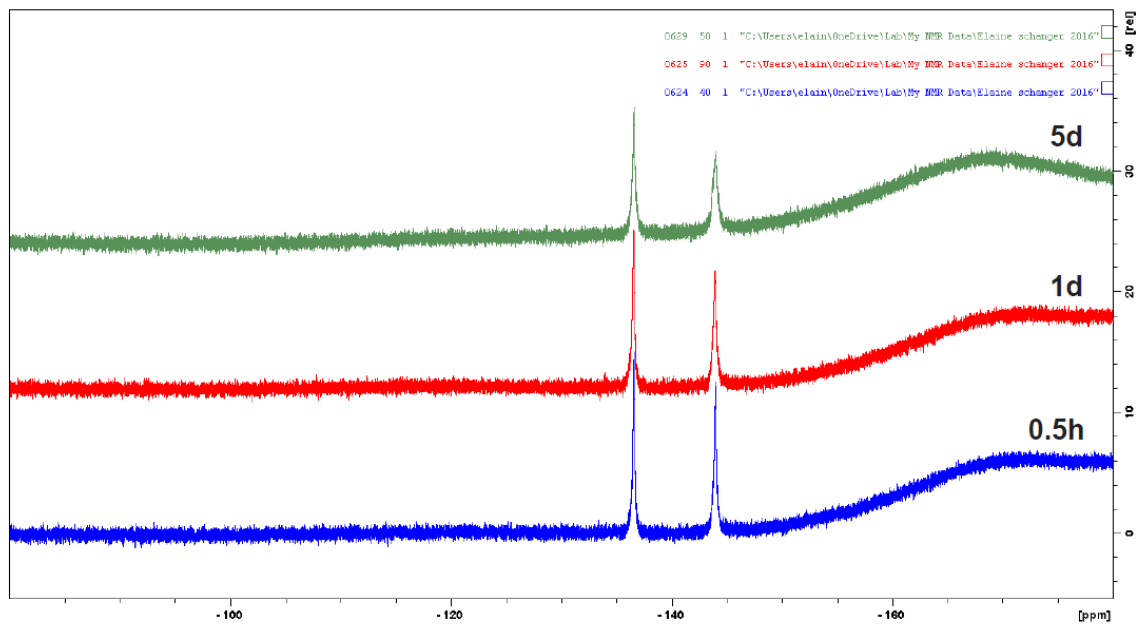


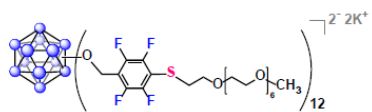
### Stability of 2i at pH 5 <sup>11</sup>B NMR



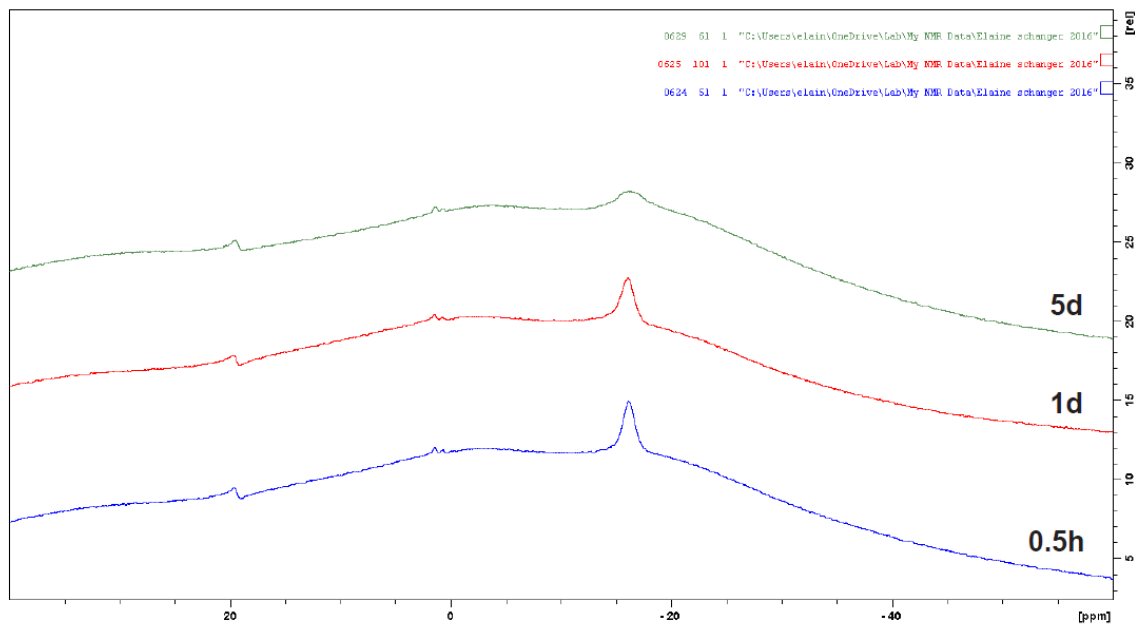


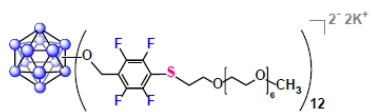
Stability of 2i at pH 5  
<sup>19</sup>F NMR



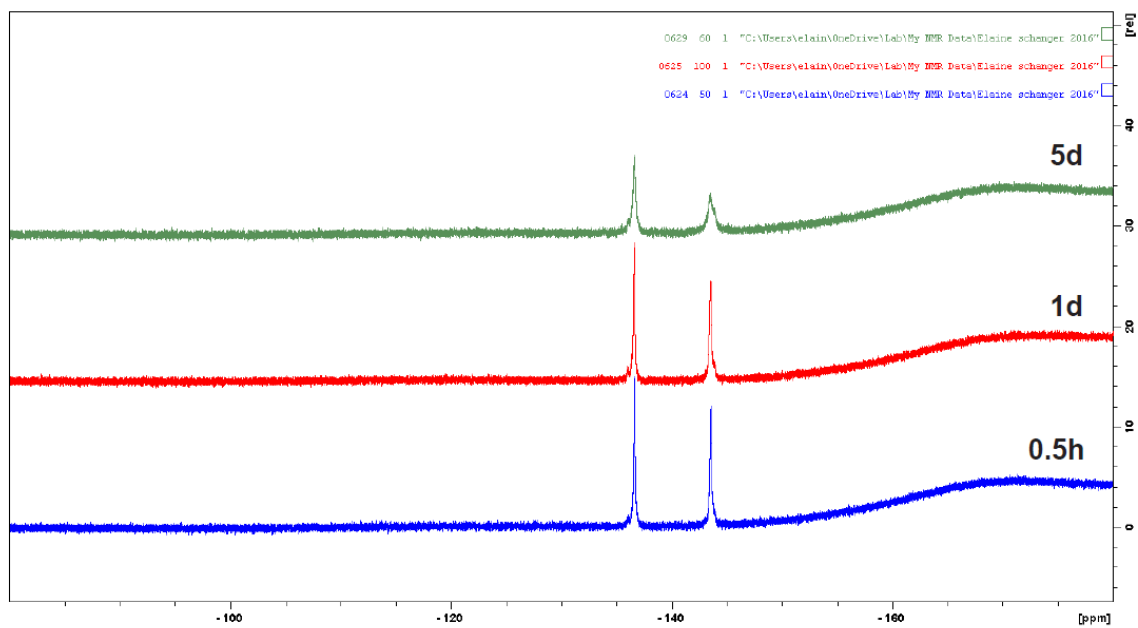


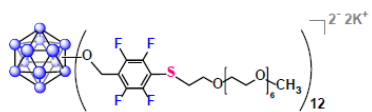
### Stability of 2i at pH 7 <sup>11</sup>B NMR



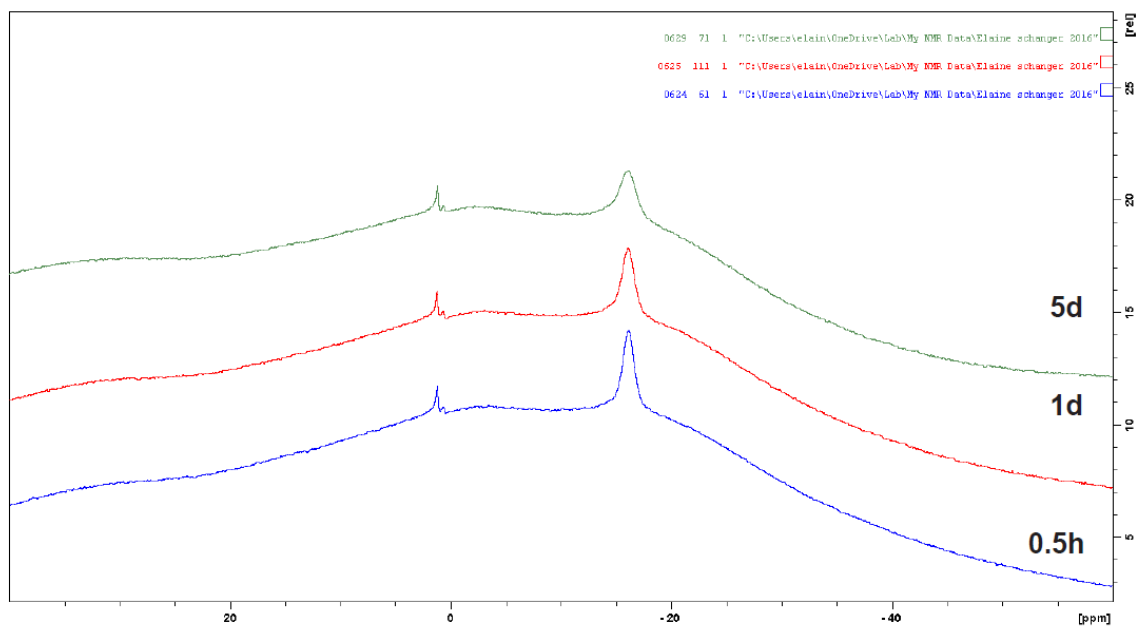


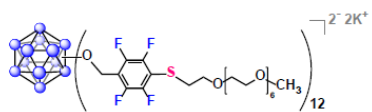
Stability of 2i at pH 7  
<sup>19</sup>F NMR



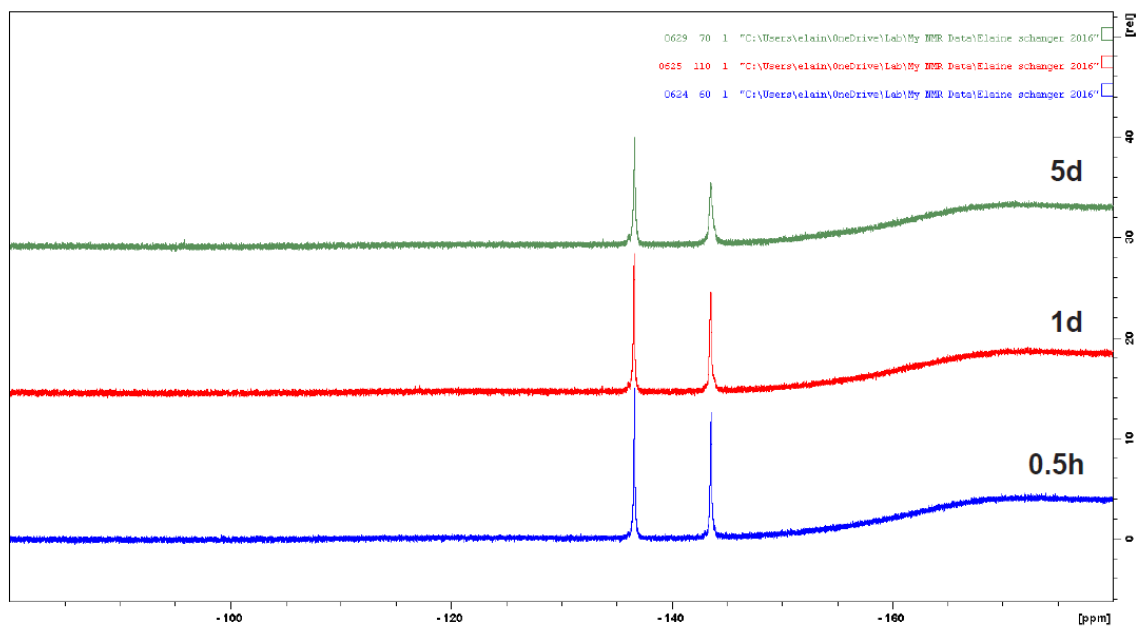


### Stability of 2i at pH 9 <sup>11</sup>B NMR

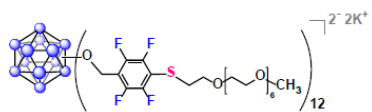




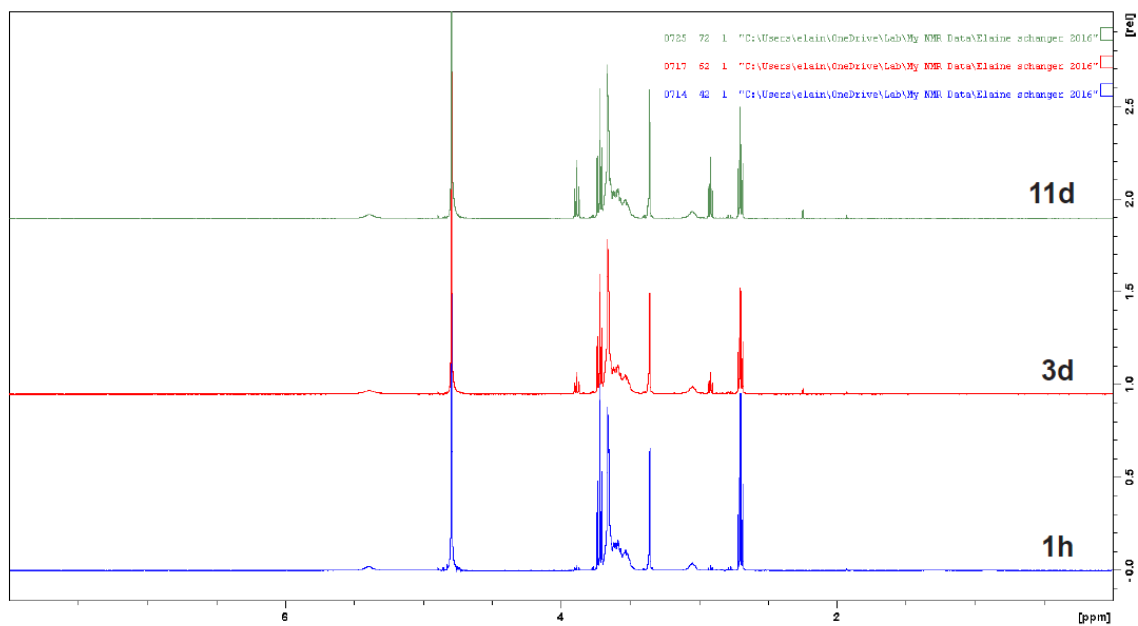
### Stability of 2i at pH 9 $^{19}\text{F}$ NMR

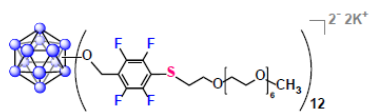




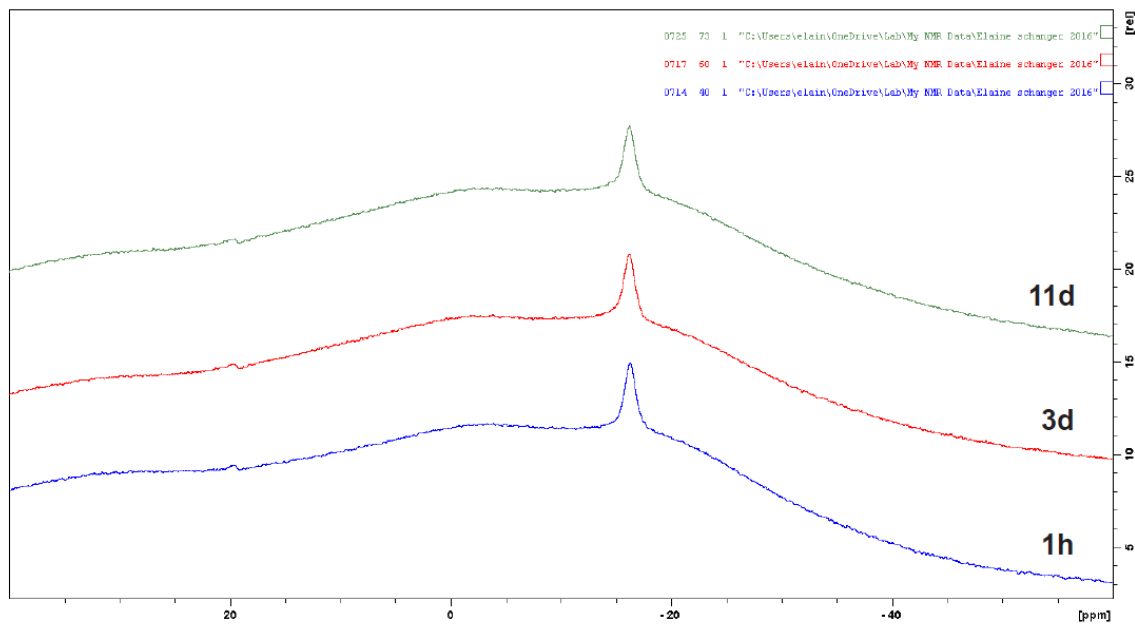


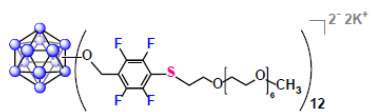
### Stability of 2i in 2-Mercaptoethanol $^1\text{H}$ NMR



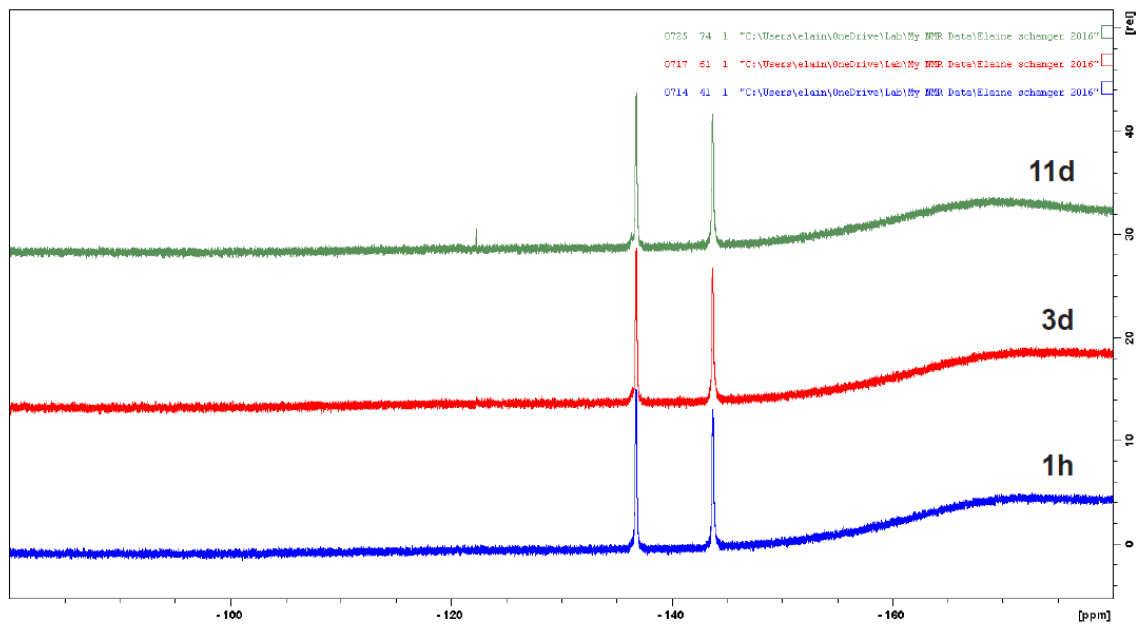


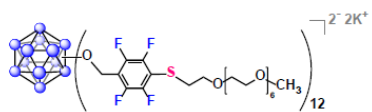
Stability of 2i in 2-Mercaptoethanol  
<sup>11</sup>B NMR





Stability of 2i in 2-Mercaptoethanol  
<sup>19</sup>F NMR

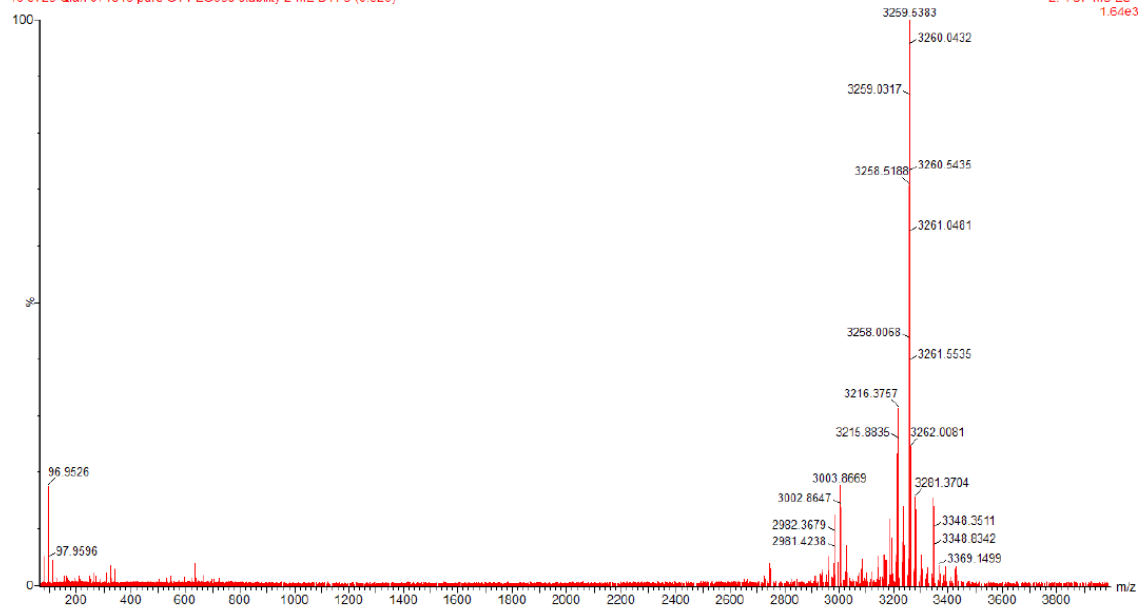


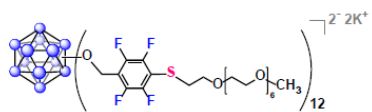


Stability of 2i in 2-Mercaptoethanol - Day 11  
Waters Mass Spec

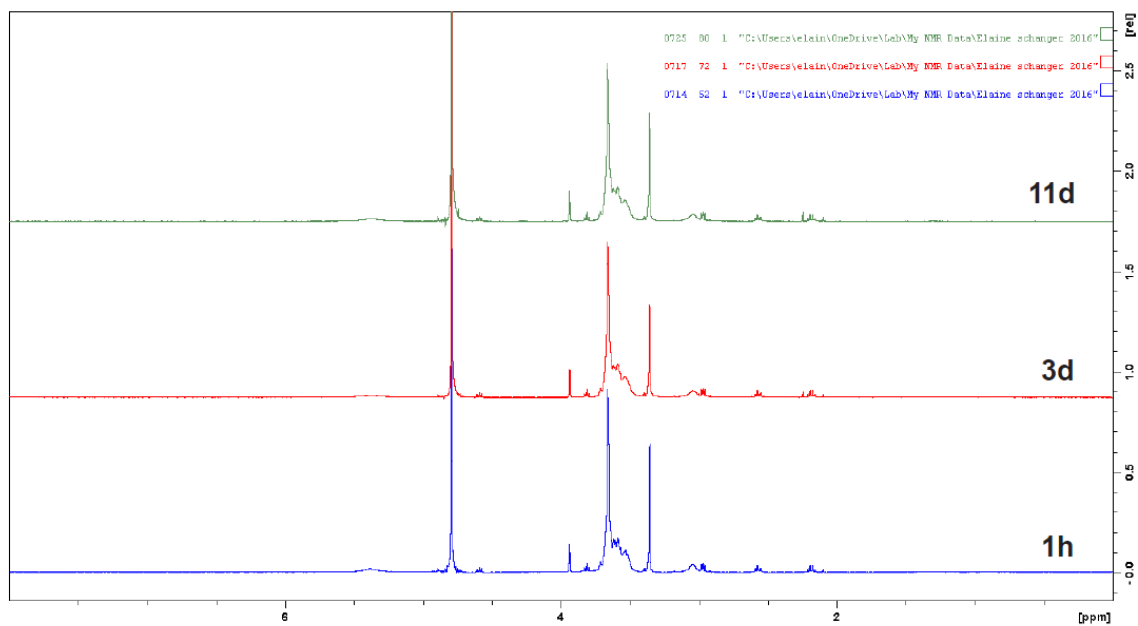
16 0725 Qian 071016 pure G1 PEG350 stability 2-ME D11 9 (0.523)

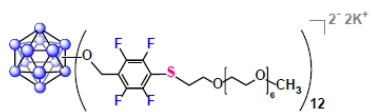
2: TOF MS ES-  
1.64e3



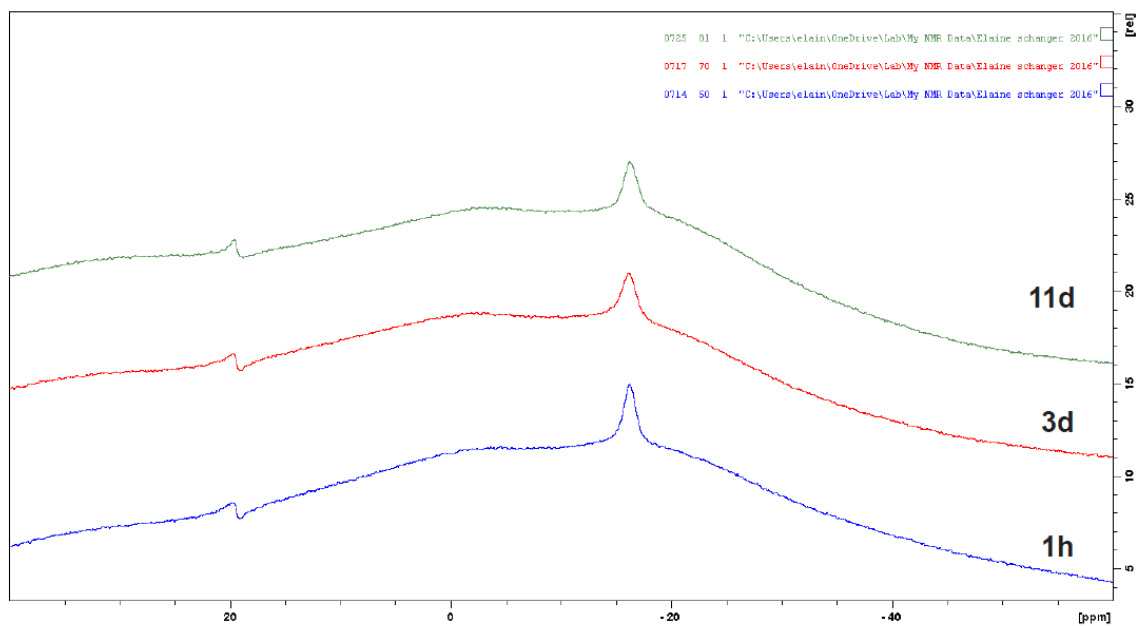


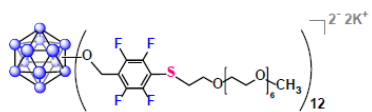
### Stability of 2i in Glutathione <sup>1</sup>H NMR



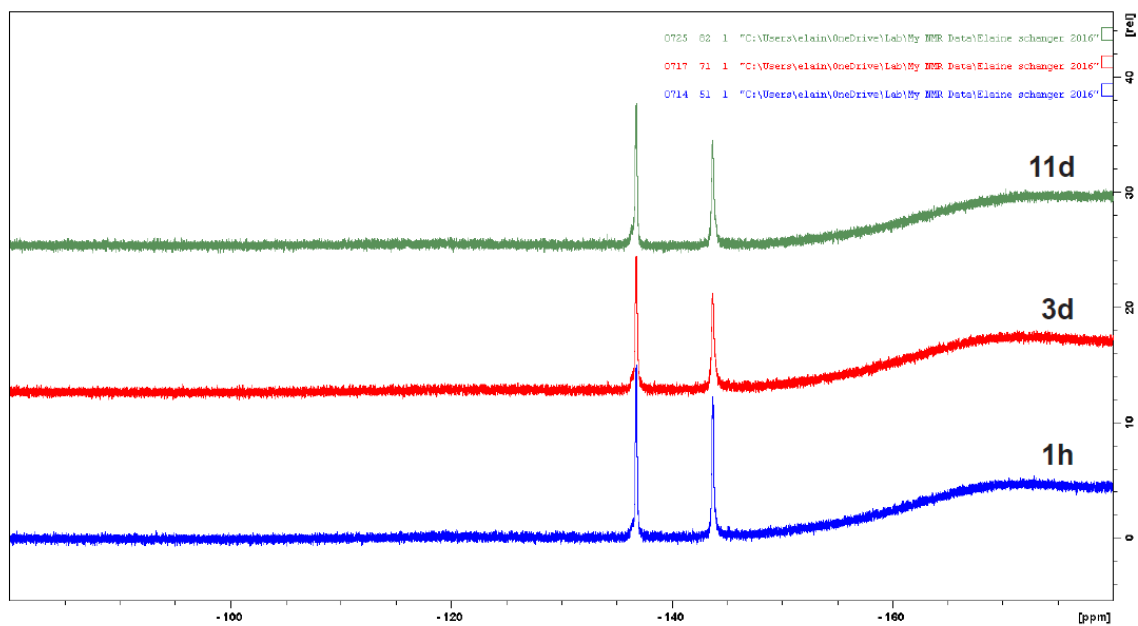


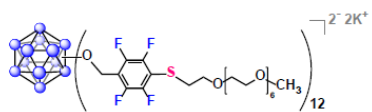
### Stability of 2i in Glutathione $^{11}B$ NMR





Stability of 2i in Glutathione  
<sup>19</sup>F NMR

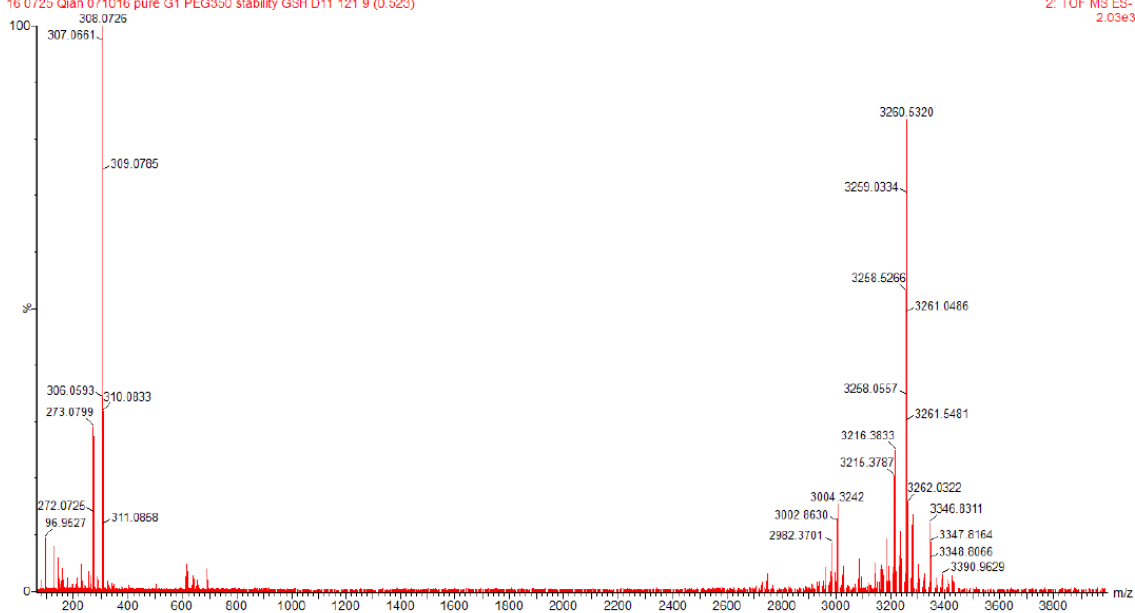




### Stability of 2i in Glutathione - Day 11 Waters Mass Spec

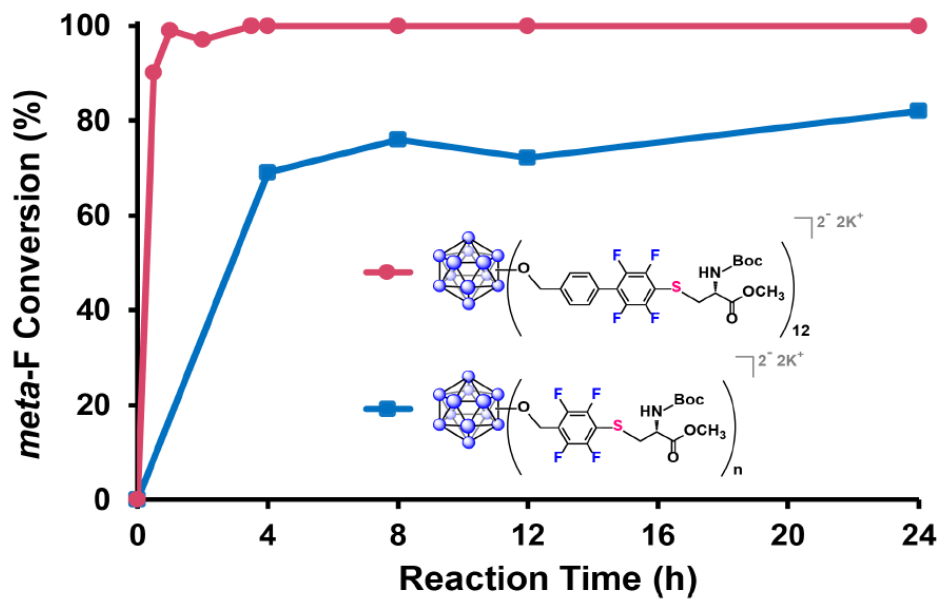
16 0725 Qian 071016 pure G1 PEG350 stability GSH D11 121 9 (0.523)

2: TOF MS ES-  
2.03e3

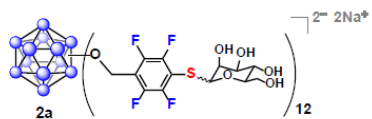




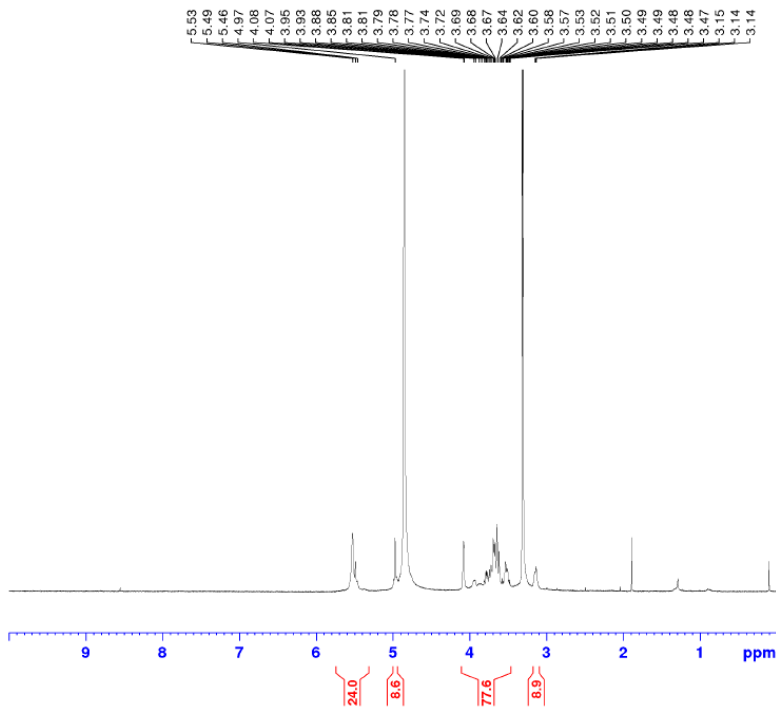
Plot of Conjugation Progress of Boc-cysteine (g)  
onto Clusters 2/3



# Supplementary Data Relevant to Chapter Three



<sup>1</sup>H NMR



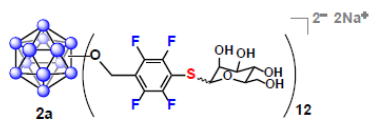
Current Data Parameters

NAME 0518  
EXPNO 120  
PROCNO 1

F2 - Acquisition Parameters  
Date\_ 20180518  
Time 11.59  
INSTRUM av400  
PROBHD 5 mm PABBO BB/  
PULPROG zg30  
TD 52882  
SOLVENT MeOD  
NS 64  
DS 0  
SWH 8012.820 Hz  
FIDRES 0.151523 Hz  
AQ 3.2998369 sec  
RG 189.85  
DW 62.400 usec  
DE 6.50 usec  
TE 298.2 K  
D1 2.00000000 sec  
TD0 1

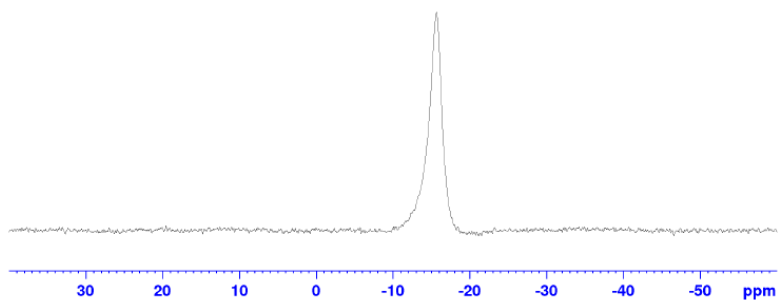
===== CHANNEL f1 =====  
SFO1 400.1324008 MHz  
NUC1 1H  
P1 15.00 usec  
PLW1 13.00000000 W

F2 - Processing parameters  
SI 65536  
SF 400.1300078 MHz  
WDW EM  
SSB 0  
LB 0.30 Hz  
GB 0  
PC 1.00



# <sup>11</sup>B NMR

-15.66

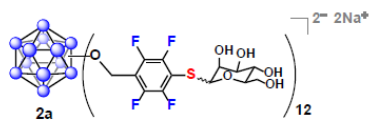


Current Data Parameters  
 NAME 0518  
 EXPNO 122  
 PROCNO 1

F2 - Acquisition Parameters  
 Date\_ 20180518  
 Time 12.18  
 INSTRUM av400  
 PROBHD 5 mm PABBO BB/  
 PULPROG zg  
 TD 5096  
 SOLVENT MeOD  
 NS 2048  
 DS 0  
 SWH 51020.406 Hz  
 FIDRES 10.011854 Hz  
 AQ 0.0499408 sec  
 RG 189.85  
 DW 9.800 usec  
 DE 6.50 usec  
 TE 298.4 K  
 D1 0.0500000 sec  
 TD0 1

===== CHANNEL f1 =====  
 SFO1 128.3776052 MHz  
 NUC1 11B  
 P1 10.00 usec  
 PLW1 52.00000000 W

F2 - Processing parameters  
 SI 32768  
 SF 128.3776161 MHz  
 WDW EM  
 SSB 0  
 LB 10.00 Hz  
 GB 0  
 PC 1.40



<sup>19</sup>F NMR

-136.60  
-137.02  
-144.57  
-144.86

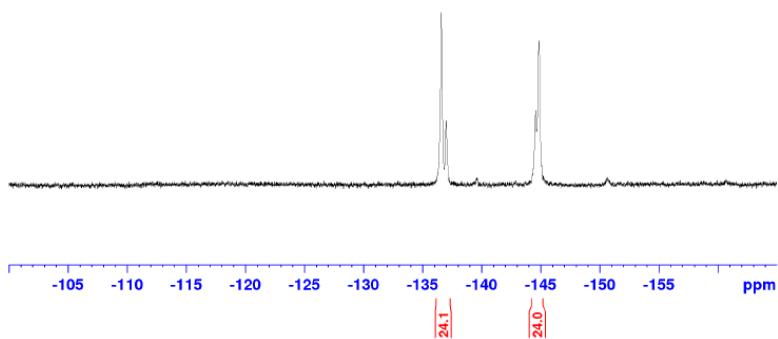


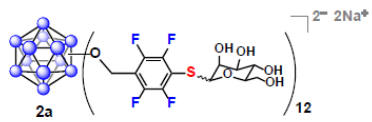
Current Data Parameters  
NAME 0518  
EXPNO 121  
PROCNO 1

F2 - Acquisition Parameters  
Date\_ 20180518  
Time 12.13  
INSTRUM av400  
PROBHD 5 mm PABBO BB/  
PULPROG zgpg30  
TD 262144  
SOLVENT MeOD  
NS 256  
DS 0  
SWH 150000.000 Hz  
FIDRES 0.572205 Hz  
AQ 0.8738133 sec  
RG 189.85  
DW 3.333 usec  
DE 6.50 usec  
TE 298.4 K  
D1 2.0000000 sec  
TD0 1

===== CHANNEL f1 =====  
SFO1 376.4983660 MHz  
NUC1 19F  
P1 14.50 usec  
PLW1 17.00000000 W

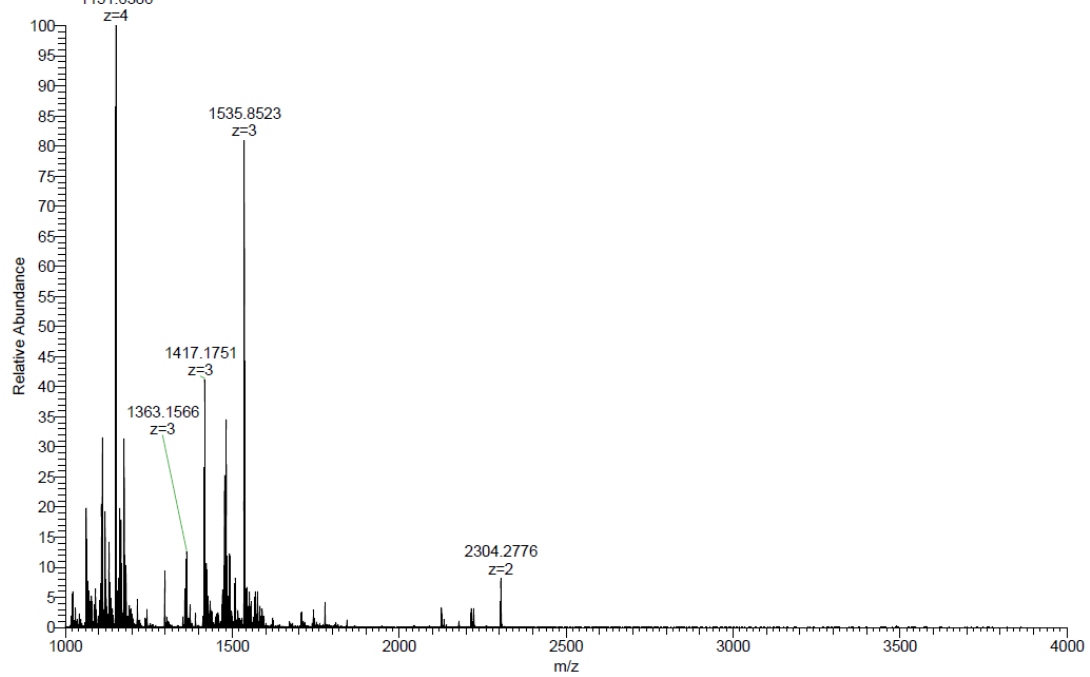
F2 - Processing parameters  
SI 262144  
SF 376.4983660 MHz  
WDW EM  
SSB 0  
LB 3.00 Hz  
GB 0  
PC 1.00

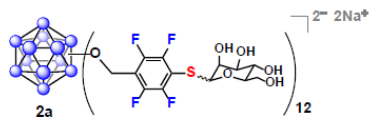




2a #1-50 RT: 0.02-0.96 AV: 50 NL: 5.48E5  
 T: FTMS - p ESI Full ms [500.0000-4000.0000]  
 1151.6386

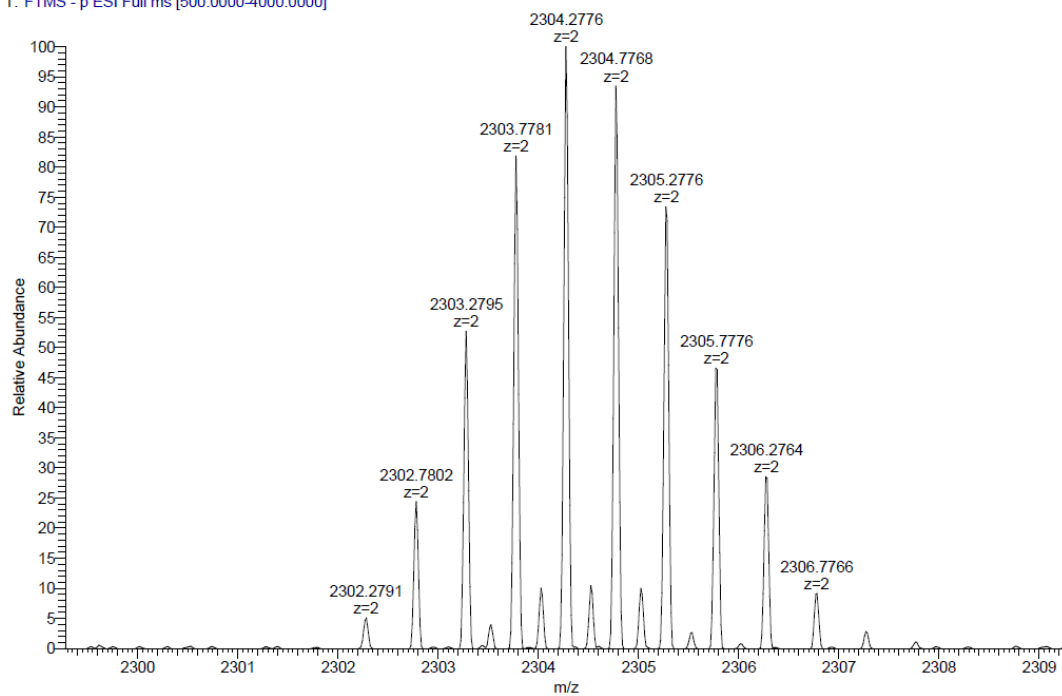
### ESI-HRMS

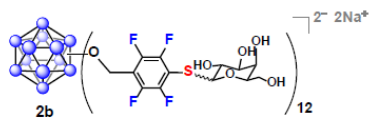




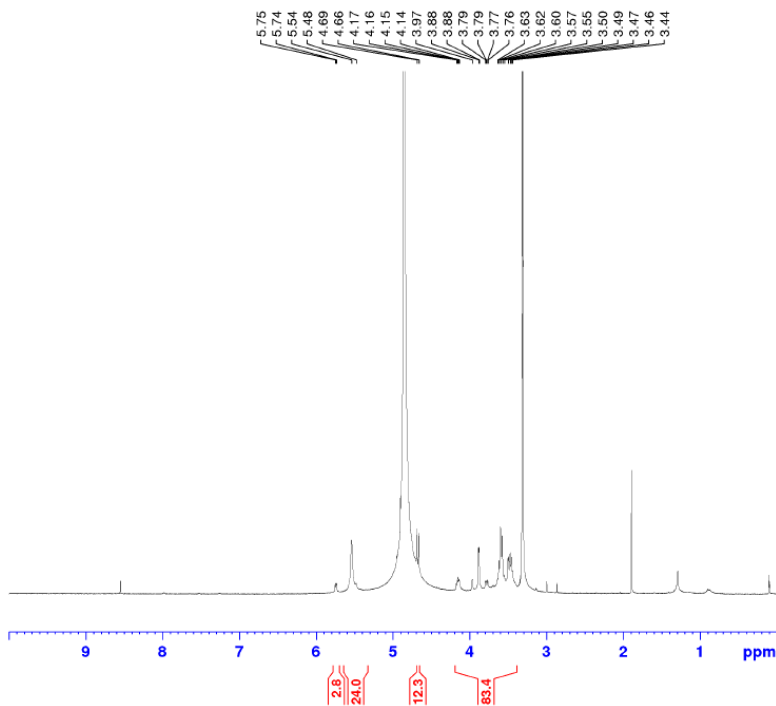
2a #1-50 RT: 0.02-0.96 AV: 50 NL: 4.43E4  
 T: FTMS - p ESI Full ms [500.0000-4000.0000]

### ESI-HRMS





# <sup>1</sup>H NMR

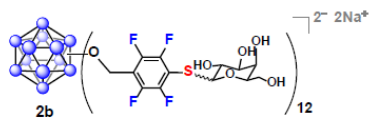


Current Data Parameters  
 NAME 0109  
 EXPNO 70  
 PROCNO 1

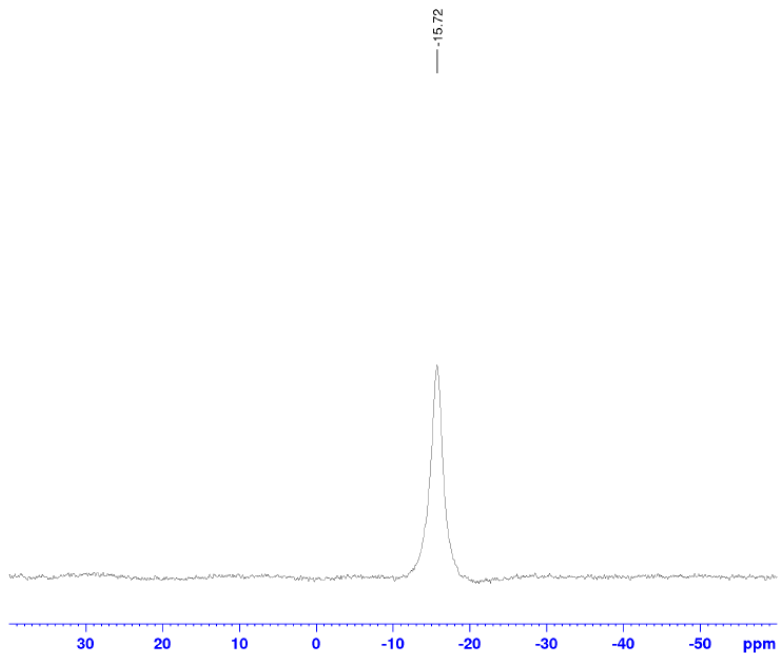
F2 - Acquisition Parameters  
 Date\_ 20190109  
 Time 13.12  
 INSTRUM av400  
 PROBHD 5 mm PABBO BB/  
 PULPROG zg30  
 TD 52882  
 SOLVENT MeOD  
 NS 64  
 DS 0  
 SWH 8012.820 Hz  
 FIDRES 0.151523 Hz  
 AQ 3.2998369 sec  
 RG 155.85  
 DW 62.400 usec  
 DE 6.50 usec  
 TE 298.7 K  
 D1 2.0000000 sec  
 TD0 1

===== CHANNEL f1 =====  
 SFO1 400.1324008 MHz  
 NUC1 <sup>1</sup>H  
 P1 15.00 usec  
 PLW1 13.0000000 W

F2 - Processing parameters  
 SI 65536  
 SF 400.1300080 MHz  
 WDW EM  
 SSB 0  
 LB 0.30 Hz  
 GB 0  
 PC 1.00



<sup>11</sup>B NMR



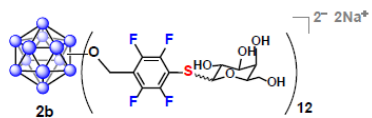
Current Data Parameters  
 NAME 0109  
 EXPNO 72  
 PROCNO 1

F2 - Acquisition Parameters  
 Date\_ 20190109  
 Time 13.24  
 INSTRUM av400  
 PROBHD 5 mm PABBO BB/  
 PULPROG zg  
 TD 5096  
 SOLVENT MeOD  
 NS 1024  
 DS 0  
 SWH 51020.406 Hz  
 FIDRES 10.011854 Hz  
 AQ 0.0499408 sec  
 RG 189.85  
 DW 9.800 usec  
 DE 6.50 usec  
 TE 299.4 K  
 D1 0.05000000 sec  
 TD0 1

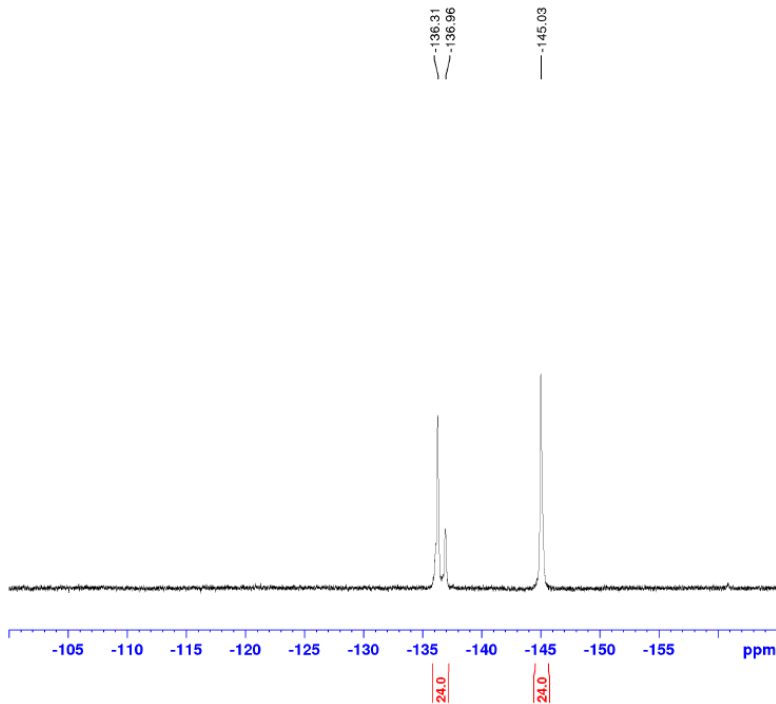
===== CHANNEL f1 =====  
 SFO1 128.3776052 MHz  
 NUC1 11B  
 P1 10.00 usec  
 PLW1 52.00000000 W

F2 - Processing parameters  
 SI 32768  
 SF 128.3776161 MHz  
 WDW EM  
 SSB 0  
 LB 10.00 Hz  
 GB 0  
 PC 1.40





<sup>19</sup>F NMR

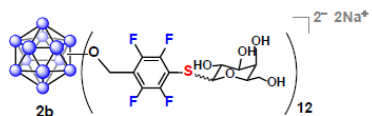


Current Data Parameters  
NAME 0109  
EXPNO 71  
PROCNO 1

F2 - Acquisition Parameters  
Date\_ 20190109  
Time 13.20  
INSTRUM av400  
PROBHD 5 mm PABBO BB/  
PULPROG zgpg30  
TD 262144  
SOLVENT MeOD  
NS 128  
DS 0  
SWH 150000.000 Hz  
FIDRES 0.572205 Hz  
AQ 0.8738133 sec  
RG 189.85  
DW 3.333 usec  
DE 6.50 usec  
TE 299.2 K  
D1 2.0000000 sec  
TD0 1

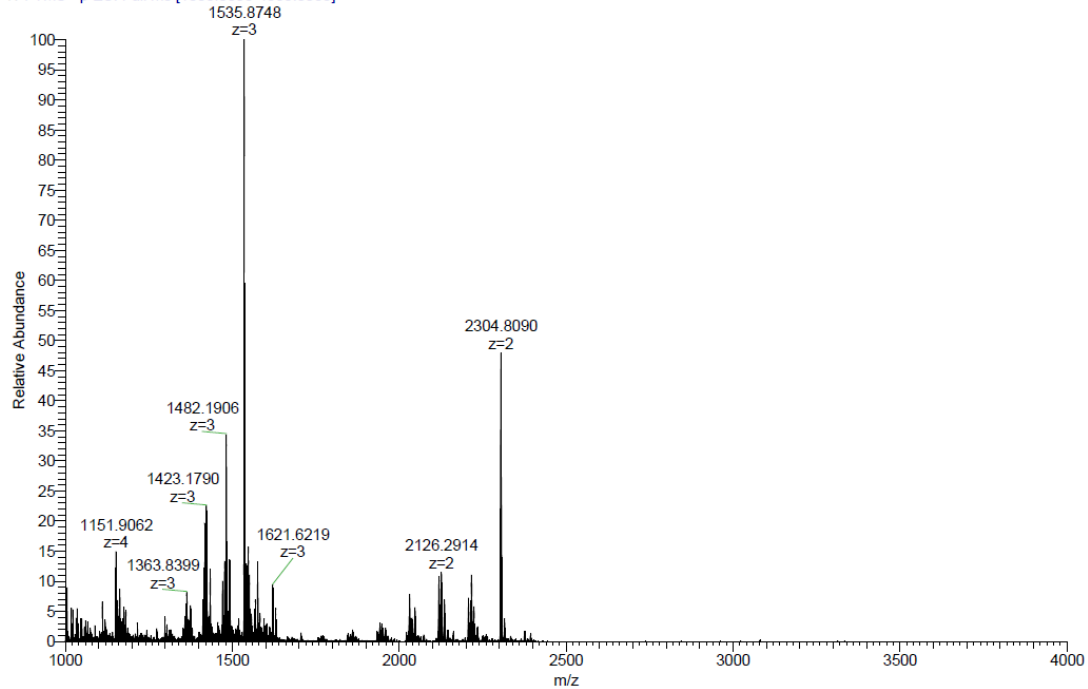
===== CHANNEL f1 =====  
SFO1 376.4983660 MHz  
NUC1 19F  
P1 14.50 usec  
PLW1 17.00000000 W

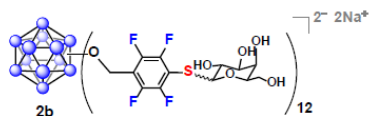
F2 - Processing parameters  
SI 262144  
SF 376.4983660 MHz  
WDW EM  
SSB 0  
LB 3.00 Hz  
GB 0  
PC 1.00



### ESI-HRMS

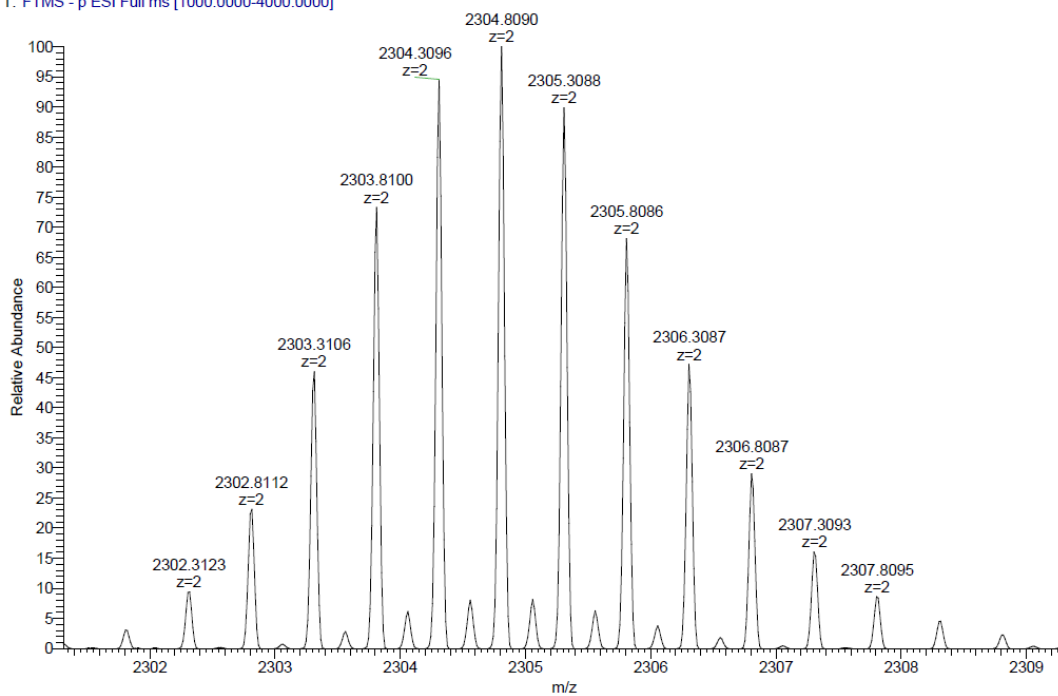
2b #1-50 RT: 0.01-0.47 AV: 50 NL: 4.32E6  
 T: FTMS - p ESI Full ms [1000.0000-4000.0000]

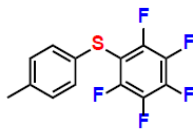




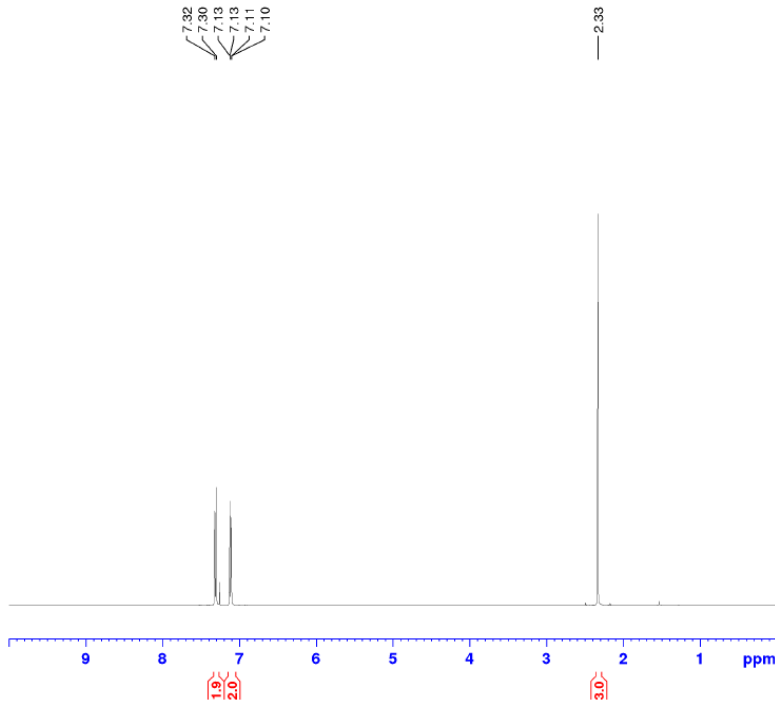
2b #1-50 RT: 0.01-0.47 AV: 50 NL: 2.07E6  
 T: FTMS - p ESI Full.ms [1000.0000-4000.0000]

### ESI-HRMS





<sup>1</sup>H NMR

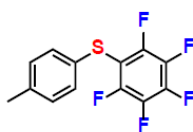


Current Data Parameters  
 NAME 1201  
 EXPNO 21  
 PROCNO 1

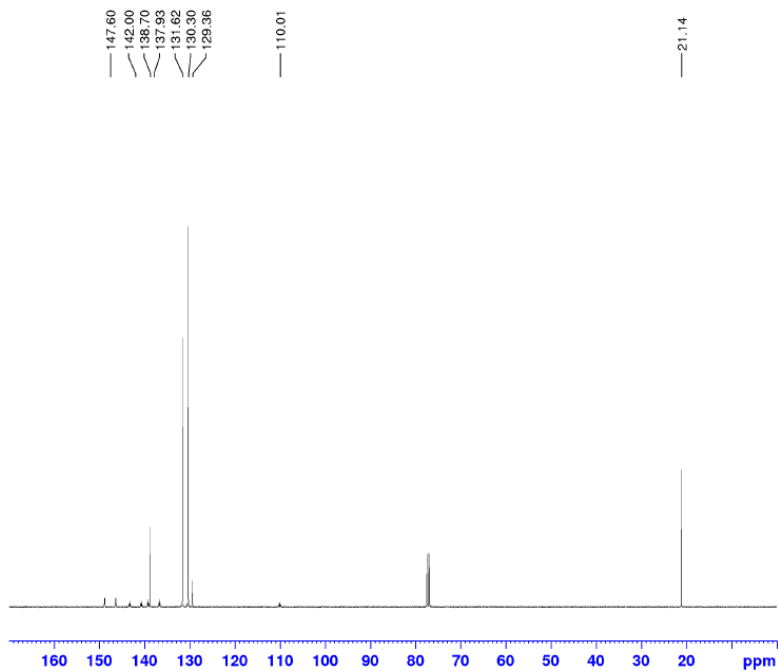
F2 - Acquisition Parameters  
 Date\_ 20181201  
 Time 13.03  
 INSTRUM av400  
 PROBHD 5 mm PABBO BB/  
 PULPROG zg30  
 TD 52882  
 SOLVENT CDCl3  
 NS 32  
 DS 0  
 SWH 8012.820 Hz  
 FIDRES 0.151523 Hz  
 AQ 3.2998369 sec  
 RG 107.83  
 DW 62.400 usec  
 DE 6.50 usec  
 TE 298.2 K  
 D1 2.0000000 sec  
 TD0 1

===== CHANNEL f1 =====  
 SFO1 400.1324008 MHz  
 NUC1 1H  
 P1 15.00 usec  
 PLW1 13.00000000 W

F2 - Processing parameters  
 SI 65536  
 SF 400.1300177 MHz  
 WDW EM  
 SSB 0  
 LB 0.30 Hz  
 GB 0  
 PC 1.00



$^{13}\text{C}\{^1\text{H}\}$  NMR

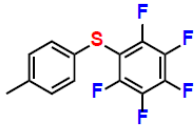


Current Data Parameters  
 NAME 1201  
 EXPNO 10  
 PROCNO 1

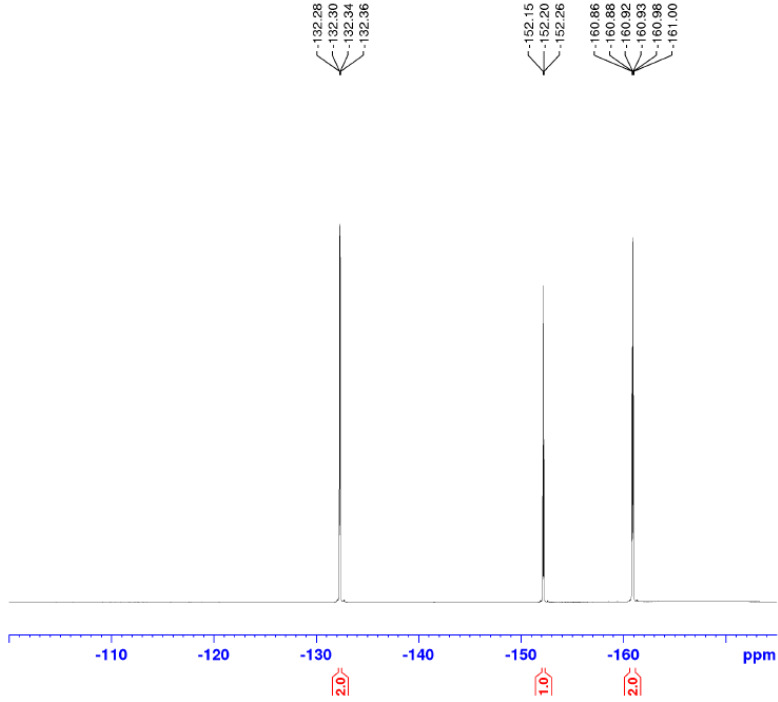
F2 - Acquisition Parameters  
 Date\_ 20181201  
 Time 12.13  
 INSTRUM av400  
 PROBHD 5 mm PABBO BB/  
 PULPROG zgpg30  
 TD 65536  
 SOLVENT CDCl3  
 NS 256  
 DS 0  
 SWH 25252.525 Hz  
 FIDRES 0.385323 Hz  
 AQ 1.2976128 sec  
 RG 189.85  
 DW 19.800 usec  
 DE 6.50 usec  
 TE 299.0 K  
 D1 2.00000000 sec  
 D11 0.03000000 sec  
 TD0 1

===== CHANNEL f1 =====  
 SFO1 100.6243395 MHz  
 NUC1  $^{13}\text{C}$   
 P1 10.00 usec  
 PLW1 52.00000000 W

===== CHANNEL f2 =====  
 SFO2 400.1324008 MHz  
 NUC2  $^1\text{H}$   
 CPDPRG2 waltz16  
 PCPD2 90.00 usec  
 PLW2 13.00000000 W  
 PLW12 0.36111000 W  
 PLW13 0.29249999 W



<sup>19</sup>F NMR

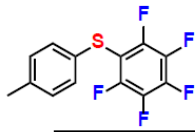


Current Data Parameters  
 NAME 1201  
 EXPNO 20  
 PROCNO 1

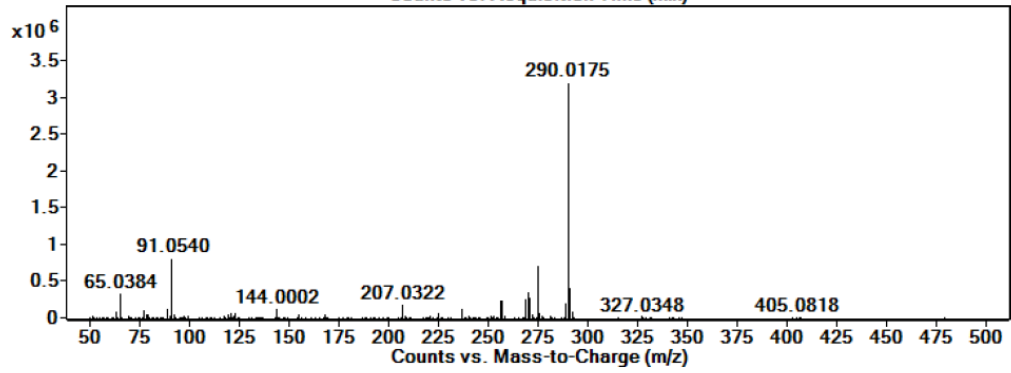
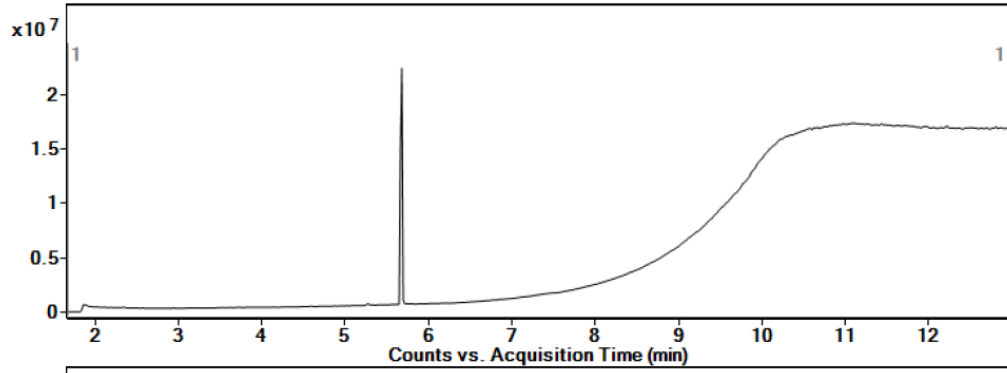
F2 - Acquisition Parameters  
 Date\_ 20181201  
 Time 12.59  
 INSTRUM av400  
 PROBHD 5 mm PABBO BB/  
 PULPROG zgpg30  
 TD 262144  
 SOLVENT CDCl3  
 NS 64  
 DS 0  
 SWH 150000.000 Hz  
 FIDRES 0.572205 Hz  
 AQ 0.8738133 sec  
 RG 189.85  
 DW 3.333 usec  
 DE 6.50 usec  
 TE 298.2 K  
 D1 2.0000000 sec  
 TD0 1

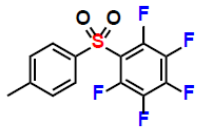
===== CHANNEL f1 =====  
 SFO1 376.4983660 MHz  
 NUC1 19F  
 P1 14.50 usec  
 PLW1 17.00000000 W

F2 - Processing parameters  
 SI 262144  
 SF 376.4984658 MHz  
 WDW EM  
 SSB 0  
 LB 1.00 Hz  
 GB 0  
 PC 1.00



GC-MS

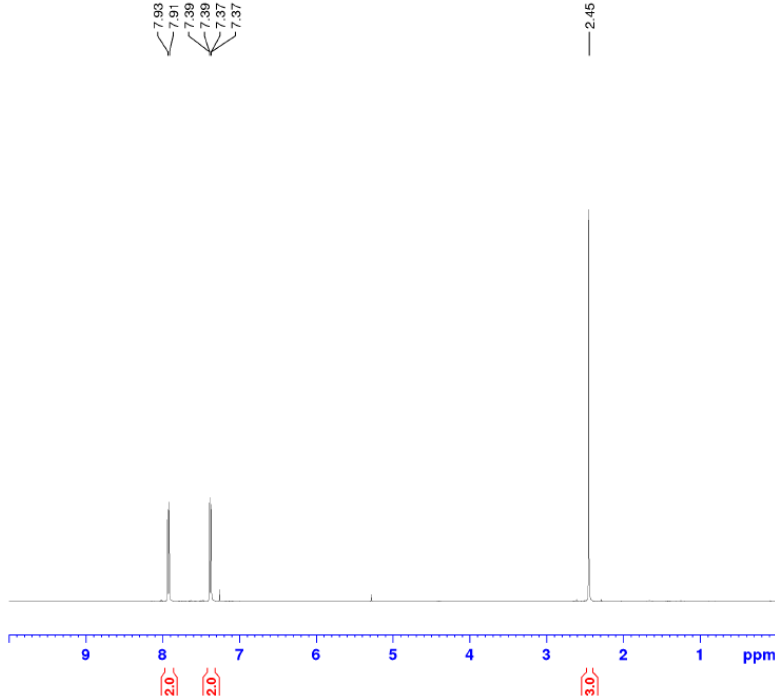




<sup>1</sup>H NMR

7.89  
7.81  
7.30  
7.39  
7.37  
7.37

2.45



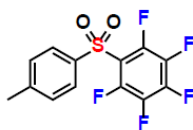
Current Data Parameters  
NAME 1202  
EXPNO 82  
PROCNO 1

F2 - Acquisition Parameters  
Date\_ 20181202  
Time 18.18  
INSTRUM av400  
PROBHD 5 mm PABBO BB/  
PULPROG zg30  
TD 52882  
SOLVENT CDCl3  
NS 16  
DS 0  
SWH 8012.820 Hz  
FIDRES 0.151523 Hz  
AQ 3.2998369 sec  
RG 60.34  
DW 62.400 usec  
DE 6.50 usec  
TE 298.3 K  
D1 2.0000000 sec  
TD0 1

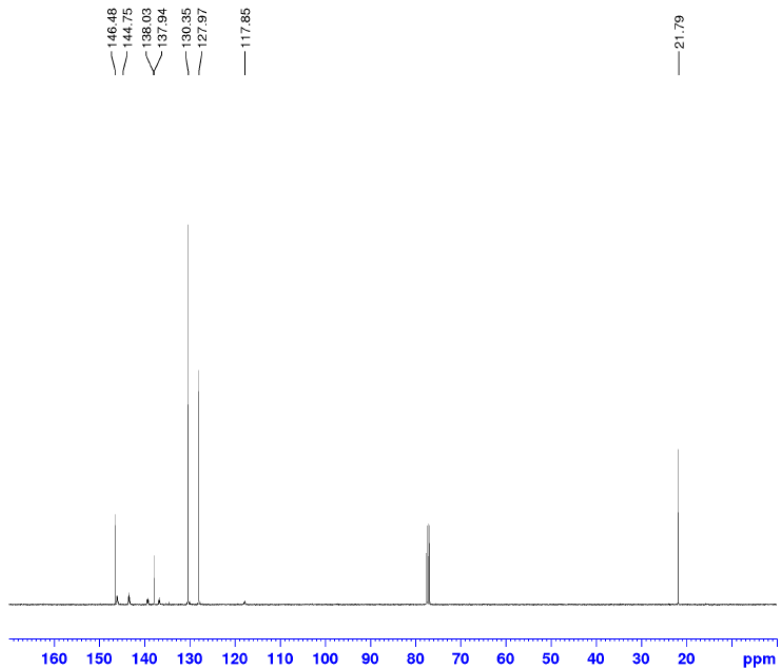
===== CHANNEL f1 =====  
SFO1 400.1324008 MHz  
NUC1 1H  
P1 15.00 usec  
PLW1 13.00000000 W

F2 - Processing parameters  
SI 65536  
SF 400.1300171 MHz  
WDW EM  
SSB 0  
LB 0.30 Hz  
GB 0  
PC 1.00





$^{13}\text{C}\{^1\text{H}\}$  NMR

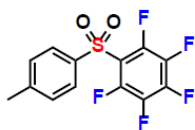


Current Data Parameters  
 NAME 1202  
 EXPNO 80  
 PROCNO 1

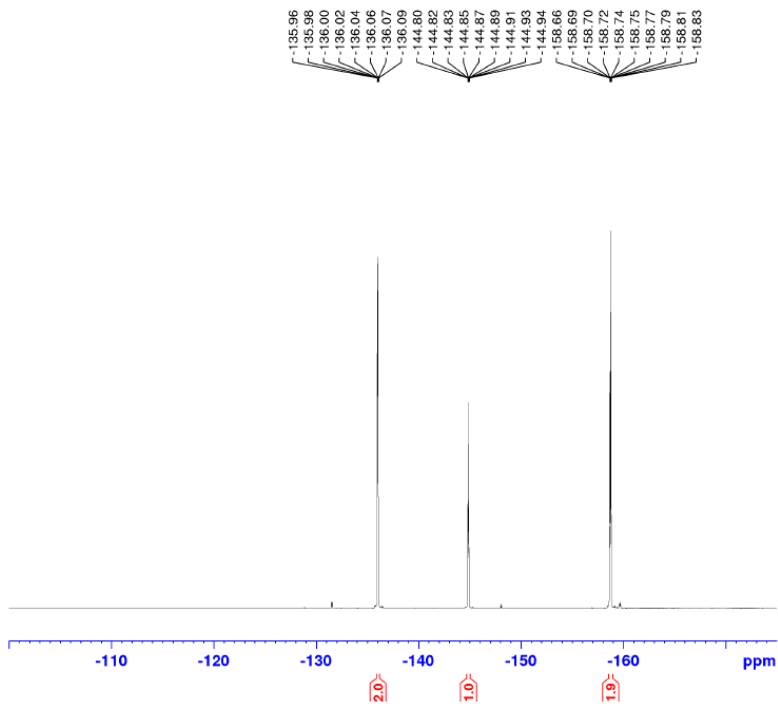
F2 - Acquisition Parameters  
 Date\_ 20181202  
 Time 18.13  
 INSTRUM av400  
 PROBHD 5 mm PABBO BB/  
 PULPROG zgpg30  
 TD 65536  
 SOLVENT CDCl3  
 NS 256  
 DS 0  
 SWH 25252.525 Hz  
 FIDRES 0.385323 Hz  
 AQ 1.2976128 sec  
 RG 189.85  
 DW 19.800 usec  
 DE 6.50 usec  
 TE 299.0 K  
 D1 2.00000000 sec  
 D11 0.03000000 sec  
 TD0 1

===== CHANNEL f1 =====  
 SFO1 100.6243395 MHz  
 NUC1  $^{13}\text{C}$   
 P1 10.00 usec  
 PLW1 52.00000000 W

===== CHANNEL f2 =====  
 SFO2 400.1324008 MHz  
 NUC2  $^1\text{H}$   
 CPDPRG2 waltz16  
 PCPD2 90.00 usec  
 PLW2 13.00000000 W  
 PLW12 0.36111000 W  
 PLW13 0.29249999 W



<sup>19</sup>F NMR

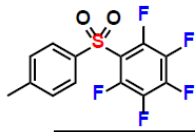


Current Data Parameters  
 NAME 1202  
 EXPNO 81  
 PROCNO 1

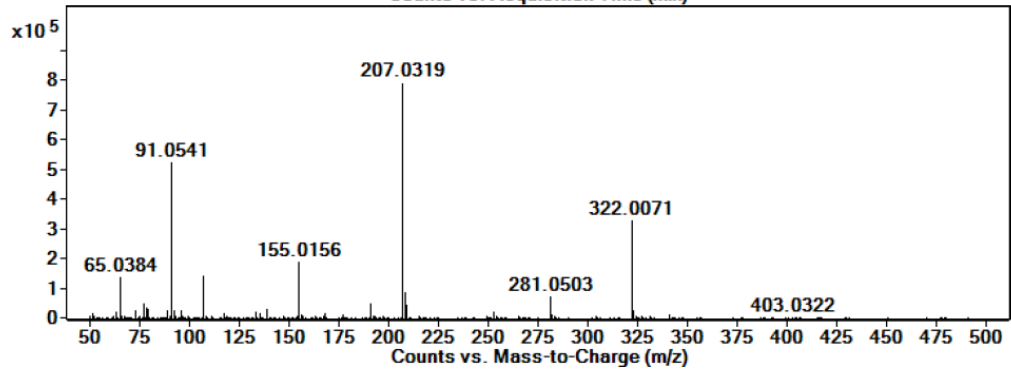
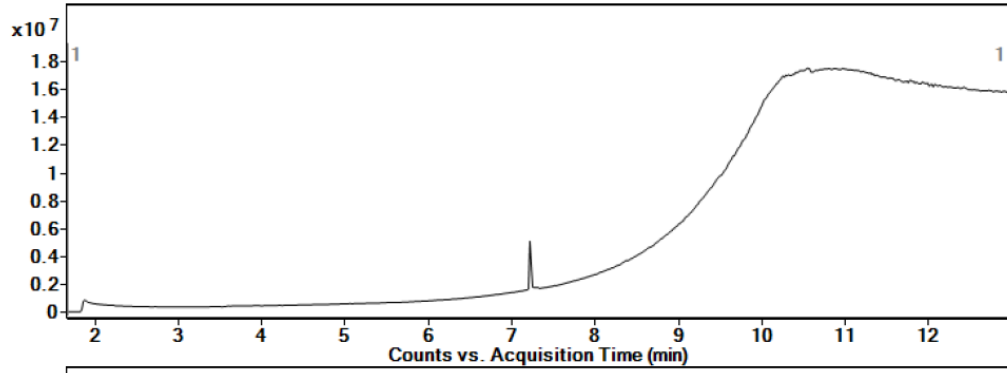
F2 - Acquisition Parameters  
 Date\_ 20181202  
 Time 18.15  
 INSTRUM av400  
 PROBHD 5 mm PABBO BB/  
 PULPROG zgpg30  
 TD 262144  
 SOLVENT CDCl3  
 NS 32  
 DS 0  
 SWH 150000.000 Hz  
 FIDRES 0.572205 Hz  
 AQ 0.8738133 sec  
 RG 189.85  
 DW 3.333 usec  
 DE 6.50 usec  
 TE 298.4 K  
 D1 2.0000000 sec  
 TD0 1

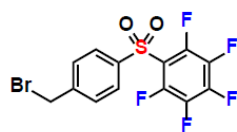
===== CHANNEL f1 =====  
 SFO1 376.4983660 MHz  
 NUC1 19F  
 P1 14.50 usec  
 PLW1 17.0000000 W

F2 - Processing parameters  
 SI 262144  
 SF 376.4984596 MHz  
 WDW EM  
 SSB 0  
 LB 3.00 Hz  
 GB 0  
 PC 1.00

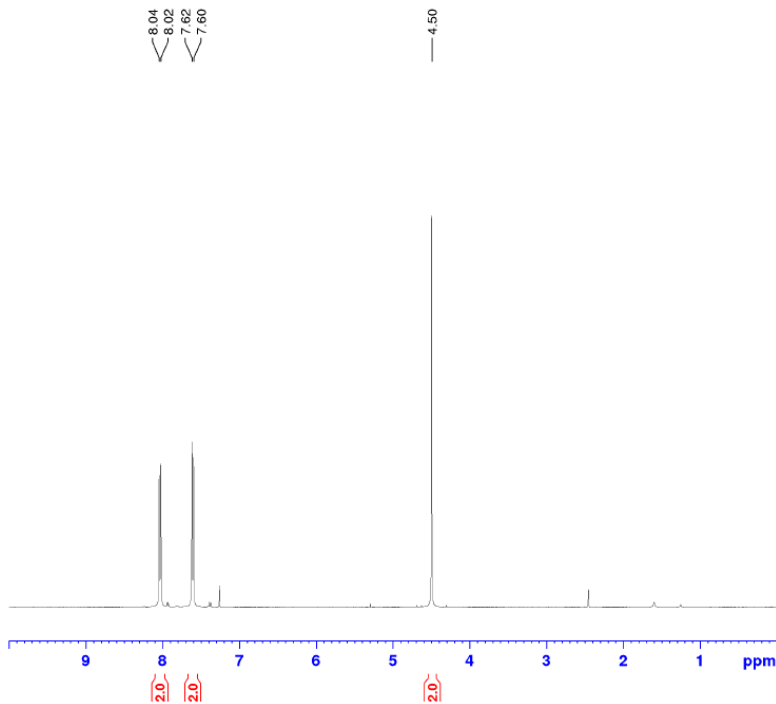


GC-MS





<sup>1</sup>H NMR

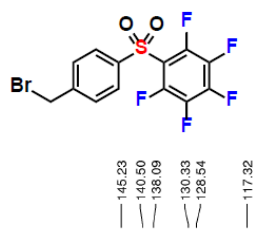


Current Data Parameters  
 NAME 1205  
 EXPNO 100  
 PROCNO 1

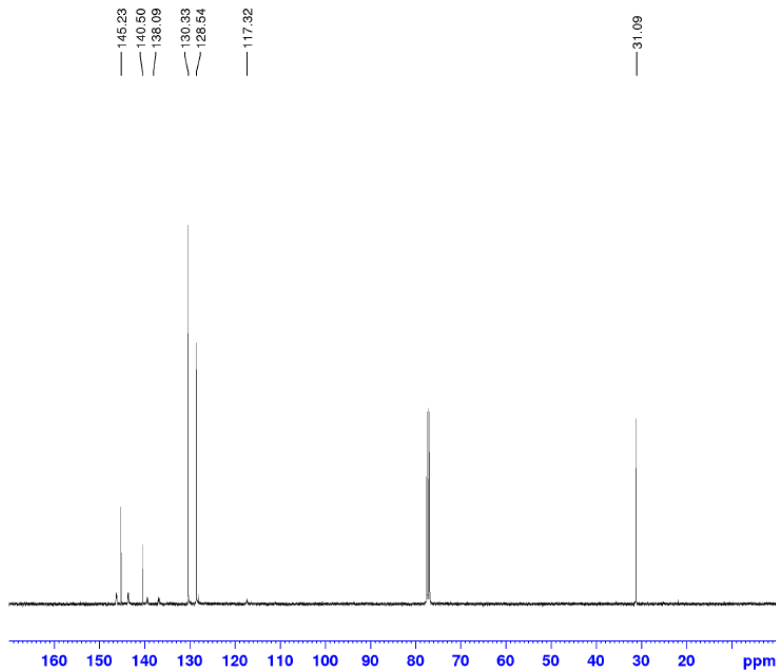
F2 - Acquisition Parameters  
 Date\_ 20181205  
 Time 18.37  
 INSTRUM av400  
 PROBHD 5 mm PABBO BB/  
 PULPROG zg30  
 TD 52882  
 SOLVENT CDCl3  
 NS 16  
 DS 0  
 SWH 8012.820 Hz  
 FIDRES 0.151523 Hz  
 AQ 3.2998369 sec  
 RG 155.85  
 DW 62.400 usec  
 DE 6.50 usec  
 TE 298.3 K  
 D1 2.0000000 sec  
 TD0 1

===== CHANNEL f1 =====  
 SFO1 400.1324008 MHz  
 NUC1 1H  
 P1 15.00 usec  
 PLW1 13.00000000 W

F2 - Processing parameters  
 SI 65536  
 SF 400.1300179 MHz  
 WDW EM  
 SSB 0  
 LB 0.30 Hz  
 GB 0  
 PC 1.00



$^{13}\text{C}\{^1\text{H}\}$  NMR

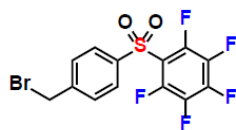


Current Data Parameters  
 NAME 1205  
 EXPNO 102  
 PROCNO 1

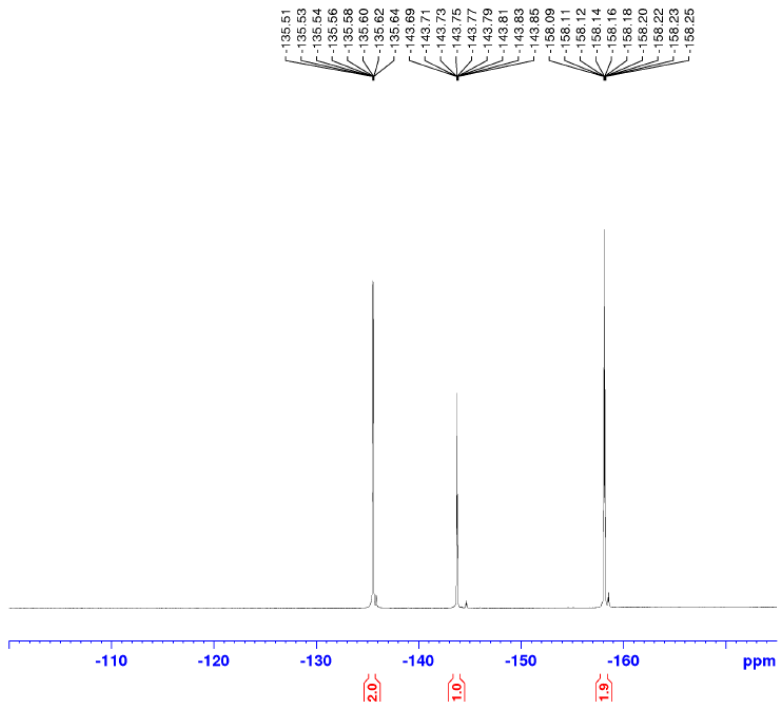
F2 - Acquisition Parameters  
 Date\_ 20181205  
 Time 19.03  
 INSTRUM av400  
 PROBHD 5 mm PABBO BB/  
 PULPROG zgpg30  
 TD 65536  
 SOLVENT CDCl3  
 NS 384  
 DS 0  
 SWH 25252.525 Hz  
 FIDRES 0.385323 Hz  
 AQ 1.2976128 sec  
 RG 189.85  
 DW 19.800 usec  
 DE 6.50 usec  
 TE 299.4 K  
 D1 2.00000000 sec  
 D11 0.03000000 sec  
 TD0 1

===== CHANNEL f1 =====  
 SFO1 100.6243395 MHz  
 NUC1  $^{13}\text{C}$   
 P1 10.00 usec  
 PLW1 52.00000000 W

===== CHANNEL f2 =====  
 SFO2 400.1324008 MHz  
 NUC2  $^1\text{H}$   
 CPDPRG2 waltz16  
 PCPD2 90.00 usec  
 PLW2 13.00000000 W  
 PLW12 0.36111000 W  
 PLW13 0.29249999 W



<sup>19</sup>F NMR

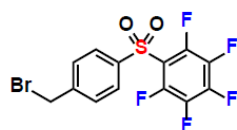


Current Data Parameters  
 NAME 1205  
 EXPNO 101  
 PROCNO 1

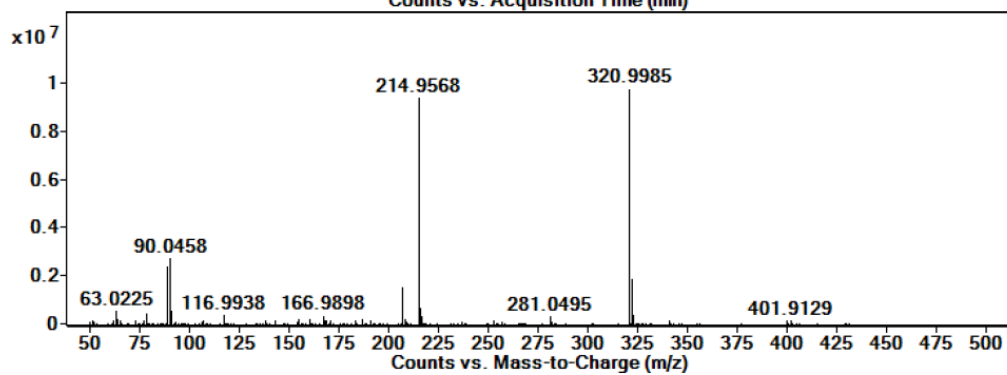
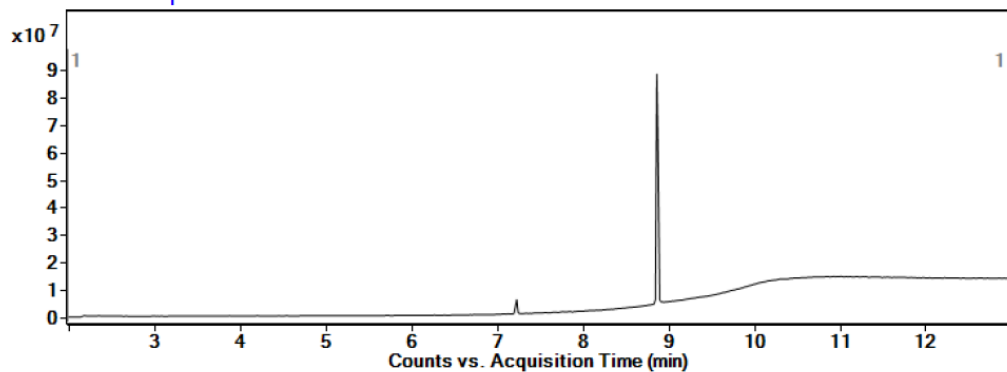
F2 - Acquisition Parameters  
 Date\_ 20181205  
 Time 18.40  
 INSTRUM av400  
 PROBHD 5 mm PABBO BB/  
 PULPROG zgpg30  
 TD 262144  
 SOLVENT CDCl3  
 NS 32  
 DS 0  
 SWH 150000.000 Hz  
 FIDRES 0.572205 Hz  
 AQ 0.8738133 sec  
 RG 189.85  
 DW 3.333 usec  
 DE 6.50 usec  
 TE 298.3 K  
 D1 2.0000000 sec  
 TD0 1

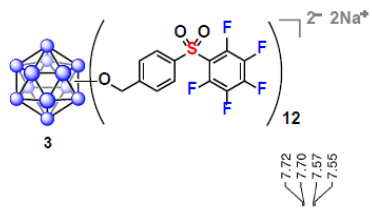
===== CHANNEL f1 =====  
 SFO1 376.4983660 MHz  
 NUC1 19F  
 P1 14.50 usec  
 PLW1 17.00000000 W

F2 - Processing parameters  
 SI 262144  
 SF 376.4984562 MHz  
 WDW EM  
 SSB 0  
 LB 3.00 Hz  
 GB 0  
 PC 1.00

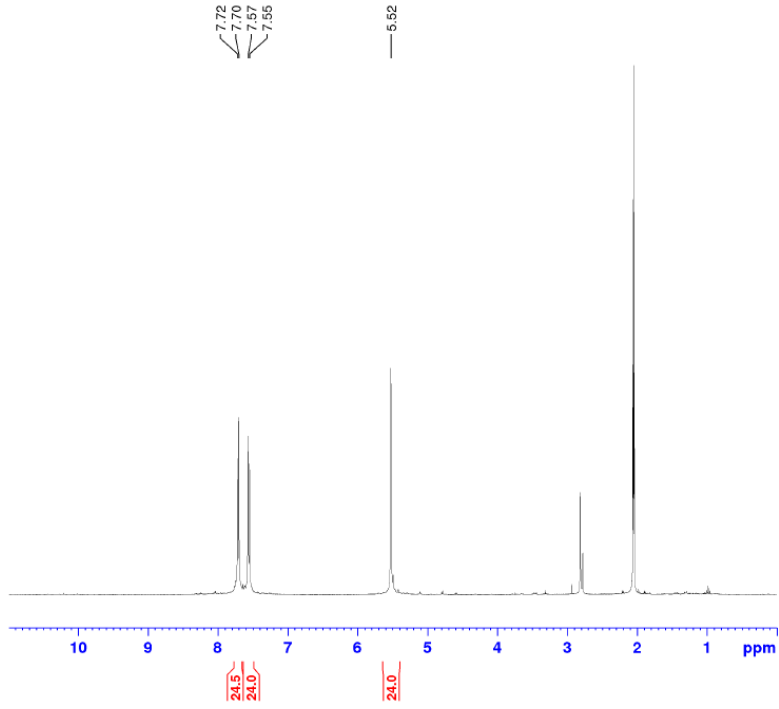


GC-MS





<sup>1</sup>H NMR



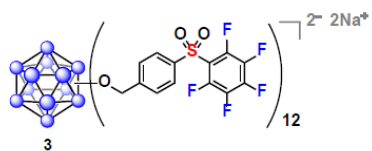
Current Data Parameters  
 NAME 1214  
 EXPNO 130  
 PROCNO 1

F2 - Acquisition Parameters  
 Date\_ 20181214  
 Time 17.58  
 INSTRUM av400  
 PROBHD 5 mm PABBO BB/  
 PULPROG zg30  
 TD 52882  
 SOLVENT Acetone  
 NS 64  
 DS 0  
 SWH 8012.820 Hz  
 FIDRES 0.151523 Hz  
 AQ 3.2998369 sec  
 RG 189.85  
 DW 62.400 usec  
 DE 6.50 usec  
 TE 298.3 K  
 D1 2.0000000 sec  
 TD0 1

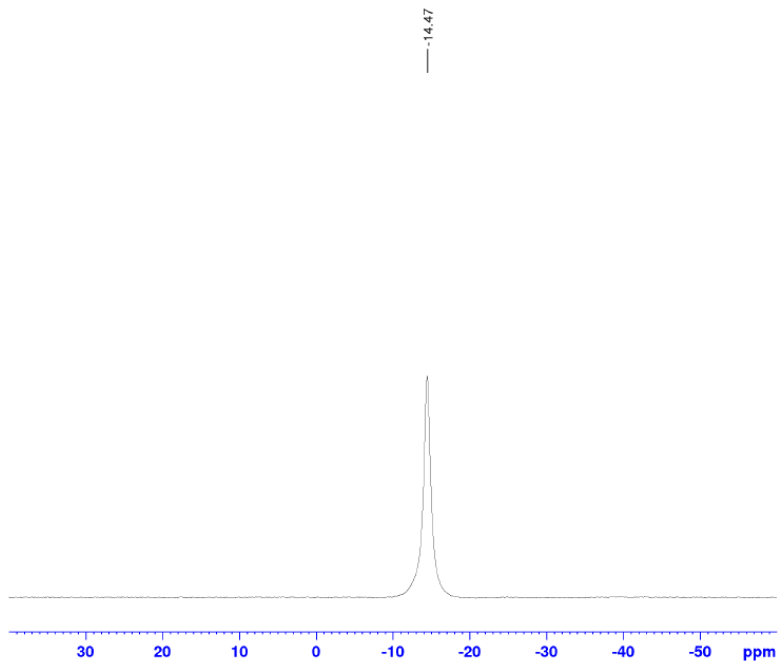
===== CHANNEL f1 =====  
 SFO1 400.1324008 MHz  
 NUC1 1H  
 P1 15.00 usec  
 PLW1 13.00000000 W

F2 - Processing parameters  
 SI 65536  
 SF 400.1300068 MHz  
 WDW EM  
 SSB 0  
 LB 0.30 Hz  
 GB 0  
 PC 1.00





<sup>11</sup>B NMR

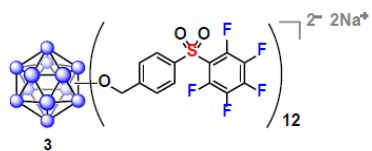


Current Data Parameters  
 NAME 1214  
 EXPNO 131  
 PROCNO 1

F2 - Acquisition Parameters  
 Date\_ 20181214  
 Time 18.03  
 INSTRUM av400  
 PROBHD 5 mm PABBO BB/  
 PULPROG zg  
 TD 5096  
 SOLVENT Acetone  
 NS 2048  
 DS 0  
 SWH 51020.406 Hz  
 FIDRES 10.011854 Hz  
 AQ 0.0499408 sec  
 RG 189.85  
 DW 9.800 usec  
 DE 6.50 usec  
 TE 298.3 K  
 D1 0.0500000 sec  
 TD0 1

===== CHANNEL f1 =====  
 SFO1 128.3776052 MHz  
 NUC1 11B  
 P1 10.00 usec  
 PLW1 52.00000000 W

F2 - Processing parameters  
 SI 32768  
 SF 128.3775198 MHz  
 WDW EM  
 SSB 0  
 LB 10.00 Hz  
 GB 0  
 PC 1.40



### <sup>19</sup>F NMR

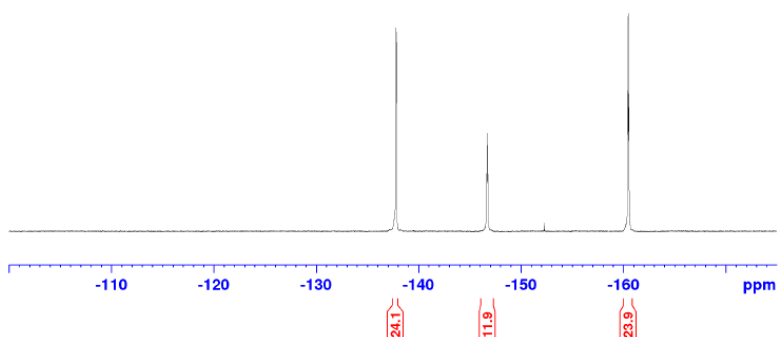


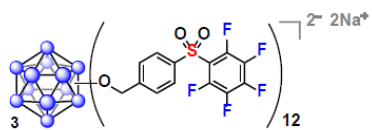
Current Data Parameters  
NAME 1214  
EXPNO 132  
PROCNO 1

F2 - Acquisition Parameters  
Date\_ 20181214  
Time 18.12  
INSTRUM av400  
PROBHD 5 mm PABBO BB/  
PULPROG zgpg30  
TD 262144  
SOLVENT Acetone  
NS 128  
DS 0  
SWH 150000.000 Hz  
FIDRES 0.572205 Hz  
AQ 0.8738133 sec  
RG 189.85  
DW 3.333 usec  
DE 6.50 usec  
TE 298.3 K  
D1 2.0000000 sec  
TD0 1

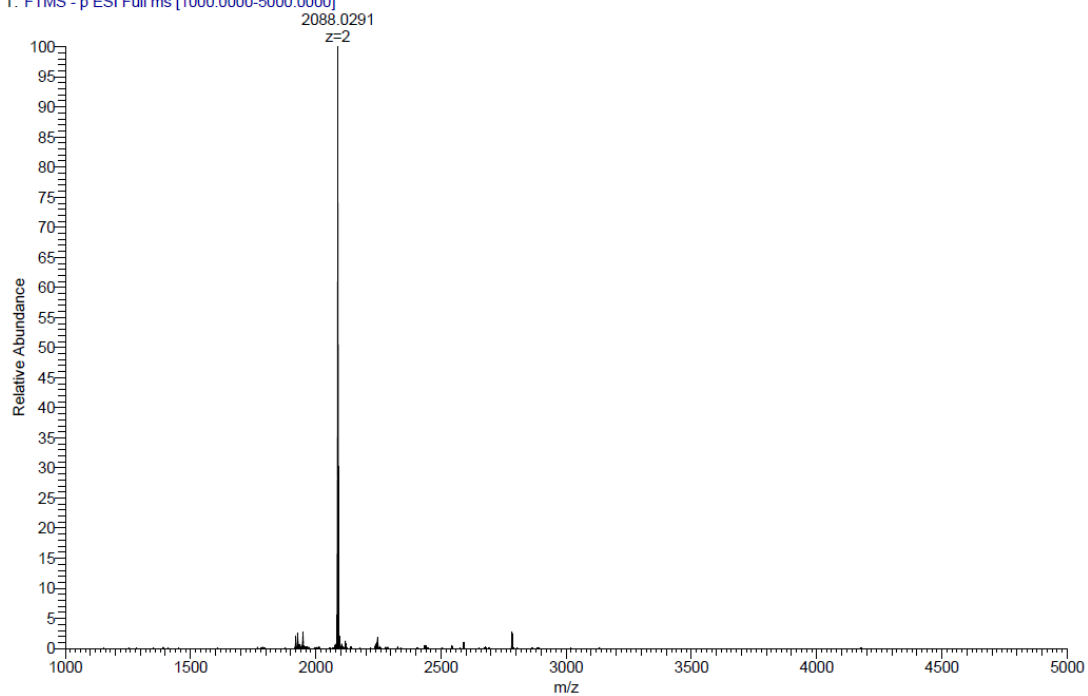
===== CHANNEL f1 =====  
SFO1 376.4983660 MHz  
NUC1 19F  
P1 14.50 usec  
PLW1 17.00000000 W

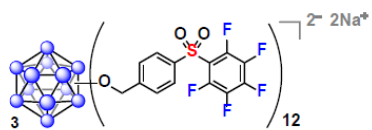
F2 - Processing parameters  
SI 262144  
SF 376.4980654 MHz  
WDW EM  
SSB 0  
LB 3.00 Hz  
GB 0  
PC 1.00



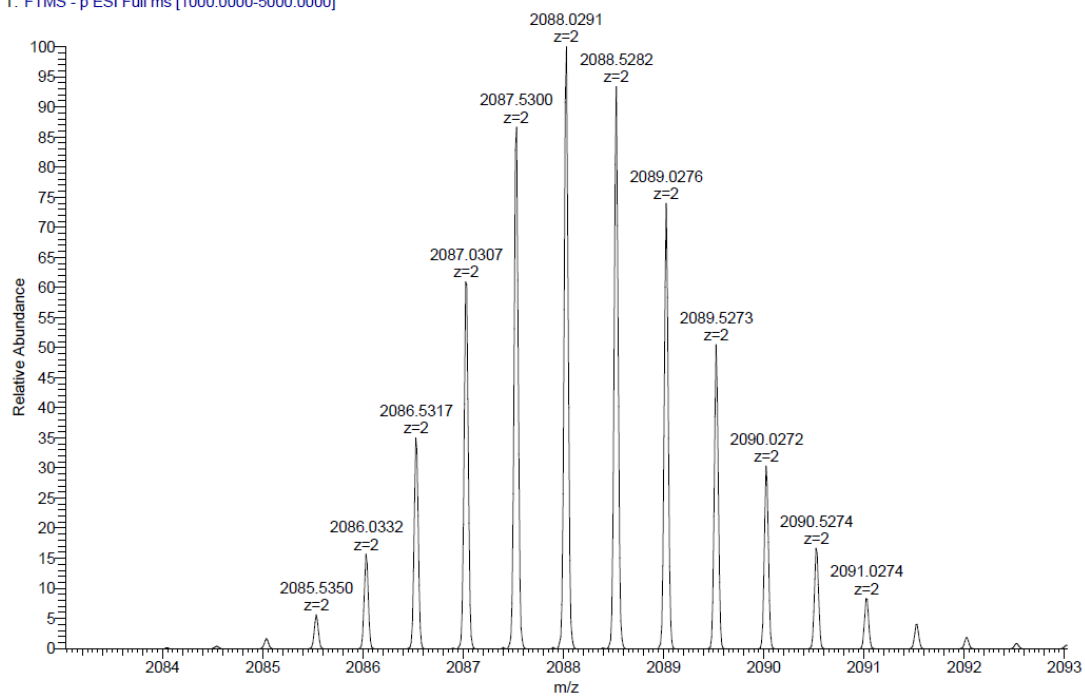


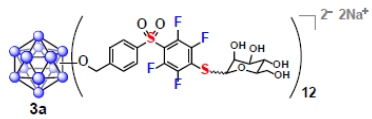
### ESI-HRMS



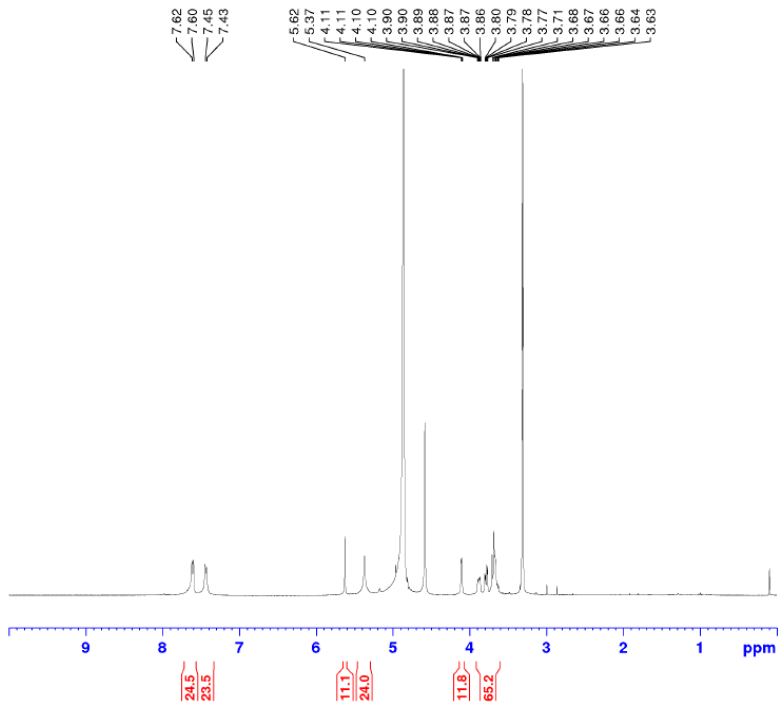


### ESI-HRMS





# <sup>1</sup>H NMR

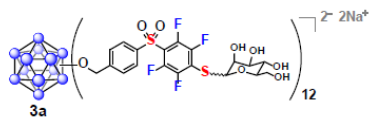


Current Data Parameters  
 NAME 0110  
 EXPNO 10  
 PROCNO 1

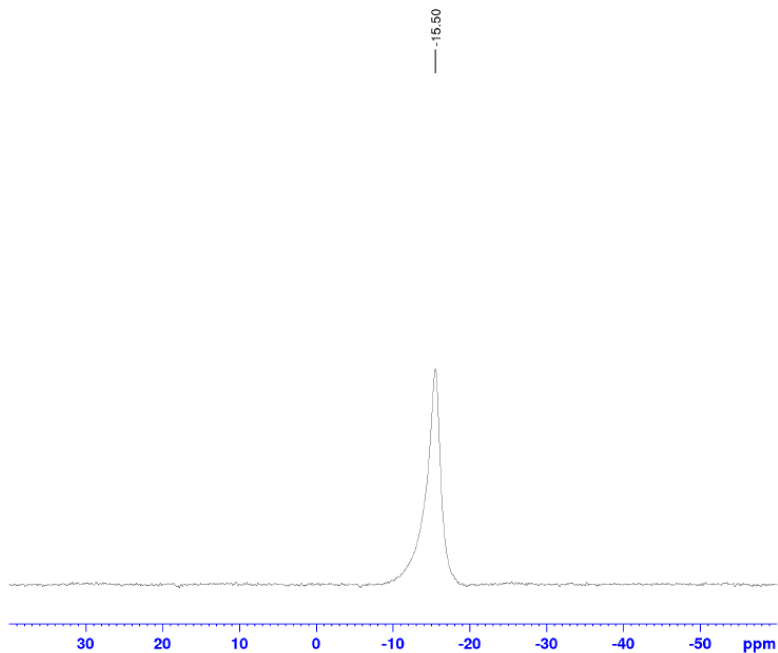
F2 - Acquisition Parameters  
 Date\_ 20190110  
 Time 10.51  
 INSTRUM av400  
 PROBHD 5 mm PABBO BB/  
 PULPROG zg30  
 TD 52882  
 SOLVENT MeOD  
 NS 128  
 DS 0  
 SWH 8012.820 Hz  
 FIDRES 0.151523 Hz  
 AQ 3.2998369 sec  
 RG 155.85  
 DW 62.400 usec  
 DE 6.50 usec  
 TE 298.2 K  
 D1 2.0000000 sec  
 TD0 1

===== CHANNEL f1 =====  
 SFO1 400.1324008 MHz  
 NUC1 <sup>1</sup>H  
 P1 15.00 usec  
 PLW1 13.00000000 W

F2 - Processing parameters  
 SI 65536  
 SF 400.1300079 MHz  
 WDW EM  
 SSB 0  
 LB 0.30 Hz  
 GB 0  
 PC 1.00



$^{11}\text{B}$  NMR

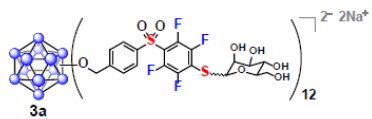


Current Data Parameters  
 NAME 0110  
 EXPNO 12  
 PROCNO 1

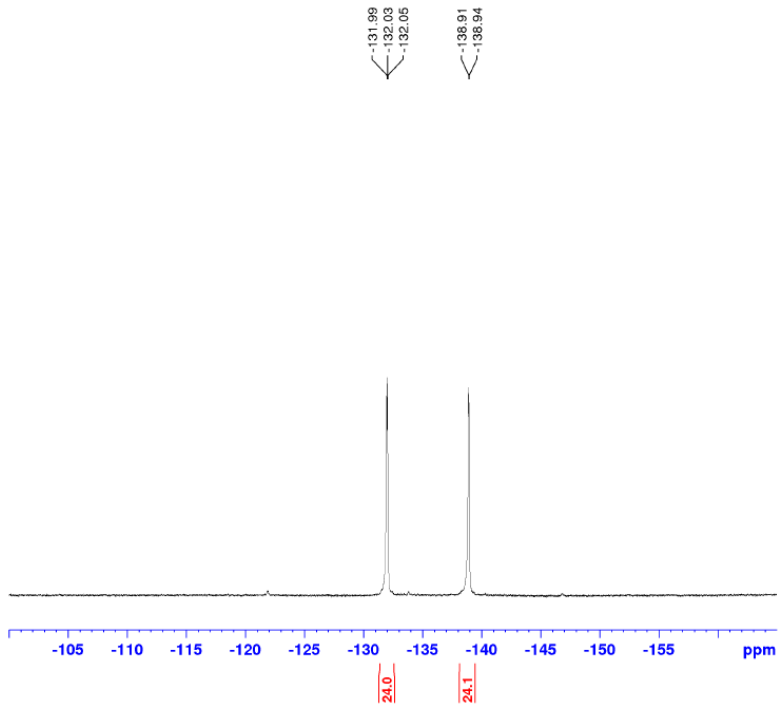
F2 - Acquisition Parameters  
 Date\_ 20190110  
 Time 11.10  
 INSTRUM av400  
 PROBHD 5 mm PABBO BB/  
 PULPROG zg  
 TD 5096  
 SOLVENT MeOD  
 NS 2048  
 DS 0  
 SWH 51020.406 Hz  
 FIDRES 10.011854 Hz  
 AQ 0.0499408 sec  
 RG 189.85  
 DW 9.800 usec  
 DE 6.50 usec  
 TE 298.3 K  
 D1 0.0500000 sec  
 TD0 1

===== CHANNEL f1 =====  
 SFO1 128.3776052 MHz  
 NUC1  $^{11}\text{B}$   
 P1 10.00 usec  
 PLW1 52.00000000 W

F2 - Processing parameters  
 SI 32768  
 SF 128.3776161 MHz  
 WDW EM  
 SSB 0  
 LB 10.00 Hz  
 GB 0  
 PC 1.40



$^{19}F$  NMR

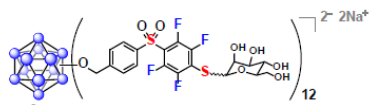


Current Data Parameters  
 NAME 0110  
 EXPNO 11  
 PROCNO 1

F2 - Acquisition Parameters  
 Date\_ 20190110  
 Time 11.04  
 INSTRUM av400  
 PROBHD 5 mm PABBO BB/  
 PULPROG zgpg30  
 TD 262144  
 SOLVENT MeOD  
 NS 256  
 DS 0  
 SWH 150000.000 Hz  
 FIDRES 0.572205 Hz  
 AQ 0.8738133 sec  
 RG 189.85  
 DW 3.333 usec  
 DE 6.50 usec  
 TE 298.2 K  
 D1 2.0000000 sec  
 TD0 1

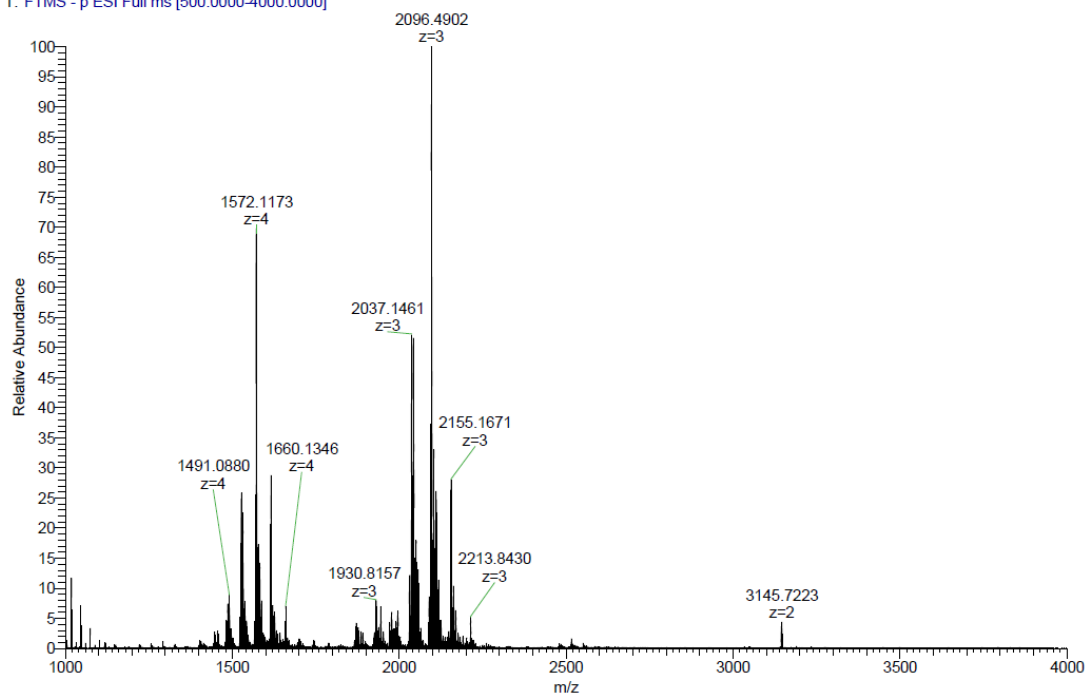
===== CHANNEL f1 =====  
 SFO1 376.4983660 MHz  
 NUC1  $^{19}F$   
 P1 14.50 usec  
 PLW1 17.00000000 W

F2 - Processing parameters  
 SI 262144  
 SF 376.4983660 MHz  
 WDW EM  
 SSB 0  
 LB 3.00 Hz  
 GB 0  
 PC 1.00

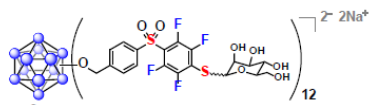


3a #1-50 RT: 0.01-0.43 AV: 50 NL: 1.80E7  
 T: FTMS - p ESI Full ms [500.0000-4000.0000]

### ESI-HRMS

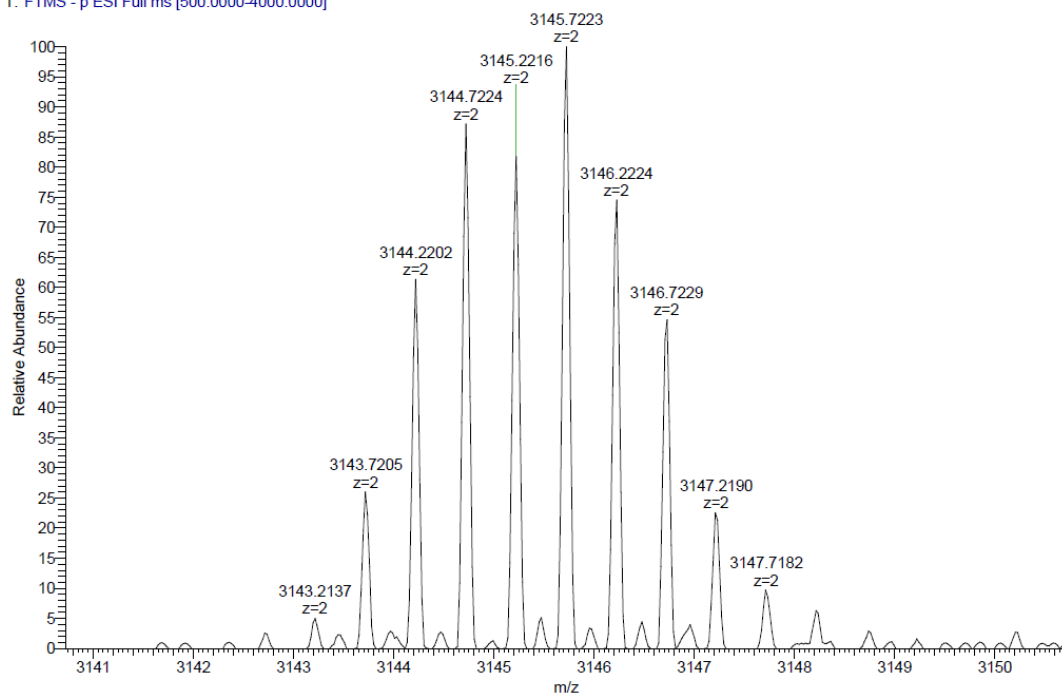


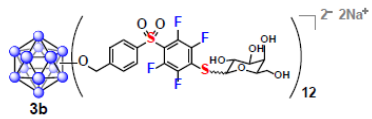




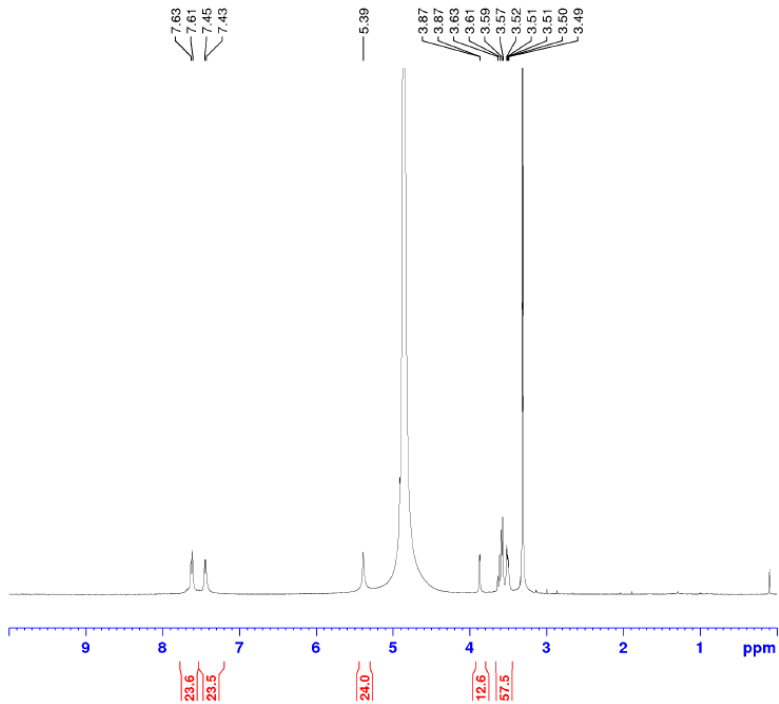
3a #1-50 RT: 0.01-0.43 AV: 50 NL: 7.82E5  
 T: FTMS - p ESI Full ms [500.0000-4000.0000]

### ESI-HRMS





# <sup>1</sup>H NMR

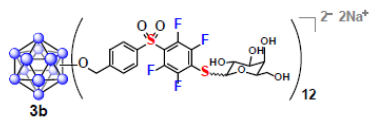


Current Data Parameters  
 NAME 0109  
 EXPNO 90  
 PROCNO 1

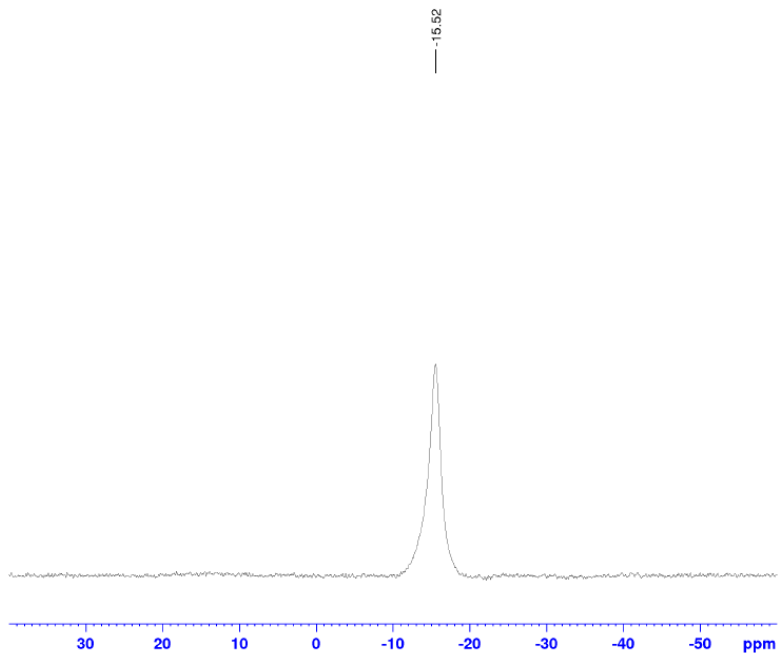
F2 - Acquisition Parameters  
 Date\_ 20190109  
 Time 14.47  
 INSTRUM av400  
 PROBHD 5 mm PABBO BB/  
 PULPROG zg30  
 TD 52882  
 SOLVENT MeOD  
 NS 128  
 DS 0  
 SWH 8012.820 Hz  
 FIDRES 0.151523 Hz  
 AQ 3.2998369 sec  
 RG 155.85  
 DW 62.400 usec  
 DE 6.50 usec  
 TE 298.8 K  
 D1 2.0000000 sec  
 TD0 1

===== CHANNEL f1 =====  
 SFO1 400.1324008 MHz  
 NUC1 <sup>1</sup>H  
 P1 15.00 usec  
 PLW1 13.00000000 W

F2 - Processing parameters  
 SI 65536  
 SF 400.1300082 MHz  
 WDW EM  
 SSB 0  
 LB 0.30 Hz  
 GB 0  
 PC 1.00



<sup>11</sup>B NMR

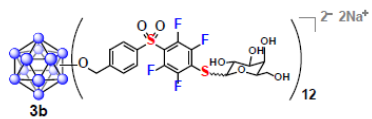


Current Data Parameters  
 NAME 0109  
 EXPNO 92  
 PROCNO 1

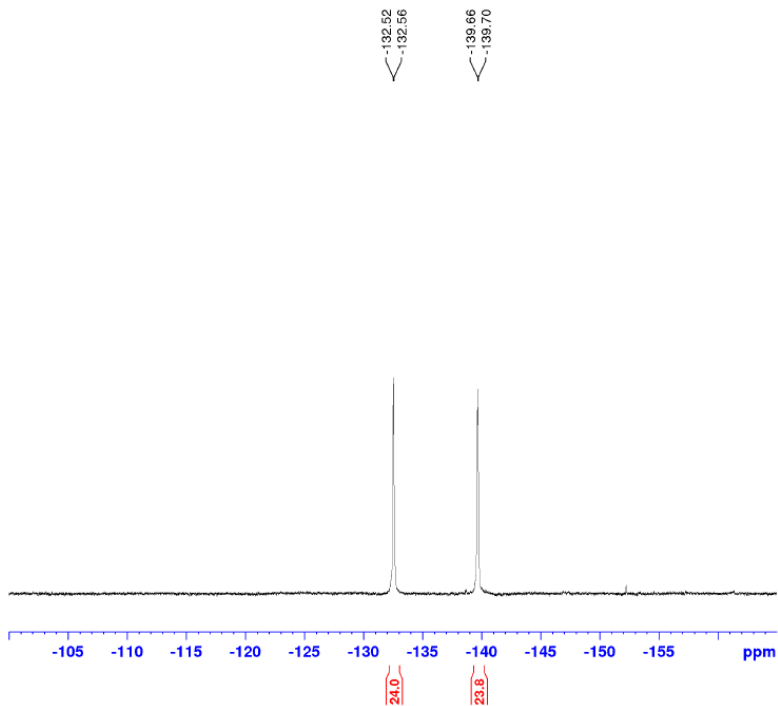
F2 - Acquisition Parameters  
 Date\_ 20190109  
 Time 15.06  
 INSTRUM av400  
 PROBHD 5 mm PABBO BB/  
 PULPROG zg  
 TD 5096  
 SOLVENT MeOD  
 NS 2048  
 DS 0  
 SWH 51020.406 Hz  
 FIDRES 10.011854 Hz  
 AQ 0.0499408 sec  
 RG 189.85  
 DW 9.800 usec  
 DE 6.50 usec  
 TE 299.5 K  
 D1 0.0500000 sec  
 TD0 1

===== CHANNEL f1 =====  
 SFO1 128.3776052 MHz  
 NUC1 11B  
 P1 10.00 usec  
 PLW1 52.00000000 W

F2 - Processing parameters  
 SI 32768  
 SF 128.3776161 MHz  
 WDW EM  
 SSB 0  
 LB 10.00 Hz  
 GB 0  
 PC 1.40



<sup>19</sup>F NMR

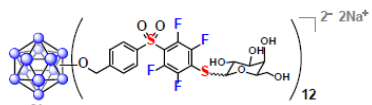


Current Data Parameters  
 NAME 0109  
 EXPNO 91  
 PROCNO 1

F2 - Acquisition Parameters  
 Date\_ 20190109  
 Time 15.00  
 INSTRUM av400  
 PROBHD 5 mm PABBO BB/  
 PULPROG zgpg30  
 TD 262144  
 SOLVENT MeOD  
 NS 256  
 DS 0  
 SWH 150000.000 Hz  
 FIDRES 0.572205 Hz  
 AQ 0.8738133 sec  
 RG 189.85  
 DW 3.333 usec  
 DE 6.50 usec  
 TE 299.3 K  
 D1 2.0000000 sec  
 TD0 1

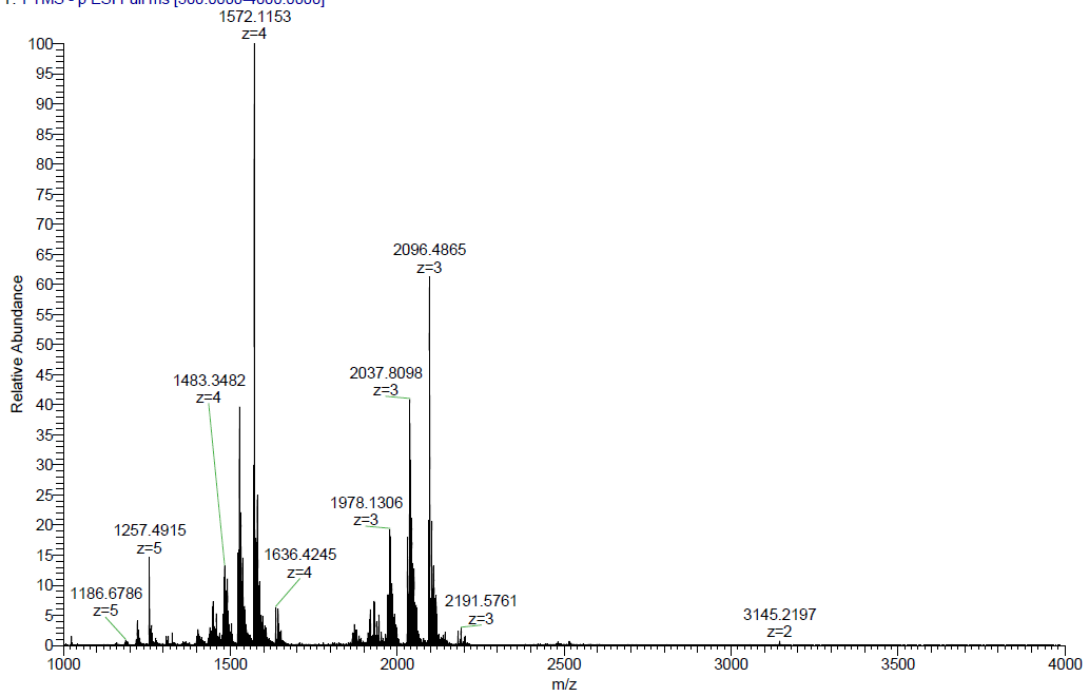
===== CHANNEL f1 =====  
 SFO1 376.4983660 MHz  
 NUC1 19F  
 P1 14.50 usec  
 PLW1 17.00000000 W

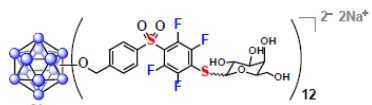
F2 - Processing parameters  
 SI 262144  
 SF 376.4983660 MHz  
 WDW EM  
 SSB 0  
 LB 3.00 Hz  
 GB 0  
 PC 1.00



### ESI-HRMS

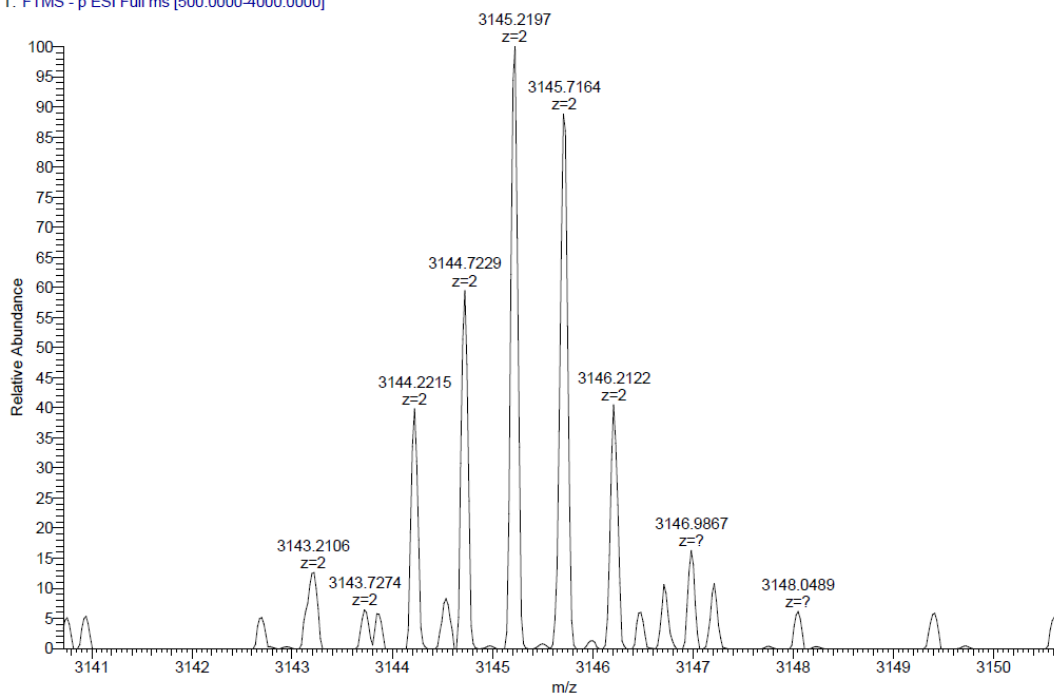
3b  
 3b #1-50 RT: 0.01-0.43 AV: 50 NL: 2.03E7  
 T: FTMS - p ESI Full ms [500.0000-4000.0000]

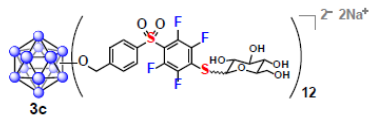




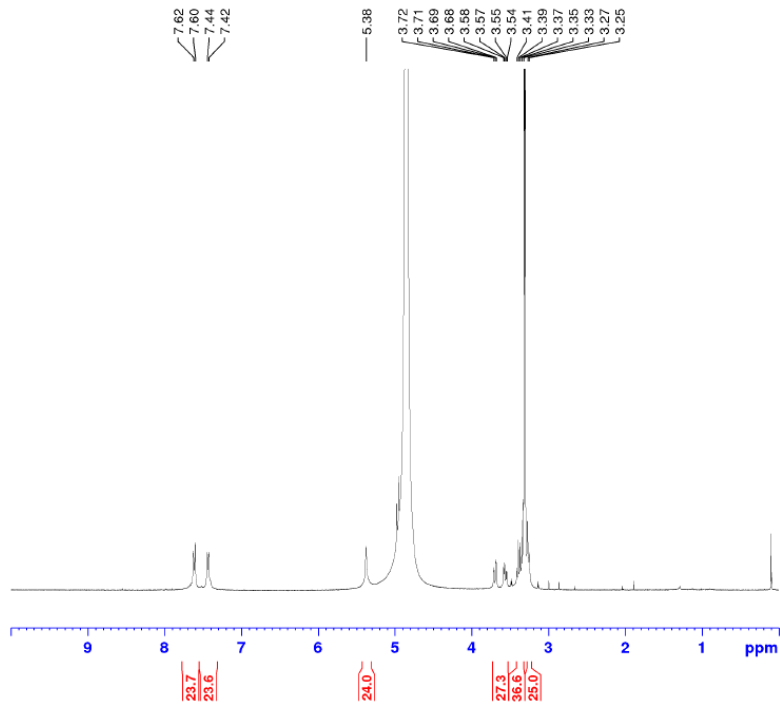
**3b**  
 3b #1-50 RT: 0.01-0.43 AV: 50 NL: 1.46E5  
 T: FTMS - p ESI Full ms [500.0000-4000.0000]

### ESI-HRMS





# <sup>1</sup>H NMR

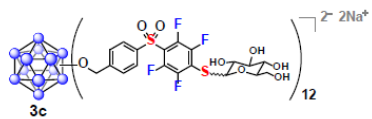


Current Data Parameters  
 NAME 0109  
 EXPNO 80  
 PROCNO 1

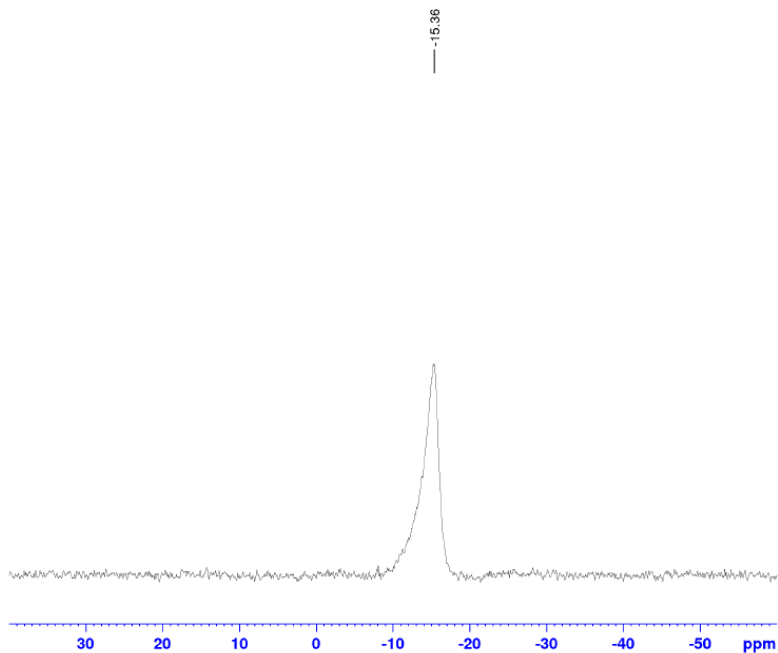
F2 - Acquisition Parameters  
 Date\_ 20190109  
 Time 17.44  
 INSTRUM av400  
 PROBHD 5 mm PABBO BB/  
 PULPROG zg30  
 TD 52882  
 SOLVENT MeOD  
 NS 128  
 DS 0  
 SWH 8012.820 Hz  
 FIDRES 0.151523 Hz  
 AQ 3.2998369 sec  
 RG 155.85  
 DW 62.400 usec  
 DE 6.50 usec  
 TE 298.3 K  
 D1 2.0000000 sec  
 TD0 1

===== CHANNEL f1 =====  
 SFO1 400.1324008 MHz  
 NUC1 <sup>1</sup>H  
 P1 15.00 usec  
 PLW1 13.00000000 W

F2 - Processing parameters  
 SI 65536  
 SF 400.1300077 MHz  
 WDW EM  
 SSB 0  
 LB 0.30 Hz  
 GB 0  
 PC 1.00



$^{11}B$  NMR



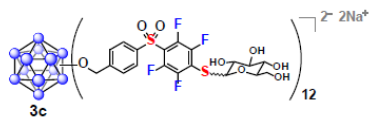
Current Data Parameters  
 NAME 0109  
 EXPNO 82  
 PROCNO 1

F2 - Acquisition Parameters  
 Date\_ 20190109  
 Time 14.22  
 INSTRUM av400  
 PROBHD 5 mm PABBO BB/  
 PULPROG zg  
 TD 5096  
 SOLVENT MeOD  
 NS 2048  
 DS 0  
 SWH 51020.406 Hz  
 FIDRES 10.011854 Hz  
 AQ 0.0499408 sec  
 RG 189.85  
 DW 9.800 usec  
 DE 6.50 usec  
 TE 298.3 K  
 D1 0.0500000 sec  
 TD0 1

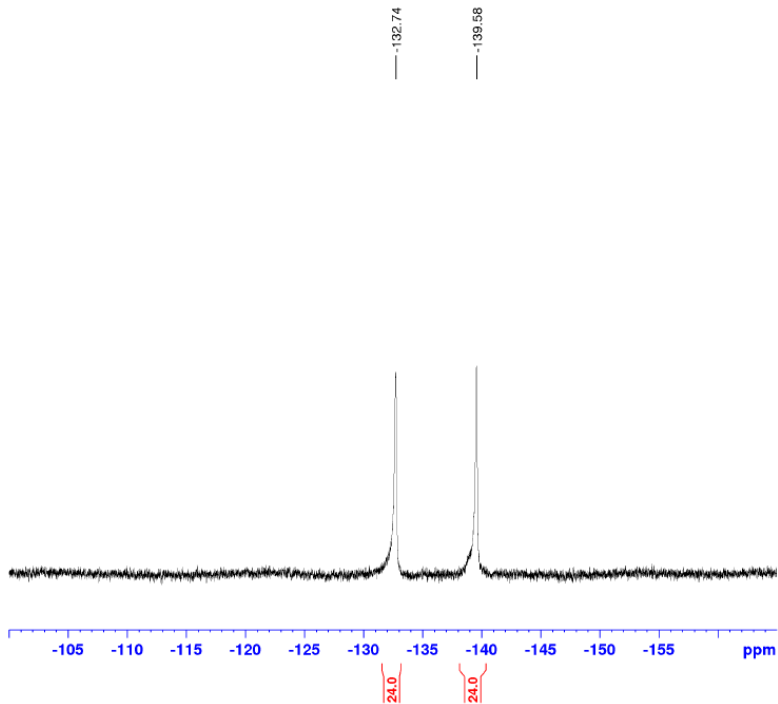
===== CHANNEL f1 =====  
 SFO1 128.3776052 MHz  
 NUC1  $^{11}B$   
 P1 10.00 usec  
 PLW1 52.00000000 W

F2 - Processing parameters  
 SI 32768  
 SF 128.3776161 MHz  
 WDW EM  
 SSB 0  
 LB 10.00 Hz  
 GB 0  
 PC 1.40





$^{19}F$  NMR

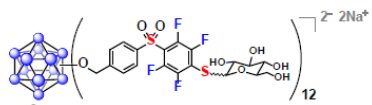


Current Data Parameters  
 NAME 0109  
 EXPNO 81  
 PROCNO 1

F2 - Acquisition Parameters  
 Date\_ 20190109  
 Time 14.16  
 INSTRUM av400  
 PROBHD 5 mm PABBO BB/  
 PULPROG zgpg30  
 TD 262144  
 SOLVENT MeOD  
 NS 256  
 DS 0  
 SWH 150000.000 Hz  
 FIDRES 0.572205 Hz  
 AQ 0.8738133 sec  
 RG 189.85  
 DW 3.333 usec  
 DE 6.50 usec  
 TE 298.3 K  
 D1 2.0000000 sec  
 TD0 1

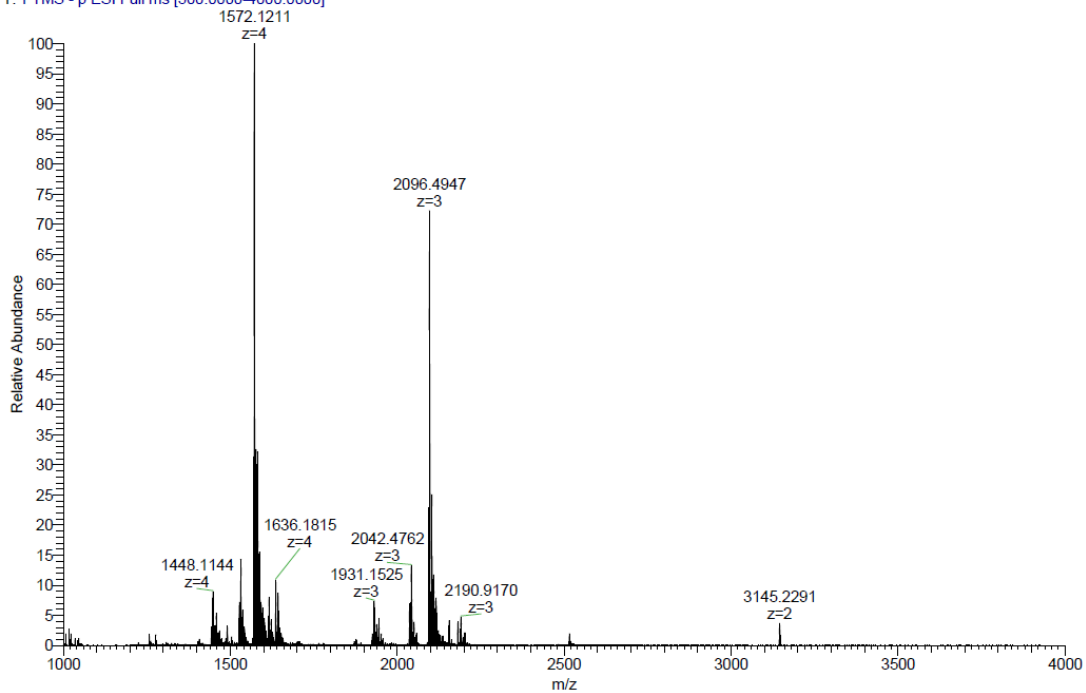
===== CHANNEL f1 =====  
 SFO1 376.4983660 MHz  
 NUC1  $^{19}F$   
 P1 14.50 usec  
 PLW1 17.00000000 W

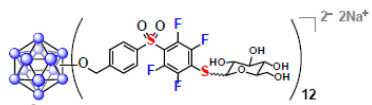
F2 - Processing parameters  
 SI 262144  
 SF 376.4983660 MHz  
 WDW EM  
 SSB 0  
 LB 3.00 Hz  
 GB 0  
 PC 1.00



### ESI-HRMS

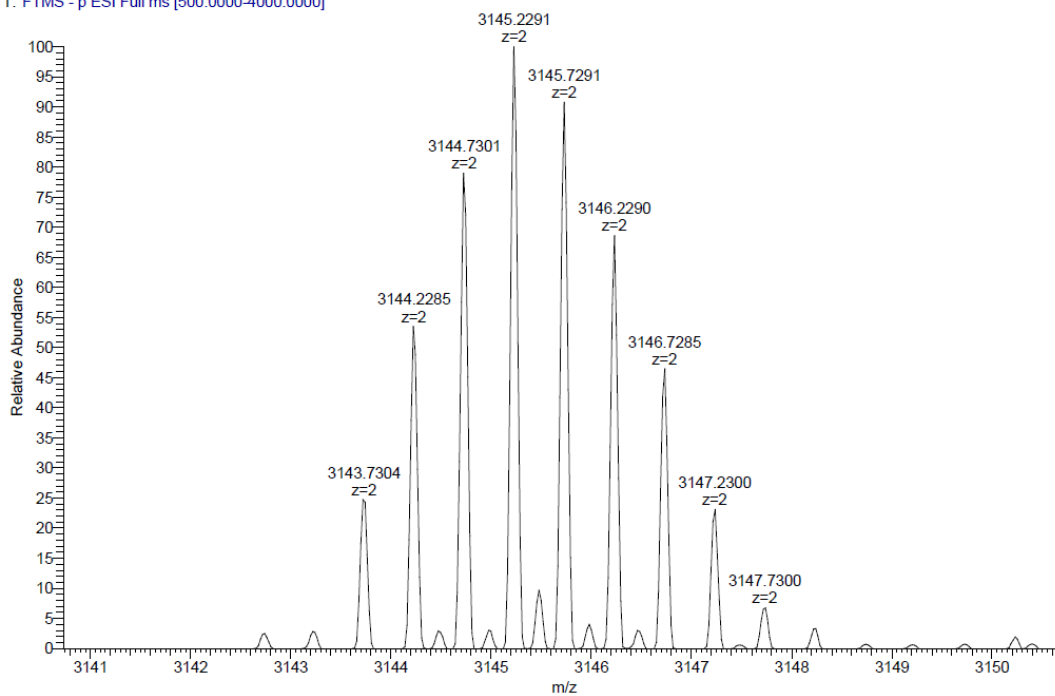
3c  
 3c #1-50 RT: 0.02-0.86 AV: 50 NL: 2.11E7  
 T: FTMS - p ESI Full ms [500.0000-4000.0000]

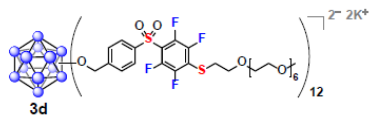




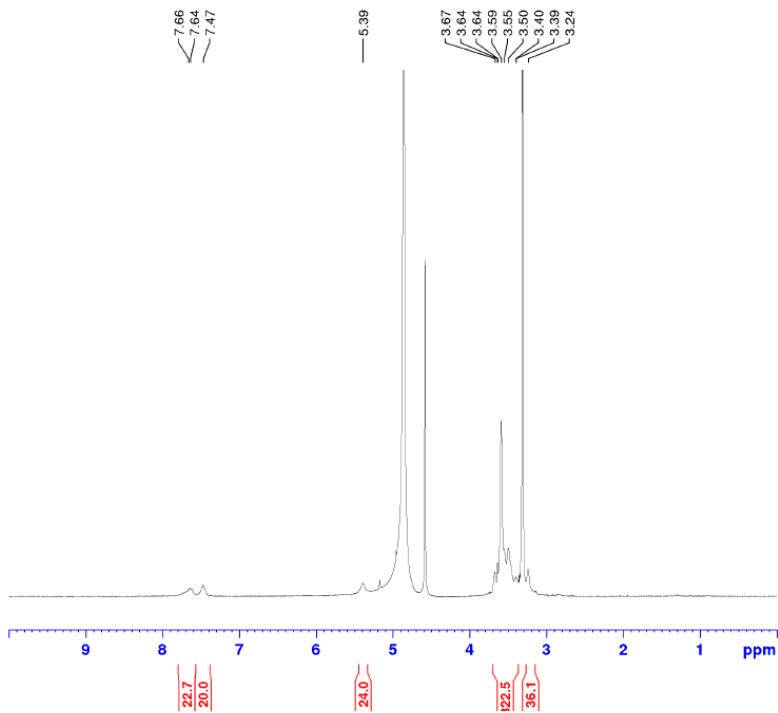
3c  
 3c #1-50 RT: 0.02-0.86 AV: 50 NL: 7.70E5  
 T: FTMS - p ESI Full ms [500.0000-4000.0000]

### ESI-HRMS





<sup>1</sup>H NMR

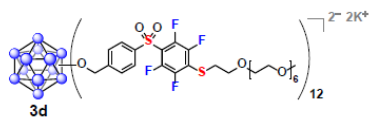


Current Data Parameters  
 NAME 0110  
 EXPNO 30  
 PROCNO 1

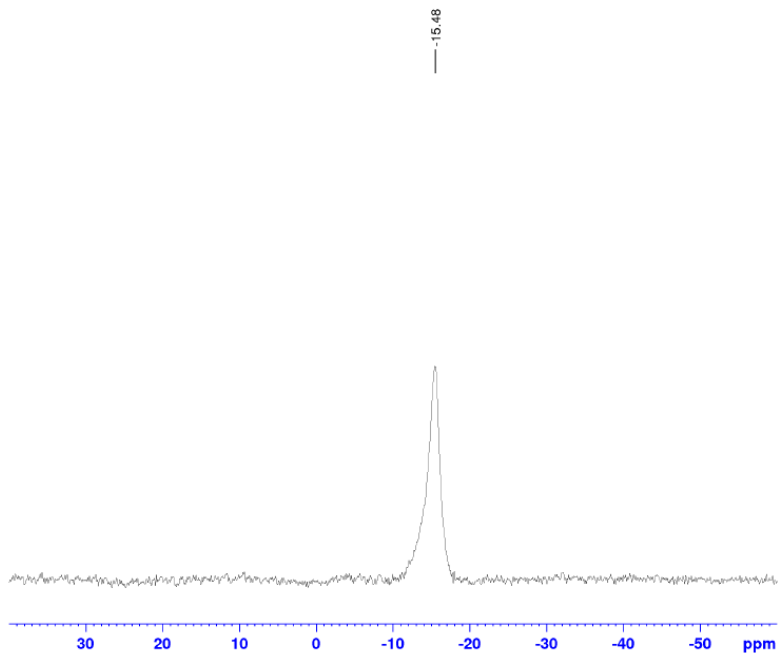
F2 - Acquisition Parameters  
 Date\_ 20190110  
 Time 12.00  
 INSTRUM av400  
 PROBHD 5 mm PABBO BB/  
 PULPROG zg30  
 TD 52882  
 SOLVENT MeOD  
 NS 128  
 DS 0  
 SWH 8012.820 Hz  
 FIDRES 0.151523 Hz  
 AQ 3.2998369 sec  
 RG 155.85  
 DW 62.400 usec  
 DE 6.50 usec  
 TE 298.3 K  
 D1 2.0000000 sec  
 TD0 1

===== CHANNEL f1 =====  
 SFO1 400.1324008 MHz  
 NUC1 <sup>1</sup>H  
 P1 15.00 usec  
 PLW1 13.00000000 W

F2 - Processing parameters  
 SI 65536  
 SF 400.1300079 MHz  
 WDW EM  
 SSB 0  
 LB 0.30 Hz  
 GB 0  
 PC 1.00



<sup>11</sup>B NMR

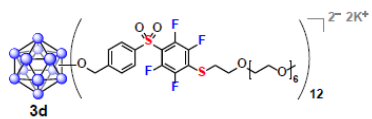


Current Data Parameters  
 NAME 0110  
 EXPNO 32  
 PROCNO 1

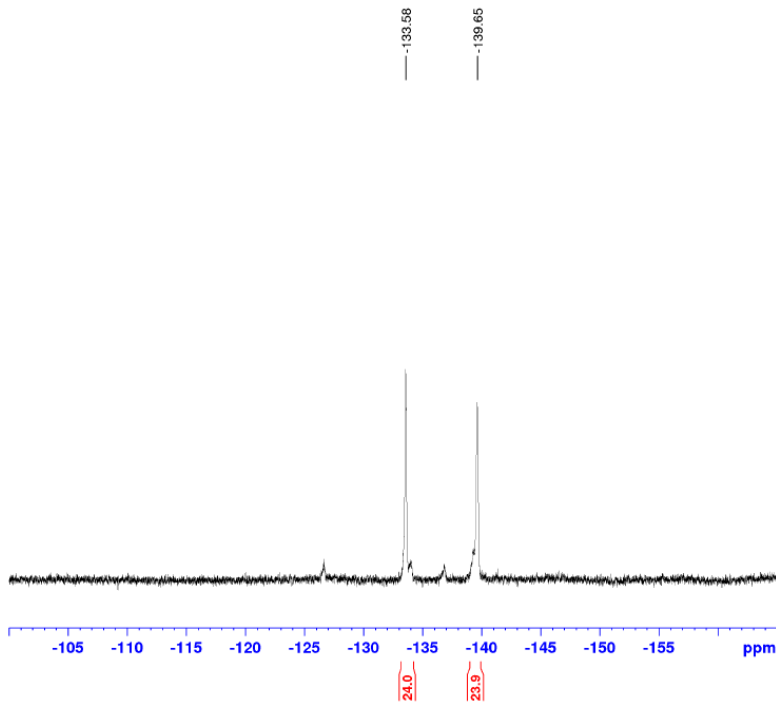
F2 - Acquisition Parameters  
 Date\_ 20190110  
 Time 12.20  
 INSTRUM av400  
 PROBHD 5 mm PABBO BB/  
 PULPROG zg  
 TD 5096  
 SOLVENT MeOD  
 NS 2048  
 DS 0  
 SWH 51020.406 Hz  
 FIDRES 10.011854 Hz  
 AQ 0.0499408 sec  
 RG 189.85  
 DW 9.800 usec  
 DE 6.50 usec  
 TE 298.4 K  
 D1 0.05000000 sec  
 TD0 1

===== CHANNEL f1 =====  
 SFO1 128.3776052 MHz  
 NUC1 11B  
 P1 10.00 usec  
 PLW1 52.00000000 W

F2 - Processing parameters  
 SI 32768  
 SF 128.3776161 MHz  
 WDW EM  
 SSB 0  
 LB 10.00 Hz  
 GB 0  
 PC 1.40



<sup>19</sup>F NMR

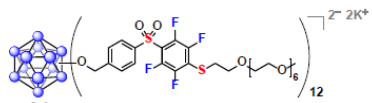


Current Data Parameters  
 NAME 0110  
 EXPNO 31  
 PROCNO 1

F2 - Acquisition Parameters  
 Date\_ 20190110  
 Time 12.14  
 INSTRUM av400  
 PROBHD 5 mm PABBO BB/  
 PULPROG zgpg30  
 TD 262144  
 SOLVENT MeOD  
 NS 256  
 DS 0  
 SWH 150000.000 Hz  
 FIDRES 0.572205 Hz  
 AQ 0.8738133 sec  
 RG 189.85  
 DW 3.333 usec  
 DE 6.50 usec  
 TE 298.4 K  
 D1 2.0000000 sec  
 TD0 1

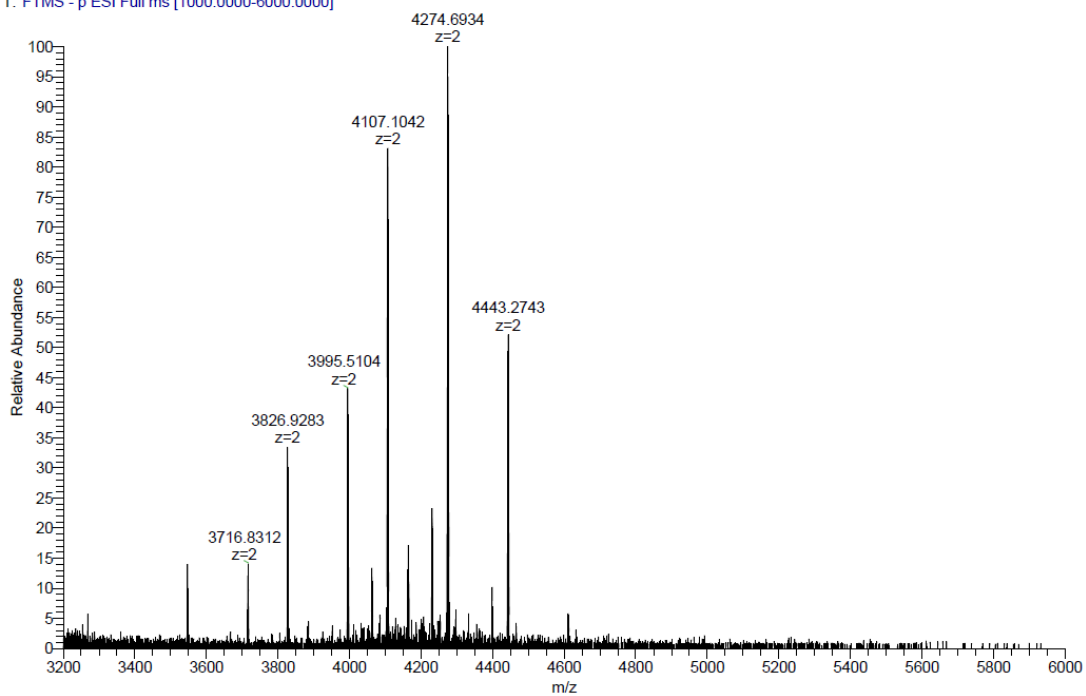
===== CHANNEL f1 =====  
 SFO1 376.4983660 MHz  
 NUC1 19F  
 P1 14.50 usec  
 PLW1 17.00000000 W

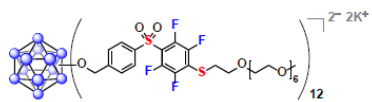
F2 - Processing parameters  
 SI 262144  
 SF 376.4983660 MHz  
 WDW EM  
 SSB 0  
 LB 3.00 Hz  
 GB 0  
 PC 1.00



### ESI-HRMS

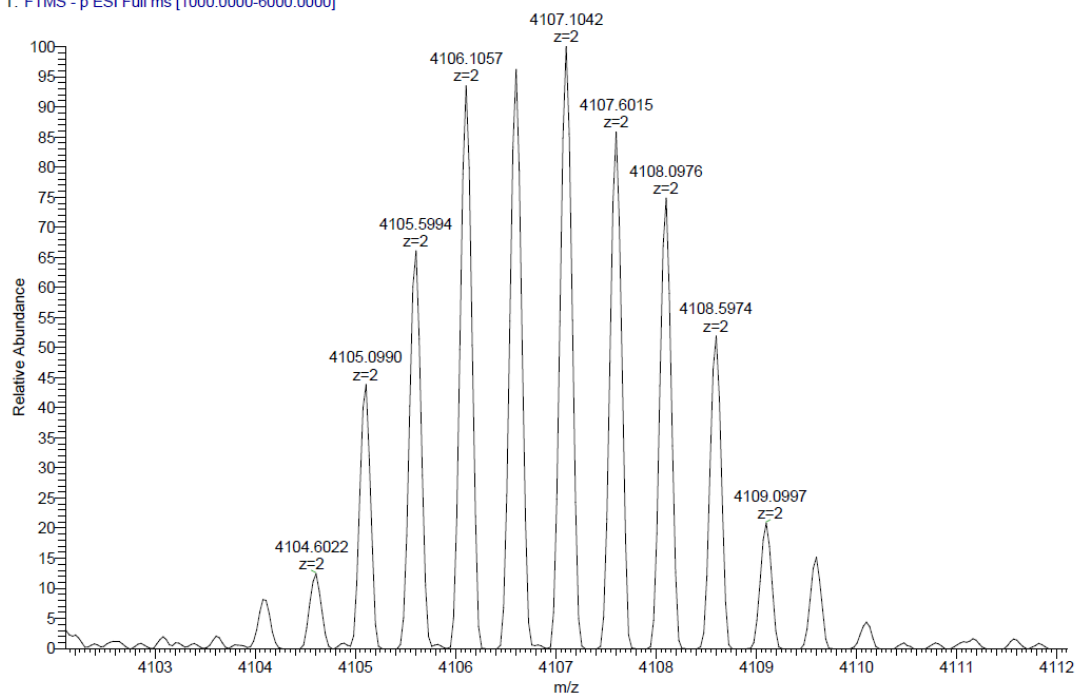
3d  
 3d #1-50 RT: 0.01-0.43 AV: 50 NL: 3.95E5  
 T: FTMS - p ESI Full ms [1000.0000-6000.0000]





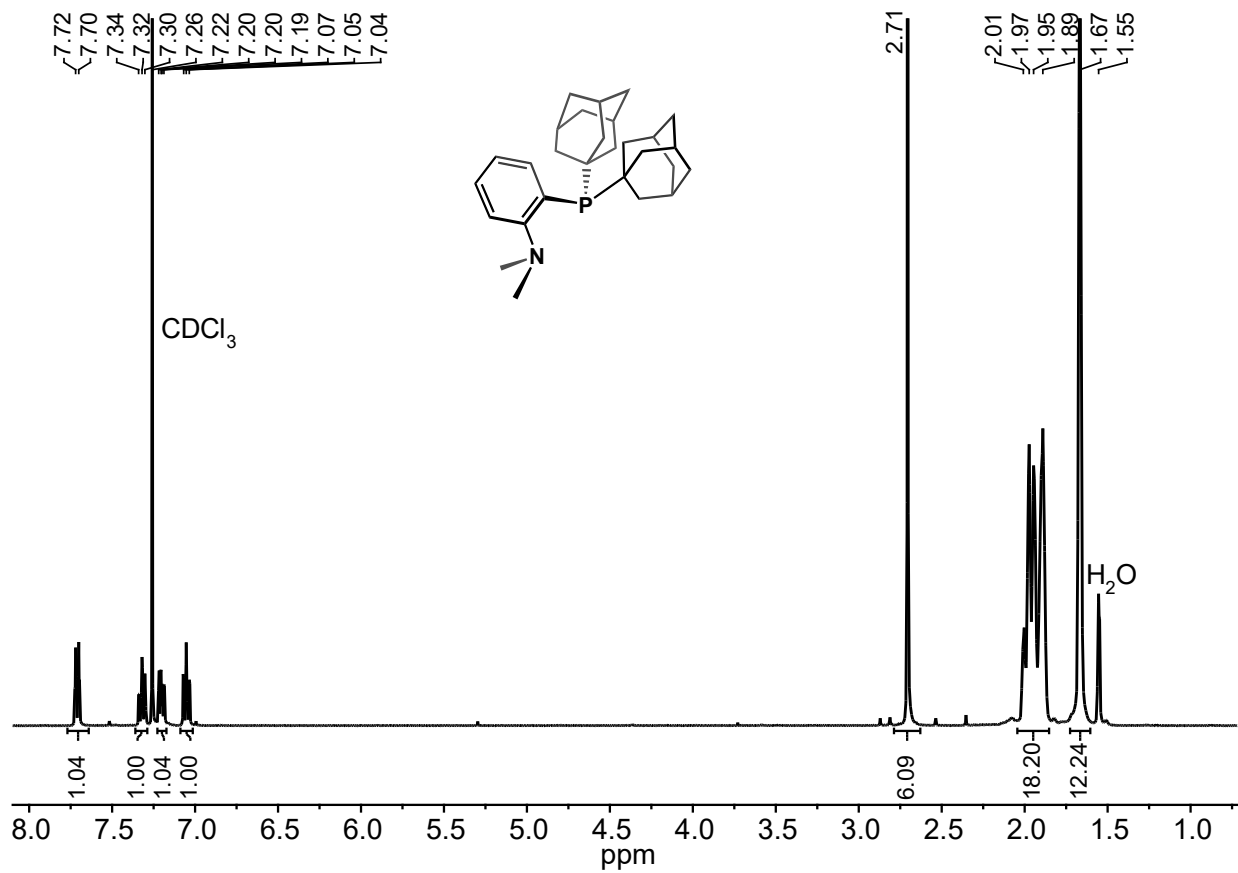
### ESI-HRMS

3d  
3d #1-50 RT: 0.01-0.43 AV: 50 NL: 3.28E5  
T: FTMS - p ESI Full ms [1000.0000-6000.0000]

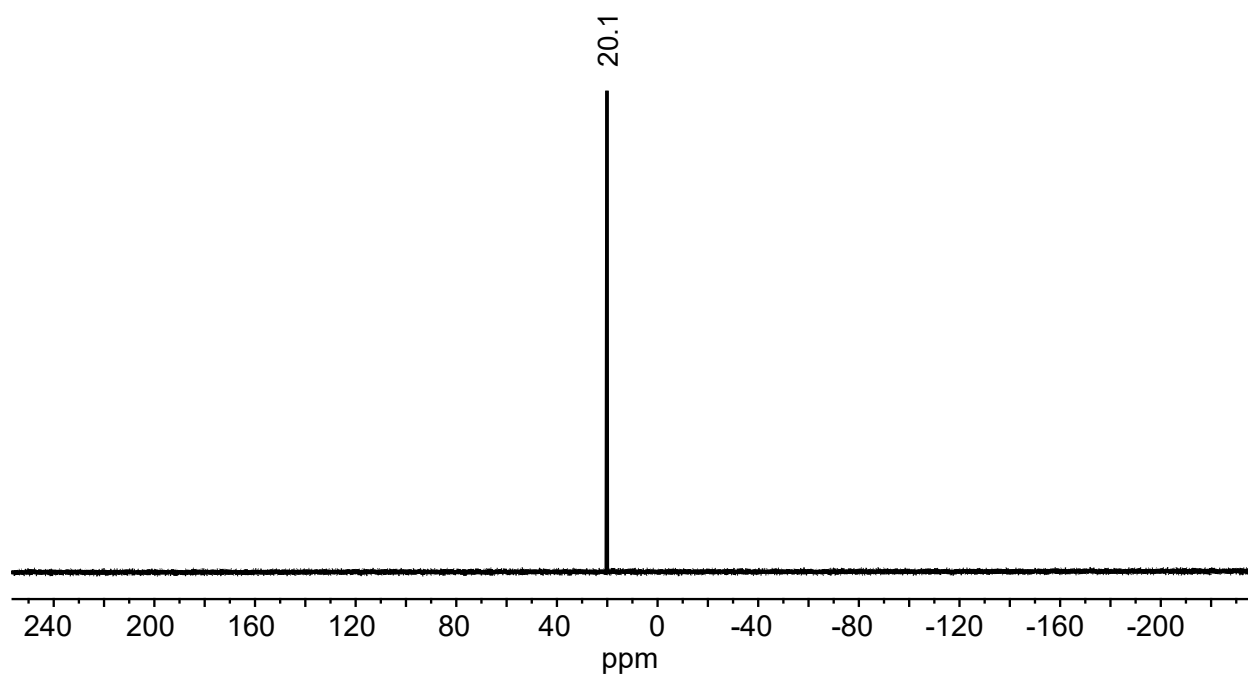




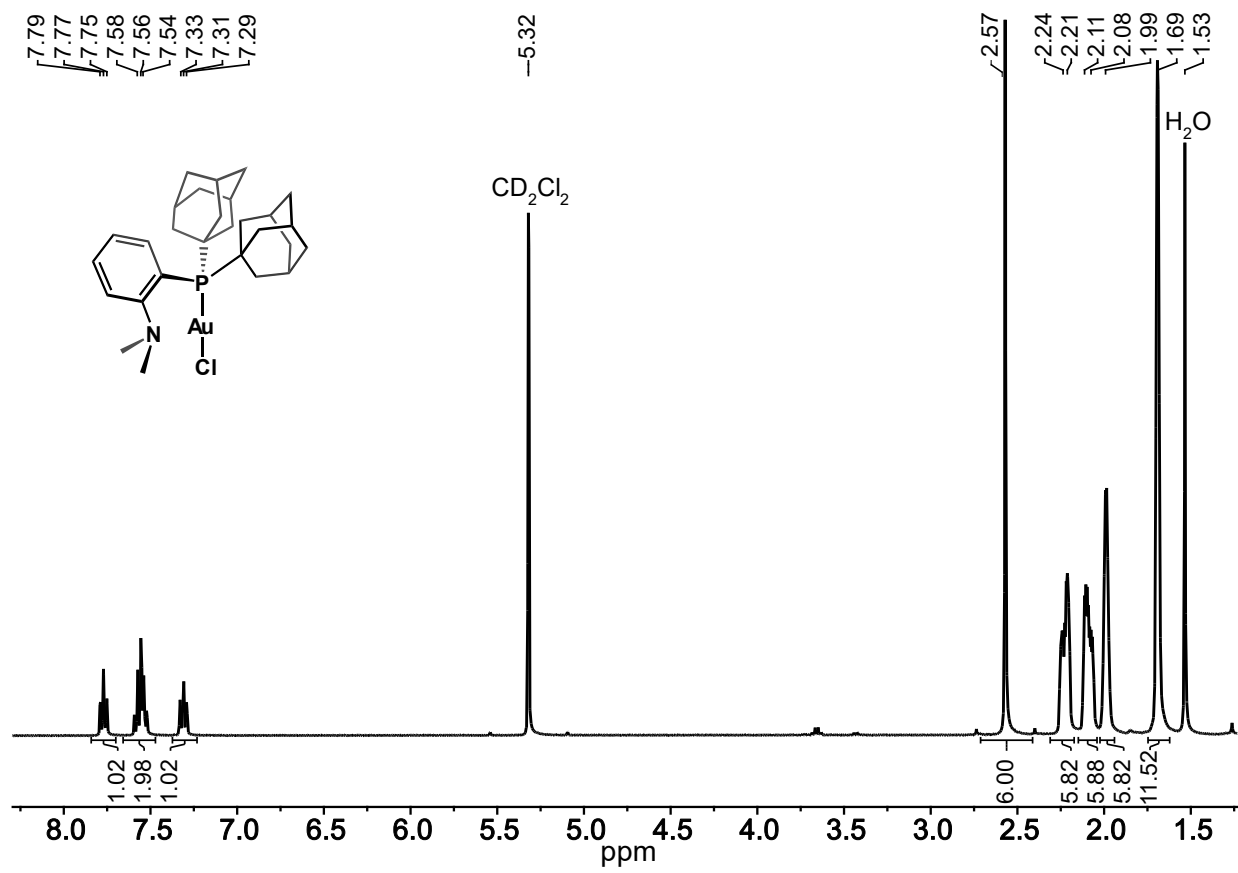
### Supplementary Data Relevant to Chapter Four



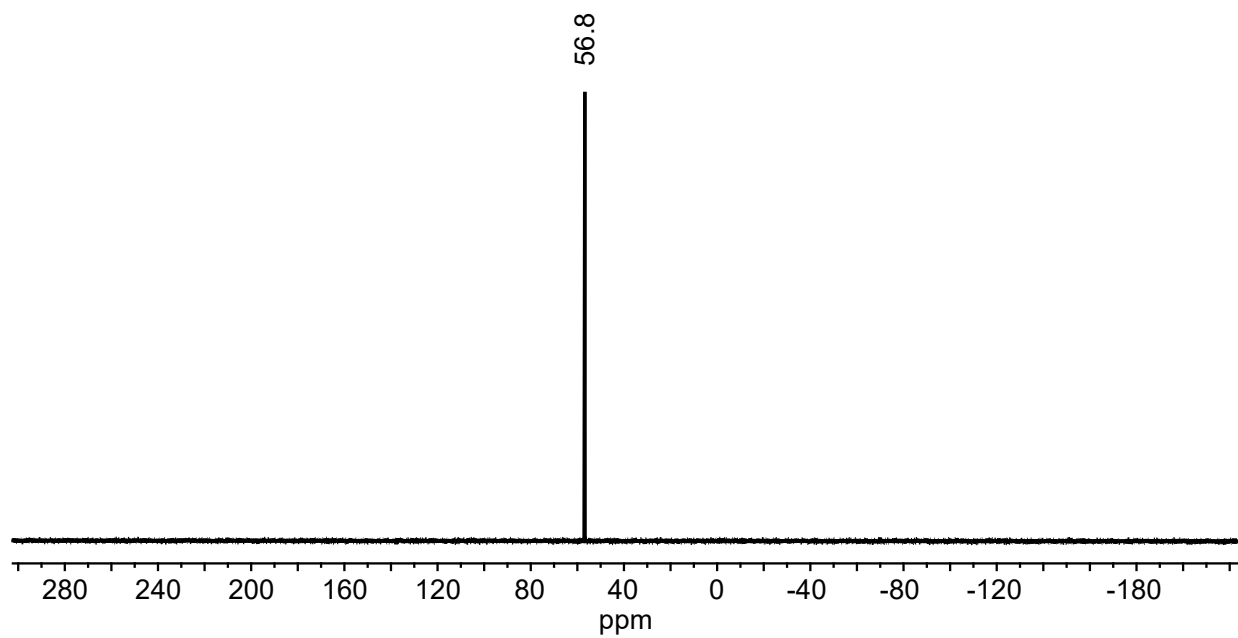
$^1\text{H}$  NMR spectrum of Me-DalPhos ( $\text{CDCl}_3$ , 400 MHz, 25 °C).



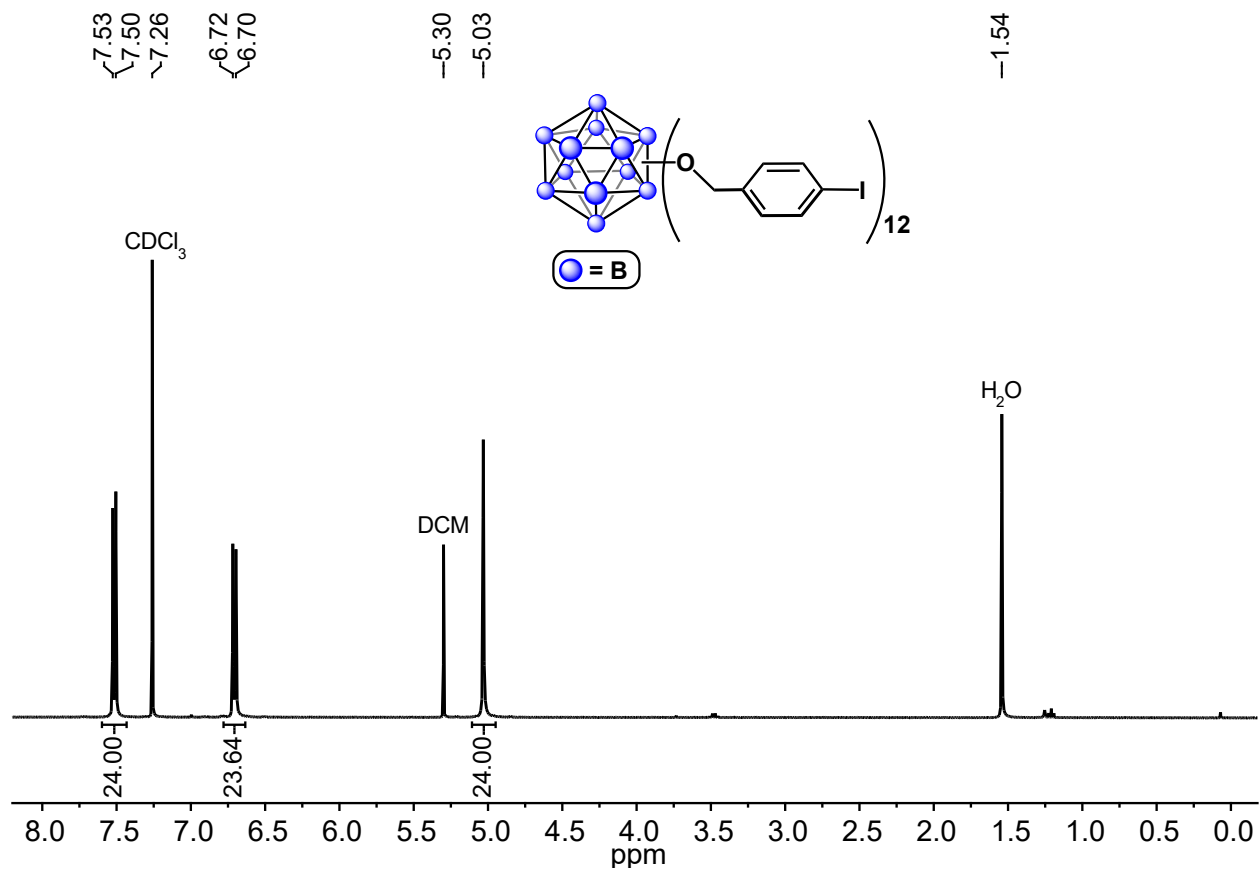
$^{31}\text{P}\{^1\text{H}\}$  NMR spectrum of Me-DalPhos ( $\text{CDCl}_3$ , 162 MHz, 25 °C).



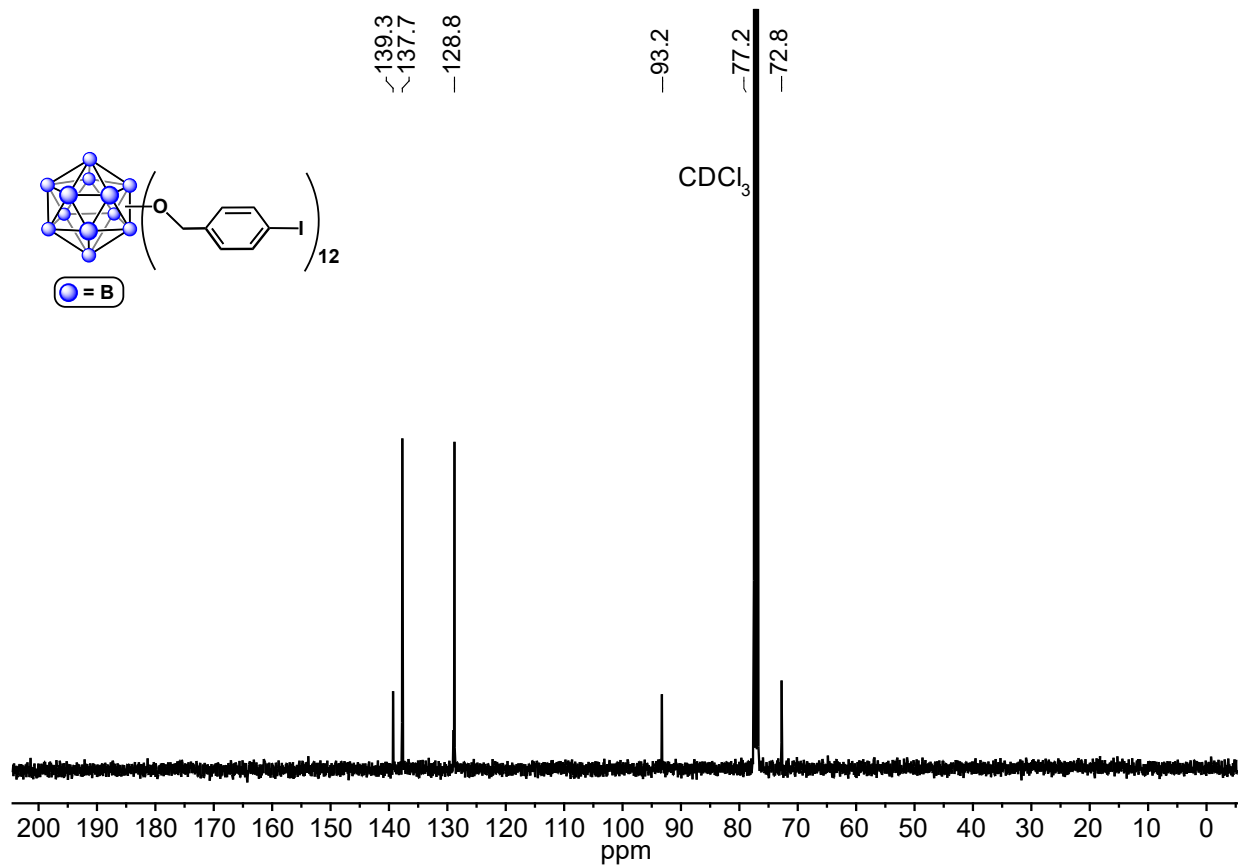
$^1\text{H}$  NMR spectrum of (Me-DalPhos)AuCl ( $\text{CD}_2\text{Cl}_2$ , 400 MHz, 25 °C).



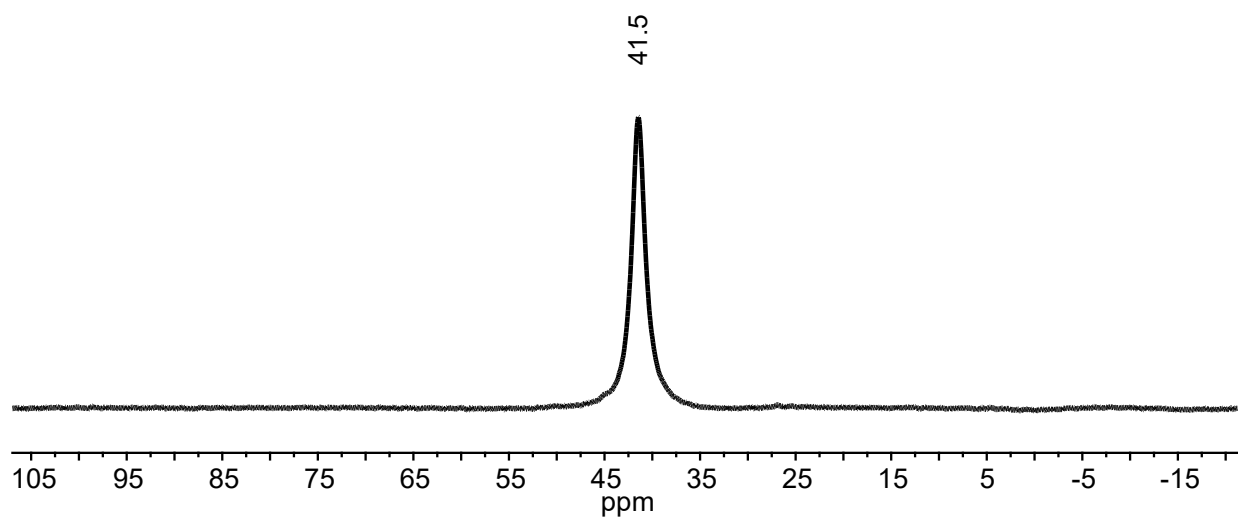
$^{31}\text{P}\{^1\text{H}\}$  NMR spectrum of (Me-DalPhos)AuCl ( $\text{CD}_2\text{Cl}_2$ , 162 MHz, 25 °C).



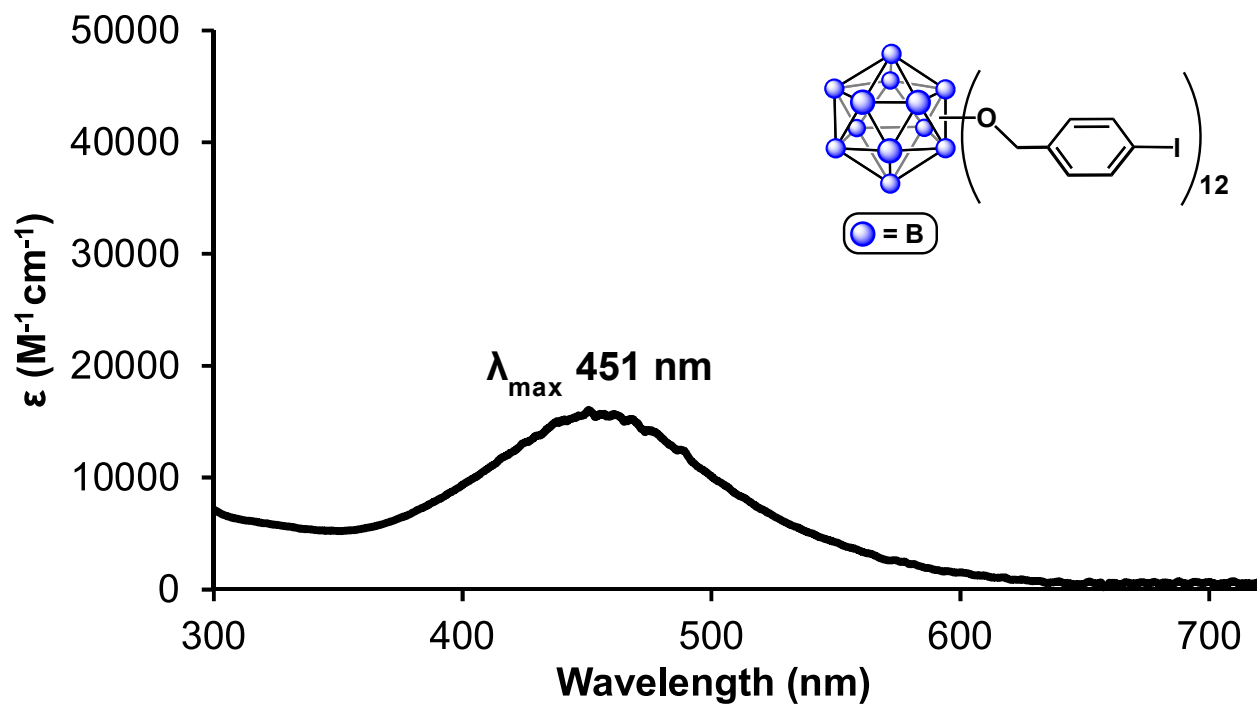
$^1H$  NMR spectrum of  $B_{12}(OCH_2C_6H_4I)_{12}$  ( $CDCl_3$ , 400 MHz, 25 °C).



$^{13}\text{C}\{^1\text{H}\}$  NMR spectrum of  $\text{B}_{12}(\text{OCH}_2\text{C}_6\text{H}_4\text{I})_{12}$  ( $\text{CDCl}_3$ , 101 MHz, 25 °C).

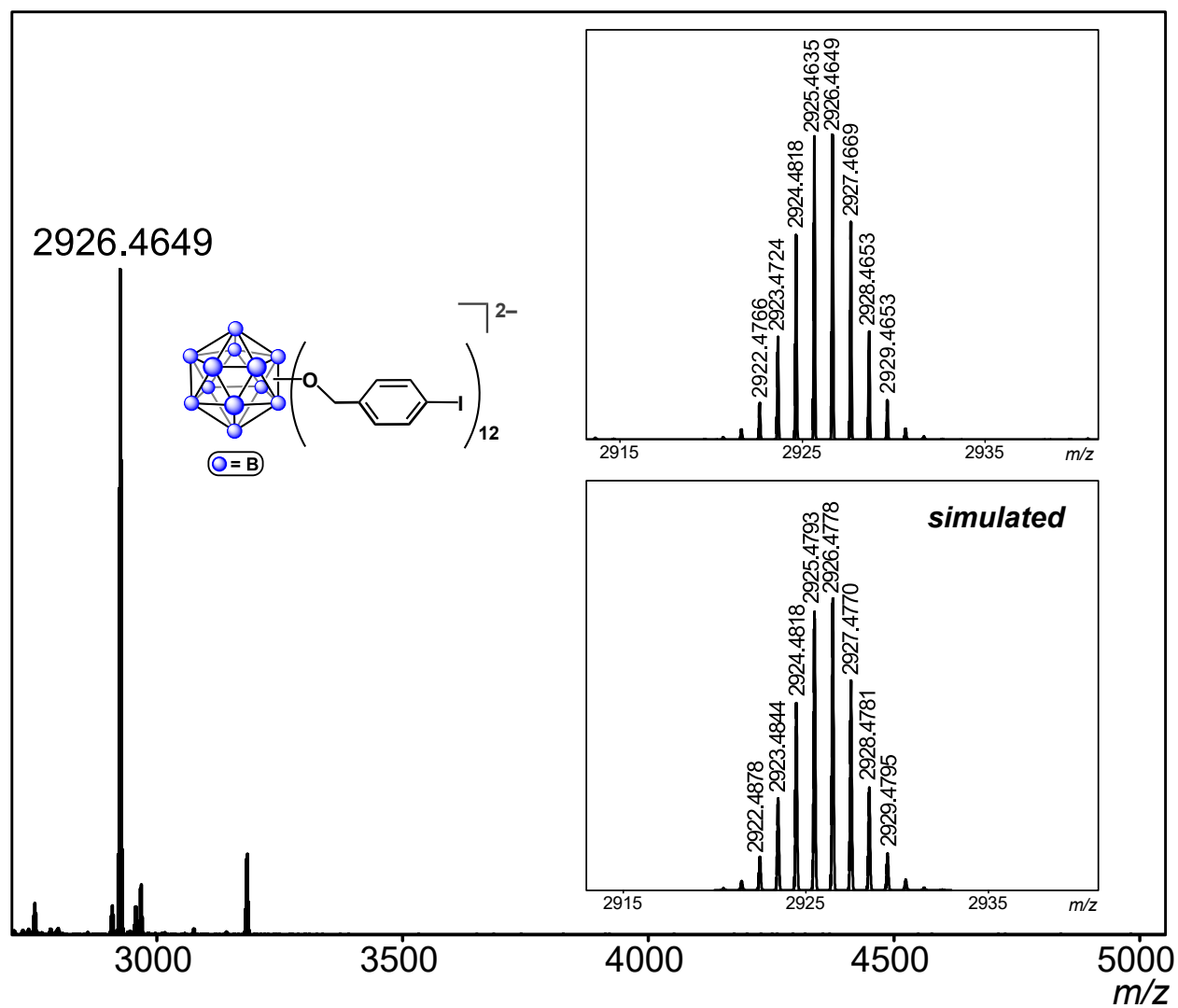


$^{11}\text{B}\{^1\text{H}\}$  NMR spectrum of  $\text{B}_{12}(\text{OCH}_2\text{C}_6\text{H}_4\text{I})_{12}$  ( $\text{CDCl}_3$ , 128 MHz, 25 °C).

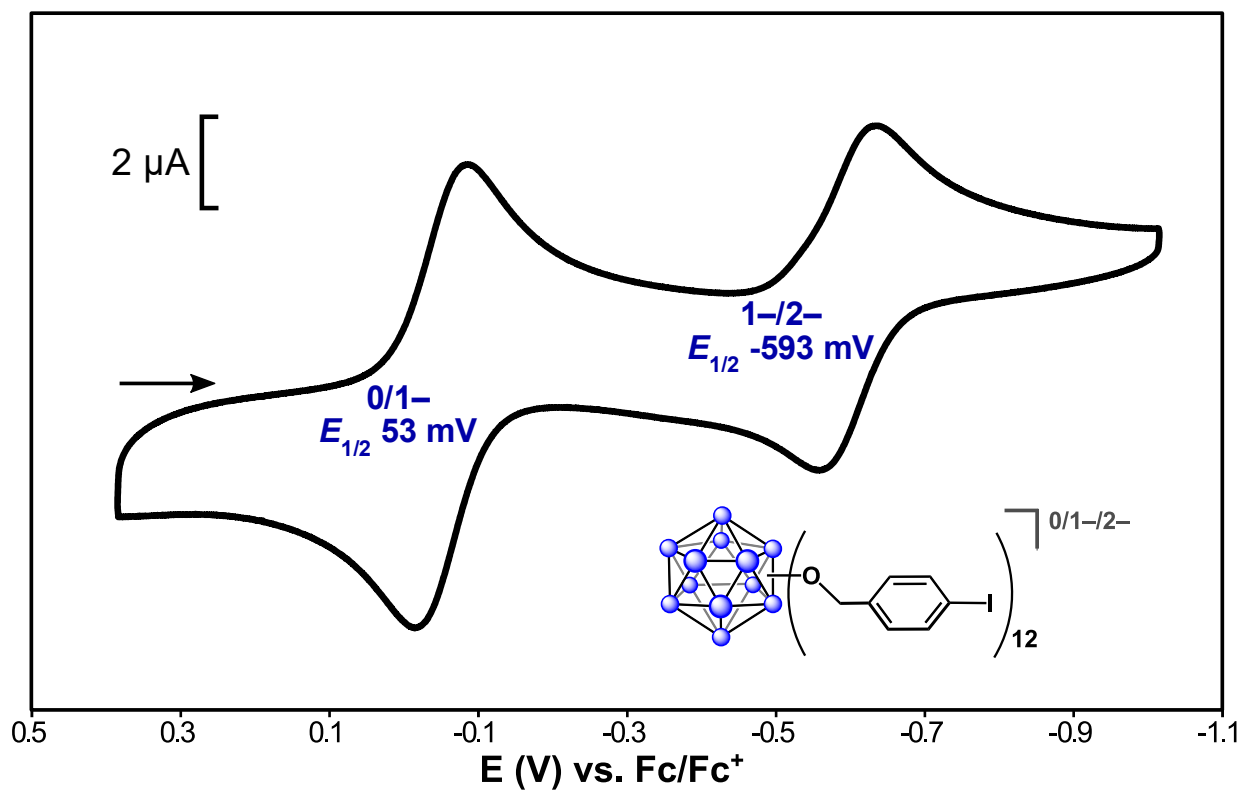


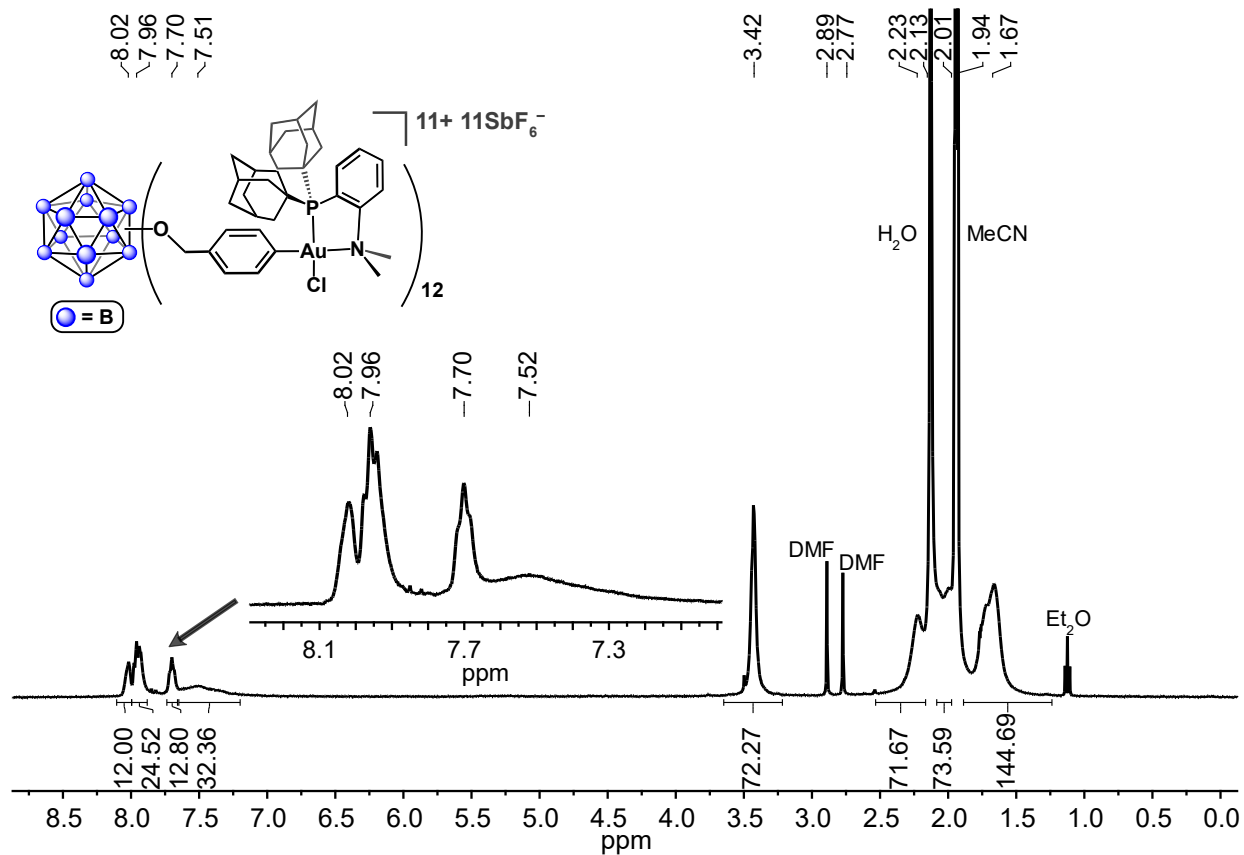
UV-vis spectrum of  $B_{12}(OCH_2C_6H_4I)_{12}$  (DCM, 0.1 mM, 25 °C).



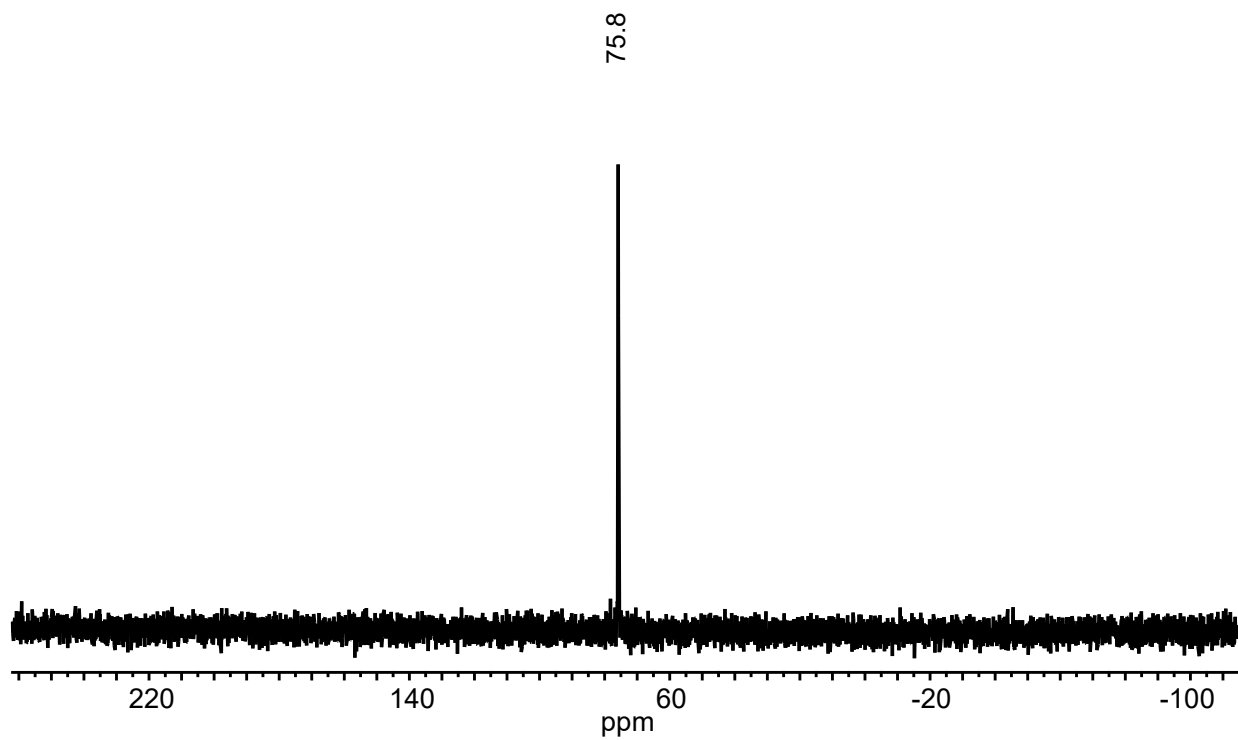


ESI-MS(-) of  $B_{12}(OCH_2C_6H_4I)_{12}$  (MeCN, 1.5 kV). This species is observed as a dianion under ESI-MS conditions in MeCN.

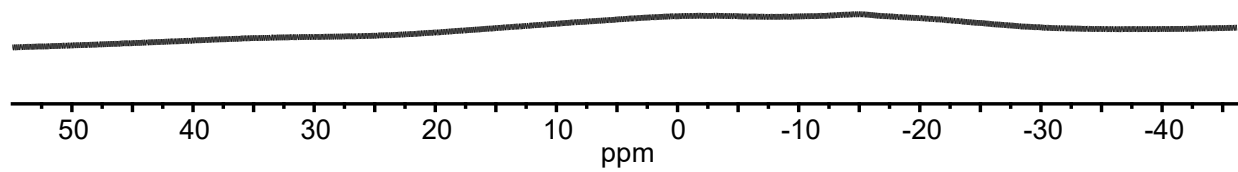




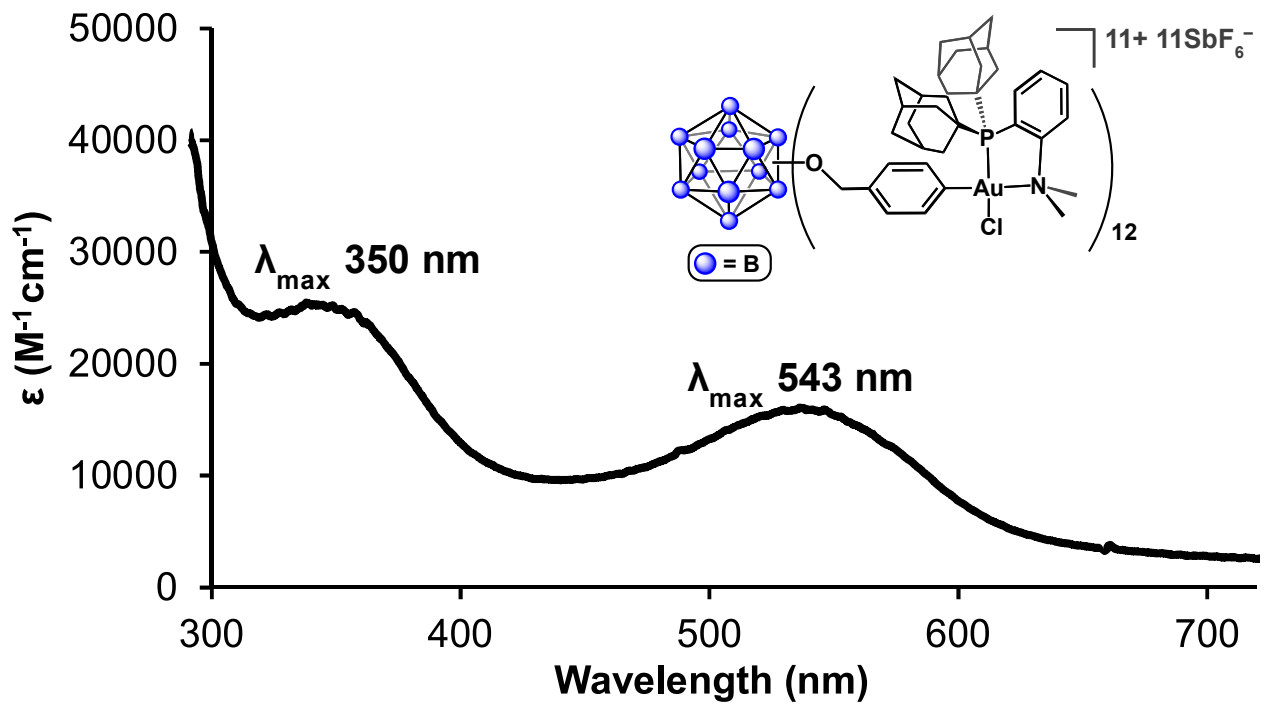
$^1H$  NMR spectrum of  $[B_{12}(OCH_2C_6H_4(Me-DalPhos)AuCl)_{12}][SbF_6]_{11}$  (CD<sub>3</sub>CN, 400 MHz, 25 °C).



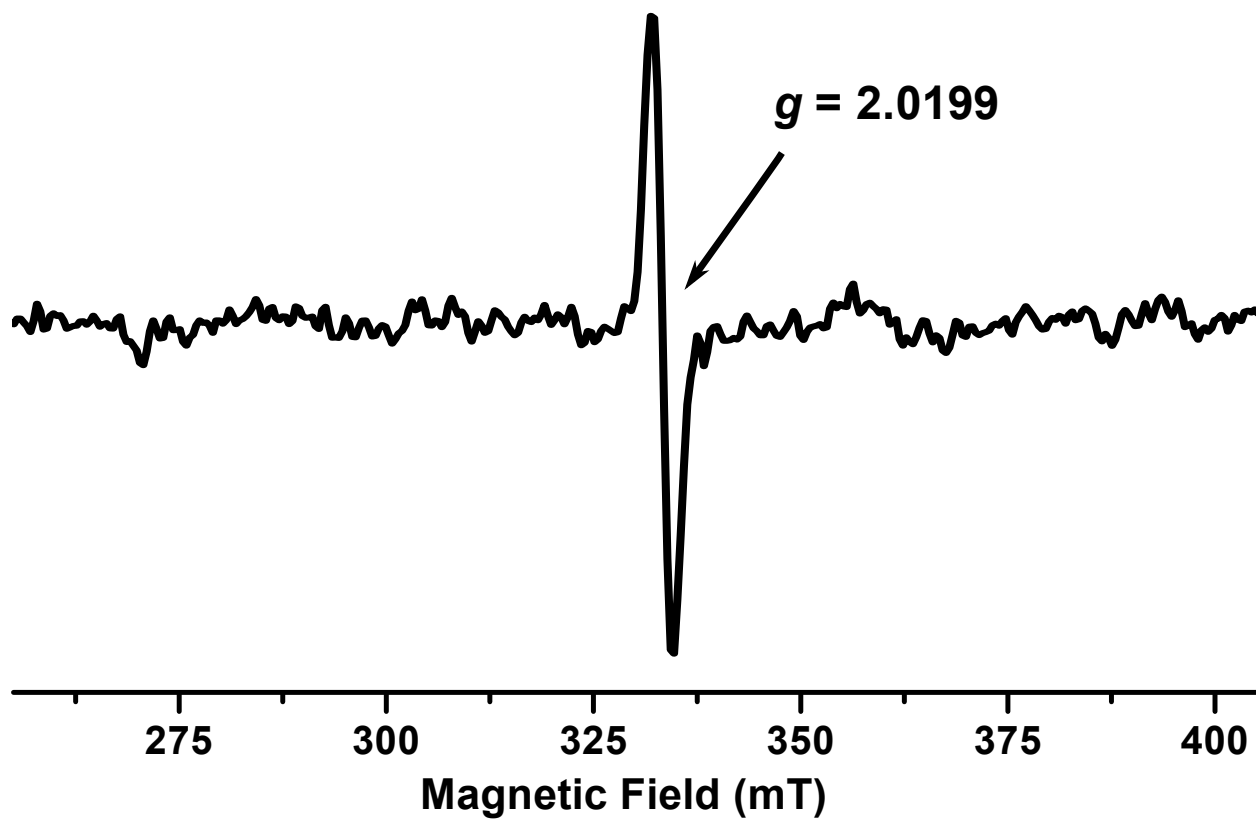
$^{31}\text{P}\{^1\text{H}\}$  NMR spectrum of  $[\text{B}_{12}(\text{OCH}_2\text{C}_6\text{H}_4(\text{Me-DalPhos})\text{AuCl})_{12}][\text{SbF}_6]_{11}$  ( $\text{CD}_3\text{CN}$ , 162 MHz, 25 °C).



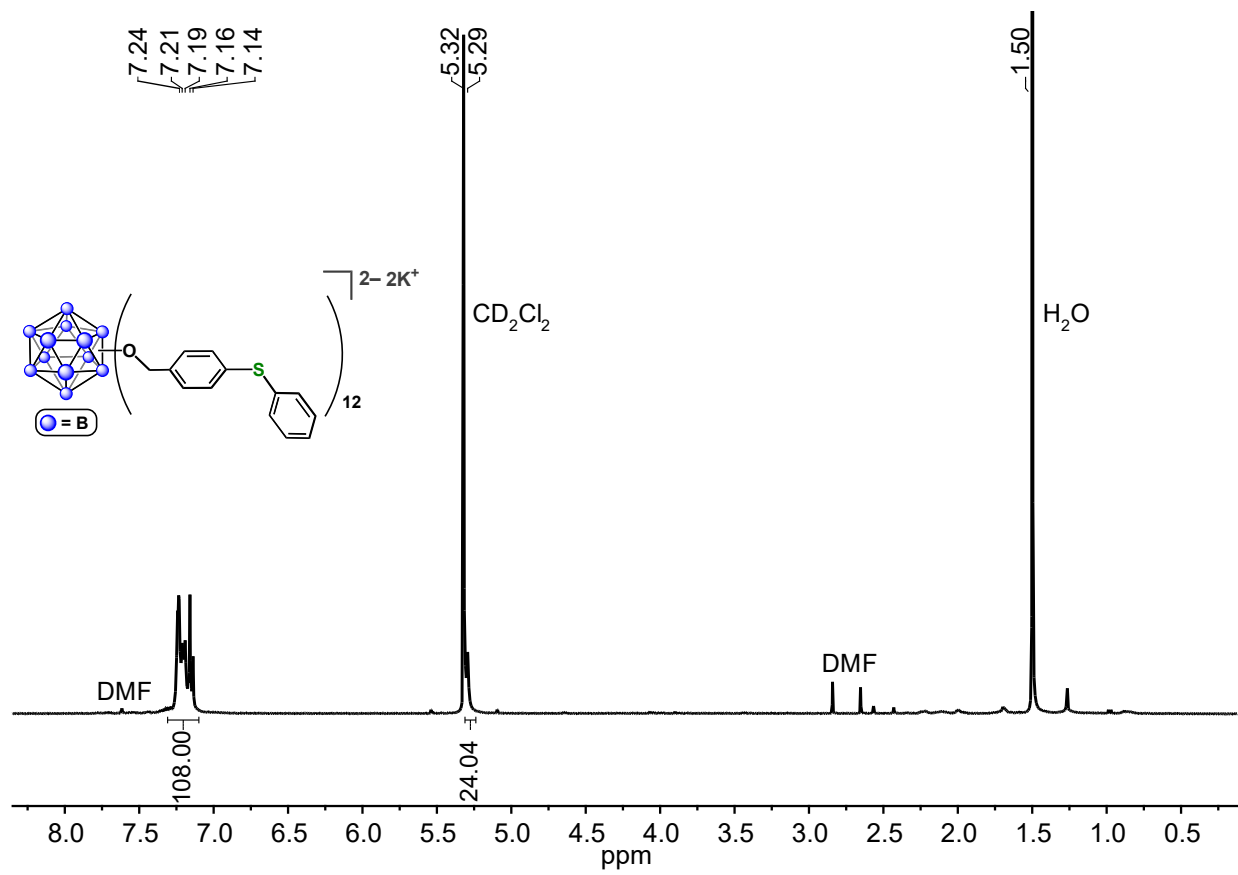
$^{11}\text{B}\{^1\text{H}\}$  NMR spectrum of  $[\text{B}_{12}(\text{OCH}_2\text{C}_6\text{H}_4((\text{Me-DalPhos})\text{AuCl})_{12})][\text{SbF}_6]_{11}$  ( $\text{CD}_3\text{CN}$ , 128 MHz, 25 °C).



UV-vis spectrum of  $[\text{B}_{12}(\text{OCH}_2\text{C}_6\text{H}_4((\text{Me-DalPhos})\text{AuCl})_{12})][\text{SbF}_6]_{11}$  (MeCN, 0.06 mM, 25 °C).

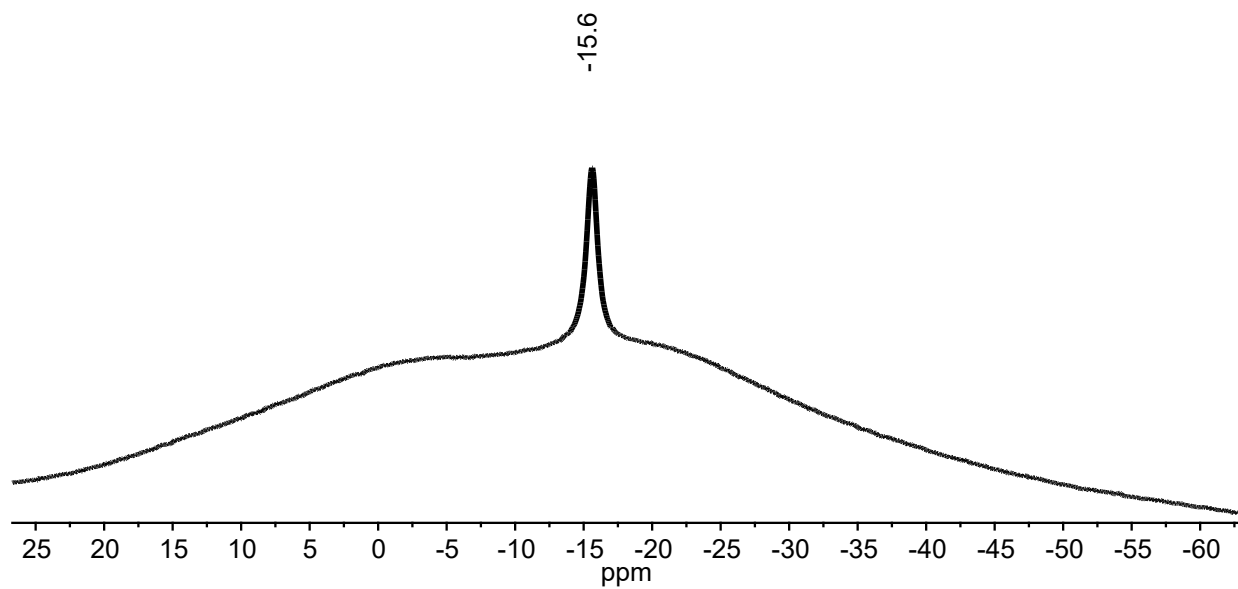


EPR spectrum of  $[\text{B}_{12}(\text{OCH}_2\text{C}_6\text{H}_4((\text{Me-DalPhos})\text{AuCl})_{12})[\text{SbF}_6]_{11}$  (1:9 MeCN:toluene, 9.42 GHz MW frequency, 32 °C cavity temperature).

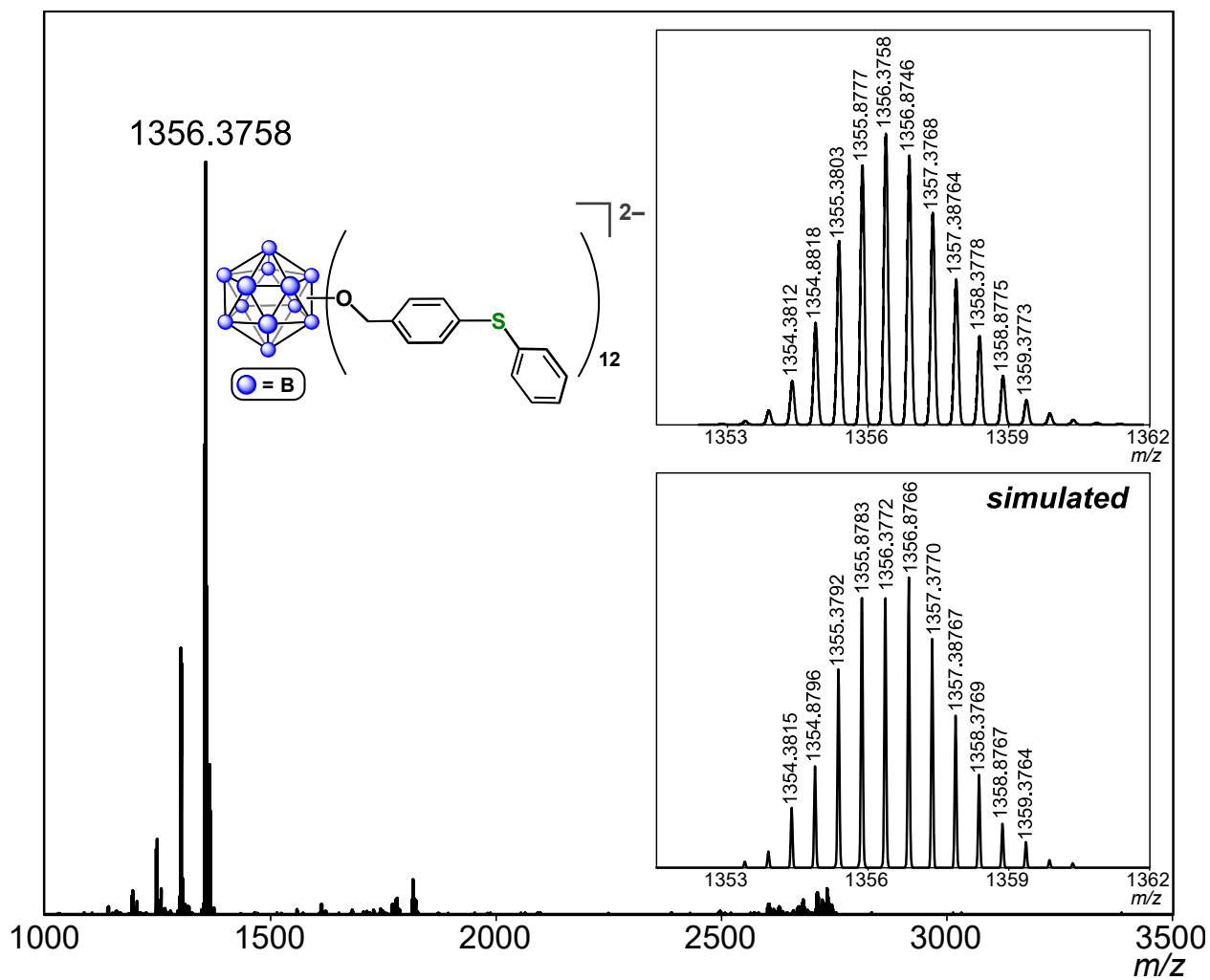


$^1H$  NMR spectrum of  $[K_2][B_{12}(OCH_2C_6H_4SPh)_{12}]$  (400 MHz,  $CD_2Cl_2$ , 25 °C).

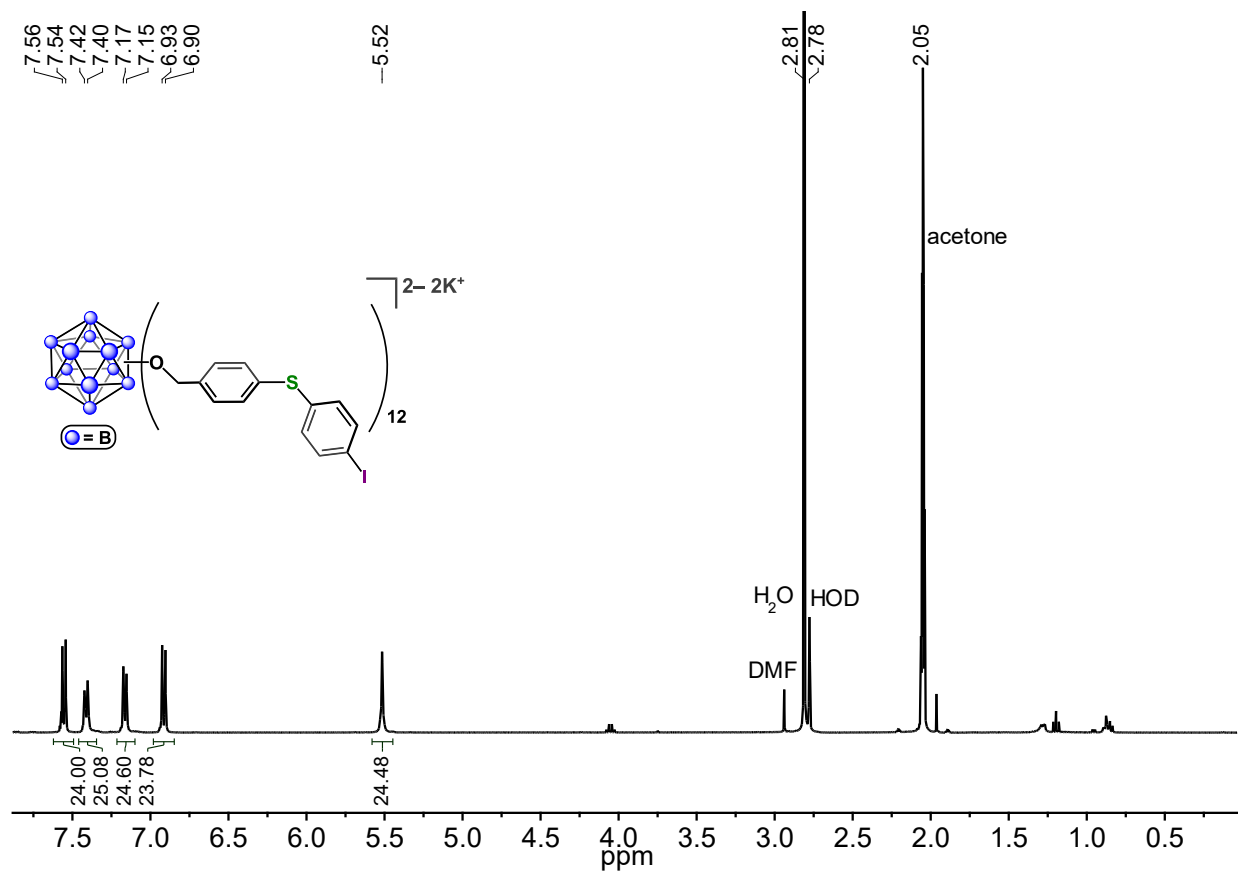




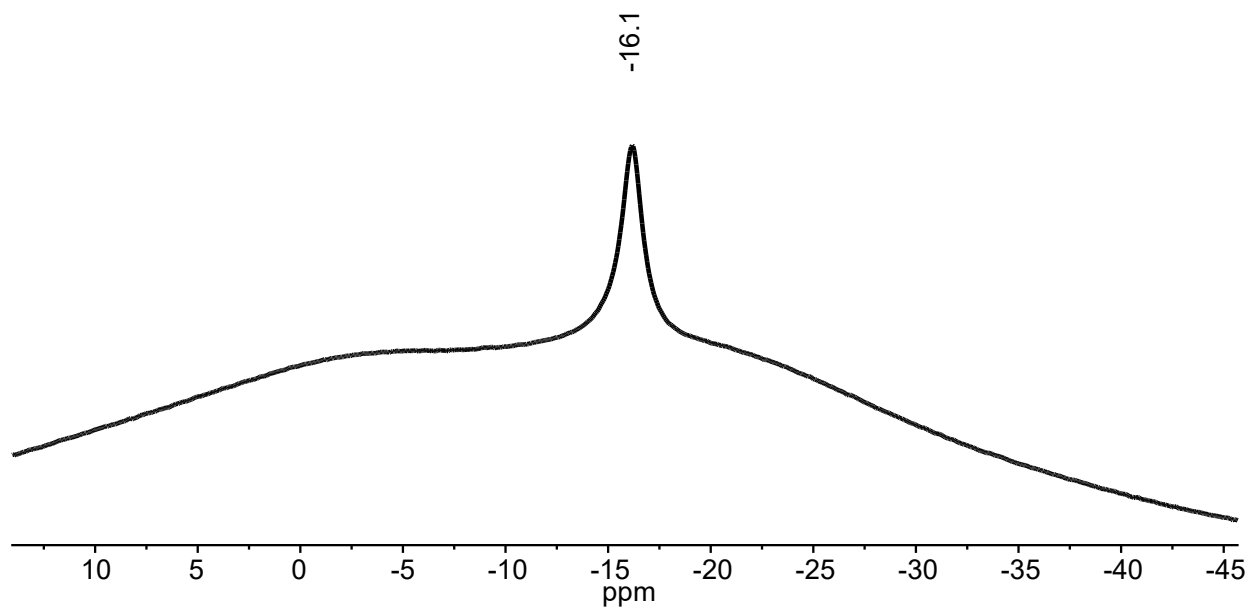
$^{11}\text{B}\{^1\text{H}\}$  NMR spectrum of  $[\text{K}_2][\text{B}_{12}(\text{OCH}_2\text{C}_6\text{H}_4\text{SPh})_{12}]$  (128 MHz,  $\text{CD}_2\text{Cl}_2$ , 25 °C).



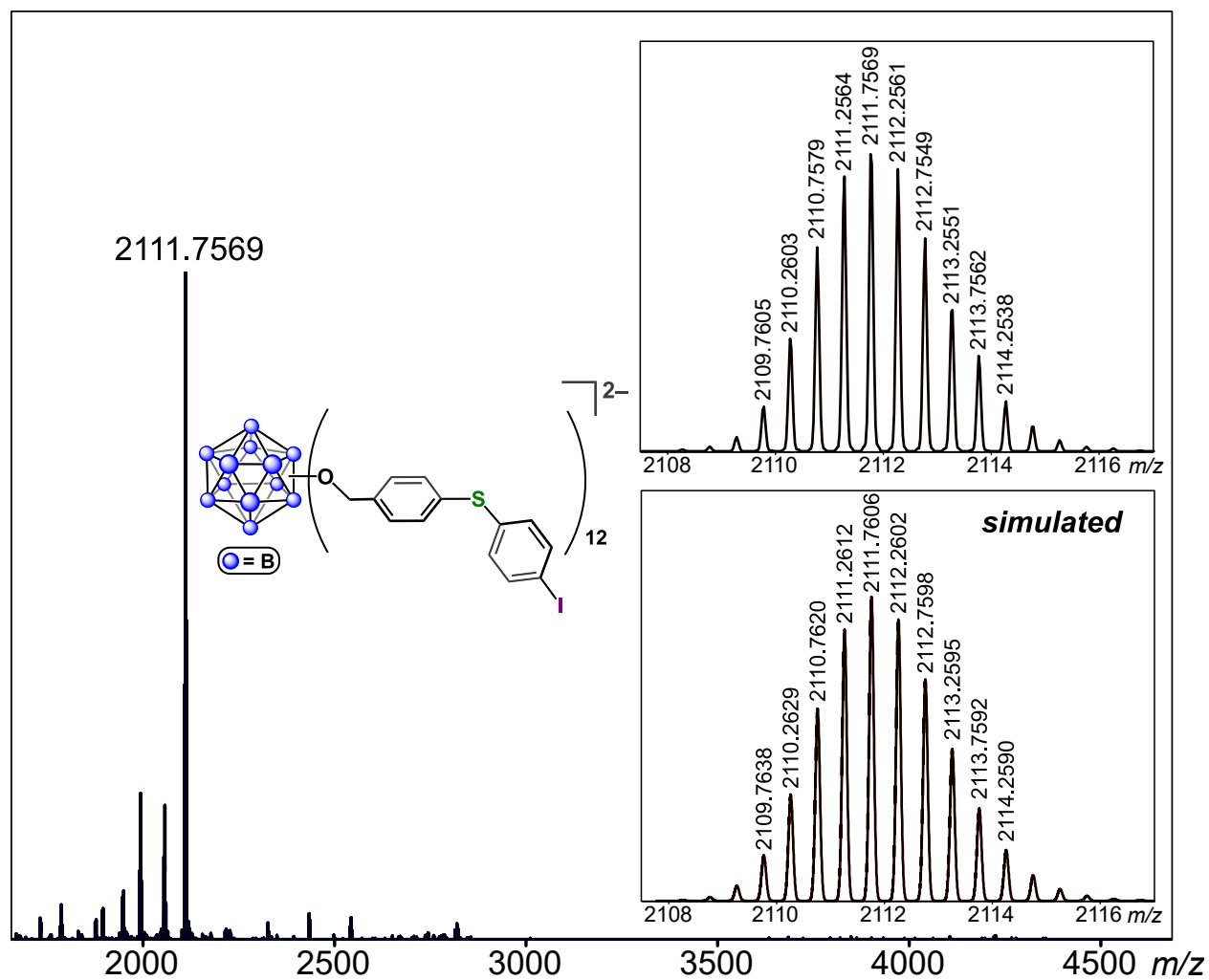
ESI-MS(-) of  $[B_{12}(OCH_2C_6H_4SPh)_{12}]^{2-}$  (MeCN, 1.5 kV).



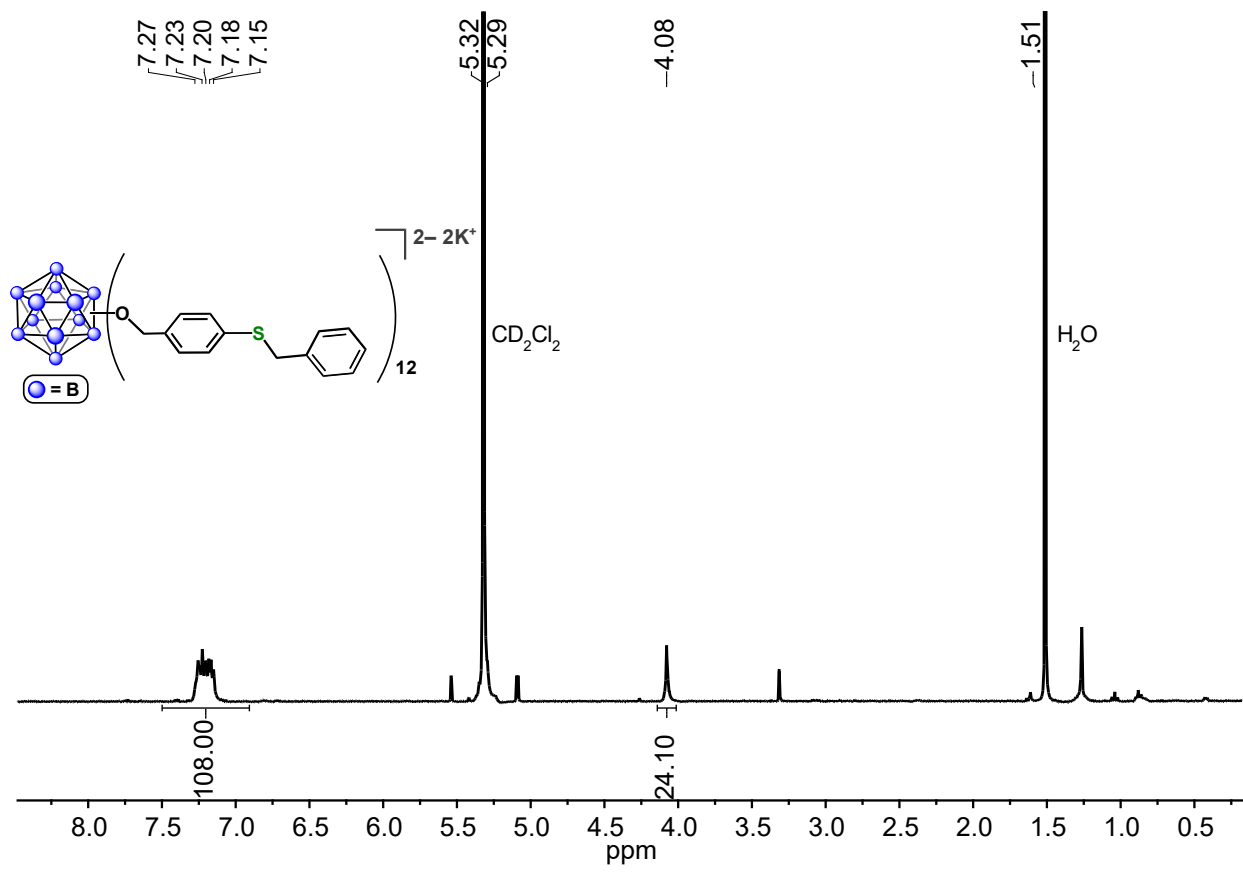
$^1H$  NMR spectrum of  $[K_2][B_{12}(OCH_2C_6H_4SC_6H_4I)_{12}]$  (400 MHz, acetone- $d_6$ , 25 °C).



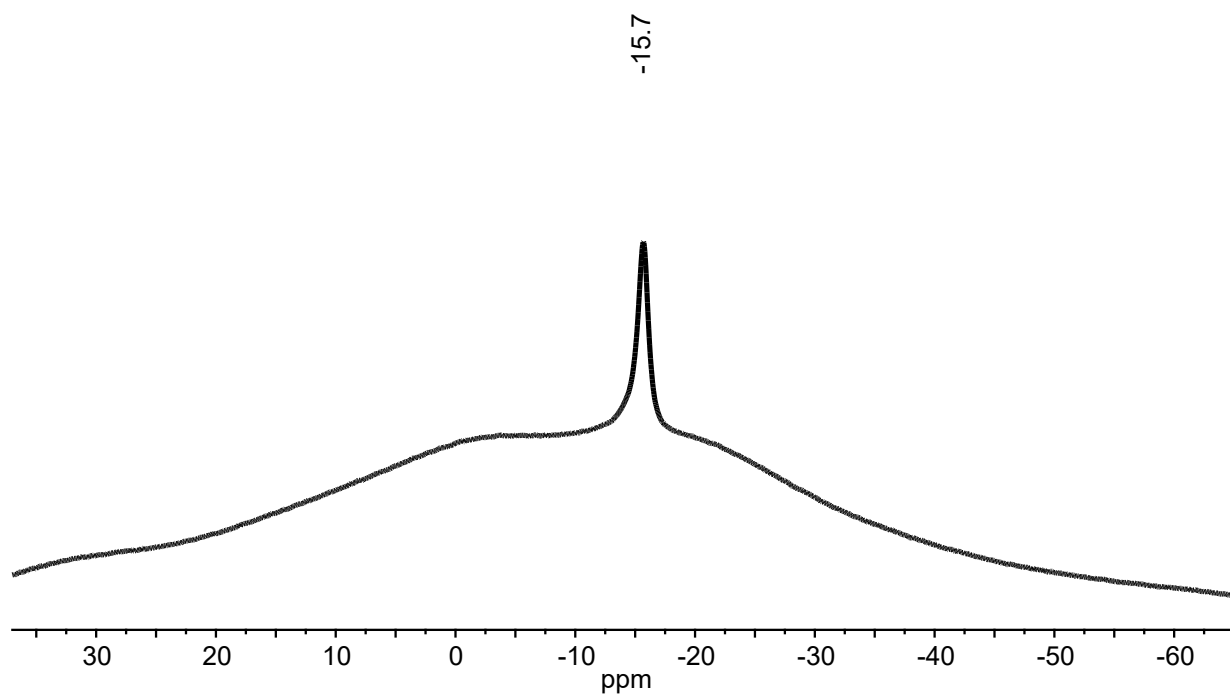
$^{11}\text{B}\{^1\text{H}\}$  NMR spectrum of  $[\text{K}_2][\text{B}_{12}(\text{OCH}_2\text{C}_6\text{H}_4\text{SC}_6\text{H}_4\text{I})_{12}]$  (128 MHz, acetone- $d_6$ , 25 °C).



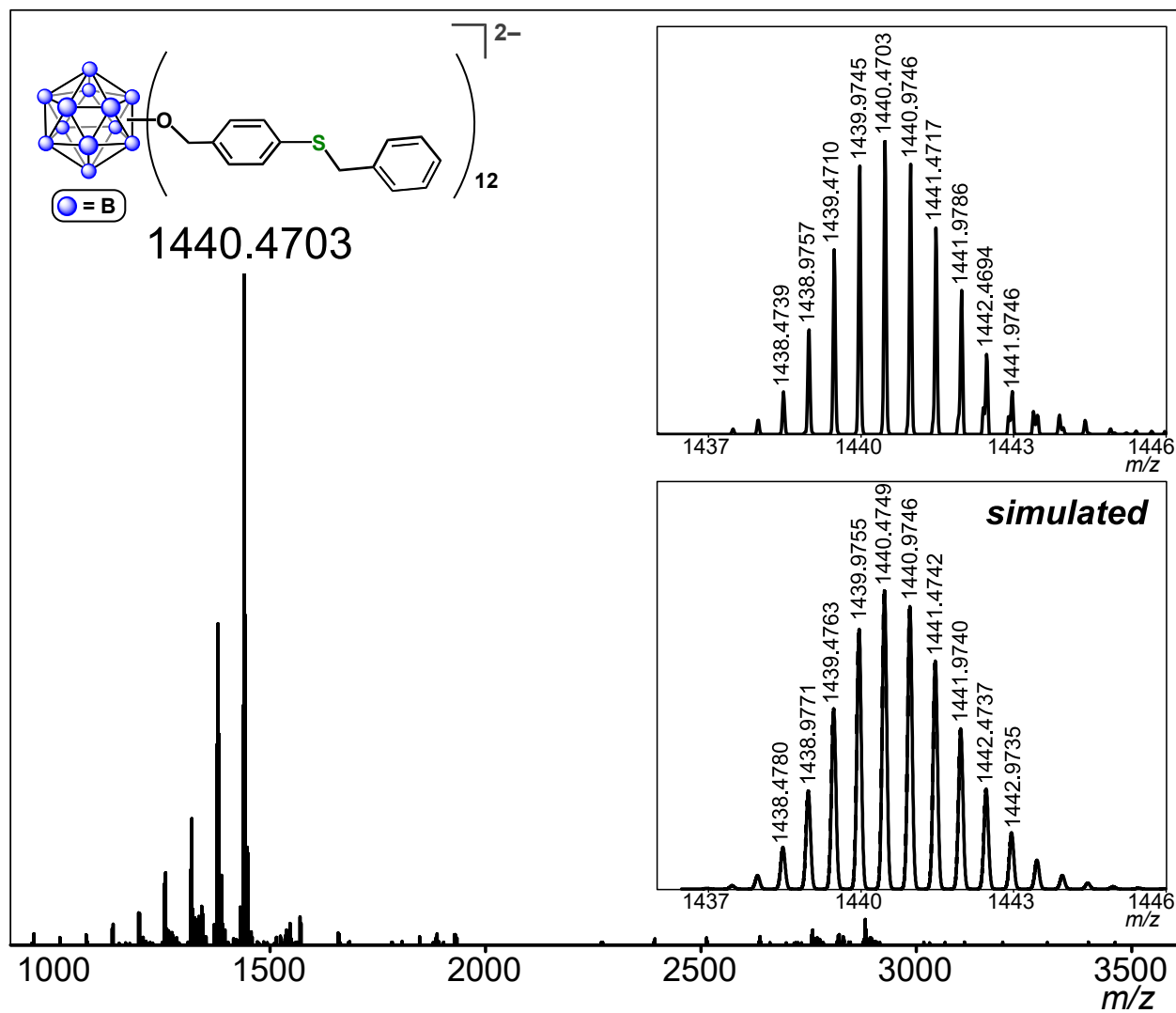
ESI-MS(-) of  $[B_{12}(OCH_2C_6H_4SC_6H_4I)_{12}]^{2-}$  (MeCN, 1.5 kV).



$^1H$  NMR spectrum of  $[K_2][B_{12}(OCH_2C_6H_4SCH_2C_6H_5)_{12}]$  (400 MHz,  $CD_2Cl_2$ , 25 °C).

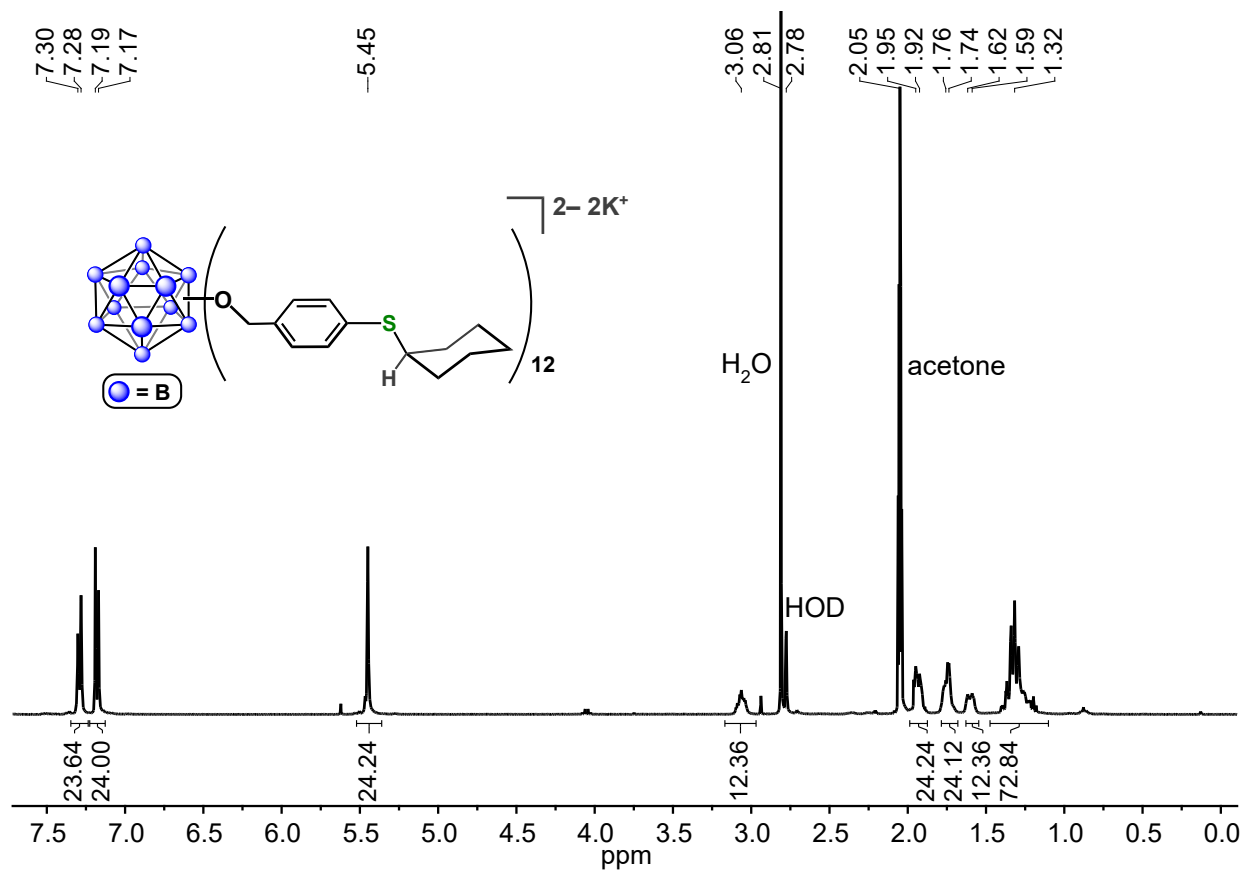


$^{11}\text{B}\{^1\text{H}\}$  NMR spectrum of  $[\text{K}_2][\text{B}_{12}(\text{OCH}_2\text{C}_6\text{H}_4\text{SCH}_2\text{C}_6\text{H}_5)_{12}]$  (128 MHz,  $\text{CD}_2\text{Cl}_2$ , 25 °C).

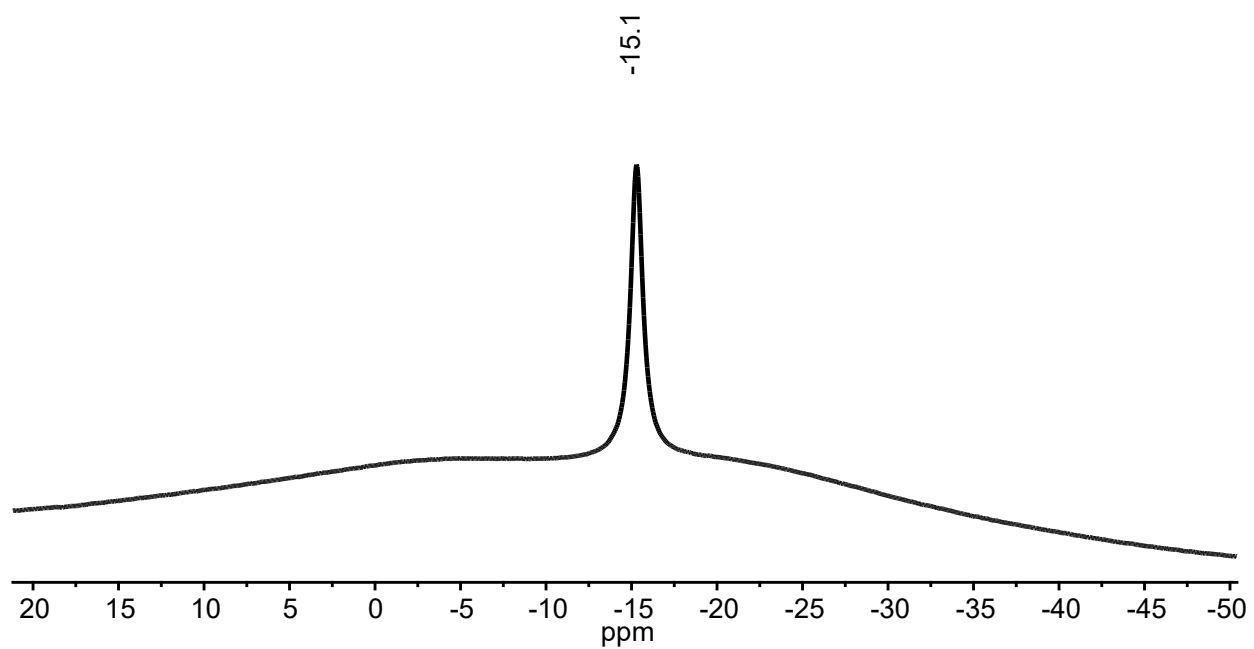


ESI-MS(-) of  $[B_{12}(OCH_2C_6H_4SCH_2C_6H_5)_{12}]^{2-}$  (MeCN, 1.5 kV).

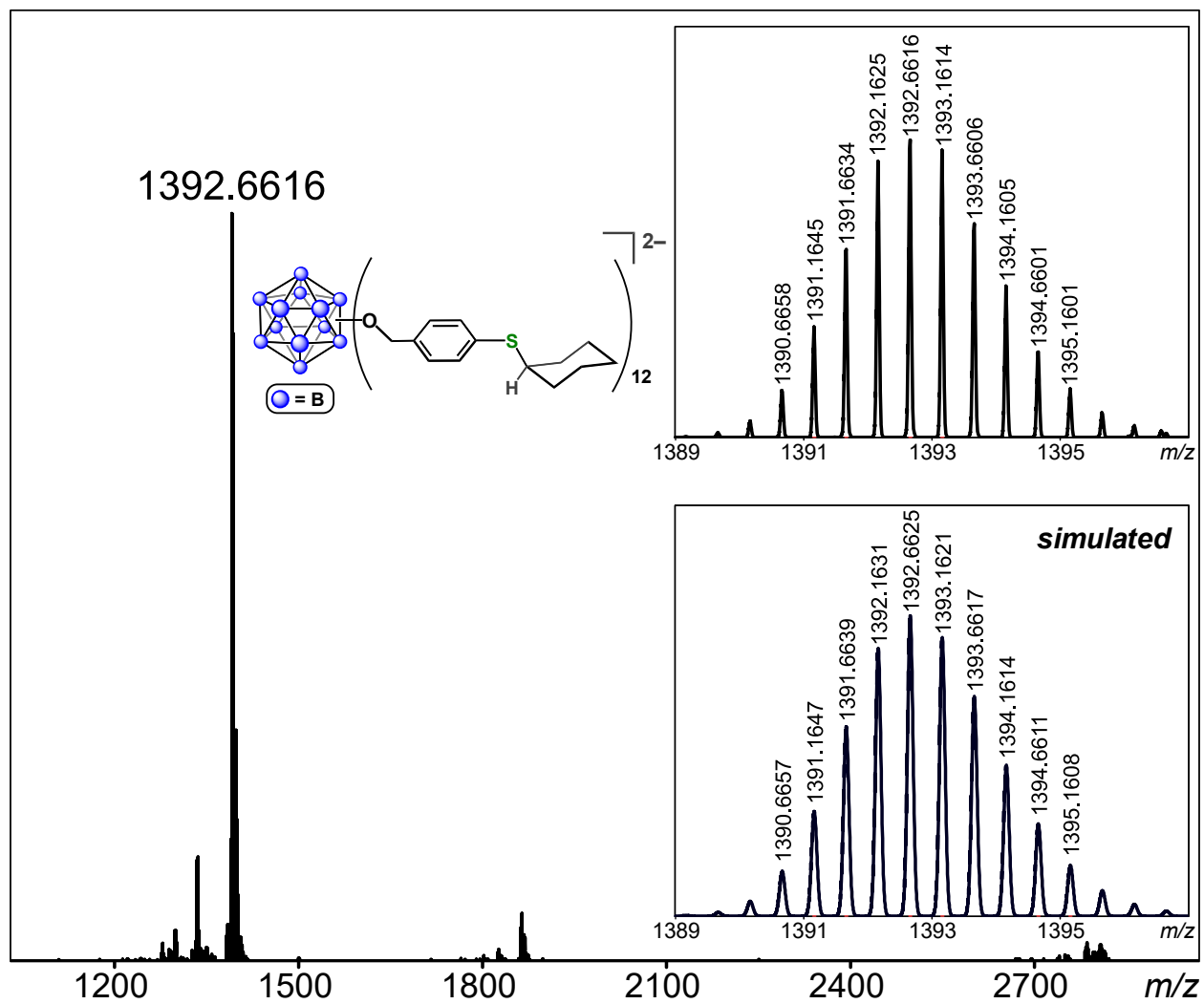




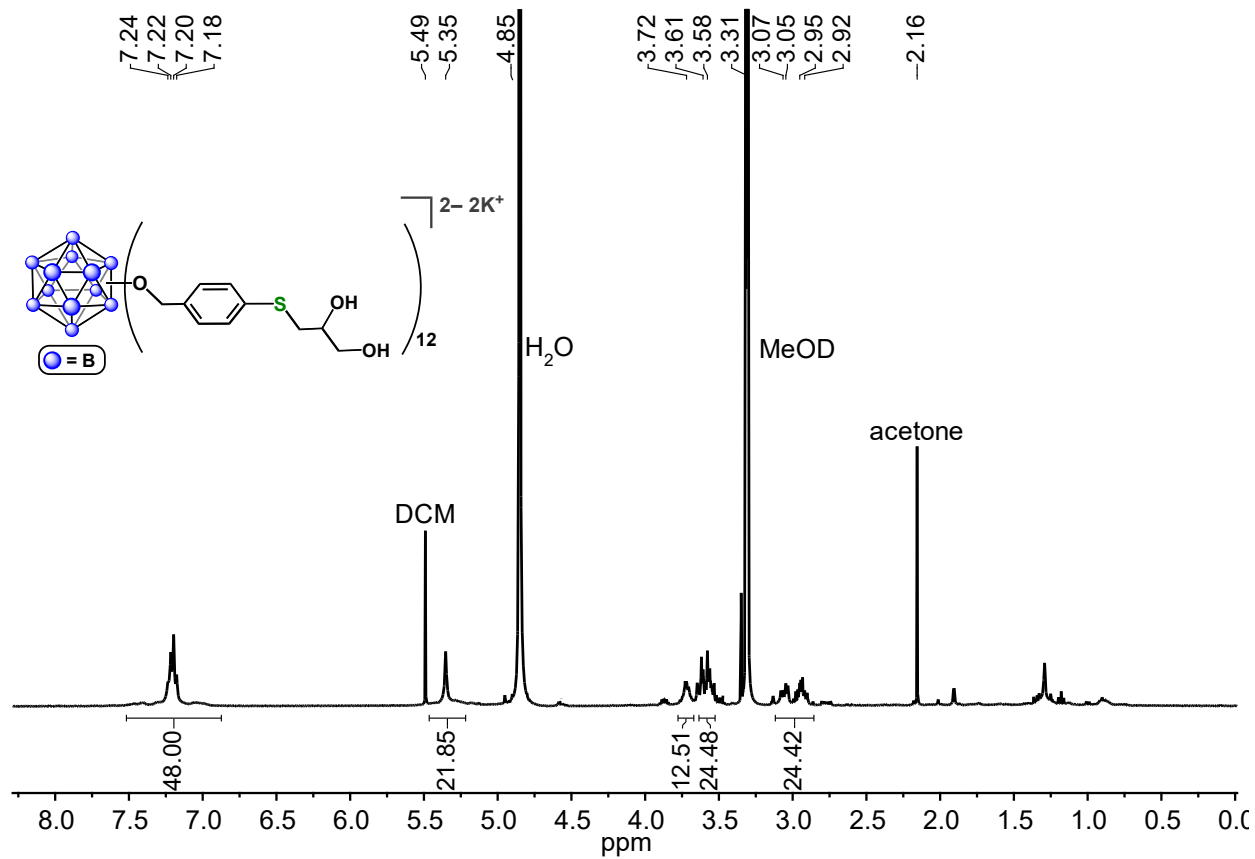
$^1H$  NMR spectrum of  $[K_2][B_{12}(OCH_2C_6H_4(cyclohexanethiol))_{12}]$  (400 MHz,  $acetone-d_6$ , 25 °C).



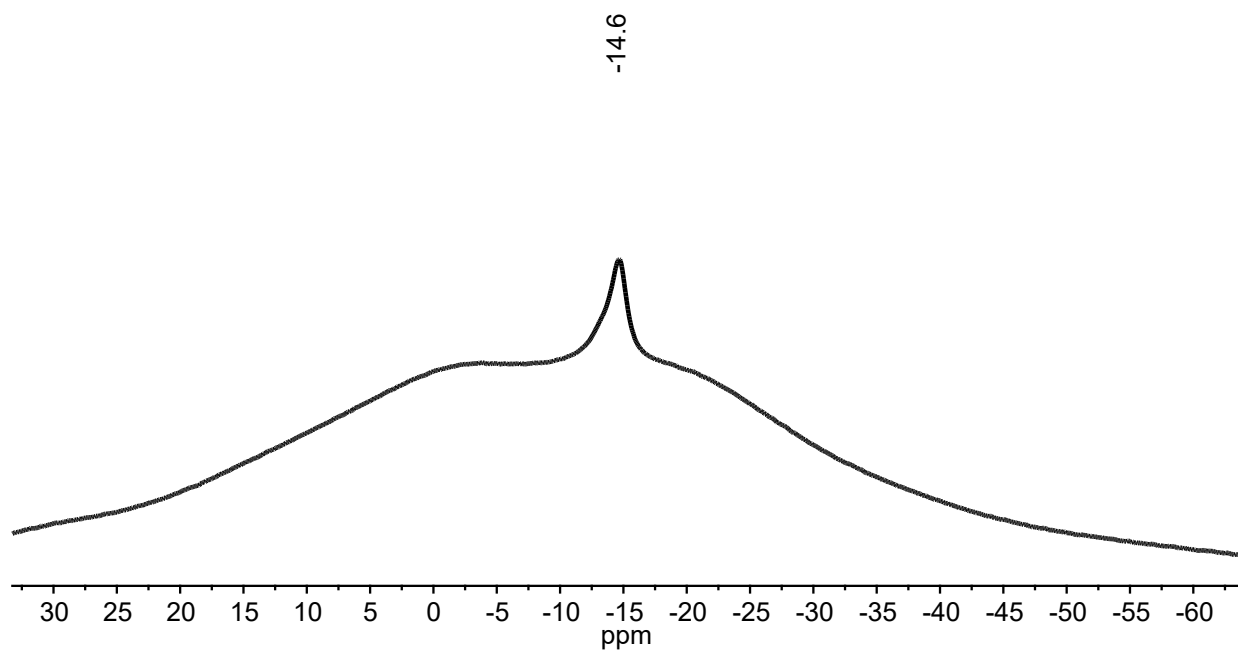
$^{11}\text{B}\{^1\text{H}\}$  NMR spectrum of  $[\text{K}_2][\text{B}_{12}(\text{OCH}_2\text{C}_6\text{H}_4(\text{cyclohexanethiol}))_{12}]$  (128 MHz, acetone- $d_6$ , 25 °C).



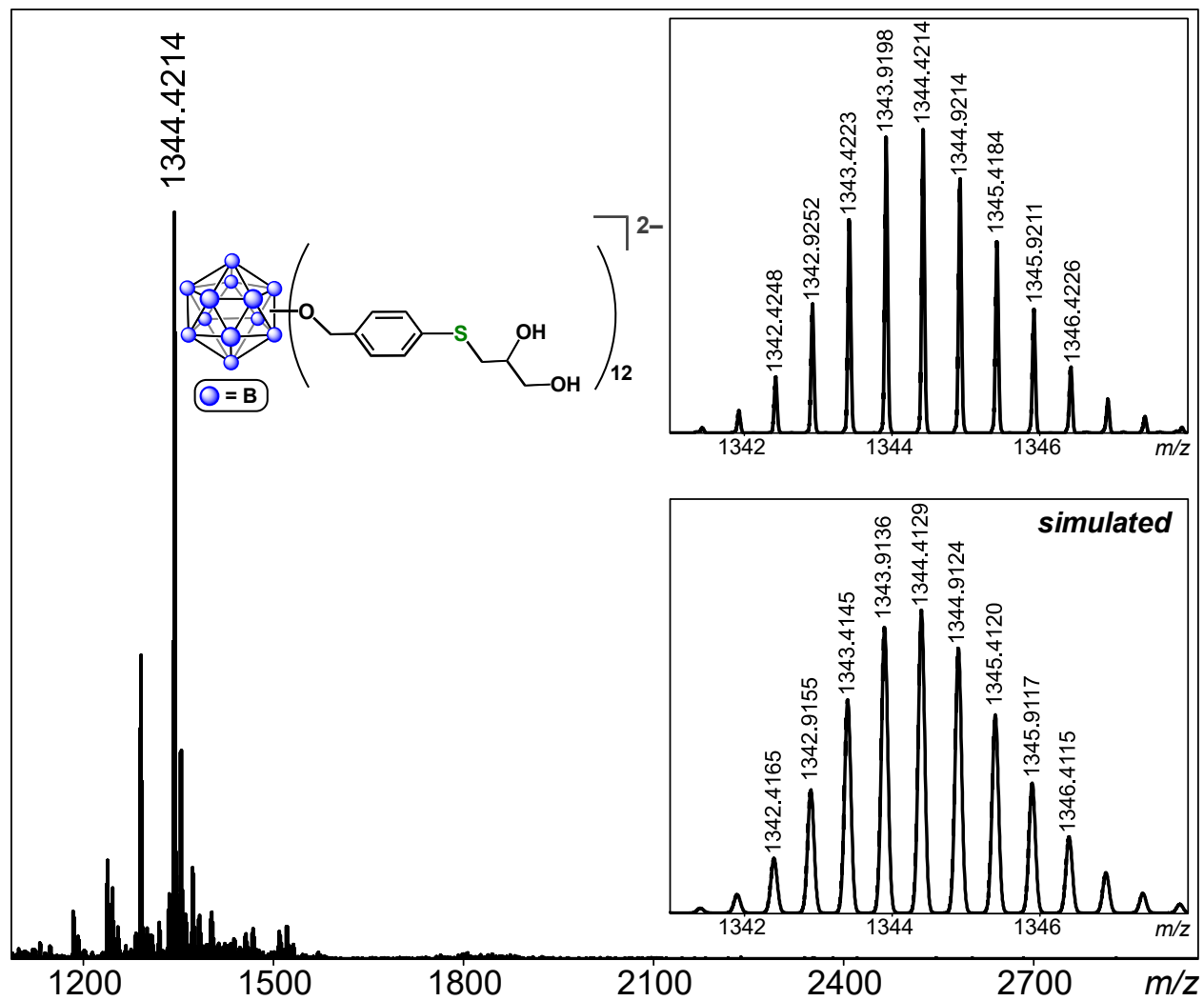
ESI-MS(-) of  $[B_{12}(OCH_2C_6H_4(\text{cyclohexanethiol}))_{12}]^{2-}$  (MeCN, 1.5 kV).



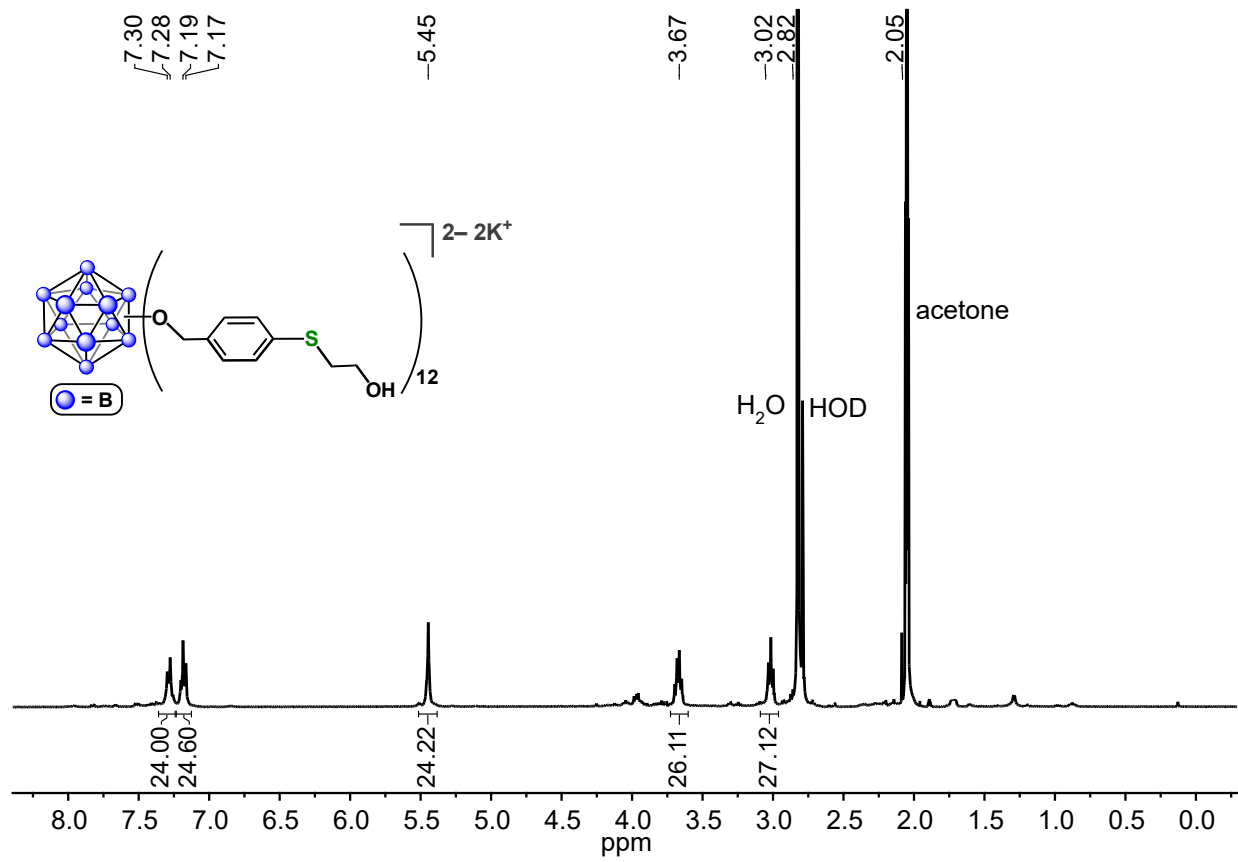
<sup>1</sup>H NMR spectrum of [K<sub>2</sub>][B<sub>12</sub>(OCH<sub>2</sub>C<sub>6</sub>H<sub>4</sub>(1-thioglycerol))<sub>12</sub>] (400 MHz, CD<sub>3</sub>OD, 25 °C).



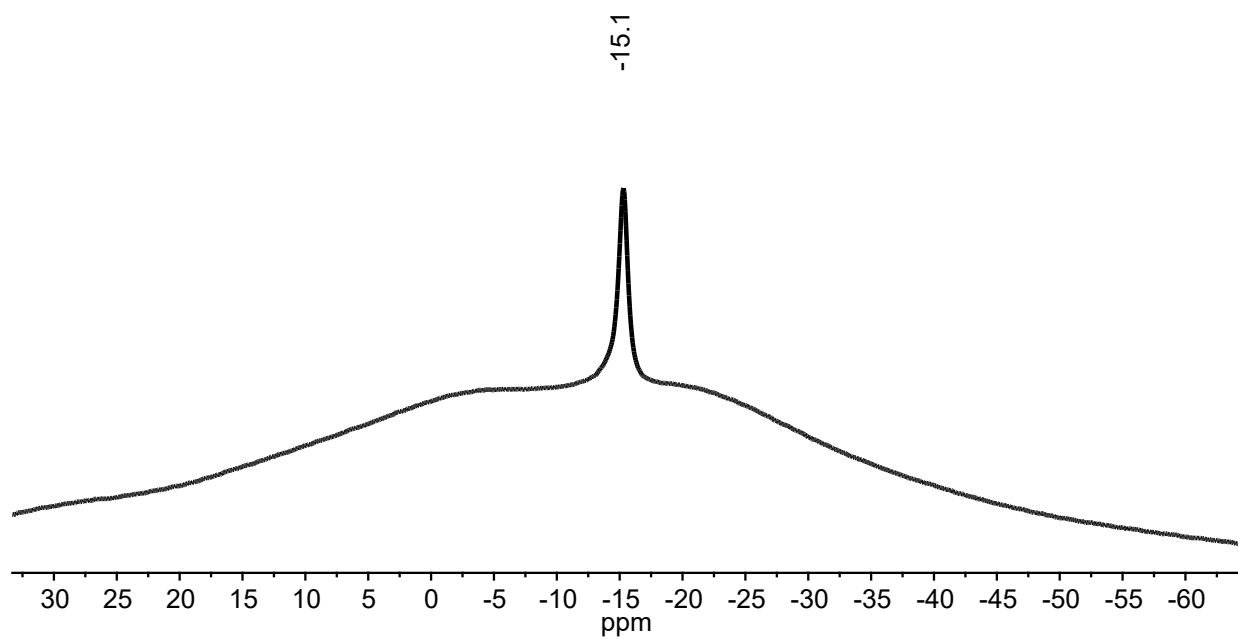
$^{11}\text{B}\{^1\text{H}\}$  NMR spectrum of  $[\text{K}_2][\text{B}_{12}(\text{OCH}_2\text{C}_6\text{H}_4(1\text{-thioglycerol}))_{12}]$  (128 MHz,  $\text{CD}_3\text{OD}$ , 25 °C).



ESI-MS(-) of  $[B_{12}(OCH_2C_6H_4(1\text{-thioglycerol}))_{12}]^{2-}$  (MeOH, 1.5 kV).

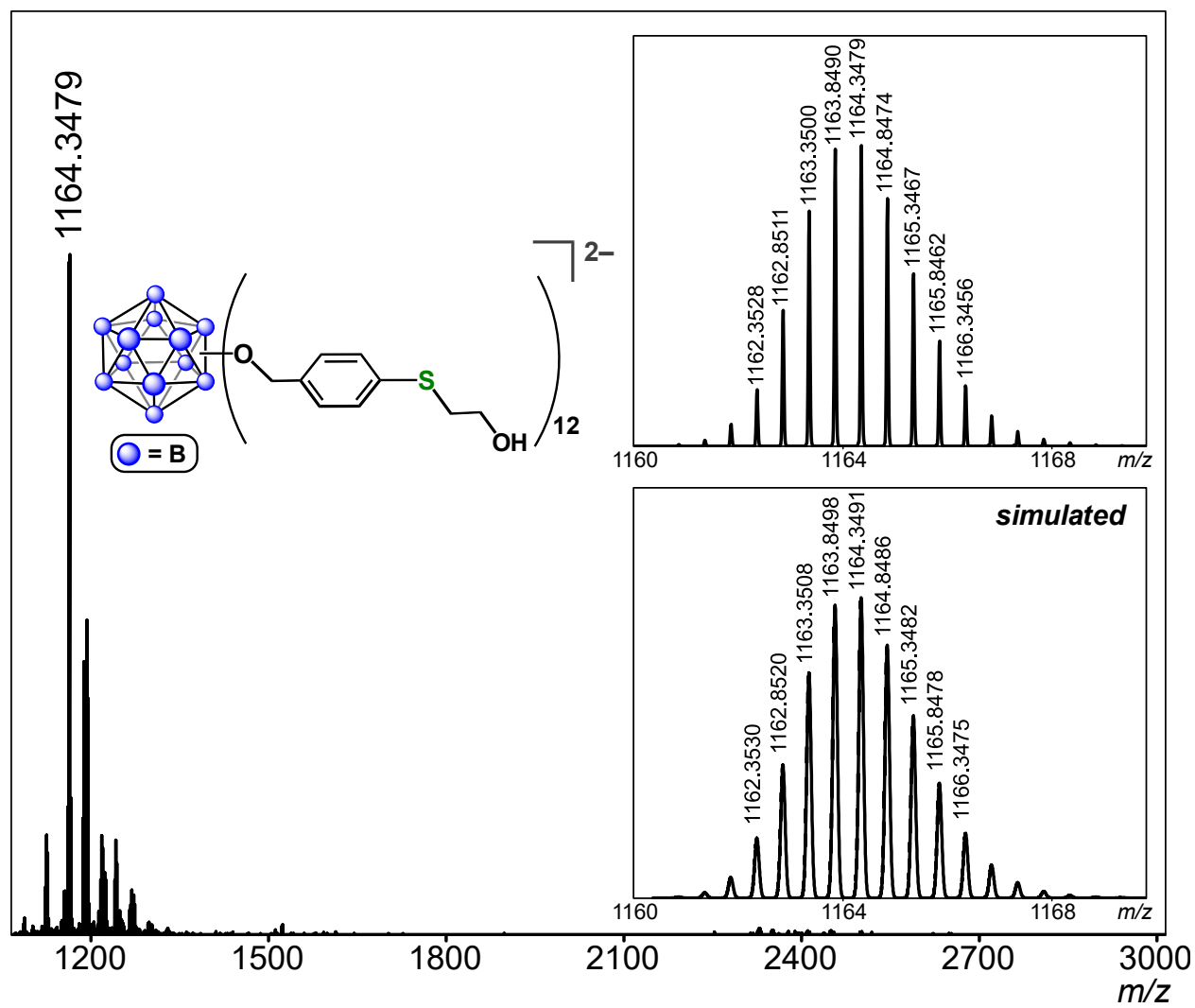


$^1\text{H}$  NMR spectrum of  $[K_2][B_{12}(OCH_2C_6H_4(2\text{-mercaptoethanol}))_{12}]$  (400 MHz, acetone- $d_6$ , 25 °C).

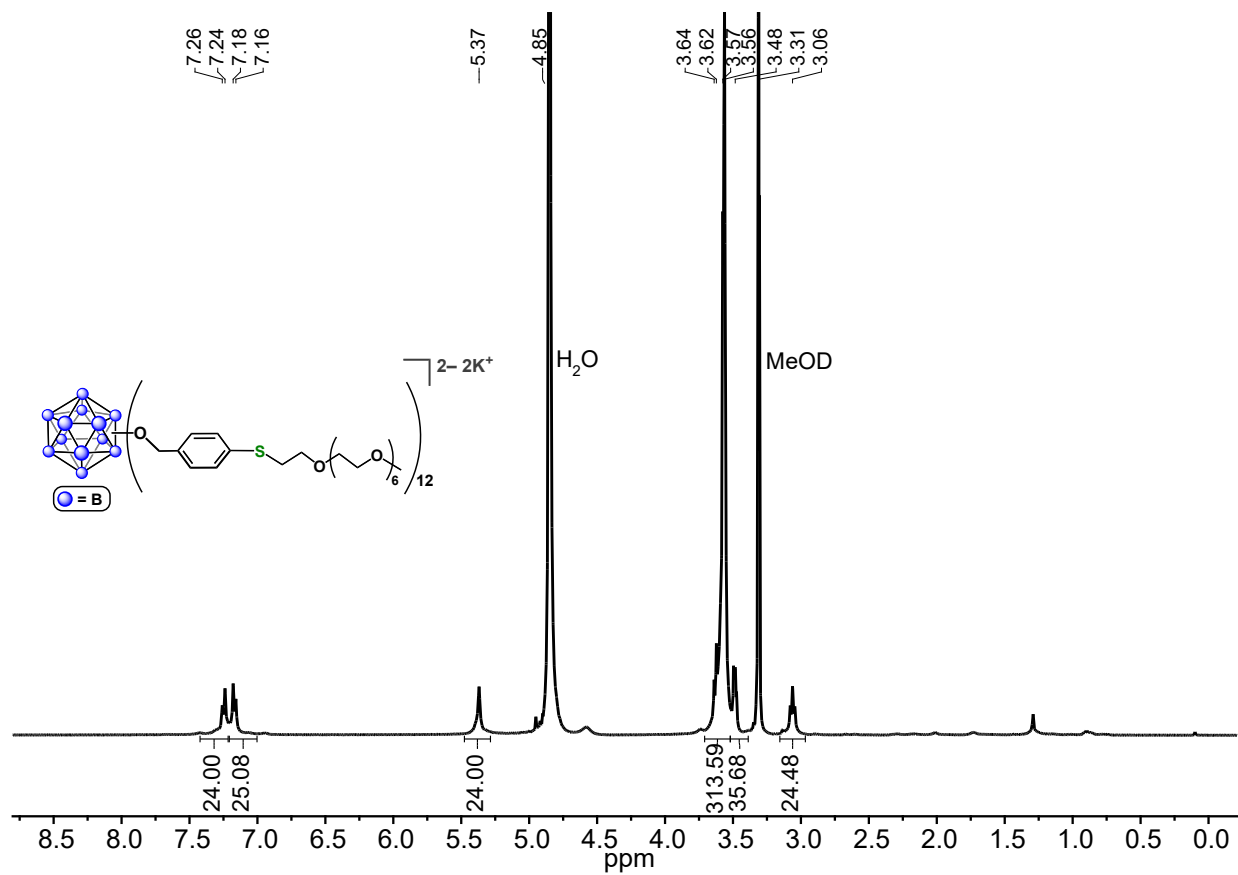


$^{11}\text{B}\{^1\text{H}\}$  NMR spectrum of  $[\text{K}_2][\text{B}_{12}(\text{OCH}_2\text{C}_6\text{H}_4(2\text{-mercaptoethanol}))_{12}]$  (128 MHz, acetone- $d_6$ , 25 °C).

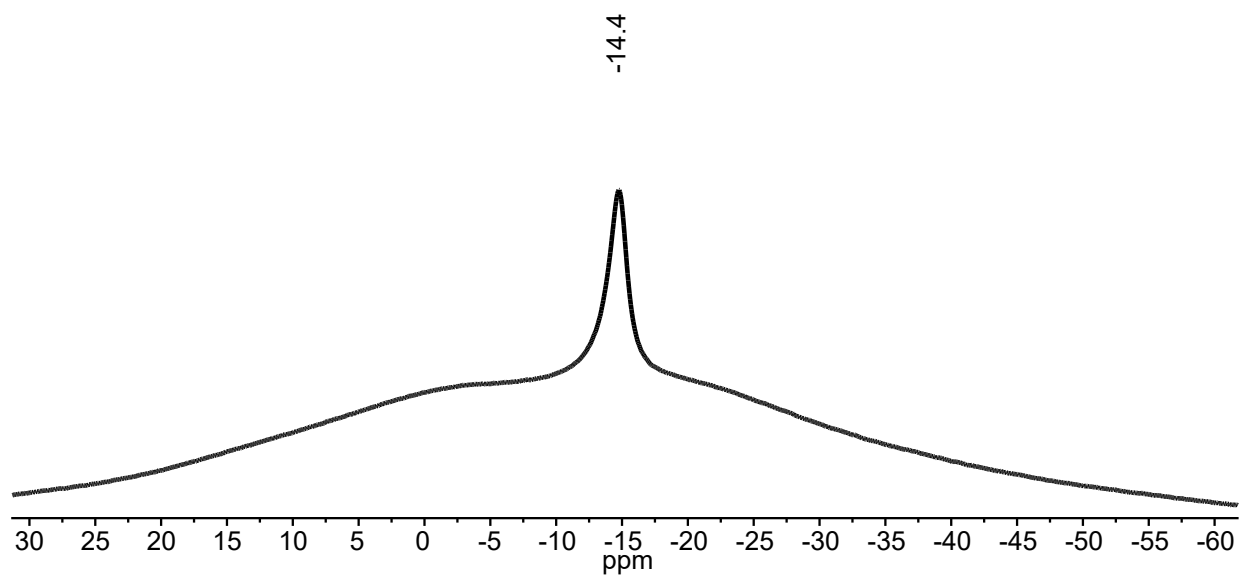




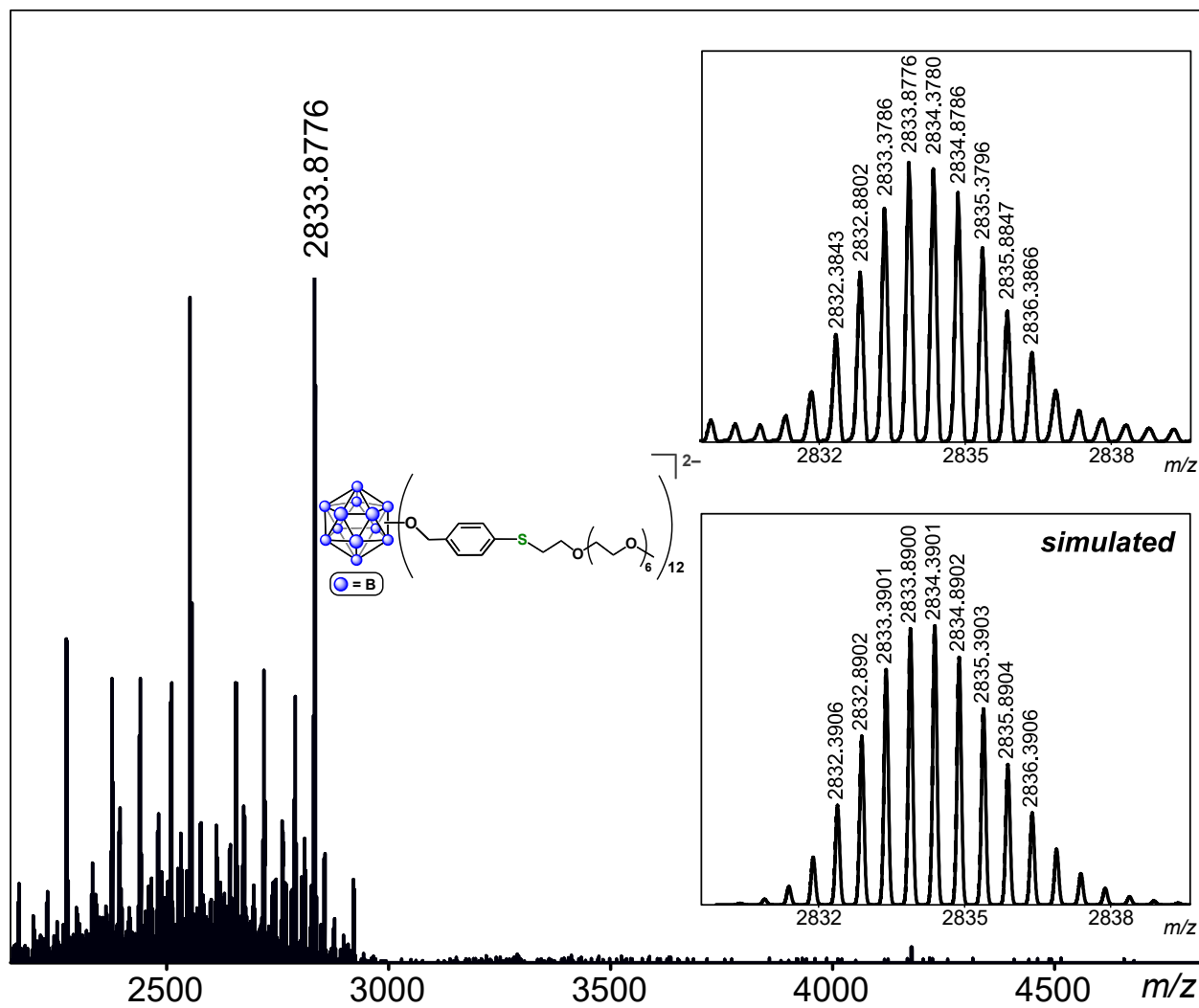
ESI-MS(-) of  $[B_{12}(OCH_2C_6H_4(2\text{-mercaptoethanol}))_{12}]^{2-}$  (MeOH, 1.5 kV).



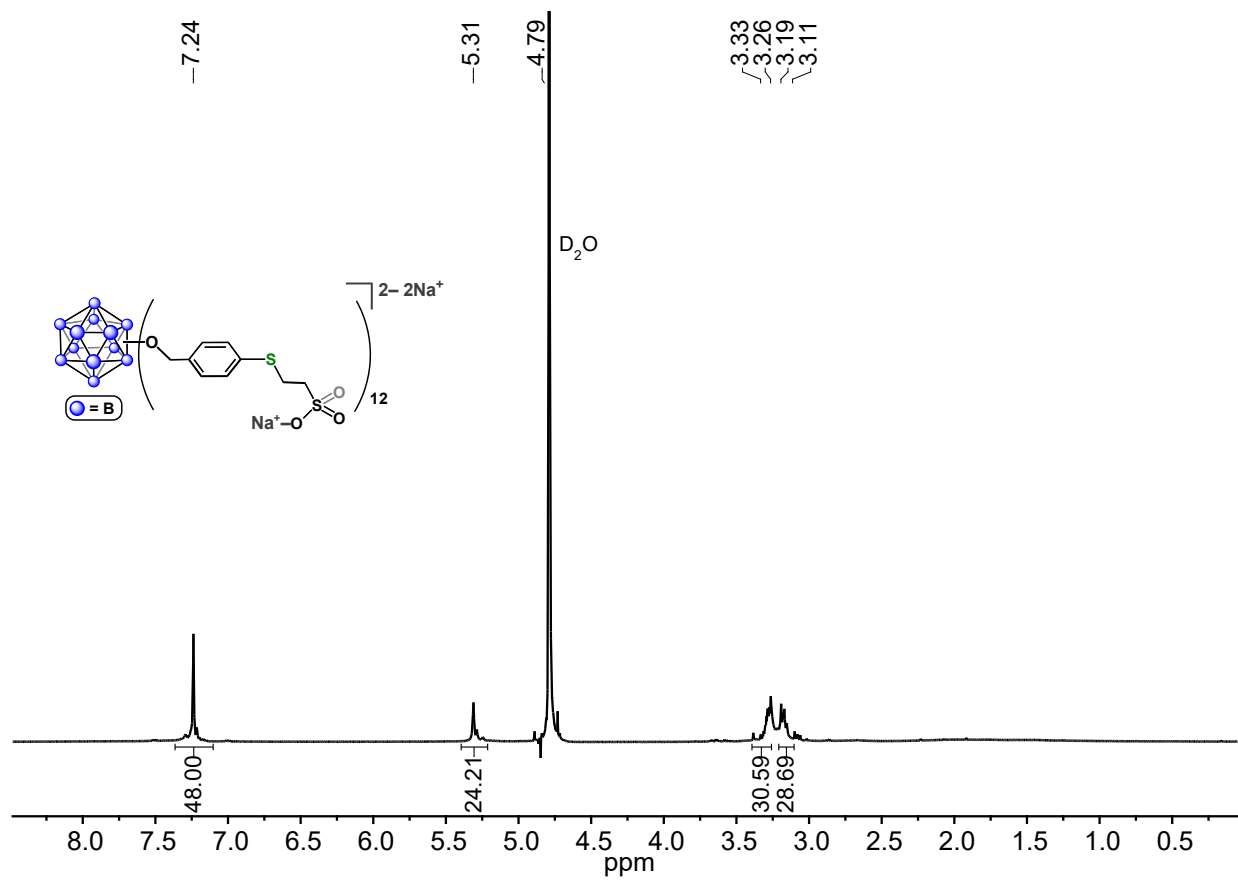
$^1H$  NMR spectrum of  $[K_2][B_{12}(OCH_2C_6H_4(mPEG_{350} \text{ thiol}))_{12}]$  ( $CD_3OD$ , 400 MHz, 25 °C).



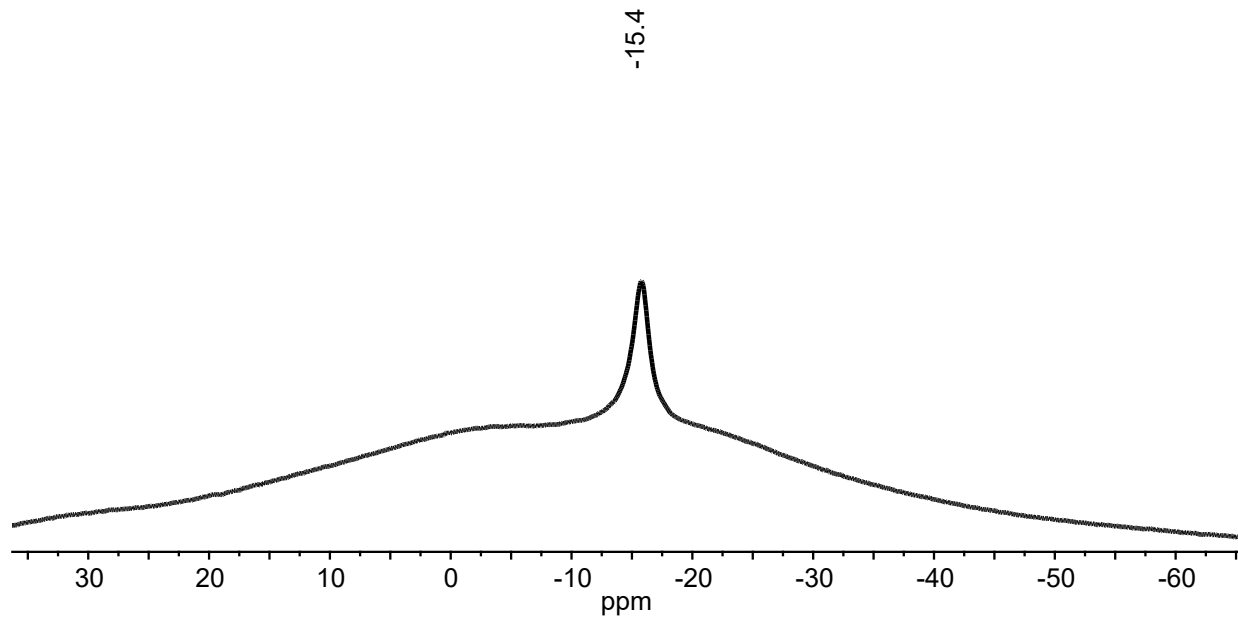
$^{11}\text{B}\{^1\text{H}\}$  NMR spectrum of  $[\text{K}_2][\text{B}_{12}(\text{OCH}_2\text{C}_6\text{H}_4(m\text{PEG}_{350}\text{ thiol}))_{12}]$  (128 MHz,  $\text{CD}_3\text{OD}$ , 25 °C).



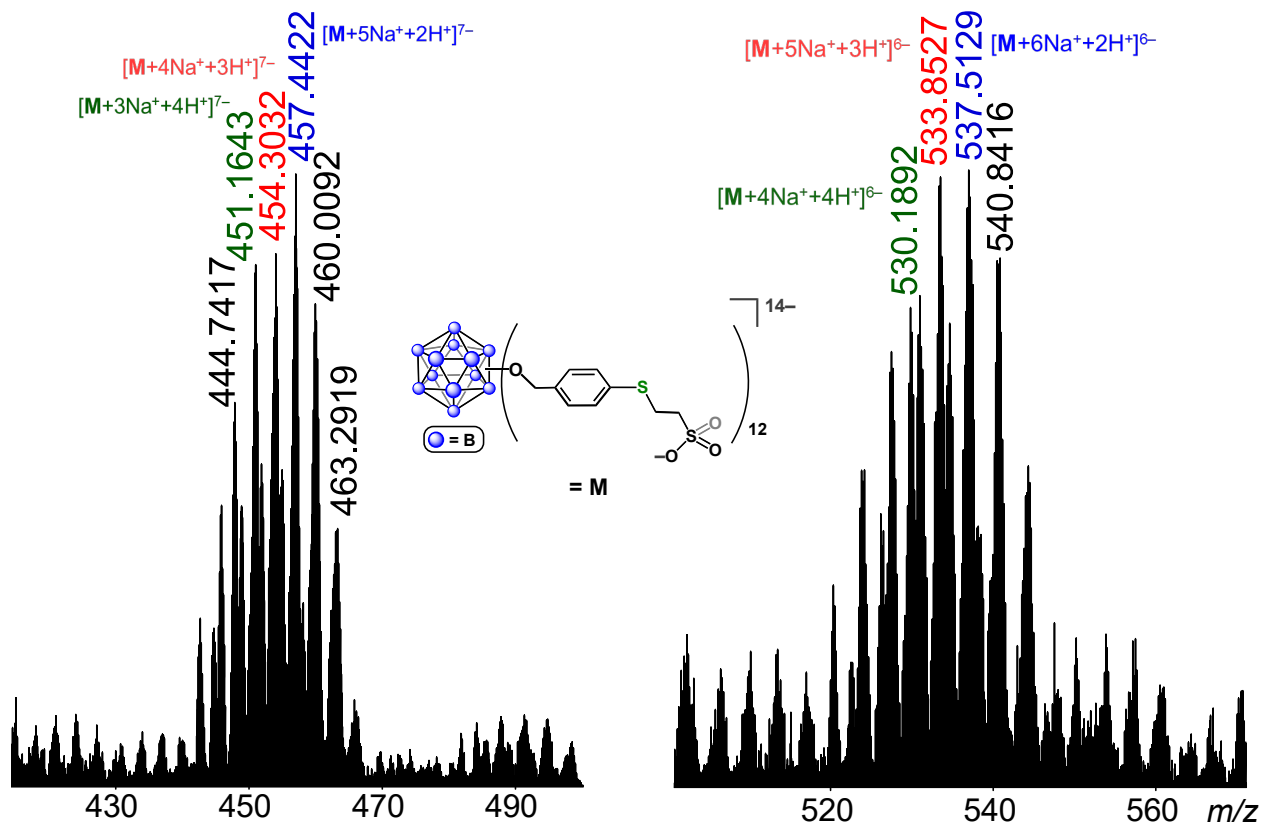
ESI-MS(-) of  $[B_{12}(OCH_2C_6H_4(mPEG_{350} \text{ thiol}))_{12}]^{2-}$  (MeOH, 1.5 kV). A significant amount of fragmentation of the PEG polymer ( $-OCH_2CH_2-$  units) is observed under ESI-MS conditions.



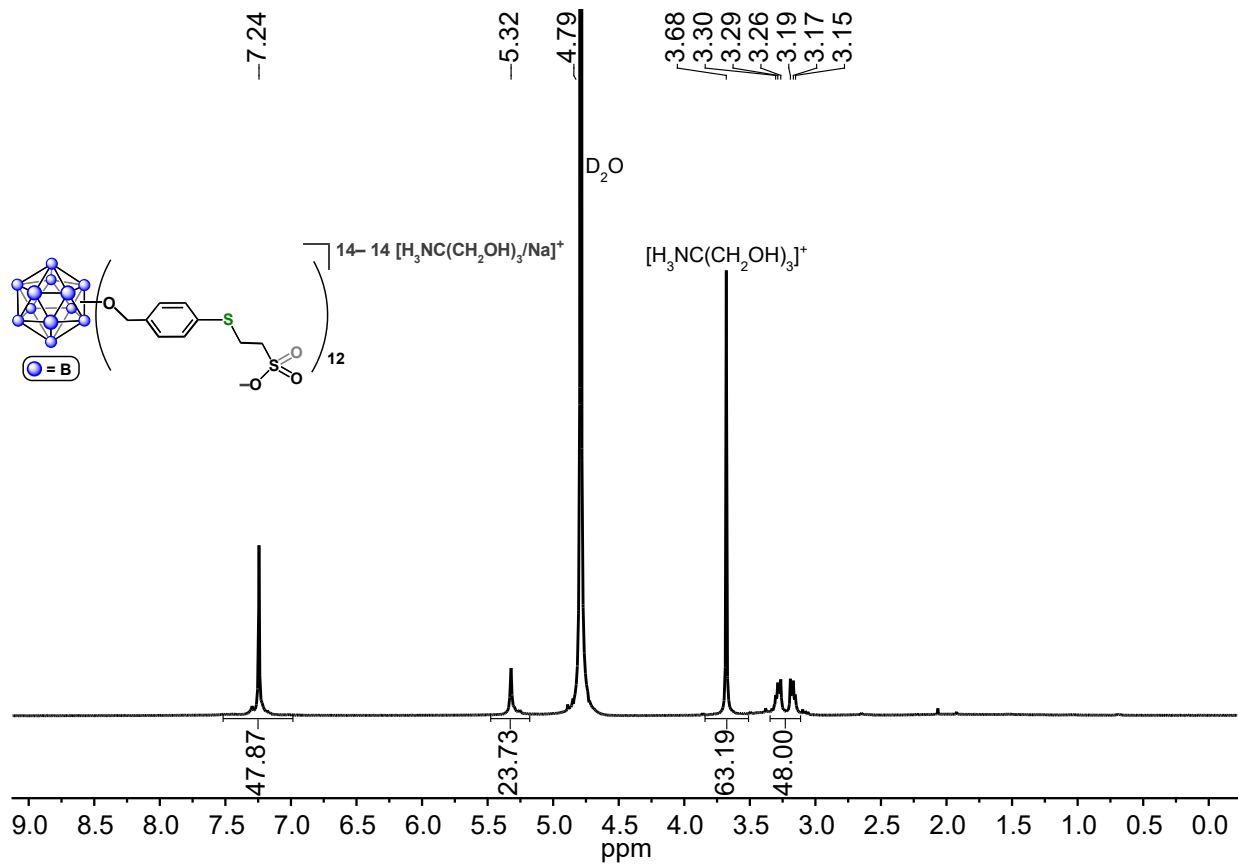
$^1\text{H}$  NMR spectrum of  $[\text{Na}]_{14}[\text{B}_{12}(\text{OCH}_2\text{C}_6\text{H}_4(2\text{-thioethanesulfonate}))_{12}]$  ( $\text{D}_2\text{O}$ , 400 MHz, 25 °C).



$^{11}\text{B}\{^1\text{H}\}$  NMR spectrum of  $[\text{Na}]_{14}[\text{B}_{12}(\text{OCH}_2\text{C}_6\text{H}_4(2\text{-thioethanesulfonate}))_{12}]$  ( $\text{D}_2\text{O}$ , 128 MHz, 25  $^\circ\text{C}$ ).

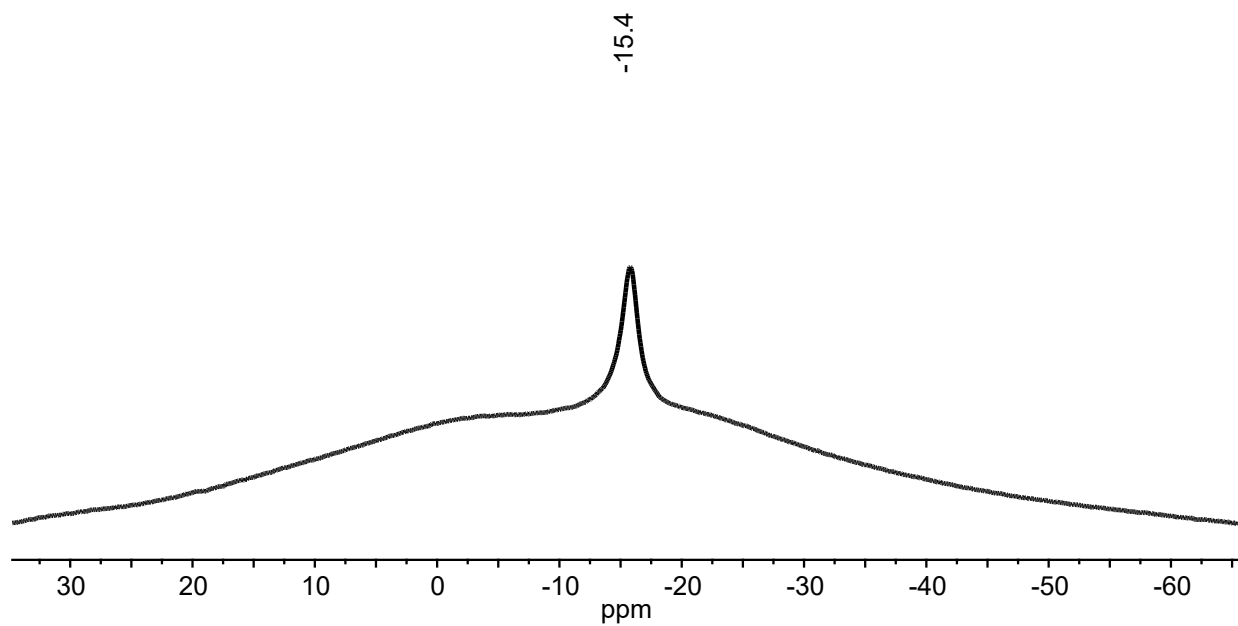


ESI-MS(-) of  $[B_{12}(OCH_2C_6H_4(2\text{-thioethanesulfonate}))_{12}]^{14-}$  (MeOH, 1.5 kV) showing a distribution of species with charge-compensating cations ( $Na^+$  and  $H^+$ ) due to the highly anionic nature of the  $[B_{12}(OCH_2C_6H_4(2\text{-thioethanesulfonate}))_{12}]^{14-}$  cluster.

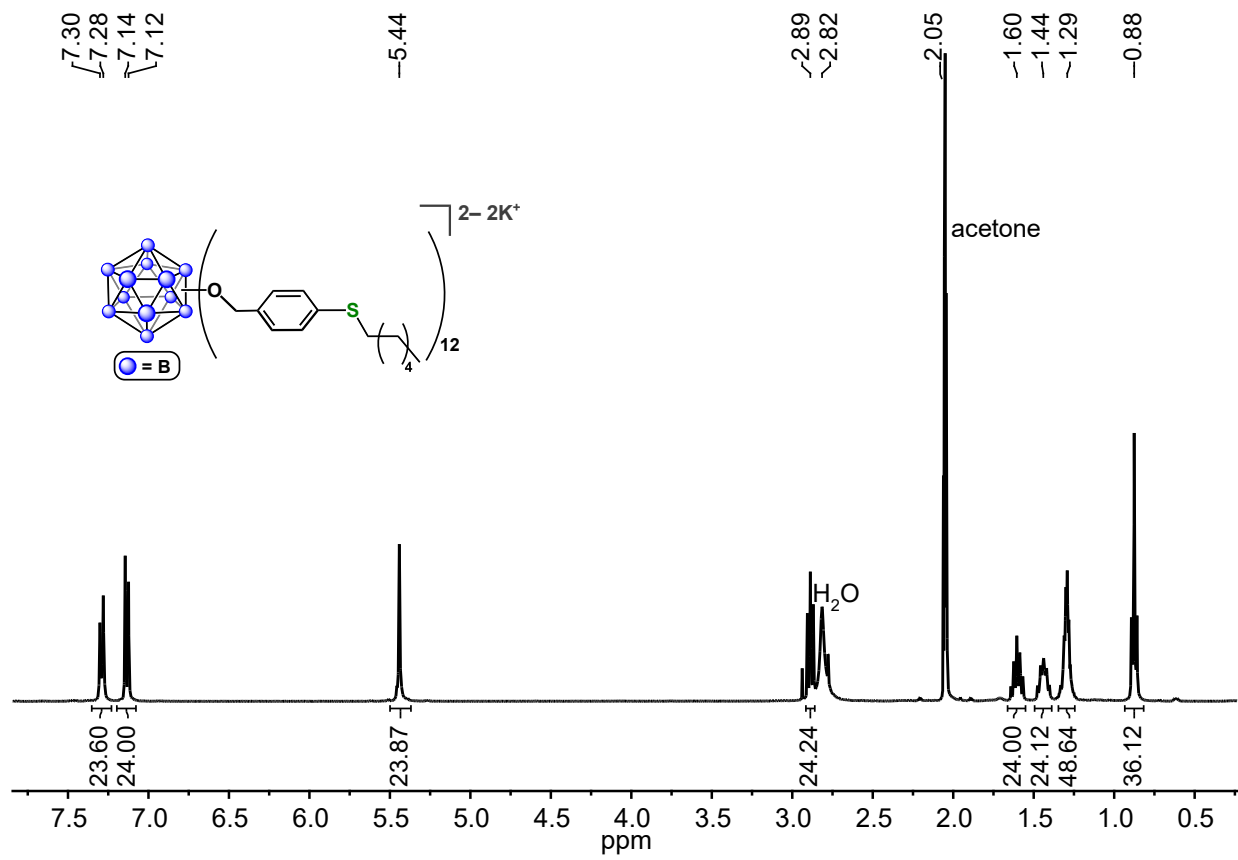


$^1\text{H}$  NMR spectrum of  $[\text{H}_3\text{NC}(\text{CH}_2\text{OH})_3/\text{Na}]_{14}[\text{B}_{12}(\text{OCH}_2\text{C}_6\text{H}_4(2\text{-thioethanesulfonate}))_{12}]$  ( $\text{D}_2\text{O}$ , 400 MHz, 25 °C).

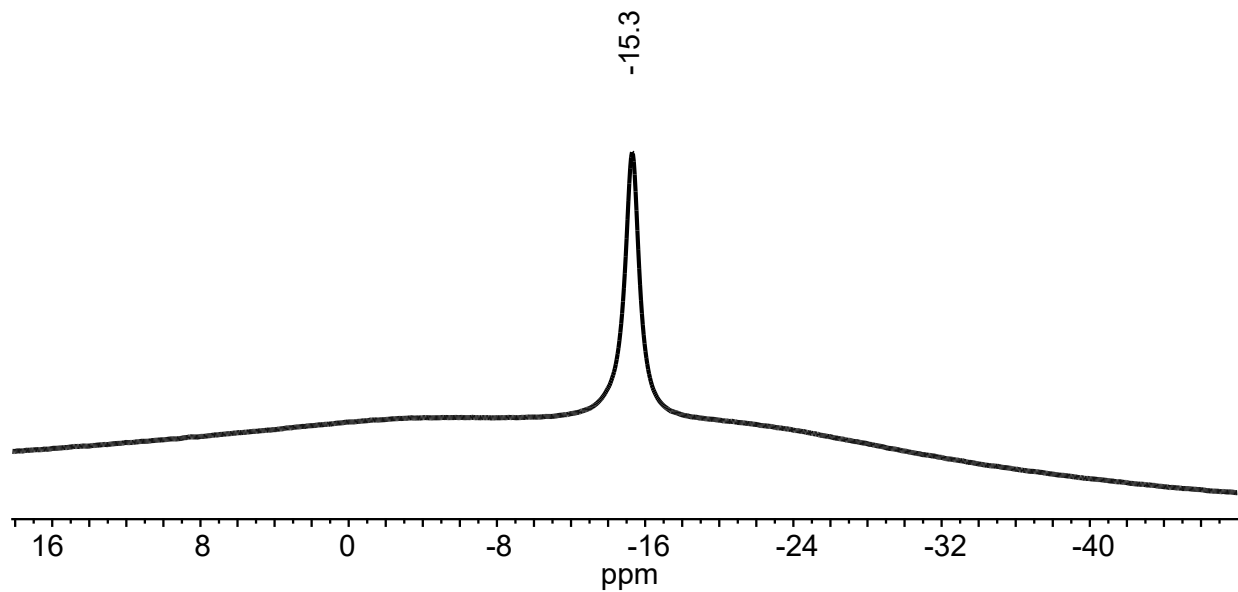




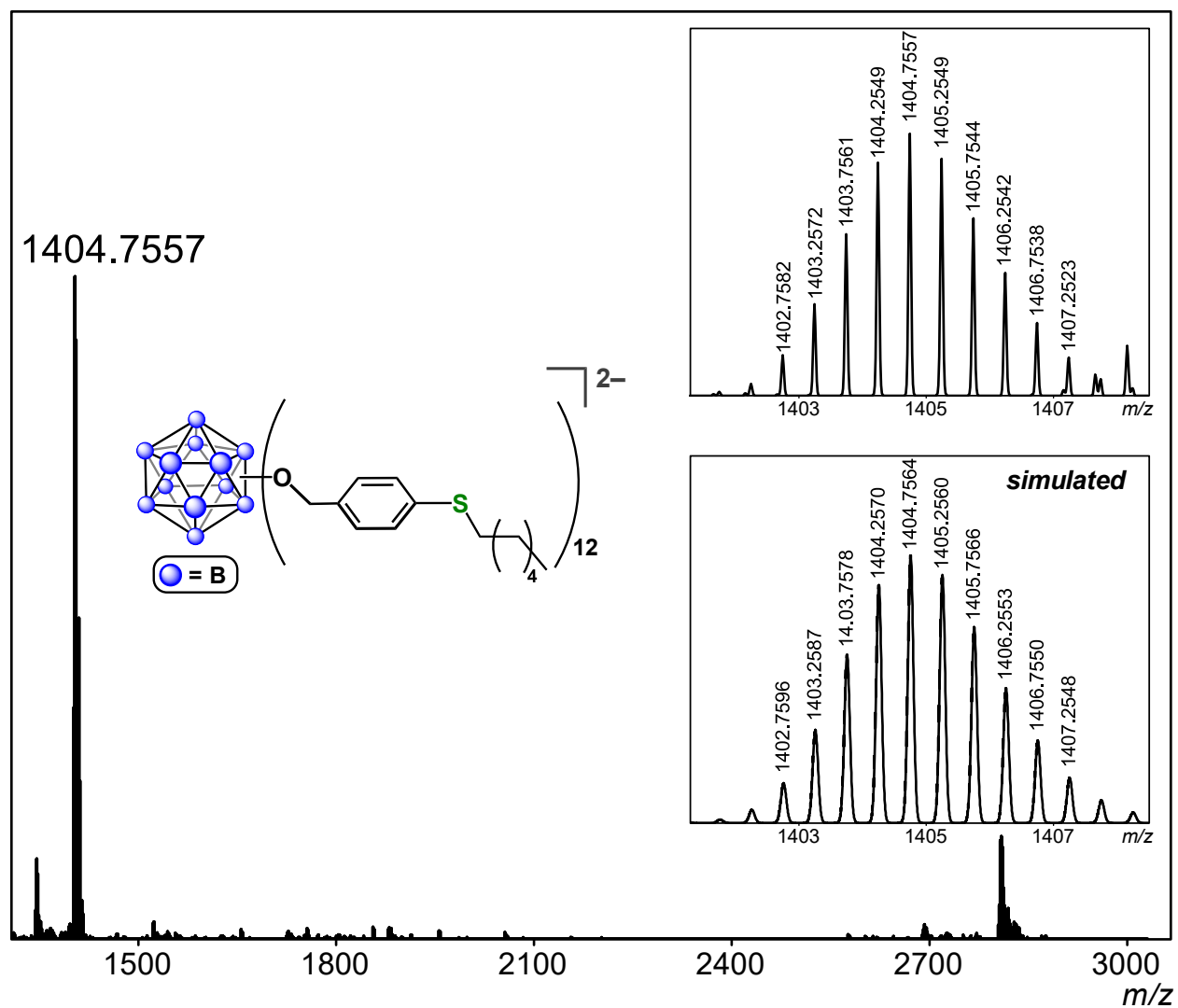
$^{11}\text{B}\{^1\text{H}\}$  NMR spectrum of  $[\text{H}_3\text{NC}(\text{CH}_2\text{OH})_3/\text{Na}]_{14}[\text{B}_{12}(\text{OCH}_2\text{C}_6\text{H}_4(2\text{-thioethanesulfonate}))_{12}]$   
( $\text{D}_2\text{O}$ , 128 MHz, 25 °C).



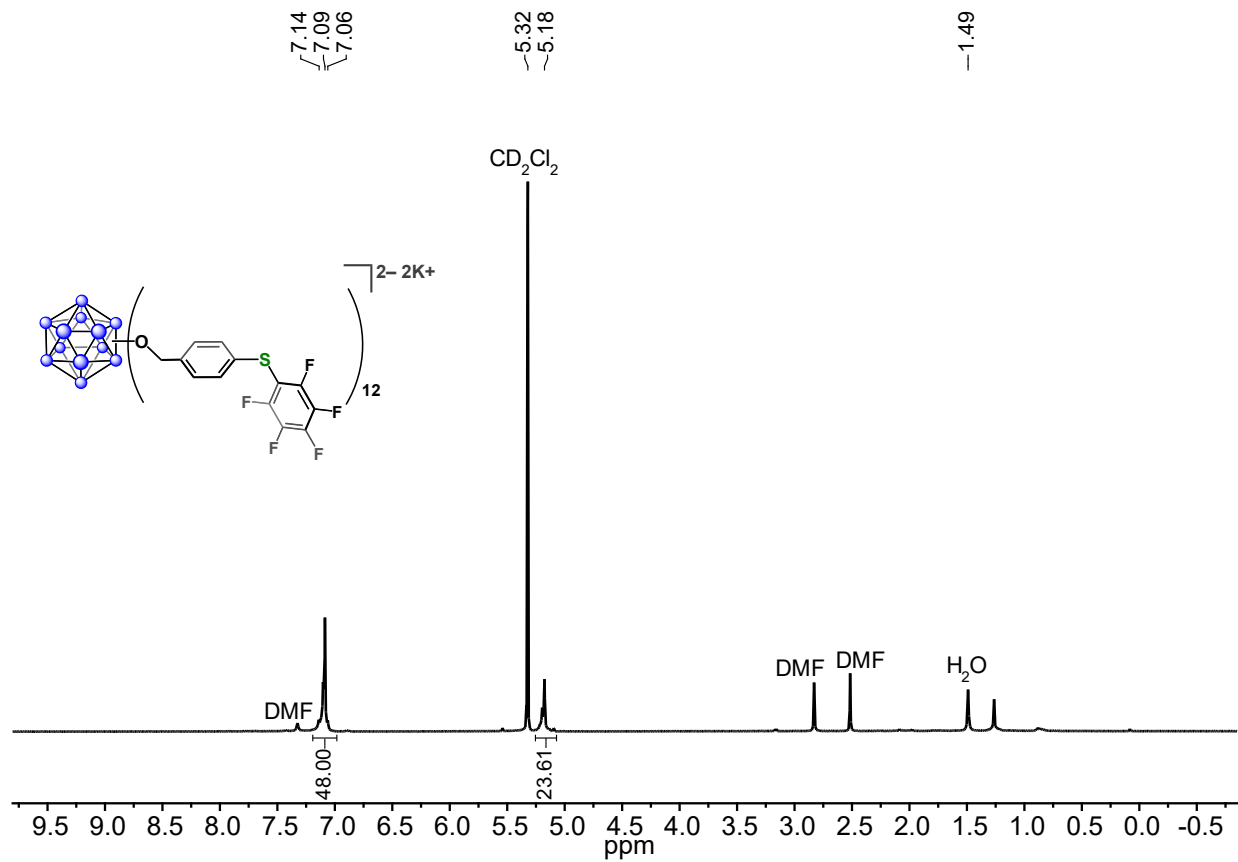
$^1H$  NMR spectrum of  $[K_2][B_{12}(OCH_2C_6H_4S(CH_2)_5CH_3)_{12}]$  (400 MHz, acetone- $d_6$ , 25 °C).



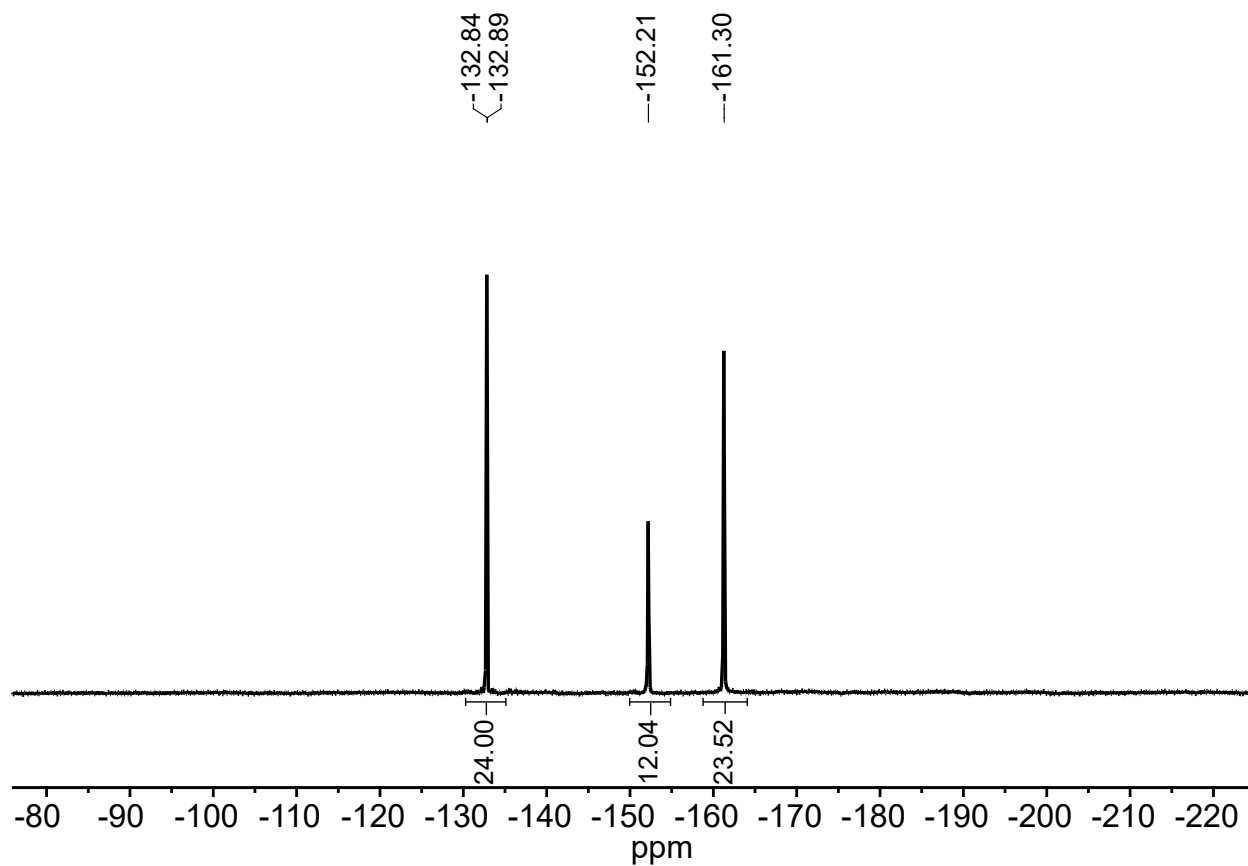
$^{11}\text{B}\{^1\text{H}\}$  NMR spectrum of  $[\text{K}_2][\text{B}_{12}(\text{OCH}_2\text{C}_6\text{H}_4\text{S}(\text{CH}_2)_5\text{CH}_3)_{12}]$  (128 MHz, acetone- $d_6$ , 25 °C).



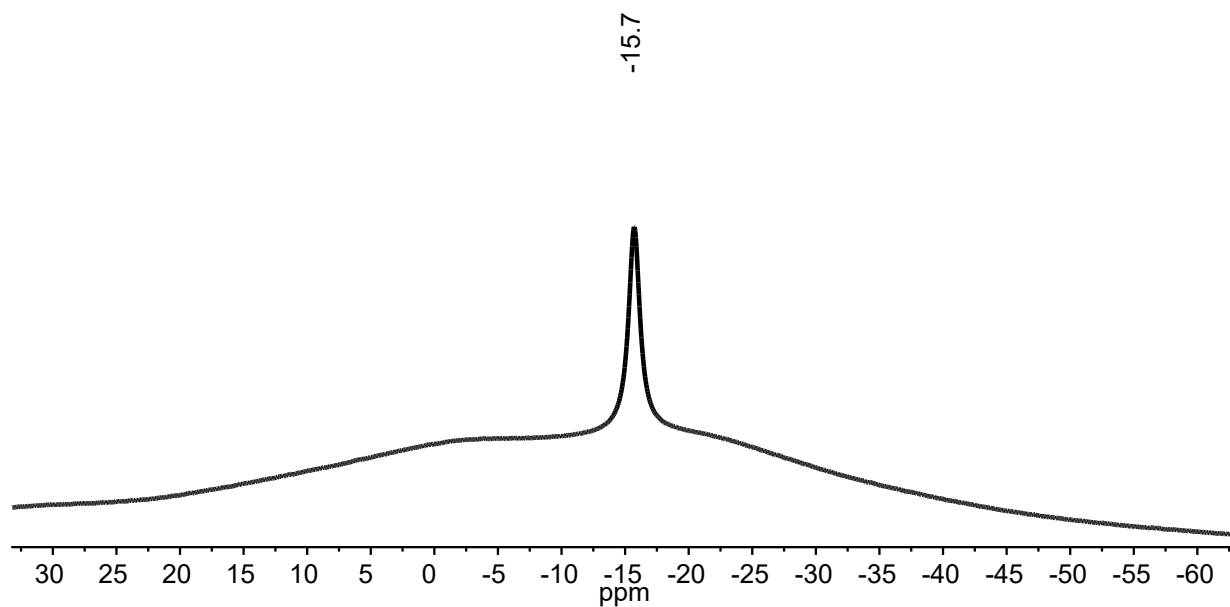
ESI-MS(-) of  $[B_{12}(OCH_2C_6H_4S(CH_2)_5CH_3)_{12}]^{2-}$  (MeCN, 1.5 kV).



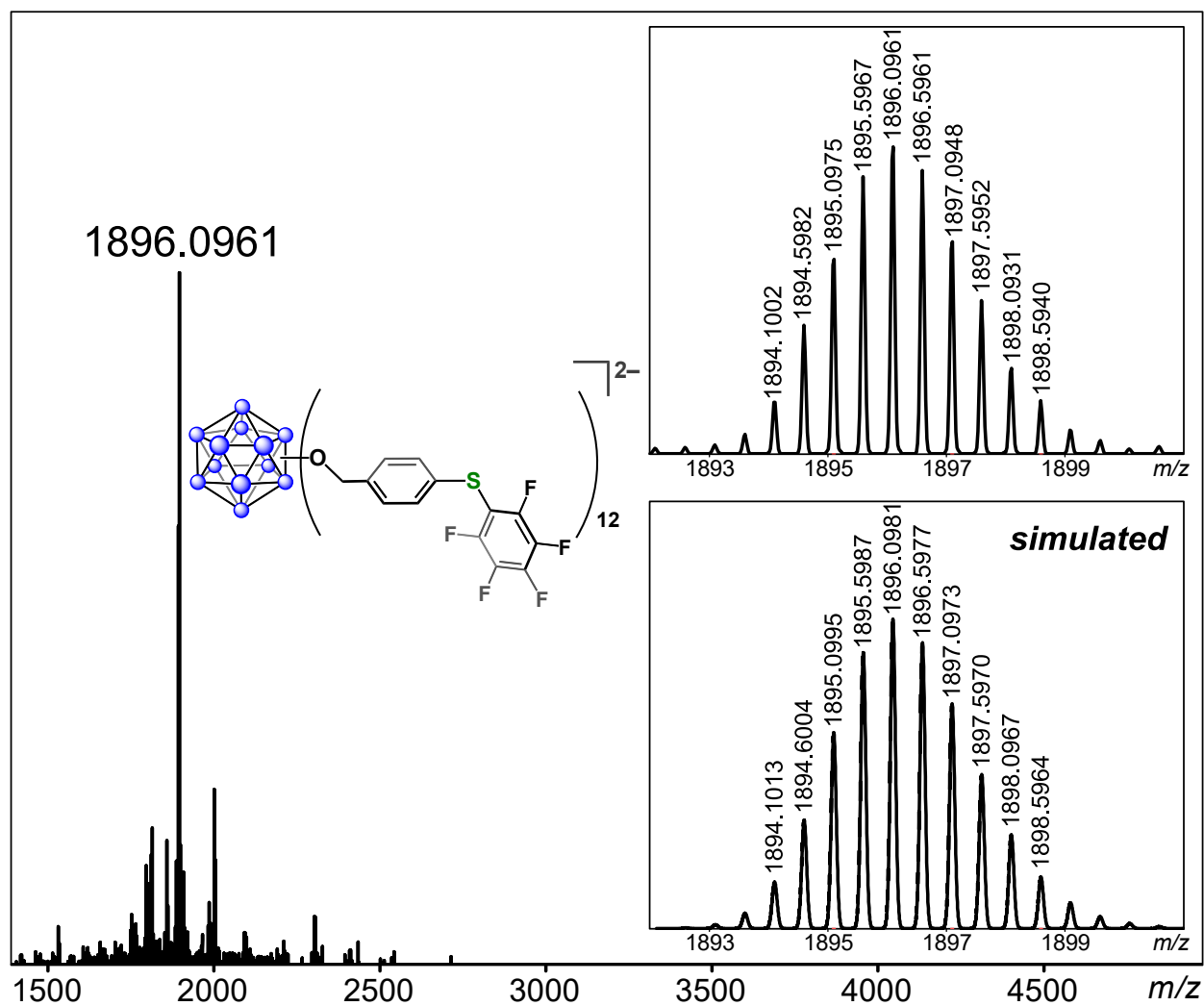
$^1\text{H}$  NMR spectrum of  $[\text{K}_2][\text{B}_{12}(\text{OCH}_2\text{C}_6\text{H}_4\text{SC}_6\text{F}_5)_{12}]$  (400 MHz,  $\text{CD}_2\text{Cl}_2$ , 25 °C).



$^{19}\text{F}\{^1\text{H}\}$  NMR spectrum of  $[\text{K}_2][\text{B}_{12}(\text{OCH}_2\text{C}_6\text{H}_4\text{SC}_6\text{F}_5)_{12}]$  (376 MHz,  $\text{CD}_2\text{Cl}_2$ , 25 °C).

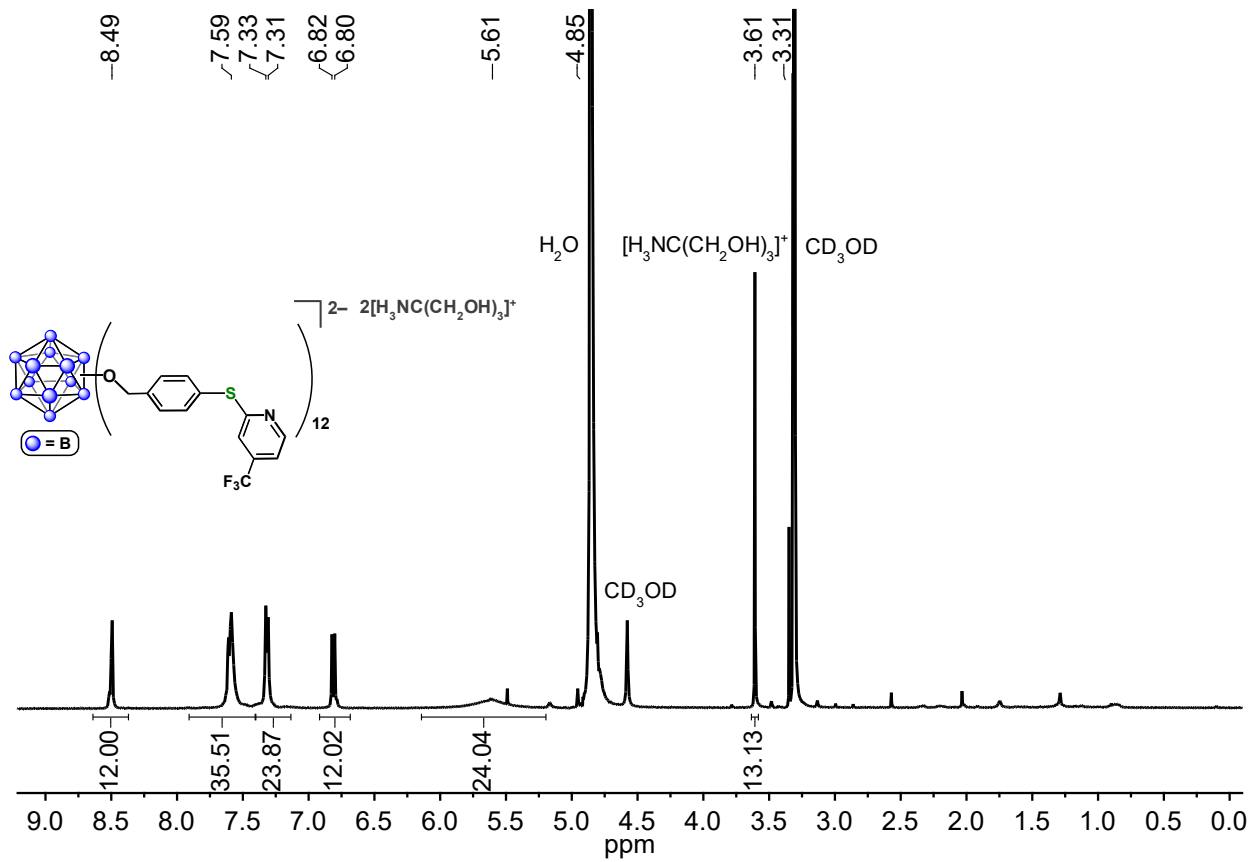


$^{11}\text{B}\{^1\text{H}\}$  NMR spectrum of  $[\text{K}_2][\text{B}_{12}(\text{OCH}_2\text{C}_6\text{H}_4\text{SC}_6\text{F}_5)_{12}]$  (128 MHz,  $\text{CD}_2\text{Cl}_2$ , 25 °C).

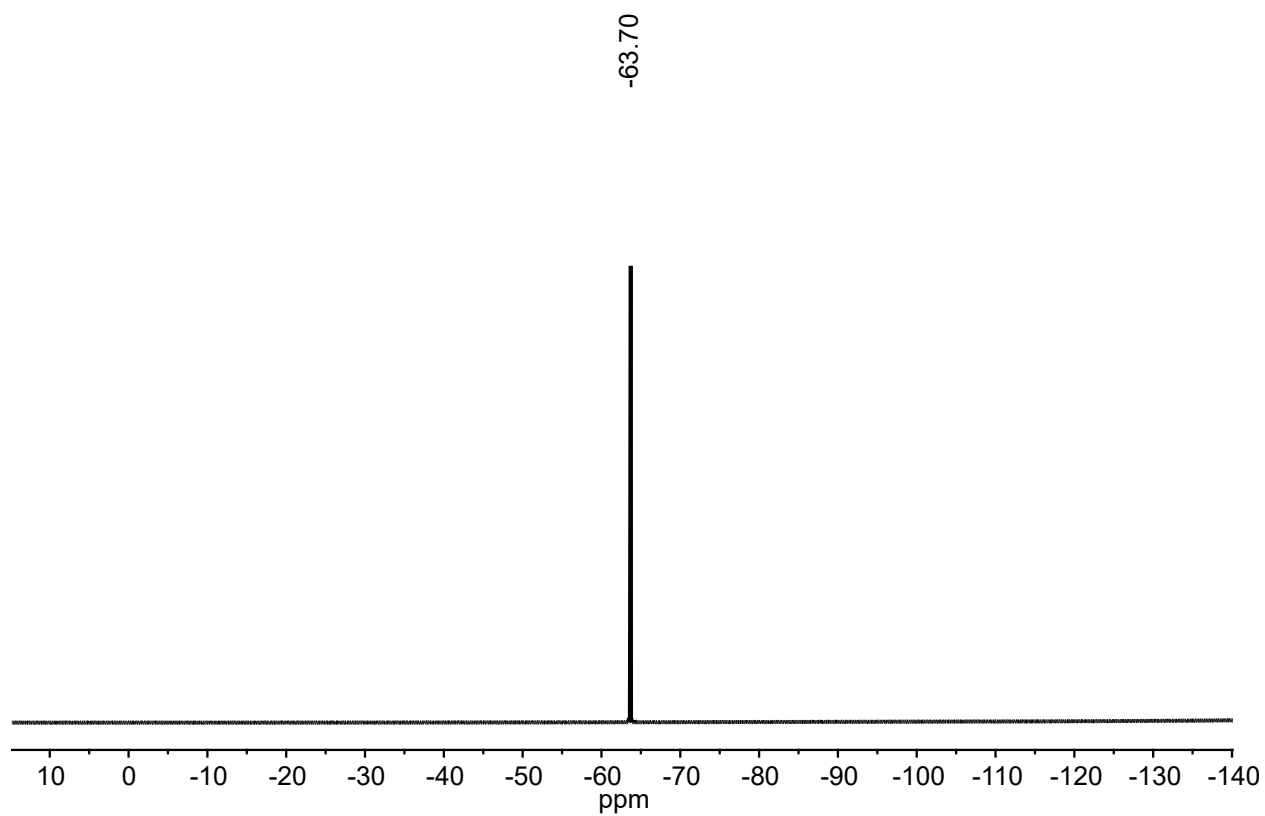


ESI-MS(-) of  $[B_{12}(OCH_2C_6H_4SC_6F_5)_{12}]^{2-}$  (MeCN, 1.5 kV).

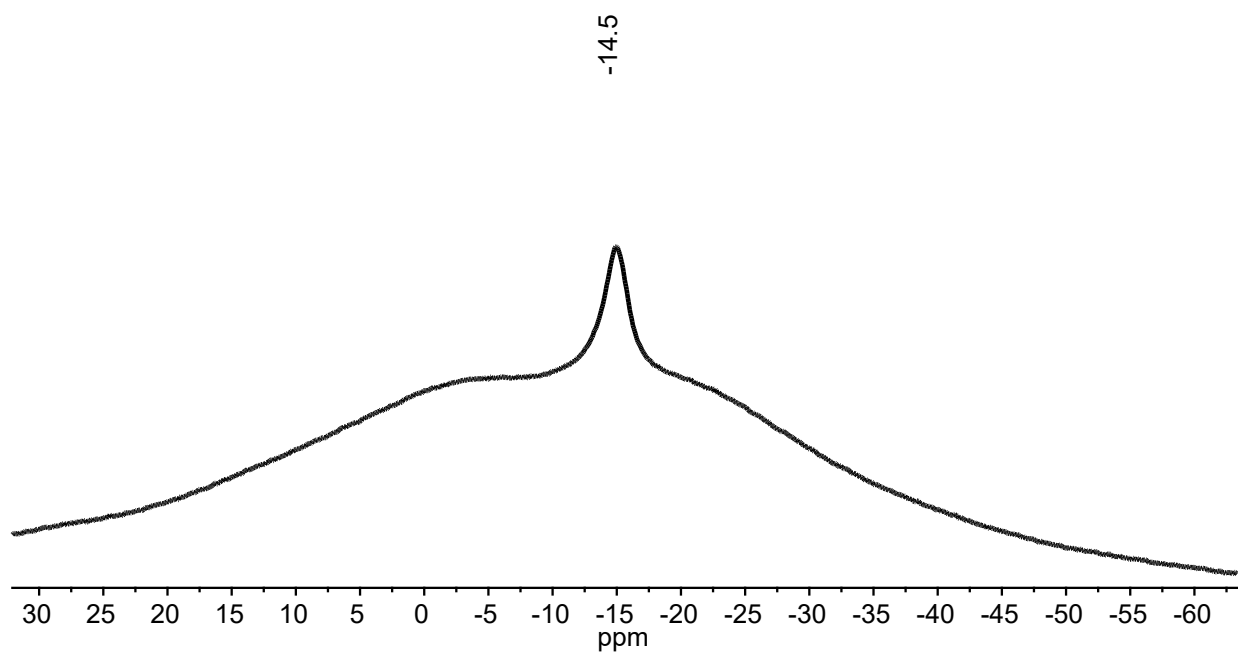




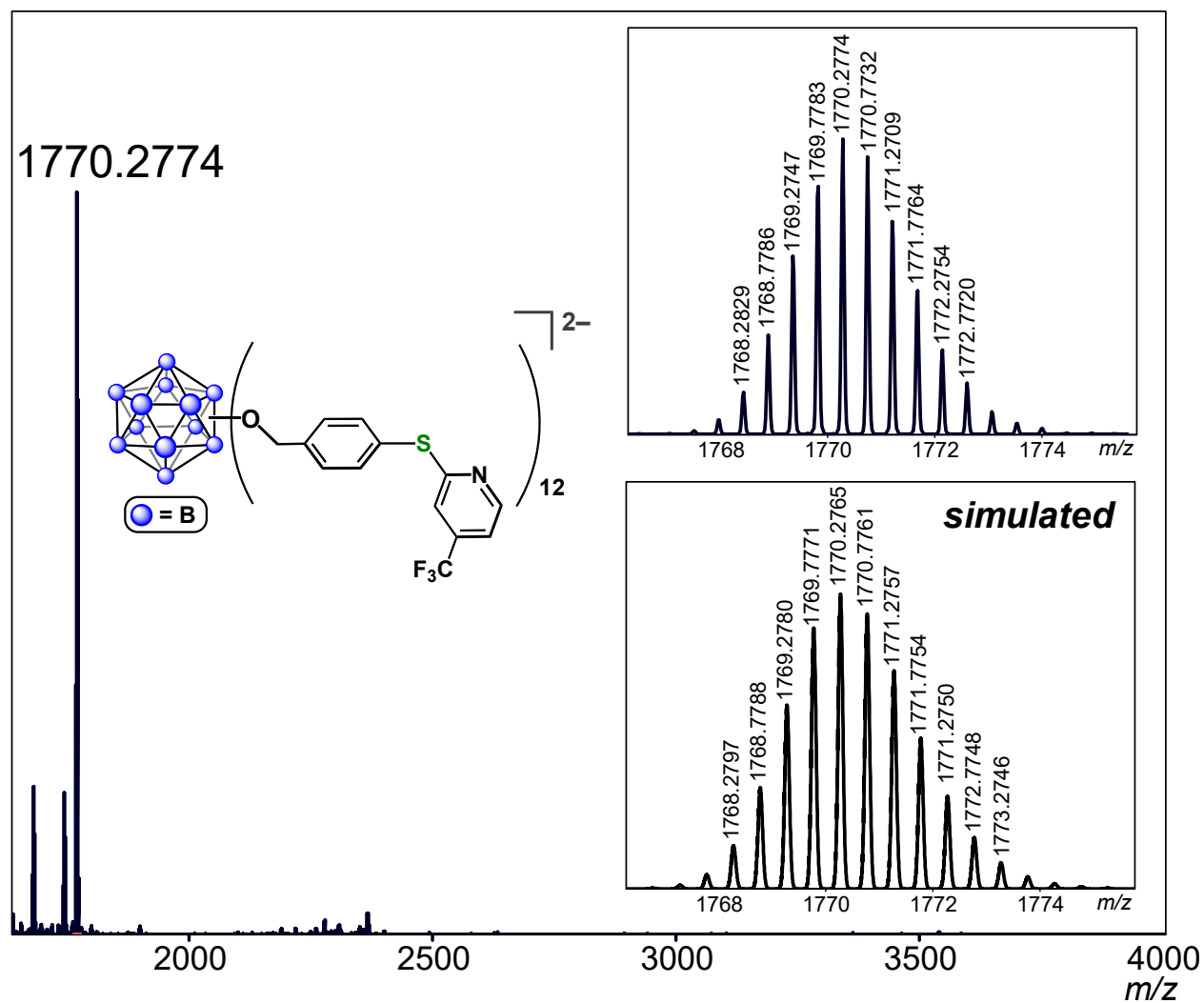
$^1H$  NMR spectrum of  $[H_3NC(CH_2OH)_3]_2[B_{12}(OCH_2C_6H_4(2\text{-thio-5-trifluoromethylpyridine}))_{12}]$  (CD<sub>3</sub>OD, 400 MHz, 25 °C).



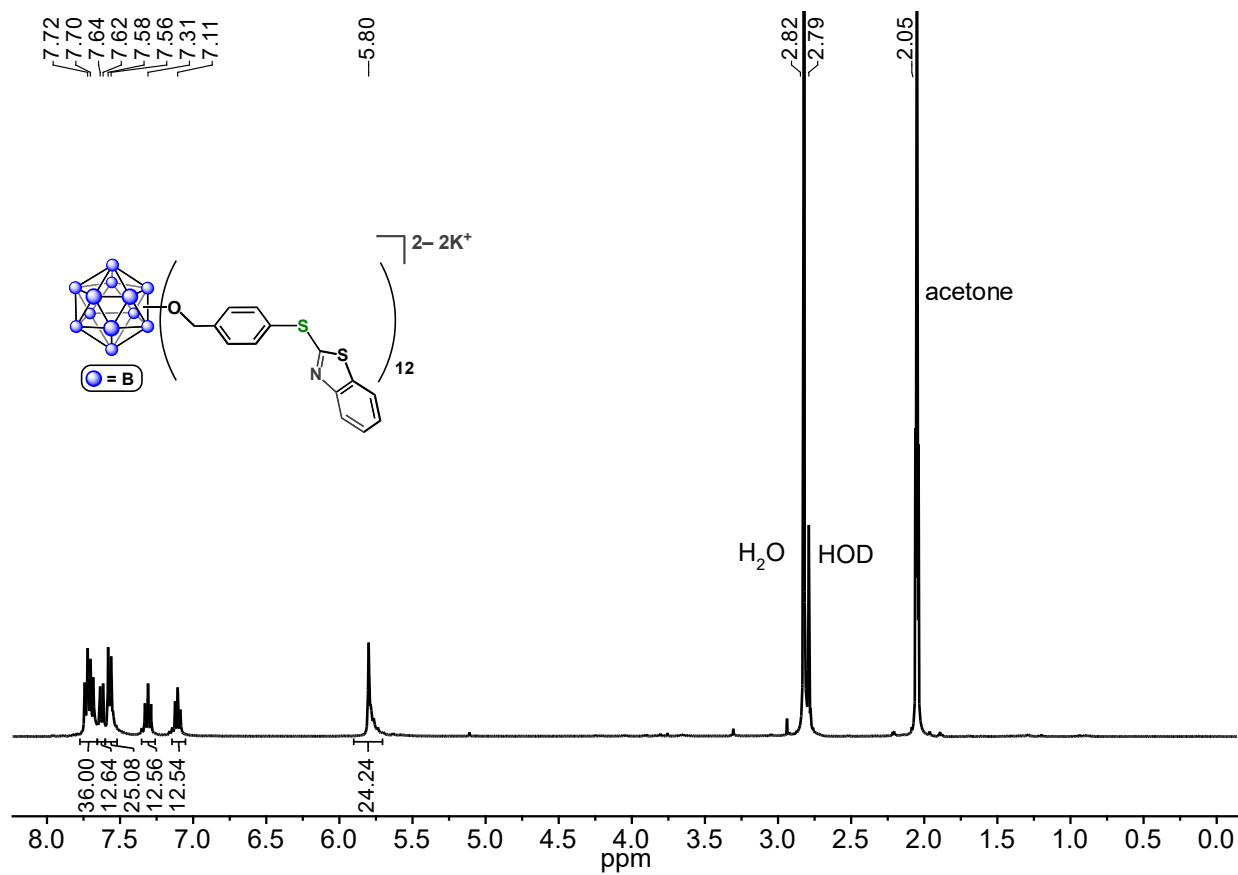
$^{19}\text{F}$   $\{^1\text{H}\}$  NMR spectrum of  $[\text{H}_3\text{NC}(\text{CH}_2\text{OH})_3]_2[\text{B}_{12}(\text{OCH}_2\text{C}_6\text{H}_4(2\text{-thio-5-trifluoromethylpyridine}))_{12}]$  ( $\text{CD}_3\text{OD}$ , 376 MHz, 25 °C).



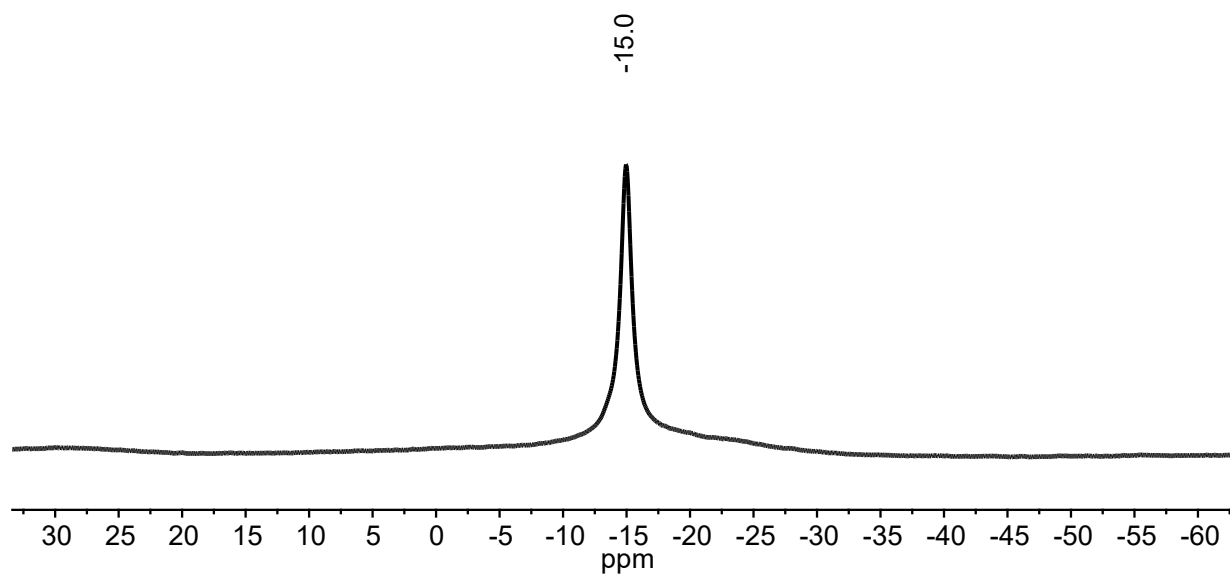
$^{11}\text{B}\{^1\text{H}\}$  NMR spectrum of  $[\text{H}_3\text{NC}(\text{CH}_2\text{OH})_3]_2[\text{B}_{12}(\text{OCH}_2\text{C}_6\text{H}_4(2\text{-thio-5-trifluoromethylpyridine}))_{12}]$  ( $\text{CD}_3\text{OD}$ , 128 MHz, 25 °C).



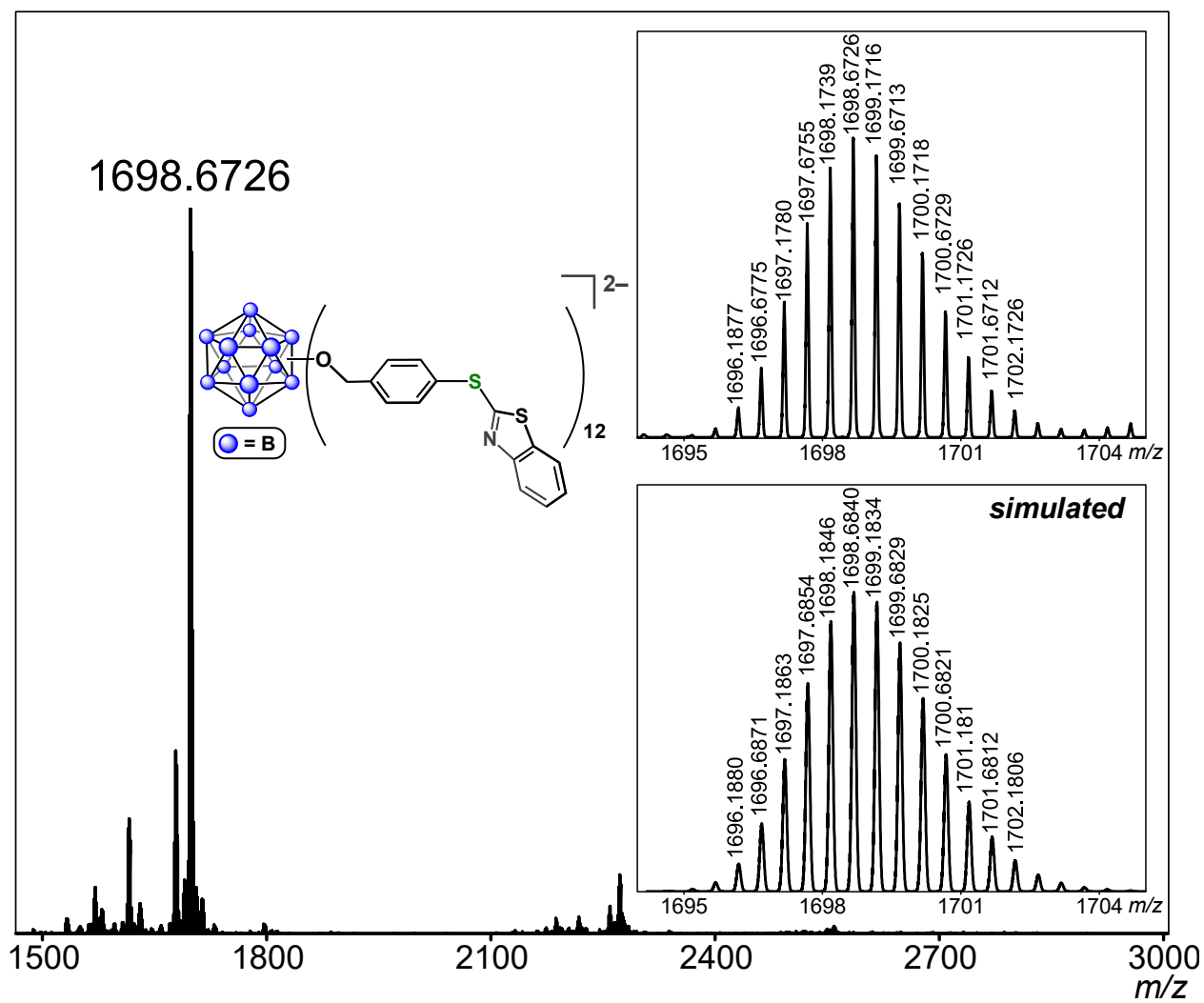
ESI-MS(-) of  $[\text{B}_{12}(\text{OCH}_2\text{C}_6\text{H}_4(2\text{-thio-5-trifluoromethylpyridine}))_{12}]^{2-}$  (MeCN, 1.5 kV).



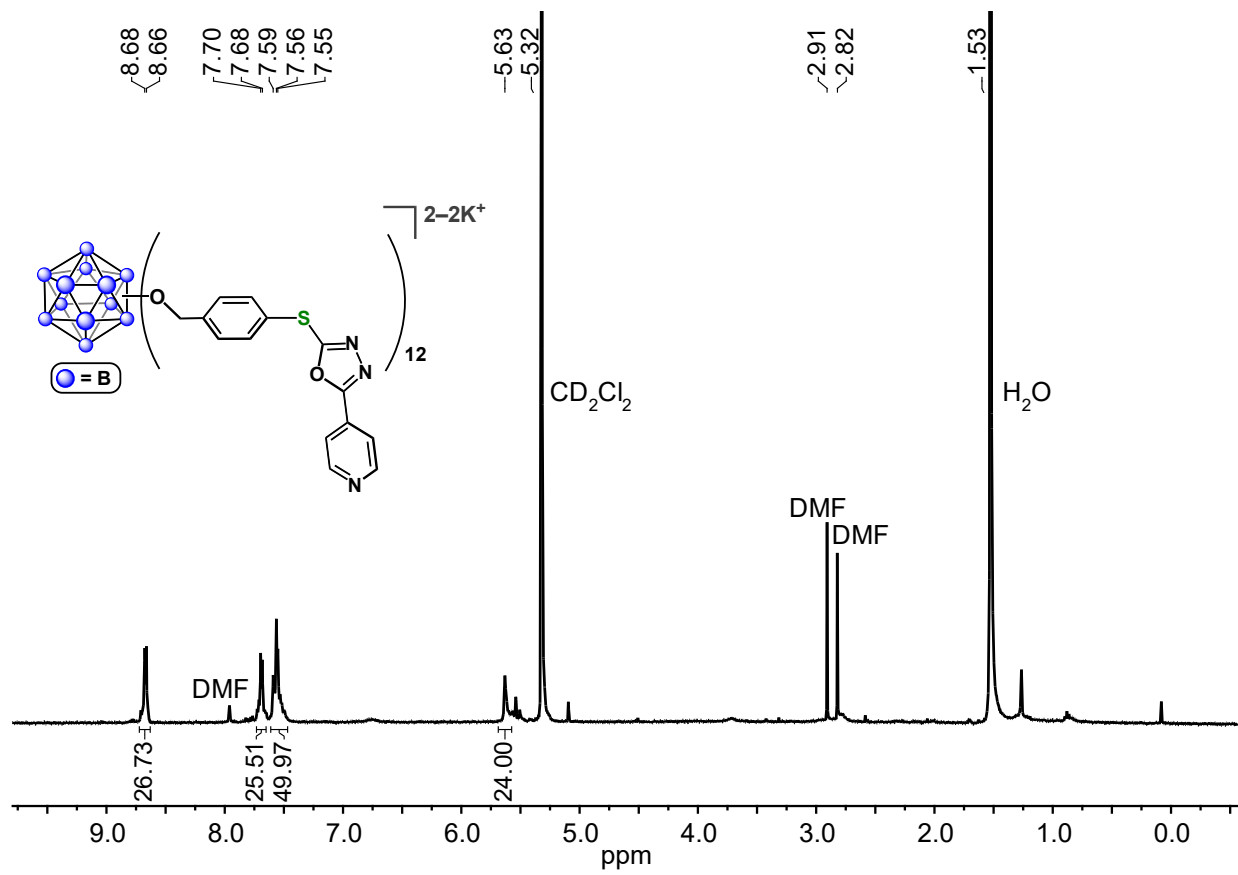
$^1H$  NMR spectrum of  $[K_2][B_{12}(OCH_2C_6H_4(2\text{-mercaptobenzothiazole}))_{12}]$  (acetone- $d_6$ , 400 MHz, 25 °C).



$^{11}\text{B}\{^1\text{H}\}$  NMR spectrum of  $[\text{K}_2][\text{B}_{12}(\text{OCH}_2\text{C}_6\text{H}_4(2\text{-mercaptobenzothiazole}))_{12}]$  (acetone- $d_6$ , 128 MHz, 25 °C).

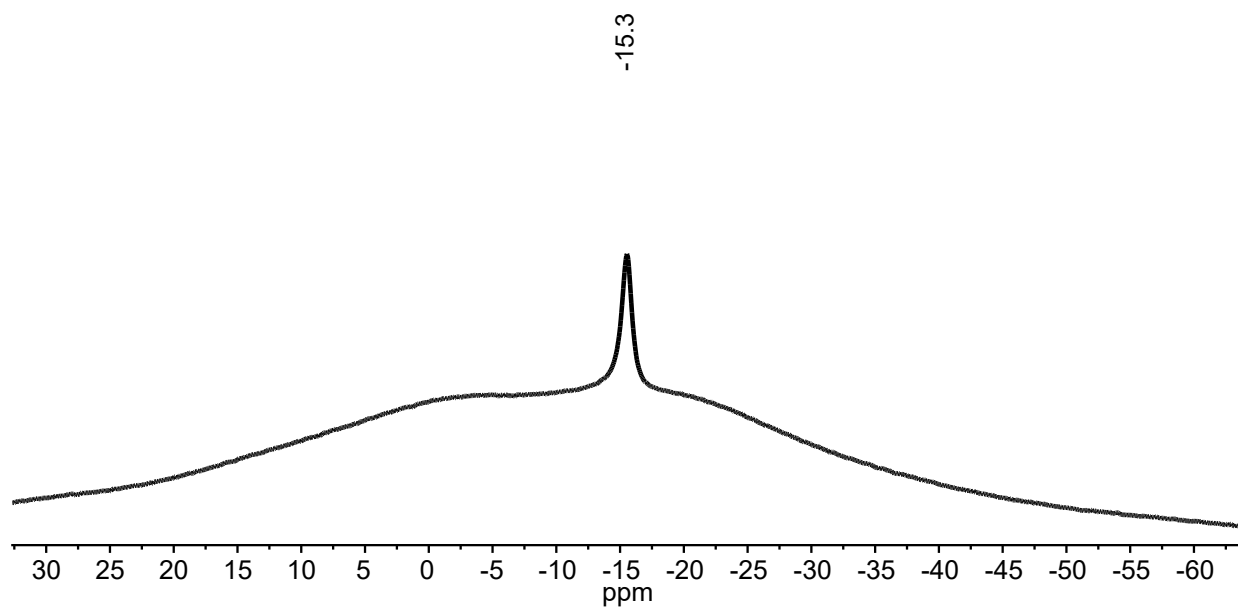


ESI-MS(-) of  $[B_{12}(OCH_2C_6H_4(2\text{-mercaptobenzothiazole}))_{12}]^{2-}$  (MeCN, 1.5 kV).

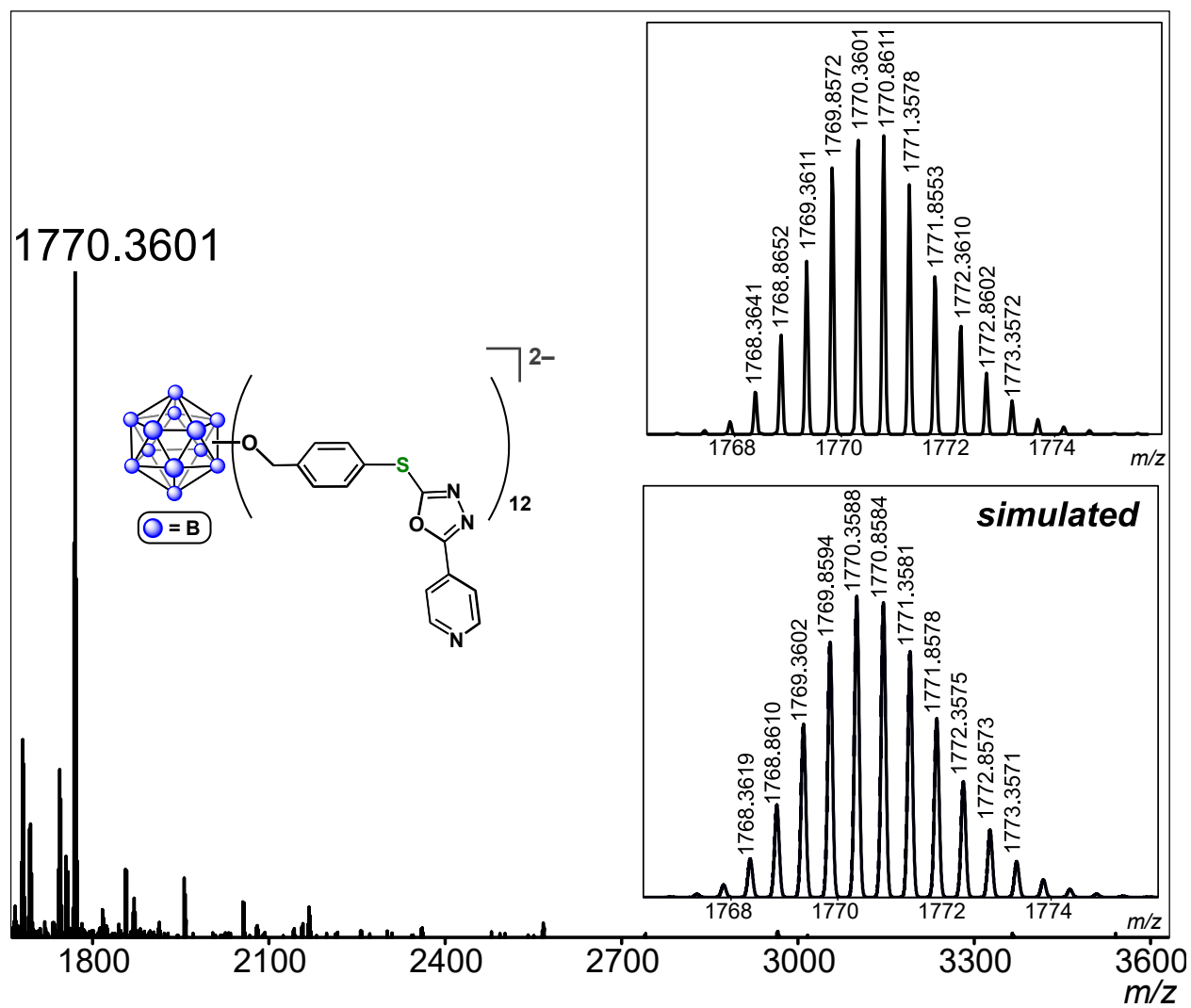


<sup>1</sup>H NMR spectrum of [K<sub>2</sub>][B<sub>12</sub>(OCH<sub>2</sub>C<sub>6</sub>H<sub>4</sub>(2-thio-5-(4-pyridyl)-1,3,4-oxadiazole))<sub>12</sub>] (CD<sub>2</sub>Cl<sub>2</sub>, 400 MHz, 25 °C).

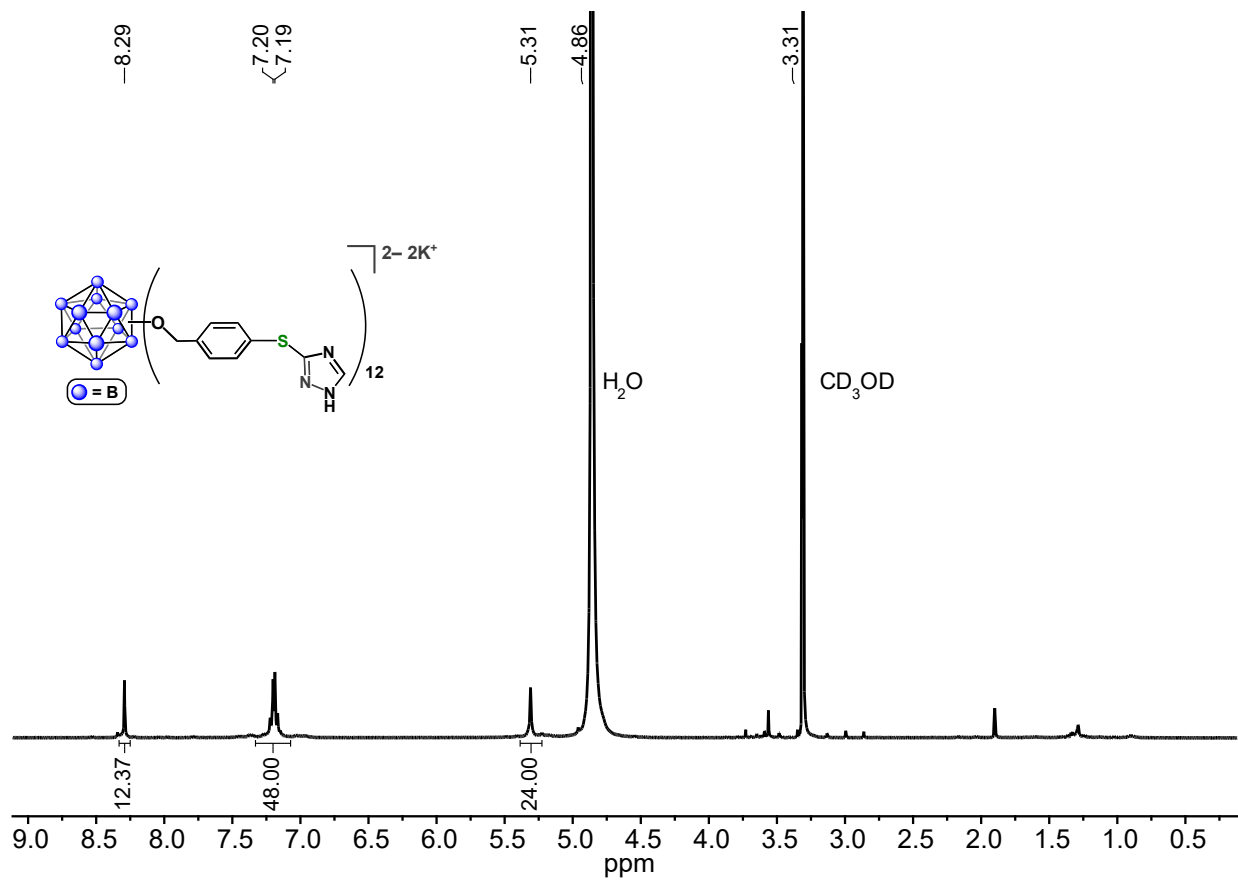




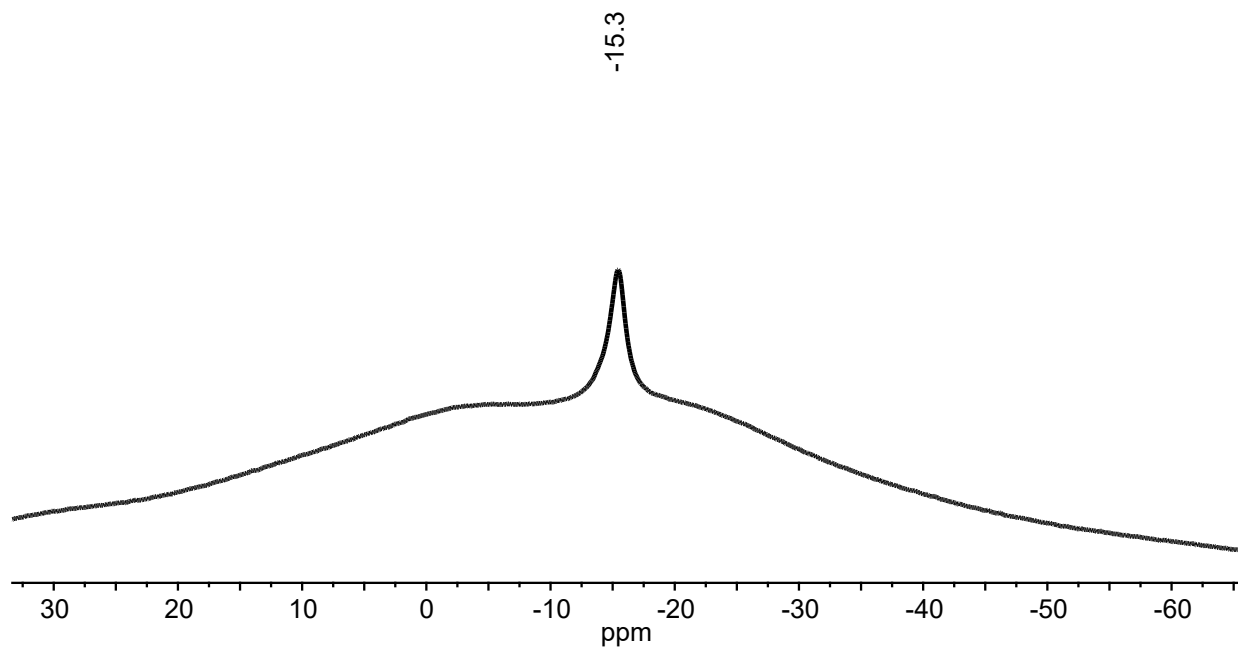
$^{11}\text{B}\{^1\text{H}\}$  NMR spectrum of  $[\text{K}_2][\text{B}_{12}(\text{OCH}_2\text{C}_6\text{H}_4(2\text{-thio-5-(4\text{-pyridyl)-1,3,4\text{-oxadiazole}))}_{12}]$   
( $\text{CD}_2\text{Cl}_2$ , 128 MHz, 25 °C).



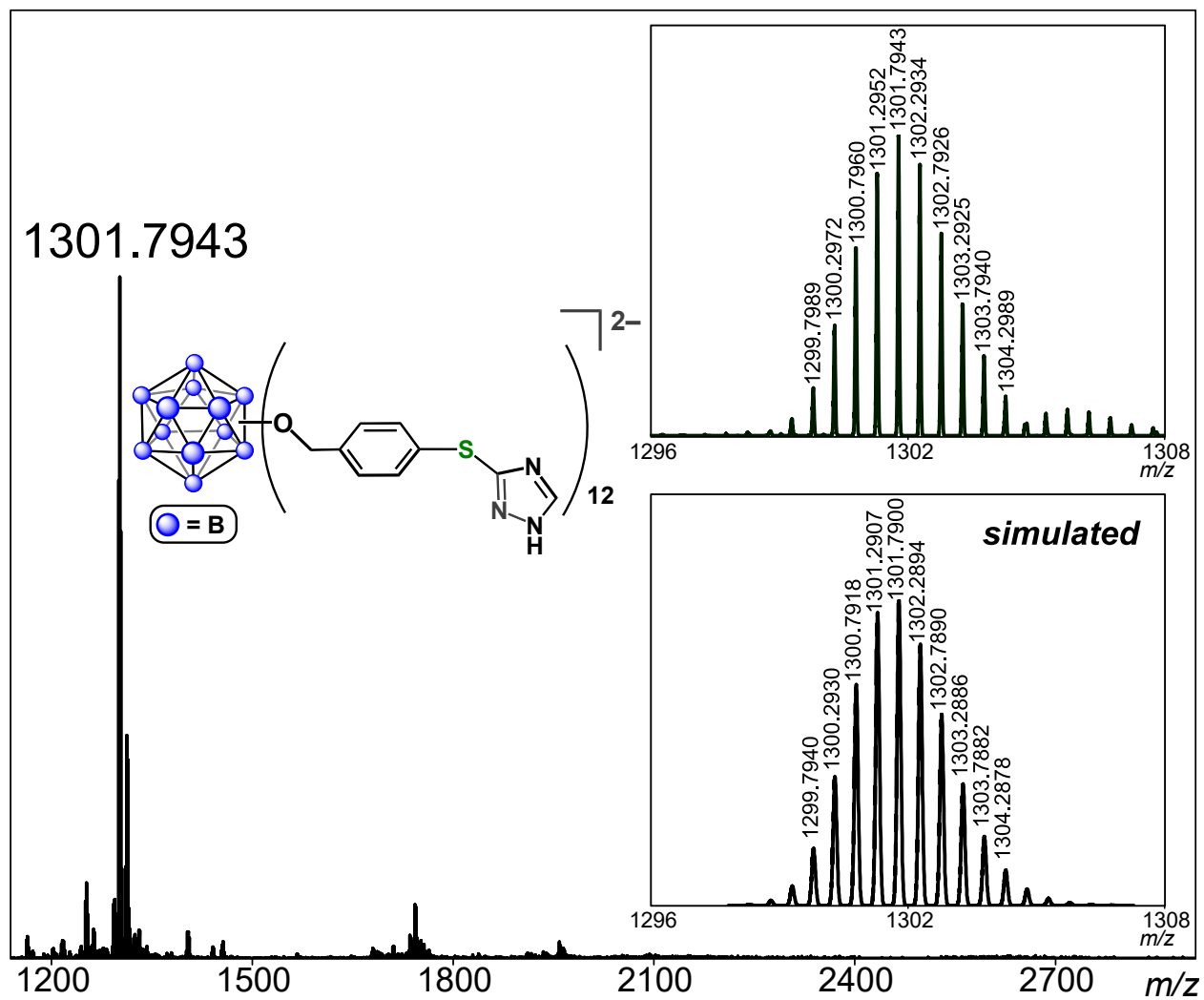
ESI-MS(-) of  $[B_{12}(OCH_2C_6H_4(2\text{-thio-5-(4-pyridyl)-1,3,4-oxadiazole}))_{12}]^{2-}$  (MeCN, 1.5 kV).



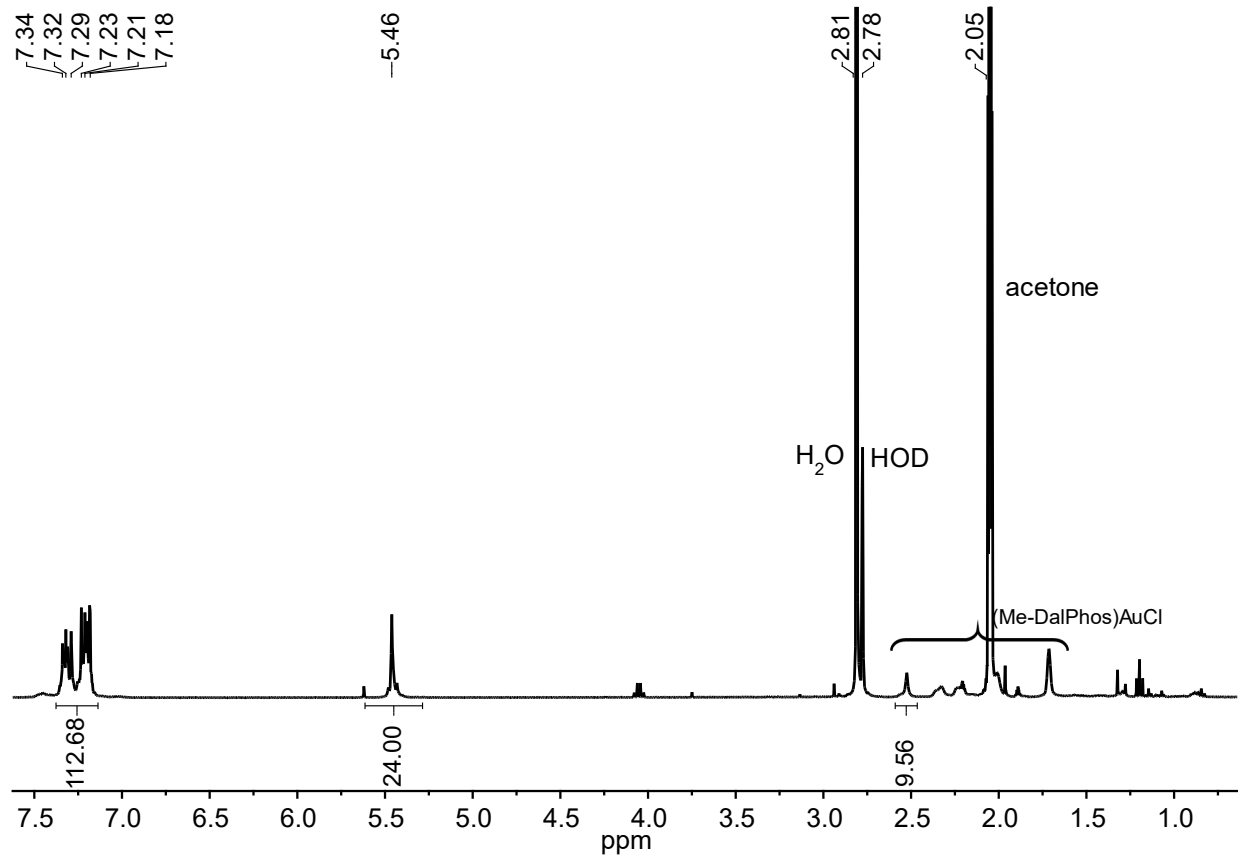
$^1\text{H}$  NMR spectrum of  $[\text{K}_2][\text{B}_{12}(\text{OCH}_2\text{C}_6\text{H}_4(3\text{-thio-1,2,4-triazole}))_{12}]$  ( $\text{CD}_3\text{OD}$ , 400 MHz, 25 °C).



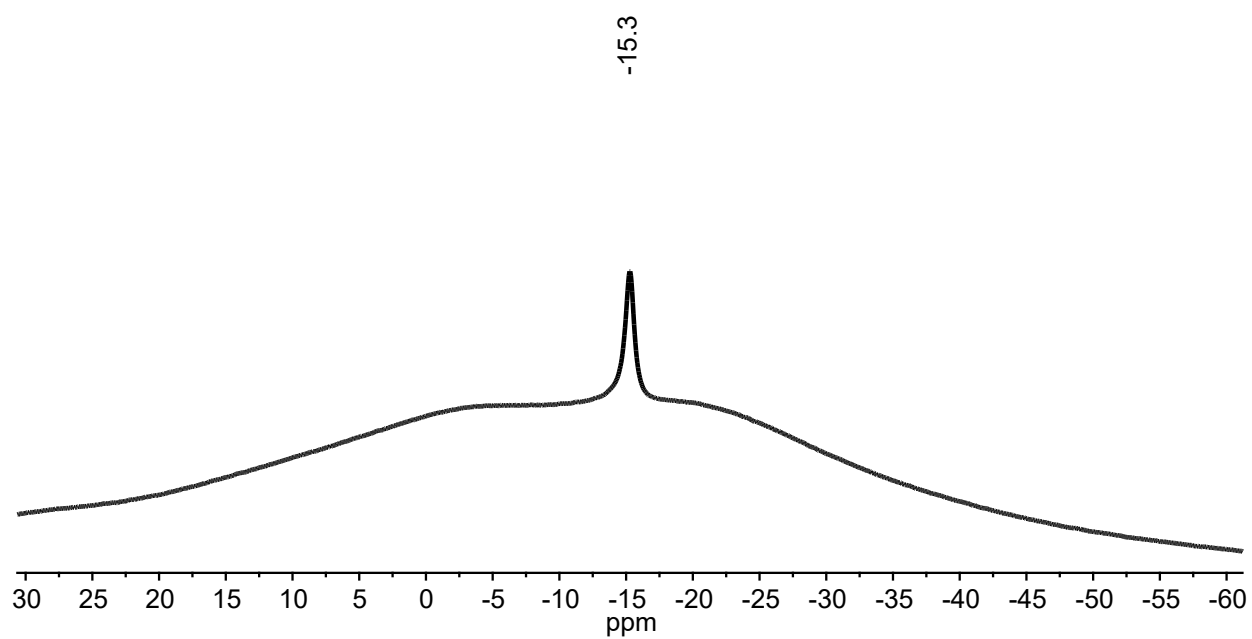
$^{11}\text{B}\{^1\text{H}\}$  NMR spectrum of  $[\text{K}_2][\text{B}_{12}(\text{OCH}_2\text{C}_6\text{H}_4(3\text{-thio-1,2,4\text{-triazole}))}_{12}]$  ( $\text{CD}_3\text{OD}$ , 128 MHz, 25  $^\circ\text{C}$ ).



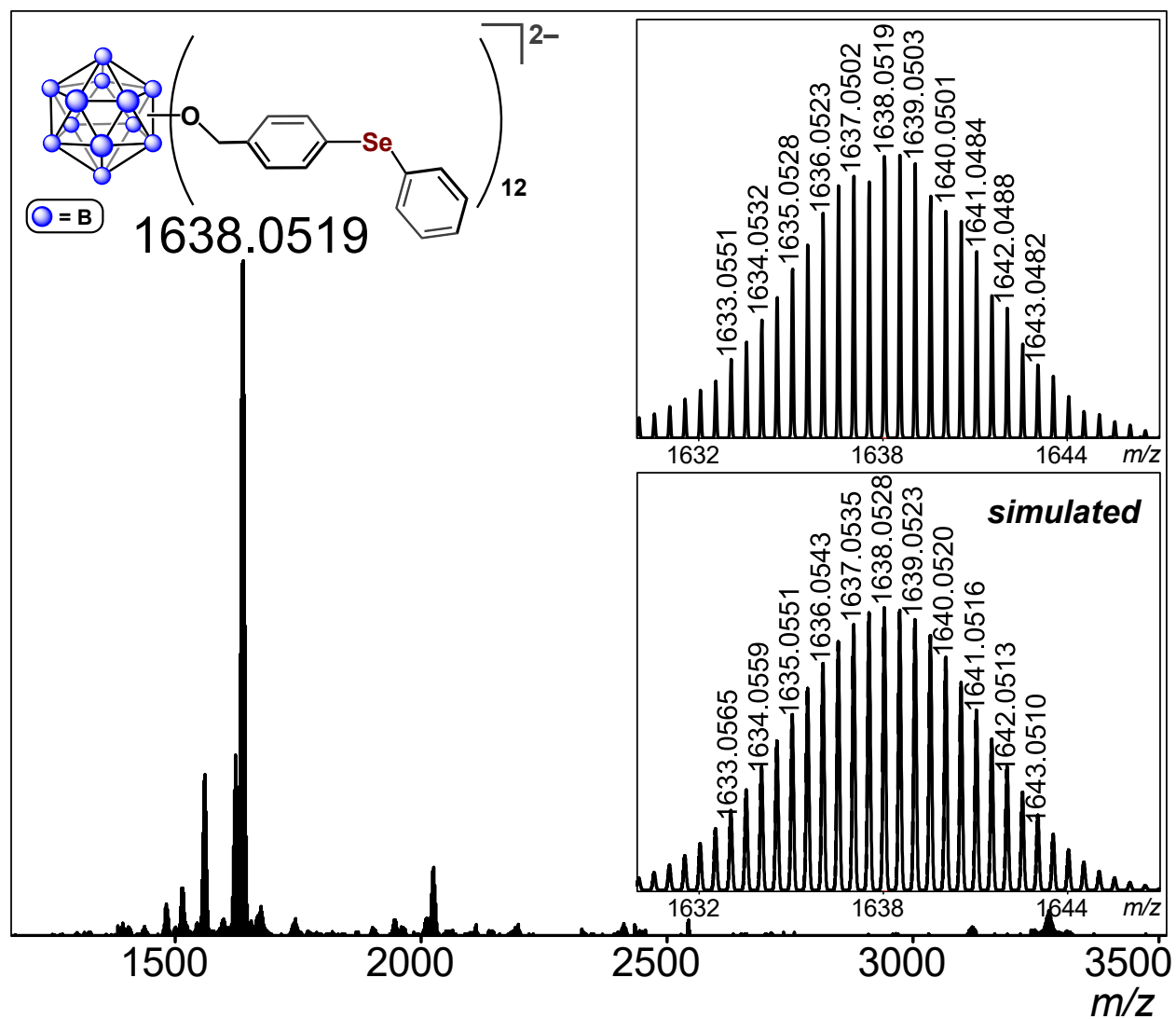
ESI-MS(-) of  $[B_{12}(OCH_2C_6H_4(3\text{-thio-1,2,4-triazole}))_{12}]^{2-}$  (MeCN, 1.5 kV).



$^1\text{H}$  NMR spectrum of  $[\text{K}_2][\text{B}_{12}(\text{OCH}_2\text{C}_6\text{H}_4\text{SePh})_{12}]$  (400 MHz, acetone- $d_6$ , 25 °C).

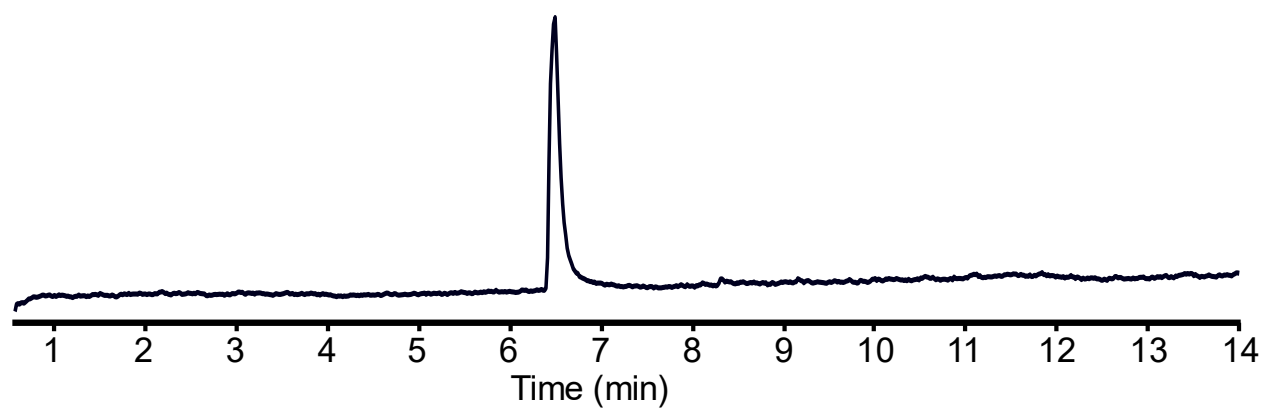


$^{11}\text{B}\{^1\text{H}\}$  NMR spectrum of  $[\text{K}_2][\text{B}_{12}(\text{OCH}_2\text{C}_6\text{H}_4\text{SePh})_{12}]$  (128 MHz, acetone- $d_6$ , 25 °C).

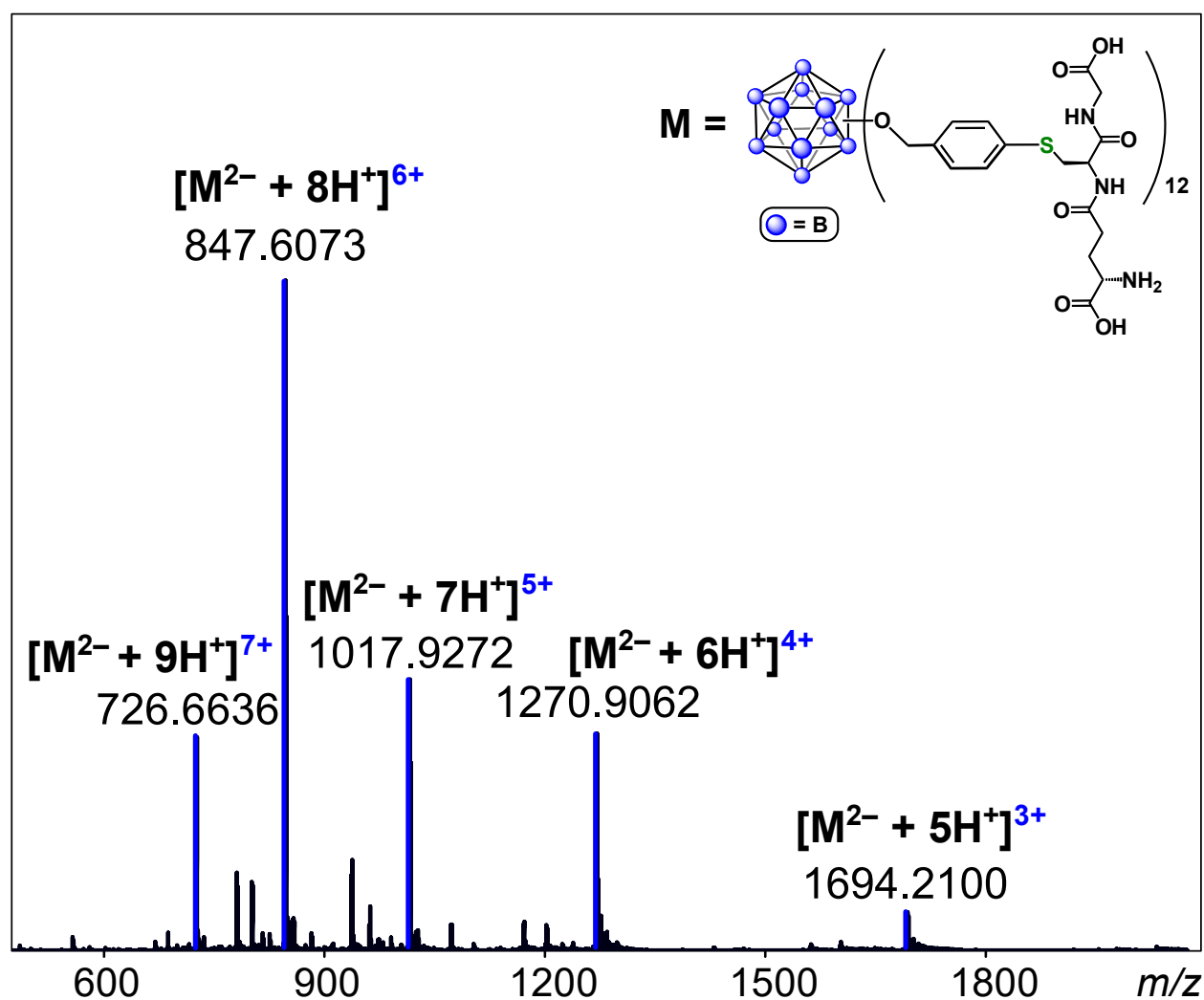
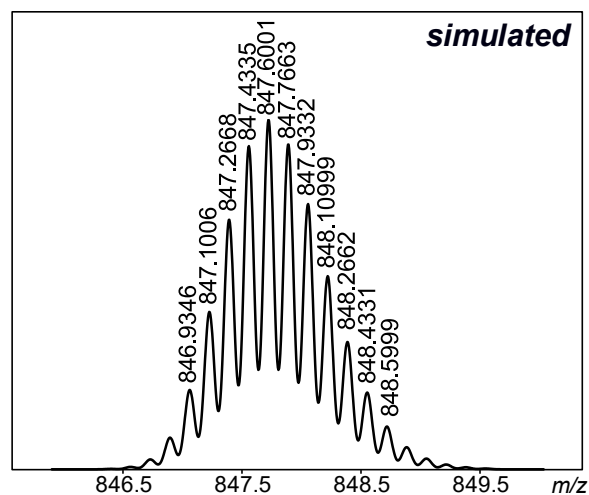
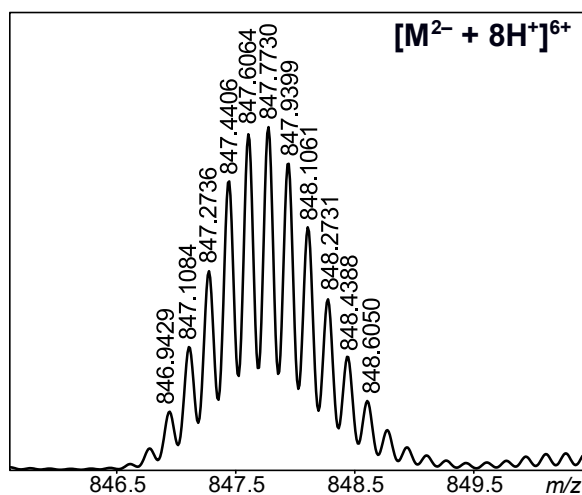


ESI-MS(-) of  $[B_{12}(OCH_2C_6H_4SePh)_{12}]^{2-}$  (MeCN, 1.5 kV).

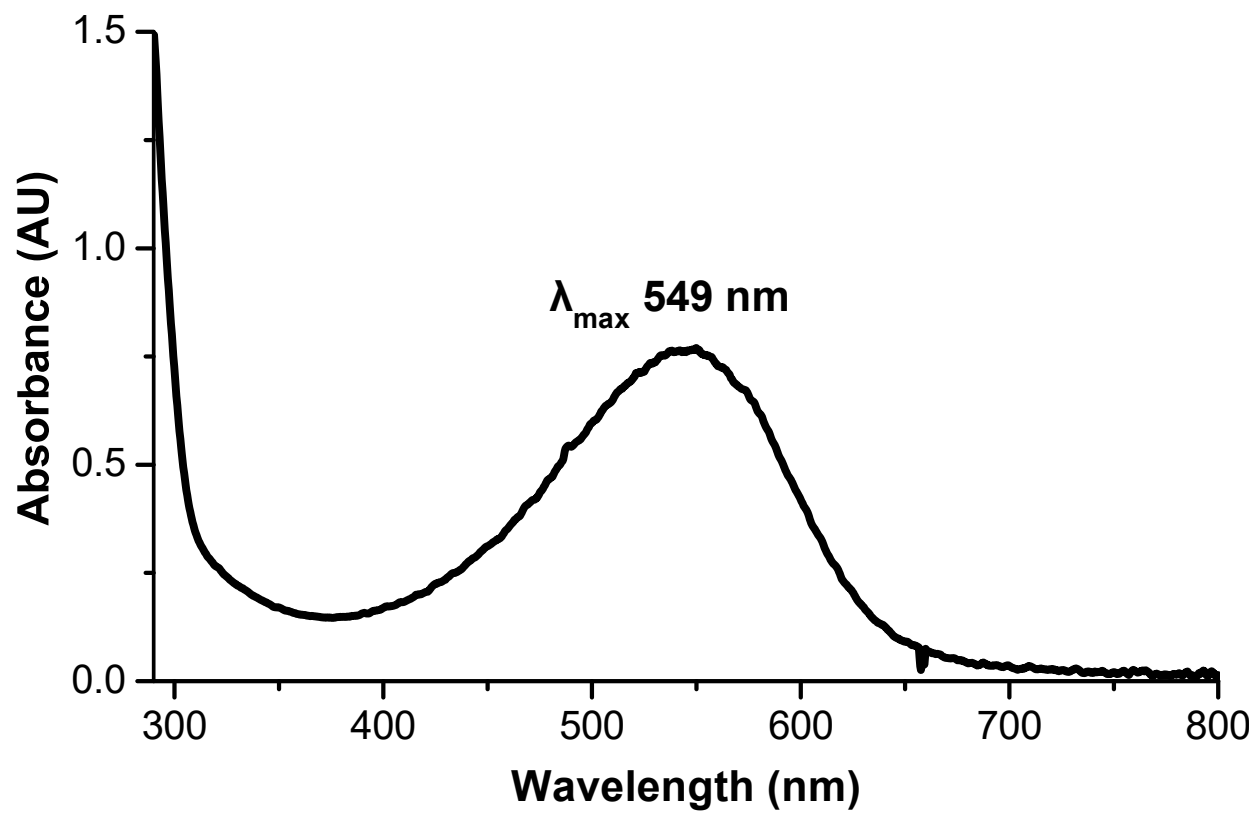




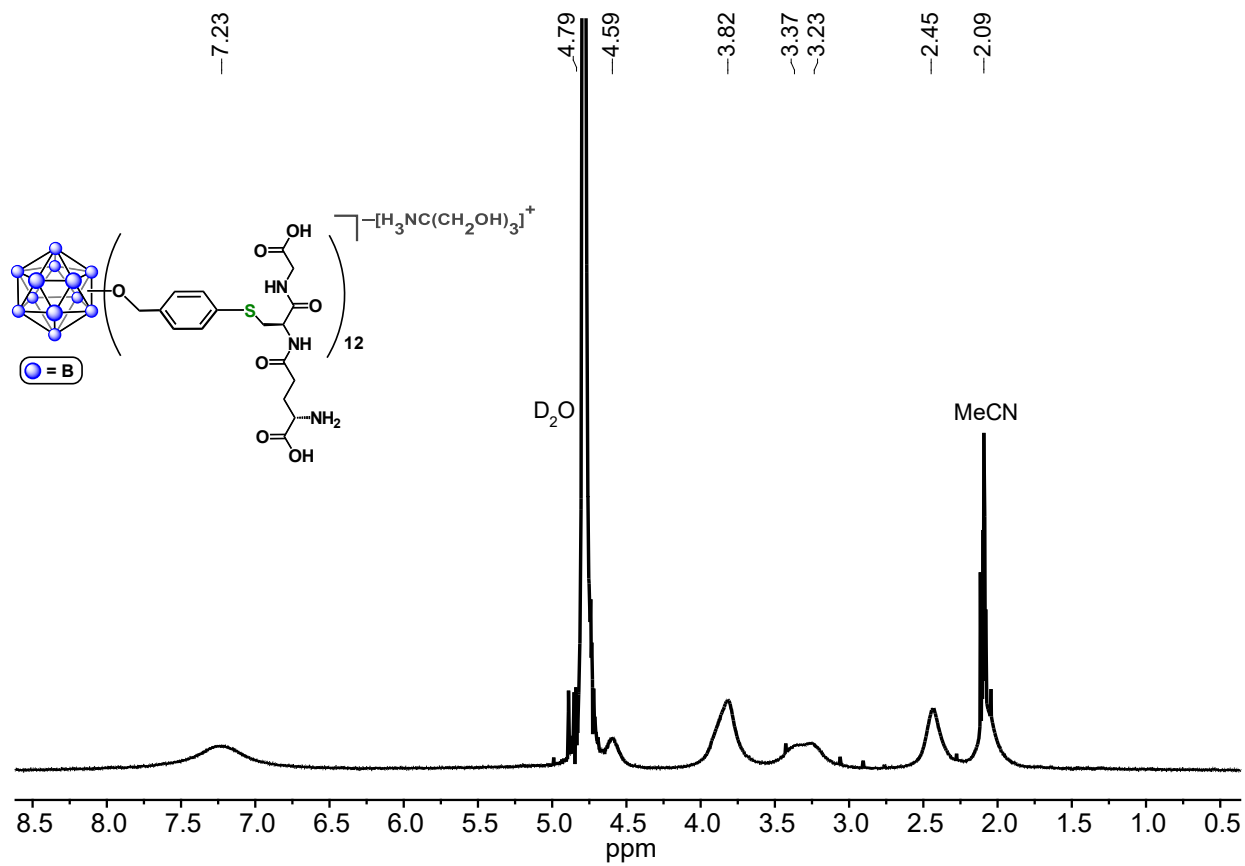
LC-trace of  $[\text{H}_3\text{NC}(\text{CH}_2\text{OH})_3][\text{B}_{12}(\text{OCH}_2\text{C}_6\text{H}_4(\text{glutathione}))_{12}]$ . LC-MS method (solvent A:  $\text{H}_2\text{O}$  with 0.1% formic acid; solvent B: MeCN with 0.1% formic acid): 0–2 min, A (100%) : B (0%); 2–11 min, A (100–5%) : B (0–95%); 11–12 min, A (5–0%) : B (95–100%); 12–14 min, A (0%) : B (100%).



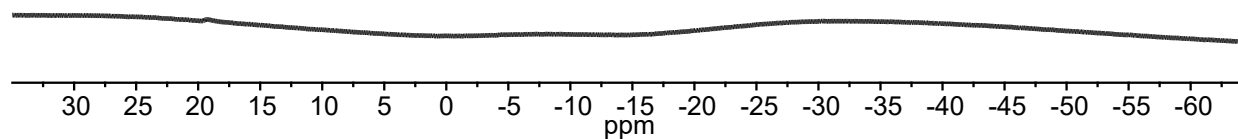
ESI-MS(+) of  $[\text{H}_3\text{NC}(\text{CH}_2\text{OH})_3][\text{B}_{12}(\text{OCH}_2\text{C}_6\text{H}_4(\text{glutathione}))_{12}]$  (at 6.6 min retention time from the LC-MS data; 50:50  $\text{H}_2\text{O}/\text{MeCN}$  v/v with 0.1% formic acid).



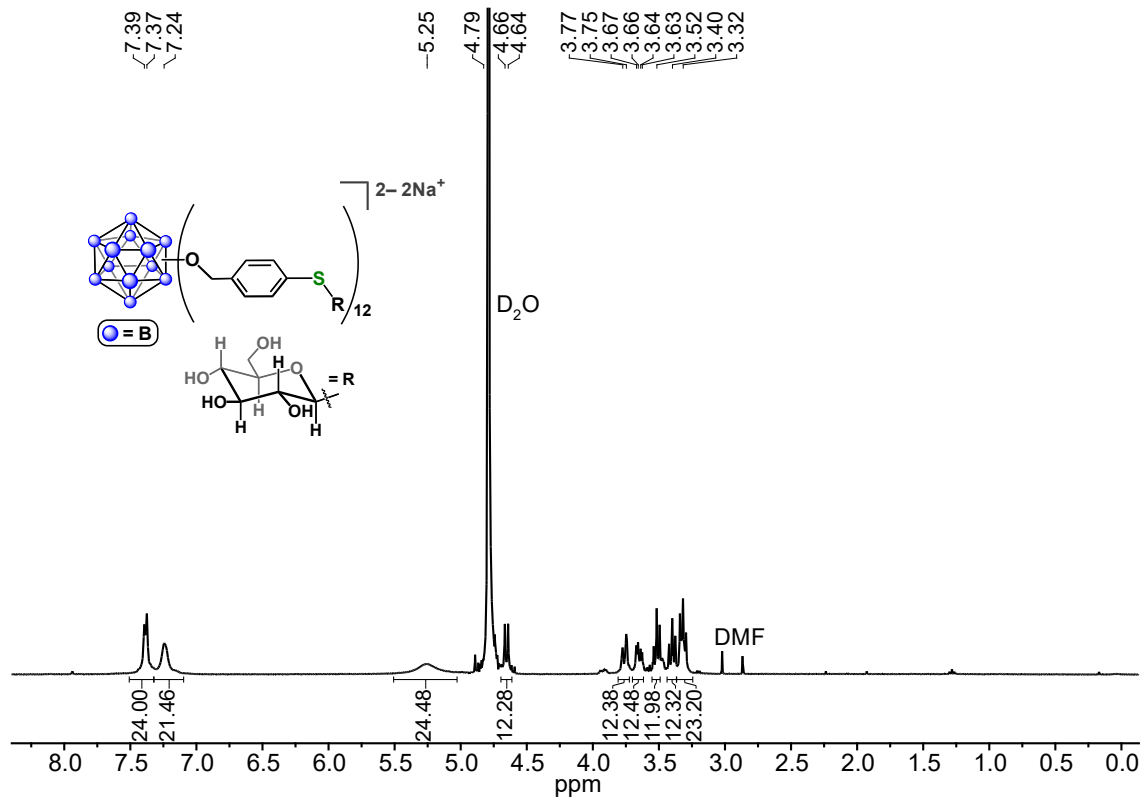
UV-vis spectrum of  $[\text{H}_3\text{NC}(\text{CH}_2\text{OH})_3][\text{B}_{12}(\text{OCH}_2\text{C}_6\text{H}_4(\text{glutathione}))_{12}]$  ( $\text{H}_2\text{O}$ ,  $25\text{ }^\circ\text{C}$ ).



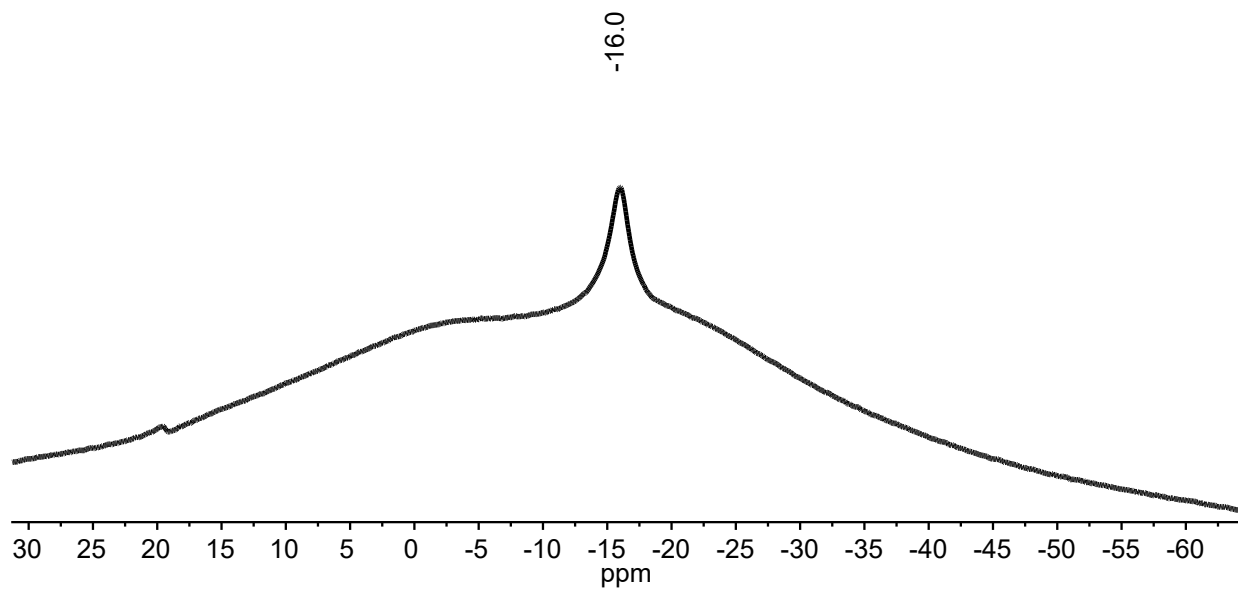
$^1H$  NMR spectrum of  $[H_3NC(CH_2OH)_3][B_{12}(OCH_2C_6H_4(glutathione))_{12}]$  ( $D_2O$  spiked with  $CD_3CN$ , 400 MHz, 25 °C).



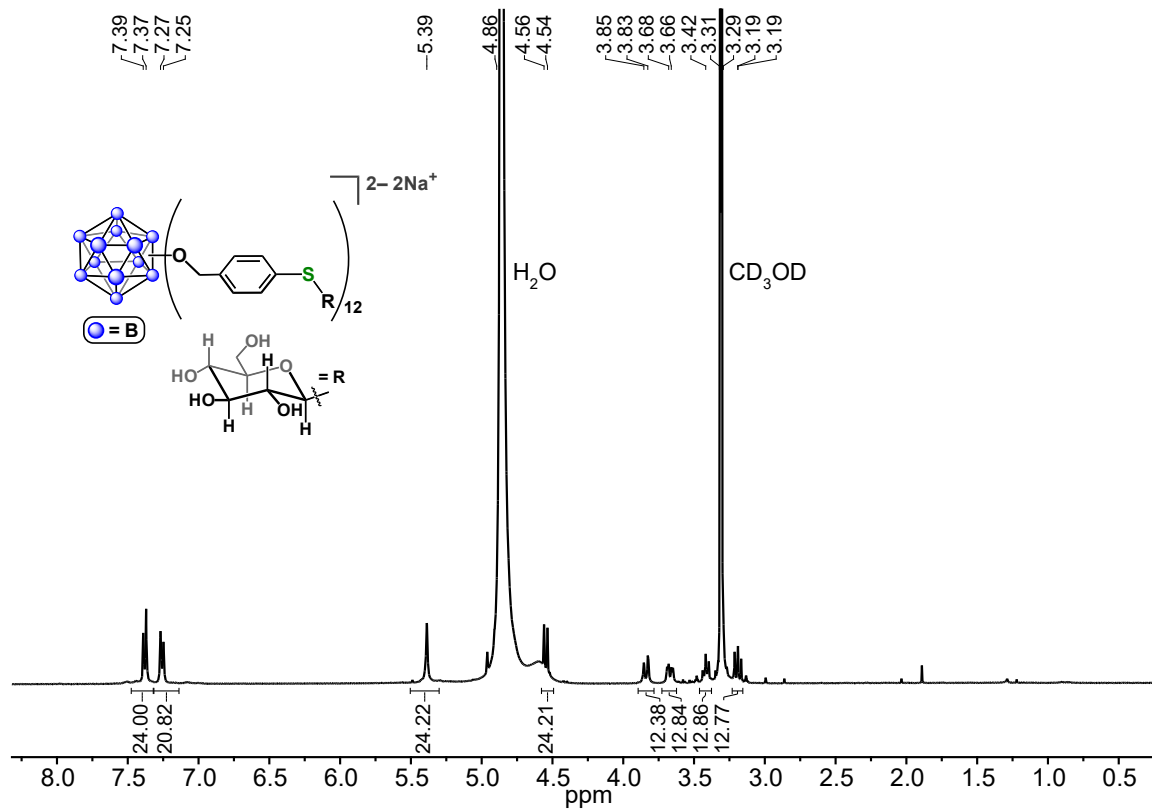
$^{11}\text{B}\{^1\text{H}\}$  NMR spectrum of  $[\text{H}_3\text{NC}(\text{CH}_2\text{OH})_3][\text{B}_{12}(\text{OCH}_2\text{C}_6\text{H}_4(\text{glutathione}))_{12}]$  ( $\text{D}_2\text{O}$  spiked with  $\text{CD}_3\text{CN}$ , 128 MHz, 25 °C).



<sup>1</sup>H NMR spectrum of  $[\text{Na}_2][\text{B}_{12}(\text{OCH}_2\text{C}_6\text{H}_4(1\text{-thio-}\beta\text{-D-glucose}))_{12}]$  (D<sub>2</sub>O, 400 MHz, 25 °C).

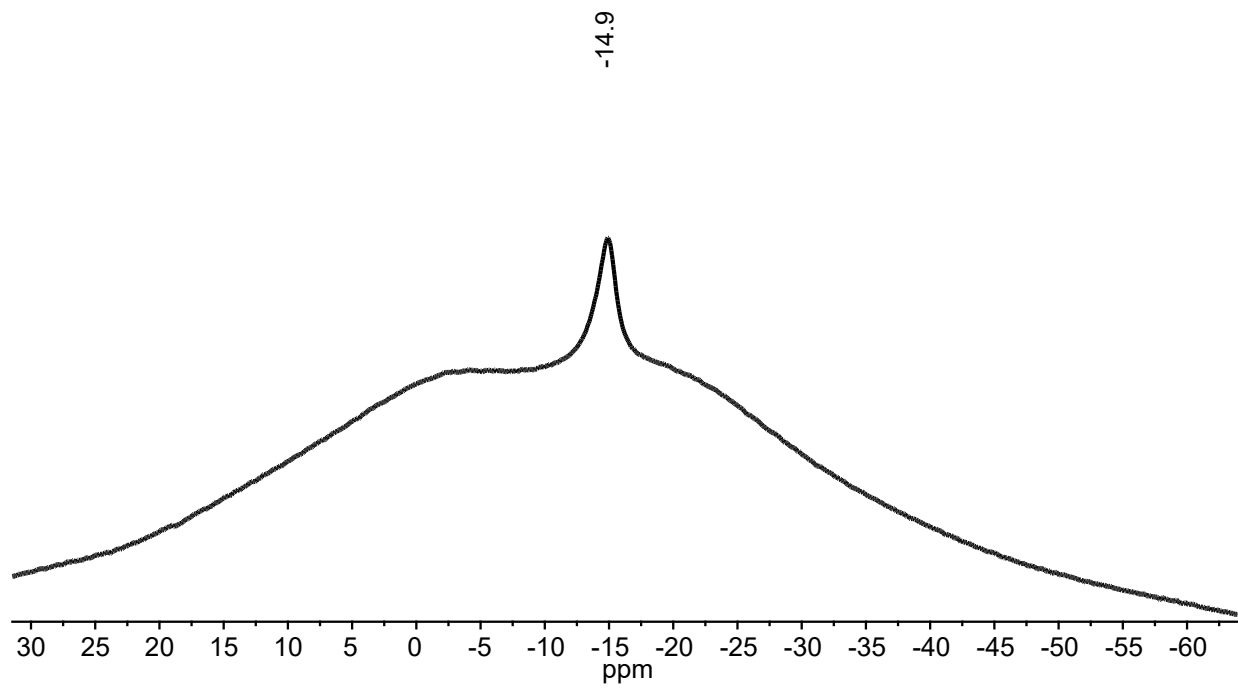


$^{11}\text{B}\{^1\text{H}\}$  NMR spectrum of  $[\text{Na}_2][\text{B}_{12}(\text{OCH}_2\text{C}_6\text{H}_4(1\text{-thio-}\beta\text{-D-glucose}))_{12}]$  ( $\text{D}_2\text{O}$ , 128 MHz, 25  $^\circ\text{C}$ ).

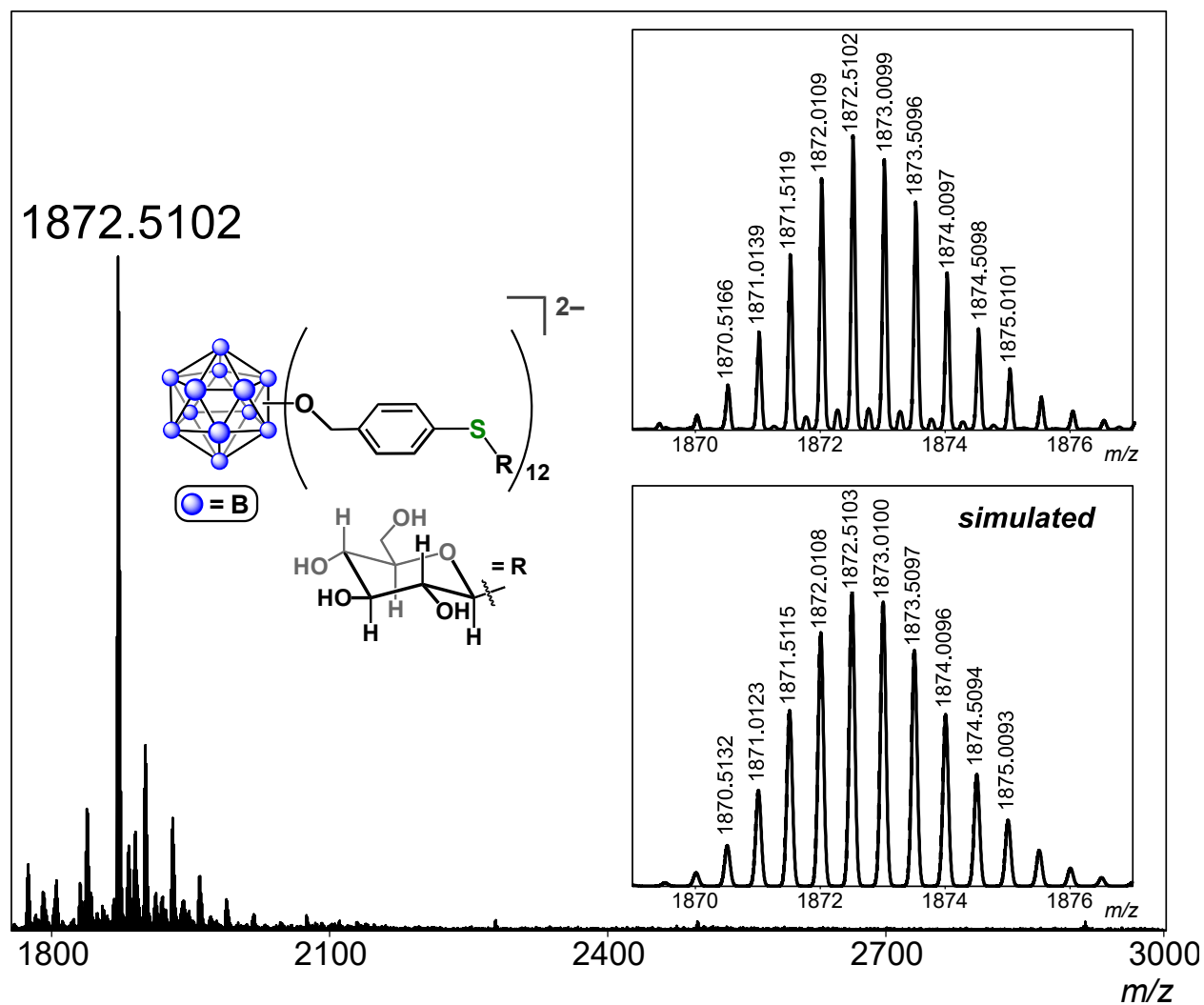


$^1\text{H}$  NMR spectrum of  $[\text{Na}_2][\text{B}_{12}(\text{OCH}_2\text{C}_6\text{H}_4(1\text{-thio-}\beta\text{-D-glucose}))_{12}]$  ( $\text{CD}_3\text{OD}$ , 400 MHz, 25 °C).

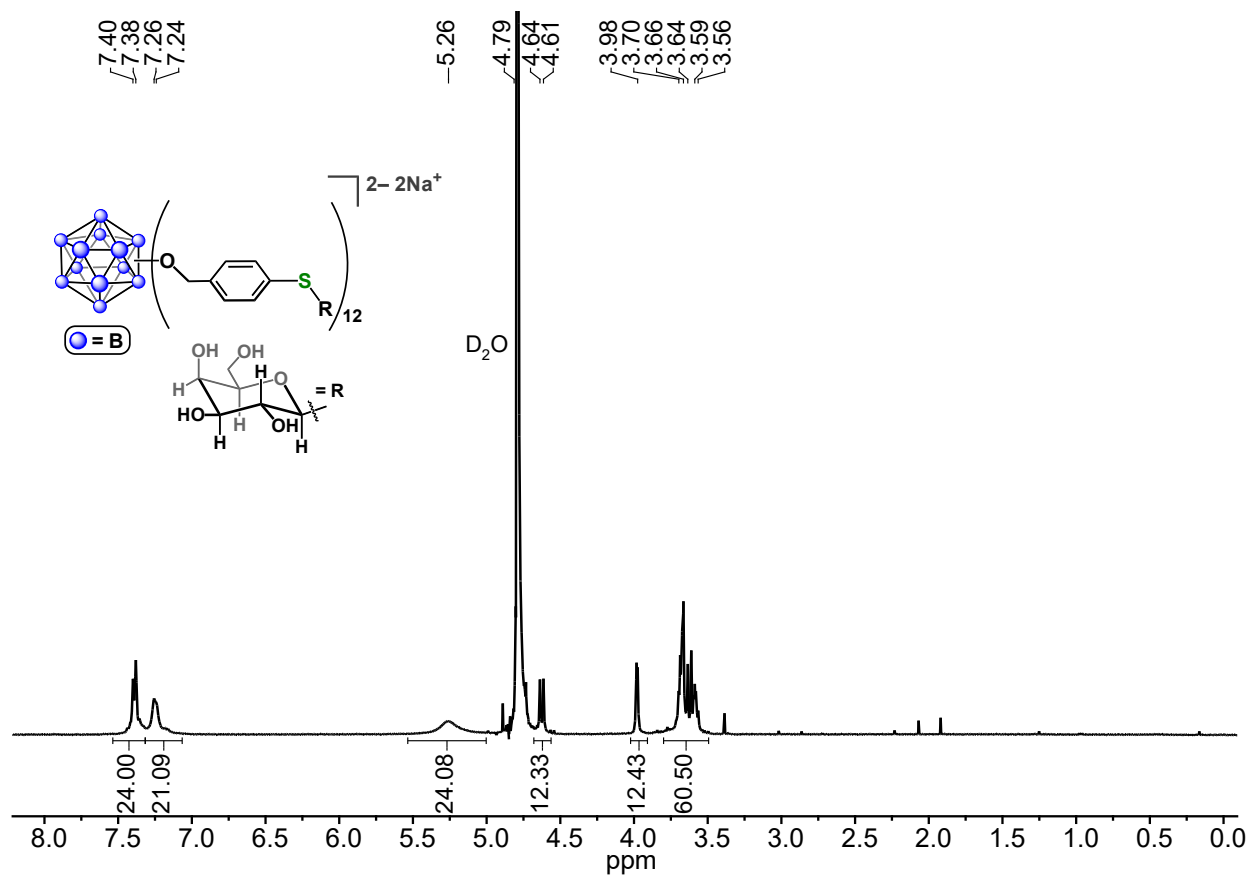




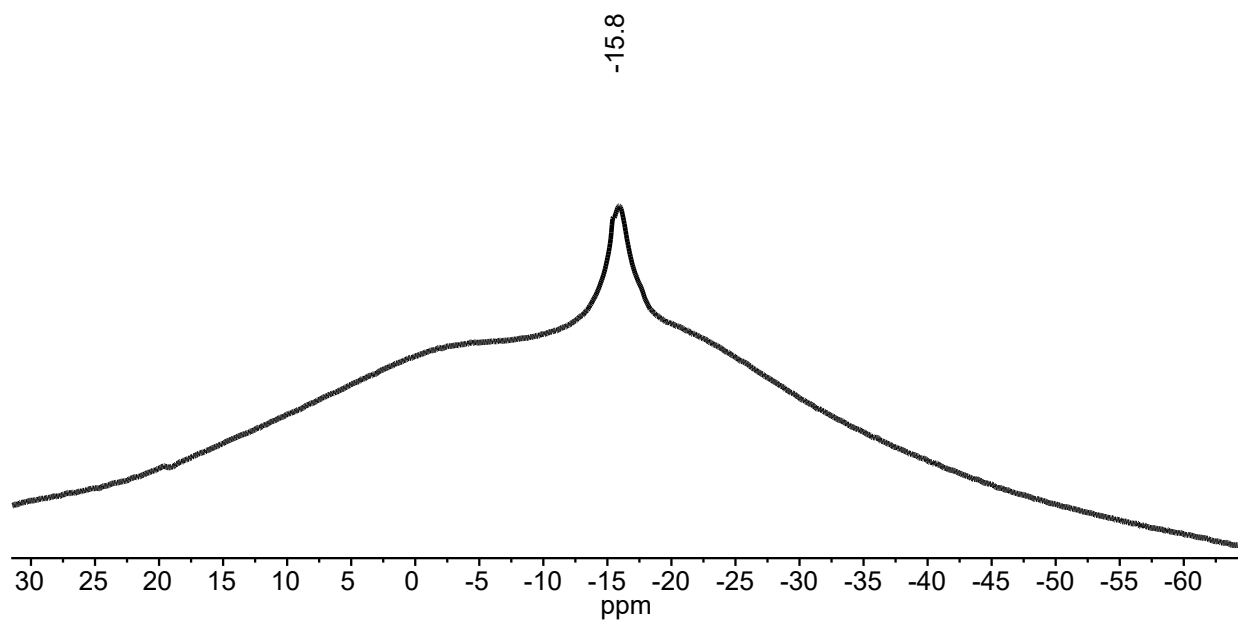
$^{11}\text{B}\{^1\text{H}\}$  NMR spectrum of  $[\text{Na}_2][\text{B}_{12}(\text{OCH}_2\text{C}_6\text{H}_4(1\text{-thio-}\beta\text{-D-glucose}))_{12}]$  ( $\text{CD}_3\text{OD}$ , 128 MHz, 25 °C).



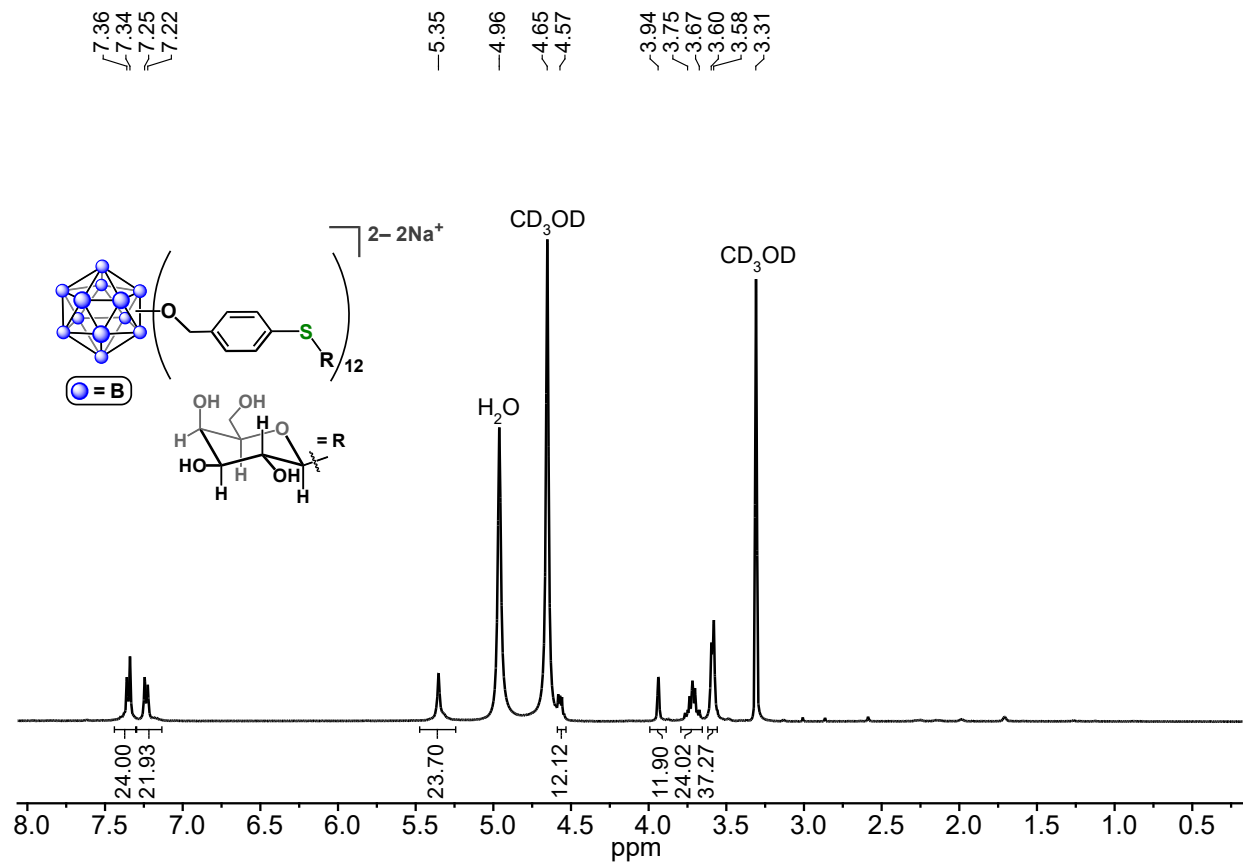
ESI-MS(-) of  $[B_{12}(OCH_2C_6H_4(1\text{-thio-}\beta\text{-D-glucose}))_{12}]^{2-}$  (MeOH, 1.5 kV).



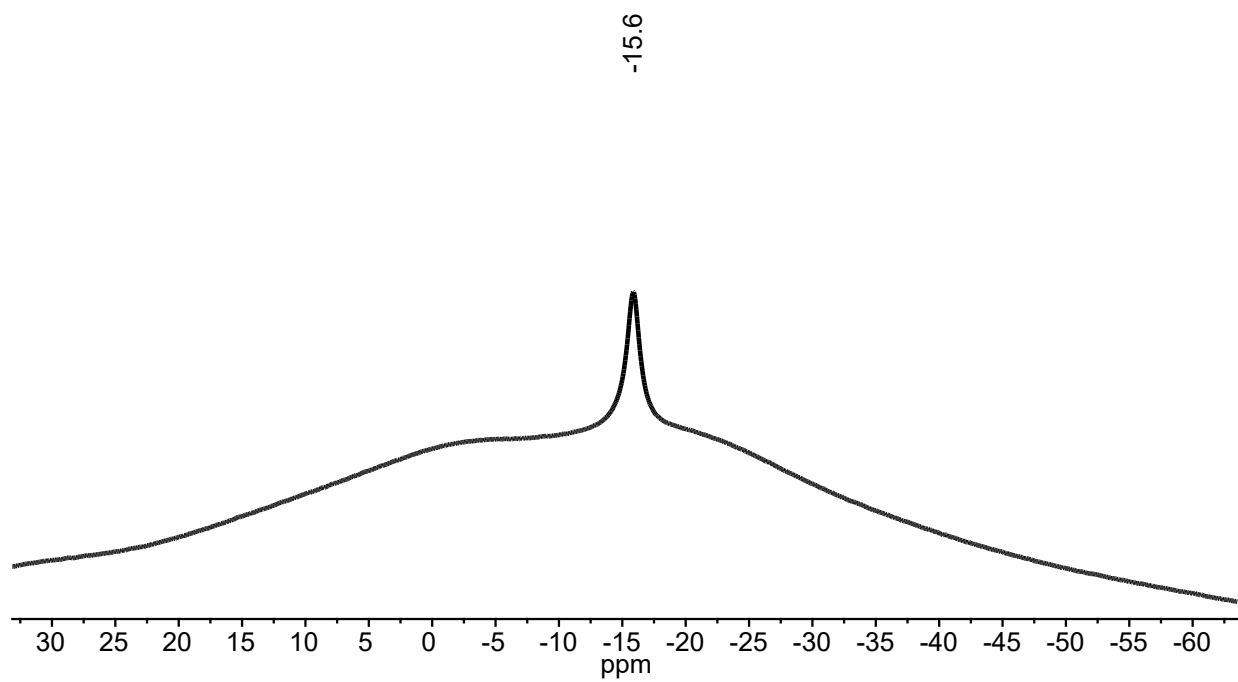
$^1\text{H}$  NMR spectrum of  $[\text{Na}_2][\text{B}_{12}(\text{OCH}_2\text{C}_6\text{H}_4(1\text{-thio-}\beta\text{-D-galactose}))_{12}]$  ( $\text{D}_2\text{O}$ , 400 MHz, 25 °C).



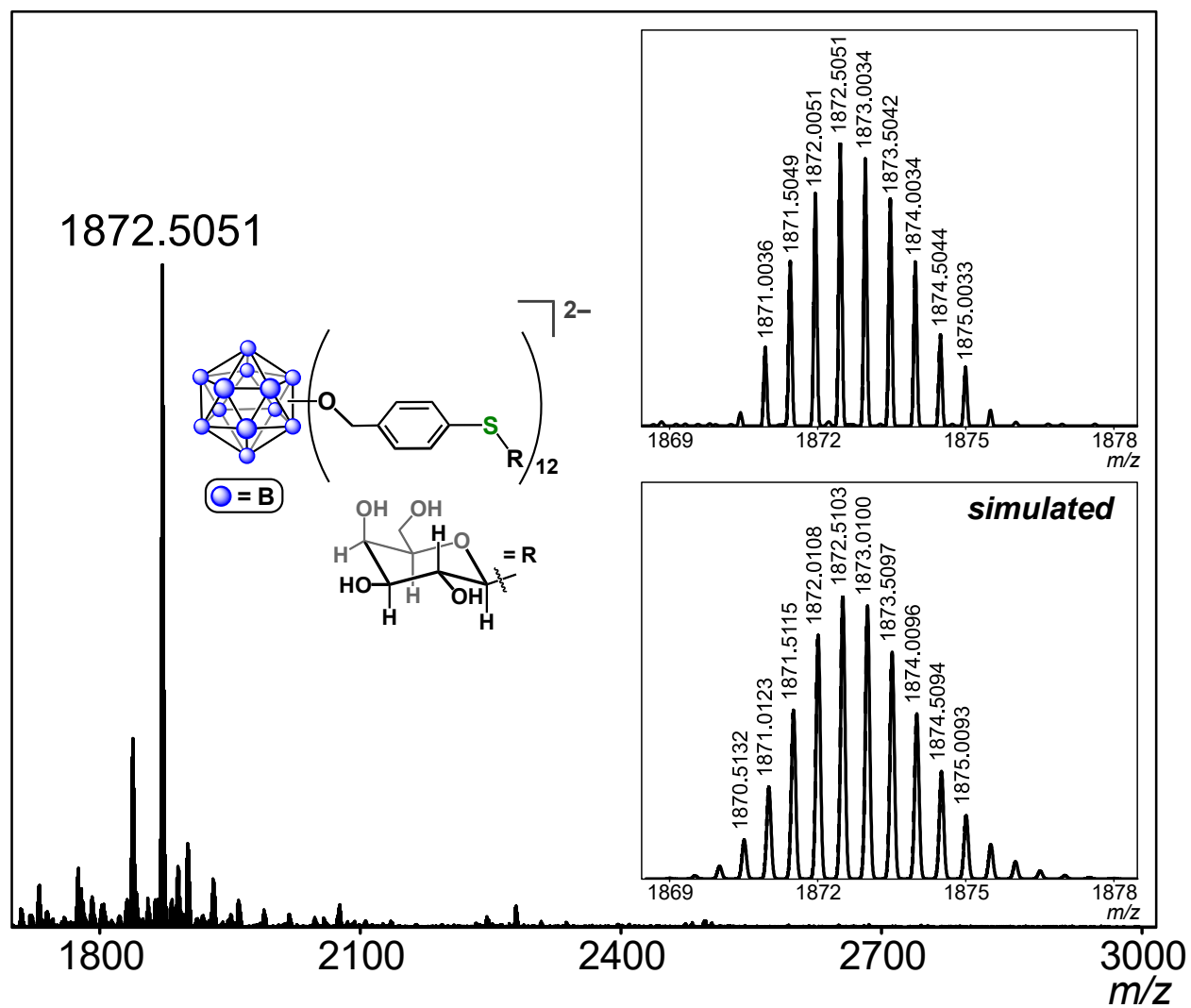
$^{11}\text{B}\{^1\text{H}\}$  NMR spectrum of  $[\text{Na}_2][\text{B}_{12}(\text{OCH}_2\text{C}_6\text{H}_4(1\text{-thio-}\beta\text{-D-galactose}))_{12}]$  ( $\text{D}_2\text{O}$ , 128 MHz, 25  $^\circ\text{C}$ ).



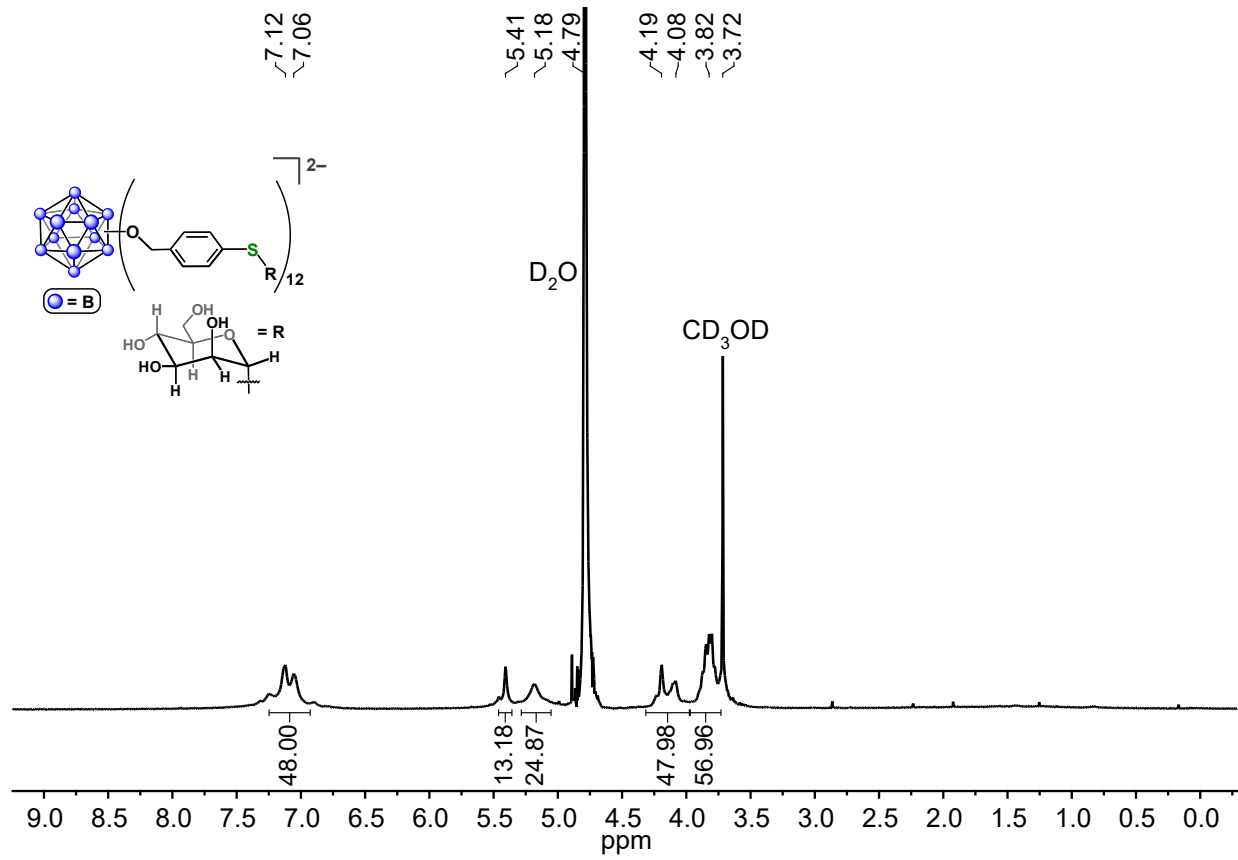
$^1H$  NMR spectrum of  $[Na_2][B_{12}(OCH_2C_6H_4(1-thio-\beta-D-galactose))_{12}]$  (CD<sub>3</sub>OD spiked with D<sub>2</sub>O, 400 MHz, 25 °C).



$^{11}\text{B}\{^1\text{H}\}$  NMR spectrum of  $[\text{Na}_2][\text{B}_{12}(\text{OCH}_2\text{C}_6\text{H}_4(1\text{-thio-}\beta\text{-D-galactose}))_{12}]$  ( $\text{CD}_3\text{OD}$  spiked with  $\text{D}_2\text{O}$ , 128 MHz, 25 °C).

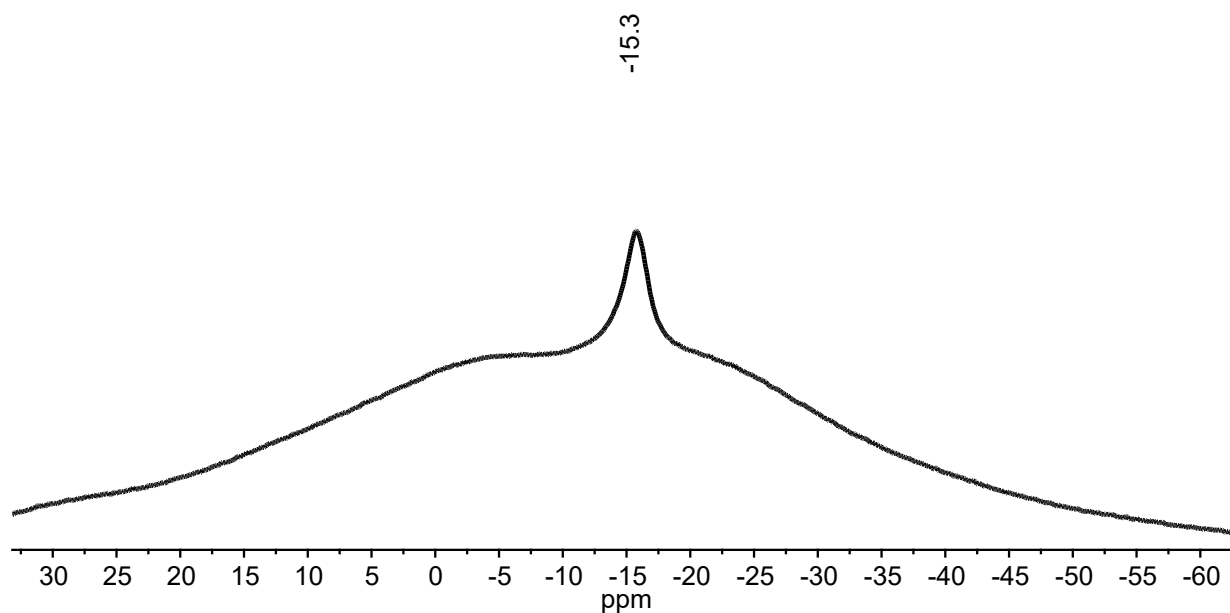


ESI-MS(-) of  $[B_{12}(OCH_2C_6H_4(1\text{-thio-}\beta\text{-D-galactose}))_{12}]^{2-}$  (MeOH, 1.5 kV).

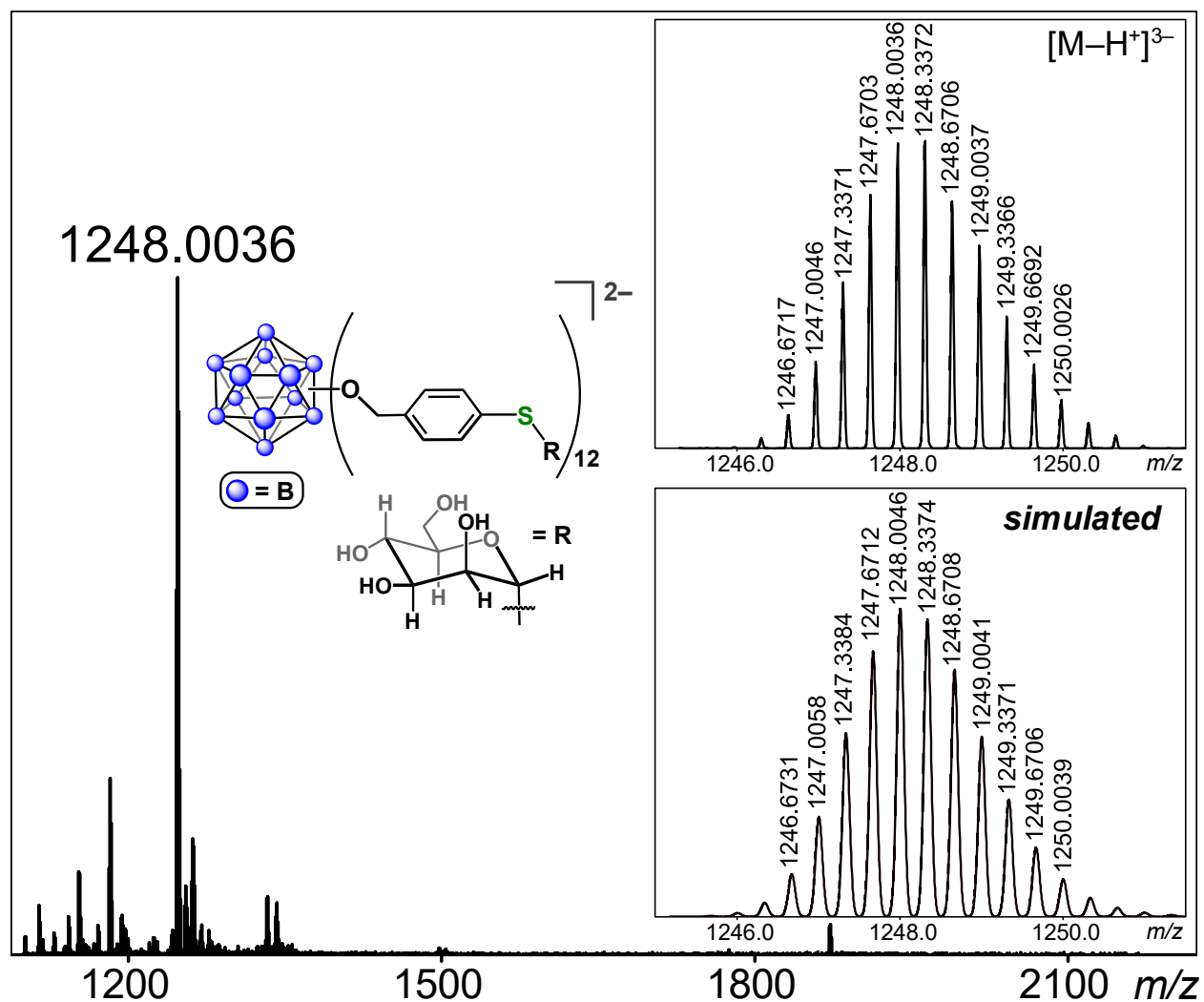


<sup>1</sup>H NMR spectrum of [Na<sub>2</sub>][B<sub>12</sub>(OCH<sub>2</sub>C<sub>6</sub>H<sub>4</sub>(1-thio-β-D-mannose))<sub>12</sub>] (D<sub>2</sub>O spiked with CD<sub>3</sub>OD, 400 MHz, 25 °C).

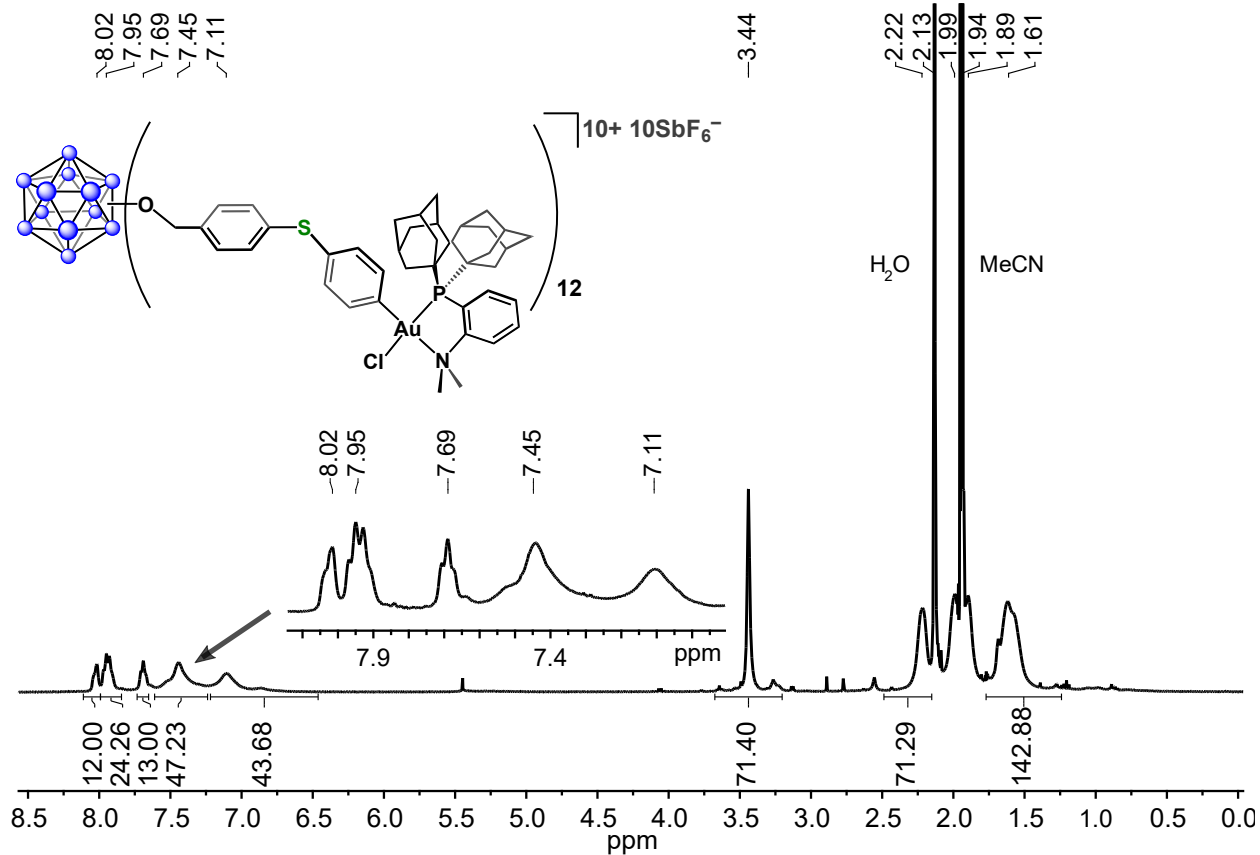




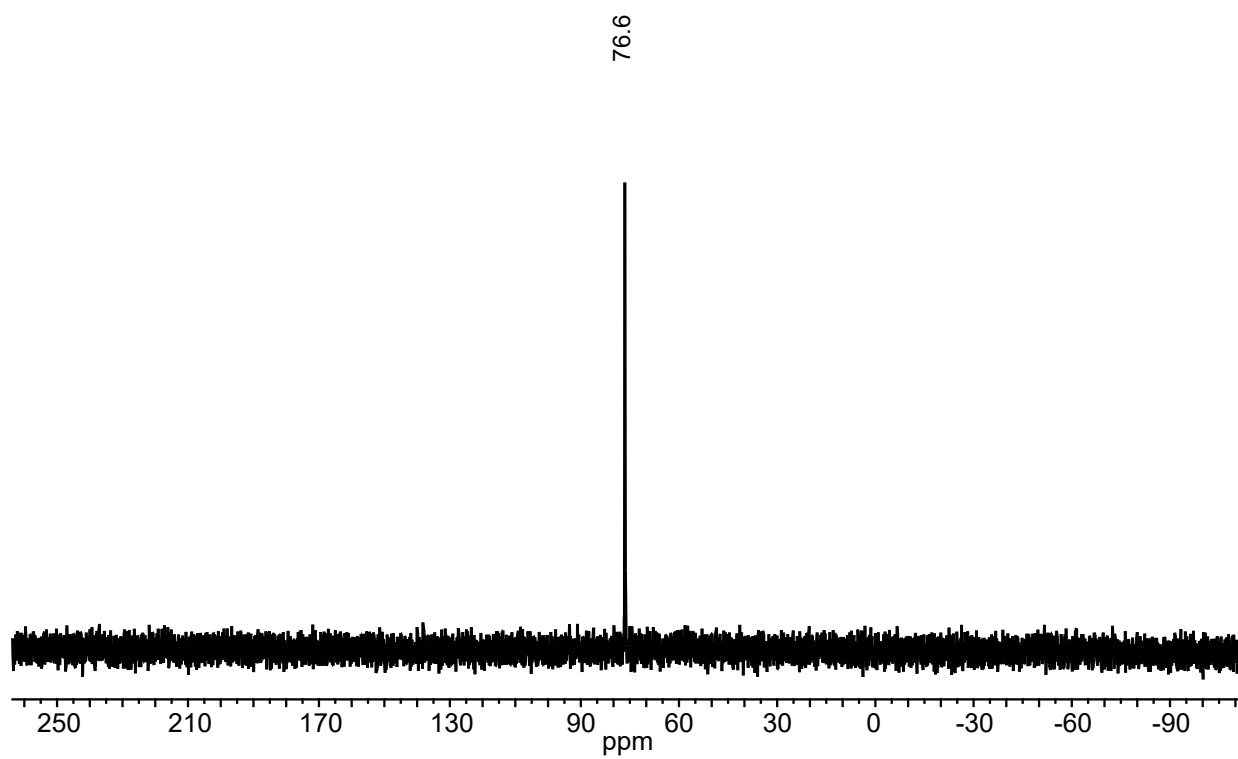
$^{11}\text{B}\{^1\text{H}\}$  NMR spectrum of  $[\text{Na}_2][\text{B}_{12}(\text{OCH}_2\text{C}_6\text{H}_4(1\text{-thio-}\beta\text{-D-mannose}))_{12}]$  ( $\text{D}_2\text{O}$  spiked with  $\text{CD}_3\text{OD}$ , 128 MHz, 25 °C).



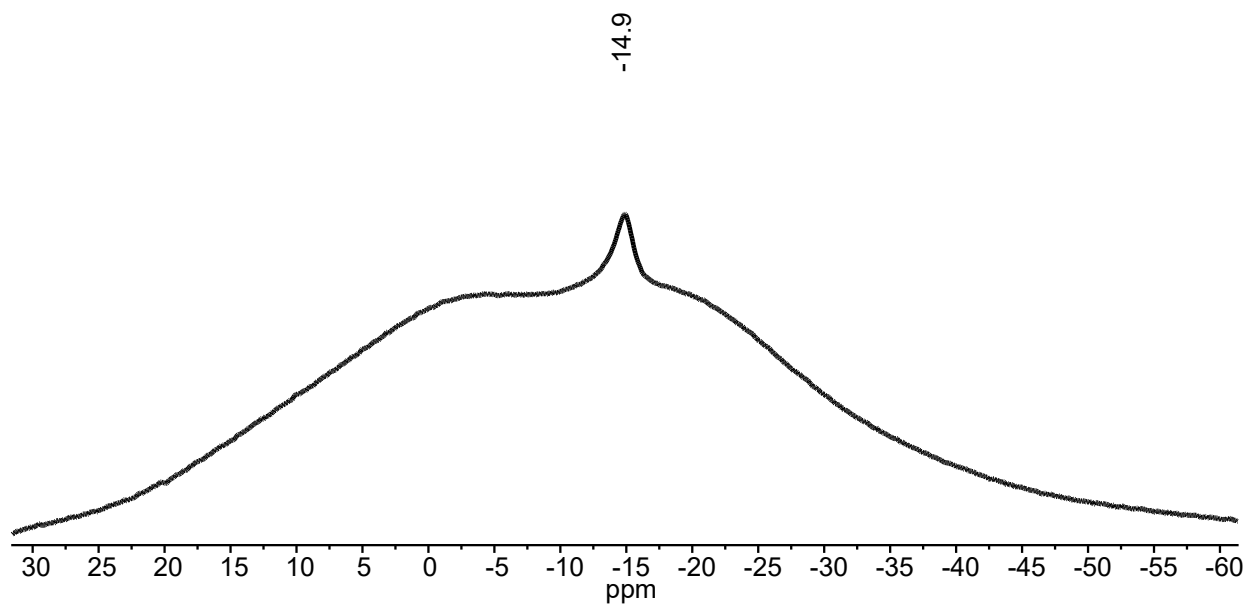
ESI-MS(-) of  $[B_{12}(OCH_2C_6H_4(1\text{-thio-}\alpha\text{-D-mannose}))_{12}]^{2-}$  (MeOH, 1.5 kV). The monodeprotonated species,  $[B_{12}(OCH_2C_6H_4(1\text{-thio-}\alpha\text{-D-mannose}))_{12} - H^+]^{3-}$ , is observed under ESI-MS conditions.



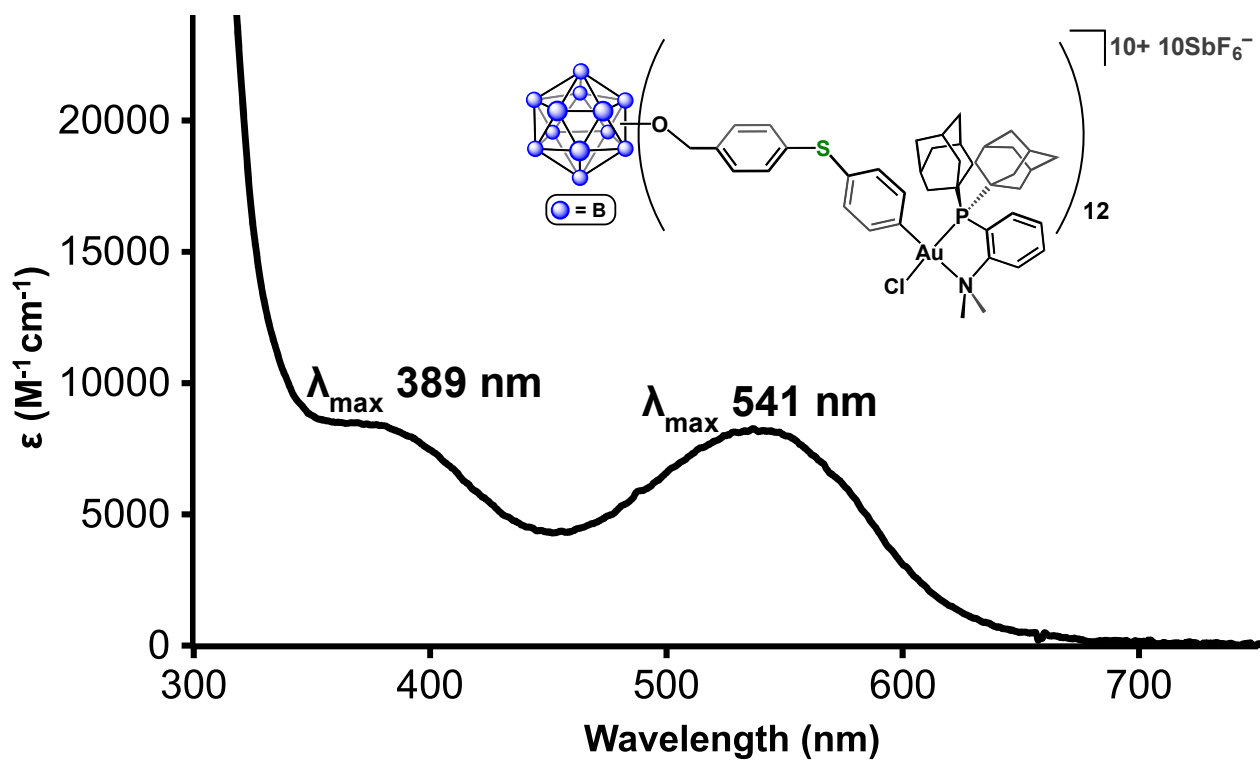
$^1\text{H}$  NMR spectrum of  $[\text{B}_{12}(\text{OCH}_2\text{C}_6\text{H}_4\text{SC}_6\text{H}_4(\text{Me-DalPhos})\text{AuCl})_{12}][\text{SbF}_6]_{10}$  ( $\text{CD}_3\text{CN}$ , 400 MHz, 25 °C).



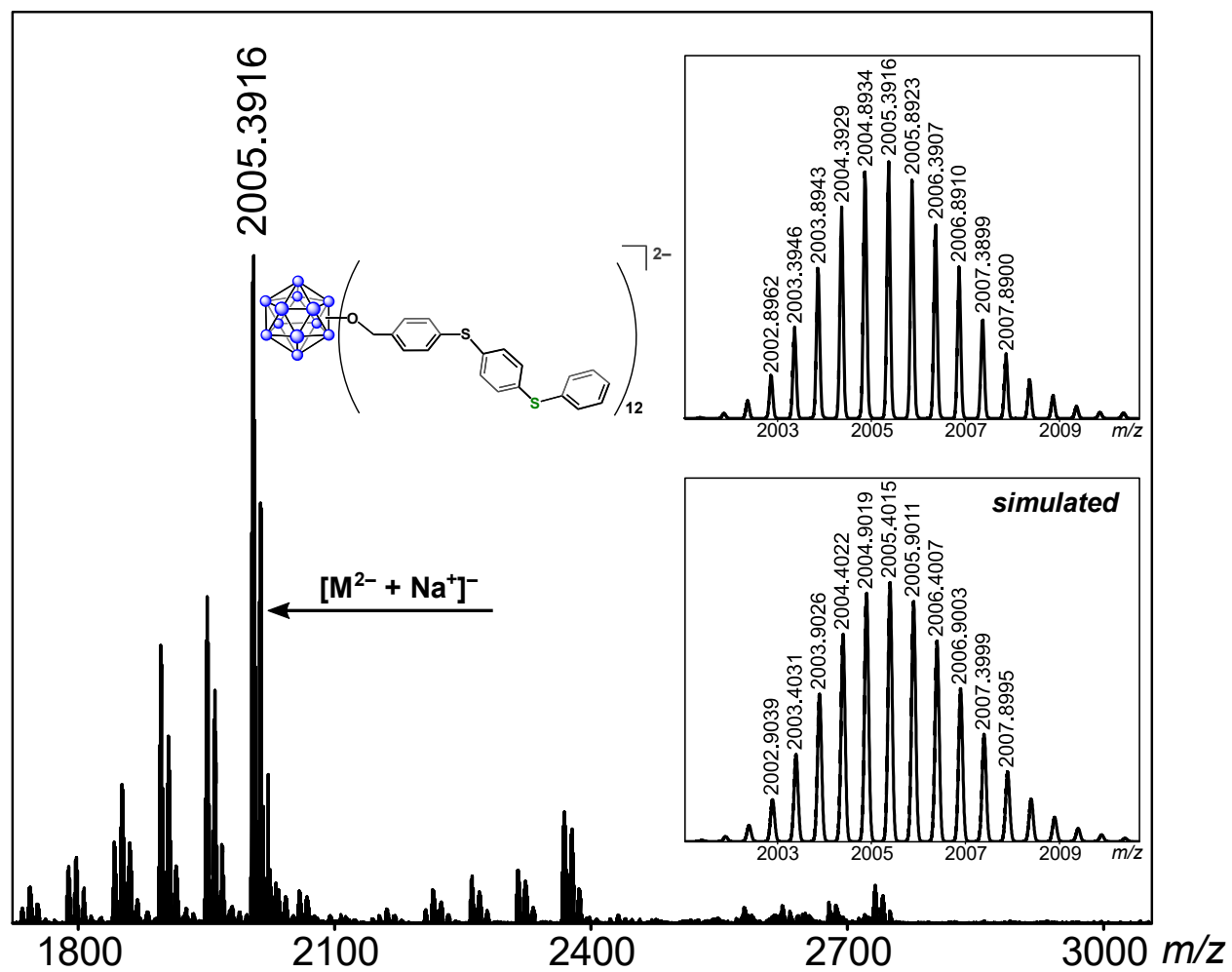
$^{31}\text{P}\{^1\text{H}\}$  NMR spectrum of  $[\text{B}_{12}(\text{OCH}_2\text{C}_6\text{H}_4\text{SC}_6\text{H}_4(\text{Me-DalPhos})\text{AuCl})_{12}][\text{SbF}_6]_{10}$  ( $\text{CD}_3\text{CN}$ , 162 MHz, 25 °C).



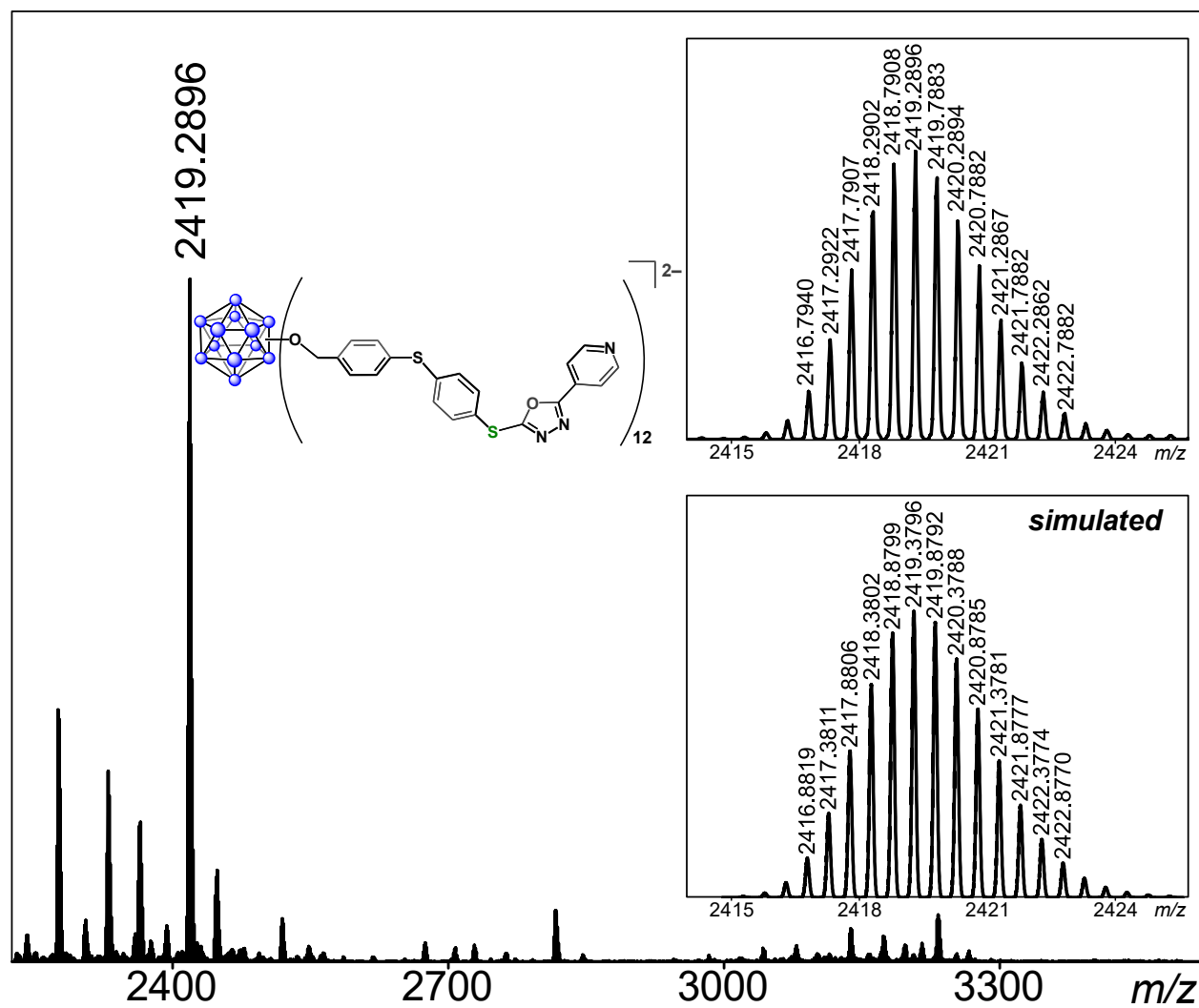
$^{11}\text{B}\{^1\text{H}\}$  NMR spectrum of  $[\text{B}_{12}(\text{OCH}_2\text{C}_6\text{H}_4\text{SC}_6\text{H}_4(\text{Me-DalPhos})\text{AuCl})_{12}][\text{SbF}_6]_{10}$  ( $\text{CD}_3\text{CN}$ , 128 MHz, 25 °C).



UV-vis spectrum of  $[B_{12}(OCH_2C_6H_4SC_6H_4(Me-DalPhos)AuCl)_{12}][SbF_6]_{10}$  (MeCN, 0.06 mM, 25 °C).

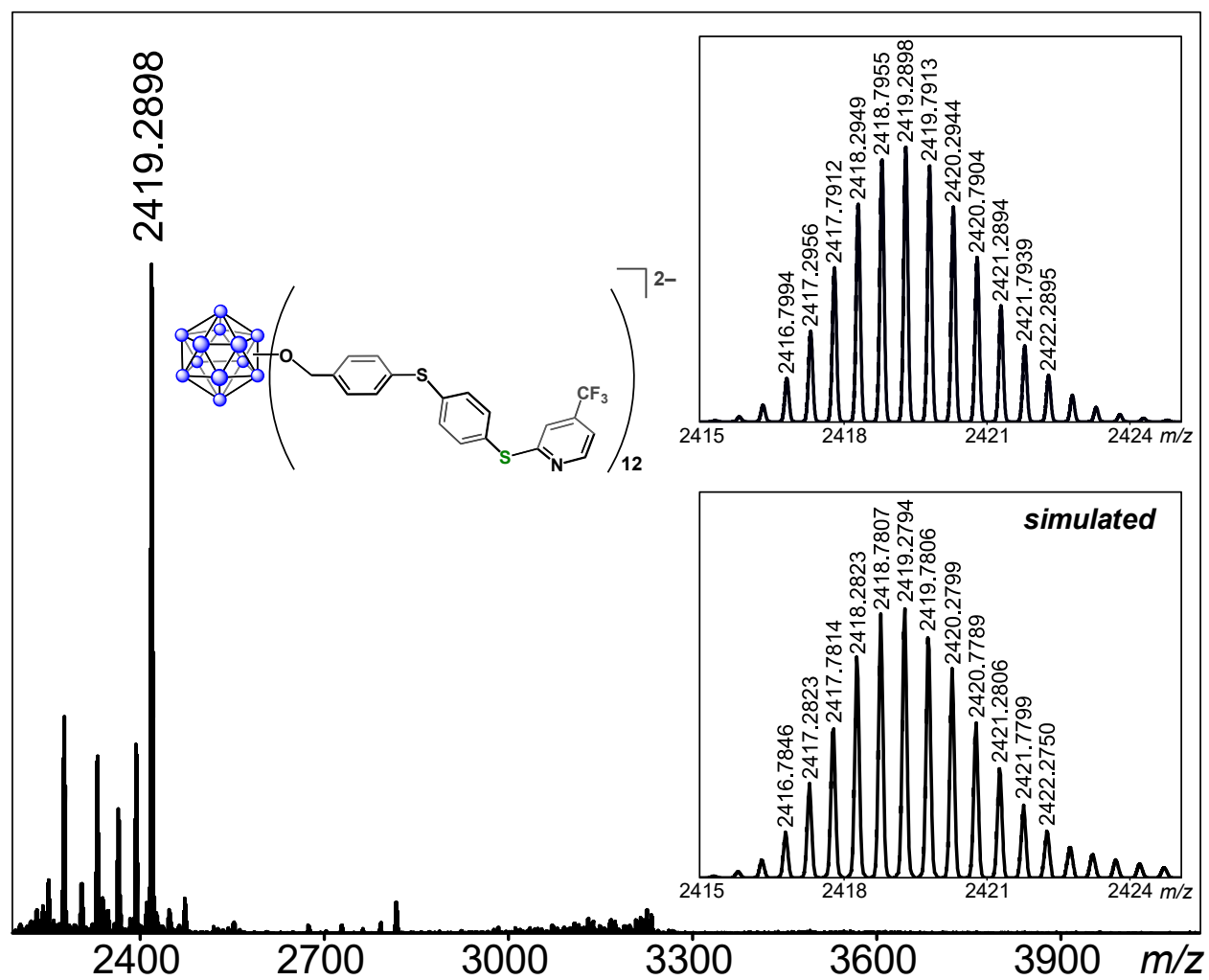


ESI-MS(-) of  $[B_{12}(OCH_2C_6H_4SC_6H_4SPh)_{12}]^{2-}$  (MeCN, 1.5 kV).

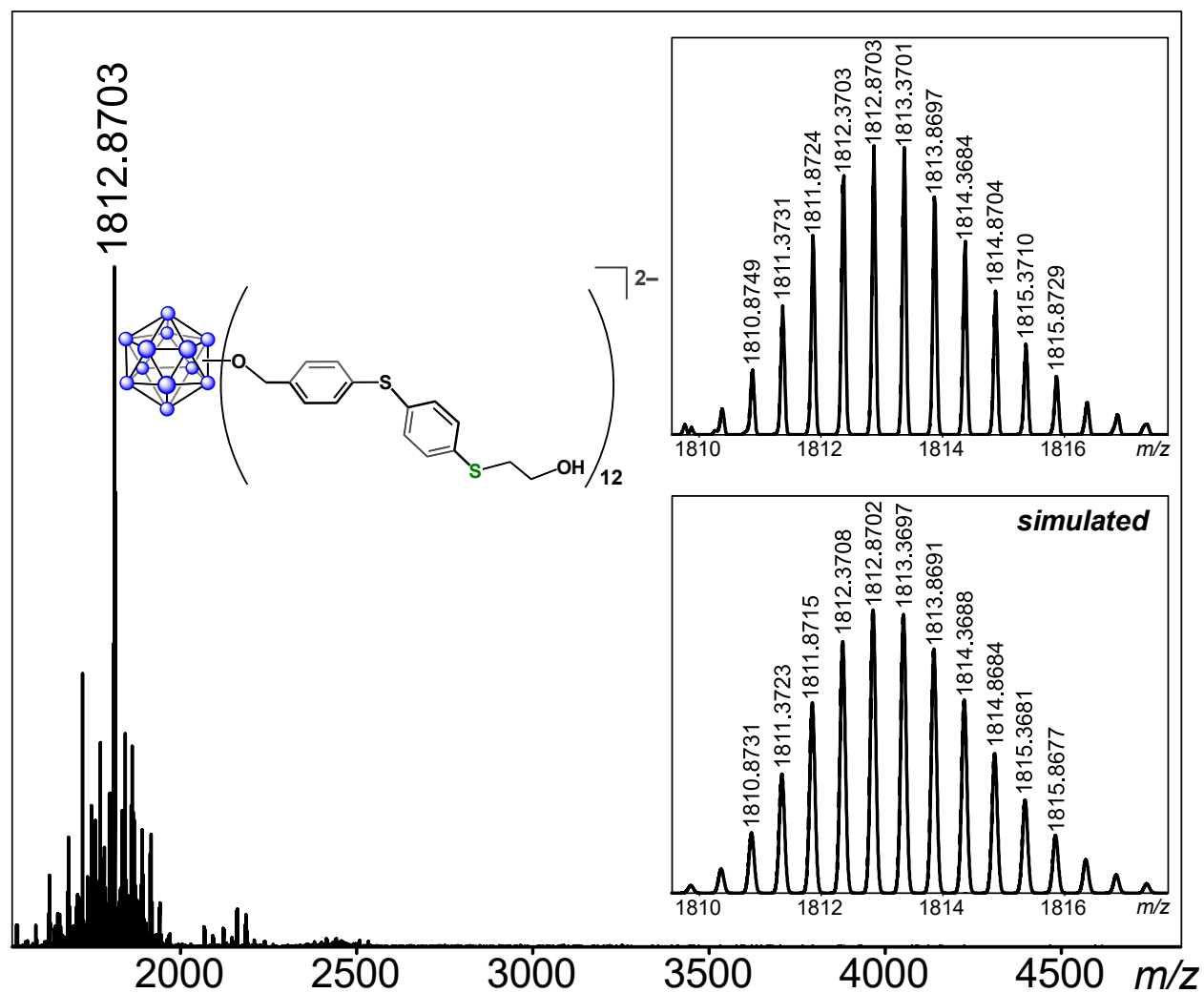


ESI-MS(-) of  $[B_{12}(OCH_2C_6H_4SC_6H_4(5-(4\text{-pyridyl})\text{-oxadiazole-2-thiol}))_{12}]^{2-}$  (MeCN, 1.5 kV).

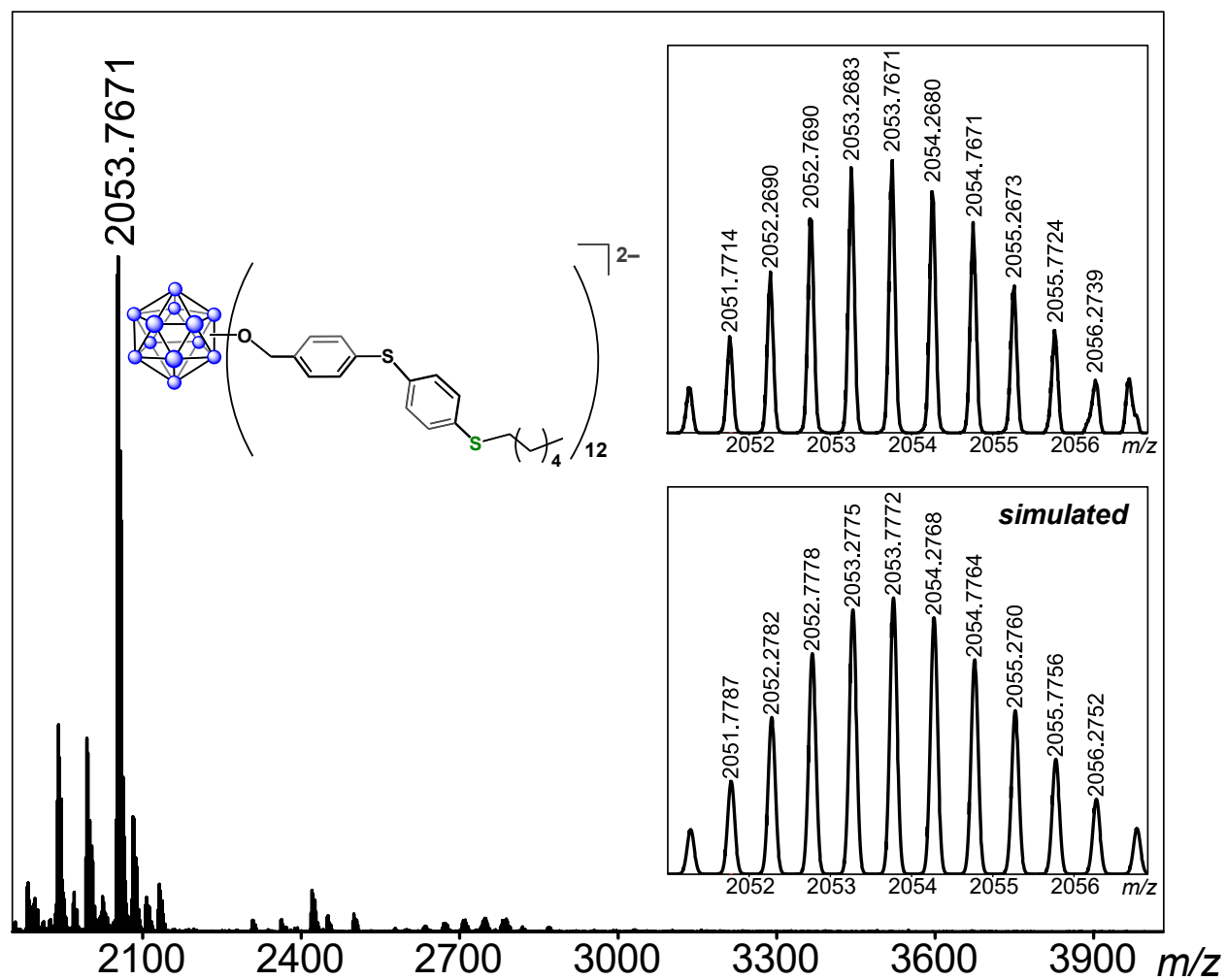




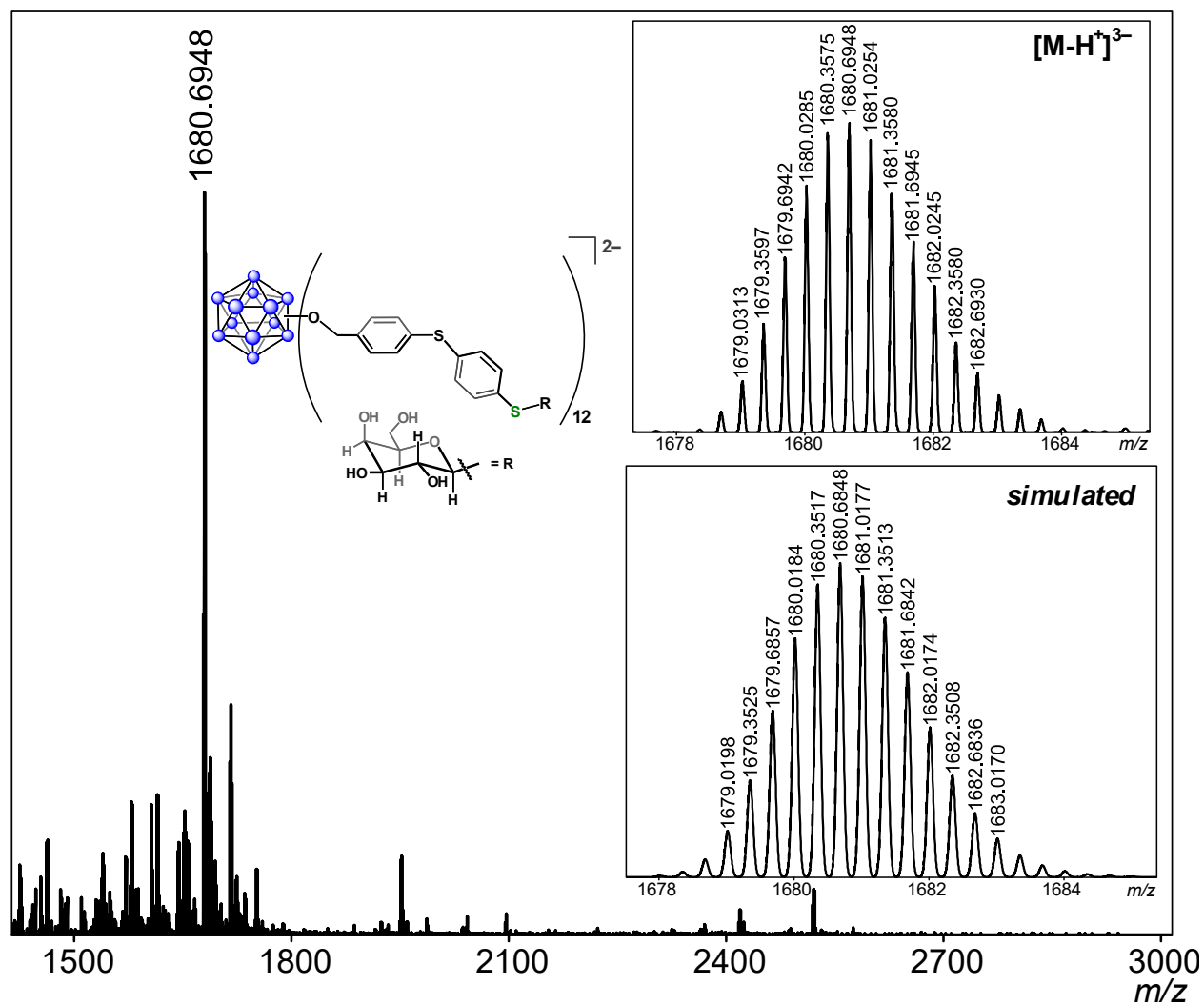
ESI-MS(-) of  $[B_{12}(OCH_2C_6H_4SC_6H_4(2\text{-thio-5-trifluoromethylpyridine}))_{12}]^{2-}$  (MeCN, 1.5 kV).



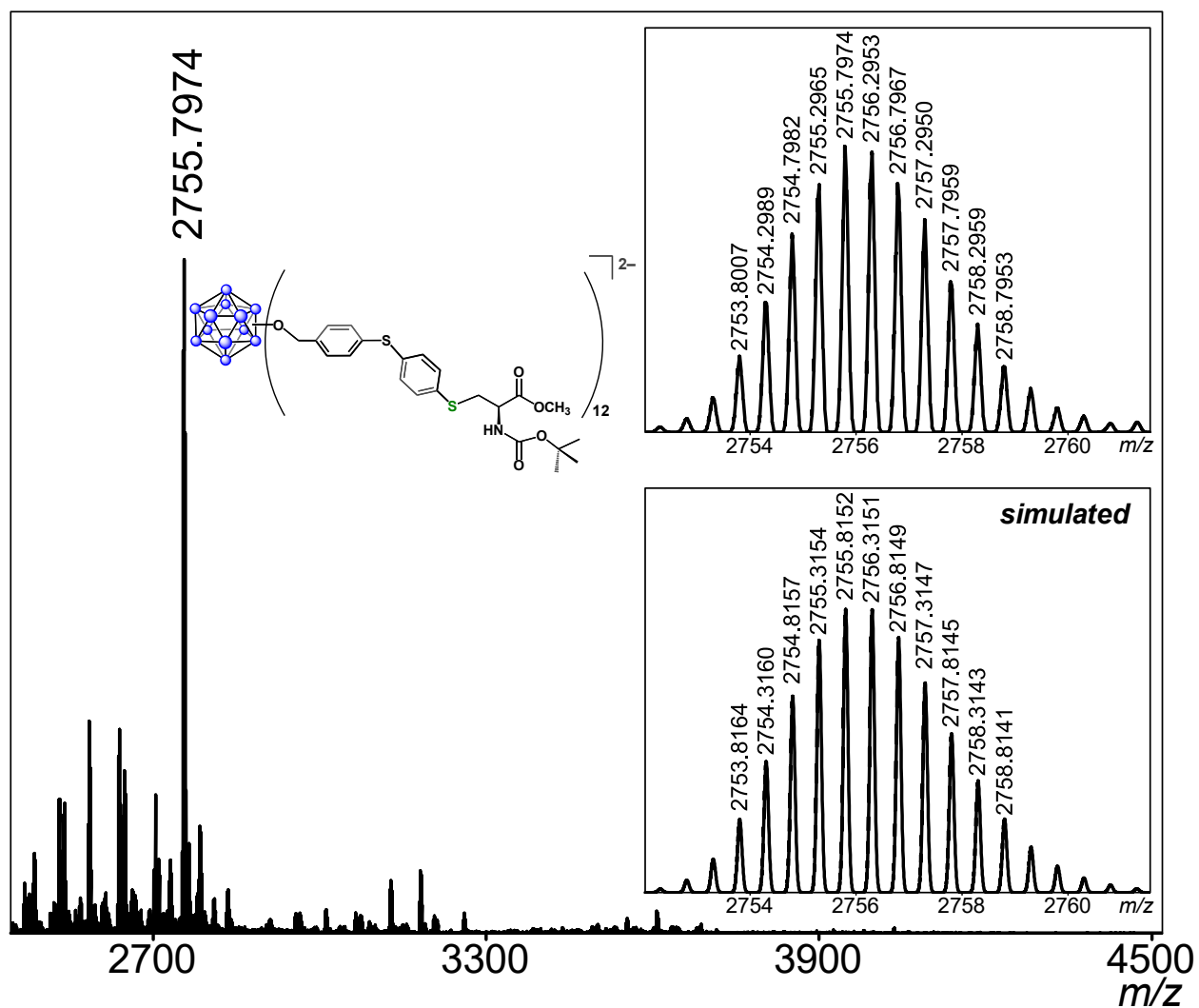
ESI-MS(-) of  $[B_{12}(OCH_2C_6H_4SC_6H_4(2\text{-mercaptoethanol}))_{12}]^{2-}$  (MeCN, 1.5 kV).



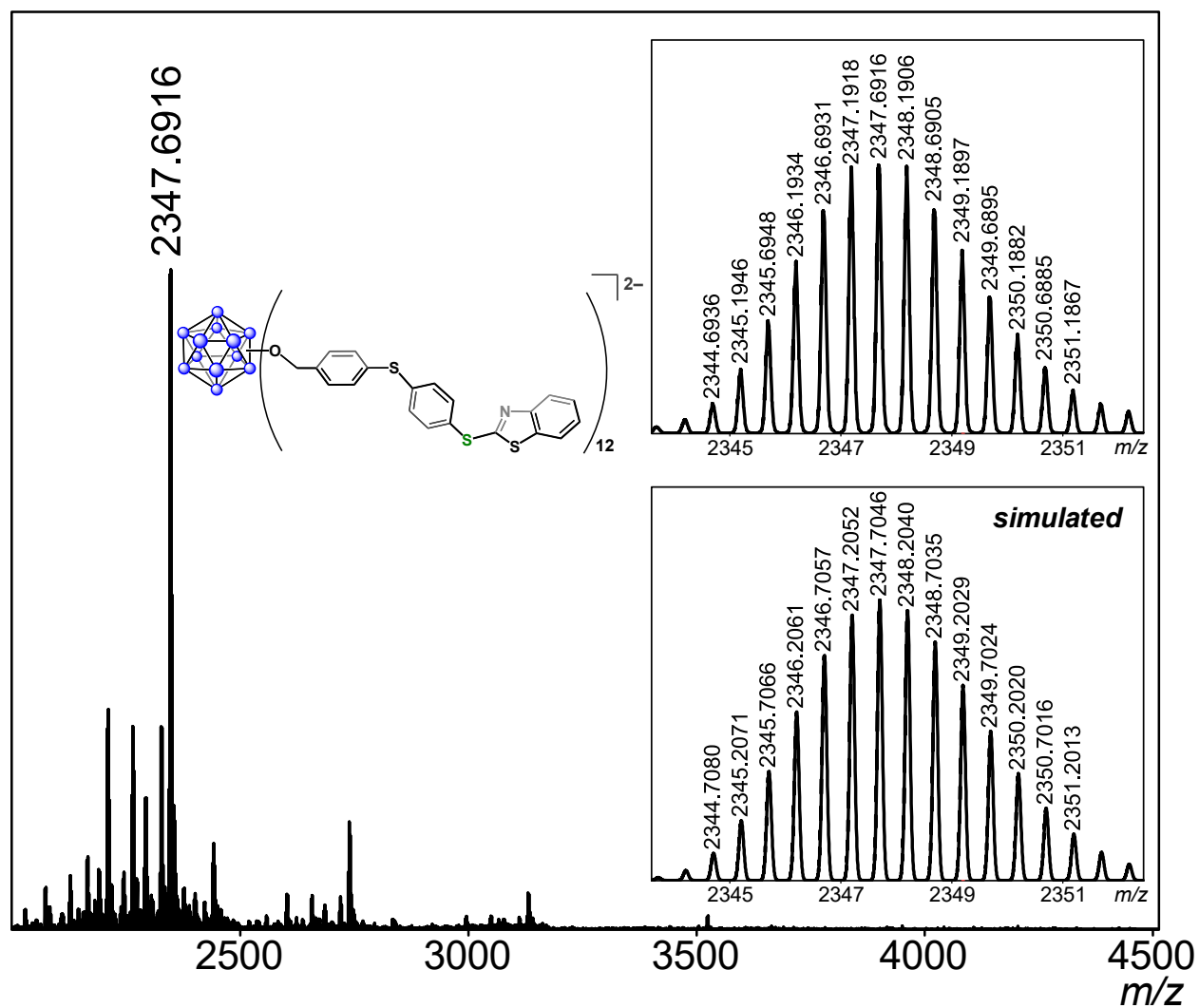
ESI-MS(-) of  $[B_{12}(OCH_2C_6H_4SC_6H_4S(CH_2)_5CH_3)_{12}]^{2-}$  (MeCN, 1.5 kV).



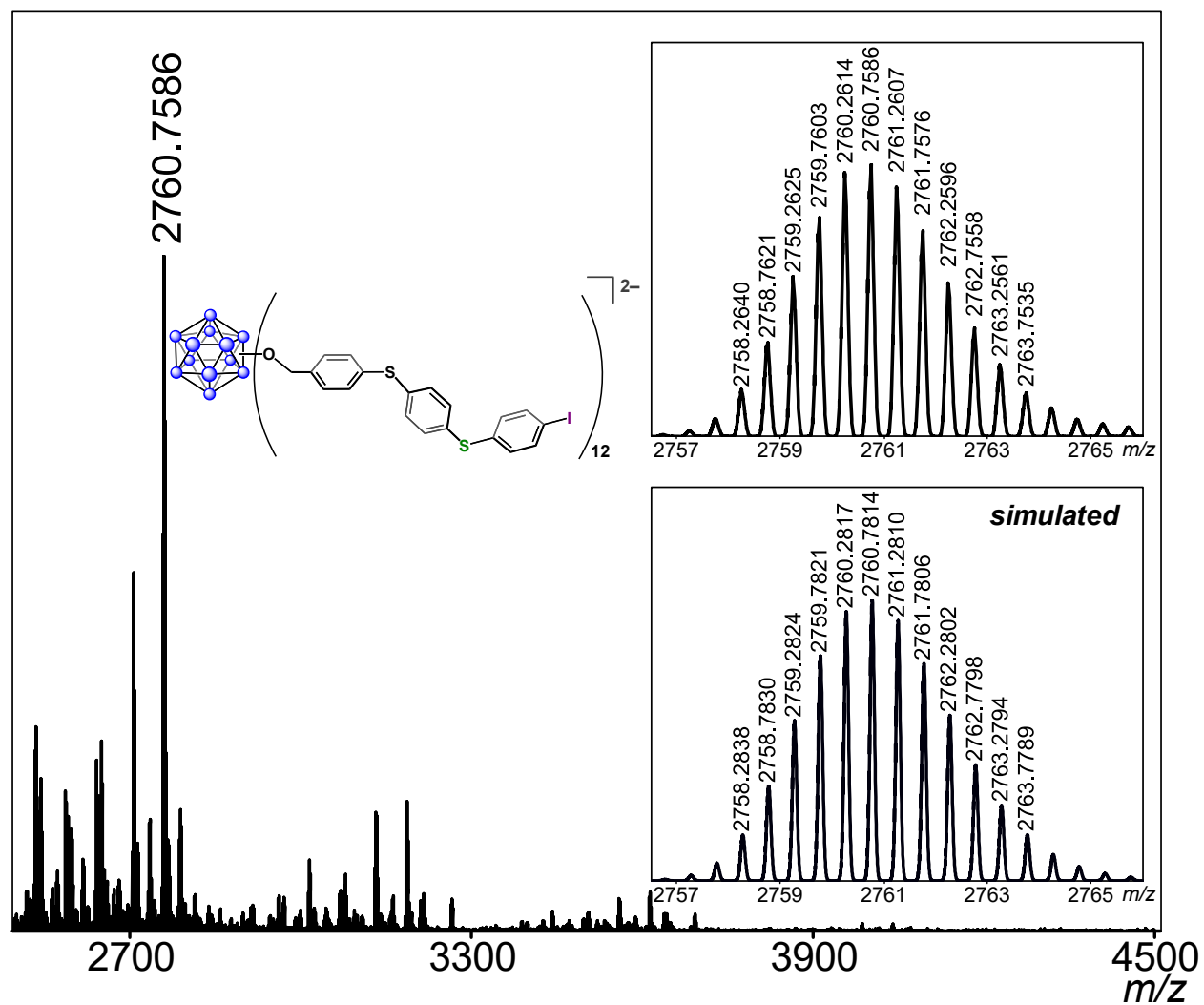
ESI-MS(-) of  $[B_{12}(OCH_2C_6H_4SC_6H_4(1\text{-thio-}\beta\text{-D-galactose}))_{12}]^{2-}$  (MeOH, 1.5 kV). The monodeprotonated, trianionic species,  $[M^{2-}-H^+]^{3-}$ , is observed under ESI-MS conditions.



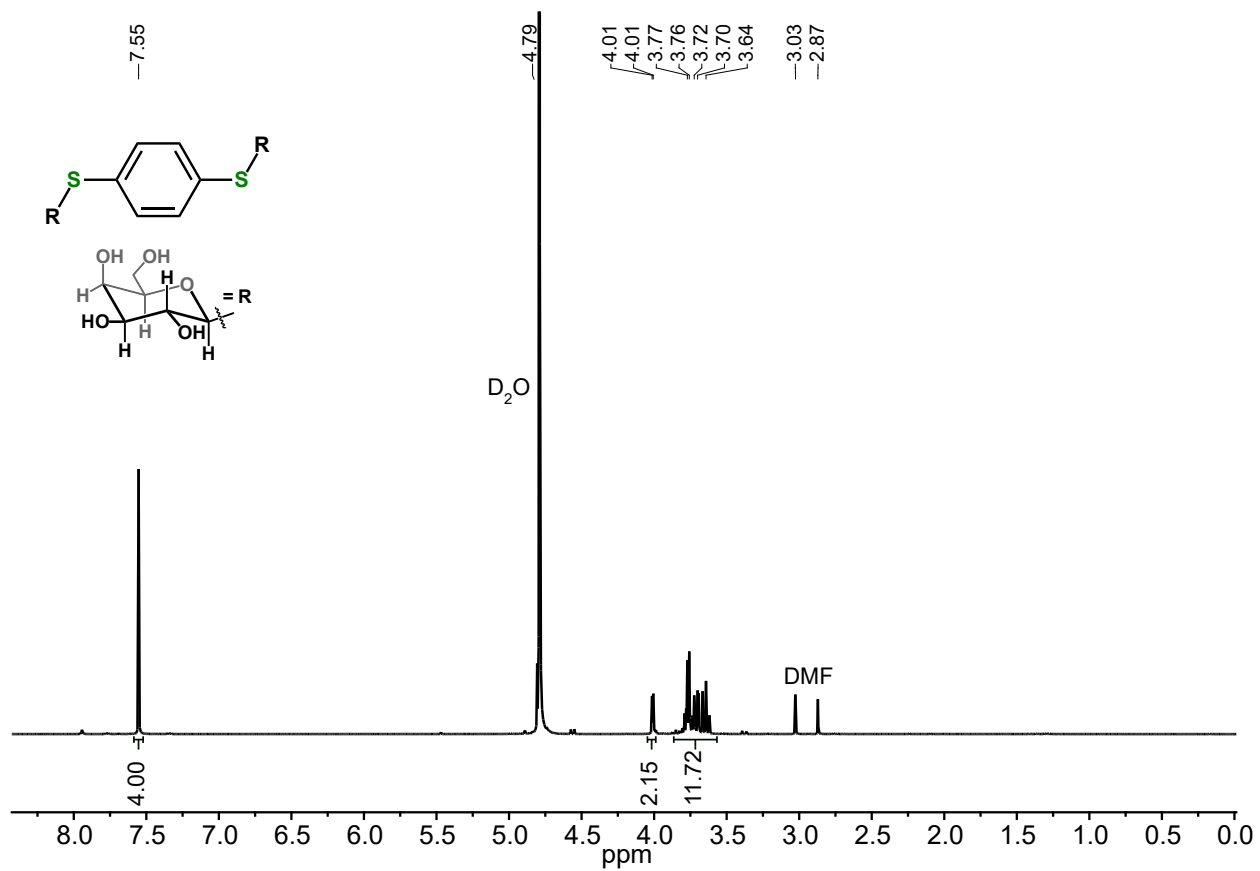
ESI-MS(-) of  $[B_{12}(OCH_2C_6H_4SC_6H_4(N-(tert-butoxycarbonyl)-L-cysteine\ methyl\ ester))_{12}]^{2-}$  (MeCN, 1.5 kV).



ESI-MS(-) of  $[B_{12}(OCH_2C_6H_4SC_6H_4(2\text{-mercaptobenzothiazole}))_{12}]^{2-}$  (MeCN, 1.5 kV).

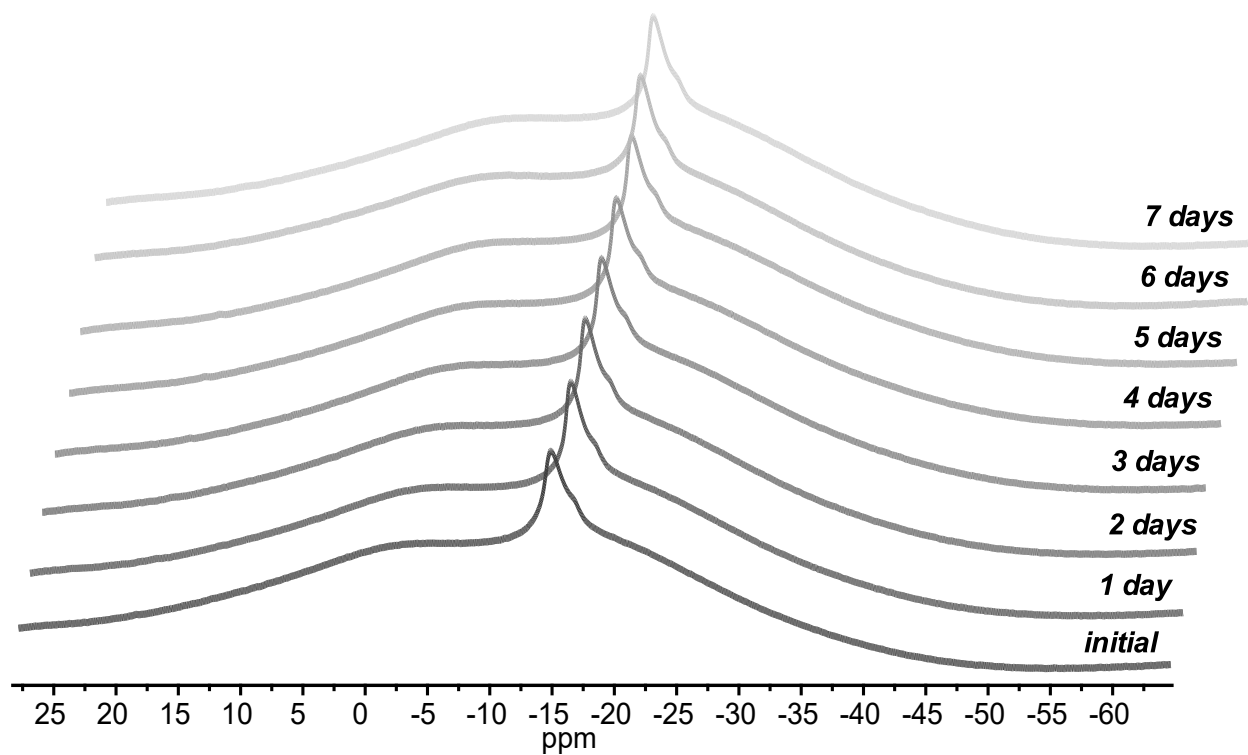


ESI-MS(-) of  $[B_{12}(OCH_2C_6H_4SC_6H_4SC_6H_4I)_{12}]^{2-}$  (MeCN, 1.5 kV).

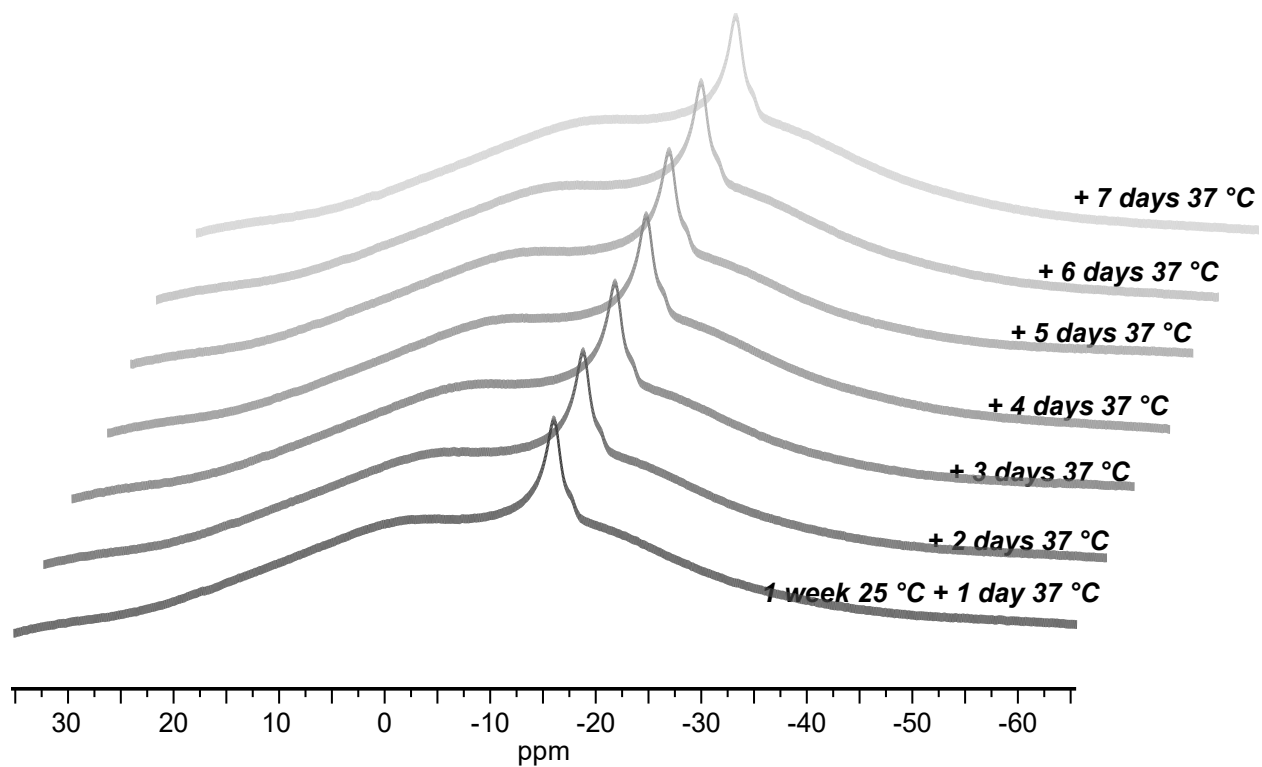


<sup>1</sup>H NMR spectrum of (1-thio-β-D-galactose)<sub>2</sub>C<sub>6</sub>H<sub>4</sub> (D<sub>2</sub>O, 400 MHz, 25 °C).

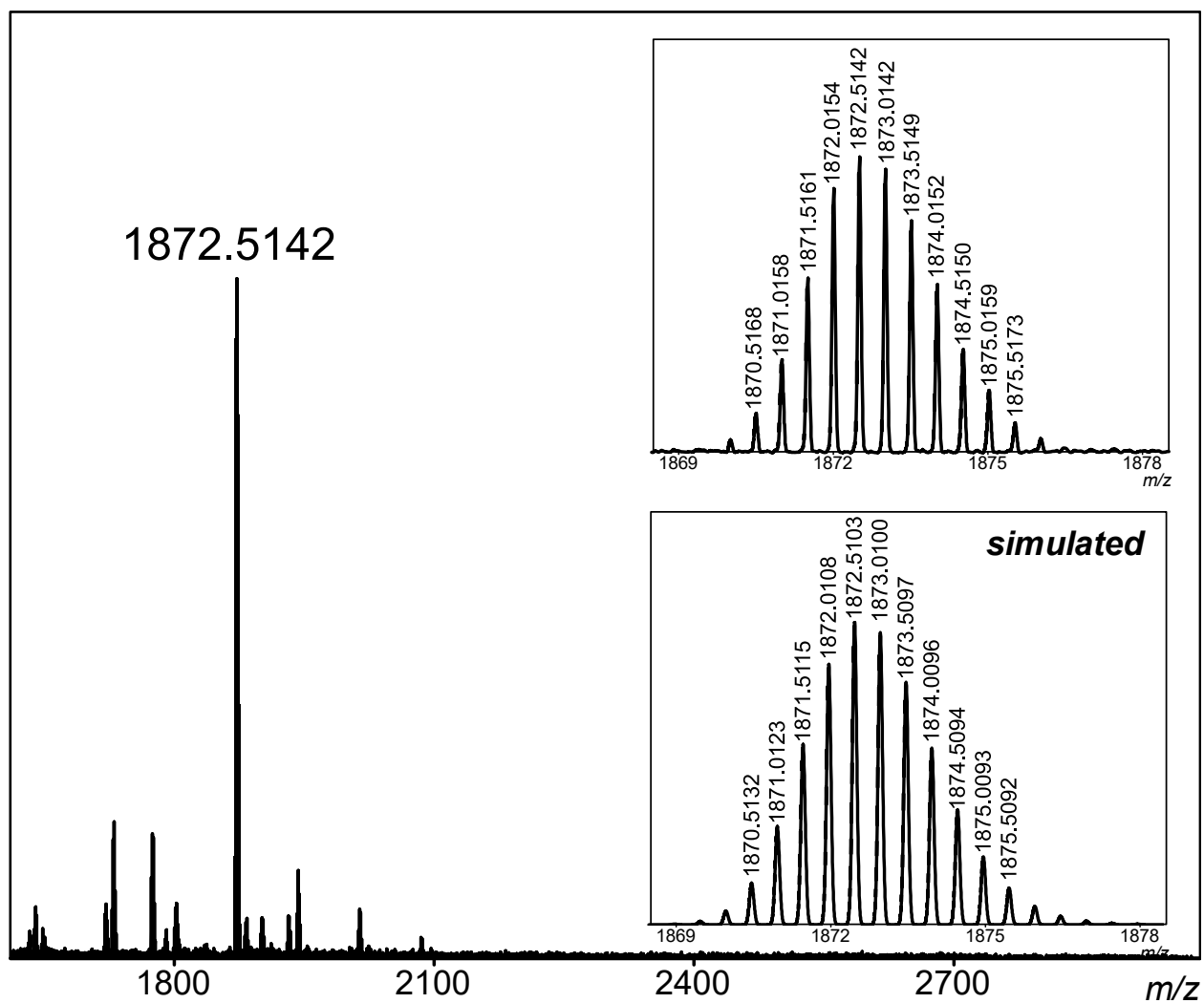




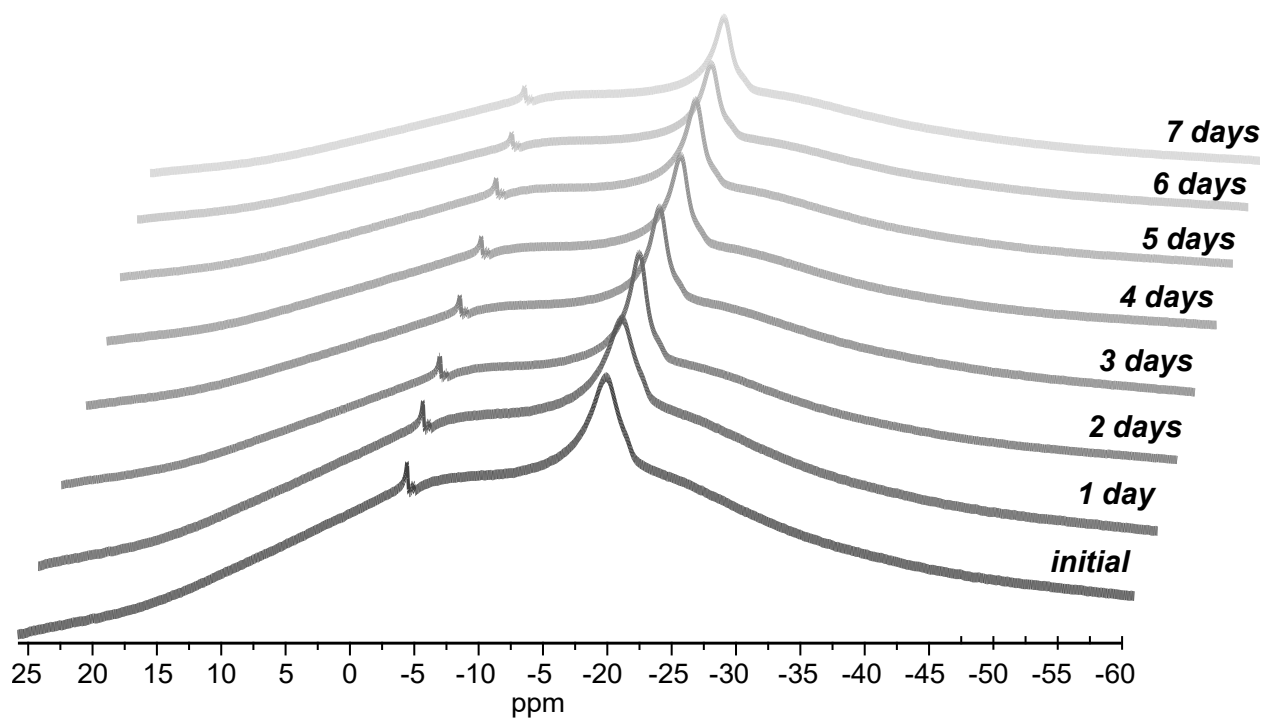
$^{11}\text{B}\{^1\text{H}\}$  NMR spectra of  $[\text{Na}_2][\text{B}_{12}(\text{OCH}_2\text{C}_6\text{H}_4(1\text{-thio-}\beta\text{-D-glucose}))_{12}]$  collected throughout the course of 7 days at 25 °C in fetal bovine serum cell culture medium (128 MHz, 25 °C).



$^{11}\text{B}\{^1\text{H}\}$  NMR spectra of  $[\text{Na}_2][\text{B}_{12}(\text{OCH}_2\text{C}_6\text{H}_4(1\text{-thio-}\beta\text{-D-glucose}))_{12}]$  collected throughout the course of an additional 7 days at 37 °C in fetal bovine serum cell culture medium (128 MHz, 25 °C).



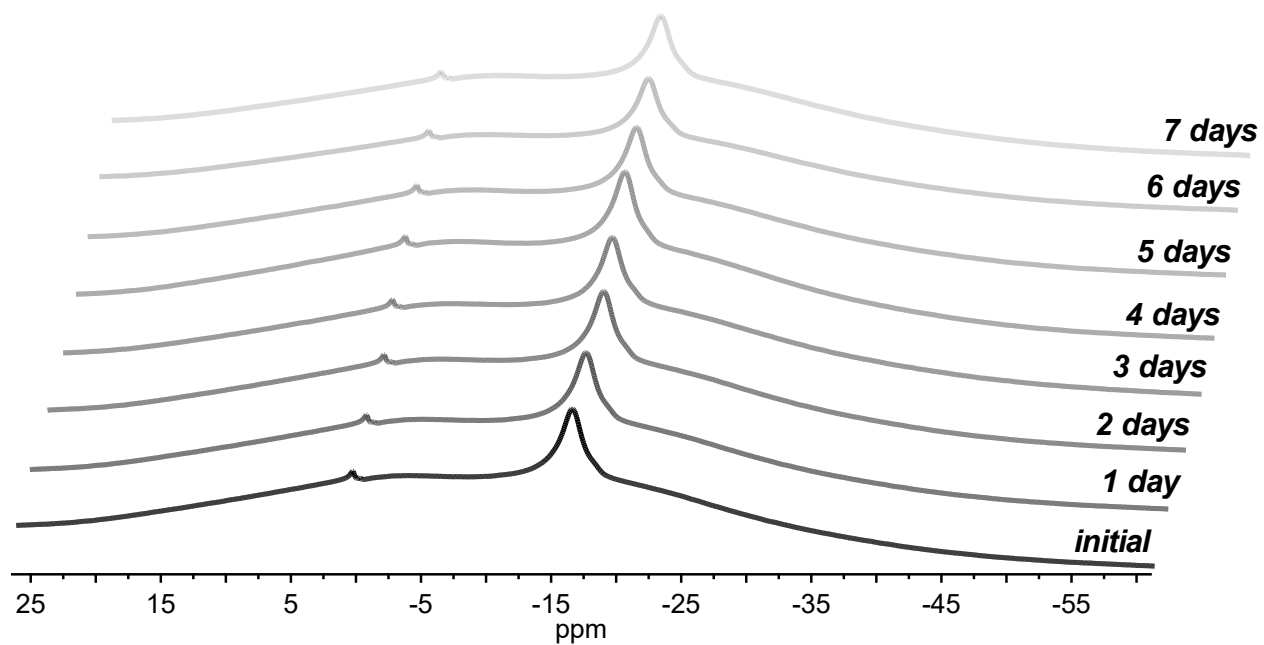
ESI-MS(-) of  $[\text{Na}_2][\text{B}_{12}(\text{OCH}_2\text{C}_6\text{H}_4(1\text{-thio-}\beta\text{-D-glucose}))_{12}]$  collected after 14 days in fetal bovine serum cell culture medium (sample diluted with MeOH, 1.5 kV).



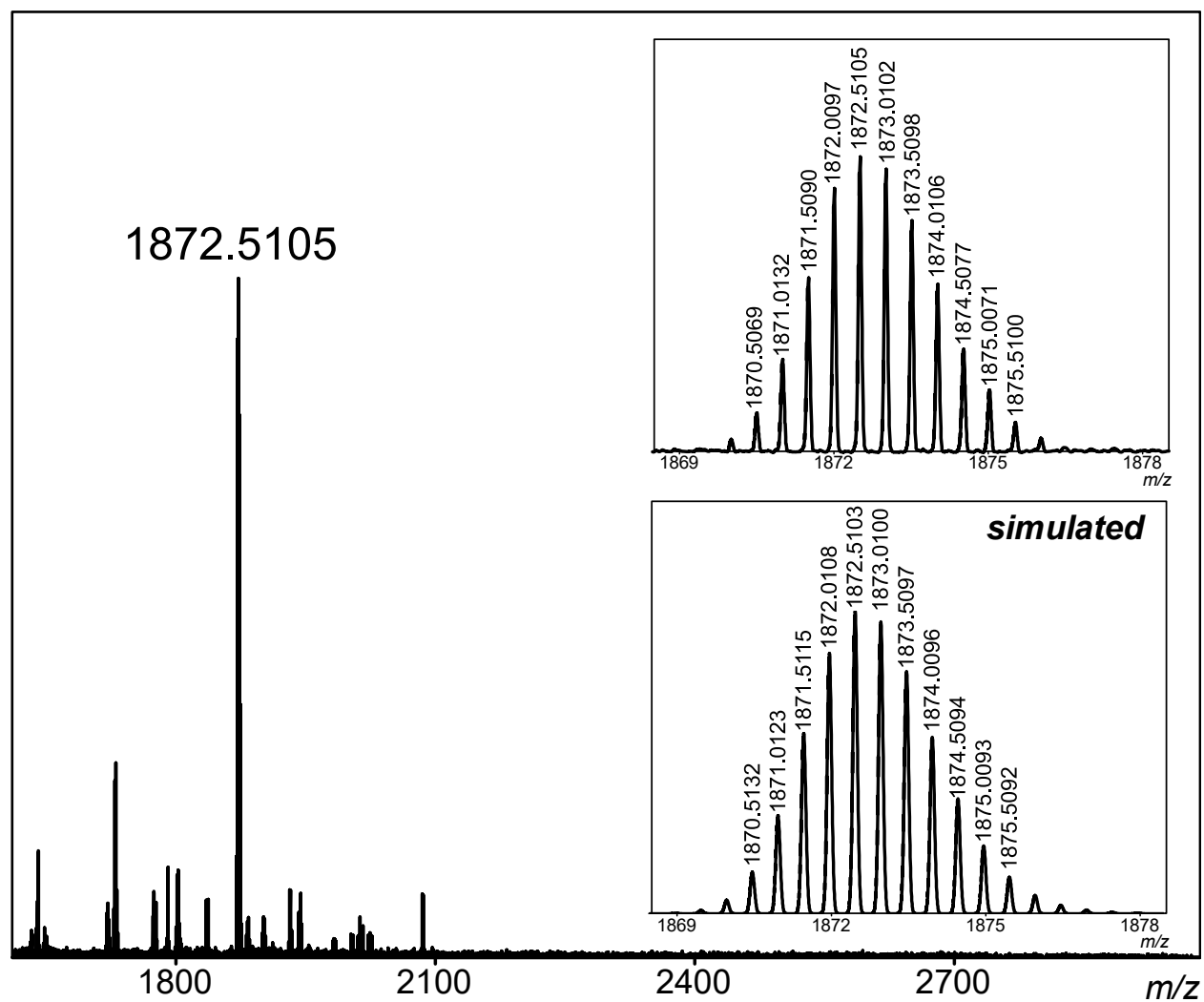
$^{11}\text{B}\{^1\text{H}\}$  NMR spectra of  $[\text{Na}_2][\text{B}_{12}(\text{OCH}_2\text{C}_6\text{H}_4(1\text{-thio-}\beta\text{-D-glucose}))_{12}]$  collected throughout the course of 7 days at 25 °C in an aqueous solution of TRIS buffer (pH 10) (128 MHz, 25 °C).



ESI-MS(-) of  $[\text{Na}_2][\text{B}_{12}(\text{OCH}_2\text{C}_6\text{H}_4(1\text{-thio-}\beta\text{-D-glucose}))_{12}]$  collected after 7 days at 25 °C in an aqueous solution of TRIS buffer (pH 10) (sample diluted with MeOH, 1.5 kV).



$^{11}\text{B}\{^1\text{H}\}$  NMR spectra of  $[\text{Na}_2][\text{B}_{12}(\text{OCH}_2\text{C}_6\text{H}_4(1\text{-thio-}\beta\text{-D-glucose}))_{12}]$  collected throughout the course of 7 days at 25 °C in an aqueous solution of acetate buffer (pH 5) (128 MHz, 25 °C).



ESI-MS(-) of  $[\text{Na}_2][\text{B}_{12}(\text{OCH}_2\text{C}_6\text{H}_4(1\text{-thio-}\beta\text{-D-glucose}))_{12}]$  collected after 7 days at 25 °C in an aqueous solution of acetate buffer (pH 5) (sample diluted with MeOH, 1.5 kV).

## A Cluster-based Approach for Peptide Macrocyclization

We hypothesized that the previously described cluster scaffolds could serve as robust and well-defined 3D building blocks for assembling complex, abiotic peptidic architectures. To test our hypothesis, we investigated the macrocyclization of unprotected multi-cysteine peptides by pentafluoroaryl-perfunctionalized dodecaborate clusters *via* perfluoroaryl-thiol S<sub>N</sub>Ar chemistry.<sup>6,82,89</sup>

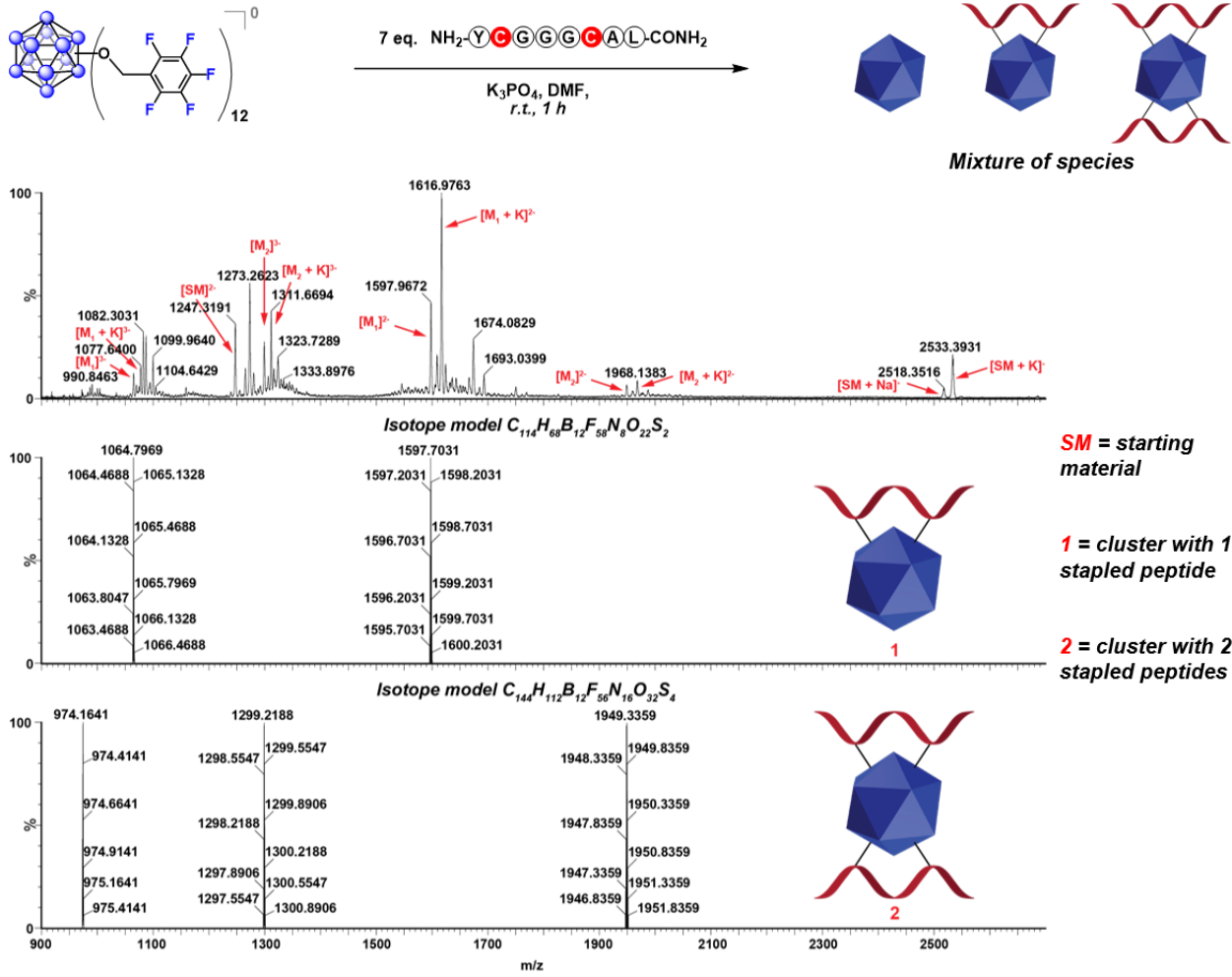
First, we treated a small pentafluoroaryl cluster<sup>6,82</sup> with a di-cysteine ( $i, i + 4$ ) peptide under mild reaction conditions,<sup>89</sup> and observed conversion to a mixture of starting material and clusters grafted with 1–2 cyclized peptides, as suggested by ESI-MS and <sup>19</sup>F NMR spectroscopy. Next, we prepared a series of tri-cysteine peptides with varied spacing between the cysteine residues ( $i, i + 2$ ,  $i, i + 3$ , and  $i, i + 4$ ) for cluster conjugation reactions, which also resulted in conversion to a mixture of starting material and clusters with 1–2 cyclized peptides. Following these conjugation experiments, we investigated several separation strategies to potentially isolate the different species in the reaction mixtures, and we have determined that size exclusion chromatography may be a promising approach.

Subsequently, we moved to test whether an extended pentafluoroaryl cluster could accommodate the installation of a higher number of cyclized peptides, due to its more favorable sterics and enhanced S<sub>N</sub>Ar reactivity toward thiols.<sup>6</sup> After treating the extended cluster with several previously prepared multi-cysteine peptides under similar reaction conditions, we observed the major product to be a fully functionalized cluster grafted with four tri-cysteine peptides, as suggested by the presence of a single major species in the ESI-MS and a nearly quantitative conversion in the <sup>19</sup>F NMR spectra.

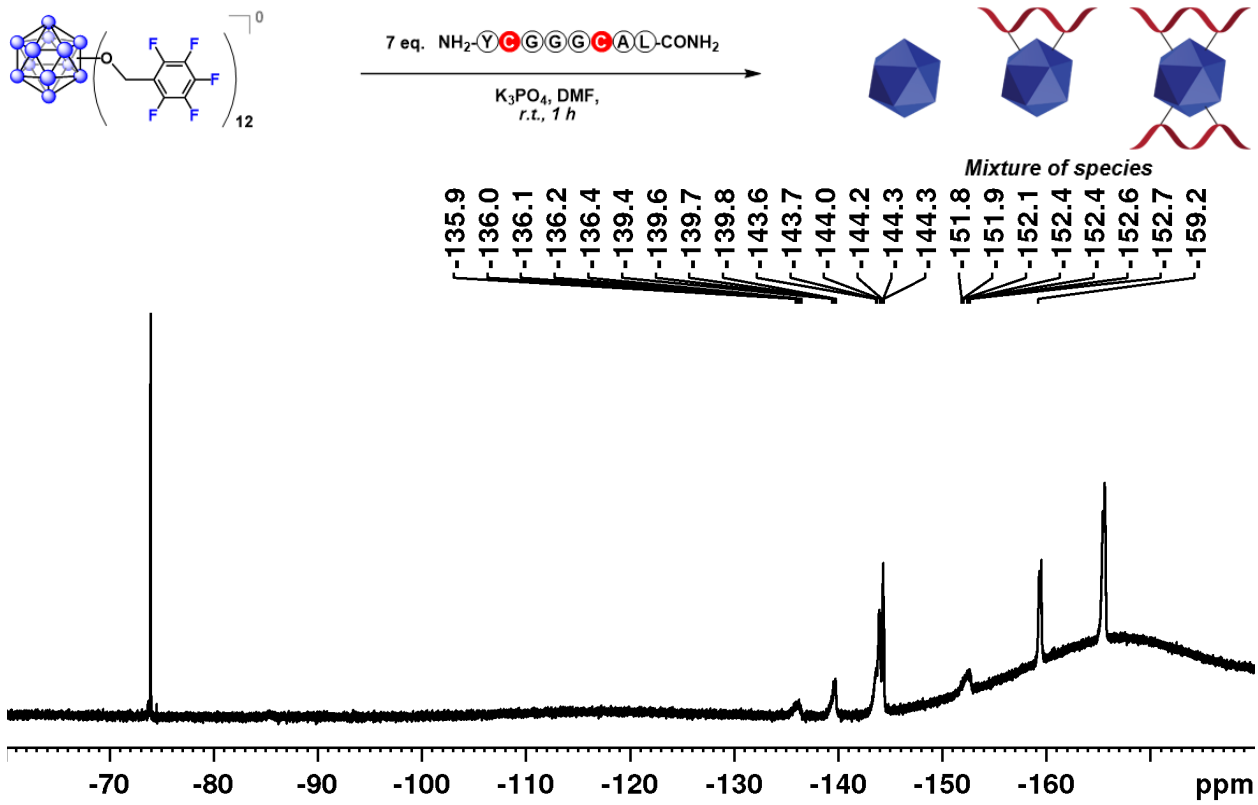


Ultimately, we discovered that perfluoroaryl-based dodecaborate clusters can facilitate the 3D macrocyclization of various unprotected multi-cysteine peptides *via* S<sub>N</sub>Ar chemistry. Moreover, we have shown that an extended cluster scaffold is able to be completely grafted with cyclized peptides, giving rise to a new class of abiotic macromolecules with a fully peptidic periphery.

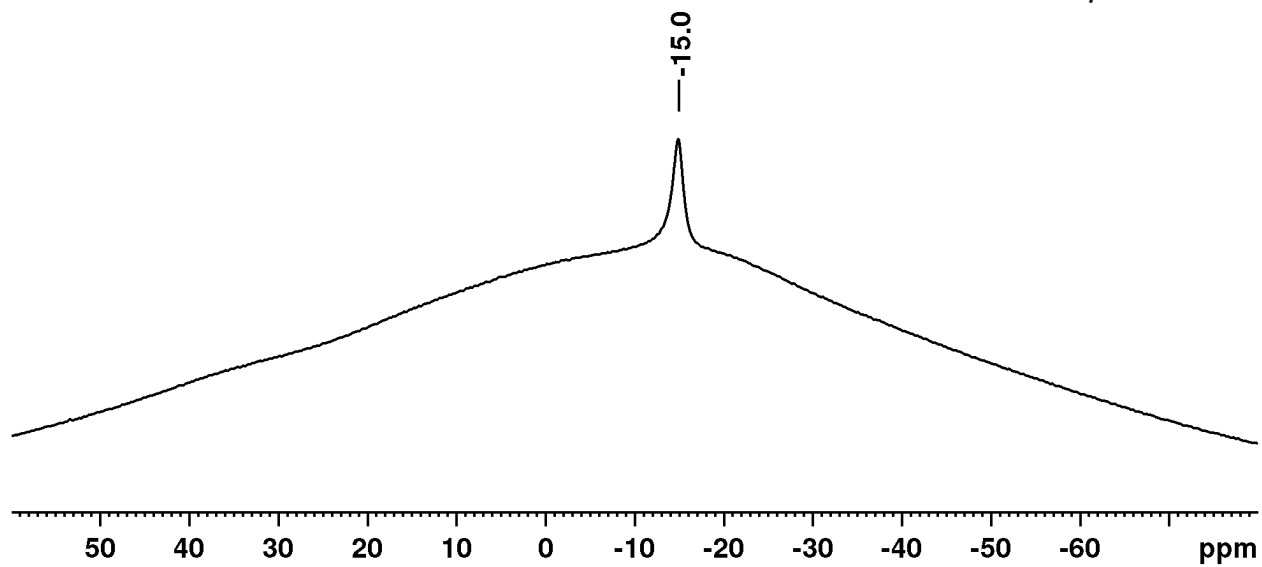
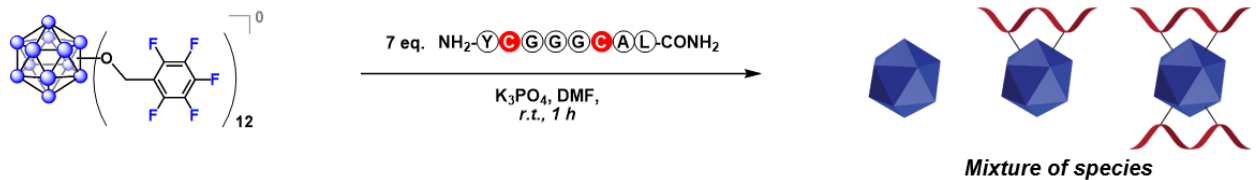
## Selected Data



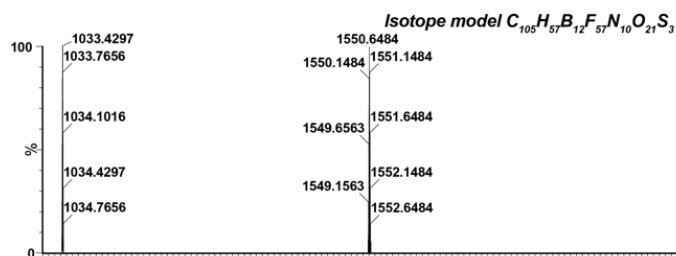
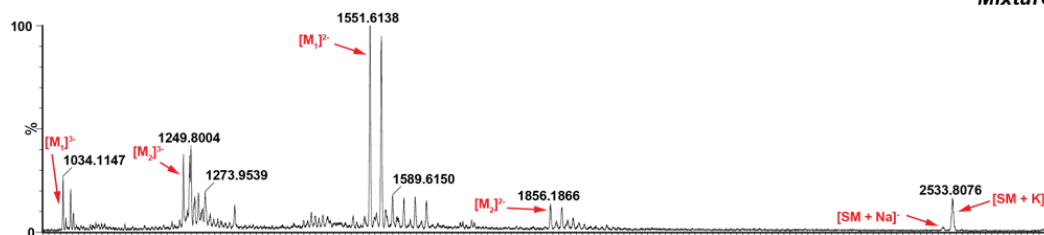
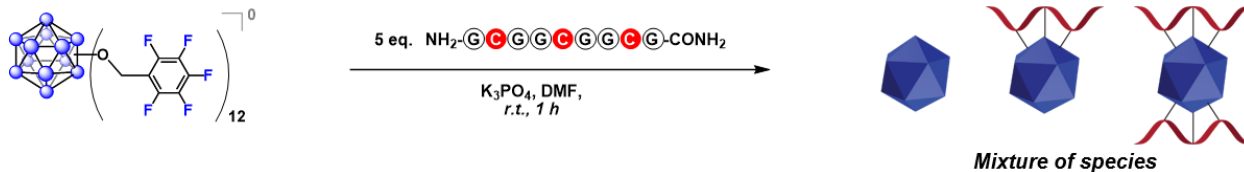
ESI-MS of the reaction mixture.



*In situ*  $^{19}\text{F}$  NMR spectrum of the reaction mixture.



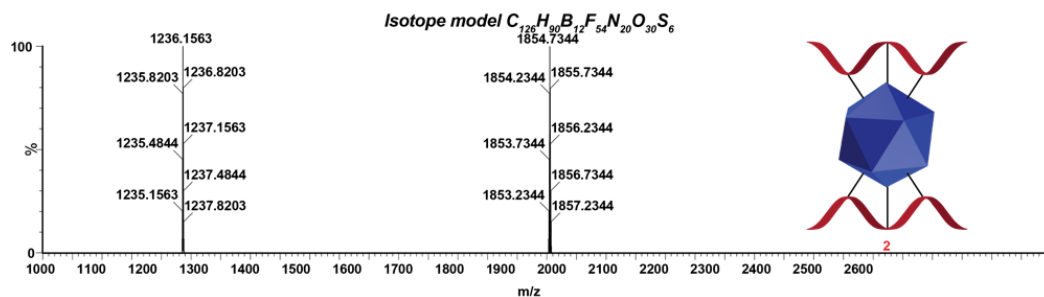
*In situ*  $^{11}\text{B}$  NMR spectrum of the reaction mixture.



SM = starting material

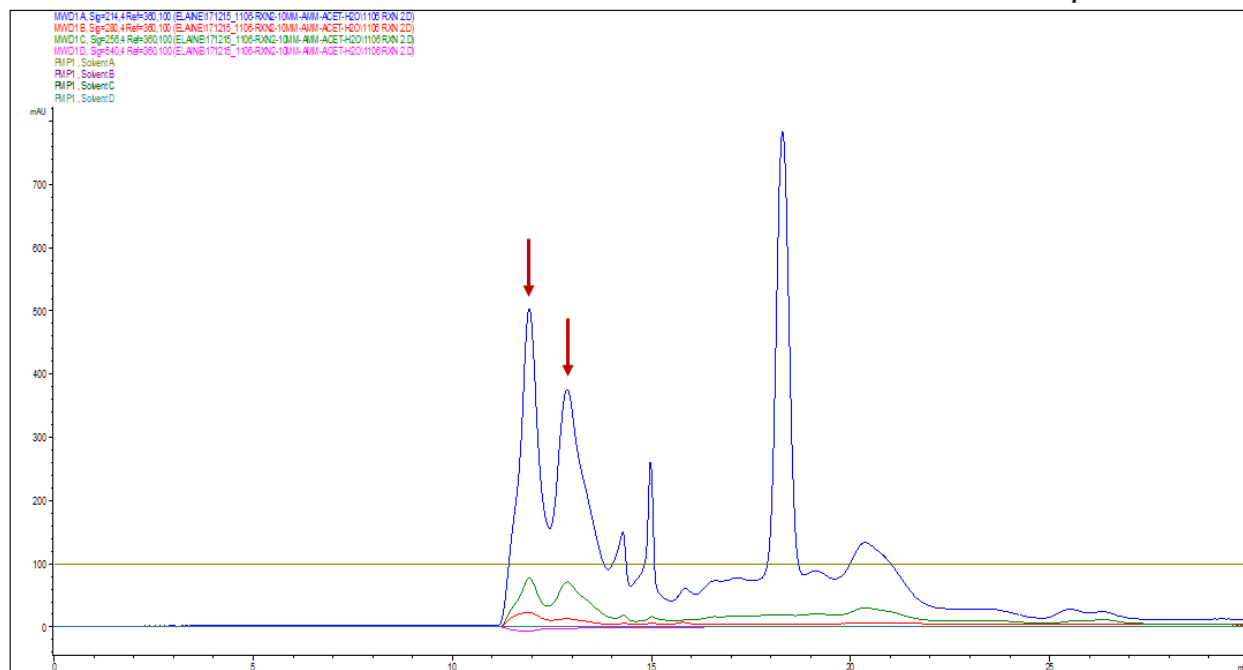
1 = cluster with 1 bicyclized peptide

2 = cluster with 2 bicyclized peptides

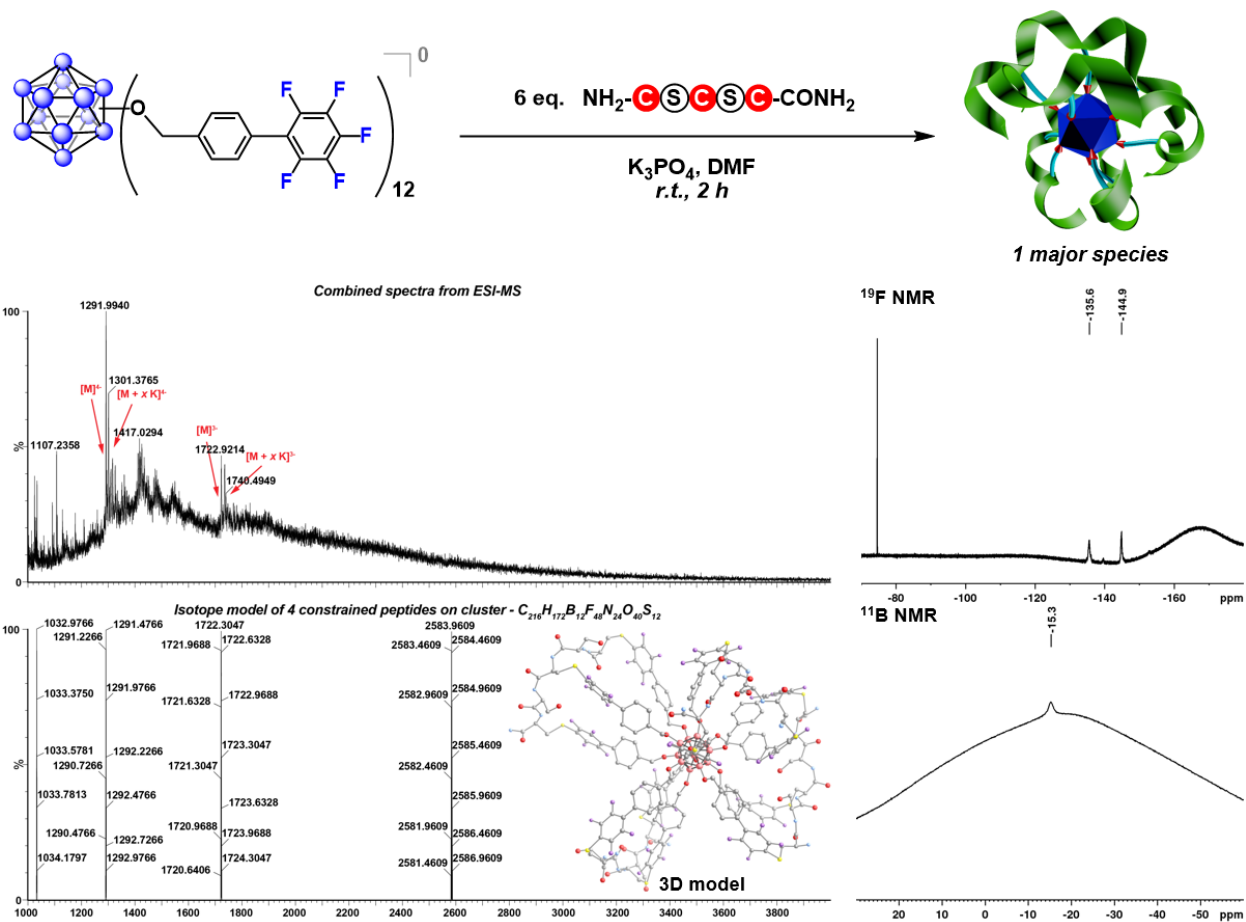


\*For clarity, peaks of conjugates with K<sup>+</sup> adducts are not labeled.

ESI-MS of the reaction mixture.



UV traces from size exclusion chromatography of the reaction mixture.



ESI-MS and *in situ* NMR spectra of the reaction mixture.

## REFERENCES

- (1) Muetterties, E. L.; Balthis, J. H.; Chia, Y. T.; Knoth, W. H.; Miller, H. C. Chemistry of boranes. VIII. Salts and acids of  $B_{10}H_{10}^{-2}$  and  $B_{12}H_{12}^{-2}$ . *Inorg. Chem.* **1964**, *3*, 444–451.
- (2) Hawthorne, M. F. The role of chemistry in the development of boron neutron capture therapy of cancer. *Angew. Chem., Int. Ed. Engl.* **1993**, *32*, 950–984.
- (3) Plesek, J. Potential applications of the boron cluster compounds. *Chem. Rev.* **1992**, *92*, 269–278.
- (4) Grimes, R. N. Boron clusters come of age. *J. Chem. Educ.* **2004**, *81*, 657–672.
- (5) Hawthorne, M. F.; Maderna, A. Applications of radiolabeled boron clusters to the diagnosis and treatment of cancer. *Chem. Rev.* **1999**, *99*, 3421–3434.
- (6) Qian, E. A.; Wixtrom, A. I.; Axtell, J. C.; Saebi, A.; Jung, D.; Rehak, P.; Han, Y.; Mouilly, E. H.; Mosallaei, D.; Chow, S.; Messina, M. S.; Wang, J. Y.; Royappa, A. T.; Rheingold, A. L.; Maynard, H. D.; Král, P.; Spokoiny, A. M. Atomically precise organomimetic cluster nanomolecules assembled via perfluoroaryl-thiol  $S_NAr$  chemistry. *Nat. Chem.* **2017**, *9*, 333–340.
- (7) Locher, G. L. Biological effects and therapeutic possibilities of neutrons. *Am. J. Roentgenol. Radium Ther.* **1936**, *36*, 1–13.
- (8) Hawthorne, M. F. New horizons for therapy based on the boron neutron capture reaction. *Mol. Med. Today* **1998**, *4*, 174–181.
- (9) Sivaev, I. B.; Bregadze, V. V. Polyhedral boranes for medical applications: current status and perspectives. *Eur. J. Inorg. Chem.* **2009**, *2009*, 1433–1450.
- (10) Moss, R. L. Critical review, with an optimistic outlook, on boron neutron capture therapy (BNCT). *Appl. Radiat. Isot.* **2014**, *88*, 2–11.
- (11) Slatkin, D. N. A history of boron neutron capture therapy of brain tumours: postulation of a brain radiation dose tolerance limit. *Brain* **1991**, *114*, 1609–1629.
- (12) Hawthorne, M. F.; Pitochelli, A. R. The reactions of bis-acetonitrile decaborane with amines. *J. Am. Chem. Soc.* **1959**, *81*, 5519.
- (13) Lipscomb, W. N.; Pitochelli, A. R.; Hawthorne, M. F. Probable structure of the  $B_{10}H_{10}^{-2}$  ion. *J. Am. Chem. Soc.* **1959**, *81*, 5833–5834.
- (14) Pitochelli, A. R.; Hawthorne, M. F. The isolation of the icosahedral  $B_{12}H_{12}^{-2}$  ion. *J. Am. Chem. Soc.* **1960**, *82*, 3228–3229.
- (15) Asbury, A. K.; Ojemann, R. G.; Nielsen, S. L.; Sweet, W. H. Neuropathologic study of fourteen cases of malignant brain tumor treated by boron-10 slow neutron capture radiation. *J. Neuropathol. Exp. Neurol.* **1972**, *31*, 278–303.
- (16) Barth, R. F.; Soloway, A. H.; Fairchild, R. G.; Brugger, R. M. Boron neutron capture



- therapy for cancer. Realities and prospects. *Cancer* **1992**, *70*, 2995–3007.
- (17) Soloway, A. H.; Hatanaka, H.; Davis, M. A. Penetration of brain and brain tumor. VII. Tumor-binding sulfhydryl boron compounds. *J. Med. Chem.* **1967**, *10*, 714–717.
- (18) Ciani, L.; Ristori, S. Boron as a platform for new drug design. *Expert Opin. Drug Discov.* **2012**, *7*, 1017–1027.
- (19) Barth, R. F.; Coderre, J. A.; Vicente, M. G. H.; Blue, T. E. Boron neutron capture therapy of cancer: current status and future prospects. *Clin. Cancer Res.* **2005**, *11*, 3987–4002.
- (20) Nakamura, H.; Kirihata, M. Boron compounds: new candidates for boron carriers in BNCT. In *Neutron Capture Therapy*; Sauerwein, W., Wittig, A., Moss, R., Nakagawa, Y., Eds.; Springer: Berlin, 2012.
- (21) Soloway, A. H.; Tjarks, W.; Barnum, B. A.; Rong, F.-G.; Barth, R. F.; Codogni, I. M.; Wilson, J. G. The chemistry of neutron capture therapy. *Chem. Rev.* **1998**, *98*, 1515–1562.
- (22) Sumitani, S.; Nagasaki, Y. Boron neutron capture therapy assisted by boron-conjugated nanoparticles. *Polym. J.* **2012**, *44*, 522–530.
- (23) Zhu, Y. Z.; Lin, Y.; Zhu, Y. Z.; Lu, J.; Maguire, J. A.; Hosmane, N. S. Boron drug delivery via encapsulated magnetic nanocomposites: a new approach for BNCT in cancer treatment. *J. Nanomater.* **2010**, *2010*, 1–8.
- (24) Mandal, S.; Bakeine, G. J.; Krol, S.; Ferrari, C.; Clerici, A. M.; Zonta, C.; Cansolino, L.; Ballarini, F.; Bortolussi, S.; Stella, S.; Protti, N.; Bruschi, P.; Altieri, S. Design, development and characterization of multi-functionalized gold nanoparticles for biodetection and targeted boron delivery in BNCT applications. *Appl. Radiat. Isot.* **2011**, *69*, 1692–1697.
- (25) Umamo, M.; Uechi, K.; Uriuda, T.; Murayama, S.; Azuma, H.; Shinohara, A.; Liu, Y.; Ono, K.; Kirihata, M.; Yanagie, H.; Nagasaki, T. Tumor accumulation of  $\epsilon$ -poly-lysines-based polyamines conjugated with boron clusters. *Appl. Radiat. Isot.* **2011**, *69*, 1765–1767.
- (26) Yanagië, H.; Tomita, T.; Kobayashi, H.; Fujii, Y.; Takahashi, T.; Hasumi, K.; Nariuchi, H.; Sekiguchi, M. Application of boronated anti-CEA immunoliposome to tumour cell growth inhibition in in vitro boron neutron capture therapy model. *Br. J. Cancer* **1991**, *63*, 522–526.
- (27) Shelly, K.; Feakes, D. A.; Hawthorne, M. F.; Schmidt, P. G.; Krisch, T. A.; Bauer, W. F. Model studies directed toward the boron neutron-capture therapy of cancer: boron delivery to murine tumors with liposomes. *Proc. Natl. Acad. Sci. U. S. A.* **1992**, *89*, 9039–9043.
- (28) Pan, X. Q.; Wang, H.; Shukla, S.; Sekido, M.; Adams, D. M.; Tjarks, W.; Barth, R. F.; Lee, R. J. Boron-containing folate receptor-targeted liposomes as potential delivery agents for neutron capture therapy. *Bioconjugate Chem.* **2002**, *13*, 435–442.
- (29) Maruyama, K.; Ishida, O.; Kasaoka, S.; Takizawa, T.; Utoguchi, N.; Shinohara, A.; Chiba, M.; Kobayashi, H.; Eriguchi, M.; Yanagie, H. Intracellular targeting of sodium mercaptoundecahydrododecaborate (BSH) to solid tumors by transferrin-PEG liposomes,

- for boron neutron-capture therapy (BNCT). *J. Controlled Release* **2004**, *98*, 195–207.
- (30) Feakes, D. A.; Shelly, K.; Hawthorne, M. F. Selective boron delivery to murine tumors by lipophilic species incorporated in the membranes of unilamellar liposomes. *Proc. Natl. Acad. Sci. U. S. A.* **1995**, *92*, 1367–1370.
- (31) Hawthorne, M. F.; Shelly, K. Liposomes as drug delivery vehicles for boron agents. *J. Neuro-Oncol.* **1997**, *33*, 53–58.
- (32) Feakes, D. A.; Spinler, J. K.; Harris, F. R. Synthesis of boron-containing cholesterol derivatives for incorporation into unilamellar liposomes and evaluation as potential agents for BNCT. *Tetrahedron* **1999**, *55*, 11177–11186.
- (33) Lee, J.-D.; Ueno, M.; Miyajima, Y.; Nakamura, H. Boron cluster lipid *closo*-dodecaborate as alternative hydrophilic function boronated liposome for neutron capture therapy. *Org. Lett.* **2007**, *9*, 323–326.
- (34) Heber, E. M.; Hawthorne, M. F.; Kueffer, P. J.; Garabalino, M. A.; Thorp, S. I.; Pozzi, E. C. C.; Hughes, A. M.; Maitz, C. A.; Jalisatgi, S. S.; Nigg, D. W.; Curotto, P.; Trivillin, V. A.; Schwint, A. E. Therapeutic efficacy of boron neutron capture therapy mediated by boron-rich liposomes for oral cancer in the hamster cheek pouch model. *Proc. Natl. Acad. Sci. U. S. A.* **2014**, *111*, 16077–16081.
- (35) Thomas, J.; Hawthorne, M. F. Dodeca(carboranyl)-substituted closomers: toward unimolecular nanoparticles as delivery vehicles for BNCT. *Chem. Commun.* **2001**, 1884–1885.
- (36) Ma, L.; Hamdi, J.; Wong, F.; Hawthorne, M. F. Closomers of high boron content: synthesis, characterization, and potential application as unimolecular nanoparticle delivery vehicles for boron neutron capture therapy. *Inorg. Chem.* **2006**, *45*, 278–285.
- (37) Kuperman, M. V.; Losytskyy, M. Y.; Bykov, A. Y.; Yarmoluk, S. M.; Zhizhin, K. Y.; Kuznetsov, N. T.; Varzatskii, O. A.; Gumienna-Kontecka, E.; Kovalska, V. B. Effective binding of perhalogenated *closo*-borates to serum albumins revealed by spectroscopic and ITC studies. *J. Mol. Struct.* **2017**, *1141*, 75–80.
- (38) Losytskyy, M. Y.; Kovalska, V. B.; Varzatskii, O. A.; Kuperman, M. V.; Potocki, S.; Gumienna-Kontecka, E.; Zhdanov, A. P.; Yarmoluk, S. M.; Voloshin, Y. Z.; Zhizhin, K. Y.; Kuznetsov, N. T.; Elskaya, A. V. An interaction of the functionalized *closo*-borates with albumins: the protein fluorescence quenching and calorimetry study. *J. Lumin.* **2016**, *169*, 51–60.
- (39) Bondarev, O.; Khan, A. A.; Tu, X.; Sevryugina, Y. V.; Jalisatgi, S. S.; Hawthorne, M. F. Synthesis of [*closo*-B<sub>12</sub>(OH)<sub>11</sub>NH<sub>3</sub>]<sup>-</sup>: a new heterobifunctional dodecaborane scaffold for drug delivery applications. *J. Am. Chem. Soc.* **2013**, *135*, 13204–13211.
- (40) Sarma, S. J.; Khan, A. A.; Goswami, L. N.; Jalisatgi, S. S.; Hawthorne, M. F. A trimodal closomer drug-delivery system tailored with tracing and targeting capabilities. *Chem. - Eur. J.* **2016**, *22*, 12715–12723.

- (41) Pushechnikov, A.; Jalisatgi, S. S.; Hawthorne, M. F. Dendritic closomers: novel spherical hybrid dendrimers. *Chem. Commun.* **2013**, *49*, 3579–3581.
- (42) Kojima, C.; Kono, K.; Maruyama, K.; Takagishi, T. Synthesis of polyamidoamine dendrimers having poly(ethylene glycol) grafts and their ability to encapsulate anticancer drugs. *Bioconjugate Chem.* **2000**, *11*, 910–917.
- (43) Agarwal, H.; Hasabelnaby, S.; Tiwari, R.; Tjarks, W. Boron cluster (radio)halogenation in biomedical research. In *Boron Science: New Technologies and Applications*; CRC Press: Boca Raton, FL, 2011.
- (44) Armstrong, A. F.; Valliant, J. F. The bioinorganic and medicinal chemistry of carboranes: from new drug discovery to molecular imaging and therapy. *Dalt. Trans.* **2007**, 4240–4251.
- (45) Goswami, L. N.; Ma, L.; Chakravarty, S.; Cai, Q.; Jalisatgi, S. S.; Hawthorne, M. F. Discrete nanomolecular polyhedral borane scaffold supporting multiple gadolinium(III) complexes as a high performance MRI contrast agent. *Inorg. Chem.* **2013**, *52*, 1694–1700.
- (46) Caravan, P. Protein-targeted gadolinium-based magnetic resonance imaging (MRI) contrast agents: design and mechanism of action. *Acc. Chem. Res.* **2009**, *42*, 851–862.
- (47) Langereis, S.; de Lussanet, Q. G.; van Genderen, M. H. P.; Backes, W. H.; Meijer, E. W. Multivalent contrast agents based on gadolinium–diethylenetriaminepentaacetic acid-terminated poly(propylene imine) dendrimers for magnetic resonance imaging. *Macromolecules* **2004**, *37*, 3084–3091.
- (48) Goswami, L. N.; Ma, L.; Cai, Q.; Sarma, S. J.; Jalisatgi, S. S.; Hawthorne, M. F. cRGD peptide-conjugated icosahedral *closo*-B<sub>12</sub><sup>2-</sup> core carrying multiple Gd<sup>3+</sup>-DOTA chelates for  $\alpha_v\beta_3$  integrin-targeted tumor imaging (MRI). *Inorg. Chem.* **2013**, *52*, 1701–1709.
- (49) Mammen, M.; Choi, S.-K.; Whitesides, G. M. Polyvalent interactions in biological systems: implications for design and use of multivalent ligands and inhibitors. *Angew. Chem., Int. Ed.* **1998**, *37*, 2754–2794.
- (50) Kiessling, L. L.; Gestwicki, J. E.; Strong, L. E. Synthetic multivalent ligands as probes of signal transduction. *Angew. Chem., Int. Ed.* **2006**, *45*, 2348–2368.
- (51) Jones, L. H. Recent advances in the molecular design of synthetic vaccines. *Nat. Chem.* **2015**, *7*, 952–960.
- (52) Elsabahy, M.; Wooley, K. L. Design of polymeric nanoparticles for biomedical delivery applications. *Chem. Soc. Rev.* **2012**, *41*, 2521–3012.
- (53) Rao, J. P.; Geckeler, K. E. Polymer nanoparticles: preparation techniques and size-control parameters. *Prog. Polym. Sci.* **2011**, *36*, 887–913.
- (54) Tomalia, D. A.; Baker, H.; Dewald, J.; Hall, M.; Kallos, G.; Martin, S.; Roeck, J.; Ryder, J.; Smith, P. A new class of polymers: starburst-dendritic macromolecules. *Polym. J.* **1985**, *17*, 117–132.
- (55) Hawker, C. J.; Frechet, J. M. J. Preparation of polymers with controlled molecular

- architecture. A new convergent approach to dendritic macromolecules. *J. Am. Chem. Soc.* **1990**, *112*, 7638–7647.
- (56) Farokhzad, O. C.; Langer, R. Impact of nanotechnology on drug delivery. *ACS Nano* **2009**, *3*, 16–20.
- (57) Peer, D.; Karp, J. M.; Hong, S.; Farokhzad, O. C.; Margalit, R.; Langer, R. Nanocarriers as an emerging platform for cancer therapy. *Nat. Nanotechnol.* **2007**, *2*, 751–760.
- (58) Daniel, M.; Astruc, D. Gold nanoparticles: assembly, supramolecular chemistry, quantum-size-related properties, and applications toward biology, catalysis, and nanotechnology. *Chem. Rev.* **2004**, *104*, 293–346.
- (59) Dreaden, E. C.; Alkilany, A. M.; Huang, X.; Murphy, C. J.; El-Sayed, M. A. The golden age: gold nanoparticles for biomedicine. *Chem. Soc. Rev.* **2012**, *41*, 2740–2779.
- (60) Brust, M.; Walker, M.; Bethell, D.; Schiffrin, D. J.; Whyman, R. Synthesis of thiol-derivatised gold nanoparticles in a two-phase liquid–liquid system. *J. Chem. Soc., Chem. Commun.* **1994**, 801–802.
- (61) Giljohann, D. A.; Seferos, D. S.; Patel, P. C.; Millstone, J. E.; Rosi, N. L.; Mirkin, C. A. Oligonucleotide loading determines cellular uptake of DNA-modified gold nanoparticles. *Nano Lett.* **2007**, *7*, 3818–3821.
- (62) Zhao, H.; Sen, S.; Udayabhaskararao, T.; Sawczyk, M.; Kučanda, K.; Manna, D.; Kundu, P. K.; Lee, J.-W.; Král, P.; Klajn, R. Reversible trapping and reaction acceleration within dynamically self-assembling nanoflasks. *Nat. Nanotechnol.* **2015**, *11*, 82–88.
- (63) Jones, M. R.; Seeman, N. C.; Mirkin, C. A. Programmable materials and the nature of the DNA bond. *Science* **2015**, *347*, 1260901.
- (64) Suzuki, K.; Sato, S.; Fujita, M. Template synthesis of precisely monodisperse silica nanoparticles within self-assembled organometallic spheres. *Nat. Chem.* **2010**, *2*, 25–29.
- (65) Heindl, C.; Peresypkina, E. V.; Virovets, A. V.; Kremer, W.; Scheer, M. Giant rugby ball [ $\{\text{Cp}^{\text{Bn}}\text{Fe}(\eta^5\text{-P}_5)\}_2\text{Cu}_9\text{Br}_6$ ] derived from pentaphosphaferrocene and  $\text{CuBr}_2$ . *J. Am. Chem. Soc.* **2015**, *137*, 10938–10941.
- (66) Ambrogio, M. W.; Thomas, C. R.; Zhao, Y.-L.; Zink, J. I.; Stoddart, J. F. Mechanized silica nanoparticles: a new frontier in theranostic nanomedicine. *Acc. Chem. Res.* **2011**, *44*, 903–913.
- (67) Love, J. C.; Estroff, L. A.; Kriebel, J. K.; Nuzzo, R. G.; Whitesides, G. M. Self-assembled monolayers of thiolates on metals as a form of nanotechnology. *Chem. Rev.* **2005**, *105*, 1103–1170.
- (68) Hostetler, M. J.; Green, S. J.; Stokes, J. J.; Murray, R. W. Monolayers in three dimensions: synthesis and electrochemistry of  $\omega$ -functionalized alkanethiolate-stabilized gold cluster compounds. *J. Am. Chem. Soc.* **1996**, *118*, 4212–4213.
- (69) Hostetler, M. J.; Templeton, A. C.; Murray, R. W. Dynamics of place-exchange reactions

- on monolayer-protected gold cluster molecules. *Langmuir* **1999**, *15*, 3782–3789.
- (70) MacLeod, M. J.; Johnson, J. A. PEGylated N-heterocyclic carbene anchors designed To stabilize gold nanoparticles in biologically relevant media. *J. Am. Chem. Soc.* **2015**, *137*, 7974–7977.
- (71) Häkkinen, H. The gold–sulfur interface at the nanoscale. *Nat. Chem.* **2012**, *4*, 443–455.
- (72) Yvon, C.; Surman, A. J.; Hutin, M.; Alex, J.; Smith, B. O.; Long, D.-L.; Cronin, L. Polyoxometalate clusters integrated into peptide chains and as inorganic amino acids: solution- and solid-phase approaches. *Angew. Chem., Int. Ed.* **2014**, *53*, 3336–3341.
- (73) Lachkar, D.; Vilona, D.; Dumont, E.; Lelli, M.; Lacôte, E. Grafting of secondary diolamides onto  $[P_2W_{15}V_3O_{62}]^{9-}$  generates hybrid heteropoly acids. *Angew. Chem., Int. Ed.* **2016**, *55*, 5961–5965.
- (74) Gouzerh, P.; Proust, A. Main-group element, organic, and organometallic derivatives of polyoxometalates. *Chem. Rev.* **1998**, *98*, 77–112.
- (75) Müller, A.; Gouzerh, P. From linking of metal-oxide building blocks in a dynamic library to giant clusters with unique properties and towards adaptive chemistry. *Chem. Soc. Rev.* **2012**, *41*, 7431.
- (76) Li, G.; Wang, L.; Ni, H.; Pittman, C. U. Polyhedral oligomeric silsesquioxane (POSS) polymers, copolymers, and resin nanocomposites. *J. Inorg. Organomet. Polym.* **2002**, *11*, 123–154.
- (77) Spokoyny, A. M. New ligand platforms featuring boron-rich clusters as organomimetic substituents. *Pure Appl. Chem.* **2013**, *85*, 903–919.
- (78) Lee, I. S.; Long, J. R.; Prusiner, S. B.; Safar, J. G. Selective precipitation of prions by polyoxometalate complexes. *J. Am. Chem. Soc.* **2005**, *127*, 13802–13803.
- (79) Farha, O. K.; Julius, R. L.; Lee, M. W.; Huertas, R. E.; Knobler, C. B.; Hawthorne, M. F. Synthesis of stable dodecaalkoxy derivatives of *hypercloso*- $B_{12}H_{12}$ . *J. Am. Chem. Soc.* **2005**, *127*, 18243–18251.
- (80) Jalisatgi, S. S.; Kulkarni, V. S.; Tang, B.; Houston, Z. H.; Lee, M. W.; Hawthorne, M. F. A convenient route to diversely substituted icosahedral closomer nanoscaffolds. *J. Am. Chem. Soc.* **2011**, *133*, 12382–12385.
- (81) Wixtrom, A. I.; Shao, Y.; Jung, D.; Machan, C. W.; Kevork, S. N.; Qian, E. A.; Axtell, J. C.; Khan, S. I.; Kubiak, C. P.; Spokoyny, A. M. Rapid synthesis of redox-active dodecaborane  $B_{12}(OR)_{12}$  clusters under ambient conditions. *Inorg. Chem. Front.* **2016**, *3*, 711–717.
- (82) Messina, M. S.; Axtell, J. C.; Wang, Y.; Chong, P.; Wixtrom, A. I.; Kirlikovali, K. O.; Upton, B. M.; Hunter, B. M.; Shafaat, O. S.; Khan, S. I.; Winkler, J. R.; Gray, H. B.; Alexandrova, A. N.; Maynard, H. D.; Spokoyny, A. M. Visible-light-induced olefin activation using 3D aromatic boron-rich cluster photooxidants. *J. Am. Chem. Soc.* **2016**, *138*, 6952–6955.

- (83) Haynes, W. M. *CRC Handbook of Chemistry and Physics*; Haynes, W. M., Ed.; CRC Press/Taylor and Francis: Boca Raton, FL, 2016.
- (84) Lundquist, J. J.; Toone, E. J. The cluster glycoside effect. *Chem. Rev.* **2002**, *102*, 555–578.
- (85) Moore, J. S.; Xu, Z. Synthesis of rigid dendritic macromolecules: enlarging the repeat unit size as a function of generation, permitting growth to continue. *Macromolecules* **1991**, *24*, 5893–5894.
- (86) Birchall, J. M.; Green, M.; Haszeldine, R. N.; Pitts, A. D. The mechanism of the nucleophilic substitution reactions of polyfluoroarenes. *Chem. Commun.* **1967**, 338.
- (87) Remzi Becer, C.; Hoogenboom, R.; Schubert, U. S. Click chemistry beyond metal-catalyzed cycloaddition. *Angew. Chem., Int. Ed.* **2009**, *48*, 4900–4908.
- (88) Becer, C. R.; Babiuch, K.; Pilz, D.; Hornig, S.; Heinze, T.; Gottschaldt, M.; Schubert, U. S. Clicking pentafluorostyrene copolymers: synthesis, nanoprecipitation, and glycosylation. *Macromolecules* **2009**, *42*, 2387–2394.
- (89) Spokoyny, A. M.; Zou, Y.; Ling, J. J.; Yu, H.; Lin, Y.-S.; Pentelute, B. L. A perfluoroaryl-cysteine  $S_NAr$  chemistry approach to unprotected peptide stapling. *J. Am. Chem. Soc.* **2013**, *135*, 5946–5949.
- (90) Zhang, C.; Welborn, M.; Zhu, T.; Yang, N. J.; Santos, M. S.; Van Voorhis, T.; Pentelute, B. L.  $\pi$ -clamp-mediated cysteine conjugation. *Nat. Chem.* **2015**, *8*, 120–128.
- (91) Hoffman, A. S. The origins and evolution of “controlled” drug delivery systems. *J. Controlled Release* **2008**, *132*, 153–163.
- (92) Alconcel, S. N. S.; Baas, A. S.; Maynard, H. D. FDA-approved poly(ethylene glycol)–protein conjugate drugs. *Polym. Chem.* **2011**, *2*, 1442.
- (93) Veronese, F. M.; Pasut, G. PEGylation, successful approach to drug delivery. *Drug Discovery Today* **2005**, *10*, 1451–1458.
- (94) Dam, T. K.; Roy, R.; Das, S. K.; Oscarson, S.; Brewer, C. F. Binding of multivalent carbohydrates to concanavalin A and *Dioclea grandiflora* lectin. Thermodynamic analysis of the “multivalency effect.” *J. Biol. Chem.* **2000**, *275*, 14223–14230.
- (95) Müller, C.; Despras, G.; Lindhorst, T. K. Organizing multivalency in carbohydrate recognition. *Chem. Soc. Rev.* **2016**, *45*, 3275–3302.
- (96) Muñoz, A.; Sigwalt, D.; Illescas, B. M.; Luczkowiak, J.; Rodríguez-Pérez, L.; Nierengarten, I.; Holler, M.; Remy, J. S.; Buffet, K.; Vincent, S. P.; Rojo, J.; Delgado, R.; Nierengarten, J. F.; Martín, N. Synthesis of giant globular multivalent glycofullerenes as potent inhibitors in a model of Ebola virus infection. *Nat. Chem.* **2016**, *8*, 50–57.
- (97) Bhatia, S.; Camacho, L. C.; Haag, R. Pathogen inhibition by multivalent ligand architectures. *J. Am. Chem. Soc.* **2016**, *138*, 8654–8666.
- (98) Bernardi, A.; Jiménez-Barbero, J.; Casnati, A.; De Castro, C.; Darbre, T.; Fieschi, F.; Finne,

- J.; Funken, H.; Jaeger, K.-E.; Lahmann, M.; Lindhorst, T. K.; Marradi, M.; Messner, P.; Molinaro, A.; Murphy, P. V.; Nativi, C.; Oscarson, S.; Penadés, S.; Peri, F.; et al. Multivalent glycoconjugates as anti-pathogenic agents. *Chem. Soc. Rev.* **2013**, *42*, 4709–4727.
- (99) Munoz, E. M.; Correa, J.; Riguera, R.; Fernandez-Megia, E. Real-time evaluation of binding mechanisms in multivalent interactions: a surface plasmon resonance kinetic approach. *J. Am. Chem. Soc.* **2013**, *135*, 5966–5969.
- (100) Fernandez-Megia, E.; Correa, J.; Rodríguez-Meizoso, I.; Riguera, R. A click approach to unprotected glycodendrimers. *Macromolecules* **2006**, *39*, 2113–2120.
- (101) Kamiya, N.; Tominaga, M.; Sato, S.; Fujita, M. Saccharide-coated M<sub>12</sub>L<sub>24</sub> molecular spheres that form aggregates by multi-interaction with proteins. *J. Am. Chem. Soc.* **2007**, *129*, 3816–3817.
- (102) Safina, G.; Duran, I. B.; Alasel, M.; Danielsson, B. Surface plasmon resonance for real-time study of lectin–carbohydrate interactions for the differentiation and identification of glycoproteins. *Talanta* **2011**, *84*, 1284–1290.
- (103) Sheldrick, G. M. SHELXT – integrated space-group and crystal-structure determination. *Acta Crystallogr.* **2015**, *A71*, 3–8.
- (104) Sheldrick, G. M. A short history of SHELX. *Acta Crystallogr.* **2008**, *A64*, 112–122.
- (105) Dolomanov, O. V.; Bourhis, L. J.; Gildea, R. J.; Howard, J. A. K.; Puschmann, H. OLEX2 : a complete structure solution, refinement and analysis program. *J. Appl. Crystallogr.* **2009**, *42*, 339–341.
- (106) Hood, C. A.; Fuentes, G.; Patel, H.; Page, K.; Menakuru, M.; Park, J. H. Fast conventional Fmoc solid-phase peptide synthesis with HCTU. *J. Pept. Sci.* **2008**, *14*, 97–101.
- (107) Phillips, J. C.; Braun, R.; Wang, W.; Gumbart, J.; Tajkhorshid, E.; Villa, E.; Chipot, C.; Skeel, R. D.; Kalé, L.; Schulten, K. Scalable molecular dynamics with NAMD. *J. Comput. Chem.* **2005**, *26*, 1781–1802.
- (108) MacKerell, A. D.; Bashford, D.; Bellott, M.; Dunbrack, R. L.; Evanseck, J. D.; Field, M. J.; Fischer, S.; Gao, J.; Guo, H.; Ha, S.; Joseph-McCarthy, D.; Kuchnir, L.; Kuczera, K.; Lau, F. T.; Mattos, C.; Michnick, S.; Ngo, T.; Nguyen, D. T.; Prodhom, B.; et al. All-atom empirical potential for molecular modeling and dynamics studies of proteins. *J. Phys. Chem. B* **1998**, *102*, 3586–3616.
- (109) Vanommeslaeghe, K.; MacKerell, A. D. Automation of the CHARMM general force field (CGenFF) I: bond perception and atom typing. *J. Chem. Inf. Model.* **2012**, *52*, 3144–3154.
- (110) Vanommeslaeghe, K.; Raman, E. P.; MacKerell, A. D. Automation of the CHARMM general force field (CGenFF) II: assignment of bonded parameters and partial atomic charges. *J. Chem. Inf. Model.* **2012**, *52*, 3155–3168.
- (111) Yu, W.; He, X.; Vanommeslaeghe, K.; MacKerell, A. D. Extension of the CHARMM general force field to sulfonyl-containing compounds and its utility in biomolecular

- simulations. *J. Comput. Chem.* **2012**, *33*, 2451–2468.
- (112) Mackerell, A. D.; Feig, M.; Brooks, C. L. Extending the treatment of backbone energetics in protein force fields: limitations of gas-phase quantum mechanics in reproducing protein conformational distributions in molecular dynamics simulations. *J. Comput. Chem.* **2004**, *25*, 1400–1415.
- (113) Vanommeslaeghe, K.; Hatcher, E.; Acharya, C.; Kundu, S.; Zhong, S.; Shim, J.; Darian, E.; Guvench, O.; Lopes, P.; Vorobyov, I.; Mackerell, A. D. CHARMM general force field: a force field for drug-like molecules compatible with the CHARMM all-atom additive biological force fields. *J. Comput. Chem.* **2010**, *31*, 671–690.
- (114) Frisch, M. J.; Trucks, G. W.; Schlegel, H. B.; Scuseria, G. E.; Robb, M. A.; Cheeseman, J. R.; Scalmani, G.; Barone, V.; Mennucci, B.; Petersson, G. A.; Nakatsuji, H.; Caricato, M.; Li, X.; Hratchian, H. P.; Izmaylov, A. F.; Bloino, J.; Zheng, G.; Sonnenb, D. J. *Gaussian 09*; Gaussian, Inc.: Wallingford, CT, 2013.
- (115) Breneman, C. M.; Wiberg, K. B. Determining atom-centered monopoles from molecular electrostatic potentials. The need for high sampling density in formamide conformational analysis. *J. Comput. Chem.* **1990**, *11*, 361–373.
- (116) Mayne, C. G.; Saam, J.; Schulten, K.; Tajkhorshid, E.; Gumbart, J. C. Rapid parameterization of small molecules using the force field toolkit. *J. Comput. Chem.* **2013**, *34*, 2757–2770.
- (117) Darden, T.; York, D.; Pedersen, L. Particle mesh Ewald: An N·log(N) method for Ewald sums in large systems. *J. Chem. Phys.* **1993**, *98*, 10089–10092.
- (118) Loris, R.; Hamelryck, T.; Bouckaert, J.; Wyns, L. Legume lectin structure. *Biochim. Biophys. Acta - Protein Struct. Mol. Enzymol.* **1998**, *1383*, 9–36.
- (119) Loris, R.; Maes, D.; Poortmans, F.; Wyns, L.; Bouckaert, J. A structure of the complex between Concanavalin A and methyl-3,6-di-O-( $\alpha$ -D-mannopyranosyl)- $\alpha$ -D-mannopyranoside reveals two binding modes. *J. Biol. Chem.* **1996**, *271*, 30614–30618.
- (120) Babu, C. S.; Lim, C. Empirical force fields for biologically active divalent metal cations in water. *J. Phys. Chem. A* **2006**, *110*, 691–699.
- (121) Weis, W. I.; Taylor, M. E.; Drickamer, K. The C-type lectin superfamily in the immune system. *Immunol. Rev.* **1998**, *163*, 19–34.
- (122) Wolfert, M. A.; Boons, G. J. Adaptive immune activation: glycosylation does matter. *Nat. Chem. Biol.* **2013**, *9*, 776–784.
- (123) *Multivalency*, 1st ed.; Huskens, J., Prins, L. J., Haag, R., Ravoo, B. J., Eds.; John Wiley & Sons: Hoboken, NJ, 2018.
- (124) Conn, M. M.; Rebek, J. Self-assembling capsules. *Chem. Rev.* **1997**, *97*, 1647–1668.
- (125) Geijtenbeek, T. B. H.; Torensma, R.; Vliet, S. J. Van; Duijnhoven, G. C. F. Van; Adema, G. J.; Kooyk, Y. Van; Figdor, C. G. Identification of DC-SIGN, a novel dendritic cell-



- specific ICAM-3 receptor that supports primary immune responses. *Cell* **2000**, *100*, 575–585.
- (126) Mitchell, D. A.; Fadden, A. J.; Drickamer, K. A novel mechanism of carbohydrate recognition by the C-type lectins DC-SIGN and DC-SIGNR. Subunit organization and binding to multivalent ligands. *J. Biol. Chem.* **2001**, *276*, 28939–28945.
- (127) Feinberg, H.; Mitchell, D. a; Drickamer, K.; Weis, W. I. Structural basis for selective recognition of oligosaccharides by DC-SIGN and DC-SIGNR. *Science* **2001**, *294*, 2163–2166.
- (128) Švajger, U.; Anderluh, M.; Jeras, M.; Obermajer, N. C-type lectin DC-SIGN: An adhesion, signalling and antigen-uptake molecule that guides dendritic cells in immunity. *Cell. Signal.* **2010**, *22*, 1397–1405.
- (129) van Kooyk, Y.; Geijtenbeek, T. B. H. DC-SIGN: Escape mechanism for pathogens. *Nat. Rev. Immunol.* **2003**, *3*, 697–709.
- (130) Geijtenbeek, T. B. H.; Kwon, D. S.; Torensma, R.; Van Vliet, S. J.; Van Duijnhoven, G. C. F.; Middel, J.; Cornelissen, I. L. M. H. A.; Nottet, H. S. L. M.; KewalRamani, V. N.; Littman, D. R.; Figdor, C. G.; Van Kooyk, Y. DC-SIGN, a dendritic cell-specific HIV-1-binding protein that enhances trans-infection of T cells. *Cell* **2000**, *100*, 587–597.
- (131) Chung, N. P. Y.; Breun, S. K. J.; Bashirova, A.; Baumann, J. G.; Martin, T. D.; Karamchandani, J. M.; Rausch, J. W.; Le Grice, S. F. J.; Wu, L.; Carrington, M.; KewalRamani, V. N. HIV-1 transmission by dendritic cell-specific ICAM-3-grabbing nonintegrin (DC-SIGN) is regulated by determinants in the carbohydrate recognition domain that are absent in liver/lymph node-sign (L-SIGN). *J. Biol. Chem.* **2010**, *285*, 2100–2112.
- (132) Lepenies, B.; Lee, J.; Sonkaria, S. Targeting C-type lectin receptors with multivalent carbohydrate ligands. *Adv. Drug Deliv. Rev.* **2013**, *65*, 1271–1281.
- (133) Zhang, Q.; Savagatrup, S.; Kaplonek, P.; Seeberger, P. H.; Swager, T. M. Janus emulsions for the detection of bacteria. *ACS Cent. Sci.* **2017**, *3*, 309–313.
- (134) Sattin, S.; Daggetti, A.; Thépaut, M.; Berzi, A.; Sánchez-Navarro, M.; Tabarani, G.; Rojo, J.; Fieschi, F.; Clerici, M.; Bernardi, A. Inhibition of DC-SIGN-mediated HIV infection by a linear trimannoside mimic in a tetravalent presentation. *ACS Chem. Biol.* **2010**, *5*, 301–312.
- (135) Borrok, M. J.; Kiessling, L. L. Non-carbohydrate inhibitors of the lectin DC-SIGN. *J. Am. Chem. Soc.* **2007**, *129*, 12780–12785.
- (136) Frison, N.; Taylor, M. E.; Soilleux, E.; Bousser, M.-T.; Mayer, R.; Monsigny, M.; Drickamer, K.; Roche, A.-C. Oligolysine-based oligosaccharide clusters. *J. Biol. Chem.* **2003**, *278*, 23922–23929.
- (137) Ng, S.; Bennett, N. J.; Schulze, J.; Gao, N.; Rademacher, C.; Derda, R. Genetically-encoded fragment-based discovery of glycopeptide ligands for DC-SIGN. *Bioorganic Med. Chem.*

2018, 26, 5368–5377.

- (138) Becer, C. R.; Gibson, M. I.; Geng, J.; Ilyas, R.; Wallis, R.; Mitchell, D. A.; Haddleton, D. M. High-affinity glycopolymer binding to human DC-SIGN and disruption of DC-SIGN interactions with HIV envelope glycoprotein. *J. Am. Chem. Soc.* **2010**, *132*, 15130–15132.
- (139) Turnbull, W. B.; Stoddart, J. F. Design and synthesis of glycodendrimers. *Rev. Mol. Biotechnol.* **2002**, *90*, 231–255.
- (140) Lasala, F.; Arce, E.; Otero, J. R.; Rojo, J.; Delgado, R. Mannosyl glycodendritic structure inhibits DC-SIGN-mediated Ebola virus infection in *cis* and in *trans*. *Antimicrob. Agents Chemother.* **2003**, *47*, 3970–3972.
- (141) Tabarani, G.; Reina, J. J.; Ebel, C.; Vivès, C.; Lortat-Jacob, H.; Rojo, J.; Fieschi, F. Mannose hyperbranched dendritic polymers interact with clustered organization of DC-SIGN and inhibit gp120 binding. *FEBS Lett.* **2006**, *580*, 2402–2408.
- (142) Luczkowiak, J.; Sattin, S.; Sutkevičiute, I.; Reina, J. J.; Sánchez-Navarro, M.; Thépaut, M.; Martínez-Prats, L.; Daggetti, A.; Fieschi, F.; Delgado, R.; Bernardi, A.; Rojo, J. Pseudosaccharide functionalized dendrimers as potent inhibitors of DC-SIGN dependent Ebola pseudotyped viral infection. *Bioconjugate Chem.* **2011**, *22*, 1354–1365.
- (143) Garcia-Vallejo, J. J.; Koning, N.; Ambrosini, M.; Kalay, H.; Vuist, I.; Sarrami-Forooshani, R.; Geijtenbeek, T. B. H.; van Kooyk, Y. Glycodendrimers prevent HIV transmission via DC-SIGN on dendritic cells. *Int. Immunol.* **2013**, *25*, 221–233.
- (144) Ordanini, S.; Varga, N.; Porkolab, V.; Thépaut, M.; Belvisi, L.; Bertaglia, A.; Palmioli, A.; Berzi, A.; Trabattoni, D.; Clerici, M.; Fieschi, F.; Bernardi, A. Designing nanomolar antagonists of DC-SIGN-mediated HIV infection: Ligand presentation using molecular rods. *Chem. Commun.* **2015**, *51*, 3816–3819.
- (145) Luczkowiak, J.; Muñoz, A.; Sánchez-Navarro, M. A.; Ribeiro-viana, R.; Ginieis, A.; Illescas, B. M.; Martín, N.; Delgado, R.; Rojo, J.; Mart, N.; Delgado, R.; Rojo, J. Glycofullerenes inhibit viral infection. *Biomacromolecules* **2013**, *14*, 431–437.
- (146) Delbianco, M.; Bharate, P.; Varela-Aramburu, S.; Seeberger, P. H. Carbohydrates in supramolecular chemistry. *Chem. Rev.* **2016**, *116*, 1693–1752.
- (147) Zhang, Q.; Su, L.; Collins, J.; Chen, G.; Wallis, R.; Mitchell, D. A.; Haddleton, D. M.; Becer, C. R. Dendritic cell lectin-targeting sentinel-like unimolecular glycoconjugates to release an anti-HIV drug. *J. Am. Chem. Soc.* **2014**, *136*, 4325–4332.
- (148) Morbioli, I.; Porkolab, V.; Magini, A.; Casnati, A.; Fieschi, F.; Sansone, F. Mannosylcalix[n]arenes as multivalent ligands for DC-SIGN. *Carbohydr. Res.* **2017**, *453–454*, 36–43.
- (149) Adak, A. K.; Lin, H. J.; Lin, C. C. Multivalent glycosylated nanoparticles for studying carbohydrate-protein interactions. *Org. Biomol. Chem.* **2014**, *12*, 5563–5573.
- (150) Martínez-Ávila, O.; Hijazi, K.; Marradi, M.; Clavel, C.; Campion, C.; Kelly, C.; Penadés, S. Gold manno-glyconanoparticles: multivalent systems to block HIV-1 gp120 binding to

- the lectin DC-SIGN. *Chem. - Eur. J.* **2009**, *15*, 9874–9888.
- (151) Ribeiro-Viana, R.; Sánchez-Navarro, M.; Luczkowiak, J.; Koeppe, J. R.; Delgado, R.; Rojo, J.; Davis, B. G. Virus-like glycodendrinanoparticles displaying quasi-equivalent nested polyvalency upon glycoprotein platforms potently block viral infection. *Nat. Commun.* **2012**, *3*, 1303.
- (152) Floyd, N.; Vijayakrishnan, B.; Koeppe, J. R.; Davis, B. G. Thiyl glycosylation of olefinic proteins: S-linked glycoconjugate synthesis. *Angew. Chem., Int. Ed.* **2009**, *48*, 7798–7802.
- (153) Pelegri-O'Day, E. M.; Paluck, S. J.; Maynard, H. D. Substituted polyesters by thiol-ene modification: rapid diversification for therapeutic protein stabilization. *J. Am. Chem. Soc.* **2017**, *139*, 1145–1154.
- (154) Zhu, S. J.; Ying, H. Z.; Wu, Y.; Qiu, N.; Liu, T.; Yang, B.; Dong, X. W.; Hu, Y. Z. Design, synthesis and biological evaluation of novel podophyllotoxin derivatives bearing 4 $\beta$ -disulfide/trisulfide bond as cytotoxic agents. *RSC Adv.* **2015**, *5*, 103172–103183.
- (155) Kalhor-Monfared, S.; Jafari, M. R.; Patterson, J. T.; Kitov, P. I.; Dwyer, J. J.; Nuss, J. M.; Derda, R. Rapid biocompatible macrocyclization of peptides with decafluoro-diphenylsulfone. *Chem. Sci.* **2016**, *7*, 3785–3790.
- (156) Hill, R. T. Plasmonic biosensors. *Wiley Interdiscip. Rev. Nanomedicine Nanobiotechnology* **2015**, *7*, 152–168.
- (157) Olaru, A.; Bala, C.; Jaffrezic-Renault, N.; Aboul-Enein, H. Y. Surface plasmon resonance (SPR) biosensors in pharmaceutical analysis. *Crit. Rev. Anal. Chem.* **2015**, *45*, 97–105.
- (158) Tabarani, G.; Thépaut, M.; Stroebel, D.; Ebei, C.; Vivès, C.; Vachette, P.; Durand, D.; Fieschi, F.; Thepaut, M.; Stroebel, D.; Ebel, C.; Vives, C.; Vachette, P.; Durand, D.; Fieschi, F. DC-SIGN neck domain is a pH-sensor controlling oligomerization. SAXS and hydrodynamic studies of extracellular domain. *J. Biol. Chem.* **2009**, *284*, 21229–21240.
- (159) Su, S. V.; Hong, P.; Baik, S.; Negrete, O. A.; Gurney, K. B.; Lee, B. DC-SIGN binds to HIV-1 glycoprotein 120 in a distinct but overlapping fashion compared with ICAM-2 and ICAM-3. *J. Biol. Chem.* **2004**, *279*, 19122–19132.
- (160) Menon, S.; Rosenberg, K.; Graham, S. A.; Ward, E. M.; Taylor, M. E.; Drickamer, K.; Leckband, D. E. Binding-site geometry and flexibility in DC-SIGN demonstrated with surface force measurements. *Proc. Natl. Acad. Sci.* **2009**, *106*, 11524–11529.
- (161) Zhang, Q.; Collins, J.; Anastasaki, A.; Wallis, R.; Mitchell, D. A.; Becer, C. R.; Haddleton, D. M. Sequence-controlled multi-block glycopolymers to inhibit DC-SIGN-gp120 binding. *Angew. Chem., Int. Ed.* **2013**, *52*, 4435–4439.
- (162) Wang, S.-K.; Liang, P.-H.; Astronomo, R. D.; Hsu, T.-L.; Hsieh, S.-L.; Burton, D. R.; Wong, C.-H. Targeting the carbohydrates on HIV-1: Interaction of oligomannose dendrons with human monoclonal antibody 2G12 and DC-SIGN. *Proc. Natl. Acad. Sci.* **2008**, *105*, 3690–3695.
- (163) Wu, L.; Martin, T. D.; Carrington, M.; KewalRamani, V. N. Raji B cells, misidentified as

- THP-1 cells, stimulate DC-SIGN-mediated HIV transmission. *Virology* **2004**, *318*, 17–23.
- (164) Liu, J.; Bartesaghi, A.; Borgnia, M. J.; Sapiro, G.; Subramaniam, S. Molecular architecture of native HIV-1 gp120 trimers. *Nature* **2008**, *455*, 109–113.
- (165) Mangold, S. L.; Prost, L. R.; Kiessling, L. L. Quinoxalinone inhibitors of the lectin DC-SIGN. *Chem. Sci.* **2012**, *3*, 772–777.
- (166) Arnáiz, B.; Martínez-Ávila, O.; Falcon-Perez, J. M.; Penadés, S. Cellular uptake of gold nanoparticles bearing HIV gp120 oligomannosides. *Bioconjugate Chem.* **2012**, *23*, 814–825.
- (167) Boulant, S.; Stanifer, M.; Lozach, P. Y. Dynamics of virus-receptor interactions in virus binding, signaling, and endocytosis. *Viruses* **2015**, *7*, 2794–2815.
- (168) Řezáčová, P.; Pokorná, J.; Brynda, J.; Kožíšek, M.; Cígler, P.; Lepšík, M.; Fanfrlík, J.; Řezáč, J.; Šašková, K. G.; Siegllová, I.; Plešek, J.; Šícha, V.; Grüner, B.; Oberwinkler, H.; Sedláček, J.; Kräusslich, H. G.; Hobza, P.; Král, V.; Konvalinka, J. Design of HIV protease inhibitors based on inorganic polyhedral metallacarboranes. *J. Med. Chem.* **2009**, *52*, 7132–7141.
- (169) Lo Conte, M.; Staderini, S.; Chambery, A.; Berthet, N.; Dumy, P.; Renaudet, O.; Marra, A.; Dondoni, A. Glycoside and peptide clustering around the octasilsesquioxane scaffold via photoinduced free-radical thiol-ene coupling. The observation of a striking glycoside cluster effect. *Org. Biomol. Chem.* **2012**, *10*, 3269–3277.
- (170) Levine, D. J.; Stöhr, J.; Falese, L. E.; Ollesch, J.; Wille, H.; Prusiner, S. B.; Long, J. R. Mechanism of scrapie prion precipitation with phosphotungstate anions. *ACS Chem. Biol.* **2015**, *10*, 1269–1277.
- (171) Pöhlmann, S.; Baribaud, F.; Lee, B.; Leslie, G. J.; Sanchez, M. D.; Hiebenthal-Millow, K.; Münch, J.; Kirchhoff, F.; Doms, R. W. DC-SIGN interactions with human immunodeficiency virus type 1 and 2 and simian immunodeficiency virus. *J. Virol.* **2001**, *75*, 4664–4672.
- (172) Peach, M. E.; Sutherland, D. J. Reactions of some bromofluorobenzenes with copper(I) benzenethiolate. *J. Fluor. Chem.* **1981**, *17*, 225–231.
- (173) Feinberg, H.; Castelli, R.; Drickamer, K.; Seeberger, P. H.; Weis, W. I. Multiple modes of binding enhance the affinity of DC-SIGN for high mannose N-linked glycans found on viral glycoproteins. *J. Biol. Chem.* **2007**, *282*, 4202–4209.
- (174) Pieters, R. J. Maximising multivalency effects in protein–carbohydrate interactions. *Org. Biomol. Chem.* **2009**, *7*, 2013.
- (175) Turnbull, W. B.; Kalovidouris, S. A.; Stoddart, J. F. Large oligosaccharide-based glycodendrimers. *Chem. - Eur. J.* **2002**, *8*, 2988.
- (176) Nishikawa, K.; Matsuoka, K.; Kita, E.; Okabe, N.; Mizuguchi, M.; Hino, K.; Miyazawa, S.; Yamasaki, C.; Aoki, J.; Takashima, S.; Yamakawa, Y.; Nishijima, M.; Terunuma, D.; Kuzuhara, H.; Natori, Y. A therapeutic agent with oriented carbohydrates for treatment of

- infections by Shiga toxin-producing *Escherichia coli* O157:H7. *Proc. Natl. Acad. Sci.* **2002**, *99*, 7669–7674.
- (177) Disney, M. D.; Zheng, J.; Swager, T. M.; Seeberger, P. H. Detection of bacteria with carbohydrate-functionalized fluorescent polymers. *J. Am. Chem. Soc.* **2004**, *126*, 13343–13346.
- (178) Polizzotti, B. D.; Kiick, K. L. Effects of polymer structure on the inhibition of cholera toxin by linear polypeptide-based glycopolymers. *Biomacromolecules* **2006**, *7*, 483–490.
- (179) Baldini, L.; Casnati, A.; Sansone, F.; Ungaro, R. Calixarene-based multivalent ligands. *Chem. Soc. Rev.* **2007**, *36*, 254–266.
- (180) Castro, E.; Garcia, A. H.; Zavala, G.; Echegoyen, L. Fullerenes in biology and medicine. *J. Mater. Chem. B* **2017**, *5*, 6523–6535.
- (181) Marra, A.; Staderini, S.; Berthet, N.; Dumy, P.; Renaudet, O.; Dondoni, A. ThiyI glycosylation of propargylated octasilsesquioxane: synthesis and lectin-binding properties of densely glycosylated clusters on a cubic platform. *European J. Org. Chem.* **2013**, *2013*, 1144–1149.
- (182) Smith, A. M.; Marbella, L. E.; Johnston, K. A.; Hartmann, M. J.; Crawford, S. E.; Kozycz, L. M.; Seferos, D. S.; Millstone, J. E. Quantitative analysis of thiolated ligand exchange on gold nanoparticles monitored by <sup>1</sup>H NMR spectroscopy. *Anal. Chem.* **2015**, *87*, 2771–2778.
- (183) Chakraborty, P.; Nag, A.; Chakraborty, A.; Pradeep, T. Approaching materials with atomic precision using supramolecular cluster assemblies. *Acc. Chem. Res.* **2019**, *52*, 2–11.
- (184) Verma, A.; Stellacci, F. Effect of surface properties on nanoparticle-cell interactions. *Small* **2010**, *6*, 12–21.
- (185) Pinkard, A.; Champsaur, A. M.; Roy, X. Molecular clusters: nanoscale building blocks for solid-state materials. *Acc. Chem. Res.* **2018**, *51*, 919–929.
- (186) Zhukhovitskiy, A. V.; MacLeod, M. J.; Johnson, J. A. Carbene ligands in surface chemistry: from stabilization of discrete elemental allotropes to modification of nanoscale and bulk substrates. *Chem. Rev.* **2015**, *115*, 11503–11532.
- (187) Man, R. W. Y.; Li, C.-H.; MacLean, M. W. A.; Zenkina, O. V.; Zamora, M. T.; Saunders, L. N.; Rousina-Webb, A.; Nambo, M.; Crudden, C. M. Ultrastable gold nanoparticles modified by bidentate *N*-heterocyclic carbene ligands. *J. Am. Chem. Soc.* **2018**, *140*, 1576–1579.
- (188) Chu, Z.; Han, Y.; Král, P.; Klajn, R. “Precipitation on nanoparticles”: attractive intermolecular interactions stabilize specific ligand ratios on the surfaces of nanoparticles. *Angew. Chem., Int. Ed.* **2018**, *57*, 7023–7027.
- (189) Tang, Q.; Hu, G.; Fung, V.; Jiang, D. Insights into interfaces, stability, electronic properties, and catalytic activities of atomically precise metal nanoclusters from first principles. *Acc. Chem. Res.* **2018**, *51*, 2793–2802.

- (190) Jadzinsky, P. D.; Calero, G.; Ackerson, C. J.; Bushnell, D. A.; Kornberg, R. D. Structure of a thiol monolayer-protected gold nanoparticle at 1.1 Å resolution. *Science* **2007**, *318*, 430–433.
- (191) Zeng, C.; Chen, Y.; Kirschbaum, K.; Lambright, K. J.; Jin, R. Emergence of hierarchical structural complexities in nanoparticles and their assembly. *Science* **2016**, *354*, 1580–1584.
- (192) Gorin, D. J.; Sherry, B. D.; Toste, F. D. Ligand effects in homogeneous Au catalysis. *Chem. Rev.* **2008**, *108*, 3351–3378.
- (193) Yang, H.; Gabbai, F. P. Activation of a hydroamination gold catalyst by oxidation of a redox-noninnocent chlorostibine z-ligand. *J. Am. Chem. Soc.* **2015**, *137*, 13425–13432.
- (194) Messina, M. S.; Stauber, J. M.; Waddington, M. A.; Rheingold, A. L.; Maynard, H. D.; Spokoyny, A. M. Organometallic gold(III) reagents for cysteine arylation. *J. Am. Chem. Soc.* **2018**, *140*, 7065–7069.
- (195) Joost, M.; Amgoune, A.; Bourissou, D. Reactivity of gold complexes towards elementary organometallic reactions. *Angew. Chem., Int. Ed.* **2015**, *54*, 15022–15045.
- (196) Scott, V. J.; Labinger, J. A.; Bercaw, J. E. Mechanism of reductive elimination of methyl iodide from a novel gold(III)–monomethyl complex. *Organometallics* **2010**, *29*, 4090–4096.
- (197) Axtell, J. C.; Saleh, L. M. A.; Qian, E. A.; Wixtrom, A. I.; Spokoyny, A. M. Synthesis and applications of perfunctionalized boron clusters. *Inorg. Chem.* **2018**, *57*, 2333–2350.
- (198) Zeineddine, A.; Estévez, L.; Mallet-Ladeira, S.; Miqueu, K.; Amgoune, A.; Bourissou, D. Rational development of catalytic Au(I)/Au(III) arylation involving mild oxidative addition of aryl halides. *Nat. Commun.* **2017**, *8*, 565.
- (199) Hesp, K. D.; Stradiotto, M. Stereo- and regioselective gold-catalyzed hydroamination of internal alkynes with dialkylamines. *J. Am. Chem. Soc.* **2010**, *132*, 18026–18029.
- (200) Cook, A. W.; Jones, Z. R.; Wu, G.; Scott, S. L.; Hayton, T. W. An organometallic Cu<sub>20</sub> nanocluster: synthesis, characterization, immobilization on silica, and “click” chemistry. *J. Am. Chem. Soc.* **2018**, *140*, 394–400.
- (201) Bai, J.; Virovets, A. V.; Scheer, M. Synthesis of inorganic fullerene-like molecules. *Science* **2003**, *300*, 781–783.
- (202) Fields-Zinna, C. A.; Sampson, J. S.; Crowe, M. C.; Tracy, J. B.; Parker, J. F.; DeNey, A. M.; Muddiman, D. C.; Murray, R. W. Tandem mass spectrometry of thiolate-protected Au nanoparticles Na<sub>x</sub>Au<sub>25</sub>(SC<sub>2</sub>H<sub>4</sub>Ph)<sub>18–y</sub>(S(C<sub>2</sub>H<sub>4</sub>O)<sub>5</sub>CH<sub>3</sub>)<sub>y</sub>. *J. Am. Chem. Soc.* **2009**, *131*, 13844–13851.
- (203) Thapa, B.; Schlegel, H. B. Density functional theory calculation of pK<sub>a</sub>'s of thiols in aqueous solution using explicit water molecules and the polarizable continuum model. *J. Phys. Chem. A* **2016**, *120*, 5726–5735.
- (204) Jencks, W. P.; Salvesen, K. Equilibrium deuterium isotope effects on the ionization of thiol

- acids. *J. Am. Chem. Soc.* **1971**, *93*, 4433–4436.
- (205) Zhang, C.; Vinogradova, E. V.; Spokoyny, A. M.; Buchwald, S. L.; Pentelute, B. L. Arylation chemistry for bioconjugation. *Angew. Chem., Int. Ed.* **2019**, *58*, 4810–4839.
- (206) Liu, R.; Priestley, R. D. Rational design and fabrication of core–shell nanoparticles through a one-step/pot strategy. *J. Mater. Chem. A* **2016**, *4*, 6680–6692.
- (207) Yan, Y.; Björnmalm, M.; Caruso, F. Assembly of layer-by-layer particles and their interactions with biological systems. *Chem. Mater.* **2014**, *26*, 452–460.
- (208) Melton-Celsa, A. R. Shiga toxin (Stx) classification, structure, and function. *Microbiol. Spectr.* **2014**, *2*, 1–13.
- (209) Jennum, K.; Vestergaard, M.; Pedersen, A.; Fock, J.; Jensen, J.; Santella, M.; Led, J.; Kilså, K.; Bjørnholm, T.; Nielsen, M. Synthesis of oligo(phenyleneethynylene)s with vertically disposed tetrathiafulvalene units. *Synthesis* **2011**, *2011*, 539–548.
- (210) Lundgren, R. J.; Sapping-Kumankumah, A.; Stradiotto, M. A highly versatile catalyst system for the cross-coupling of aryl chlorides and amines. *Chem. - Eur. J.* **2010**, *16*, 1983–1991.
- (211) Lee, M. W.; Farha, O. K.; Hawthorne, M. F.; Hansch, C. H. Alkoxy derivatives of dodecaborate: discrete nanomolecular ions with tunable pseudometallic properties. *Angew. Chem., Int. Ed.* **2007**, *46*, 3018–3022.
- (212) Barton, J. L.; Wixtrom, A. I.; Kowalski, J. A.; Qian, E. A.; Jung, D.; Brushett, F. R.; Spokoyny, A. M. Perfunctionalized dodecaborate clusters as stable metal-free active materials for charge storage. *ACS Appl. Energy Mater.* **2019**, *2*, 4907–4913.
- (213) Heravi, M. M.; Ghavidel, M.; Mohammadkhani, L. Beyond a solvent: triple roles of dimethylformamide in organic chemistry. *RSC Adv.* **2018**, *8*, 27832–27862.
- (214) Jacobson, J. M.; Yin, J.; Kitov, P. I.; Mulvey, G.; Griener, T. P.; James, M. N. G.; Armstrong, G.; Bundle, D. R. The crystal structure of Shiga toxin type 2 with bound disaccharide guides the design of a heterobifunctional toxin inhibitor. *J. Biol. Chem.* **2014**, *289*, 885–894.
- (215) Becke, A. D. Density-functional exchange-energy approximation with correct asymptotic behavior. *Phys. Rev. A* **1988**, *38*, 3098–3100.
- (216) Bayly, C. I.; Cieplak, P.; Cornell, W.; Kollman, P. A. A well-behaved electrostatic potential based method using charge restraints for deriving atomic charges: the RESP model. *J. Phys. Chem.* **1993**, *97*, 10269–10280.
- (217) Ling, H.; Boodhoo, A.; Hazes, B.; Cummings, M. D.; Armstrong, G. D.; Brunton, J. L.; Read, R. J. Structure of the Shiga-like toxin I B-pentamer complexed with an analogue of its receptor Gb<sub>3</sub>. *Biochemistry* **1998**, *37*, 1777–1788.
- (218) Spek, A. L. Structure validation in chemical crystallography. *Acta Crystallogr. Sect. D Biol. Crystallogr.* **2009**, *65*, 148–155.